NASA CR-66731

AN INVESTIGATION OF SOME THERMAL AND MECHANICAL PROPERTIES OF A LOW-DENSITY PHENOLIC-NYLON ABLATION MATERIAL

by H. G. Sanders, E. D. Smyly, and C. D. Pears

Prepared by
SOUTHERN RESEARCH INSTITUTE
Birmingham, Alabama
for Langley Research Center

NATIONAL AERONAUTICS AND SPACE ADMINISTRATION

February 1969

AN INVESTIGATION OF SOME THERMAL AND MECHANICAL PROPERTIES OF A LOW-DENSITY PHENOLIC-NYLON **ABLATION** MATERIAL

By H. G. Sanders, E. D. Smyly,
and C. D. Pears

Prepared under Contract No. NAS **1-5448**
SOUTHERN RESEARCH INSTITUTE
Birmingham, Alabama

for Langley Research Center

NATIONAL AERONAUTICS AND SPACE ADMINISTRATION

CONTENTS

CONTENTS - continued

PART II

CONTENTS - continued

LIST OF ILLUSTRATIONS

LIST OF ILLUSTRATIONS - continued

LIST OF ILLUSTRATIONS - continued

LIST OF ILLUSTRATIONS - continued

LIST OF ILLUSTRATIONS - continued

LIST OF ILLUSTRATIONS - continued

LIST OF ILLUSTRATIONS - continued

LIST OF ILLUSTRATIONS - continued

LIST OF ILLUSTRATIONS - continued

LIST OF ILLUSTRATIONS - continued

LIST OF ILLUSTRATIONS - continued

LIST OF ILLUSTRATIONS - continued

LIST OF TABLES

LIST OF TABLES - continued

LIST OF TABLES - continued

LIST OF TABLES - continued

LIST OF TABLES - continued

AN INVESTIGATION OF SOME THERMAL AND MECHANICAL PROPERTIES OF A LOW-DENSITY PHENOLIC-NYLON ABLATION MATERIAL

By H. G. Sanders, E. D. Smyly
and C. D. Pears

ABSTRACT

The thermal and mechanical properties of low-density phenolic-nylon were studied. The studies consisted of two separate parts. Part I consisted of studies of the tensile and compressive properties of the nondegraded material to isolate the effects of variations in experimental techniques, test conditions and environmental parameters from the intrinsic properties. Part II consisted of characterization of the charred material, definition of its thermal conductivity and the development of an analysis so that the data could be extrapolated to conditions other than those under which the measurements were made.

Under Part I, the studies of the nondegraded low-density phenolic-nylon revealed that specimen configuration, specimen size, stress rate, heating rate, and time at elevated temperature had little effect on the tensile and compressive properties over relatively large ranges. Other factors such as density and moisture were revealed to have an overbearing effect on these properties, perhaps to the extent of masking the effect of the variables first investigated. The effects of these variables were isolated, and the results provide guide lines for characterization of this material.

Under Part II, a characterization study was made to determine the bulk density, true density, permeability and characteristic X-ray diffraction patterns of low-density phenolic-nylon chars prepared in both an arc-jet and a high temperature furnace. Thermal conductivity measurements were made to 3033°K on chars prepared at different heating rates and to different temperature levels. The studies revealed that the char was more carbon-like than graphite-like when charring was performed in an arc-jet to about 2000°K (heat flux of 1.13 MW/m^2 to 2.27 MW/m^2) or in a furnace at a low heating rate to 3033°K. The char exhibited a significant trend toward graphite-like behavior when prepared by rapid heating (heat flux of 4.9 MW/m^2) in a furnace to 3033°K. The thermal conductivity of the carbon-like char was found to increase significantly with temperature. A significant portion of this increase was attributable to an increase in the thermal conductivity of the matrix (solid) portion of the char as the maximum exposure temperature increased. The radiation heat transfer through

the char was not experimentally separated from the contributions by solid conduction and gas conduction. Analyses of the possible mechanisms for radiation heat transfer in the porous char led to the conclusion that the char must become transparent at high temperatures if radiation is to explain the significant increase in thermal conductivity with temperature. It was determined that if radiation is not predominant in the carbon-like char the thermal conductivity of the matrix, after stabilization by heat treatment at 3033°K, must increase by a factor of two between 500°K and 3033°K. An equation was developed to allow the reduction of the thermal conductivity of the matrix from the effective thermal conductivity measurements. Using the equation, values of the thermal conductivity of the matrix are reduced from measurements on chars prepared at different temperature levels. The values of the thermal conductivity of the matrix at each precharring temperature level (boxing values) when used with the equation form the basis for extrapolating the steady-state thermal conductivity values to the values expected under flight conditions. The uncertainty in the extrapolation procedure relates directly to the uncertainty in the radiation heat transfer component. Extrapolated values for the effective thermal conductivity of the char are compared with values reduced from transient temperature measurements made during ablation tests by other laboratories. It was found that the thermal conductivity values reduced from the transient measurements with an equation which included heat absorption by the pyrolysis gases were several times higher than the values obtained when the gas effects were neglected in the analysis. That is, the major thermal resistance is the consequence of the gas generation.

INTRODUCTION

This is the final report to the National Aeronautics and Space Administration, Langley Research Center, under Task Order 4 of Contract NAS 1-5448. This task was for thermophysical property measurements on a low-density phenolic-nylon ablation material. The effort consisted of mechanical property studies of the nondegraded material and characterization and thermal conductivity and permeability measurements of the char formed from the degradation of the material.

The objectives of the program were (1) to obtain data for which the effects of variations in experimental techniques, test conditions, and environmental parameters could be isolated from the intrinsic mechanical properties of the ablation material, and (2) to obtain and analyze data which could be used to predict the flight performance of the char. These objectives were pursued in two separate efforts. Under Part I, the mechanical properties of the nondegraded material were studied, and under Part II, the char was characterized and its thermal conductivity was studied.

Prior to this program, the characterization of the mechanical properties of nondegraded phenolic-nylon consisted of preliminary investigations to establish test methods based on the use of the material. Evaluations were made for temperatures from 144°K (-200°F) to 477°K (400°F). In the prior programs considerable data scatter was observed, especially at temperatures below ambient temperature. This scatter could have been an intrinsic property of the material, could have resulted from the effects of variation in experimental technique, or could have resulted from a combination of both suppositions. The manufacture of this ablative material consisted of:

1. dry blending of several finely powdered ingredients
2. compressive molding under heat and pressure to reduce the bulk and cure the resin matrix
3. postcuring of the molded material at elevated temperature to assure full cure and thermal stability

Because of the complications involved in each of these processes, even to the degree of reproducibility of the raw materials themselves, the intrinsic property supposition could have been the predominant factor affecting data scatter. Therefore, in order to test this supposition, the objective of the mechanical property studies was to evaluate the effects of experimental techniques in order to determine optimum test conditions. Some of the parameters studied were:

1. the effects of specimen size and shape at room temperature on measured values of tensile and compressive elastic modulus and ultimate strength
2. the effects of stress rates at room temperature on tensile and compressive elastic modulus and ultimate strength, Stress rates from 172 x 10^3 to approximately 6900 x 10^3 $N/m^2/sec$ were used
3. the effects of heating rate and time at temperature on tensile and compressive elastic modulus and ultimate strength. Heating rates of 22 to 111°K/min to test temperatures of 422°K to 477°K were used

Then, utilizing the results of these evaluations, testing was conducted at 144°K (-200°F) and at room temperature to evaluate the nature of the material and to determine if the data scatter is greater at 144°K than at room temperature.

The objective in investigating the degraded material was to determine its influence on the ablative process during entry conditions. Phenolic-nylon has been used for several years as an ablative material because of its ability to provide thermal protection against the high heat flux densities

encountered at entry. It provides good thermal protection because of its low thermal conductivity and because it generates gaseous products during degradation which absorb significant amounts of heat. Also, the gases transpire through the char layer formed on the surface and alter the boundary layer heating effects. Since it is a serviceable thermal protection system, considerable effort has been expended toward understanding the ablative behavior of this material. This effort has taken the form of performing theoretical analyses of the ablating system and of measuring the thermophysical properties required in the analyses. A correlation of the analyses with simulated-flight test and/or flight test data, using the proper thermophysical properties, is required to confirm the analyses and thus allow the design of an optimum weight heat shield for a particular mission.

The measurements of the thermophysical properties during the active ablation process is not within the present state of the art. Consequently, analytical predictions of the performance of charring ablators depend upon the use of thermophysical properties measured on material which has been precharred. Therefore, when disagreements between theoretical predictions and experimental observations and measurements of the degrading system exist it is difficult to evaluate the source of these differences. Differences can arise because of the assumptions inherent in the Analyses or because the thermophysical properties measured on the precharred materials are different from the properties of the material during the short-time exposure during active ablation.

Of all the properties of the phenolic-nylon, the two which are open to the most question are the enthalpy of the gaseous products of pyrolysis and the thermal conductivity of the char. To make matters worse, these two properties have the greatest influence on the thermal performance of phenolic-nylon. Of the two, the enthalpy of the pyrolysis products is the most difficult to determine experimentally because of the multitude of gas species present and the complex interactions which occur as the relative concentrations change as a function of temperature.[1] Therefore, considerable attention has been directed toward defining the thermal conductivity of the char so that gas effects can be studied from correlations of the analytical predictions with experimental data.

The most precise measurements of the thermal conductivity of phenolic-nylon char have been made with steady-state apparatuses. These measurements show a thermal conductivity which increases by nearly a factor of 10 as the temperature is increased from 500°K to 3000°K.[2] Some authors have taken exception to this behavior, claiming that the time required for the steady-state measurements allows additional graphitization of the solid to occur which would not occur in flight.[3] Further, some mea-

surements of the overall conductance of the char layer have indicated that the thermal conductivity of the char during ablation is lower than the values measured with steady-state techniques. The analysis commonly used for reducing the thermal conductivity from the overall conductance measurements neglects heat absorption by the pyrolysis gases, but it is agreed that these effects are small.

Swann, Pittman, and Smith[4] have developed a one-dimensional analysis of the transient behavior of charring ablators. Two different reports have been written which correlate this analysis with measurements made under simulated flight conditions.[5,7] Pittman and Brewer[7] found that good agreement could be obtained by using the steady-state values for conductivity if the theoretical gas enthalpy curves developed by Kratsch[7] were used. McLain, et al,[6] concluded that the steady-state thermal conductivity values were high by a factor a three when carbon monoxide was assumed to be the pyrolysis gas. Thus, one can see that neither the thermal conductivity nor the gas effects can be studied by correlation of the thermal model with experimental data until one or the other is accurately known.

The objective of Part II of this program was to study the effects of thermal history on the thermal conductivity of the char and to analytically separate the relative contributions of the various modes of heat transfer to the effective thermal conductivity of the char. With this knowledge one could develop analytical expressions which could be used to predict the thermal conductivity of the char under flight conditions, Thus, the goal of this work was to isolate the intrinsic properties of the phenolic-nylon char so that the flight performance of the material could be predicted under actual use conditions.

SPECIMEN MATERIAL

The low-density phenolic-nylon was supplied by the NASA Langley Research Center in both nondegraded and thermally degraded forms. The nondegraded material was supplied in the form of discs 7.6 cm thick by 30.4 cm in diameter. The charred material was supplied in the form of discs 5.4 cm in diameter by about 0.635 cm thick.

This low-density phenolic-nylon had a nominal density of 0.65 gm/cm^3, was molded, and consisted of the following constituents: (1) 40 percent (by weight) Zytel 103 (120 mesh) nylon powder, (2) 23 percent phenolic Microballoons (-50 to 230 mesh fraction), (3) 37 percent Hughes HFN Novolac phenolic resin. The molding was performed at a temperature of 408°K for

three hours. The molding pressure was not specified. The documentation of the formulation and molding conditions supplied by the manufacturer of the material is given in Appendix A. A complete description of the general processing of the phenolic-nylon is given in Reference 7. Some physical properties of the materials from which this low-density phenolic-nylon was made or for similar materials are given in Appendix B.

The Phenolic-novolac resin in the material is a condensation polymer formed by the reaction of phenol and formaldehyde. The product is a thermoplastic resin. The thermoplastic novolac polymer is converted to an infusible cross linked polymer by the addition of additional sources of methylene linkages. The final product is similar to resole formation and results in a highly cross linked infusible product. The phenolic Microballoons are made of cured phenolic resin and as such are also probably infusible cross linked polymers.

The thermally degraded material was produced in an arc-jet at the NASA Langley Research Center. Half of the 5.4 cm disks of phenolic-nylon char supplied were exposed to the following conditions during charring: a stagnation enthalpy of 2.8 MJ/Kg (1200 Btu/lb), pressure of 2×10^3 N/m^2 (0.290 lb/in.^{2}), heat flux of 1.13 MW/m^2 (100 Btu/sec-ft^2) and an exposure time of 130 seconds. The charring conditions for the remainder of the disks were as follows: a stagnation enthalpy of 2.8 MJ/Kg (1200 Btu/lb), pressure of 5×10^3 N/m^2 (0.73 lb/in.^{2}), heat flux of 2.27 MW/m^2 (200 Btu/sec-ft^2) and an exposure time of 135 seconds.

The bulk densities of the charred materials varied, but the nominal values were 0.25 gm/cm^3 for the material charred at 1.13 MW/m^2 and 0.30 gm/cm^3 for the material charred at 2.27 MW/m^2.

PART I

MECHANICAL PROPERTY STUDIES OF NONDEGRADED MATERIAL

Introduction

The scope of this part of the program was to obtain a better characterization of low-density phenolic-nylon through the study of environmental parameters and test conditions resulting in an improved test configuration and improved methods of testing. In order to efficiently carry out the mechanical testing for this part of the program, the work was divided into two phases.

Phase I. - The objectives of this phase of the program were to provide:

1. A reliable specimen design for both tensile and compressive specimens;
2. Data to determine whether a relationship exists between specimen strength and specimen size or configuration;
3. Data to determine the effects of stress rate on the elastic moduli and ultimate strengths of tensile and compressive specimens.

Several tensile and compressive specimen designs were available. For example, the specimen could have a rectangular, square, or a circular cross section within the gage length. For ductile materials, this consideration may not be of any consequence. However, for brittle or semibrittle materials the presence of corners could affect the data, especially for low temperature applications when the material becomes increasingly brittle. Also, heretofore, the compressive specimens used were boxlike, usually $\frac{1}{2}$ in. x $\frac{1}{2}$ in. x 1 in. making it more difficult to measure true strain.

The selection of a specimen design for the tensile and compressive specimens was made by preparing specimens having rectangular, square, and circular cross sections. Each of the tensile and compressive specimens of the different shapes had identical volumes and were tested at the same stress rate. Also, a study was made to determine the effects on initial elastic moduli resulting from slight variations in slenderness ratio of the different compressive configurations.

After the specimen configurations were selected for both the tensile and compressive evaluations, the effects of gage volume and stress rate were studied. To determine the volume effect on the tensile specimen, two gage volumes were tested (0.80 and 6.44 cm^3). Similarly, the volume effect on the compressive specimen was studied using two volumes (0.40 and 3.21 cm^3). From these data, the Weibull constant for the material was determined in order that effects for smaller and larger volumes than these could be extrapolated. The effects of stress rate on tensile and compressive elastic moduli and strength were studied using stress rates of 172 x 10^3, 690 x 10^3, and 1860 x 10^3 $N/m^2/sec$. Because these stress rates were considerably lower than those experienced in flight, a limited number of compressive and tensile tests were performed at a stress rate in the range of 6900 x 10^3 $N/m^2/sec$.

Phase II. - The objectives of this portion of the program were to provide:

1. Data for studying the effects of time at temperature in the range of 422°K to 477°K on initial elastic moduli and strength in compression and tension;
2. Data for investigating data scatter at 144°K (-200°F).

The shapes and sizes of the specimens, both tensile and compressive, and the stress rate used in this phase of the program were selected based on the results of Phase I.

Three important factors were considered during the high temperature studies (422°K to 477°K): (1) the heating rate; (2) the loading rate; (3) the total time at temperature, The third variable, total time at temperature, was of primary concern being, of course, influenced by the other two factors. In order to consider the effect of heating rate, two tensile runs were conducted at each of three different heating rates (22, 55.5, and 111.0°K/min) to the three different test temperatures (422°K, 450°K, and 477°K). Loading was initiated immediately when the surface of the specimen reached the prescribed test temperature. A constant loading rate (determined from Phase I testing - 690 x 10^3 $N/m^2/sec$) was used for all tests. Then compressive and tensile runs were made holding constant the time of heating to the test temperature.

The low temperature tests were conducted at 144°K. Additional runs were made at room temperature to provide data for statistical

analysis. It was felt that 15 runs at room temperature and 20 runs at 144°K would provide a meaningful analysis.

During the actual running of the tests, care was taken to prevent the occurrence of systematic errors which could affect the data. For example, each specimen tested at 144°K was dryed at 377°K for 24 hours in order to remove any moisture which would cause prestressing of the specimen when the moisture froze at low temperature.

In pursuing the scope of this program, some other parameters which significantly affected the characterization of low-density phenolic-nylon were studied. For example, as a result of variations in mechanical properties for evaluations made several months apart for Specimens from the same billet, a study was made to determine if moisture content affected mechanical properties. For this study, tensile and compressive specimens from adjacent positions within a single billet were selected. Two were dried for 24 or 40 hours at 377°K in an oven before testing, and two were tested at the same time without any conditioning. Another parameter investigated and determined to be a factor affecting characterization was density (to the extent that the light colored areas within the billets were denser than the dark and yielded higher values of elastic moduli and strength).

Apparatuses and Procedures

Tensile Evaluations. - The tensile evaluations from 144°K (-200°F) to 477°K (400°F) were determined using a Tinius-Olsen universal testing machine with mechanical screw loading as the basic apparatus. Threaded loading rods were used for the load train for both the room temperature and high temperature evaluations. The ultimate strengths measured using this apparatus were comparable with values measured in our gas-bearing testing facility described in Appendix C. For the cold runs, in order to minimize parasitic stresses, a universal joint was added to the lower loading rod; and a loading chain was used as the upper loading mechanism to complete the load train. This type of system has been used here before for measuring the tensile strength of brittle materials such as graphite. The results of these tests were also comparable to those obtained from our gas-bearing tensile facility.

The output load signal from the Tinius-Olsen was fed into the ordinate of a Model 135 Mosely recorder. A final calibration of pen travel of X-Y recorder was made by dead weight loading. The calibration was checked regularly throughout the runs to maintain an accurate calibration;

Also, a comparison of the recorded load to the visual dial gage of the Tinius-Olsen during each run was made to further check calibration.

The axial strain was measured by clip-on extensometers. The basic features of the clip-on extensometers are shown in figure 1. An extensometer was clipped on each side of the specimen. Insulators of steatite ceramic were used as the rigid contact arms. While providing electrical and thermal insulation for the extensometer springs, the ceramic contact arms translated the elongation within the gage length of the specimen into flexure of the springs. Type SR-4 strain gages were mounted on both sides of the springs and connected electrically into a bridge circuit. With two strain gages in tension and two in compression, all four gages in the bridge circuit served as both strain-measuring and as temperature-compensating gages. The output of the extensometer was an electrical signal proportional to the average strain along two edges of the specimen.

The free lengths of the clip-on extensometers were about 10 percent greater than the gage length. The extensometers were attached to the specimen by depressing the free ends of the contact arms sufficiently to insert them between the gage point yokes attached to the specimen. The restoring forces of the springs were small yet sufficient to cause the extensometers to support themselves between the yokes and to follow the elongation of the specimen. Thus, as the specimen was strained during a run, the springs relaxed proportionately incurring a change in the strain which was sensed by the SR-4 strain-gage bridge.

The clip-on extensometers were calibrated using a shunt resistor calibration circuit and a micrometer accurate to 0.0001 inch. The electrical signal from the extensometers was fed into the abscissa of the *X*-Y recorder, thus producing a complete, calibrated load-elongation curve to failure.

For high-temperature evaluations, two five-element quartz infrared lamps (controlled by a Powerstat for variability in heat output) located approximately three inches from opposing sides of the test specimen were used for heating. Temperature gradients and heating rates were determined from heat runs made with specimens instrumented with six thermocouples (chromel/alumel). For this determination, the gage length was instrumented with four surface thermocouples ($\frac{1}{32}$ inch within the outer surface of the specimen — one located at the upper extremity and three located about the center perimeter of the gage length) and two interior thermocouples (installed at the bottom of drilled holes to the center of the specimen — one located at the lower extremity and one located at the center of the gage length). Powerstat settings required to incur the proper heating rate and the final, stable test temperature were determined by time versus temperature runs made with the instrumented specimen. For actual test runs, these Powerstat settings versus time were used to heat and maintain the test temperature of the test specimen.

For the low-temperature evaluations, the specimen was cooled with vapors from liquid nitrogen. An insulated, cylindrical shell was placed around the specimen, and the vapors were blown into it. Again, temperature gradients were determined from runs made with a specimen instrumented with six thermocouples (chromel/alumel). One of the three surface thermocouples was taped to the outside surface while the other two were installed similarly to those used in the high temperature evaluations. All three surface thermocouples indicated equivalent temperatures. Thus, each specimen tested for cold-temperature effects was monitored by a thermocouple taped to the gage-length surface.

All specimens tested for low-temperature effects were dried for 24 hours at 377°K (220°F) in order to prevent any prestressing incurred by the freezing of moisture within the specimen.

Compressive Evaluations. - The compressive evaluations were made in our Tinius-Olsen universal testing machine and our gas-bearing compressive facility described in Appendix D. The specimen configuration studies of Phase I were conducted using the Tinius-Olsen setup which utilized the clip-on extensometers (described in the previous section on apparatuses used for the tensile evaluations) for measuring axial strain. The gas-bearing facility was used for the remaining runs of Phase I and for all the runs of Phase II. Results of tests conducted at room temperature in the two apparatuses were comparable.

As described in Appendix D, a typical gas-bearing compressive facility primarily includes a compressive frame with two gas bearings, a graphite resistance furnace, and an optical strain analyzer for measuring axial strain. For these evaluations, the optical strain analyzer for measuring lateral strains and the graphite resistance furnace were not used. The optical strain analyzer for measuring axial strain was used for the room temperature and high temperature evaluations. Axial strain for the cold temperature evaluations had to be measured with the clip-on extensometers, previously described, because of the inability of the optical extensometer system to see the flags through the dense vapor around the specimen.

For the high temperature evaluations, the five element quartz infrared lamps were again used. For the cold temperature evaluations, the specimen was again cooled with vapors from liquid nitrogen. This equipment and the test procedures associated with it were discussed in the previous section describing apparatuses used for the tensile determinations.

Bulk Density Measurements. - Each test specimen blank was sawed from the billet as furnished (12 in. diameter x 3 in. thick) and machined to blank size for accurate measurement. Lengths were measured with micrometers accurate to 0.0005 in., and weights were determined on an analytical balance sensitive to 0.0001 gm. After the densities were recorded, the specimen blanks were machined to final test configurations.

NDT Evaluations. - Sonic velocity measurements were made using our ultrasonic test system utilizing a longitudinal wave motion at frequencies in the range of 1 MHz. A pulsed ultrasonic generator provided the voltage to both the transmitting SFZ crystal and the trigger input to the oscilloscope, from which delay time was measured. The receiver signal was fed to the vertical axis of the oscilloscope. Pulse travel time in the material was measured accurately by adjusting the delay time multiplier until the first received peak was realigned to its calibration position on the CRT. Delay time was then recorded from the product of the delay time setting and the delay time multiplier. Division of the specimen thickness by the delay time provided the desired V_L value,

Transducers having resonance frequencies of 1 MHz and 1.127 cm diameters were used. To avoid errors induced by solid couplants, isopropyl alcohol was used.

Data and Results – Phase I Testing

Specimen Configuration Studies. - The three basic specimen configurations studied were: (1) circular cross section (1.270 cm dia); (2) square cross section (1.125 x 1.125 cm); (3) 2:1 width-to-thickness rectangular cross section (1.588 x 0.800 cm). Because of the brittle nature of phenolic-nylon, some of the compressive and tensile specimens were ground finished while others were machined finished in order to evaluate surface finish effects on ultimate strength.

The four basic compressive configurations evaluated are described in figures 2 through 5. These specimens had a constant gage-section volume (3.21 cm^3) with fairly uniform values of minimum slenderness ratio (circular configuration 8.0, square configuration 7.8, rectangular configuration 11.0). The specimen configurations used to evaluate the changes in slenderness ratio for the three basic configurations are described in figures 6 through 8.

The three basic tensile specimens evaluated are described in figures 9 through 11. These specimens also had approximately equal gage-section volumes (circular configuration, 6.44 cm^3; square configuration, 6.44 cm^3; rectangular configuration, 6.46 cm^3). In addition to studying these basic tensile configurations, evaluations were also made on the basic square cross section (1.125 x 1.125 cm) with a thick shank (1.67 cm), on the basic 2:1 width-to-thickness rectangular cross section (1.588 x 0.800 cm) with a thin shank (0.800 cm), and on a 4:1 width-to-thickness rectangular cross section (2.260 x 0.559 cm) shown in figure 12. The purpose of this testing was to measure any effects on tensile strength incurred by shank thickness between loading grips and to include a 4:1 width-to-thickness configuration which had indicated higher measurements of strength than similar configurations to these under a previous testing program conducted here on composite materials.

Compressive specimen configuration studies: The results of the specimen configuration studies in compression are tabulated in table 1. The results of this study comparing compressive strength, offset yield strength (0.2 percent), and initial elastic moduli to bulk density for the various configurations are plotted in figures 13 through 15. Typical stress-strain curves from these determinations are shown in figures 16 through 19.

As shown in table 1, the circular, the dumbbell, and the square configurations provided approximately equal mean values for elastic moduli and ultimate strength:

Cross Section Configuration	Compressive Elastic Modulus (10^9 N/m^2)	Compressive Strength (10^6 N/m^2)
Circular (1.270 cm dia)	1.08	30.0
Dumbbell (1.270 cm dia)	1.07	29.4
Square (1.125 x 1.125 cm)	1.10	29.6

The rectangular configuration, however, indicated lower average values for modulus (1.04 x 10^9 N/m^2) and compressive strength (26.6 x 10^6 N/m^2). These evaluations indicated, therefore, that either the circular, dumbbell, or the square configuration could be used to characterize compressive properties without incurring variations as a result of cross section configuration.

Note in table 1 that the results of evaluations on the circular configuration tested in the Tinius-Olsen apparatus and the dumbbell

configuration tested in the gas-bearing compressive facility were in good agreement. The average ultimate strength determined in the gas-bearing was 29.4 x 10^6 N/m^2 compared to 30.0 x 10^6 N/m^2 in the Tinius-Olsen, and the average elastic modulus was evaluated at approximately 1.07 x 10^9 N/m^2 in both apparatuses. Thus, the Tinius-Olsen setup should be suitable for testing from room temperature to 477°K. However, because brittleness increases with decreasing temperature, testing below room temperature should be done in the gas-bearing apparatus.

Normally, the gas-bearing apparatus measures higher ultimate strengths as a result of precise alignment of the loading train to the specimen. However, for the billets tested, 4 and 5, variations in bulk density within the billet (up to 20 percent) had been measured. These variations, as depicted by figure 13, seemed to affect the strength property, possibly offsetting the advantages of precise alignment provided by the gas-bearing apparatus. Such inconsistency within the material could have caused an inherent eccentric loading condition on the specimen. For example, if the density parameter were determined to be a factor affecting strength, then density variations within the gage section would result in areas of nonuniform stiffness resulting in an eccentrically-loaded specimen which would fail prematurely at a load level not indicative of the capability of the material.

In order to check for specimen bending, a limited number of runs were made in the Tinius-Olsen apparatus using the clip-on extensometers. For this determination, the clip-ons were connected electrically into a bridge circuit for measuring bending. The results of this evaluation are plotted as compressive stress versus bending strain in figures 20 through 22. Specimens for two directions of interest were considered (ab and c). Note that bending effects occurred at low values of stress and that the percentage of bending strain to axial strain at yield strength (0.2 percent) was as high as 19 percent in the ab direction. The results of this evaluation indicated that (1) bending was present during the compressive evaluations regardless of the precautions taken to control misalignment within the load train, possibly because of the density variations within the material resulting in unequal loading across the cross section, and (2) the variance in ultimate strength measured in the ab and c directions indicated anisotropic properties for the two directions.

The results of the slenderness-ratio studies on the basic cross section configurations to determine effects on the elastic modulus resulting from slight variations in slenderness ratio are tabulated in table 2. Slenderness ratio is defined as the ratio of specimen length to

radius of gyration. This nomenclature was used instead of the normal l/d due to the different cross sectional shapes. The results of the slenderness ratio studies comparing the elastic moduli, compressive yield strength (0.2 percent offset), and the ultimate strength to the slenderness ratio of the basic cross section configurations are plotted in figure 23. As shown in figure 23, all three configurations indicated a constant level of modulus for the varying values of slenderness ratio; therefore, the slight variations incurred in slenderness ratio had no effect on the results of the tests. Note that two curves were plotted for initial elastic moduli versus slenderness ratio. The slightly higher values measured for the 1.27 cm diameter circular cross section perhaps reflect the effects of the proportions of the specimen shape (diameter or minimum cross section dimension to height ratio). As the dimension in the direction of load decreases, the frictional effects incurred between the end of the specimen and the loading heads become more pronounced.

Tensile specimen configuration studies: Results of the specimen configuration studies in tension are tabulated in table 3. Typical tensile stress-strain curves for the basic circular (1.270 cm diameter), square (1.125 cm), 2:1 width-to-thickness (1.588 x 0.800 cm), and the 4:1 width-to-thickness (2.260 x 0.559 cm) configurations are given in figures 24 through 27. The results comparing tensile strength, yield strength, and initial elastic moduli to density for the various configurations are given in figures 28 through 30.

Typical for brittle materials, the data scatter was large. As shown in figure 28, little if any dependence of ultimate tensile strength on gage section configuration was discernible. Data scatter caused by density effects and frequent failures outside the gage section tended to screen configuration effects. Of the 36 tensile tests conducted on all configurations, 30 specimens (83 percent) failed at a strength level within the range of 8×10^6 N/m^2 to 10.5×10^6 N/m^2. Within this range, the data from all tensile specimen configurations were scattered throughout the range. Therefore, it appeared that the specimen gage section configuration (including shank thickness between grips) did not have any significant effect on ultimate strength. However, this evaluation was expanded to investigate surface effects; ground cross sections were tested. The data from these evaluations indicated that higher values of ultimate strength with somewhat less scatter resulted from tensile specimens having ground gage sections. Of the three machining processes used to finish the tensile specimens (milling, turning, and grinding), the smoothest surface was, of course, produced by grinding. The milling

process, and the turning process to a lesser degree, had a tendency of knocking particles from the composite material leaving voids in the new surface. This event occurred frequently at corners where the particle being exposed from two surfaces offered less resistance to displacement. In the case of brittle materials, such voids represent crack starters which often result in premature failure. Grinding at high speed (perhaps due to a high concentration of heat on the surface at the point of contact between the specimen and the grinding wheel) smeared these same particles resulting in a much smoother, improved finish. Therefore, ground gage surfaces assure that the surface flaws incurred by milling or turning are not more detrimental than the flaws inherent in the material resulting in premature failures.

Variations in the elastic properties (yield strength and initial elastic modulus) for the various configurations versus density are shown in figures 29 and 30. The data scatter for yield strength was quite large. Although the ground gage section indicated less scatter in the yield strength, it did not affect any reduction in scatter for measurements of elastic moduli. Again, the data indicated no apparent dependence of tensile properties on gage section configuration. Although no notable tensile property variations were measured within a single billet, some elastic property variations between billets were noted. Generally, billets 4 and 5 indicated higher values than billet 8 for the elastic properties for all configurations tested.

Volume Effect Studies. - The compressive and tensile specimen configurations evaluated for volume effects are shown in figures 31 through 33. These specimens were geometrically scaled down to one-half scale from the basic 1.27 cm diameter specimens (shown in figures 3 and 9). The compressive configuration shown in figure 31 had a gage section volume of 0.40 cm^3 compared to a gage section volume of 3.21 cm^3 for the basic 1.27 cm diameter dumbbell configuration (shown in figure 3). Two tensile configurations of the reduced section were used, shown in figures 32 and 33. The specimen shown in figure 32 was used in the Tinius-Olsen apparatus, and the specimen shown in figure 33 was used in the gas-bearing tensile facility. The gage section of both specimens were geometrically scaled down identically with the compressive specimen. The gage section volume of the scaled-down tensile specimens was 0.80 cm^3 compared to a gage section volume or 6.44 cm^3 for the basic 1.27 cm diameter cross section specimen.

Because past experience has shown that the smaller volumes usually produce the most pronounced volume effects, initially only the

volumes just described were considered for volume effects. Also, using the results from the room temperature tensile evaluations from Phase II of this part of the program, Weibull's constants for this material were determined in order to further extrapolate the effects of larger and smaller volumes.

Volume effects in compression: Results of the compressive tests for volumetric effects are tabulated in table 4; also see table 6. The results of this study comparing the 1.270 cm diameter to the one-half scale configuration versus ultimate compressive strength and elastic moduli are given in figures 34 and 35. A typical stress-strain curve for the scaled-down specimen is given in figure 36.

As shown in figure 34, runs from both volumes resulted with failures at a constant level of compressive strength (24.9×10^6 N/m^2 for the half-scale specimen and 24.6×10^6 N/m^2 for the 1.270 cm diameter specimen). Unexpectedly, however, a significant variance in modulus was measured. As shown in figure 35, the half-scale configuration had what appeared to be a significantly higher modulus (19 percent). In compression, an increase in modulus with decrease in gage length would normally suggest that any added stiffness was incurred by friction effects between the specimen and the loading head. However, in this case, the slenderness ratio of the gage section for both specimens was the same, but the modulus decreased with increase in specimen size. This effect might suggest that the 1.270 cm diameter specimen (shown in figure 3) incurred less lateral restraint from the loading head than the half-scale configuration (shown in figure 31). However, if this were the case, the load carrying capability for the smaller, laterally restrained specimen would have been greater resulting in higher measured values of strength. However, this was not the case, both configurations failed at the same strength level. Since the same apparatus (gas-bearing compressive facility), the same instrumentation, and the same testing procedures were used for evaluations on both configurations, these evaluations indicate that an elastic modulus-size effect may exist. However, further work is needed in this area before a definite conclusion can be reached.

Volume effects in tension: Results of the tensile tests for determining volume effects are tabulated in table 5; also see table 3. The results of these studies comparing the 1.270 cm diameter configuration to the half-scale configuration versus elastic moduli and ultimate tensile strength are given in figures 37 through 39. Typical tensile stress-strain curves for the one-half scale specimen tested in the Tinius-Olsen setup and the tensile gas-bearing facility are given in figures 40 and 41, respectively.

As shown in figure 37, runs from both volumes and both apparatuses (Tinius-Olsen setup and gas-bearing tensile facility) resulted with failures at a constant level of strength (10.7×10^6 to 11.1×10^6 N/m^2). Normally, according to Weibull's volume theory, when equal values of tensile strength are measured for volumes differing by a factor approaching 10, one would expect to be testing on the lower level of the Weibull curve. The Weibull volume theory is based on the assumption that the ultimate tensile strengths of brittle materials are determined by the "weakest link" resulting from a combination of stress intensity and a defective state of the material; thus, large test pieces fail at lower stress levels than small test pieces. The reduction in measured strength results, therefore, because the large test piece has a higher probability of containing weak spots than the small test piece. Figure 39 describes the volumetric effect on tensile strength based on these tests for two volumes and the expected trend should larger or smaller volumes than these be tested.

Again a significant variance in moduli was measured. As shown in figure 38, the half-scale configuration had a lower modulus (28 percent). For this evaluation, both the Tinius-Olsen and the gas-bearing tensile facility setups measured equal values of moduli, thus somewhat confirming a modulus size effect observed in the compressive evaluations.

Stress Rate Effect Studies. - Stress rates of 172×10^3, 690×10^3, and 1860×10^3 N/m^2/sec (25, 100, and 270 psi/sec) were used. Because these stress rates were considerably lower than those expected in flight, a limited number of tests was conducted at stress rates in the range of 6900×10^3 N/m^2/sec (1000 psi/sec) in order to predict more accurately the effects which occur during flight. The basic 1.270 cm diameter .dumb-bell configuration (shown in figure 3) was used in the compressive evaluations, and the basic 1.270 cm diameter circular cross section specimen (shown in figure 9) was used in the tensile evaluations.

Stress rate effects in compression: Results of the study on stress rate effects in compression are tabulated in table 6. These results comparing compressive strength and elastic moduli to the various stress rates are given in figures 42 through 45. Typical compressive stress-strain curves for the various stress rates are given in figures 46 through 49.

This evaluation indicates that this material does not conform to viscoelastic theory, at least for the stress rates investigated. Although some scatter is reflected in the data, a constant level of compressive strength and modulus was indicated for all stress rates evaluated. For example, the mean values for strength at the stress rates of 170×10^3,

690 x 103, 1860 x 10^3 and 4720 x 10^3 to 8600 x 10^3 N/m^2/sec were 24.1 x 10^6, 24.6 x 10^6, 25.7 x 10^6, and 25.6 x 10^6 N/m^2, respectively. Similarly, the mean values for elastic moduli were 0.78 x 10^9, 0.73 x 10^9, 0.87 x 10^9, and 0.74 x 10^9 N/m^2, respectively. Thus, this evaluation indicates that valid measurements of compressive strength and moduli can be made at room temperature using any stress rate within the 170 x 10^3 to 6900 x 10^3 N/m^2/sec range.

It should be noted that two sets of compressive evaluations for compressive strength and elastic moduli are plotted in figures 42 and 43 at the 690 x 10^3 N/m^2/sec stress rate. For the two sets of tests, one conducted in February and the other in May, both conducted seemingly under the same conditions in the gas-bearing compressive apparatus using identical test specimens from the same billets of material, the material indicated significant decreases in compressive elastic moduli (32 percent) and ultimate compressive strength (16 percent). The total strain in failure in February averaged approximately 0.040 m/m; whereas, in May, it exceeded 0.060 m/m. Therefore, because of this anomaly, other parameters which could possibly affect the characterization of this material were considered.

Moisture absorption was adjudged to be the most likely parameter. Thus, in order to get a better understanding for characterizing this material, a study on moisture effects was undertaken. The results of this study were considered to be significant and will, therefore, be reported later under its own heading.

Stress rate effects in tension: Results of the studies on stress rate effects in tension are tabulated in table 7. The results comparing tensile strength and elastic moduli to the various stress rates are plotted in figures 50 through 53. Typical tensile stress-strain curves for the various stress rates are given in figures 54 through 57.

This evaluation also indicated this material to be a nonconformer to the viscoelastic theory. Thus, since comparable values for tensile strength and elastic moduli were measured for all stress rates evaluated from 170 x 10^3 to 7000 x 10^3 N/m^2/sec, this material can be characterized at room temperature for tensile properties at any stress rate within the range of 170 x 10^3 to 7000 x 10^3 N/m^2/sec.

Moisture Effect Studies. - As mentioned earlier in the discussion on stress-rate effects in compression, moisture effects on the characterization of low-density phenolic-nylon could be severe. It was pointed out

in that discussion for two sets of tests conducted in February and May, both conducted seemingly under the same conditions in the gas-bearing compressive facility using identical test specimens from the same billets of material, significant decreases in compressive elastic moduli (32 percent) and ultimate strength (16 percent) were measured. Also, the total strain to failure in February averaged approximately 0.040 m/m; whereas, in May, it exceeded 0.060 m/m. Because moisture absorption was adjudged as being the cause of this anomaly, a study was made to determine its effects on mechanical properties.

Two types of tests were conducted. The first test consisted of mechanical property evaluations in compression and tension (dupiicate data). Two types of specimens were used: dried and undried. The dried and undried. The dried specimens were maintained at a temperature of 377°K (220°F) in a thermostatically-controlled oven for 24 hours or more. The undried specimens were taken from adjacent locations within the same billet of material as the dried specimens with no environmental controls being imposed to control the moisture content. Testing was done on both types of specimens at the same time using the same testing conditions and procedures. The basic 1.270 cm diameter dumbbell specimen was used for the compressive evaluations, and the basic 1.270 cm diameter cross section tensile specimen was used for the tensile evaluations. The second test consisted of monitoring the moisture absorption rate and the moisture content variations over a prolonged period of time. This test was conducted using three specimens having the approximate dimensions of 1.273 x 2.288 x 6.279 cm. Before testing, the specimens were dried at a temperature of 377°K (220°F) for 40 hours. The weights of the specimens were measured immediately prior to placing in oven and immediately after removal from oven. After removal from the oven, the specimens were left in an air-conditioned laboratory for moisture absorption in an area adjacent to the location where the unused billets of material were stored.

Moisture effects in compression: Results of the study to determine moisture effects in compression are tabulated in table 8. The results comparing the compressive ultimate strength and elastic moduli with the dried and undried specimens in retrospect to the stress-rate effect studies in compression are plotted in figures 58 and 59. Typical compressive stress-strain curves for the dried and undried specimens are given in figures 60 and 61.

The dried specimens had a significant increase in elastic moduli compared to the undried specimens (27 percent). Also, but not surprising, the compressive strength of the dried specimens increased significantly above that of the undried specimens (24 percent). It is interesting to note that the undried specimens yielded values of mechanical properties which lie within the range of values inscribed by the compressive stress rate tests conducted a week earlier; whereas, the dried specimens provided values equal to some of those determined back in February. Also, note in figures 60 and 61 that the total strain to failure of the dried specimen was approximately 0.037 m/m as opposed to approximately 0.063 m/m for the undried specimen. Therefore, total strain-to-failure seems to be affected by moisture along with compressive elastic moduli and ultimate strength.

This consequence leads to the perception that the billets, having not been stored in a humidity controlled area may have had varying mechanical properties depending on the amount of moisture contained within the billet. If this observation were correct, then variances between billets and within a billet would be expected should billets not be stored under controlled environmental conditions and if samples to be tested were taken from the billet at different times and not maintained under the same environmental conditions.

Moisture effects in tension: The results of the study to determine moisture effects in tension are tabulated in table 9. The results comparing the tensile strength and elastic moduli with the dried and undried specimens are plotted in figures 62 and 63. Typical tensile stress-strain curves for the dried and undried specimens are given in figures 64 and 65.

The results of this study also indicate a moisture effect. The dried specimens had only a slightly higher elastic modulus (5 percent) but a significantly lower ultimate strength (14 percent). These results indicate two possibilities. One is that drying has an embrittlement effect resulting in a stiffer material becoming more susceptible to brittle fracture, which would explain the significant decrease in tensile strength. Another possibility is that the nylon particles (40 percent of mixture by weight) is the predominant material affecting stiffness. The modulus of nylon drops significantly with absorption of moisture (66 Nylon, for example, has a modulus of 4.1 x 10^5 psi with 0.2 percent water but only 1.75 x 10^5 psi with 2.5 percent water). Also note for this study, that two sets of dried specimens were prepared. One set was dried at 377°K (220°F) for 24 hours and the other was dried for 42 hours before testing. The extended drying

time did not affect the tensile properties but did result in a greater loss of volatiles (presumably moisture), 2.97 percent compared to 3.38 percent, respectively.

Moisture absorption study: Results of the moisture absorption study are plotted in figure 66. Based on weights after drying, the specimens contained (by weight) moisture in excess of 2 percent (8W-2B contained 2.29 percent, 8W-2C, 2.54 percent; 8X-3C, 2.42 percent). This moisture content was less than that measured for the tensile specimens tested for moisture effects but in line with that measured for the compressive specimens tested (shown in tables 8 and 9).

After removal from the oven, the specimens started absorbing moisture immediately. The highest rate of absorption was during the first four hours of the test. After 120 hours, approximately half of the moisture that had been given up by drying had been absorbed once again (8W-2B absorbed 0.92 percent; 8W-2C, 1.56 percent; 8W-3C, 1.21 percent). All three specimens regained the original amount of moisture that they contained before drying within 480 to 624 hours. It is interesting to note that moisture absorption for all three specimens leveled out on reaching the original level of moisture contained before drying. Then, after 624 hours, the rate of absorption increased again and leveled out at a higher level after about 960 hours. From 960 hours to 1416 hours, the moisture content remained constant. Based on the dry weights, the specimens contained approximately from 3 to $3\frac{1}{2}$ percent moisture (8W-2B contained 2.83 percent; 8X-2C, 3.49 percent; 8X-3C, 3.28 percent) at the end of the test. The reason for this increase in moisture content is not certain. However, one possible explanation might be that during the test, the specimens were open to the environment of the laboratory; whereas, before the test, they were stored in separate manila envelopes making them less susceptable to environmental changes within the laboratory.

Moisture Effects on Density Variation and Anisotropic Properties. - Because a large variance in bulk density (in the magnitude of 20 percent) was measured, the bulk densities of several specimens were measured to determine if moisture content caused the variation in density. Thirteen specimens taken from the top two layers (1.9 cm thick) of billet 8 were machined to blank size (1.270 x 2.286 x 6.350 cm) and dryed for 24 hours at 377°K (220°F). Measurements and weights (accurate to within 0.0002 inch and 0.0002 gram) were taken before drying, two hours after drying, and 72 hours after drying. After removal from the oven, the test specimens were stored in the laboratory with no special provisions being made to control their environment.

The results of these measurements are given in table 10. Although the density variance between these specimens was only approximately 8 percent, the volatiles removed (moisture) ranged from only 1 to 1.5 percent. Therefore, a variance in density caused by moisture content in the magnitude of 20 percent is highly unlikely since all the billets have been stored in the same location and environment. Also during this determination, a small but consistent shrinkage was noted after the specimens were dried. Based on the average change for similar dimensions, the dimensional changes (expressed as percent shrinkage of measurements taken before drying) were as follows;

Sequence / Dimension	% Shrinkage before Drying	% Shrinkage 2 Hours after Drying	% Shrinkage 72 Hours after Drying
Thickness	0.00	0.14	0.10
Width	0.00	0.22	0.11
Length	0.00	0.25	0.16
Average	0.00	0.20	0.12

$$\% \text{ Shrinkage} = -\left[\frac{\text{Length after drying}}{\text{Length before drying}} - \right] \times 100$$

This test suggests, therefore, that small dimensional changes might be expected when events occur which change the moisture content of this material.

Anisotropic evaluations were made by testing several compressive specimens (1.127 x 1.125 cm square cross section) taken in the "c" direction (thickness direction) from several billets from which evaluations had been made in the ab direction (diametrical direction). These tests were conducted in the same apparatus using the same testing procedures.

Results of this evaluation are tabulated in table 11. The results of this study comparing compressive strength in the "c" direction to bulk density is shown in figure 67. A typical stress-strain curve measured

in the c direction is given in figure 68. Note that the average compressive strength for the circular, dumbbell, and square configurations in the ab direction (table 1) was 29.7 x 10^6 N/m^2; whereas, in the c direction, the average strength was only 20.8 x 10^6 N/m^2— a significant drop in strength (30 percent). Similarly the compressive modulus dropped from an average of 1.08 x 10^9 N/m^2 to 0.88 x 10^9 N/m^2, also a significant drop (18$\frac{1}{2}$ percent). Thus, based on this study, these billets of material possess anisotropic properties for the ab and the c directions.

In order to confirm the evaluations made on density variations and anisotropy, sonic velocity measurements through the material were made. The results of these measurements are tabulated in tables 12 and 13.

The results of sonic velocity measurements through a constant thickness (c direction) of billet 13 are given in table 12. Variations in sonic velocity ranged from 0.158 x 10^6 cm/sec to 0.164 x 10^6 cm/sec. Because sonic velocity is a function of elastic modulus and material density, these velocity variations therefore reflect either variations in the elastic modulus, variations of material density, or an accumulative variation of both properties.

The results of sonic velocity measurements on some failed tensile specimens on which values of elastic moduli and density have been measured are tabulated in table 13. Similar velocity measurements in the b and c directions were made on both halves of the failed specimen. For all measurements made, the sonic velocity in the c direction was from 3 to 11 percent lower (average of 6$\frac{1}{2}$ percent) than in the b direction. Thus, anisotropic properties in the a-b and c directions in compression are confirmed and would be expected should additional mechanical testing be conducted in the c direction.

Data and Results - Phase II Testing

High Temperature Studies. - The compressive and tensile test specimens used in these studies (determined from Phase I testing) were primarily the 1.270 cm diameter x 2.54 cm gage length compressive specimen (figure 3) and the 1.270 diameter x 5.08 cm gage length tensile specimen (figure 9).

Two preliminary heat runs during Phase I were made at 477°K (400°F) on the 1.270 cm diameter x 5.08 cm gage length (figure 9) and the 1.125 cm square x 5.08 cm gage length (figure 10) tensile specimens. These

runs were made primarily to measure the thermal gradients within each specimen configuration, to compare the gradients between the configurations, and to study the surface thermal effects of the two configurations (especially at sharp corners). Each specimen used in this study was instrumented with four thermocouples as shown in figure 69. Heating rates and thermal gradients for the circular and the square configurations are shown in figures 70 and 71. The interior temperature lagged the surface temperature during heating, but the temperatures leveled out after soaking at temperature for 8 to 10 minutes. The circular configuration provided a maximum thermal gradient of approximately 10°K (18°F) compared to 20°K (36°F) for the square configuration. The thermal gradients indicated were within the acceptable range (normally for this apparatus gradients within 50°F are considered acceptable). Also, no adverse thermal effects were incurred on the surfaces (including the corners of the square configuration). These data indicate that either the circular or square (rectangular) specimen could be used without incurring adverse thermal effects at temperatures up to 477°K.

Six thermocouples were used for measuring thermal gradients for the tensile heating-rate effect studies. These thermocouples were located as shown in figure 72. Typical heating curves for the three heating rates (22.0, 55.5, and 111°K/min) to the three test temperatures (422°K, 450°K, and 477°K) are shown in figures 73 through 81. Note that the specimen was loaded immediately when the middle-surface thermocouples indicated test temperature.

Six thermocouples were also used for determining thermal gradients for the effects of time at temperature in compression and tension. The location of the thermocouples for the compressive evaluations is shown in figure 82, and the location for the tensile evaluations was the same used in the study on tensile heating-rate effects (figure 72). For these evaluations, the specimens were heated ta the three test temperatures (422°K, 450°K and 477°K) in $2\frac{1}{4}$ minutes. Typical heating curves for the compressive and the tensile evaluations are shown in figures 83 and 84. Note that time at temperature was measured from the time that the middle surface thermocouples indicated test temperature.

Heating rate effects in tension: Results of this study are tabulated in table 14. These results comparing values of tensile strength and elastic moduli to the heating rates for each test temperature are given in figures 85 and 86. Typical tensile stress-strain curves for some of these runs are given in figures 87 through 89.

Although only duplicate data were determined for each test condition, several definite trends were in evidence. As shown in figures 85 and 86, these trends were (1) the strength level decreased as the test temperature increased, (2) the strength level was seemingly not affected by heating rates in the range of 22°K/min to 111°K/min, (3) modulus decreased as the test temperature increased, (4) modulus increased only slightly with increase in heating rate in the range of 22°K/min to 111°K/min. Based on these results, the heating rate effect for test temperatures and heating rates in these ranges was negligible.

Time at temperature effects in compression: The results of this study are tabulated in table 15. The results comparing compressive strength and elastic moduli with time at temperature are shown in figures 90 and 91. Some typical compressive stress-strain curves are given in figures 92 through 94. Evaluations were made primarily at time t = 5, t = 15, and t = 25 minutes. Runs at t = 0 for the three test temperatures were made in order to screen for initial temperature-time effects since heating rate effects in compression were not included in the test program. Testing was not extended beyond t = 25 minutes because the results indicated a plateau in the data for time at temperature well beyond the length of time expected during actual application of the material.

As shown in figures 90 and 91, triplicate data with good reproducibility were obtained for this study. The results of this testing indicate that time at temperature is not a significant parameter affecting characterization for the temperatures evaluated. As shown in figure 90, no significant variations were measured for compressive strength from time t = 0 to t = 25 minutes. The average values for compressive strength at t = 0 and t = 25 for the 450°K evaluation, for example, were 13.4 x 10^6 and 14.3 x 10^6 N/m^2. As shown in figure 91, although a very slight increase in modulus with time at temperature is indicated, no significant variations in modulus were measured. The average values for elastic moduli at t = 0 and t = 25 for the 450°K evaluation, for example, were 0.30 x 10^9 and 0.36 x 10^9 N/m^2. This is not a significant variation for this type of material. Note also that modulus and ultimate strength decreased with increase in test temperature.

Time at temperature effects in tension: The results of this study are tabulated in table 16. The results comparing tensile strength and elastic moduli with time at temperature as shown in figures 95 and 96. Some typical tensile stress-strain curves are given in figures 97 through 99. Again, evaluations were made primarily at time t = 5, t = 15, and t = 25 minutes. As in the case of the compressive evaluations, testing was not

extended beyond t = 25 minutes because the results indicated a plateau in the data for time at temperature well beyond the length of time expected during actual application of the material.

As shown in figures 95 and 96, triplicate data were obtained, but the reproducibility was not as good as it was for the compressive evaluations which in some cases necessitated reruns in order to more clearly characterize properties of the material. More scatter should be expected in tension than in compression for brittle and semi-brittle type materials. In tension the crack-opening mode of failure is incurred which induces high stress concentrations; whereas, in compression the load only acts to close any crack openings of flaws inherent in the material. However, considering that scatter is present, the results of this testing indicate that time at temperature does not appreciably affect characterization for the temperatures evaluated. As shown in figure 95, no significant variations were measured for tensile strength from t = 0 to t = 25 minutes. The presence of data scatter is evidenced by the overlapping of values for the various test temperatures and the low values of strength measured at t = 15 and t = 25 minutes for the 422°K evaluations. As shown in figure 96, again no real significant variations in modulus with time at temperature is indicated. The difference in modulus between the 450°K - 477°K and 422°K evaluation at t = 5 could possibly be meaningful. However, because the modulus for both the 450°K and 477°K evaluations showed a marked increase at t = 15 minutes, it was concluded that additional runs would not have affected the overall plateau indicated, but would have only resulted in bringing the average values of the 450°K - 477°K and 422°K evaluations closer together. Note that the modulus again decreased with increase in test temperature.

Low Temperature Studies. - The compressive and tensile specimens used in this study (determined from Phase I testing) were the same basic specimens (shown in figures 3 and 9) used in the high temperature studies. A uniform stress rate of 690 x 10^3 $N/m^2/sec$ was used for both the room temperature and the low temperature evaluations for this study. During cooldown for the low temperature tests, each specimen was cooled slowly to the test temperature (144°K). After reaching test temperature, from $2\frac{1}{2}$ to $3\frac{1}{2}$ minutes elapsed to allow for temperature stabilization before loading. The thermal gradient between the exterior surface and the center of the specimen in the compressive and tensile specimens were measured to be approximately 13°K (23°F) and 20°K (36°F), respectively.

As mentioned previously, the specimens to be tested at low temperature were dried before testing. These specimens were maintained at 377°K (220°F) for 24 hours; after which, they were sealed individually in cellophane bags until test. Before the actual testing began, the apparatus was checked for stress rate and performance by testing some undried specimens. The results of these runs were also included in the data for comparison with the actual runs, but they were not included with the data used in the statistical analysis.

The room temperature tests in tension were actually conducted with two purposes in mind. The first, of course, was to obtain data for a statistical analysis to evaluate data scatter at low temperature, The second, however, was to verify and possibly determine the effects of density hetergeneity on data scatter. Sampling was accomplished by taking specimens from within single billets and from several different billets by the color of the material. This technique was used because distinct light and dark colored areas within the material had been noted which consistently had shown a variance in density.

The statistical calculations were made using "standard" statistical formula. For example, the mean property value, standard deviation, and coefficient of variation were calculated from the equations:

$$\overline{X} = \frac{1}{N} \sum_{i=1}^{N} X_i \qquad (1)$$

$$s^2 = \frac{1}{N-1} \sum_{i=1}^{N} (X_i - \overline{X})^2 \qquad (2)$$

and

$$V = \frac{s}{\overline{X}} \quad (100 \text{ percent}) \qquad (3)$$

where

$\overline{X}$ = mean (average property value)
X_i = individual measure of property

N = number of specimens tested
s = standard deviation
V = coefficient of variation

Perhaps it should be mentioned that a somewhat different equation is sometimes used in statistical analysis to calculate the standard deviation, The equation sometimes used is

$$\sigma^2 = \frac{1}{N} \sum_{i=1}^{N} (X_i - \overline{X})^2 \qquad (4)$$

where σ is the standard deviation. Equations (2) and (4) are different in that equation (4) represents a standard deviation from a true mean value of the parameter being evaluated; whereas, in equation (2) the mean property value was estimated. For this case, one degree of freedom in the data was lost when the mean property value was estimated by a previous calculation, equation (1). Also, in order to emphasize that equation (2) is an estimate of the true population standard deviation, the symbol s is used rather than σ. The confidence interval at the 95 percent confidence level was calculated for both ultimate strength and modulus in compression and tension. These calculations were made assuming the data followed the normal distribution law. The equation used was

$$D = t_{(1 - \frac{\alpha}{2})} \, s/\sqrt{N} \qquad (5)$$

where

α = allowable risk of error
$t_{(1 - \frac{\alpha}{2})}$ = Student's t value for N-1 degrees of freedom
D = deviation from the mean

In layman's terms, the results of the calculations permit the statement with $(1 - \alpha)$ 100 percent confidence that the true mean property value is within $\pm$ D units of the reported value.

Low temperature studies in compression: The statistical correlation of the mechanical property data for the compressive evaluations are tabulated in table 17. The data from the 15 tests evaluated at 294°K and the 22 tests (20 dried and 2 undried) at 144°K from which the statistical calculations were made are tabulated in table 18. The average values of compressive strength and elastic moduli at 294°K and 144°K are plotted showing the 95 percent confidence interval in figures 100 and 101. A typical compressive stress-strain curve measured at 144°K is given in figure 102.

As shown in figures 100 and 101, the compressive strength and modulus was much higher at 144°K than at 294°K (strength: 36.2 x 10^6 compared to 24.2 x 10^6 N/m^2; modulus: 1.85 x 10^9 compared to 0.75 x 10^9 N/m^2). The coefficient of variation averaged from approximately 5 percent to 15 percent, and the 95 percent confidence level ranged from only 2.4 percent to 5.6 percent, see table 17. The higher values for the coefficient of variation for both strength and modulus occurred at the cold temperature (strength: 7.39 percent opposed to 5.25 percent; modulus: 14.59 percent opposed to 6.12 percent). Thus, low temperature effects on data scatter were more predominant in determining modulus than in determining compressive strength.

The reason for the high variability in modulus could have resulted from two variations: (1) differences among true values measured, (2) differences in observed values resulting from limitations of measuring equipment. If it could be shown that the occurence of the variance was highly unlikely as result of limitations in the measuring equipment, then the scatter measured could have resulted from differences among the true values measured. As discussed under the section on apparatuses and procedures, the clip-on extensometers were used to measure unit axial strain for these evaluations. Two parameters could have possibly altered the output signal for axial strain: (1) temperature effects on extensometer strain gages, (2) freezing of hinge-point between clip-on andyoke attachment to specimens. As discussed in the section on apparatuses and procedures, the clip-on extensometer consisted in part of two clip-on springs which were instrumented with four SR-4 strain gages back-to-back. These gages were electrically connected into a bridge circuit which served the dual purpose of measuring strain and compensating for temperature variance. Freezing, the second parameter, did occur at the hinge points on the first trial run as result of condensation of moisture from the atmosphere during cooldown. This occurrence would have altered the loading characteristic of the clip-on spring resulting in less measured output strain for unit axial strain on the specimen. It can readily be seen that this effect would reflect a higher modulus for the specimen. However,

during the test runs, motion was frequently incurred relative to the extensometer hinge point and the yoke by jiggling the extensometers. This procedure prevented freezing at the hinge point and thus maintained the original calibration of the clip-ons. Confidence in the test equipment was thus established.

It should be pointed out here that moisture too was a parameter in this. As shown in Phase I in the discussion of moisture effects in compression, dried compressive specimens (duplicate data) indicated higher values of strength and modulus than did undried specimens. Therefore, if the specimens used for the tests at 294°K of this study had been dried, there is a good possibility that the difference in strength and modulus measured at the two temperatures (144°K and 294°K) would not have been as large.

Note in figures 100 and 101 that an embrittlement effect was indicated by these evaluations. For example, the elastic modulus increased from 0.75 x 10^9 N/m^2 at 294°K to 1.85 x 10^9 N/m^2 at 144°K and the compressive strength increased from 24.2 x 10^8 N/m^2 to 294°K to 36.2 x 10^8 N/m^2 at 144°K.

Low temperature studies in tension: The statistical correlation of the mechanical property data for the tensile evaluations are tabulated in table 17. The data from the 15 tests evaluated at 294°K and the 24 (22 dried and 2 undried) at 144°K from which the statistical calculations were made are tabulated in table 19. The average values of tensile strength and elastic moduli at 294°K and 144°K are plotted showing the 95 percent confidence interval in figures 103 and 104. A typical tensile stress-strain curve measured at 144°K is given in figure 105.

Before getting into the statistical analysis, it should be pointed out that the room temperature evaluations in tension were conducted with two purposes in mind: (1) obtain data for a statistical analysis on the low temperature effects on data scatter, (2) verify and determine effects of material density on data scatter. Ten of the specimens used in the room temperature tests (5 light and 5 dark) were chosen carefully. They represented either totally light or totally dark colored samples of material from different billets and different locations within a single billet. The results of these tests comparing density, tensile elastic moduli, and tensile strength to the light and dark colored specimens are given in figures 106 through 108. Note that all the light colored specimens had a higher density, higher modulus, and higher strength than the dark colored specimens. Also note that specimens were taken from four different billets with both light and dark specimens being taken from billet 13. Therefore, these tests surely indicate the light and dark areas of this material to have different mechanical properties.

To confirm the results of the mechanical testing which indicated mechanical property variations with density variations on the light and dark colored specimens, sonic velocity measurements were made. The results of these measurements are tabulated along with values of experimental tensile elastic moduli in table 20. The results comparing tensile elastic moduli to sonic velocity in the a direction (see table 20) for the various light and dark specimens are also shown in figure 107. The sonic velocity of the light colored specimens varied from approximately 0.172×10^6 to 0.176×10^6 cm/sec while the measured tensile modulus varied from 1.14×10^9 to 1.52×10^9 N/m^2. The sonic velocity of the dark colored specimens varied from approximately 0.159×10^6 to 0.163×10^6 cm/sec while the tensile modulus varied from 0.98×10^9 to 1.12×10^9 N/m^2. Therefore, since sonic velocity is equal to the square root of elastic modulus divided by the density, these tests substantiate each other in indicating a variance in mechanical properties for the light and dark colored areas between separate billets and within a single billet.

The effect of cold temperature on tensile strength and elastic modulus is shown in figures 103 and 104. Keeping in mind the specimens tested at 144°K were dried while those tested at 294°K were not, the strength decreased from an average of 9.9×10^6 N/m^2 at 294°K to 9.4×10^6 N/m^2 at 144°K while the average elastic modulus increased from 1.12×10^9 N/m^2 at 294°K to 2.45×10^9 N/m^2 at 144°K. The coefficient of variation ranged from 9.38 percent to 17.15 percent, and the 95 percent confidence level ranged from 3.4 percent to 6.3 percent, see table 17. The higher value for coefficient of variation for tensile strength (12.07 percent) occurred at 294°K instead of 144°K as might normally be expected for a material which becomes increasingly brittle with decreasing temperature. However, the additional parameter (density) which was purposely introduced resulted in the mixing of two somewhat dissimilar universes. The net effect was that a higher data scatter was perhaps reflected than would have been had only the light and dark colored specimens been used. Again, low temperature effects on data scatter were reflected primarily in the measurement of elastic moduli. The clip-on extensometers were again used to measure axial strain, but the same procedures outlined for the low temperature evaluations in compression were used to assure valid measurements of unit axial strain.

Note that the embrittlement effect was also indicated by the tensile evaluations. For example, the elastic modulus increased from 1.12×10^9 N/m^2 at 294°K to 2.45×10^9 N/m^2 at 144°K; whereas, the tensile strength decreased from 9.9×10^6 n/m^2 at 294°K to 9.4×10^6 N/m^2 at 144°K. With

the embrittlement effect, the elastic modulus increases, but in tension the ultimate strength decreases. The reason for this is that brittle materials are susceptable to premature failure, especially when loaded in tension when the inherent flaws within a material are being opened up incurring high values of stress concentration at the tips of cracks.

Summary and Discussion

In general, the results of Phase I testing indicated that the 1.270 cm diameter cross section is a reliable configuration for measuring ultimate strength and elastic moduli in compression and tension. Of the three cross sections considered (circular, 1.270 cm diameter; square, 1.125 x 1.125 cm; rectangular, 1.588 x 0.800 cm), the compressive evaluations resolved that either the circular or square cross section (machine finished) with a 2.54 cm gage length would indicate valid values for ultimate strength and elastic modulus; whereas, the rectangular cross section yielded somewhat smaller values for both properties. The tensile evaluations resolved that the circular cross section (ground finished) with a 5.08 cm gage length yielded higher values of ultimate strength with less scatter. As a result, the 1.270 cm diameter circular cross section was adopted as the cross section to be evaluated for the remainder of the program. The compressive specimen gage section was turned in a lathe to conserve program funding, but the tensile specimen gage section was ground finished.

Specimen size effect at room temperature on ultimate strength in compression and tension was negligible. However, evidence of a definite size effect on elastic modulus was measured in compression and tension. Two sizes were evaluated: the basic 1.270 cm diameter cross section and a one-half scale specimen. In compression, the half-scale specimen indicated a higher average modulus (0.87×10^9 N/m^2 compared to 0.73×10^9 N/m^2). In tension, the half-scale specimen indicated a lower average modulus for runs made in both the Tinius-Olsen testing machine and the gas-bearing tensile facility (0.75×10^9 N/m^2 compared to 1.05×10^9 N/m^2). This apparent size effect was unexpected, and at the present, is not explainable.

In order to further extrapolate the effects of larger and smaller volumes on ultimate strength, the results from the room temperature tensile evaluations from Phase II of this part of the program (table 19) were evaluated for Weibull's material constants. Then the Weibull equation

$$\frac{\sigma_2 - \sigma_u}{\sigma_1 - \sigma_u} = \left(\frac{V_1}{V_2}\right)^{1/m} \qquad (6)$$

where

a_1 = average experimental value of strength
σ_u = stress below which failure cannot occur
m = constant representative of flaw density of material
V_1, V_2 = respective volumes of material for which stresses σ_1 and a_1 are being evaluated

was evaluated and the results plotted in figure 109. The departure of the experimental data from the theoretical curve resulted because the theoretical curve was defined for an isotropic material subjected to a uniform stress field. Also, note that the determinations used for this evaluation were tested three months apart, 6.44 cm^3 in July and 0.80 cm^3 in May, thus incurring the moisture effect again. Had both determinations been tested at the same time, the experimental data for the smaller volume should have fallen closer to the theoretical curve. In comparison, the experimental data indicated values of strength for volumes sufficiently large to provide valid measurements of strength without excessive scatter in the data.

Evaluations for stress rate effects at room temperature on ultimate strength and elastic moduli in compression and tension indicated that this material did not conform to viscoelastic theory. These evaluations were made for stress rates ranging from 170×10^3 to approximately 6900×10^3 $N/m^2/sec$. Although the tensile evaluations indicated data scatter, a constant level of ultimate strength and elastic moduli was reflected (figures 44, 45, 52 and 53).

The effects of heating rate and time at temperature on ultimate strength and elastic moduli in compression and tension were negligible for the range of temperatures and heating rates used (422 - 477°K at rates of 22 - 111°K/min). Having good reproducibility, the data for time at temperature effects (figures 90 and 91) indicated a constant level for strength and moduli up to t = 25 minutes. A slight but consistent drop in both properties with increase in temperature was evident. The tensile data from the tests on heating rate effects and time at temperature effects contained more scatter than the compressive evaluations; however, sufficient agreement was present to determine that the heating rate did not appreciably influence the strength of the material for these heating rates.

The data scatter was somewhat higher at low temperature (144°K) than at room temperature (table 17). This effect was consistent for both the compressive and tensile evaluations; however, again the tensile loading

condition resulted in more data scatter. The coefficient of variation for some of the determinations was somewhat higher than had been anticipated. A coefficient of variation of 10 percent or less should probably be considered good data scatter. As shown in table 17, the coefficient of variation varied from 5.25 percent to 17.15 percent. However, it should be pointed out that the density parameter was introduced fur the tensile evaluations at room temperature which undoubtedly increased the coefficient of variation for ultimate strength and modulus to 12.07 and 11.47 percent, respectively.

Some previous work done here on low-density phenolic-nylon included measurements of ultimate strength and elastic moduli at 144°K and 294°K in compression and in tension. However, only 2 to 4 runs for each condition were made, thus, making a statistical correlation between the two programs impossible. [8] However, even considering the small number of runs for that program, fairly good agreement in the measurements of ultimate strength and elastic moduli was obtained:

Property	Temp. "K	Average value [1] for Contract NAS1-2978	Average value for [1] current program
Ultimate strength in compression	294	28.7 (2) [2]	24.2 (15)
	144	38.7 (2)	36.2 (20)
Elastic modulus in compression	294	0.86 (2)	0.75 (14)
	144	2.34 (2)	1.85 (20)
Ultimate strength in tension	294	9.40 (4)	9.90 (15)
	144	9.90 (3)	9.40 (22)
Elastic modulus in tension	294	0.79 (4)	1.12 (15)
	144	1.30 (4)	2.45 (22)

Notes:
1. The values for ultimate strength are in 10^6 N/m^2 and elastic moduli are in 10^9 N/m^2.
2. The number within parenthesis is the number of runs on which the average value is based.

It has been reported[7] that billets are not homogeneous in density and that density measurements might be the most precise and useful test for analysis of variance. Testing conducted under this program supported these findings. Density variances were measured from point to point within a single billet frequently up to 10 - 12 percent. These variances occurred in an orderly arranged fashion. The referenced report indicated that the distribution of densities within a billet could be represented by a model consisting of a low density core encased in a high density shell. However, our findings indicated the opposite model existed; that is, a high density core encased by a low density shell. This seemingly contradiction indicates that both types of variations could randomly occur depending on, say, the behavior of the molding material under pressure for that particular molding process. A variance in compressive properties with density hetergeneity is somewhat distinguishable in results for the configuration studies in compression (figures 13 through 15). The results of the room temperature evaluations on light and dark colored material in tension for evaluating data scatter strongly indicate this effect (table 19). For five each of the light and dark colored specimens, the light colored specimens yielded higher measurements of density, ultimate strength, and elastic moduli in all cases. For example, the average values for density, strength, and modulus for the light and dark specimens were 0.603 gm/cm^3 opposed to 0.568 gm/cm^3, 11.1 x 10^6 N/m^2 opposed to 8.9 x 10^6 N/m^2, and 1.25 x 10^9 N/m^2 opposed to 1.06 x 10^9 N/m^2, respectively. To support the mechanical effects measured, sonic velocity measurements were made on light and dark colored blank tensile specimens. Again, in all cases, the light colored samples produced the highest sonic velocities indicating higher values of elastic moduli for the light material (table 20).

Anisotropy in the ab and *c* directions was measured in compression for several of these billets (4, 5, 8, and 10). The average values measured for compressive strength and moduli in the ab and c directions were 29.6 x 10^6 N/m^2 and 1.10 x 10^9 N/m^2 opposed to 22.3 x 10^6 N/m^2 and 0.88 x 10^9 N/m^2, respectively (tables 1 and 11). These results were confirmed by sonic velocity measurements in the ab and c directions (table 13). Again, for all cases, the sonic velocity was higher in the ab direction indicating a higher modulus for the ab direction.

Moisture content appeared to have a definite effect on material embrittlement. Phenolic-nylon has an affinity for moisture, note results of moisture absorption test in figure 66. Normally, from our experience, moisture absorption in the range of at least 2 or 3 percent can be expected when no environmental controls are used. Tests results have shown that this amount of moisture content can appreciably affect the characterization

of ultimate strength, modulus, and total strain to failure (figures 58, 59, 62 and 63). Moisture absorption affects characterization by causing the material to become less brittle resulting in a lower modulus and a higher total-strain-to-failure. Ultimate strength in compression is reduced with moisture absorption; whereas, tensile strength is increased because the material is less brittle, therefore less susceptible to brittle fracture. For example, the results of the compressive testing (figures 58 and 59) yielded higher values for both compressive strength and modulus for the dried specimen over the undried specimen (24 and 27 percent higher, respectively). The total strain to failure of the dried specimen was approximately 0.037 m/m; undried, 0.063 m/m (figures 60 and 61).

The characterization of the mechanical properties of low-density phenolic-nylon, ultimate strength and initial elastic modulus in compression and tension, as determined by this testing are given in figures 110 through 113. The general trend of these data was that ultimate strength and modulus decreased with increase in temperature from 144°K (-200°F) to 477°K (400°F) as shown. However, these data, of course, included the parameters of moisture and density rendering such values as arithmetic mean of experimental results, the true trend of mechanical properties as affected by temperature, and the true variance of experimental results for each test condition still somewhat undefined. For example, consider moisture effects as shown in figures 110 and 112, from 294°K (70°F) to 477°K (400°F), higher values of ultimate strength would have been measured in compression but lower in tension had dried specimens been used. Similarly, as shown in figures 111 and 113, from 294°K to 477°K, higher values of modulus would have been measured in compression and in tension had dried specimens been used. Thus, the overall trend of the effects of temperature on the characterization of the mechanical properties was affected by testing with dried specimens having practically no moisture content and with undried specimens having perhaps from 2 to 3 percent moisture content. Consider density effects for example. As shown in figure 112, as result of selecting specimens of high density, higher values of ultimate strength in tension were measured at 294°K than at 144°K. The lower values at 144°K were due, of course, in part to the embrittlement effect; however, in looking at the data of these two determinations, one can readily see that had specimens randomly selected been used at 294°K, probably somewhat smaller values in ultimate strength would have been measured resulting in approximately equivalent values of strength at 144°K and 294°K. Thus, characterization of these billets from the standpoint of an overall trend and of each test condition was influenced appreciably by moisture and density effects.

Conclusions and Recommendations

The data scatter obtained in Phase II testing was higher than was anticipated. The test program involved primarily an investigation of the effects of several parameters on characterization of low-density phenolic-nylon; namely,

1. specimen shape effects
2. specimen size effects
3. stress rate effects
4. heating rate effects
5. time at temperature effects
6. low temperature effects

Except for a size effect on moduli, none of these parameters appreciably affected characterization within rather broad ranges. In pursuing the scope of the program, however, some additional parameters which did appreciably affect characterization were isolated and studied:

1. surface finish effects (in tension)
2. density effects
3. moisture effects

Surface finish was a parameter which affected only ultimate strength in tension. Brittle and semi-brittle materials often fracture prematurely due to high stress fields at crack fronts caused by flaws inherent in the material. The data scatter was reduced to a minimum by grinding the gage section thus providing a smooth surface having the least detrimental effect on the strength of the material.

Density effects were inherent in the material and could not be controlled at testing. Density variations occurred from point to point within a single billet and from billet to billet. Therefore, data scatter was influenced by this parameter throughout the program.

Moisture effects could and probably should be controlled throughout a testing program such as this on this type of material. If not controlled, at least the data should be qualified as to moisture content at time of testing. Such information should be of considerable interest to the design engineer. Data scatter from moisture effects were incurred throughout the program.

A reduction in data scatter could be affected by reducing the density variation and by controlling moisture content. In order to reduce the density variation, the reproducibility in the material from billet to billet would have to be improved while variances within billets were reduced. This would perhaps entail the securing of batches of raw material with more certainty of characterization, improvements in dry blending of finely powdered ingredients, and improved controls on behavior of the molding material under pressure. The moisture content throughout testing could be controlled at a minimum level in a programmed humidity atmosphere. Results thus reported, would indicate truer mechanical properties for design purposes. On the other hand, reliable design data could be obtained by simply characterization of the material as a function of either moisture content or density, or both. This would give the designer a more definite control over the end product's performance. This report should provide specific guide lines for the design data in either case.

PART II

STUDIES OF DEGRADED MATERIAL

Summary

A sufficiently detailed characterization of arc-jet and furnace chars was made to allow the results of the thermal conductivity measurements on furnace chars to be extrapolated to flight chars. The major variables defined were the bulk density and true density of both the arc-jet and furnace chars. This allows the determination of the porosity of both types of char and hence, allows the thermal conductivity measurements made on furnace chars to be reduced to intrinsic property values which can be extrapolated to calculate the heat transfer by solid conduction under active ablation conditions. In addition, the chars were characterized in terms of lattice spacings from X-ray diffraction measurements and other monitors such as electrical resistivity and sonic velocity. Char prepared at a hot face temperature of about 2050°K in the arc-jet and chars prepared at 3033°K in the furnace (at a low heating rate) were found to be carbon-like since the lattice spacings as well as the properties and monitors did not conform to those of graphite. Char prepared to 3033°K at a high heating rate (4.9 MW/m^2) was found to be more graphite-like since its lattice spacing, monitors, and properties more nearly conformed to that of graphite. The results of the lattice spacings of the rapid char are included in Appendix C.

Chemical analyses were made of the arc-jet and slow furnace chars. The arc-jet chars were nearly completely degraded throughout the char layer as evidenced by the large amounts of carbon and the small amounts of nitrogen and hydrogen which remained in the char. The furnace chars also consisted primarily of carbon; however, the furnace chars prepared at 812°K and 1366°K contained more nitrogen and hydrogen than the arc-jet chars which indicates that they were not totally degraded.

The objectives of thedegraded material studies were to (1)define the effect of charring temperature level, time at temperature and heating rate on the thermal conductivity of the matrix, K_m, and (2) define the heat transported through the char by radiation. An equation was developed to allow the apparent thermal conductivity measurements to be reduced to intrinsic char properties (thermal conductivity of matrix) which could be extrapolated to conditions other than those of the measurements. The

equation is an acceptable thermal model for the char except that the transparency radiation term needs more definition. The effects of the several variables on the matrix conductivity at temperatures below 2000°K were defined. An uncertainty remains in whether or not the increase in apparent thermal conductivity of the stable (3033°K) slow furnace char above 2000°K is primarily an increase in the thermal conductivity of the matrix or a thermal radiation effect. A qualitative assessment of the possibility of assigning this increase to solid conduction (increased K_m) indicates that this behavior seems reasonable in view of the behavior of the electrical resistivity. The analysis of the radiation heat transfer through the material led to the conclusion that the char must become transparent to thermal radiation at temperatures above 2000°K if the significant increase in thermal conductivity is to be explained as thermal radiation.

The thermal conductivity of the matrix at temperatures to 2000°K was found to be controlled more by temperature than by time at temperature. This was established by the fact that chars prepared in the arc-jet in two to three minutes had about the same value of matrix conductivity as chars prepared by heating slowly in the furnace and holding for 30 minutes. Also, chars held at a given temperature for various times had the same values for thermal conductivity at low temperatures. The time effects observed were in the opposite direction to that normally expected for graphitizing materials. It was found that heating to high temperatures (3033°K) in a short time resulted in a more graphite-like behavior. Chars prepared by heating slowly to 3033°K never reached the same level of thermal conductivity as those heated rapidly. Also, the arc-jet chars, even though exhibiting carbon-like behavior, tended to have slightly higher values of matrix thermal conductivity than the slow furnace chars,

The thermal conductivity values measured for chars produced under different conditions were reduced to values of the thermal conductivity of the matrix. The values of the thermal conductivity of the matrix at each precharring temperature level are called the "boxing" values and are the values of thermal conductivity which the char matrix should assume the first time it reaches that temperature level. The boxing values of matrix conductivity were presented as a function of temperature. Use of these values in equation (23) along with the correct values for porosity, pore size, etc., provides the extrapolation of the data to transient conditions. The boxing values of thermal conductivity are uncertain to the extent that the transparency of the char to thermal radiation is undefined. It is intrinsic in the ablation system that the carbon-like structure and its lower matrix conductivity at lower temperatures as obtained for "boxing chars" does not influence the overall conductivity to a large degree.

Thermal conductivity values were reduced from transient temperature measurements made during steady-state ablation tests by other laboratories. A reduction of the data which did not include the effects of heat absorption by the pyrolysis gases gave values for the thermal conductivity of the char which were about one-fifth of those predicted from the results of our studies of the char. The analysis was modified to include pyrolysis gas effects under the assumptions that the gases reached the same temperature as the char and that the enthalpies of the gases were the same as those given by Kratsch.[1] Using the modified analysis, the values of thermal conductivity reduced from the transient measurements were found to be in good agreement with the values obtained by extrapolating the results of the steady-state measurements

Introduction

The char formed from the thermal degradation of the phenolic-nylon was studied in an attempt to develop a more complete understanding of the factors which influence the thermal conductivity of the char. The effort was directed toward defining the intrinsic properties of the char so that an analytical model could be developed which would allow the prediction of the flight properties of the material. The intrinsic properties of greatest concern were the thermal conductivity of the matrix or solid portion of the char and the ability of the char to transmit thermal radiation. The thermal radiation characteristics are separated into two mechanisms. The first is direct transmission through the cell walls due to the transparency of the char matrix. The second is transmission of thermal radiation through the holes and pores in the material. We shall keep these radiant mechanisms separate by referring to the former as radiation through a transparent media and the latter as radiation through a porous media. Thus, there were three intrinsic properties which required separation for a complete understanding of the behavior of the thermal conductivity of the char.

Arc-jet chars and furnace chars were physically characterized from measurements of the lattice spacings (X-ray diffraction), bulk density, true density, pore size, chemical composition, open porosity, closed porosity and sonic velocity. The chemical analysis and X-ray diffraction studies were made to provide information about the effects of thermal history on the char. The other measurements were made to characterize the char for heat transfer analysis.

Laboratory chars were prepared in our high temperature furnaces. Most of the chars for the measurements were prepared at low heating rates and were stabilized at temperatures of 700 and 922°K for extended times to

allow thermal degradation and dimensional changes to occur. Acceptable specimen blanks could not be obtained from chars prepared at low and moderate linear heating rates. The charring temperature and time at temperature were varied and some specimens were prepared by heating rapidly to 3033°K.

Thermal conductivity and permeability measurements were made on the arc-jet chars and on the furnace chars. Other measurements were also made in an effort to gain additional information about the intrinsic properties of the chars. These other measurements included room temperature measurements of the radiation through the porous media, electrical resistivity measurements as a function of temperature, measurements of the thermal conductivity of powders prepared from the char and sonic velocity measurements at room temperature. The transmittance measurements were made to aid in analyzing the radiation component through the char and the measurements of the electrical resistivity of the char, the thermal conductivity of the powder and the sonic velocity were made to provide information about the thermal conductivity of the solid matrix. Further, considerable effort was expended in attempting to impregnate a char with a material which would absorb the thermal radiation being transmitted through the char and thus remove this component from the effective thermal conductivity measurements.

Apparatuses and Procedures

Chemical Analysis. - The chemical analysis of the chars for C, H, and N was made with a Perkin-Elmer Model 240 elemental analyzer. This apparatus performs as follows: A sample of known weight is placed in a platinum "boat" and combusted at about 1155-1255°K in a static oxygen atmosphere. The products of combustion are flushed by a helium stream through a reduction tube. Excess oxygen and unwanted combustion products are removed, and the oxides of nitrogen are reduced to molecular nitrogen. The remaining mixture, now consisting of only water vapor, carbon dioxide, nitrogen and the helium diluent are gathered into a mix vessel, pressurized to about 2 atmospheres and held at a constant temperature. After the mixture thermally equilibrates, it is expanded into a sampling system, then swept through a series of thermal conductivity cells. An adsorption trap which removes the H_2O is situated between the first two thermal conductivity cells. The thermal conductivity difference before and after the trap, as read on a potentiometric recorder, reflects the amount of hydrogen in the original sample. A similar measurement is made of the signal output of a second pair of conductivity cells between which is a trap

which removes CO_2. The remaining gas, which consists of helium and nitrogen, passes through a conductivity cell whose output is compared with that of a reference cell through which flows pure helium from the supply gas cylinder. This gives the nitrogen content.

The potentiometric outputs from the apparatus are calibrated by combusting a sample of known concentrations. From this a response factor in microvolts per microgram of element is obtained. In use, the potentiometric outputs for each element are converted to micrograms which are ratioed with the sample weight to obtain the percents by weight of the elements. The measurements of the amounts of C, H, and N are normally the true values within ± 0.3 percent for any species.

Also a Bausch and Lomb Type 33-84-69 emission spectrograph was used to determine what elements other than C, H, and N were present in the chars. This apparatus operates by burning a sample in an electric arc. The emitted light is analyzed for characteristic emission lines, which are recorded on photographic plates. These emission lines correspond to certain wavelengths which are associated with a particular element. The measured intensity of a line for a given element related to the known intensity for that element indicates the relative concentration. The absolute concentrations of the elements were not obtained. However, the relative concentrations of the impurities found were qualitatively determined.

X-ray Diffraction. - X-ray diffraction measurements were made with a Siemens X-ray diffraction apparatus. Debye-Scherrer patterns were made for all samples using a chromium tube operating at 30KV and 15 mA. The incident radiation was vanadium filtered, and a 4 hour exposure was used. The film patterns were reproduced on a strip chart using a Siemens photometer. All aspects of the X-ray procedure and strip chart reproduction were held as uniform as possible for each specimen.

Figure 114 shows a drawing of the critical planes for synthetic graphite in accordance with ASTM Card 12-212. The crystallographic planes defined in figure 114 shall be referred to in discussing the results.

The X-ray diffraction measurements gave the characteristic spacings of the atoms within the crystalline portion of the material. However, they did not allow a measurement of the amount of material within the sample which had that spacing. In order to gather some qualitative information about the relative amount of material in a crystalline state, the intensity of the diffraction peaks were referenced to the measured intensity of that sample which had the most intense peak in the radiation from the 002 plane.

Liquid Absorption. - Liquid adsorption measurements were made to determine the open porosity, bulk density and apparent density of the char. These measurements were made by first floating the specimens on a liquid and then pulling a vacuum above the specimen. This caused the liquid to penetrate into the open pores of the material. The penetration had to occur to a degree sufficient to allow the specimens to entirely submerge in the liquid before the measurements could be made. Mineral spirits was used as the liquid media because of its low density which enhances the submersion of the material.

The measurements which are made on the specimens are the dry weight, weight when saturated with mineral spirits, and weight when suspended in mineral spirits. From these measurements the percent water absorption, open porosity, bulk density and apparent density may be obtained directly. The total porosity of the material can be derived from the measurements if the true density of the material is known. These values are calculated as follows:

$$WA = \left(\frac{W_{SA} - W_D}{W_D}\right)\left(\frac{\rho_W}{\rho_M}\right) \times 100 \text{ percent} \tag{7}$$

$$P_O = \left(\frac{W_{SA} - W_D}{W_{SA} - W_{SU}}\right) \times 100 \text{ percent} \tag{8}$$

$$\rho_B = \left(\frac{W_D}{W_{SA} - W_{SU}}\right) \times \rho_M \tag{9}$$

$$\rho_A = \left(\frac{W_D}{W_D - W_{SU}}\right) \times \rho_M \tag{10}$$

$$P_T = \frac{\left(\frac{W_{SA} - W_{SU}}{\rho_M} - \frac{W_D}{\rho_t}\right)}{\left(\frac{W_{SA} - W_{SU}}{\rho_M}\right)} \tag{11}$$

where

WA	=	water absorption
W_{SA}	=	weight of sample when saturated with liquid M
W_D	=	dry weight of sample
W_{SU}	=	weight of sample when suspended in liquid M
ρ_M	=	density of liquid M
ρ_W	=	density of liquid water
ρ_t	=	true density of sample
ρ_B	=	bulk density of sample
ρ_A	=	apparent density of sample
P_O	=	open porosity
P_T	=	total porosity

Note that the true density of the material must be known in order to calculate the total porosity of the material from equation (11).

Bulk Density. - Two methods used to measure the bulk density of the arc-jet chars. One method was to make the measurement in accordance with ASTM D311-58. This entails weighing the sample and then coating it with paraffin and determining the volume by water immersion of the coated specimen. The second method was to machine the samples to a known geometry, calculate the volume from measurements of the dimensions and then weigh the samples. For the arc-jet chars this required impregnating the samples with polyalphamethylstyrene prior to machining so that they could be machined. After determining the dimensions of the impregnated sample, the impregnant was baked out, the weight was obtained, and the bulk density was calculated. It is our judgement that the densities determined from calculations of the volume provided the best values for this low-density material.

True Density. - The true density was measured with a pycnometer, using the procedure outlined in ASTM C 135-66. Prior to making the measurements the samples were pulverized to as fine a particle size as was possible. Normally, the particles were passed through a U. S. Standard 325 mesh screen which has an opening of 44 microns. This is the smallest opening size available in the standard series. However, most of the particles were probablysmaller than 44 microns. This same procedure has been used in the past on arc-jet chars, and measurements of the particle sizes after pulverization showed that nearly all of the particles were less than 12 microns in size and that 75 percent were less than 2 microns in size.

Both water and ethanol were used as fluids for the pycnometer. A wetting agent, Tergitol TNN, a nonionic detergent, which is a product of Union Carbide, was used for the measurements with water to reduce surface tension effects. Nevertheless, a small amount of flotation occurred which lent inaccuracy to the measurements. We estimate that the true density measurements themselves had an uncertainty of about ± 5 percent. The major uncertainty in the measurements, however, is that some entrained porosity may be retained after pulverization.

Pore Size Distribution. - The pore size distribution measurements were made by viewing the samples under a microscope at 100X magnification. The specimens were impregnated with Koldmount prior to polishing for the measurement. The impregnant did not fill the voids as well as had been hoped and the impregnant also picked up a dark coloration from the char. A filar eyepiece was used to measure the pore diameters. The filar eyepiece was calibrated against a calibration standard with scribed lines of known separation. The pores were assumed to be circular and when irregular pores were found the diameter was visually approximated and this approximation was measured. From these measurement a histogram of the relative frequency distribution was developed.

Figures 115, 116, and 117 give typical views of the char structure. In making the measurements on the arc-jet chars, the cracks parallel to the charring direction were not measured. Reference to figure 116 can clarify the method in which the measurements were made. Note the picture in the upper right hand corner. At the neck of the pores a wide bright ring can be observed. This ring was not measured, but rather the fine bright ring encircling the inner ring was measured. It is not very clear in the pictures, but under the microscope it was obvious that this gave the proper dimensions of the pore. Also, the distinction was clearer under the microscope.

The measurements were made by traversing the sample along a straight line and measuring the sizes of all of the pores which intersected the line. The arc-jet chars were viewed normal to the charring direction.

Pore Continuity. - Microscopic measurements were made to obtain some understanding of the continuity of the pores in the material. This analysis consisted of grinding furnace chars to thicknesses of 0.0127 cm and 0.0254 cm and then measuring the area fraction of the holes which went all the way through the thickness. A light source was set up so that light was incident on the bottom of the sample and those areas which transmitted light were counted as connecting pores. The measurements were made by viewing the sample through an eyepiece which had nine lines scribed on it in a regular

array. The 18 ends of these lines were taken as points. The sample was viewed through the microscope and the number of points which fell inside holes (points occupied) were counted along with a count of the 18 points applied. Then the sample was randomly reoriented and the same measurement was made on the new section. Points which fell on the edge of a hole were counted as 1/2 point occupied. The measurements were repeated until about 100 points occupied had been counted. Then the area fraction of holes is given by the ratio of the points occupied to the points applied.

High Temperature Furnaces. - The high temperature furnaces described in Appendix E were used to prepare the chars. These furnaces employ a graphite heating element which operates at low voltage and high current. The furnaces can be operated to 3033°K for prolonged periods and to 3311°K for short periods (less than one hour). A helium purge was used during all of the charring. Special heater tubes of 5 cm and 7.6 cm diameter were used for most of the char preparation.

Impregnation of Char with Thermatomic Carbon. - It became obvious during the course of the work that some means of negating the radiation heat transfer during a thermal conductivity measurement was needed in order to separate this component from the effective thermal conductivity. Toward this end, attempts were made to impregnate a furnace ahar with thermatomic carbon. This material has a low thermal conductivity (0.11 W/m-°K at 1000°K). The idea was to fill the voids with this low conductivity material.

Impregnation was attempted by mixing thermatomic carbon, which had passed a U. S. Standard 325 mesh screen, with kerosene. Then the mixture and specimen were placed inside a vacuum chamber with the specimen suspended above the mixture. After a vacuum of about 200 microns was achieved the sample was lowered into the mixture and allowed to remain until it quit bubbling. Then vacuum was broken, and atmospheric pressure was placed on the surface of the mixture, with the specimen still submerged, to help drive the impregnant in. Using this method, we were able to achieve only 4 to 7 percent by weight impregnation.

Another method that was used was to place the specimen in a slot machined into a metal plate placed over a dessicator. The periphery of the specimen at the opening in the cover plate was sealed with silicone rubber (Silastic RTV 731). Next, a vacuum was pulled inside the dessicator. Then a mixture of thermatomic carbon and kerosene was poured onto the surface of the char and allowed to seep in under the influence of the pressure gradient. No significant amount of impregnation was achieved with this method.

In addition to the attempts at impregnation with thermatomic carbon, colloidal graphite in methanol and Barrett No. 30 pitch in trichloretheylene were used. These gave no better success, primarily because the solvents vaporized too rapidly in vacuum.

The main reason that successful impregnation was not achieved was probably because the impregnant blocked the small openings at the pore necks. However, the weight gain due to kerosene penetration was only about 20 percent and it should have been about 170 percent for total void filling. Therefore, the structure must have included much closed porosity.

Thermal Conductivity - Comparative Rod Apparatus. - A comparative rod apparatus was used to measure the thermal conductivity of the chars at low temperatures. This apparatus is described in detail in Appendix F and in Reference 9. Basically, it consists of cylindrical upper and lower heat meters (references of known thermal conductivity) between which the cylindrical specimen is sandwiched. Heaters, which provide the heat flow and temperature control are placed above and below the upper and lower references. The column consisting of the heaters, references and specimen is surrounded by a guard heater 10.2 cm in diameter. In operation, the temperatures in the guard are matched as closely as possible with those at the same axial location in the column to reduce radial heat flow. The annulus between the column and the guard heater is filled with thermatomic carbon powder insulation to further guard against radial heat flow.

Temperature wells are drilled into the specimen and the references at two different axial locations for the measurement of the temperature gradients. These wells are drilled along a diameter to the centerline of the specimen. Chromel/alumel thermocouples were used to measure temperatures.

The thermal conductivity of the specimen is calculated from the equation

$$K_s = \left[\frac{K_1 \triangle T_1}{l_1} + \frac{K_2 \triangle T_2}{l_2}\right] \frac{l_s}{2 \triangle T_s} \qquad (12)$$

where

K = thermal conductivity
1 = gage length (distance between two thermocouples wells)
$\triangle T$ = temperature difference over the gage length.

The subscripts s, 1 and 2 refer to the specimen, upper reference and lower reference, respectively.

The specimens used for the measurements were 1.907 cm in diameter by 2.54 cm long and had a gage length of 1.907 cm. The length and gage length of the arc-jet chars were reduced because the char supplied was only about 0.9 cm thick.

For the measurements, the apparatus was placed inside a bell jar which can be evacuated. For most of the measurements up to about 500-600°K, the apparatus was not evacuated and a nitrogen purge was used. For the measurements above 600°K the apparatus was evacuated and then back-filled with either helium or nitrogen to prevent specimen oxidation.

The normal uncertainty in the measurements with the comparative rod apparatus is ± 5 percent. This uncertainty applies to materials with a thermal conductivity above about 1.4 W/m-°K. The chars had a thermal conductivity which was lower than this value, thus the uncertainty was increased. The uncertainty increases because low thermal conductivity references must be used and the heat flow through the column relative to the extraneous radial heat flows is decreased. Most of the data were obtained using Code 9606 Pyroceram references. Some evaluations were made with Pyrex and Teflon references, which have a lower thermal conductivity than Pyroceram, in order to match the thermal conductivity of the specimens. Where data were obtained with more than one type of references, we made a judgement as to which data were the most valid and drew the curve accordingly.

We estimate that the random uncertainties in the measurements were ± 7 percent with a positive bias error of perhaps 30 percent for those cases where the thermal conductivity of the reference was considerably higher than the thermal conductivity of the specimen. The bias error can be in the negative direction when the thermal conductivity of the specimen is higher than the thermal conductivity of the references. As the thermal conductivity of the specimen is increased relative to the thermal conductivity of the references, the bias error decreases. Even though these bias uncertainties are large, the measurements do indicate differences between specimens if the same type of references are used for thedifferent specimens.

Thermal Conductivity - Radial Inflow Apparatus. - The thermal conductivity of the char at elevated temperatures was measured with a radial inflow apparatus. The basic apparatus is fully described in References 2 and 10.

This apparatus consists of a cylindrical specimen, with a hole along its axis, which is centered on a water flow calorimeter. This calorimeter consists of a hollow stainless steel tubing which contains two thermocouples

located 1.27 cm apart axially. A spiral spring around the thermocouples insures mixing of the water in the vicinity of the thermocouples. The heat flow is calculated from measurements of the water flow rate and temperature rise of the water as it flows through the 1.27 cm gage length.

The specimen is placed over the calorimeter and the annulus between the specimen and the calorimeter is filled with a packing material, either zirconia powder or graphite granules. The buildup is inserted in a high temperature furnace with a graphite heating element. The specimen is heated radiantly on its exterior surface and the heat flows radially inward. Temperatures are measured in wells drilled axially into the specimen at two different radial locations and by direct optical sightings on the face through an opening in the furnace. Below 1500°K, temperature measurements inside the specimen are made with chromel/alumel thermocouples. Above 1500°K, temperature measurements are made by direct optical sightings on the bottom of the wells with an optical pyrometer using a right angle mirror. Axial conduction in the specimen is minimized by (1) insulating the specimen on each end with graphite cylinders containing thermatomic carbon powder (thermal conductivity of about 0.2 W/m-°K at 1350°K), (2) making the specimen length at least twice the gage length, and (3) providing an isothermal hot zone over a least twice the specimen length. The upper thermatomic carbon filled graphite cylinder contains graphite sight tubes through which the specimen can be viewed from the top.

A drawing of the standard cylindrical specimen configuration is given in figure 118. For this specimen, thermal conductivity is calculated from the relation

$$K = \frac{\ln (R_o/R_i)}{2\pi l} \quad \frac{Q}{\Delta T} \tag{13}$$

where

K = thermal conductivity
R_o and R_i = outside and inside radii, respectively, at which temperatures were measured
l = 1.27 cm gage length of calorimeter
Q = heat flow into calorimeter gage length
ΔT = temperature difference measured between R_o and R_i

Below 1500°K, the mean temperature is calculated as the average of the thermocouple readings. Above 1500°K, the true internal specimen

temperatures are not known because there are losses through the sight ports through which temperatures are measured. Therefore, the true mean temperature of the specimen has to be calculated from the measurement of the temperature difference and the face temperature. The equation used is

$$T_m = T_{of} - \left[0.5 + \frac{\ln (R_{of}/R_o)}{\ln (R_o/R_i)}\right] \Delta T \qquad (14)$$

where

T_m = average of true temperatures at hot and cold holes
T_{of} = face temperature of specimen

For the particular cylindrical specimen configuration employed

$$T_m = T_{of} - 0.808\,\Delta T \qquad (15)$$

Problems associated with preparing cylindrical specimens, except for the char prepared at 812°K, dictated that a strip specimen configuration be employed for the thermal conductivity measurements. This required modification to the procedure used for the radial inflow apparatus. Four char strips 0.953 cm wide by 0.795 cm thick (in the measurement direction) and 5.08 cm long were arranged symmetrically about the water calorimeter as shown in figure 119. The dimensions of the individual strips are given in figure 120. For this configuration it was necessary that the isotherms be perpendicular to the heat flow. This condition was achieved by backing the specimens on the inside with thin strips of pyrolytic graphite. This forced the isotherms to assume a square configuration because of the high anisotropy ratio of this material (the thermal conductivity in the "a" direction is about 50 times the thermal conductivity in the "c" or thin direction). Thermatomic carbon was packed in the triangular openings at the edges of the specimen (see figure 119) to minimize heat flow other than thr ugh the specimen. This packing has a low thermal conductivity of about 0.2 W/m-°K at 1350°K. The annulus between the calorimeter and the inside of the pyrolytic graphite strips was packed with graphite granules, zirconia powder or a mixture of the two.

The basic assumption of the strip configuration method is that the heat flow divides equally between the four strips. Under this assumption the thermal conductivity is calculated from the equation

$$K = \frac{\Delta X}{A} \left(\frac{Q}{\Delta T} \right) \tag{16}$$

where

K = thermal conductivity
ΔX = distance between inside and outside temperature wells
A = total area of four strips = 4 x width of one strip x 1.27 cm gage length of calorimeter
Q = total measured heat flow
T = temperature difference between inside and outside temperature wells

Again, temperatures were measured with chromel/alumel thermocouples below 1500°K and with an optical pyrometer above 1500°K. For the thermocouple points the mean temperature was calculated as the average of the thermocouple readings. Above 1500°K the mean temperature was calculated from the outer face reading by assuming a linear temperature gradient. The equation used was

$$T_m = T_{of} - \frac{\Delta X_1}{\Delta X} \Delta T \tag{17}$$

where

T_m = mean temperature
T_{of} = measured outer face temperature
ΔX_1 = distance from outer face to midpoint between thermocouple wells
ΔX = distance between inside and outside temperature wells
ΔT = observed temperature difference between inside and outside temperature wells

The thermal conductivities of powders made from the char and from ATJ graphite were measured to aid in determining the thermal conductivity of the char solid. These measurements also required a modification to the radial inflow apparatus. The apparatus used is shown in figure 121. Briefly, it consisted of two concentric cylinders made of ATJ graphite. The powder was packed between the two cylinders and the assembly was placed on the water flow calorimeter. A graphite paste was used to cement the inner cylinder to the calorimeter. Temperatures were measured in the ATJ graphite cylinder's and a measurement of the

face temperature of the sample was made through a hole drilled in the outer ATJ cylinder. The thermal conductivity of the powder was calculated from the equation

$$K = \frac{\ln (D_o / D_i)}{2\pi l} \quad \frac{Q}{\Delta T} \tag{18}$$

where

K = thermal conductivity
D_o, D_i = inside diameter of outer ATJ cylinder and outside diameter of inner ATJ cylinder, respectively
1 = 1.27 cm gage length of calorimeter
Q = heat flow
AT = temperature difference between ATJ cylinders

For the calculations it was assumed that the temperature drop between the powder and the cylinders was negligible and that the temperature drop in the ATJ cylinders from the surface to the temperature well was negligible. The later assumption is confirmed by the fact that the thermal conductivity of the ATJ graphite is about 30 times as high as that of the powder with the highest thermal conductivity. Therefore the error should be no more than perhaps 2 percent since the distance between the temperature well and the surface of the cylinder is about half the thickness of the sample.

The mean temperature of the powder samples was calculated either as the average of the thermocouple readings or as the average of the face temperature and inside thermocouple reading. When the temperature difference between the cylinders was obtained optically, the mean temperature was calculated as the face temperature minus one-half the temperature difference.

The basic uncertainty in the radial inflow apparatus is estimated to be $\pm$ 7 percent for the standard cylindrical specimen configuration. This is based on the assumption that the temperature difference measured with an optical pyrometer gives the true temperature difference even though there is an error in the absolute values.

For the strip specimen configuration there is an additional uncertainty caused by the heat flow through the thermatomic carbon packing in the corners of the buildup. This uncertainty was estimated by making a graphical calculation of the heat flow from the cylindrical portion of the thermatomic into the specimen (note in figure 119 that all of the heat input through the thermatomic must go into the specimen). The calculations were made by assuming a temperature gradient through the specimen typical of those measured with a 50 graphite-50 zirconia mixture. The calculations showed that the total heat input to the specimen through all of the thermatomic could be approximated by the equation

$$Q_T = 16\,Kp \qquad (19)$$

where

Q_T = heat flow through insulation - watts
Kp = thermal conductivity of thermatomic

Using a thermal conductivity value for the powder of 0.5 W/m-°K at 3000°K (extrapolation of the values which we measured to 1350°K) the heat input to the specimen would be 8 watts. Correspondingly, the total measured heat flow corresponding to the same conditions was about 140 watts. Thus the extraneous heat flow was about 6 percent of the true heat flow through the specimen. However, this uncertainty would be reduced because the heat input through the thermatomic goes into the specimen and some increase in temperature difference is caused by it. Thus, some of the extraneous heat flow is accounted for in the measurement of temperature difference. Hence, we conclude that the bias in the measurements due to the extraneous heat flow is perhaps +4 percent.

The total uncertainties in the measurements are estimated to be as follows:

1. Regular cylindrical configuration - ± 7 percent random uncertainty.
2. Strip specimen configuration - ± 7 percent random uncertainty with a bias error of + 4 percent.

Permeability. - Permeability measurements were made on the chars with the apparatus and procedures described in Appendix G. A schematic diagram of the apparatus is given in figure 122. The specimens

employed were nominally 1.59 cm in diameter by 1.59 cm thick. The arc-jet specimens were about 0.635 cm thick, which was the maximum thickness available.

The arc-jet specimens were impregnated with polyalphamethylstyrene and then machined to known dimensions. Then the impregnant was removed by baking the specimen at 700°K for one hour.

The specimens were inserted in the specimen holder and the annulus between the specimen and holder was filled with silicone rubber (Dow Corning RTV-731 Silastic). This material provides an excellent leak tight seal around the specimen.

Differential pressures across the specimen were measured with U-tube manometers filled with water for the measurements on the arc-jet specimens and with U-tubes filled with mercury for the measurements on the furnace chars. Volumetric flow rates were measured with Fischer and Porter laboratory flowmeters for the measurements on the arc-jet chars and with the same flowmeters or a bubble-type flowmeter for the measurements on the furnace chars.

The data were analyzed with an analysis developed by Greenberg and Weger,[11] which considers the flow to consist of both viscous and inertial components. The equation used to determine the permeability coefficients from the data was

$$\frac{MP_m \Delta P}{LRT\mu G} = \alpha + \beta (G/\mu) \qquad (20)$$

where

$P_m = \frac{1}{2}(P_1 + P_2)$ = mean specimen pressure (absolute)
$\Delta P = (P_1 - P_2)$ = differential pressure
L = thickness of specimen
M = molecular weight of permeating gas
R = universal gas constant
T = absolute gas temperature
P = absolute pressure
G = mass velocity = ρV
ρ = density of gas
V = velocity of gas

P = absolute viscosity of gas
α = viscous flow coefficient = $1/K$
K = Darcy's constant
β = inertial flow coefficient

Since G is a constant, one may write

$$G = \frac{Q_{STP}\rho_{STP}}{A} \tag{21}$$

where

Q_{STP} = volumetric flow rate at standard conditions
ρ_{STP} = gas density at standard conditions
A = total cross section of porous media normal to flow

The dependent and independent variables in equation (20) are calculated fur each data point. Then a plot of $MP_m \Delta P/LRT\mu G$ versus G/μ is made. Such a presentation is known as a Cornell and Katz plot. A straight line is drawn through the points thus plotted and the viscous and inertial coefficients are obtained from the intercept and slope of the line, respectively. Thus, for each specimen evaluated, one viscous and one inertial coefficient is calculated. Data are obtained over a sufficient range of the parameter (G/μ) to allow a good correlation and reduce the effects of spurious readings. The uncertainty in the reduced data is estimated to be $\pm$ 5 percent.

Transmittance. - In an effort to understand more about the radiant heat transfer characteristics of the porous structure, transmittance measurements were made on samples of the char which were ground to thicknesses of 0.0127 cm and 0.0254 cm. The measurements were made with the sample at room temperature in a Cary Model 14 recording spectrophotometer. This apparatus provides wavelengths within the spectrum of 0.2 microns to 2.6 microns. A tungsten lamp is used as the source. The wavelength is controlled by a monochromator grating and the intensity of the radiant energy incident on the sample is controlled through a variable slit mechanism. The equipment measures absorptance by alternately passing the chopped source radiation through a cell containing the sample and a standard cell. The amounts of radiant energy passing through the two cells are detected by a photocell. The ratio of the energy passing

through the test cell to that passing through the standard cell is converted to an absorptance value which is recorded on a strip chart recorder in absorbance units (ranging from 0 to 2). A continuous reading in absorbance units versus wavelength is obtained. The absorptance values are then converted to transmittance values from the relation $A = \log_{10}(1/T)$, where A is the measured value in absorbance units and T is the fraction of the radiation transmitted.

The transmittance measurements were made over a range of wavelengths from the visible region (0.2 microns) to the near infrared (2.6 microns).

Electrical Resistivity. - Electrical resistivity measurements were made from 294°K to 2330°K to gather more information on the properties of the char solid. A schematic diagram of the apparatus used for the measurements is given in figure 123. The specimen used was 0.483 cm in diameter by about 3.12 cm long and was threaded on both ends. The threaded ends of the specimen were screwed into graphite rods which extended to outside the furnace. These graphite rods were connected to an external circuit through which current was supplied to the specimen. Split graphite rings were placed around the specimen at two different axial locations to serve as voltage taps. These rings were radiused on the inside so that they made line contact with the specimen. They were held in place by graphite screws which held the two halves together. A graphite fiber (Thornel) was attached to each split ring and extended through the bottom of the furnace. These fibers were attached directly to the potentiometer which was used to measure the voltage drop across the specimen. A rectified d. c. power supply was used to provide current flow through the specimen and a General Electric precision d. c. ammeter was used in the circuit to measure the current.

The apparatus was inserted in a furnace which employed a graphite heater tube. The fibers and the graphite current leads were electrically isolated from the heater tube by spacers on either end of the furnace which were made from firebrick.

In operation the following procedure was used:

1. The specimen was brought up to the desired temperature level.
2. The open circuit (no current flow) voltage across the Specimen was measured.
3. Current was passed through the specimen and the current flow and associated voltage drop were measured.

The volume electrical resistivity was calculated from the measurements with the equation

$$\rho = \frac{A}{L} \frac{V}{I} \qquad (22)$$

where

ρ = volume electrical resistivity
A = cross-sectional area of specimen
V = voltage drop across gage length of specimen (corrected for open circuit voltage)
I = current flow through specimen
L = gage length of specimen

A helium purge was used for all of the measurements.

The normal uncertainty in electrical resistivity measurements is + 2 percent. However, the uncertainty was increased fur these measurements because the method used to tap the specimen voltage made it difficult to accurately measure the gage length. Normally, pins are pressed into holes drilled into the specimen so that an accurate gage length definition is obtained. We estimate that the uncertainty in these measurements is + 10 percent, primarily because of the uncertainty in the gage length. However the precision of the measurements is $\pm$ 2 percent. Therefore, the method was completely acceptable for studying the relative change in electrical resistivity as a function of temperature.

Sonic Velocity. - Sonic velocity measurements were made with the sample at room temperature using a pulse ultrasonic through transmission technique. The measurements were made at a frequency of 1 megacycle. A Sperry Model 721 pulser unit was used with a Techtronics Model 564 oscilloscope for the measurements.

Preparation of Laboratory Chars

Chars were produced in the high temperature furnaces to provide specimens with a known thermal exposure. The first specimens made were for the chemical analysis and X-ray diffraction measurements. These specimens were made by heating linearly to different temperature levels

at a rate of 10°K/min (see figure 124). This cycle resulted in gross cracking of the material and a linear shrinkage of about 25 percent was observed. Thus, while the cracked samples could be used for the chemical analysis and X-ray diffraction measurements, they were unacceptable as specimen blanks. After experimentation, it was found that if the material were allowed *to* soak for about 30 minutes at temperature levels of 700°K and 920°K the material would thermally equilibrate sufficiently that the shrinkage would not produce gross cracking, provided the sample was not too large. Significant warpage did occur and this had to be allowed for in sizing the virgin blanks along with an allowance for shrinkage. Withregard *to* the effects of specimen size, several attempts were made to produce a standard cylindrical radial inflow specimen which required a virgin blank 4.05 cm in diameter by 7.62 cm long. An acceptable blank was obtained for one char produced at 812°K, however, the additional shrinkage which occurred above this temperature level resulted in a cracked blank after each attempt to char at higher temperature levels. The heating rate for this particular blank size was decreased until it required 10 hours to reach 1366°K and still the specimen cracked. A similar result was encountered when trying *to* produce large diameter specimens for the ASTM C177 guarded hot plate thermal conductivity apparatus. Thus, acceptable specimens could be produced only by using small blank sizes and putting steps in the temperature-time curve at low temperatures.

The blank size used for each strip for the specimensfor the radial inflow apparatus was 1.59 cm square by 18.2 cm long. The long dimension corresponded to the a-b direction of the virgin billet (normal *to* pressing direction) and the square dimensions corresponded *to* the direction parallel *to* pressing (c) and the a-b direction. Since the outgassing occurred from the center of the specimen out in both the c and a-b directions of the square dimensions, both directions were considered to be the charring direction. All measurements were made in the charring direction. For the blank sizes required, only two strips of the four required for a thermal conductivity specimen could be charred in a given furnace at one time.

The blanks for the permeability specimens were 2.54 cm cubes. These were charred in the furnace in the same manner as the thermal conductivity specimens.

The temperature-time cycles used *to* produce the majority of the samples for the thermal conductivity and permeability measurements are presented in figures 125 through 128. Note that most of the curves are similar and only the temperaturelevels and hold times at temperature were varied.

A char was produced which had a short time exposure at 1366°K by heating slowly to 922°K and then heating more rapidly to 1366°K. As soon as the specimenreached 1366°K the power to thefurnace was turned off so that the dwell time at the maximum temperature was not more than two minutes. The temperature-time curve for this specimen is given in figure 129.

Specimens were also charred by heating rapidly to 3033°K for short times. This was done by immersing the specimen in a furnace preheated to 3033°K. The approximate cold-wall heat flux density was 4.9 MW/m^2. The temperature-time history for specimens prepared by this method is given in figure 130. The specimens thus prepared were cracked similarly to the arc-jet chars. However, they did hold together and some acceptable specimens were obtained from chars prepared in this manner. These specimens exhibited a slight amount of growth after charring, rather than a shrinkage as was observed for the low heating rates. Pictures of chars prepared at a low heating rate and at a rapid heating rate are presented in figures 131 and 132.

The blanks used for the chars prepared at high heating rates were approximately 4 07 cm in diameter by 7.5 cm long. The axis of the cylinders corresponded to the pressing direction of the virgin billet.

The same procedure that was used to prepare the char to 3033°K at a high heating rate was attempted at a temperature of 1366°K. The specimen was fragmented upon removal from the furnace.

In summary, specimens were not prepared under all of the conditions which were originally anticipated because of problems with preparing acceptable specimens. However, at this point in the program, we decided to concentrate our efforts toward devising methods which would allow the mechanisms of heat transfer within the chars to be separated and thus provide us with an understanding of the behavior that was being observed in the property measurements. Some of the other charring conditions would still be of interest to see what effects they have on properties.

Data and Results

Characterization. - A quite detailed characterization was performed on the arc-jet chars supplied by the NASA Langley Research Center and a limited amount of characterization was performed on the chars prepared in the high temperature furnaces

The arc-jet chars contained the columnar structure which is invariably noted for samples prepared in the arc-jet. The chars prepared in the furnace at low heating rates were crack free and homogeneous in appearance. Pictures of the arc-jet chars prepared at the two different heating rates are presented in figure 131. The char prepared at 2.27 MW/m^2 had been removed from the substrate prior to receipt at SRI and had sufficient strength to allow handling. The char prepared at 1.13 MW/m^2 was still attached to the substrate upon receipt at SRI. Upon removal of the char from the substrate the columns of char were so loosely bonded that the material fell apart. Thus, the arc-jet char prepared at the lower heating rate was more cracked and contained fewer interconnections between columns than the char prepared at the higher heat flux density. The cracks were so large in the former char that the impregnant used to bond the material for machining could not hold the columns together well enough to provide machinability.

Chemical analyses of the amounts of carbon, hydrogen and nitrogen in arc-jet chars were made as a function of distance from the heated surface. Samples of various thickness were removed from the char by slicing with a microtome. The various samples obtained and the thicknesses of the samples are summarized in table 21. Four samples were obtained from the arc-jet char produced at 1.13 MW/m^2 and six samples were obtained from the arc-jet char produced at 2.27 MW/m^2. The results of the chemical analyses of these chars are presented in table 22. The chars consisted primarily of the element carbon with slight amounts of nitrogen and hydrogen. Note that a significant amount of unidentified elements were found in the surface layers of both arc-jet chars. Reruns were made on these two samples and the carbon content was determined to be above 98 percent. It is believed that the first values measured were low because of incomplete combustion of the sample. For the second measurements, a smaller sample size was used, the combustion time was extended and the temperature was raised about 50°K.

Emission spectrograph measurements were also made on samples 100-1 and 200-1. These measurements indicated the presence of magnesium, silicon, and calcium in the arc-jet char prepared at 1.13 MW/m^2 and the presence of manganese, magnesium, silicon and calcium in the arc-jet char prepared at 2.27 MW/m^2. These were trace impurities and probably accounted for less than 1 percent by weight.

The furnace chars were also comprised mainly of carbon. The furnace chars prepared at low temperatures contained more hydrogen and nitrogen than either than arc-jet chars or the char prepared in the furnace at 3033°K.

The percent of unidentified elements in the chars ranged from 0 to 14 percent (neglecting the first evaluations on specimens 100-1 and 200-1). No residue was noted after burning the 812°K furnace char, which had the highest percentage of unidentified material, so the balance of the elements in the char could not be attributed to ash. One is inclined to conclude that the balance was oxygen since the starting material primarily consisted of C, H, N and O. However, oxygen would most likely be bound to nitrogen and the percentages of nitrogen were small. It is not known how the oxygen was combined with the other elements.

In summary, the chemical analysis shows that the arc-jet chars consist of over 90 percent carbon and the furnace chars consist of over 80 percent carbon. The hydrogen and nitrogen content of the chars is low, generally less than 1 percent of the total composition for the arc-jet chars and less than 3 percent for the furnace chars. The balance of unidentified elements in the char ranged from 0 to 9 percent for the arc-jet chars and from 0.21 to 16 percent for the furnace chars.

X-ray diffraction measurements were made on chars which came from the same samplings of the arc-jet chars as the chemical analysis samples. Measurements were also made on chars prepared in the furnace at 1922°K and 3033°K at low heating rates and on chars prepared at a rapid heating rate to 3033°K.

The X-ray diffraction data acquired are presented in table 23 and figure 133 and Appendix C. Figure 114 shows the orientations of the crystalline planes. Of the many distinguishing lines produced by well-oriented or crystallized graphite, only three appear on most of the patterns produced by these specimens. The first column of "d" spacings refers to the (002) plane which is the interplanar spacing along the "c" axis, while the second column refers to the (100) plane associated with rhombohedral order, a plane parallel to the "c" axis. The last column (004) plane is the second order diffraction of the (002) plane.

The relative intensities were all based on the intensity of the 3.45 Å line of specimen 200-3 which was the most intense line. Since all experimental conditions were as uniform as possible, the relative intensities may be compared to give a crude idea of the degree of perfection of the various planes.

The results of the bulk and true density measurements on the arc-jet chars are presented in table 24. True density measurements on furnace chars are also presented in table 24. Only two bulk density measurements were obtained on the char prepared in the arc-jet at 1.13 MW/m^2 because

of difficulties in obtaining a good sample for either method used to measure bulk density. The arc-jet char prepared at the lowest heat flux density had a lower bulk density, about 0.25 gm/cm³, than that of the arc-jet char prepared at the highest heat flux density, about 0.30 gm/cm³. There was considerable scatter in the bulk density measurements which probably reflects variations in the size and number of the cracks in the various samples. The sample which was prepared in the furnace at a rapid heating rate had the highest true density and the samples which were prepared in the furnace at low temperatures had the lowest true density. The true density values ranged from 1.433 gm/cm³ to 1.780 gm/cm³ (see table 24).

Data for the weight loss of the specimens during charring in the furnace are presented in table 25 and in figures 134 and 135. Figure 134 presents data for the chars which were prepared for the chemical analysis and X-ray diffraction measurements (the charring cycle for these specimens is given in figure 120). Table 24 and figure 135 percent weight loss data for the samples which were used for the thermophysical property measurements. The data presented in figure 135 show that the weight loss increases as the charring temperature is increased to 2500°K with a slight decrease occurring above 2500°K. Note the similarity between the curves presented in figures 134 and 135. It is of interest to note that the char prepared at a rapid heating rate exhibited less weight loss than the chars prepared at the low heating rates.

The data for the bulk densities of the chars prepared at various temperature levels are presented in table 25 and in figure 136. The chars prepared at 812°K had the lowest bulk density and the chars prepared at 1366°K had the highest bulk density. These results are related to the weight loss and shrinkage of the material. The bulk densities of the furnace chars were higher than those of the arc-jet chars. The char which was prepared in the furnace at a rapid heating rate had a lower bulk density than either of the other chars because the specimens did not shrink during degradation. The bulk densities of the chars prepared at low heating rates ranged from 0.29 to 0.385 gm/cm³, the bulk densities of the arc-jet chars ranged from 0.22 to 0.34 gm/cm³ and the bulk density of the char prepared at a high heating rate in the furnace was 0.21 gm/cm³.

Liquid absorption measurements were made on the arc-jet char prepared at a heat flux density of 2.27 MW/m². Measurements were also attempted on the char prepared in the arc-jet at 1.13 MW/m² and on furnace chars. These other specimens could not be saturated to a degree which would permit them to sink and hence measurements could not be made.

This probably means that they had more closed porosity. The results for the char prepared in the arc-jet at 2.27 MW/m^2 are presented in table 26. The bulk density of the specimen was 0.30 gm/cm^3 and the open porosity was 64 percent. A total porosity of 80 percent was calculated by using the measured true density of 1.5 gm/cm^3. Thus, the closed porosity of the char was 16 percent.

Pore size distributions were obtained on the arc-jet chars and on the furnace chars. Pictures of the arc-jet chars are presented in figure 115. The pore size measurements do not include the cracks shown in the pictures but were made in the areas between cracks. Photomicrographs of the samples used for the measurements are given in figures 116 and 117. The results of the pore size measurements are given in figures 137 through 142. The measurements showed that the arc-jet chars and furnace chars were very similar with regard to the mean pore size and pore size distribution. The mean pore sizes from the various distribution curves ranged from 28 to 43 microns with most of the mean pore sizes being nearer 40 microns. The similarity between the pore structures of the arc-jet and furnace chars is apparent from the photomicrographs given in figures 116 and 117.

The approximate thickness of the walls of the pores in the furnace chars was calculated from the mean pore size, bulk and true density measurements. The calculations were performed by assuming a regular arrangement of pores in a square array. Under this assumption the pore wall thickness was calculated to be 2.8 microns.

Measurements were made to ascertain the degree to which the pores were continuous through the char. Two samples of furnace char prepared at 3033°K were used. One was ground to a thickness of 0.0127 cm and the other was ground to a thickness of 0.0254 cm. Pictures of the samples are given in figure 143. For the char of 0.0127 cm thickness the holes through the char occupied 11.4 percent of the total. area and for the 0.0254 cm thick char the holes occupied 2.5 percent of the area. It was suspected that removal of material during grinding may have increased the fraction of holes in the 0.0127 cm char. However, the amount of material removed was not determined. This effect was probably less pronounced in the sample which was 0.0254 cm thick.

The results of the characterization studies are summarized in table 27. The arc-jet chars and furnace chars were similar with regard to X-ray diffraction patterns (considering the thermal history of the arc-jet char), chemical analysis, pore size and true density. The major differences were in the bulk density and the fact that the furnace char did not have the columnar structure and thus was more homogeneous.

Thermophysical Property Measurements. - Thermal conductivity measurements were made on specimens which were prepared in a furnace for different exposure times and for different exposure temperatures. The conditions which were studied are summarized in table 28. Recall that acceptable specimens were produced only at low heating rates and by immersing the specimen in a furnace preheated to 3033°K. Intermediate heating rates and rapid rates obtained by preheating to a temperature level of 1922°K or below resulted in unacceptable specimen. Therefore, the effects of heating rate were not as fully established as had been planned.

The results of the thermal conductivity measurements on the chars are presented in figures 144 and 146 through 151 and in tables 29 through 62. Shown in figure 144 are the thermal conductivity data for the char prepared at 812°K for 30 minutes. Two chars were evaluated to 3033°K with the strip specimen configuration and one char was evaluated with the standard cylindrical specimen configuration. Note that the agreement between the two types of specimens was good which indicates that the material had about the same conductivity in these two directions and that the heat flow through the thermatomic carbon does not introduce a significant error in the measurements. All of the specimens prepared at 812°K were found to be cracked after exposure to 3033°K. Pictures of strip specimens, taken after exposure to 3033°K during the thermal conductivity run, are presented in figure 145. Note that the specimen precharred at 1366°K did not crack; whereas, the specimen charred at 812°K showed gross cracking.

The data for the specimens charred at 1366°K are presented in figure 146. Specimens 5R and TC17 which were held at temperature for less than one minute and for 30 minutes, respectively, had the same value for thermal conductivity. Specimens TC2 and TC10 were evaluated in a helium purge and in an argon purge, respectively, and no consistent difference in thermal conductivity was noted for these two specimens.

The data for the chars prepared at a low heating rate to 3033°K are presented in figures 149 and 150. Shown in figure 149 are data obtained with a nitrogen purge in the comparative rod apparatus and with an argon purge in the radial inflow apparatus. Specimen 2F5000-2 was held at temperature for two hours and had been exposed to 3033°K during a first thermal conductivity run, for additional exposure time, prior to obtaining the data shown in figure 149. Specimen TC13 had been held at temperature for 30 minutes and was impregnated with 4 to 7 percent by weight of thermatomic carbon. Specimen TC5 had been held at temperature for 30 minutes. The thermal conductivity of the specimen which had been held at temperature for the longest time fell between the values for the

specimens with shorter exposure times and the specimen with the slight thermatomic carbon impregnation had the highest thermal conductivity. It is our judgement that the thermatomic carbon did not penetrate into the gage section of the specimen and hence did not affect the measurements.

Thermal conductivity data obtained in a helium purge environment on chars which had been prepared at **3033°K** are presented in figure **150.** Specimen 2F5000-2 had been held at temperature for two hours and Specimen 3F5000-3 had been held at temperature for three hours. Both specimens were precharred at **1366°K** prior to charring at **3033°K** (see figures **126** and **127).** Note that both specimens had the same thermal conductivity. The temperature gradient during the measurements was different for these two specimens. Zirconia packing was used for specimen 3F5000-3 to achieve a small temperature gradient and graphite packing was used for specimen 2F5000-2 to achieve larger temperature gradient. The temperature gradients achieved are listed in the table in figure **150.** Note that the gradient through specimen 2F5000-2 was about **2.8** times as high as the gradient through specimen 3F5000-3 at 2000°K and about **1.6** times as high at 3000°K. No effect of the gradients was noted in the thermal conductivity values.

Thermal conductivity data for chars prepared at rapid heating rates in the furnace are presented in figure **151.** The approximate cold wall heat flux fur the charring conditions was 4.9 MW/m^2 (radiant flux from heater tube at **3033°K** to cold specimen). Specimens 5000-R2 and 5000-R3 were made from virgin blanks about **4.06** cm in diameter by **7.6** cm long. The columns formed during the charring grew in from the top and sides as shown in figure 132a (picture in vicinity of end of specimen). The specimens were removed from the sides of the blanks, away from the ends, with the heat flow axis for the measurements parallel to the columns. Specimen 5000-R1 was made from a blank about **3.17** cm in diameter by **3.17** cm long and the measurements were made in the direction of the axis of the cylinder. Hence, most of the columns for this specimen were perpendicular to the heat flow and the situation is not too well defined. There were subtle differences in the conditions under which the rapid furnace chars were prepared (see notes in figure **151)** and these differences probably influenced the results to some degree. Nevertheless, each of the specimens exhibited thermal conductivity values which were higher than values for the furnace chars prepared at low heating rates and the character of the curves were different at low temperatures. Also of significance is the fact that the differences in the thermal conductivity of the solid portions of the chars prepared at the two different heating rates is even greater than the difference in the effective values shown on the curves. This is based on the fact that the porosity of the rapid chars is greater which would tend to reduce the effective thermal conductivity within this porosity (and radiation) range.

A composite plot of the thermal conductivities of the specimens prepared at low heating rates as a function of precharring temperature level is given in figure 152. The thermal conductivity data obtained in the comparative rod apparatus for the arc-jet chars are also presented in figure 152. There was a significant increase in the values of thermal conductivity at low temperatures as the precharring temperature was increased. The differences in the values of thermal conductivity at 3033°K was less than the differences at 500°K.

The thermal conductivity data obtained on powders made from ATJ graphite, thermatomic carbon and phenolic-nylon chars prepared at 3033°K are presented in figure 153 and in tables 63 and 68. For the measurements on the thermatomic carbon, specimen 1 of the ATJ powder and the powder from the chars a helium purge was used. For the measurements on specimens 2 and 3 of the ATJ powder, the apparatus was evacuated and backfilled with helium two times prior to the start of the measurements, then the measurements were made in a helium purge. The powders made from the ATJ graphite had the highest thermal conductivity, However, there was a considerable difference between the thermal conductivities of the two specimens and one showed more dependence upon temperature than the other. Likewise, there was a considerable difference in the thermal conductivities of the two specimens made from the powder of the phenolic-nylon char. Both specimens exhibited a significant increase in thermal conductivity above 2000°K. The thermatomic carbon had the lowest thermal conductivity of any of the powders.

Electrical resistivity data obtained on a specimen made from specimen 3F5000-3, which was used for thermal Conductivity measurements, are presented in table 69. The char was initially prepared by charring at 3033°K for three hours. In addition, it had been exposed to 3033°K for an additional one or two hours during a thermal conductivity measurement. The measured electrical resistivity values were multiplied by an area correction $(1 - P^{2/3})$, where P is the porosity, and the corrected values are shown in figure 154. The electrical resistivity decreased significantly with increasing temperature, Curves for the electrical resistivity of two grades of graphite are shown in the figure for comparison.

Permeability measurements were made on furnace chars which had been prepared by heating to various temperature levels at low heating rates (see figure 128), on a char which had been heated rapidly to 3033°K and on chars prepared in an arc-jet at a heat flux density of 2.27 MW/m^2. The data are presented in tables 70 through 77. The Cornell and Katz data correlations used to reduce the permeability coefficients are presented

in figures 155 through 161. The permeability coefficients for the furnace chars prepared at low heating rates are plotted as a function of charring temperature in figure 162. The permeability coefficients for all of the specimens are summarized in table 78. There were large differences in the permeability coefficients of the arc-jet chars and the furnace chars prepared at low heating rates. However, the rapid furnace chars had about the same values as the arc-jet chars. Darcy's constant for the arc-jet chars was higher than that of the furnace chars by a factor of 10^5 and the inertial flow coefficient of the arc-jet chars was lower by a factor of 10^6. The arc-jet chars and the rapid furnace chars contained cracks parallel to the charring direction (see figures 131 and 132). The major portion of the gas flow probably occurs through these cracks and hence explains the difference in values for the furnace chars prepared at low heating rates and the chars prepared at rapid heating rates.

The measurements of the sonic velocity at room temperature of chars prepared under different conditions are presented in figure 163 and in table 79. The parameter ρV^2, where ρ is the density and V is the sonic velocity, is also presented in figure 163 and table 79. The sonic velocities of the chars prepared at low heating rates increased as the heat treatment temperature was increased from 812°K to 1366°K and then remained fairly constant above 1366°K. The sonic velocity of the char prepared in the furnace at a high heating rate was about the same as the values for the chars prepared at lower heating rates. The arc-jet char had the lowest sonic velocity except for the char prepared at 812°K.

The parameter ρV^2 is similar to the dynamic modulus. Note in figure 163 that the effects of heat treatment temperature on this parameter were the same as the effects noted for the sonic velocity. However, the char prepared in the furnace at high heating rates and the arc-jet char both exhibited lower values than the values for the chars prepared at slow heating rates at temperatures of 1366°K and above.

The data for the transmittance of the char at room temperature are presented in figure 164. The measured values of transmittance were 0.114 and 0.025 for chars of 0.0127 cm and 0.0254 cm thickness, respectively. Note also that the measurements made with the microscope of the ratio of hole area to total area are presented in the figure. There was fair agreement between the two measurements for the char 0.0127 cm thick and rather poor agreement between the two measurements for the char of 0.0254 cm thickness. The measurements indicate that the only radiation which passed through the char at room temperature was that which was directly transmitted through the holes.

The data which have been presented will be correlated and discussed in more detail in a subsequent section, "Analysis and Discussion of Results."

Methods of Analysis of Thermophysical Property Data

Thermal Model for Char. - In order to attempt to reduce the intrinsic properties of the phenolic-nylon char from the measured values of thermal conductivity, an analytical expression was required. The thermal model used for the thermal conductivity of the chars was developed by superimposing the several types of heat flowwhich can occur within the char. The equation developed to correlate the thermal conductivity data was

$$K = P^{2/3} K_g + (1 - P^{2/3}) K_m + \frac{4 P^{2/3} \phi \sigma \epsilon T_m^3}{2 (\rho + \epsilon)} + 4 \tau L \sigma T_m^3 \qquad (23)$$

where

K = "effective" or measured thermal conductivity of char
P = porosity
K_g = thermal conductivity of gas in pores
K_m = thermal conductivity of matrix (solid) portion of char
ϕ = average pore diameter
ϵ = emittance of pore walls
ρ = reflectance of pore walls
τ = overall fraction transmittance of char across the length L
L = thickness of char over which measurements were made
T_m = average temperature of char (absolute)
σ = Stefan-Boltzmann constant

Equation (23) applies specifically to the furnace chars. For arc-jet, rapid or flight chars, another term accounting for radiation through the cracks should be added.

Equation (23) is less complex than the equation which we previously presented (Reference 9) for the thermal conductivity of the char. However, for studying intrinsic properties, it is an acceptable representation of the former development if the environment for the measurements is not a vacuum.

The first term in equation (23) accounts for the contribution to the "effective" thermal conductivity by the gas in the pores. Since the chars have some closed porosity, the porosity used for this component should probably be the open porosity. The second term accounts for the contribution by solid conduction through the matrix. The third term represents the contribution of the radiation across pore walls and is similar to an expression developed by Russell. [12] The final term in equation (23) accounts for radiation which is transmitted directly through the pore walls of the char.

The effective cross-sectional area for solid conduction, $(1 - P^{2/3})A$, used in equation (23) is an approximation to a more complex equation given by Russell. [12] For porosities of 70 percent or above the expression used gives values which are less than 9 percent lower than those given by Russell's equation. The difference decreases with increasing porosity so that the difference is only 3 percent for a porosity of 90 percent. Since the highly porous chars are not as continuous as the regular geometry assumed by Russell, the expression used represents a reasonable approximation.

The expression used for radiant heat transfer across the pores (third term in equation 23) has been criticized as not being an adequate model for a material as porous as the char because of the interconnectivity of the pores. Therefore, a calculation of the radiant heat transfer was made wherein it was assumed that the char consisted of a bundle of reradiating cylindrical tubes which were parallel to the direction of heat flow and occupied P percent of the area. The tubes were assumed to have a diameter of 0.0127 cm (about three times the average pore diameter of the chars) and a length of 0.475 cm (gage length for measurements). The radiant conductivity was calculated from the equation

$$K_r = 4P\sigma L F_{iR_2} T_m^3 \qquad (24)$$

where

K_r = radiant conductivity
σ = Stefan-Boltzmann constant
L = length of tubes of ϕ diameter and length over which measurements were made
F_{iR_2} = total radiation factor
T_m = mean temperature (absolute)

For the diameter to length ratio of the openings, the total radiation factor, F_{iR_2}, was found to be about 0.03 from solutions given by Jakob.[13] Assuming a porosity of 85 percent, the radiant conductivity at 3000°K was calculated to be 0.74 W/m-°K. This is about 4.5 times higher than the value calculated from the model used in equation (23). However, the absolute values in either case are not large and since the pores are not as large as was assumed and do not extend all the way through the char, it was concluded that the radiant conductivity given by the third term in equation (23) is reasonable.

The expression $4T_m^3 \Delta T$ was used in place of $(T_1^4 - T_2^4)$ in developing equation (23). It can be shown algebraically that this is a valid assumption (within less than 3 percent uncertainty) if ΔT is less than $0.346\ T_m$.

The direct transmittance term in equation (23) can be interpreted in terms of an equation which has been 'used for nonopaque materials. The equation given by Gardon[14] for the radiant conductivity in the interior of a grey material (wavelength independent absorption coefficient) in which the temperature gradients are small in relation to the product of absolute temperature and absorption coefficient is

$$K_r = \frac{16n^2\sigma T_m^3}{3B} \qquad (25)$$

where

K_r = radiant conductivity
n^r = index of refraction
B = absorption coefficient

Thus, the fraction transmittance and the optical properties of the material may be related by equating equation (25) and the last term in equation (23). From this equality one finds that

$$\tau = \frac{4n^2}{3LB} \qquad (26)$$

Equations (25) and (26) are grossly simplified approximations to the mechanisms of radiant transmission through the char. The char is not composed of a homogeneous slab of diathermanous material as was assumed

in developing equation (25). Rather, it is a random selection of thin pore walls, each of which causes some scattering of the radiation being transmitted through the char. However, in lack of a more definitive analysis of the ability of the char to transmit radiation, it was believed that equation (26) would provide some basis for interpreting the thermal conductivity measurements in terms of material properties.

Note that when the transparency term is used in equation (23), the effective thermal conductivity is no longer a material property. The effective thermal conductivity becomes dependent on the thickness through which radiation is being transmitted.

Correlation of Transmittance Data. - The data obtained for the transmittance of the char at room temperature were interpreted in terms of an analysis of the heat transfer through porous insulations given by Larkin and Churchill.[15] These equations will be mentioned briefly. These authors defined the radiant heat flux through porous materials in terms of the following structural and/or material properties:

M = interception cross section per unit volume
N = backscattering cross section per unit volume
P = absorption cross section per unit volume

Only two of these parameters are independent and they are related through the equation

$$P = M - N \tag{27}$$

If a radiant flux $I_1(O)$ is incident on a porous insulation and the transmitted flux is $I_1(L)$, then the equations given by Larkin and Churchill[15] reduce to

$$\frac{dI_1}{dx} = -MI_1 + NI_2 \tag{28}$$

$$-\frac{dI_2}{dx} = MI_1 + NI_2 \tag{29}$$

where

I_1 = radiant heat flux in forward direction
I_2 = radiant heat flux in backward direction

with the boundary conditions

$$I_1(O) = 1 \tag{30}$$

$$I_2(L) = 0 \tag{31}$$

the solution to equations (28) and (29) for the transmitted flux is

$$I_1(L) = \frac{1}{\text{Cosh } L\sqrt{M^2N^2} + \frac{M}{\sqrt{M^2N^2}} \text{ sinh } L\sqrt{M^2N^2}} \tag{32}$$

Equation (32) gives the fraction of the incident flux $I_1(L)/I_1(O)$ which reaches X = L. Thus, by measuring the radiation transmitted through samples of different thickness, L, the parameters M and N can be determined by simultaneous solutions of equation (32).

Once the parameters M and N are known, they can be used with solutions of the differential equations given by Larkin and Churchill to calculate the radiant conductivity.

Unfortunately, the measurements of transmission could be made only with the sample at room temperature. Therefore, the parameters M and N determined from the data provide information only about the structural or porous effects of the char. The optical properties of the char may change with temperature and allow radiation to be transmitted which would result in changes in the parameters M and N.

The differential equations given by Larkin and Churchill have been solved for very restrictive conditions only. For the case where absorption is dominant (M >> N)

$$K_r(O) \simeq \frac{4\sigma\epsilon_0 T^3}{M} \tag{33}$$

where

$K_r(O)$ = radiant conductivity at X = 0
ϵ_0 = boundary emissivity at X = 0

For thick slabs such that $L >> (\frac{1}{\epsilon_0} + \frac{1}{\epsilon_L} - 1)/N$, and for which absorption is small

$$K_r \cong \frac{4\sigma T^3}{N} \tag{34}$$

where

ϵ_0, ϵ_L = boundary emmissitivities at X = 0 and X = L, respectively.

Larkin and Churchill also derived an equation for the case where the net radiant heat flux is essentially constant or a small fraction of the total heat transfer rate under the assumptions that

$$L\sqrt{M^2N^2} > 5 \tag{35}$$

and

$$T_o >> \frac{3(T_o - T_1)}{(M - N)L} \tag{36}$$

where

T_o, T_1 = boundary temperatures

For the solution the reader is referred to equation (14) of their paper.[15]

If the parameters M and N are known as functions of temperature, the analysis of Larkin and Churchill can be used to replace both radiant conductivity terms given in equation (23). A particular solution would then require a numerical solution of the governing differential equations for particular boundary conditions of interest.

Correlation of Data on Thermal Conductivity of Powders. - Two different analyses were used in attempting to determine the thermal conductivity of the char solid from thermal conductivity measurements on powders made from the char. First, a correlation was attempted from the results of a correlation of experimental data given by Deissler and Boegli.[16] They correlated data on powders made from three different kinds of solids and presented the results in terms of K/K_g versus K_s/K_g

(K - thermal conductivity of powder, K_s - thermal conductivity of solid, K_g - thermal conductivity of gas). The curves presented by these authors for the range of porosities from 36 to 40.5 and from 42 to 50 percent were used.

The second analysis used for correlating the data on powders was the one given in a paper by Stevens17 which was developed by Yagi and Kunii. [18] This equation is given by

$$\frac{K_e}{K_g} = \frac{\beta\,(1-\epsilon)}{\gamma\left(\frac{K_g}{K_s}\right)+\left(\frac{1}{\phi}+\frac{D_p\,h_{rs}}{K_g}\right)-1} + \epsilon\,\beta\,\frac{D_p\,h_{rv}}{K_g} \qquad (37)$$

where the radiative heat transfer coefficients are

$$h_{rs} = 0.1952\left(\frac{p}{2-p}\right)\left(\frac{t}{100}\right)^3 \qquad (38)$$

and

$$h_{rv} = \frac{0.1952\left(\frac{t}{100}\right)^3}{1+\frac{\epsilon}{2(1-\epsilon)}\left(\frac{1-p}{p}\right)} \qquad (39)$$

The nomenclature used is as follows:

D_p = average particle diameter m
h_{rs} = heat transfer coefficient for radiation, solid to solid, kcal/(h m^2 °C)
h_{rv} = heat transfer coefficient for radiation, void to void, kcal/(h m^2 °C)
K_e = effective thermal conductivity of packed bed
K_g = thermal conductivity of gas
K_s = thermal conductivity of particles
L_p = distance between adjacent particles
L_s = effective diameter of particles relating to thermal conduction
L_v = effective thickness of fluid film adjacent to contact surface of two particles

p = emissivity of particle surface
t = temperature °K
β = L_p/D_p
γ = L_s/D_p
d = L_v/D_p
ϵ = fraction void

When applying equation (39) to the data it was assumed that β and γ were unity. The value of ϕ was determined by fitting the equation to the data obtained at the lowest temperature level and then that value was used for all subsequent calculations at higher temperature levels.

The curves used for the thermal conductivities of helium, nitrogen, and air are presented in figures 165 and 166.

Reduction of Thermal Conductivity of Char from Transient Temperature Measurements Made during Simulated Ablation Tests at Other Laboratories. - Many authors have presented thermal diffusivity values for plastic materials undergoing thermal degradation. Generally these values are "effective" values and do not represent a true thermophysical property. The values of thermal conductivity reduced from such measurements are usually much lower than the values obtained in steady-state measurements. The equations which have been much used for these transient data reductions do not include the effect of the heat of pyrolysis and the transpiration cooling by the gases evolved during ablation. However, since the spread between transient and steady-state values has been so large it has been argued that the corrections would not raise the transient thermal conductivity to the value measured in a steady-state apparatus. Thus, the steady-state values have been questioned. In an effort to gain further insight into this problem, we have first used a typical method for reduction of transient data and then have tried to correct the method for the effects of the heat of pyrolysis and the transpiration coolings of the gases.

The equation used for the data reduction was one presented in a paper by Perry, et al.[19] It has also appeared elsewhere in the literature and is sometimes called the "procedural" diffusivity. This equation applies only to steady-state ablation (char surface and pyrolysis zone receding at same rate) when the temperature profile within the degrading zone and char changes uniformly at all points with time. The equation is written

$$\alpha = \frac{\dot{V}^2 (T_x - T_\infty)}{\left(\frac{dT}{d\theta}\right)_x} \qquad (40)$$

where

α = thermal diffusivity
T_x = temperature at point **x**
$\left(\frac{dT}{d\theta}\right)_x$ = slope of temperature-time curve at point **x**
T_∞ = reference temperature that does not change **(x = ∞)**
$\dot{V}$ = ablation velocity

To solve equation **(40)** all that is needed is a temperature-time curve at one point within an ablating solid. The equation was derived based on the assumption that the derivative $(dT/d\theta)_x$ is equivalent to $\dot{V}\,(dT/dx)_x$ during steady-state ablation. However, the equation is nothing more than a manipulation of the general heat conduction equation and does not include heat absorption or generation terms other than sensible heating of the solid.

To apply equation (40) to data reduction, one has only to find the slope and temperature at any given point in time and substitute these values into the equation along with the ablation velocity. By repeating the procedure for different times, the diffusivity at different temperatures is obtained. The thermal diffusivity values thus obtained are multiplied by the density and specific heat, corresponding to the temperature level, to obtain the thermal conductivity.

In order to correct equation **(40)** far the heat absorbed by the transpiring gases another term was added to the general equation **of** heat conduction for the char layer as shown below

$$\rho_s c_s \frac{\partial T}{\partial \theta} = K \frac{\partial^2 T}{\partial x^2} - (\rho_v - \rho_s)\, C_g \dot{V} \frac{\partial T}{\partial x} \qquad (41)$$

where

ρ_s = density of solid at temperature T
ρ_c = density of char
c_s = heat capacity of solid
ρ_v = density of virgin material
K = thermal conductivity
C_g = specific heat of gaseous products of pyrolysis at temperature T

The term $(\rho_v - \rho_s) V$ in equation (41) gives the mass velocity of the pyrolysis gases. It has been assumed for this derivation that the temperature of the gases equals that of the char at any point.

Equation (41) was solved using the assumption of steady-state ablation to obtain

$$K = \left[\rho_c c_s + (\rho_v - \rho_c) C_g\right] \frac{\dot{V}^2 (T_x - T_\infty)}{(dT/d\theta)} \qquad (42)$$

Equation (42) is the corrected equation which includes a term for the heat absorption by the gases. The heat absorbed by pyrolysis has been neglected.

Equation (40) was used to reduce the thermal conductivity of the virgin material and of the char from the temperature-time data. Then, equation (42) was applied to that portion of the data above the pyrolysis temperature to ascertain what effect the neglect of transpiration cooling had on the reduced thermal conductivity values and also to check the agreement between the calculation and the values measured in a steady-state apparatus.

Unfortunately, the transient temperature measurements which have been made on phenolic-nylon provide a temperature-time curve to only 1500°K. Thus, the curve had to be extrapolated to obtain slopes at the highe'r temperatures. The extrapolation was performed as follows: The thickness of the material from the pyrolysis interface to the char surface during steady-state ablation was determined from data presented in the reports from which the temperature-time data were obtained.

Then, the time required for the pyrolysis interface to reach the surface was calculated by dividing the thickness by the ablation velocity. This time was added to the time at which the temperature was about 750°K (approximate temperature at start of pyrolysis). Then, the face temperature was plotted at that time. The temperature-time curve was then smoothly extrapolated from the last thermocouple reading to the face temperature.

The instantaneous density of the char which was required in the calculations was calculated as follows: The material was assumed to have a density of 0.65 gm/cm^3 at 800°K and 0.30 gm/cm^3 at 1650°K. The density was assumed to vary linearly with temperature. Thus, for a temperature between 800°K and 1650°K the density was determined from a linear interpolation between the two reference values.

Analysis and Discussion of Results

Chemical Analysis. - The results of the chemical analyses were presented in table 22. As expected, carbon was the predominant species in the char with small amounts of hydrogen and nitrogen. The hydrogen content in the arc-jet chars increased from the hot to the cold surface. Likewise, there was an increase in nitrogen content from the hot to the cold surface of the arc-jet chars. This trend is in agreement with the increases noted for the furnace chars as the charring temperature was lowered. The presence of these elements is probably related to incomplete degradation of the material at lower temperatures.

The percentages of unidentified elements should represent the amounts of oxygen left in the char. These percentages were significant in most cases. Without a detailed investigation of the preferrential bonding of oxygen to nitrogen and hydrogen and the molecule which might result from such bonding we cannot make a judgement as to why the percentages of oxygen are high.

Traces of magnesium, silicon, calcium and manganese were found in the chars. These impurities accounted for less than 1 percent by weight. It is not known whether these elements can affect properties in these small amounts.

X-ray Diffraction. - The results of the X-ray diffraction studies which were presented in table 23 and in figure 133 indicate the degree to which the material is ordered. None of the (002) lattice spacings

for the arc-jet and slow furnace chars corresponded to the value of 3.37 Å which corresponds to the ASTM card value for synthetic graphite. The lattice spacings reached a minimum of 3.44 Å at the hot faces of the arc-jet char and for the furnace char. See Appendix C for a discussion of the rapid furnace chars. Note in table 23 that the two evaluations on the furnace char show a decreasing lattice spacing with increasing heat treatment temperature. These results can be roughly interpreted to give some idea of the temperature gradient across the arc-jet chars. Since the surface temperature of the arc-jet char did not exceed 2500°K, it appears that the lattice spacing did not change between this temperature and 3033°K. Based on this assumption, it appears that the rear of the arc-jet char prepared at 2.27 MW/m^2 reached about 2000°K for a face temperature of perhaps 2500°K. Thus, the mean charring temperature was probably about 2250°K. It appears that the rear surface of the arc-jet char prepared at 1.13 MW/m^2 was well below 2000°K, perhaps as low as 1500°K. Assuming that the face temperature of the char was 2200°K, the mean temperature was probably about 1850°K.

Several general observations can be made regarding the X-ray diffraction data presented in table 23 for the arc-jet and furnace chars.

1. The only specimens which came near representing a well-crystallized graphite were those prepared by heating rapidly to 3033°K in the furnace (see Appendix C).
2. In each case, the specimen or that portion of the specimen which was hotter yields data more closely approaching those of graphite.
3. With regard to the 200 series (charred at heat flux density of 2.27 MW/m^2), one would assume that the first three layers removed are equivalent with respect to X-ray analysis. That is, the lattice measurements are changing as the successive layers are examined starting with the cold face. However, the change is negligible from layer three to the hot face.
4. An unexplained peak occurred at 4.14 Å on the patterns for 200-5 and 200-6. It is believed that this peak could be due to an impurity in contact with this particular specimen or due to a reaction product yielded from the removal of wax from the specimen. Wax was used to mount the chars for sectioning. It would seem.that the peak is not inherent in the material, since it did not appear on the patterns for the 100 series.
5. The 100 series char sample which was fartherest removed from the heated surface was also probably crystallized (ordered) to some degree from thermal effects. However, there is no direct experimental evidence since the virgin material was not examined to determine its characteristic lattice spacings.

6. For a comparison of the values for the 1922°K and 3033°K furnace chars with those of the 200 and 100 series arc-jet chars, the following is noted. The 1922°K and 3033°K chars gave patterns which were similar to the 100-3 and 100-2 specimens, respectively. The 3033°K char pattern was also similar to those for the 200-4 and 200-5 specimens. To compare the effect of the two different thermal fluxes used, observe the similarity between specimens 100-1 or 100-2 and 200-5. A rough conclusion from this observation is that the hot face of the 1.13 MW/m² arc-jet specimen received a thermal treatment approximately equal to that at a point 6.3 mm from the hot face of the 2.27 MW/m² arc-jet specimen. Since so many factors may influence the degree of perfection of an X-ray pattern for this type of material, one can only very loosely say that a specific layer of material from a given thermal gradient reached the same temperature as that of a specific char. One can say that the structure of a specific char and its respective material layer from the thermal gradient are equivalent with respect to X-ray diffraction analysis.

In summary, the material did become somewhat crystalline as a result of the thermal exposure. Thus, the resultant char is not a purely amorphous carbon. However, even though crystalline, the arc-jet and slow furnace chars did not reach the physical state of a well ordered graphite. Further, note in figure 133 that while both arc-jet chars achieved the same lattice spacing near the hot surface, the amount of material converted to the crystalline state was less for the phenolic-nylon charred in the arc-jet at 1.13 MW/m². This is evidenced by the fact that the relative intensity was less for this material. This behavior might be explained as resulting from either a lower exposure temperature or a shorter time at the peak temperature.

The X-ray diffraction results for the arc jet and slow furnace chars are significant in that (1) the lattice spacings do not conform to those of graphite, and (2) heating to lower temperatures (2500°K) rapidly (arc-jet char) produced the same lattice spacing as heating to 3033°K and holding at temperature. Further, the intensity of the arc-jet pattern was greater than that of the char soaked at 3033°K. Hence, the structure of the arc-jet char reached a certain level of perfection in the shorter time at a given temperature and was not affected much by longer times at temperature within these ranges. For shorter times and more rapid heating to higher temperature, the trend was reversed and the material exhibited a more graphite-like behavior.

The phenolic-nylon consists of a phenol formaldehyde binder with a nylon filler. During the charring process, the phenol formaldehyde is converted to carbon and the nylon is essentially depleted. Thus, the resultant carbonaceous material is strongly related to the behavior of a char made from the phenolic. Degraded phenol formaldehyde is classed as a "hard" carbon. This class of materials is characterized as nonmelting and "nongraphitizing." Kobayashi, Sugawara, Toyoda, and Honda[20] reported measurements of the lattice spacings of this material as a function of heat treatment temperature. Their results were similar to those for the phenolic-nylon charred in the arc-jet and in the furnace at a low heating rate in that they reported a lattice spacing of 3.44 Å for a heat treatment temperature of 3273°K. Also, their measurements showed a continuous decrease in lattice spacing as the heat treatment temperature was increased. Dollimore and Heal[21] state that Kipling made the point that, if a graphitizing carbon is to be formed, fusion of the polymer must take place, so that the polycyclic aromatic structures formed at lower temperatures readily orient to form graphite. Evidently, if this fusion does not take place, the structure will not orient to reach the lattice order of graphite.

The X-ray diffraction measurements on the phenolic-nylon are in accord with the literature. This indicates that the phenolic-nylon charred in the arc-jet and in the furnace at a low heating rate is essentially carbon-like. The properties of such a material related to those of graphite will be discussed in another section.

Density, Porosity, and Permeability. - There was a significant variation in bulk density between the chars prepared in the furnace at low heating rates and the chars prepared in the arc-jet and in the furnace at high heating rates. The densities of the slow furnace chars varied from 0.29 to 0.385 gm/cm³ with an average of about 0.34 gm/cm³ for charring temperatures above 1000°K. The arc-jet chars had average bulk densities of 0.25 gm/cm³ and 0.30 gm/cm³ for charring heat flux densities of 1.13 MW/m² and 2.27 MW/m², respectively. The bulk density of the char prepared in the furnace at a high heating rate was also low at about 0.23 gm/cm³. The differences between the bulk densities of the chars can be explained on the basis of a shrinkage effect. The linear shrinkage of the phenolic-nylon as it passes through the 800-1500°K temperature range slowly is about 25 percent. If this temperature range is passed through quickly, no shrinkage is observed. The arc-jet chars and the rapid furnace char passed through this region rapidly and did not shrink appreciably. Thus, even though the weight loss of the rapid chars was less, the retention of the original volume resulted in a lower bulk density. Further, the cracks in the arc-jet chars occupy a fairly significant volume which also decreases the bulk density.

The true densities of the chars ranged from 1.435 gm/cm^3 for the char prepared at 812°K to 1.78 gm/cm^3 for the char prepared by heating rapidly in the furnace to 3033°K (see table 24). The chars prepared at high heating rates had the highest true density values. The values shown in table 24 were used for all of the porosity calculations and hence should be used for extrapolation purpose. The values for the arc-jet chars and rapid furnace chars should be representative of flight chars,

True density measurements on chars of phenolic-carbon and phenolic-graphite composites were made by Clayton, et al.[24] The true density values ranged from 1.48 to 2.26 gm/cm^3. The lower values are in agreement with our measurements on arc-jet chars and furnace chars prepared at low heating rates. The surprising feature of the results on the phenolic-graphite and phenolic-carbon composites is that the true density was generally lowest for the char which had the highest temperature exposure. The true density of the phvnolic-nylon char either remained about constant with increasing heat treatment temperature or exhibited an increase.

The porosity of the chars is a function of the bulk density and the true density ($P = 1 - \rho_b/\rho_t$). The porosities of the slow furnace chars ranged from 74 percent to 78 percent as compared to porosities of about 82 and 86 percent forthe arc-jet and rapid furnace chars, respectively. These porosities reflect the differences in bulk and true densities of the chars prepared at low heating rates and at rapid heating rates.

The porosity of the materials consists of both open and closed porosity. These two porosities were separable only for the char prepared in the arc-jet at 2.27 MW/m^2. The open porosity of this char was 64 percent and the closed porosity was 16 percent. The remainder of the chars evaluated (1.13 MW/m^2 arc-jet char and slow furnace chars) had closed porosities exceeding 16 percent. This was evidenced by the fact that they would not absorb the liquid to a degree sufficient to cause complete submersion. These results are interesting from the standpoint that carbon-like materials are usually characterized by closed microporosity. However, this effect seems to persist to some degree in the pore size range of the chars.

One would expect that materials of 74 to 86 percent porosity would offer little resistance to gas flow. This effect was noted for the arc-jet char prepared at 2.27 MW/m^2 and for the char prepared by heating rapidly in the furnace. However, the chars prepared in the furnace at low heating rates exhibited permeability coefficients 6 to 8 orders of magnitude different than those of the other chars and thus offered a considerably larger resistance to flow. Most of the difference in the permeabilities of the char can be attributed to the cracks in the chars prepared at rapid

heating rates which were parallel to the gas flow. However, the chars prepared at the rapid heating rates may also have had more connected open porosity than the chars prepared at low heating rates which increased the permeability. This possibility is of significance in understanding the gas flows through the char during active ablation.

Relation to Properties of Carbon to Graphite Transformation. - Soft or "graphitizing" carbons usually exhibit a continual change in properties with increasing temperature. At a sufficiently high heat treatment temperature the graphitization process goes to completion and the resulting product has the properties of graphite. These graphites are characterized as being polycrystalline with large crystal sizes. Carbon-like materials also exhibit a change in structure and properties with increasing heat treatment temperature and it has been reported that the changes occur rapidly at any given temperature level. However, these materials differ from soft carbons in that the changes in the properties toward those of graphite with increasing heat treatment temperature are small for temperatures up to **3033°K.** At higher temperatures, the carbon-like materials may exhibit a drastic change to a graphitic structure.

Models have been proposed for the structure of the carbon-like material. [22, 23] Generally, these carbons are thought to consist of small mosaics (more or less flat platelets of aromatic molecules) interpersed with a disorganized phase. The mosaics formed in the carbun-like materials at low temperature from the aromatic molecules do not have the alignment of those of graphitizing carbons which tend to align to each other. It is this alignment feature of the mosaics of "soft" carbons which is thought to be favorable to crystallite growth and ordering during heat treatment at higher temperatures. The poor alignment of the crystallites in carbon-like materials appears not to be favorable to growth andordering. An interlayer spacing (002) of **3.44** Å is the dividing line between random orientation of carbon basal planes (turbostractic structure) and the advent of some three-dimensional ordering. [23]

Glass-like carbon is a typical carbon-like material, though perhaps not identical to the chars. However, for purposes of comparison we elected to compare the properties of glass-like carbon to those of ATJ graphite to indicate what monitors show the trend in changes from carbon to graphite and to ascertain how the properties of the char change from those of carbon to those of graphite. The properties of the materials are compared in figure 167. The properties of the carbon-like materials do not progress smoothly, in terms of "degree of graphitization," from those

of carbon to those of graphite as a function of heat treatment temperature. Rather, they change to a certain point and then remained fixed at different values than those of graphite. Therefore the expected trends with heat treatment temperature, given in figure 167, have been shown as a smooth curve up to a point and then a discontinuity has been drawn to show the change that would be required for the material to become graphitic. Thus, a material can be classed as carbon-like or graphite-like depending upon which side of the discontinuity it falls.

There are several property monitors which can be used to study the ability of the char to become graphite-like. These property monitors, along with the measured and reduced property values, are presented in figure 167. Shown in the lower portion of the figure is the lattice spacing. The lattice spacings of the heat treated glass-like carbon ranges from 3.43 to 3.51 Å, exhibiting a decrease with increasing heat treatment temperature. The lattice spacings of the arc-jet and slow furnace chars exhibited a similar decrease through the spacings were greater at the low temperatures, However, there was a convergence to 3.44 Å for all of the chars. This indicates that although there was some ordering of the structure with increasing heat treatment temperature, the structure probably did not become sufficiently ordered three-dimensionally to be considered graphite-like.

Clayton, et al,[24] recently made X-ray diffraction measurements on phenolic-carbon (MX4926) and phenolic-graphite (FM5014) composites. For both the virgin material and the char, (002) lattice spacings of 3.37 Å were observed. The intensity of the diffraction patterns increased as a function of precharring temperature. The char of phenolic-nylon prepared in the arc-jet and in the furnace at low heating rates did not exhibit the 3.37 Å spacing characteristic of graphite. The fact that the phenolic-carbon and phenolic-graphite had a spacing characteristic of graphite is most likely attributed to the carbon and graphite in the material, rather than "graphitization" of the phenolic.

Density is another monitor of the carbon to graphite transformation. True density would be the best monitor by which to compare the materials. However, true density values were not found for carbon. Thus, apparent densities have been presented in figure 167 for the glass-like carbon. The true density of carbon is generally believed to range from 1.8 to 2.1 gm/cm^3.[25] The true density values for the chars have been presented for comparison. The values for the chars may be low because of the inclusion of some fraction of micropores in the volume measurement. The slow furnace chars exhibited an increase in true density with increase in heat

treatment temperature. The true densities of the arc-jet chars were higher than those of the slow furnace chars. The slow furnace chars and arc-jet chars exhibited carbon-like density values since they were in general agreement with the apparent density values for glass-like carbon. The rapid furnace char exhibited a significant increase in true density and should probably be considered more graphite-like even though the value obtained was considerably below the true density of ATJ graphite. Thus, it appears that rapid heatingcan result in a more graphite-like material but only if the temperature level is high enough, perhaps about 2000°K.

Electrical resistivity at low temperatures is another monitor of the carbon to graphite transformation. Typical values for carbon and graphite are presented in figure 167. Note that the value of resistivity obtained for the char prepared at low heating rates falls in with the values for glass-like carbon.

Carbons and graphites exhibit vastly different thermal conductivities at low temperatures. The relative values of the two at high temperatures is less certain because the mechanisms of heat conduction are not totally understood. The thermal conductivity values for the chars are compared with the values for glass-like carbon and graphite in figure 167. The thermal conductivity values for the chars are the values of the matrix thermal conductivity at 500°K which were reduced by applying equation (23) to the measured values. Note that the slow furnace chars exhibited an increase in thermal conductivity with heat treatment temperature and had about the same values as the glass-like carbon for a heat treatment temperature of 3033°K. Likewise, the arc-jet chars had a value for thermal conductivity which agreed rather well with that for glass-like carbon. No significant graphite-like trend was achieved by the arc-jet or slow furnace chars. The furnace chars prepared by heating rapidly to 3033°K took a significant jump in thermal conductivity toward the value for ATJ graphite. Thus, again the effect of rapid heating to high temperatures seemed to drive the char toward a more graphite-like structure.

The final property correlated in figure 167 was the sonic velocity. Graphite exhibits a higher sonic velocity than glass-like carbon. However the difference in sonic velocity between the two materials is not extremely large. The comparison of the sonic velocities of the chars with those of glass-like carbon and graphite indicated that the chars were more carbon-like than graphite-like.

In summary, all of the monitors indicated that the "degree of graphitization" of the slow furnace chars and arc-jet chars was low in terms of the property change from carbon to graphite (for temperatures to 3033°K). However, the rapid furnace char prepared in the furnace at a high heating rate exhibited a significant "degree of graphitization" since its properties moved strongly toward those of graphite.

Thermal Conductivity of Laboratory Chars. - In this section the effects of time and temperature on the thermal conductivity of the char will be discussed. Also, the results of the reductions of the intrinsic properties of the char from the effective thermal conductivity measurements will be discussed in detail.

The measurements showed that time at temperature did not significantly alter the thermal conductivity of the chars prepared at low heating rates at either 1366°K or 3033°K. The thermal conductivities of specimens TC17 and 5R were identical at 800°K (see figure 146) even though specimen TC17 had been held at temperature for 30 minutes and specimen 5R was only briefly exposed to that temperature. Likewise, the thermal conductivity measurements on specimens prepared at 3033°K indicated no change in thermal conductivity at low or high temperatures for soak times ranging from 30 minutes to 5 hours (see figures 149 and 150). There was a considerable difference between the thermal conductivites of the two specimens charred at 3033°K for 30 minutes (see figure 149), however, the values bracketed the values for specimen 2F5000-2 which had been held at 3033°K for two hours during preparation, exposed to 3033°K during the first thermal conductivity evaluation, and then evaluated again to obtain the values given in figure 149. Thus, time at temperature seemed to have had a minimal affect upon the chars prepared at low heating rates.

There is another point concerning the effect of precharring temperature level on the thermal conductivity of the char. The thermal conductivity values are not completely "locked in" by precharring to a low temperature level and then cooling the specimen. For example, specimen 1F5000-3 was heated continuously to 3033°K; whereas, specimen 4F5000-5 was precharred to 1366°K prior to charring to 3033°K (see figure 125), yet both chars had the same values for thermal conductivity (see figure 150). Thus, the precharring at 1366°K did not "lock in" the thermal conductivity at the value for a 1366°K slow char. This point should not be confused with the point that charring slowly can "lock in" the thermal conductivity values and result in a more carbon-like material, whereas a graphite-like material results from a rapid exposure to high temperatures. Thus it is a matter of degree, but does seem separable.

For the chars prepared in the furnace at a rapid heating rate to 3033°K the thermal conductivity was significantly increased (see figure 151) above that for a slow furnace char. The cold wall heat flux to the rapid char specimens was about 4.9 MW/m^2 (more than two times as high as for the arc-jet chars) and we estimate that it took about 109 seconds to completely degrade the specimen and bring it to a temperature of 3033°K. Thus, charring to a temperature of 3033°K in a short time resulted in a char which was apparently more graphite-like since the thermal conductivity at low temperatures was increased from 91 to 270 percent above that for the char prepared to 3033°K in the furnace at a low heating rate. Also, the character of the thermal conductivity curve was altered and the thermal conductivity of the rapid furnace char decreased with temperature is is typical for graphite. The effects of rapid charring to different temperature levels has not been fully investigated. However, the arc-jet chars provide some information about other temperature levels. The major uncertainty in analyzing the arc-jet data is that the precharring temperature is not well defined. Data from Reference 26 for an arc-jet char prepared at a heat flux density of 1.58 MW/m^2 are also presented in figure 151. This specimen did not exhibit graphite-like behavior and showed a higher conductivity during cooldown which indicated that the thermal conductivity of the solid was raised by exposure to temperatures above the formation temperature. Hence, it appears that the carbon to graphite transformation is a function of both heating rate and temperature level.

The charring temperature level had a significant effect on the thermal conductivity of the chars prepared at low heating rates. The thermal conductivities of the chars prepared at different temperature levels are presented in figure 152. The thermal conductivity at 500°K increased with increasing heat treatment temperature.

The values of the matrix thermal conductivity at 500°K for the slow and rapid furnace chars and the arc-jet chars are presented in figure 168. These values were reduced from the measured thermal conductivity values by solving equation (23) for K_m. The slow furnace chars exhibited an increase in K_m with increasing heat treatment temperature. The arc-jet chars also exhibited an increase and had slightly higher values than the slow furnace chars. The chars prepared in the furnace at rapid heating rates to 3033°K exhibited a drastic change in matrix conductivity, increasing from 12.5 W/m-°K for the slow char to 40-77 W/m-°K for the rapid chars.

The values reduced for the matrix thermal conductivity at 500°K are valid because radiation was not a factor. However, the reduction of the matrix thermal conductivity at higher temperatures is affected by the

assumptions used in making the calculations. The first approach was to assume that the cell walls of the char were not transparent to thermal radiation and calculate the matrix conductivity by using equation **(23)** without the last term. The results of the calculations made under this assumption are presented in figure **169.** The matrix thermal conductivity of the **3033°K** rapid furnace char decreased with increasing temperature in the manner normally associated with graphite (see ATJ graphite reference curve on figure). The arc-jet chars and slow furnace chars exhibited a different behavior in that they showed an increase with increasing temperature. Note that some data for cellulose carbon pipe (Reference **27)** are also presented in the figure and show an increase with increasing temperature. The cellulose carbon pipe had an apparent density of about 1.5 gm/cm^3 which is near the value for the true density of the slow furnace chars. The heat treatment of the material is not known.

The "boxing" value of the thermal conductivity of the matrix when neglecting transparency effects is also given in figure **169.** This curve was developed by connecting the values of matrix conductivity which the chars had at the precharring temperature level.

The boxing value of the thermal conductivity of the matrix of the slow chars was also determined under the assumption that the material could transmit radiation. The percent transmission through the char, τ, as a function of temperature was determined from the data on the 3033°K slow furnace char by assuming that the matrix thermal conductivity remained constant at the value determined from the **500°K** data. Then using these values of τ the thermal conductivity of the matrix at the different precharring temperature levels was determined by applying equation **(23)** to the boxing values of effective thermal conductivity given in figure **152.** The results of the data reductions are presented in figure **170.**

The values of the thermal conductivity of the matrix as a function of temperature were determined under the assumption of an opaque material with radiation across pore walls only and under the assumption of transparency for the **3033°K** slow furnace char, which is a thermally stable material. Under the assumption of transparency the matrix conductivity was assumed to remain constant at the value which it had at **500°K** of **12.7** W/m-°K. The results obtained under these two assumptions are presented in figure **170.** Data from Reference 28 for a carbon prepared from phenol formaldehyde filler with a phenol benzaldehyde binder and heat treated at **3373°K** are also presented in figure **166.** This material is similar to the phenolic-nylon char except that the binder is different.

Note that whereas the values of matrix conductivity reduced from our measurements corresponded to a true density of 1.4 - 1.5 gm/cm³, the values for the reference material were measured on a sample with a bulk density of 1.36 gm/cm³. There is general agreement in the level of thermal conductivity and if it is assumed that the char is transparent, the values nearly coincide. However, under the assumption that the char is not transparent, the matrix thermal conductivity of the 3033°K slow furnace char must increase with temperature, which is in opposition to the constant thermal conductivity of the phenol formaldehyde-phenol benzaldehyde. This raises the question of whether or not an increasing thermal conductivity with temperature is reasonable for a carbon-like material.

Generally, it is believed that the thermal conductivity of dense carbons and graphites is constant or decreases with temperature because the phonon-phonon interactions reduce the lattice component of conductivity as fast or faster than the electronic component increases. However, the increase in matrix thermal conductivity with temperature, for a stable but carbon-like char, could be rationalized as follows: In graphite, at temperatures below about 2000°K, heat is conducted primarily by lattice vibrations (phonons). This is evidenced by the fact that the Lorentz number of graphiteis two hundred to several hundred times as high as that of a metallic conductor.[29] Mason and Knibbs[30] found that for a given graphite, the thermal conductivity varies inversely with electrical resistivity when either the orientation or the crystallinity varies.[29] They attributed this correlation to the fact that the flow of both heat and electricity is restricted essentially to the crystal layer planes and that in both cases, the flow is controlled by scattering at crystal boundaries.[29] The lattice of the carbon-like material does not have the perfection of the graphite lattice and the average size of the crystallite is much smaller. These factors would be expected to reduce both the lattice conduction, which is the larger, and the electronic conduction of the carbon below the values for graphite at temperatures in the vicinity of 500-1000°K. The electrical resistivity measurements bear out the suppression of the electronic component (see figure 154). As the temperature is raised, the phonon contribution to the heat flow is reduced by lattice interactions and the electronic contribution increases. In graphites this causes a significant decrease in thermal conductivity because the phonon transport predominates. However, the phonon transport in the carbon-like material is initially at a low level and the decrease in phonon transport with increasing temperature does not have as much effect on the thermal conductivity of this material as it does on a graphite. It must be remembered that the electronic conduction in the carbon is also retarded. As the temperature increases, the electronic conduction in graphite increases relative

to the phonon conduction as evidenced by the fact that the Lorentz number decreases significantly with temperature and approaches the theoretical value. This decrease in Lorentz number also occurs for the chars. Now, the lattice effects (or defects) within the carbon manifested themselves by increasing the electrical resistively at 500°K to a value well above that of graphite and by decreasing the thermal conductivity of the matrix at 500°K to a value well below that of graphite. From this it seems fair to assume that the electrical resistivity measurements reflect the suppression of both of these components of thermal conduction.

Based on this line of reasoning, it would follow that the difference in electrical resistivity values for carbons and graphites reflect the differences in thermal conductivity. Since the values of electrical resistivity for the carbon matrix and those for graphite tend to converge at higher temperatures (see figure 154) it would appear reasonable to conclude that the thermal conductivity values also tend to converge. Since the carbon has a much lower conductivity at 500°K than the graphite, the convergence would result in an increase in thermal conductivity with temperature. Further, the electrical resistivity of the phenolic-nylon char decreases faster as a function of temperature thah the electrical resistivity of the phenol formaldehyde-phenol benzaldehyde (see figure 170). This indicates that the electronic contribution in the char could be increasing at a faster rate and would help to explain the differences between the two materials.

Thermal conductivity measurements were made on powders of ATJ graphite and char prepared at 3033°K. The thermal conductivity of the solid ATJ graphite was known as a function of temperature. It was hoped that the analyses of Deissler and Boegli[16] and Yagi and Kunii[18] could be correlated with the data on the ATJ powder well enough for the thermal conductivity of the char solid to be reduced from the effective thermal conductivity measurements on its powder. The results were unsatisfactory as the data on the ATJ powder could not be correlated with the analysis to the degree of precision required to allow a reduction of the solid conductivity of the char. Unfortunately, the thermal conductivity of the gas within the powder has more effect on the effective thermal conductivity than the thermal conductivity of the solid. Hence, real precision in the measurements and a model which exactly correlates the data is required in order to determine the solid conductivity from such measurements. Within the scope of this program these problems could not be resolved.

The reasonableness of an increasing matrix thermal conductivity with temperature for a stable slow furnace char has been discussed and to some extent rationalized. Whether or not the material does behave in this manner

cannot be determined with certainty. However, the calculations of the matrix thermal conductivity under the assumption of opacity (with radiation between pore walls) do show what demands are placed on the behavior of the material if it satisfies the assumptions. If the material is transparent to radiation, the behavior required of the matrix can be easily rationalized. Next we will discuss what demands the assumption of transparency places on the optical properties of the char.

As was mentioned previously, a calculation of the radiant conductivity through the openings in the char was made. For this calculation it was assumed that the char consisted of holes which went from one side of the char to the other. The holes were assumed to be 0.0127 cm in diameter, which was larger than the average pore size measured under the microscope. Using a reasonable heat transfer calculation it was determined that the effective radiant thermal conductivity at 3000°K was 0.74 W/m-°K or about 5 times that given by the third term in equation (23). However, the value calculated was about one third of the amount required to explain the increase in thermal conductivity with temperature of the furnace char prepared by slow heating to 3033°K, assuming that the matrix conductivity remained constant. Further, the char is not as open to radiation as the calculations assumed. So it was concluded that the third term in equation (23) was a reasonable approximation to the radiation between pore walls and through openings within the char. This conclusion was substantiated by transmittance measurements with the sample at room temperature. From measurements on char ground to different thicknesses, a plot of fraction transmittance versus thickness was developed. Using the analysis of Larkin and Churchill [15] which was presented earlier (equation 32), the parameters M and N were determined. From the limited data obtained, the values of M and N could not be determined exactly. However, the value of M had to be 276 cm^{-1} or greater to satisfy the data, As higher values of M were assumed the value of N required to correlate the data increased and N could not be determined with certainty with the data available. Therefore, calculations of the radiant conductivity were made from the analyses of Larkin and Churchill [15] based on the following:

$M = 276\ cm^{-1}$ and $M \gg N$ (absorption predominates)

$M = 314\ cm^{-1}$, $N = 296\ cm^{-1}$; $M \cong N$

Both calculations gave about the same value for the radiant conductivity as that given by the third term in equation (23). Further, the char was highly absorbing at room temperature because the measured transmittance agreed closely with the area fraction of holes through the char.

From the analyses it was concluded that radiation through the openings in the material did not explain the high temperature behavior of the thermal conductivity of the char. If radiation is significant it must be because the char becomes transparent to thermal radiation at the higher temperatures. The radiant transmission required to explain the behavior of the material was calculated as follows: Equation (23) was used for the calculations. It was assumed that the solid conduction component remained constant at the 500°K value. All other terms in equation (23) except the overall fraction transmittance were known. Using these values and the measured conductivity, the fraction transmittance was calculated as a function of temperature.

The results of the calculations of the required transmittance through a stable 3033°K slow furnace char and an arc-jet char are presented in figure 171. More transmittance was required for the arc-jet char because some additional increase in solid conductivity resulted from the exposure to 3033°K during the measurement which meant that too low a solid conduction component was used (see figure 151). The approximate transmission required at temperatures above 2500°K is 8 percent. The contribution to the overall thermal conductivity, for the sample thickness used in the measurements, is given in the upper portion of figure 175.

The percent transmittance required at 3000°K through various thicknesses of char to give the required value of 8 percent, for a thickness of 0.425 cm, is given in figure 172. The equation used for the calculations was $\tau = f^x$ (where f = fraction transmittance of one layer and x = number of layers). Note that a small thickness of char must transmit significant amounts of radiation. Also shown in the figure is the result of the calculation of the percent transmittance required through each pore wall, about 96 percent. Thus, the char must be almost nonabsorbing at 3000°K if radiation transport is to account for the increase in thermal conductivity.

The absorption coefficient required by the material was calculated from equatiod (26) and the results are presented in figure 173. The values used for the index of refraction are very uncertain as they were taken from calculations of the index of refraction of a single graphite crystal and temperature effects on this property were not given.[31] A typical value for the absorption coefficient of a graphite single crystal at an unspecified temperature was calculated from values of the extinction coefficient given in Reference 31 as 386,000 cm^{-1}. No data were found for the absorption coefficient of carbon as a function of temperature. Hence, we cannot interpret the calculated values as to their reasonableness for the carbon at high temperatures.

It is important to note that equation (26) was based upon the simultaneous absorption and reradiation of the bulk material whereas the transmittance calculations were based on the assumption of direct transmission from the source. The absorption coefficient is derived from the defining equation

$$I/I_o = e^{-Bx} \qquad (43)$$

where

I = residual radiant intensity of source radiation at x
I_o = intensity of monochromatic radiation entering a transparent body at right angles to its surface
B = absorption coefficient
x = distance into the body

If the value obtained for the absorption coefficient at 3000°K ($B = 100\ cm^{-1}$) is used in equation (43) with a distance of 0.425 cm, the percent transmission obtained is negligible. Thus, it appears that the absorption coefficient can be higher than that calculated from direct transmission, if the body absorbs and reradiates simultaneously, and still provide the required radiant transport.

Clayton, et al,[24] of the Boeing Company, recently published a report on some studies which had similar objectives as this program only on reinforced materials. Namely, they are also attempting to extrapolate thermal conductivity data obtained in the laboratory to flight conditions. The materials which they studied were phenolic-carbon and phenolic-graphite laminates. These materials are significantly different than the phenolic-nylon studied in this program. However, there are from areas common to both programs and we believe that some discussion and comparison of the findings of the two programs may enhance an understanding of all of the materials.

The effects of time and temperature on the thermal conductivity of the chars is one area in which some correlation of the two programs might be expected. A comparison is not very direct since the materials which Clayton, et al, studied were made up of several constituents, all of which probably behaved differently to a given set of exposure conditions, and were highly anisotropic. Thus, the effect of environmental conditions on the overall thermal conductivity of the solid portions of the laminates should

not be expected to give a one to one correspondence with the behavior of the phenolic-nylon chars. However, trends in the behavior of the matrix (solid) thermal conductivities of the materials should show some correlation since all contained a resin which charred to a carbonaceous material.

Clayton, et al, presented their results in terms of the thermal conductivity of theoretically dense material. This was done by subtracting the radiation component from the effective thermal conductivity measurements and then correcting the solid conduction component for porosity. The radiation component was determined by extrapolating the data obtained at low temperatures, on a char prepared at 2480°K, to higher temperatures and then subtracting the extrapolated values from the measured values. Thus, the "dense" material values which they presented were actually the values for a dense composite which consisted of several components. Hence, the behavior of any given constituent cannot be ascertained. Nevertheless, the phenolic-carbon (MX4926) exhibited a significant increase in the thermal conductivity of the "dense" material in the with lamina direction as a function of heat treatment temperature, from about 2.9 W/m-°K at 812°K to about 15 W/m-°K at 2480°F. In the across lamina direction, the phenolic-carbon exhibited a low value for the thermal conductivity of the dense material throughout the temperature range of about 1.1 W/m-°K. The values which were presented for the thermal conductivity of the dense material of the phenolic-graphite (FM5014) were lower in both directions than the values for thephenolic-carbon in the with lamina direction and did not exhibit a significant increase with heat treatment temperature. However, the radiation component assumed for the phenolic-graphite was significantly larger than that assumed for the phenolic-carbon. If the radiation components of the phenolic-graphite is assumed to be the same as that estimated for the phenolic-carbon, the phenolic-carbon will also exhibit a significant increase in dense material conductivity as a function of heat treatment temperature. The radiation components which Clayton, et al, used were several times higher than the effective thermal conductivity of the phenolic-nylon char except for the phenolic-carbon laminates across lamina. The low values for the thermal conductivity of the phenolic-carbon laminates in the across lamina direction are probably related to the fact that Sterling R was used as the resin (phenolic) reinforcement or that pyrolytic deposition along the fibers gave a low conductivity in that direction. If the Sterling R material is like Sterling MT it probably has a low thermal conductivity and is not much affected by heat treatment within the conditions involved.

The amount of thermal radiation passing through the chars was the largest uncertainty in the data reductions of both Boeing and ourselves. If the radiation component is assumed to be small for both the phenolic laminates and the phenolic-nylon the following general trends are noted. The thermal conductivity of the dense materials exhibit a significant increase with heat treatment temperature except for the phenolic-carbon laminates in the across lamina direction. Further, the magnitudes of the values of the thermal conductivities of the dense materials for both the phenolic laminates and the phenolic-nylon are not vastly different which indicates that the resin may be the controlling factor for the phenolic laminates. If the reinforcement were controlling, one would expect that the phenolic-graphite laminates would exhibit a more graphite-like behavior. It was concluded in both programs that the thermal conductivity of the solid was more dependent on temperature than time for chars prepared at low heating rates. We also found that this was essentially true for high heating rates to temperatures below 2000°K. However, high heating rates to 3000°K were found to significantly increase the thermal conductivity of the phenolic-nylon char. The higher heating rate effects on thermal conductivity were not studied for the phenolic-carbon and phenolic-graphite laminates in that program.

Analysis of Transient Ablation Data Obtained by Other Laboratories. - Transient temperature measurements made by Tompkins[32] and Space General[33] were analyzed using equations (40) and (42), the latter-of which accounted for the heat absorbed by the pyrolysis gases. The data which were analyzed are presented in figure 174. The values used for the specific heat of the pyrolysis gases were those given by Kratsch' for 50 phenolic-50 nylon and are presented in figure 175. The properties assumed for the materials were those given in Reference 2 for low-density phenolic-nylon. The results of the data reductions are given in figures 176 and 177. Shown in figure 176 are the values obtained for the thermal conductivity of the virgin material. Note that the values obtained from Tompkins' data agree well with steady-state data given in Reference 2. The values obtained from the Space General data do not agree well. The disagreement may be due to some uncertainty in the ablation rate which was obtained during the measurements by Space General. The results of the data reductions for the degrading and char zones are presented in figure 177. Note that the reduced values of thermal conductivity are increased by a factor of 5 or more when account is taken of the pyrolysis gases. Further note that the values reduced from Tompkins data when accounting for gas effects converge to the values which were previously measured on an arc-jet char and also with "boxing" values calculated from equation (23) with the matrix conductivities given in figure 169.

The data reductions show how important an effect the gas has on determining the thermal conductivity from transient measurements. If the specific heat values used for the gases are correct, and if the assumption that the gases are at the same temperature as the char is valid, then the data reductions show that the level of the char thermal conductivity during ablation can approach the values measured in the steady-state apparatus. The values reduced from Tompkins' data and those predicted by the boxing analysis show general agreement from 1250°K onward.

Estimate of Thermal Conductivity during Active Ablation from Steady-State Measurements. - The analyses of the experimental steady-state thermal conductivity data provided knowledge about the intrinsic properties of the char. First, the solid or matrix thermal conductivity increases with temperature because of additional ordering or "graphitization" of the char. The exact amount of this increase could not be determined because possible transparency effects could not be separated from the contribution by the solid. These remarks apply to the char prepared at low heating rates. However, the analysis of the data obtained for the char prepared in the furnace at a high heating rate (4.9 MW/m^2 cold wall heat flux) indicated that rapid heating to 3000°K can result in significant graphitization of the matrix with the result that the matrix thermal conductivity can approach the values for graphite. Also, the measurements indicated that transparency was small for the rapid furnace char as the thermal conductivity curve tended to flatten at the higher temperatures as is typical for graphite. Thus, in applying the results to the active ablation situation the contribution by the solid at 3000°K is reasonably well defined. The effects of high heating rates at low temperatures is not known. However, the analysis of the data on the arc-jet chars indicated that significant graphitic behavior is not observed below 2000°K. Hence, the "boxing" values of matrix conductivity given in figure 169 are probably applicable at lower temperatures. Little can be said about the region between 2000 and 3000°K. The solid conduction component can then be approximated from 812°K to 2000°K by using equation (23) without the transparency term and the boxing values of matrix conductivity given in figure 169. The solid conduction component at 3000°K can be estimated by using equation (23) without the transparency term and the value determined for the matrix conductivity of the rapid furnace char at 3000°K. The results of these extrapolations of the data are presented in figure 179. Also shown in the figure is the solid conduction component which the char would have for the matrix conductivity values obtained by assuming transparency (figure 170). The solid conduction components were extrapolated between the values calculated at 2000°K and 3000°K.

Next, the transparency contribution was calculated from equation (25) using the values for the absorption coefficient B and the index of refraction shown in figure 173. Since the transmittance given in the last term in equation (23) was related to the thickness of the char for the small gradients achieved during the measurements, it is not directly applicable to different thicknesses unless the gradient is small. That is, it represents an overall value. For the small gradients that existed during the measurements it related to a point value. This would not be so for, say, 2500°K temperature differences across a thin layer of char. Thus, equation (25) is more of a point value function, though this is not entirely true for this equation either for large gradients. The transparency contribution is shown in figure 178. It has been sloped downward above 2250°K based on the assumption that it will probably decrease as the material becomes more graphite-like from rapid higher temperature exposure.

The cracks in the char also pass radiation. This component was estimated by using equation (24) with the reradiation shape factor given by Jakob [13] for a rectangular opening 0.0178 cm thick by 0.152 cm long (typical flight char thickness). The cracks were assumed to occupy 33 percent of the area. That component is also shown in figure 178.

The effective thermal conductivity of the char during transient ablation would be given as the sum of the components given in figure 178. The proper components to sum would depend upon whether or not the ablation gases blocked the radiation if the material were transparent. If the gases do not block this radiation, the effective thermal conductivity would be the same regardless of whether the char was transparent or not.

The components of thermal conductivity have been summed in figure 179 to give the thermal conductivity of the char during active ablation. The lower curve was developed by assuming that the char was transparent but that the ablation gases blocked the radiation. If the radiation were not blocked, the two curves would be about the same. The thermal conductivity values reduced from Tompkins' transient data are also presented in the figure.

Conclusions

The characterization studies were made in sufficient depth to allow the physical characteristics of the arc-jet chars to be related to those of the furnace chars. The major physical differences between the arc-jet and slow furnace chars are (1) the bulk density of the slow furnace chars is higher and (2) the furnace char does not contain the cracks parallel to the heat flow which invariably appear in arc-jet chars. The primary reason for these differences is that the phenolic-nylon shrinks if it is charred slowly and does not shrink if it is charred rapidly to perhaps 1500°K. Thus, the bulk densities, true densities and pore sizes measured on the arc-jet chars are expected to relate directly to chars prepared under more severe heating conditions than those of charring in the furnace.

Chars prepared at temperatures of 2000°K or below exhibit values for the thermal conductivity of the matrix which are dependent only upon the charring temperature and which are more carbon-like than graphite-like. These conclusions were confirmed by true density, sonic velocity and electrical resistivity measurements. High heating rates to 3033°K result in a char which has matrix thermal conductivity values which are more graphite-like.

The radiant heat transfer through the material could not be separated experimentally. However, an anlysis led to the conclusion that the char must become transparent at temperatures above 2000°K for radiation to become significant. The small pores within the char appear to significantly retard radiant transport by absorption and re-emission. Equation (23), which was the thermal model used to analyze the data and provide the basis for extrapolation, is considered an acceptable model for the char except for the uncertainty in the transparency radiation term.

The boxing values presented for the thermal conductivity of the matrix define the transient behavior of the solid to 2000°K with reasonable certainty. Between 2000°K and 3000°K the values are uncertain because the degree of transparency of the char is not well defined. For the particular thickness of chars investigated, the effective thermal conductivity in this temperature range would be the same regardless of whether it was attributed to radiation or solid conduction, provided that the gases evolved during charring do not absorb the radiant transmission. However, for different thicknesses of char and higher temperature gradients, the radiant transmission would probably be different from that through the furnace chars, if the char is transparent. At 3033°K,

the thermal conductivity of the matrix was reasonably well defined for conditions of rapid heating. This conclusion was drawn from the values of matrix thermal conductivity determined for the rapid furnace char prepared to 3033°K. The values were reduced under the assumption of an opaque material. The character of the curve followed that for a graphite and indicated that the assumption of opacity for a char prepared under this particular condition was probably valid. Hence, the values of the matrix thermal conductivity of the char are defined within a reasonable certainty from 500°K to 2000°K and at 3000°K. These values when used in equation (23) along with the proper values of other variables (also defined in this report) allow a reasonable prediction of the transient behavior of the thermal conductivity of the char.

The analysis of the transient temperature measurements during steady-state ablation reinforced the validity of extrapolating the steady-state boxing values of thermal conductivity to transient conditions. However, uncertainties in the validity of the assumptions made in developing the equation for the analysis of the data and in the enthalpy of the pyrolysis gases disallow using that comparison as final proof.

Two equations were presented for reducing the transient thermal conductivity from temperature measurements during active ablation. One equation included heat absorption by the pyrolysis gases and one did not. The former equation is much more realistic and gave values which were several times higher.

The studies of the thermal conductivity of the char provided some significant information about the behavior of the material and provided a better prospective of the total problem. However, there are three areas which require further study before the behavior of the char can be totally understood: (1) The question of the radiation heat transfer needs to be resolved through direct measurements of this component, (2) the effects of high heating rates to temperatures between 1500°K and 3000°K requires further study, and (3) continued work is necessary in relating the char structure to their carbon-like and graphite-like behaviors.

Recommendations

The thermal conductivity of the matrix could not be precisely defined above 2000°K. However, the study does provide fairly definite guide lines for making an engineering analysis of the probable flight performance and as to what additional effort would be required to provide a total solution to the problem. Our recommendations for further study are given below:

1. The radiation component of heat transfer through the char and through a carbon-like material such as glass-like carbon should be determined by direct experimental measurements. This would require an apparatus to measure the transmittance of char samples with the sample at elevated temperatures (between 2000 and 3000°K). New techniques seem to be required for these measurements. These measurements would resolve the uncertainty in the radiation component of heat transfer and thus allow a more precise definition of the thermal conductivity of the matrix.

2. The optical properties (index of refraction and absorption coefficient) of glass-like carbon and char should be measured as a function of temperature. Then, analyses of the radiation heat transfer which utilize these values should be correlated with the transmission measurements.

3. The effects of rapid heating rates on the thermal conductivity of the matrix should be studied in more detail. This would involve precharring to temperatures below 3000°K and then determining the thermal conductivity of the matrix from measurements of the effective thermal conductivity. The charring should be performed in a furnace so that the soak time, after complete degradation, could be controlled to provide a well-defined temperature level. This would allow a determination of the "break-point" at which the char becomes more graphite-like than carbon-like.

4. A limited study of the thermal conductivity of one of the carbon-like materials of a higher density should be made. The purpose of this would be to further define the thermal conductivity of the char solid. This study would be more direct if a dense material were used. Glass-like carbon or a char made from a high density phenol formaldehyde (no Microballoons) are two possible candidate materials for the study, This would enhance the knowledge about carbon-like materials in general.

5. Thermal conductivity measurements should be made on chars with a well-defined thermal history under conditions approaching those of flight. This would involve measuring the thermal conductivity of thin chars subjected to very steep temperature gradients. The measurements should then be analytically correlated with the boxing analysis and the results of the transmittance measurements.

6. The mechanisms of heat transfer between the pyrolysis gases and the char warrant detailed study. Future studies should be directed toward defining the enthalpy of the gaseous species and the efficiency of the heat transfer from the char to the gas. It appears that suitable experiments could be devised to study this phenomena. The results of such studies would provide a base for developing meaningful equations for reducing thermophysical property values from temperature measurements made during ablation.

7. Continued studies are required to explore the carbon-like and graphite-like behaviors of chars as monitored by such features as true density, X-ray diffraction, electrical resistivity, thermal expansion, thermal conductivity, sonic velocity and others.

Southern Research Institute
Birmingham, Alabama
February 11,1969

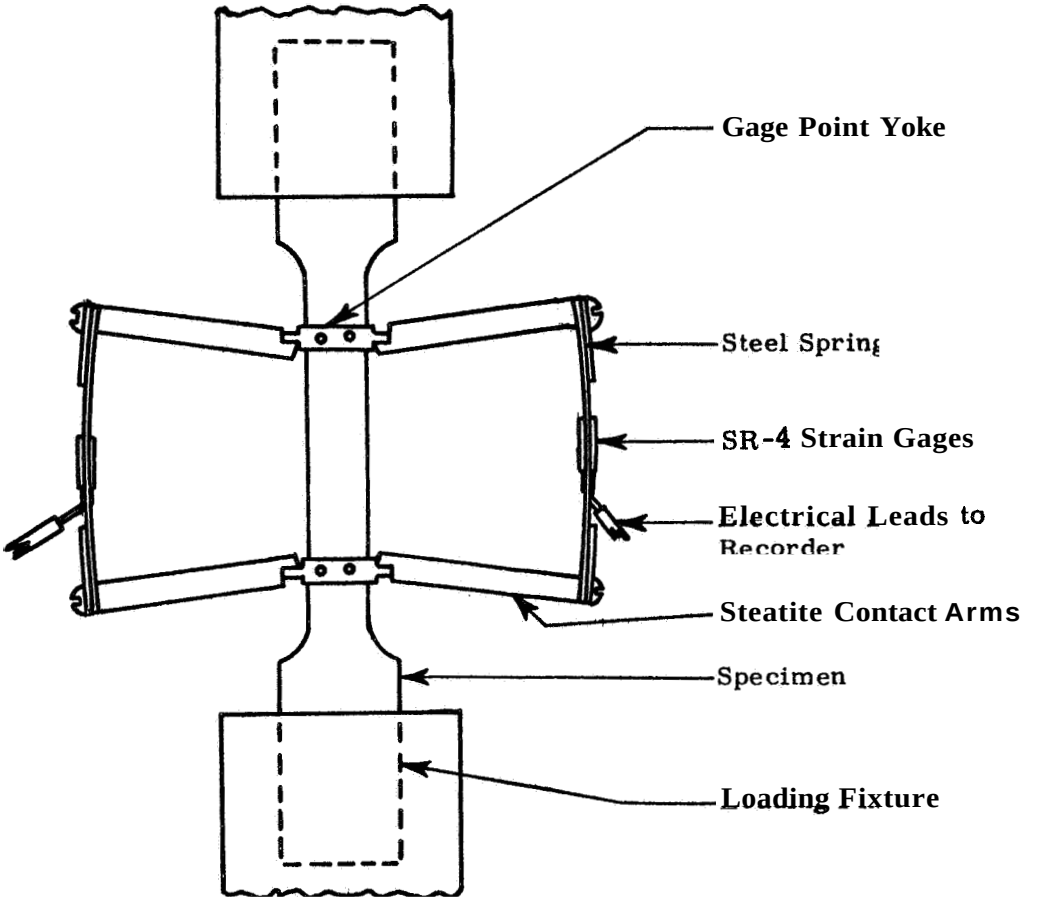

Figure 1. **"Clip-on" extensometers used to monitor axial strains**

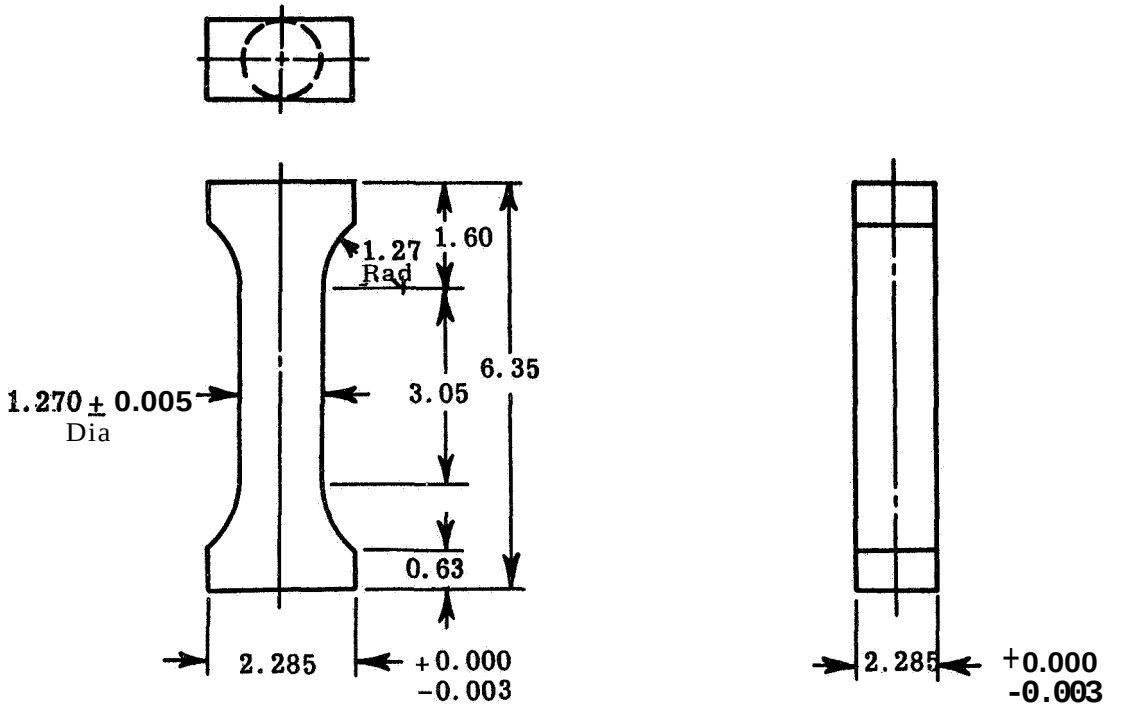

Designation -- CC1-XX-X

Notes:
1. Dimensions are in centimeters.
2. Dimensional tolerance unless noted: Decimal ~±0.013, Fraction ~± 0.080.
3. Do not undercut radii.
4. Ends to be perpendicular to $\mathbb{C}_L$ and parallel *to* each other within 0.001 cm.
5. Surface quality: Blanks ~ mill smooth and flat, reduced section **to** be determined.
6. Diameter to be true and concentric with $\mathbb{C}_L$.

Figure 2. Compressive test specimen, circular **cross** section

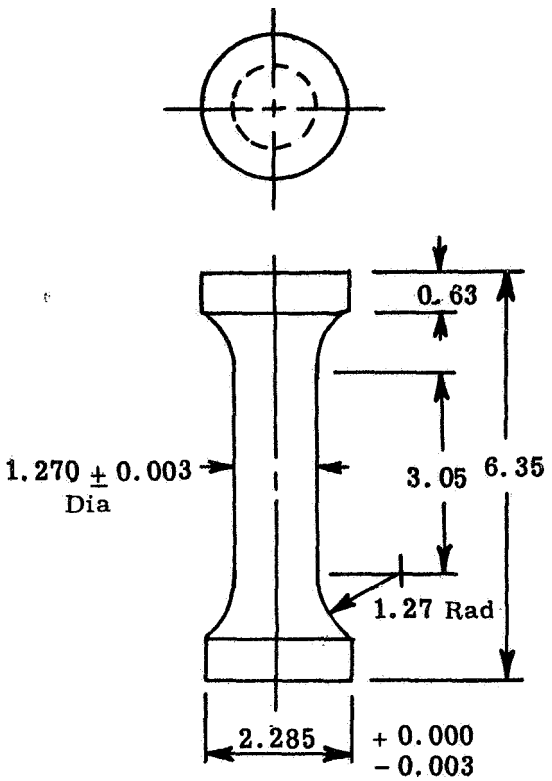

Designation -- CD-XX-X

Notes:
1. Dimensions are in centimeters.
2. Dimensional tolerance unless noted: Decimal ~ ±0.013, Fraction ~ ± 0.080.
3. Ends *to* be Perpendicular to ℄ and parallel to each other within 0.001 cm.
4. Do not undercut radii.
5. Surface quality: Blanks ~ mill smooth and flat, reduced section to be determined.
6. Diameter to be true and concentric with ℄.

Figure 3. Compression test specimen, standard dumbbell configuration

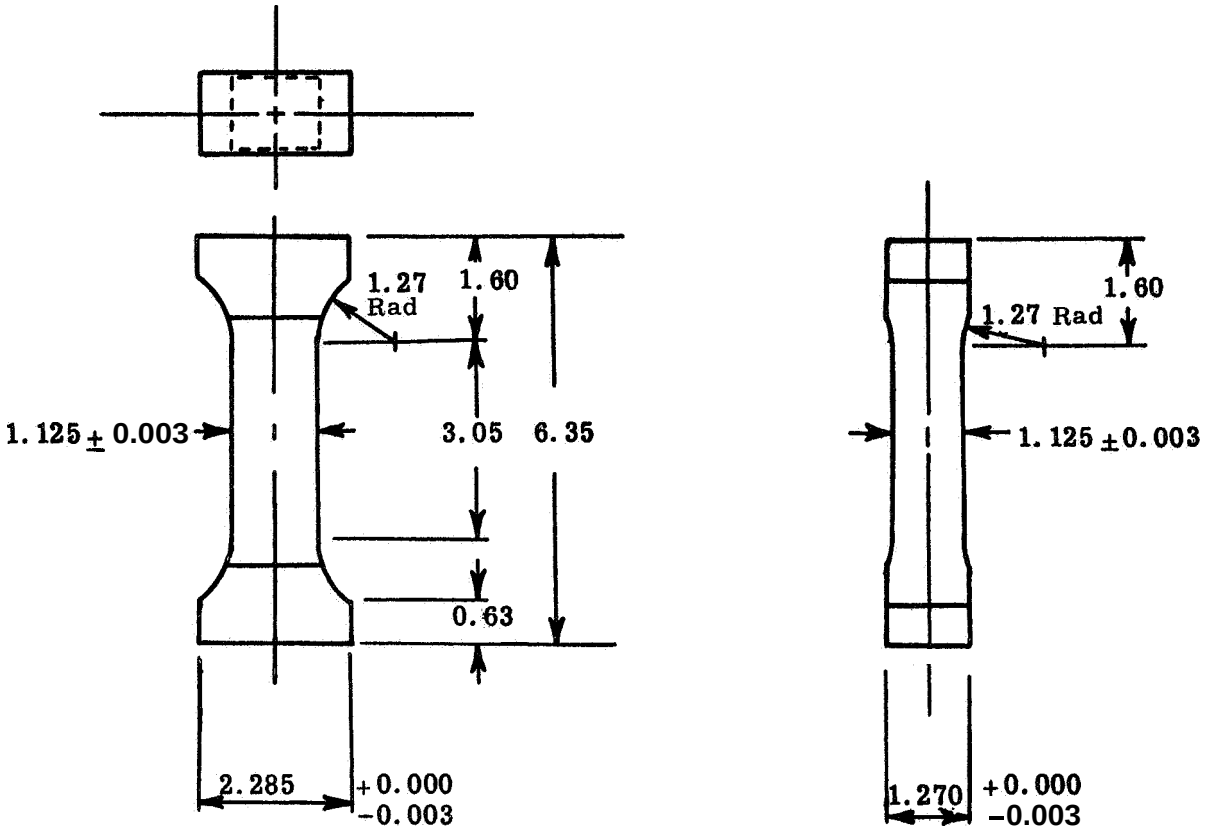

Designation -- CS1-XX-X

Notes:
1. Dimensions are in centimeters.
2. Dimensional tolerance unless noted: Decimal ~±0.013, Fraction ~± 0.080.
3. Do not undercut radii.
4. Ends to be perpendicular to ℄ and parallel to each other to within 0.001 cm.
5. Surface quality: Blanks ~mill smooth and flat, reduced section to be determined.

Figure 4. Compressive test specimen, square cross section

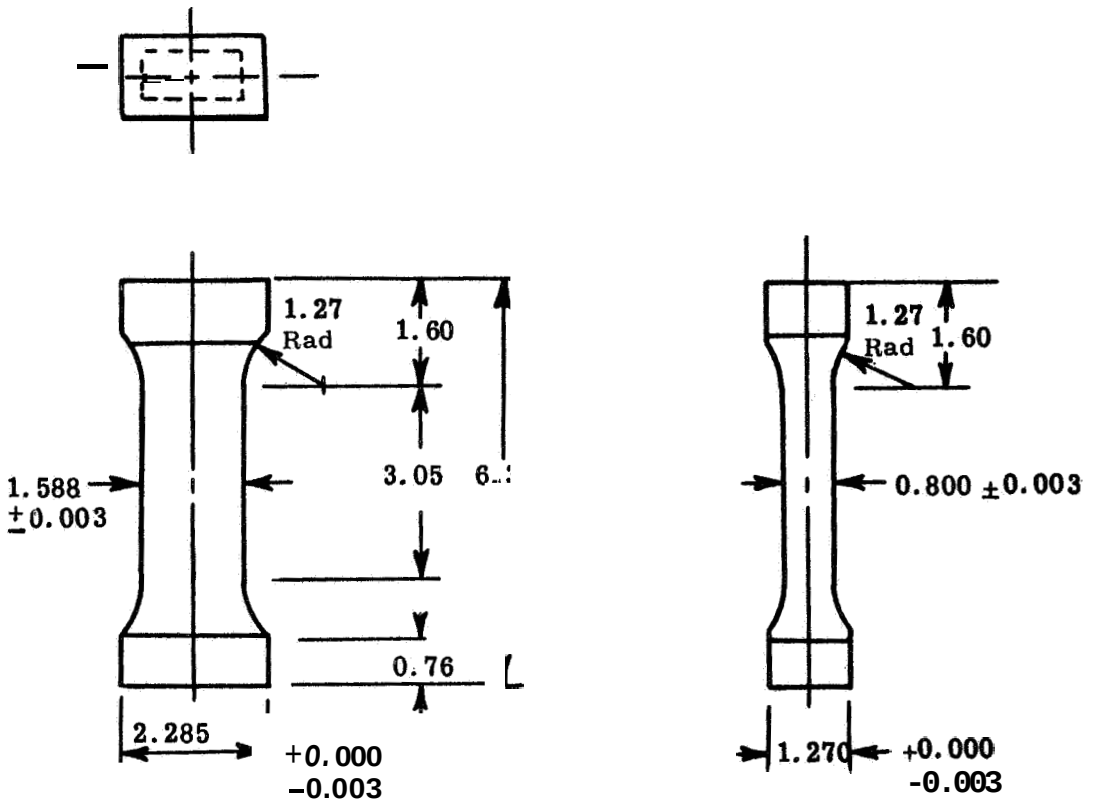

Designation -- CR1-XX-X

Notes:
1. Dimensions are in centimeters.
2. Dimensional tolerance unless noted: Decimal ~±0.013, Fraction ~± 0.080.
3. Do not undercut radii.
4. Ends to be perpendicular to ℄ and parallel to each other within 0.001 cm.
5. Surface quality: Blanks ~ mill smooth and flat, reduced section to be determined.

Figure 5. Compressive 'test specimen, 2:1 width-to-thickness, rectangular cross section

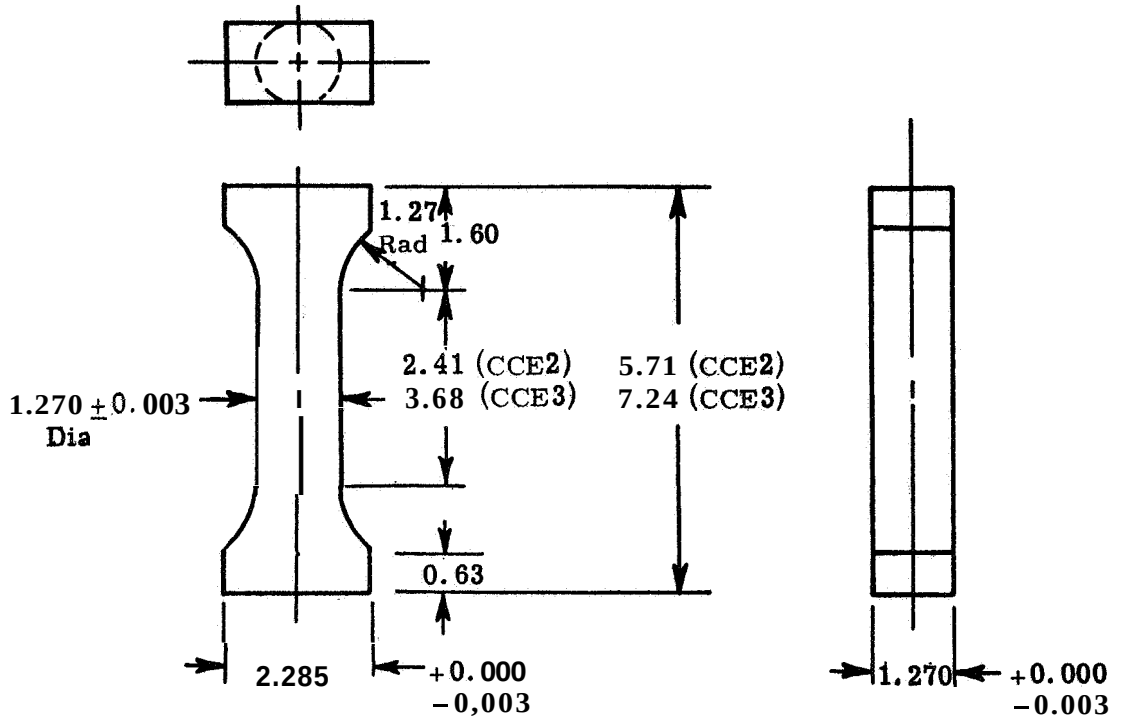

Designations --CCE2-XX-X
CCE3-XX-X

Notes:
1. Dimensions are in centimeters.
2. Dimensional tolerance unless noted: Decimal ~± 0.013, Fraction ~± 0,080.
3. Do not undercut radii.
4. Ends to be perpendicular to $\mathbb{Q}$ and parallel to each other within 0.001 cm.
5. Surface quality: Blanks ~ mill smooth and flat, reduced section to be determined.
6. Diameter to be true and concentric with $\mathbb{Q}$.

Figure 6. Experimental compressive test specimen, circular cross Section

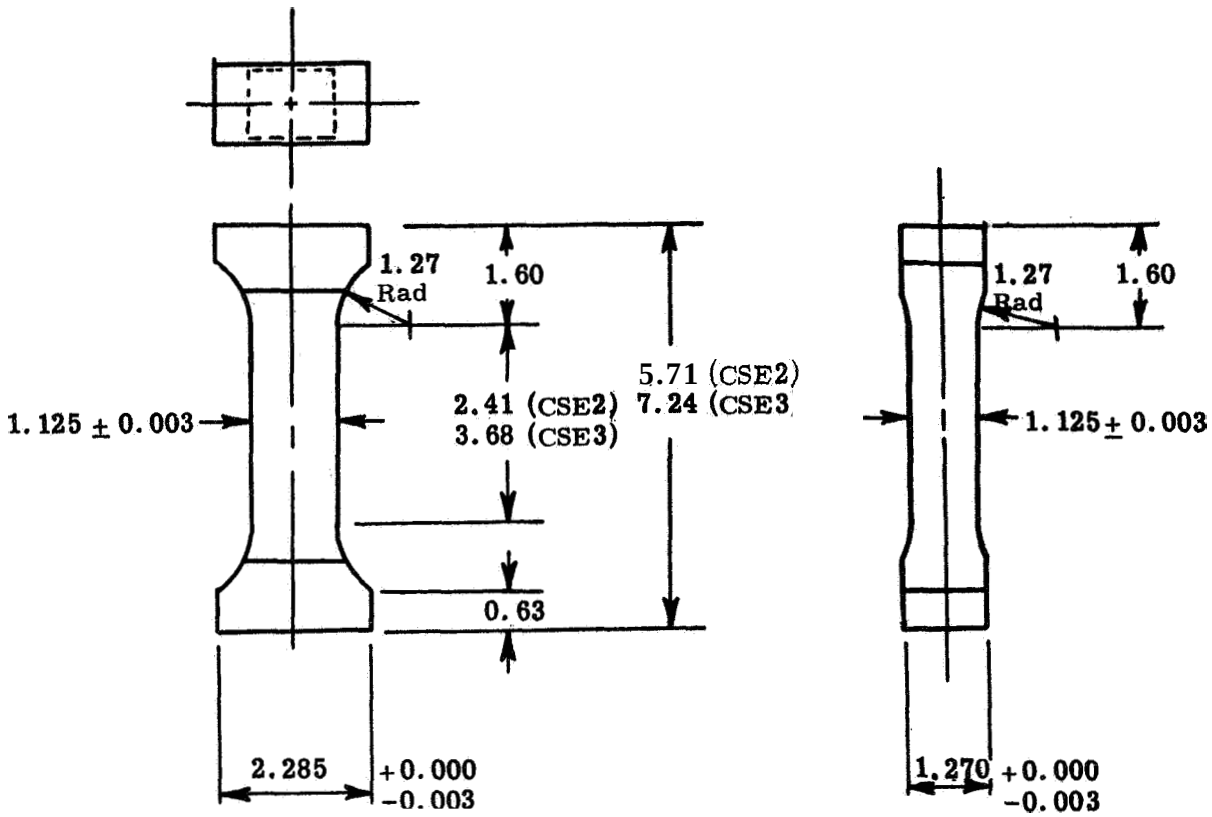

Designations -- CSE2-XX-X
CSE3-XX-X

Notes:
1. Dimensions are in centimeters.
2. Dimensional tolerance unless noted: Decimal ~±0.013, Fraction ~±0.080 cm.
3. Do not undercut radii.
4. Ends to be perpendicular to ℄ and parallel to each other to within 0.001 cm.
5. Surface qrality: Blanks ~ mill smooth and flat, reduced section to be determined.

Figure 7. Experimental compressive test specimen, square cross section

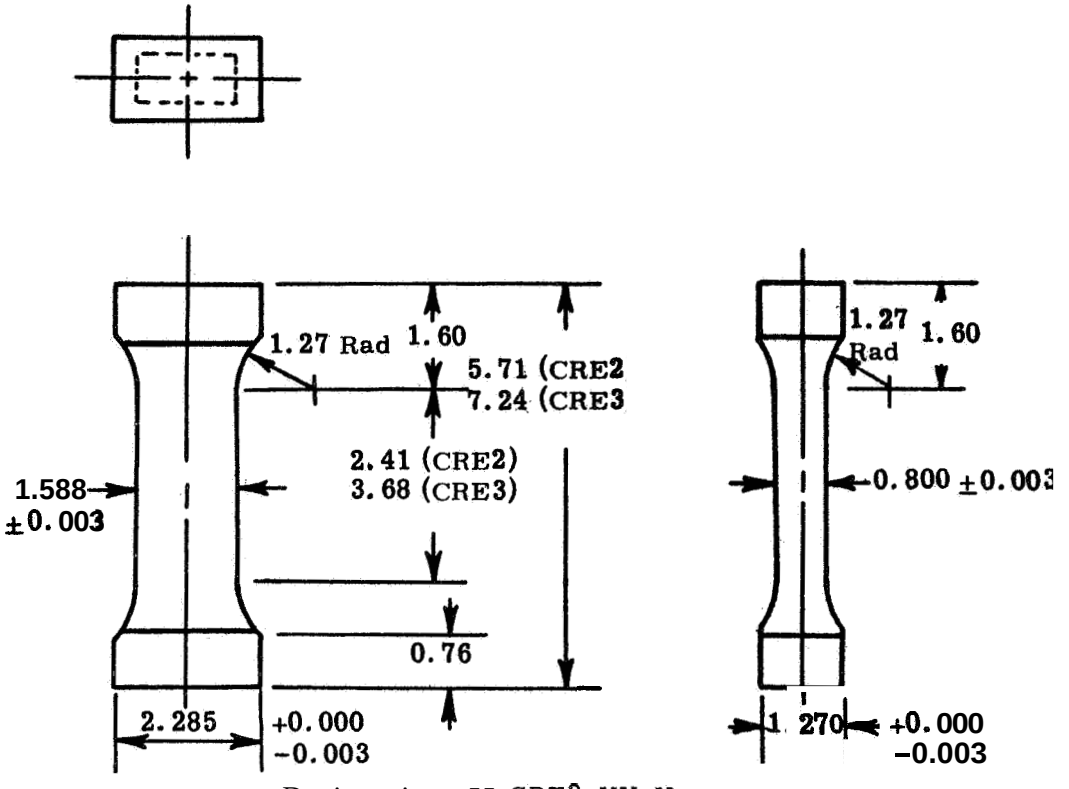

Designations -- CRE2-XX-X
CRE3-XX-X

Notes:
1. Dimensions are in centimeters.
2. Dimensional tolerance unless noted: Decimal ~±0.013, Fraction ~± 0.080.
3. Do not undercut radii.
4. Ends to be perpendicular to ℄ and parallel to each other within 0.001 cm.
5. Surface Quality: Blanks ~ mill smooth and flat, reduced section to be determined.

Figure 8. Experimental compressive test specimen, 2:1 width-to-thickness rectangular cross section

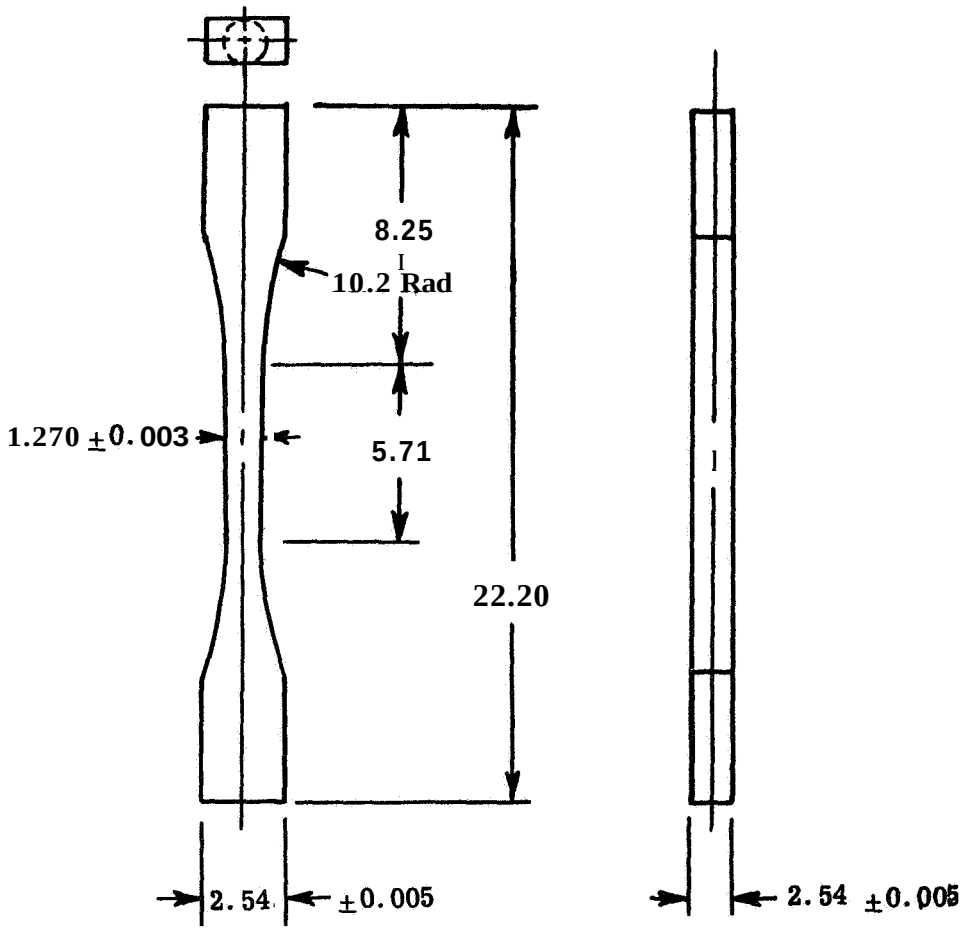

Designation -- TC1-XX-X

Notes:
1. Dimensions are in centimeters.
2. Dimensional tolerance unless noted: Decimal ~±0.013, Fraction ~± 0.080.
3. Do not undercut radii.
4. Hold diameter true and concentric with ℄.
5. Faces to be flat and parallel to ℄.
6. Surface quality: Blanks ~ mill smooth and flat, reduced section *to* be determined.

Figure 9. Tensile test specimen, circular cross section

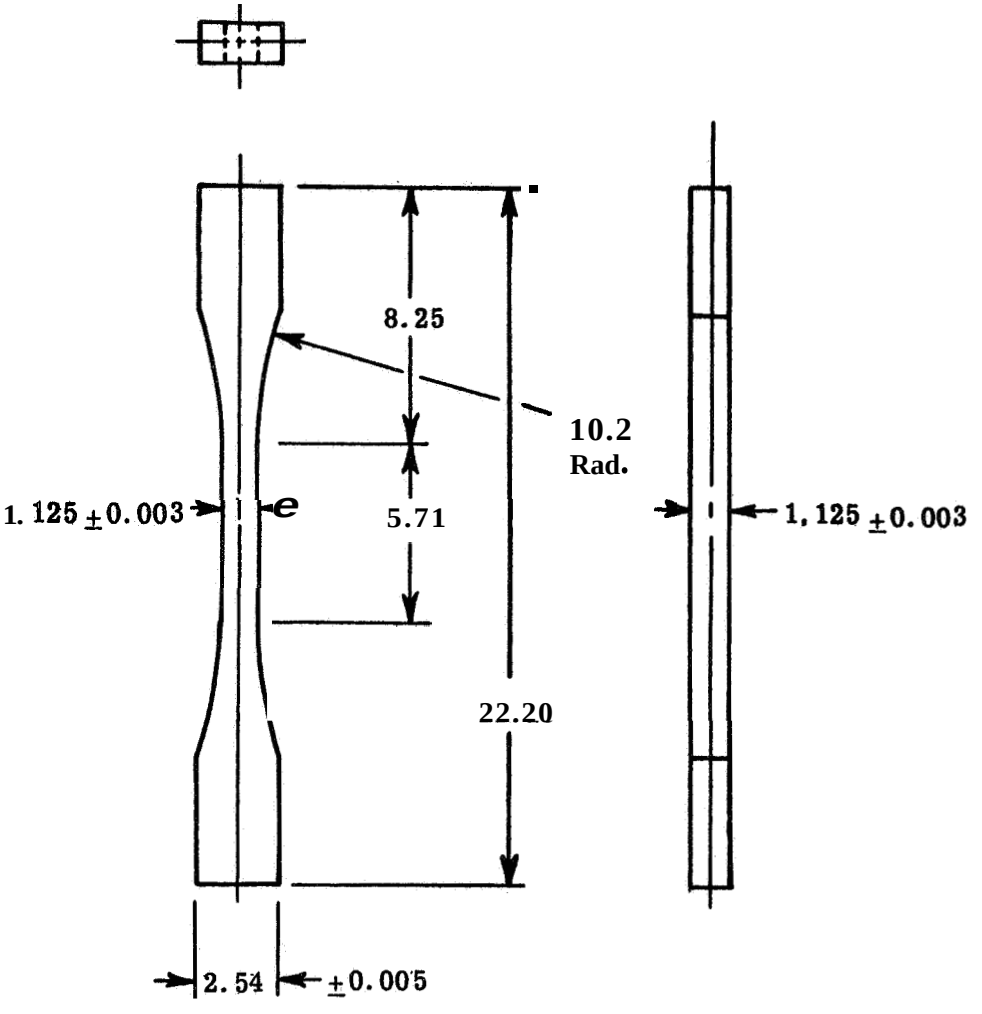

Designation -- TS1-XX-X

Notes:

1. Dimensions are in centimeters.
2. Dimensional tolerance unless noted: Decimal ~±0.013, Fraction ~± 0.080.
3. Do not undercut radii.
4. Faces to be flat and parallel to ℄.
5. Surface quality: Blanks ~ mill smooth and flat, reduced section to be determined.

Figure 10. Tensile test specimen, square cross section

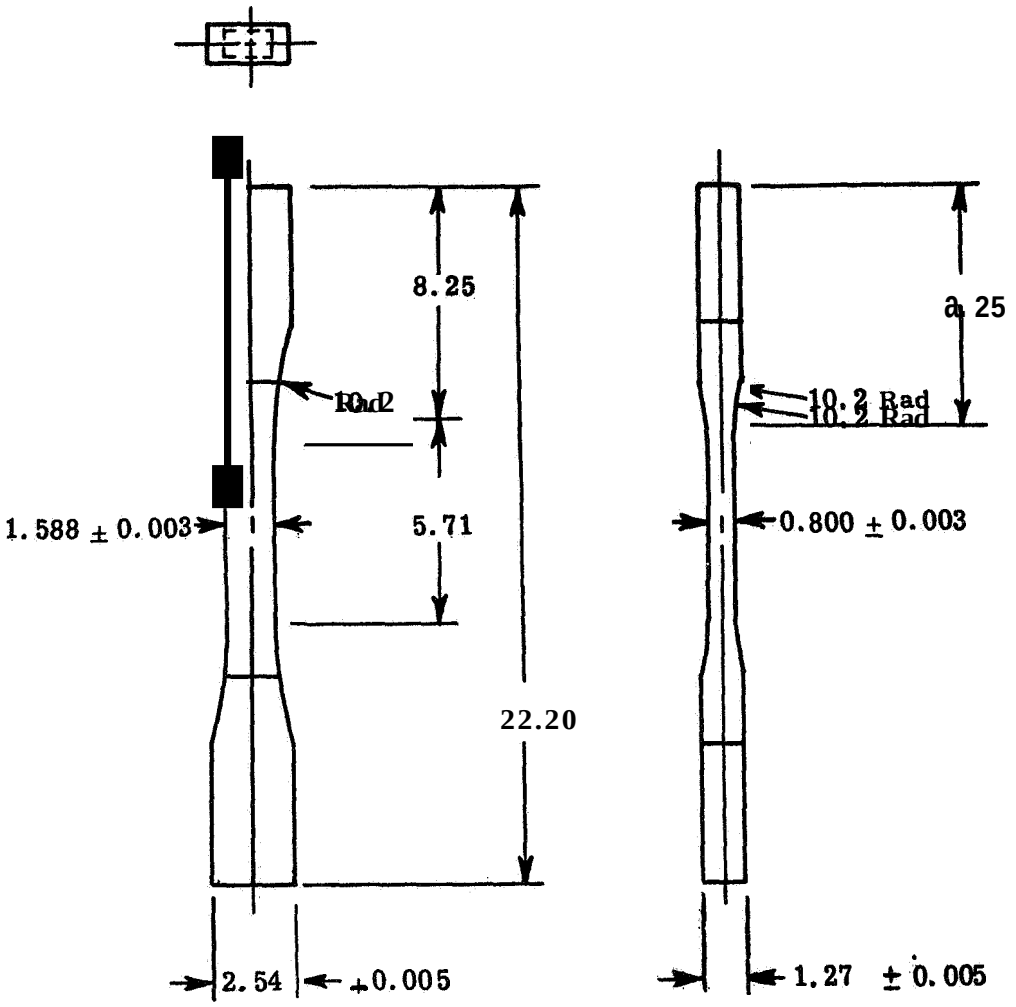

Designation -- TR1-XX-X

Notes:
1. Dimensions are in centimeters.
2. Dimensional tolerance unless noted: Decimal ~±0.013, Fraction ~±0.080.
3. Do not undercut radii.
4. Faces to be flat and parallel to ℄.
5. Surface quality: Blanks ~ mill smooth and flat, reduced section to be determined.

Figure 11. Tensile test specimen, 2:1 width-to-thickness, rectangular cross section

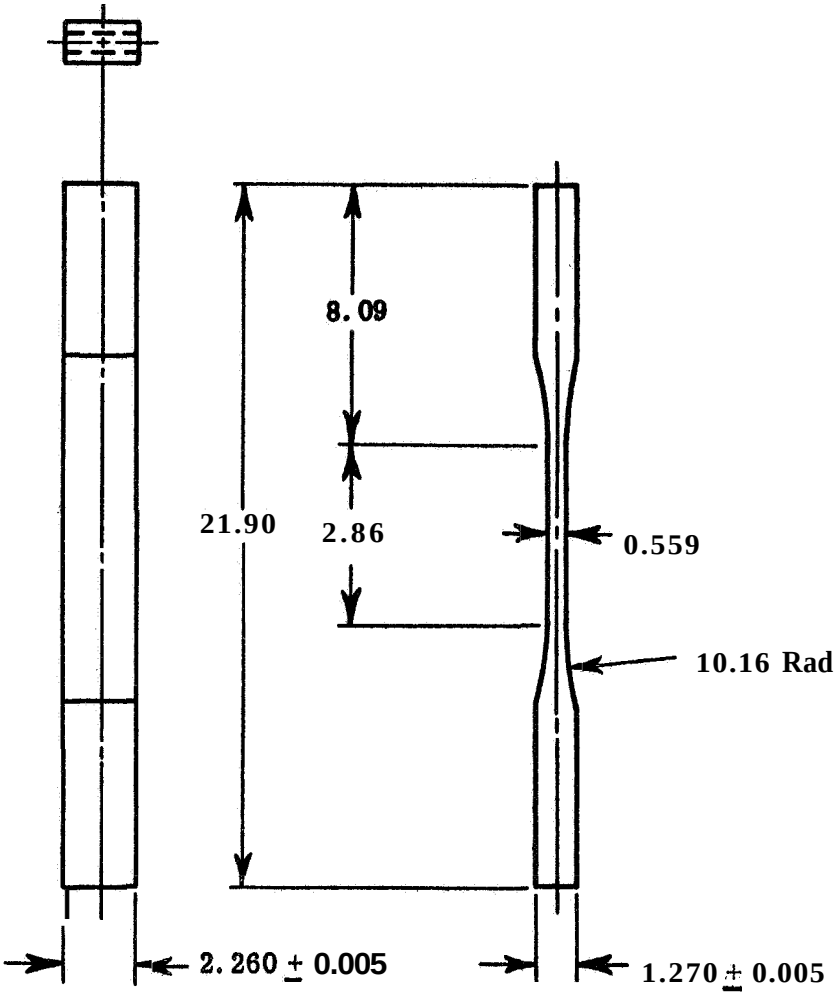

Designation - TR3-XX-X

Notes :
1. Dimensions are in centimeters.
2. Do not undercut radii.
3. Maintain gage length surface flat and parallel to centerline to within 0.0013.

Figure 12. Tensile test specimen 4:f width-to-thickness ratio (2.260 x 0.559 cm)

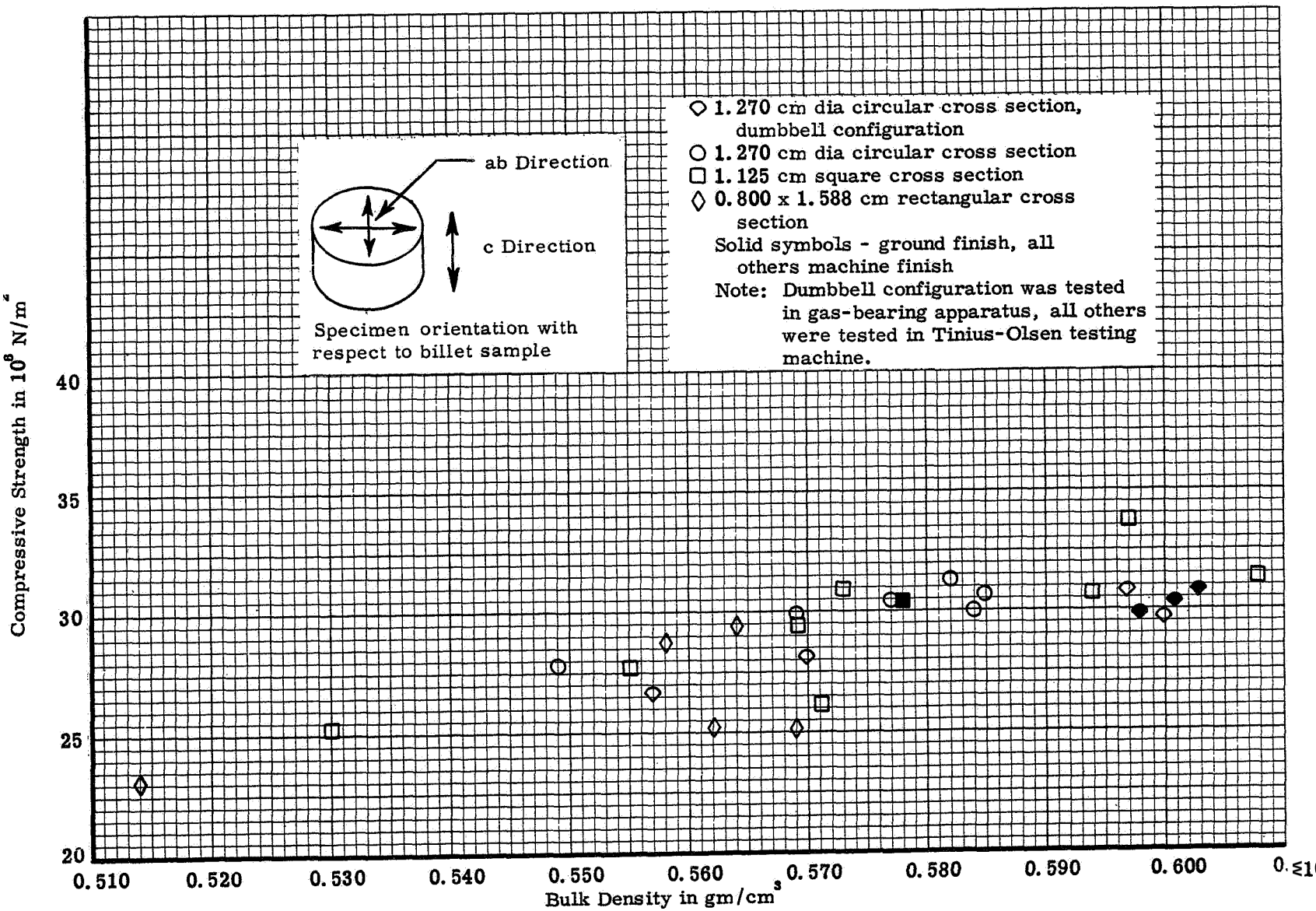

Figure 13. Compressive strength versus bulk density for various configurations in ab direction at 294°K (70°F)

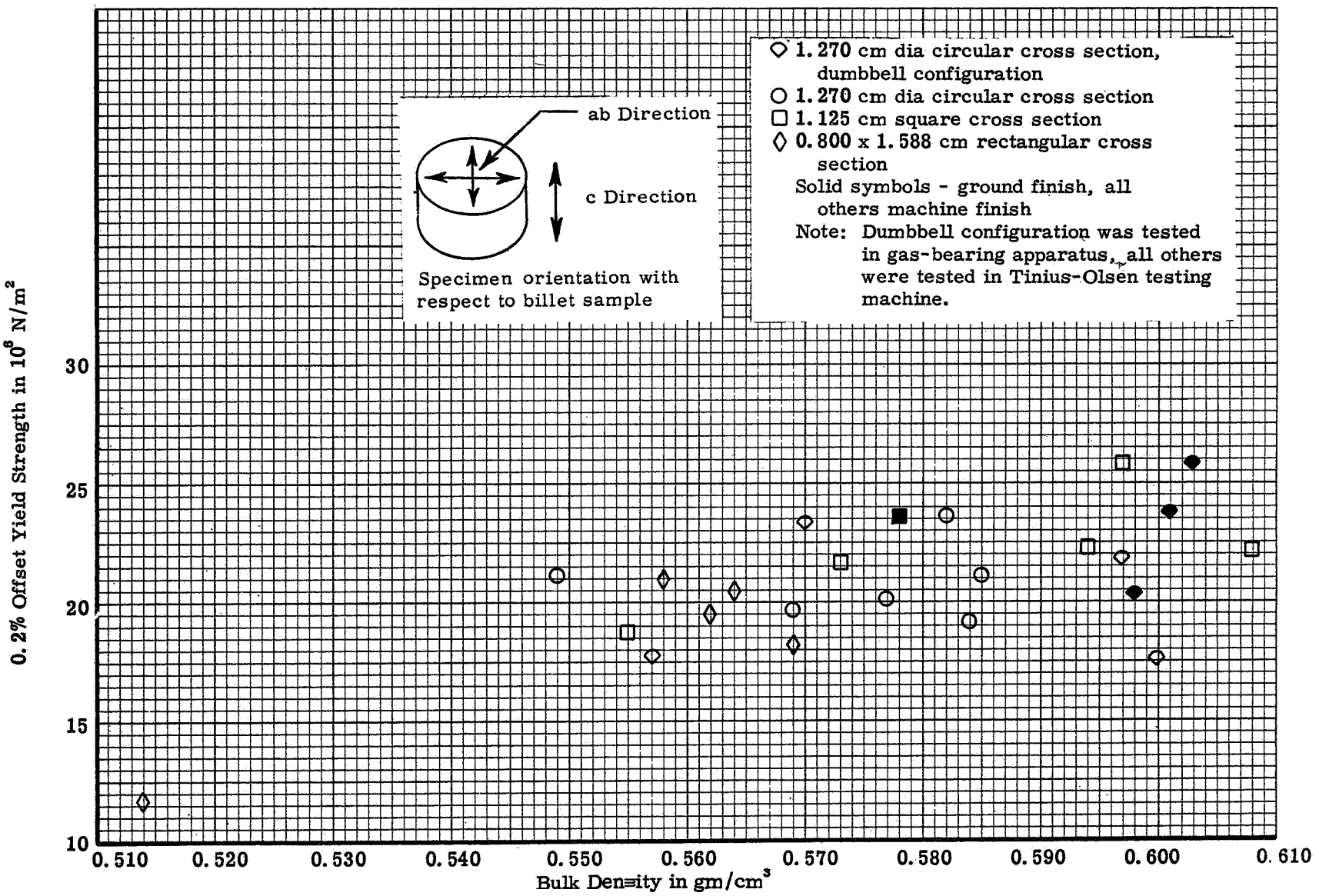

Figure 14. Compressive 0.2% offset yield strength versus density for various configurations in ab direction at 294°K (70°F)

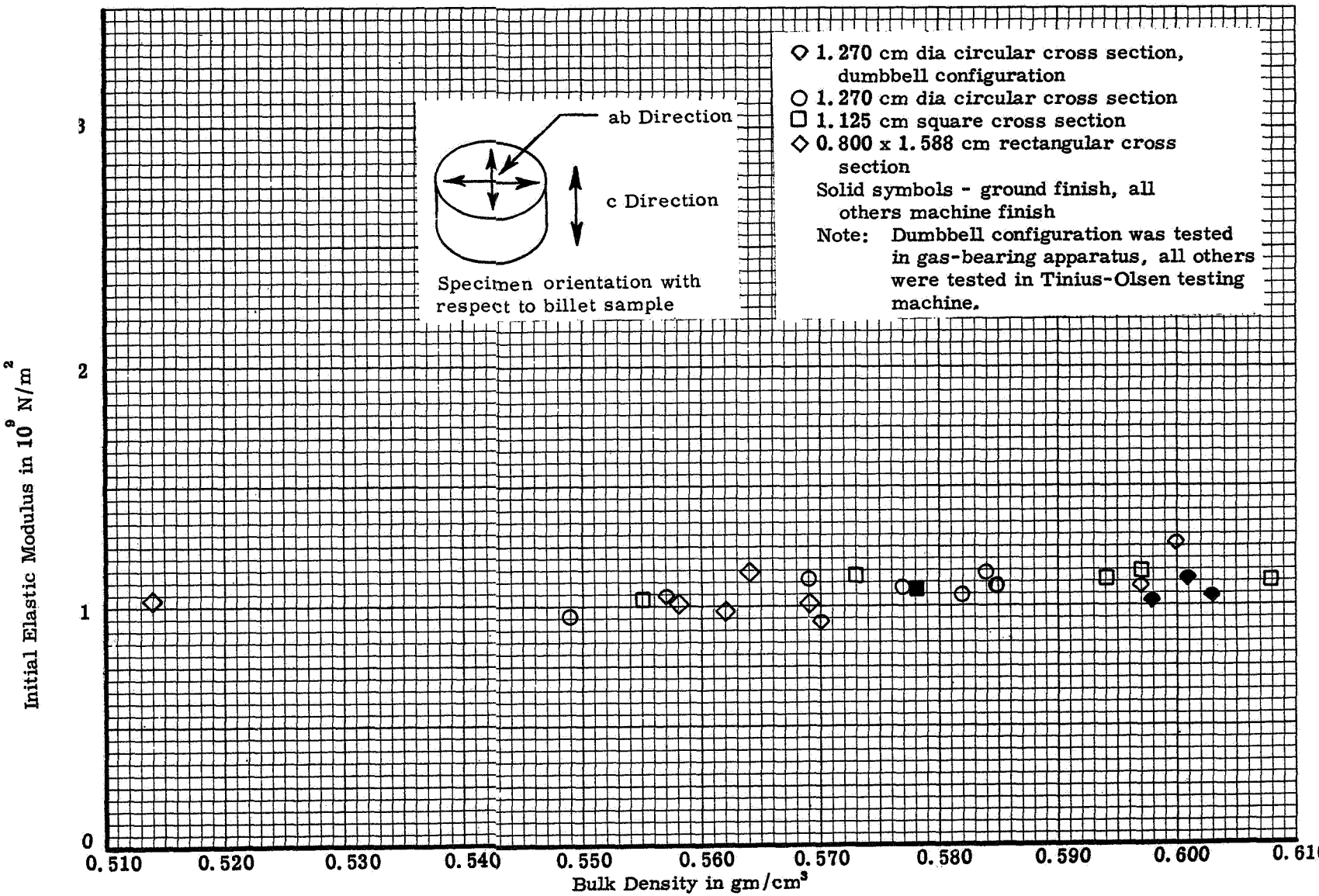

Figure 15. Compressive initial elastic modulus versus density for various configurations in ab direction at 294°K (70°F)

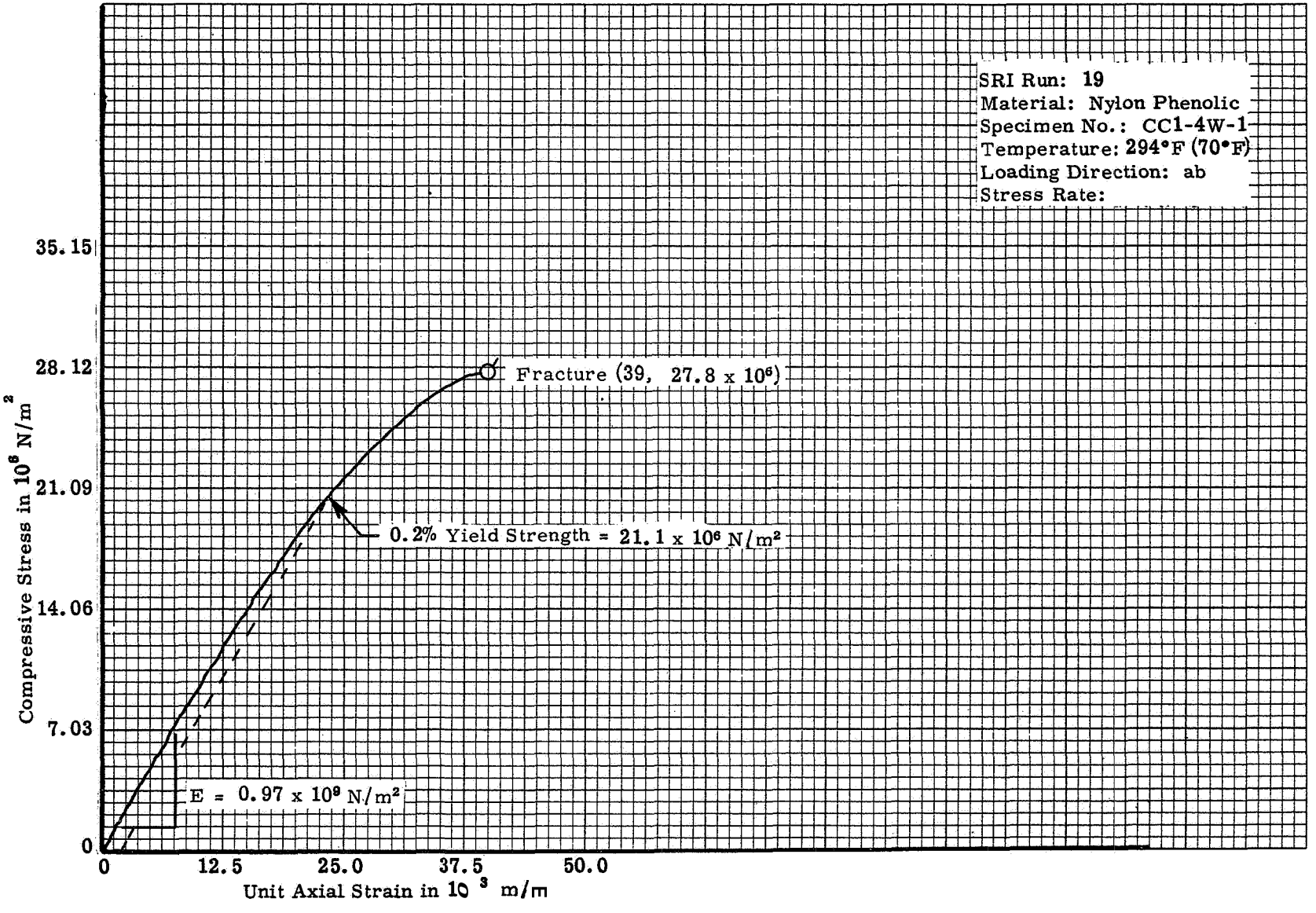

Figure 16. Typical compressive stress-strain for circular cross section in the ab direction at 294°K (70°F) tested in the Tinius Olsen apparatus

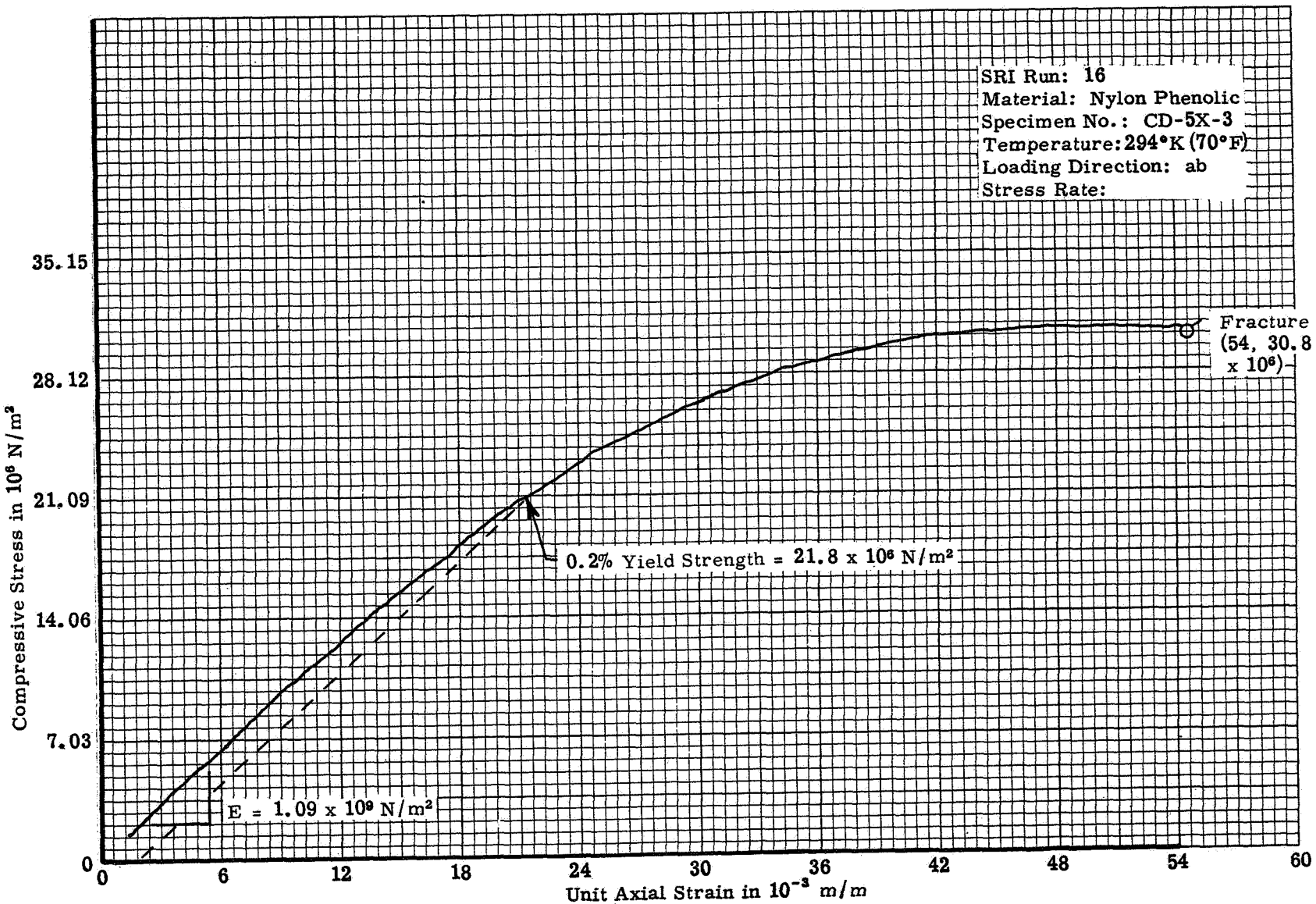

Figure 17. Typical compressive stress-strain curve for standard dumbbell configuration in the ab direction at 294°K (70°F), tested in the gas-bearing apparatus

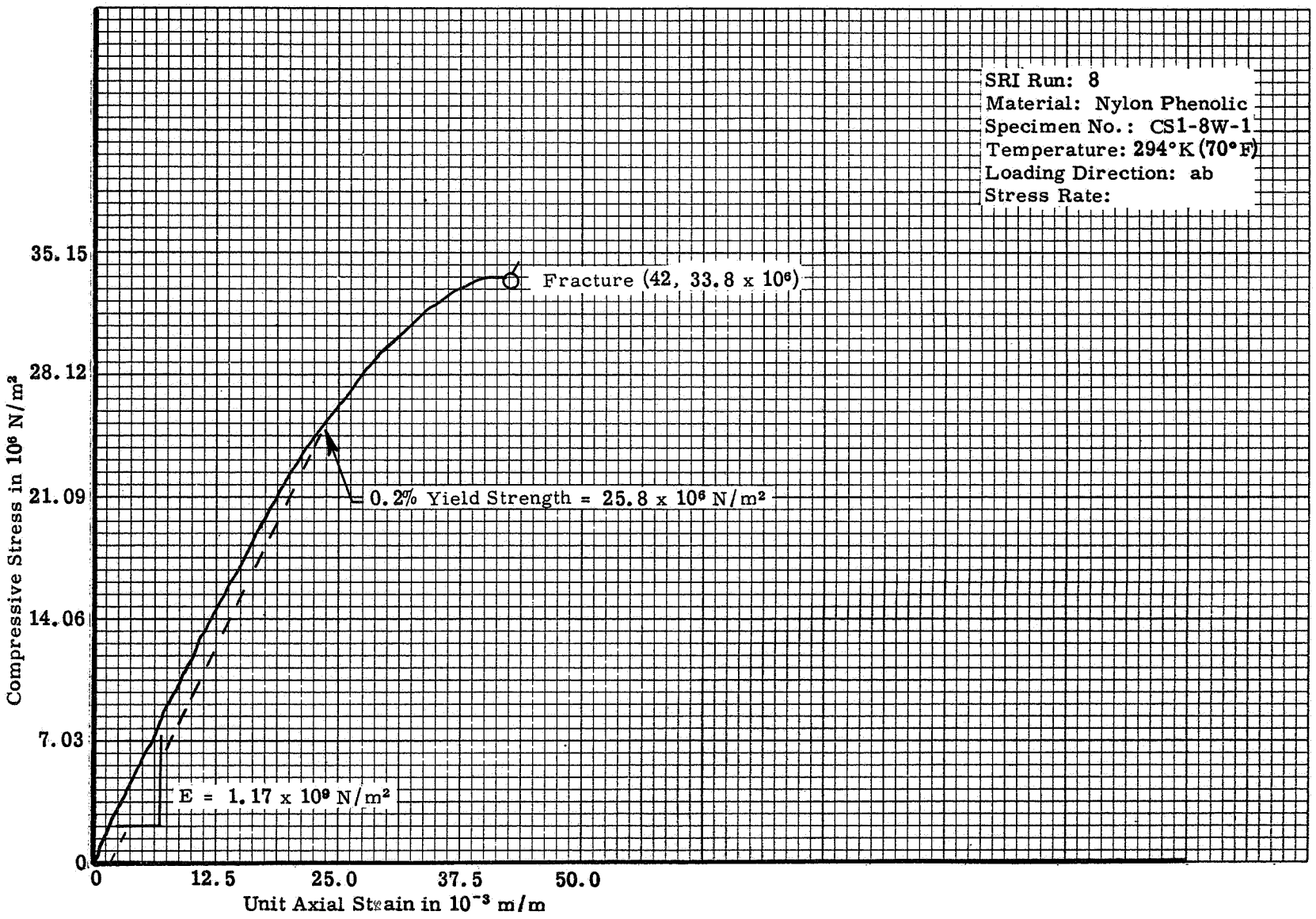

Figure 18. Typical compressive stress-strain curve for square cross section in the ab direction at 294°K (70°F) tested in the Tinius-Olsen apparatus

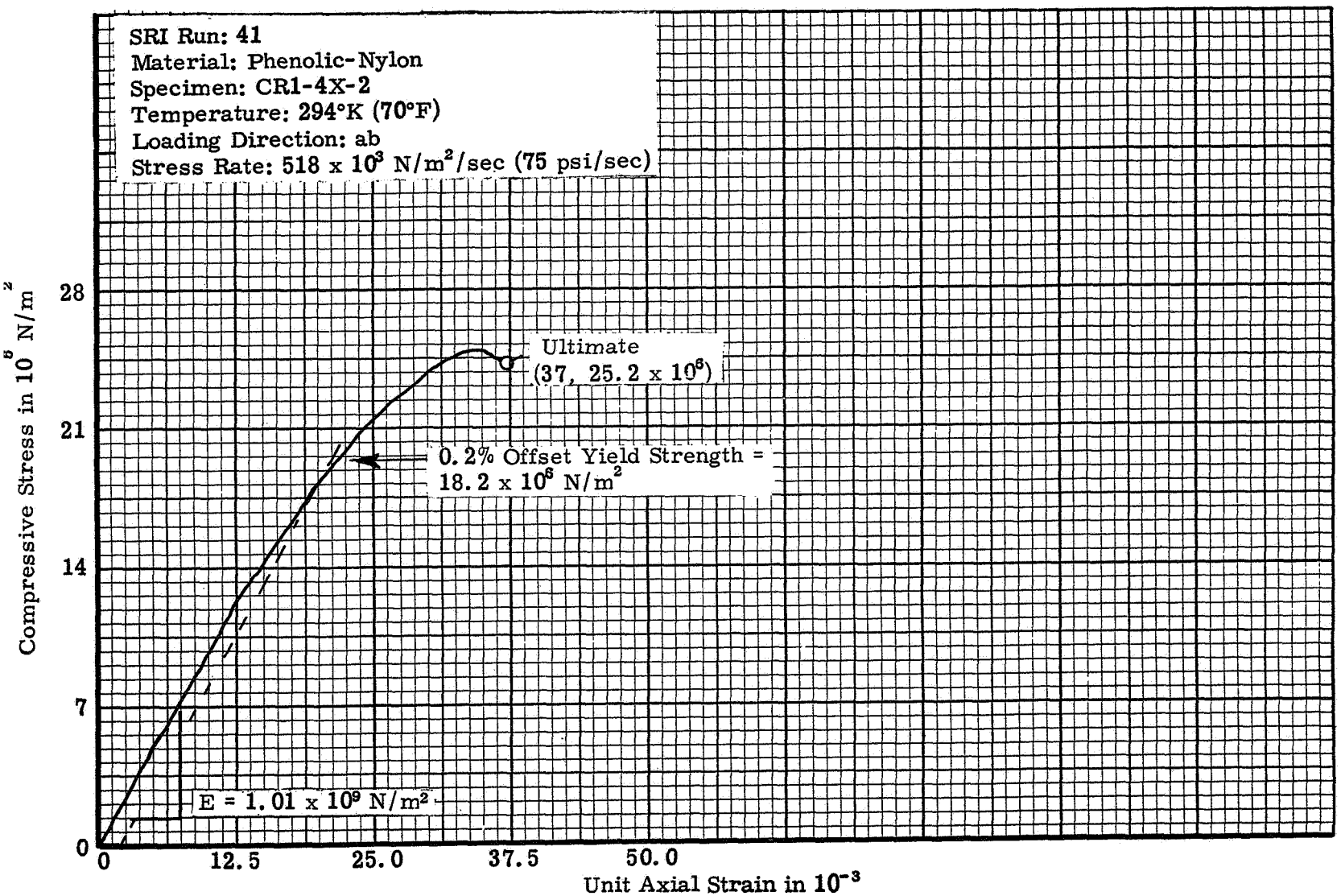

Figure 19. Typical compressive stress-strain curve for 2:1 rectangular cross section 1.588 cm (0.625 in.) x 0.800 cm (0.315 in.) in the ab direction at 294°K (70°F) tested in the Tinius-Olsen apparatus

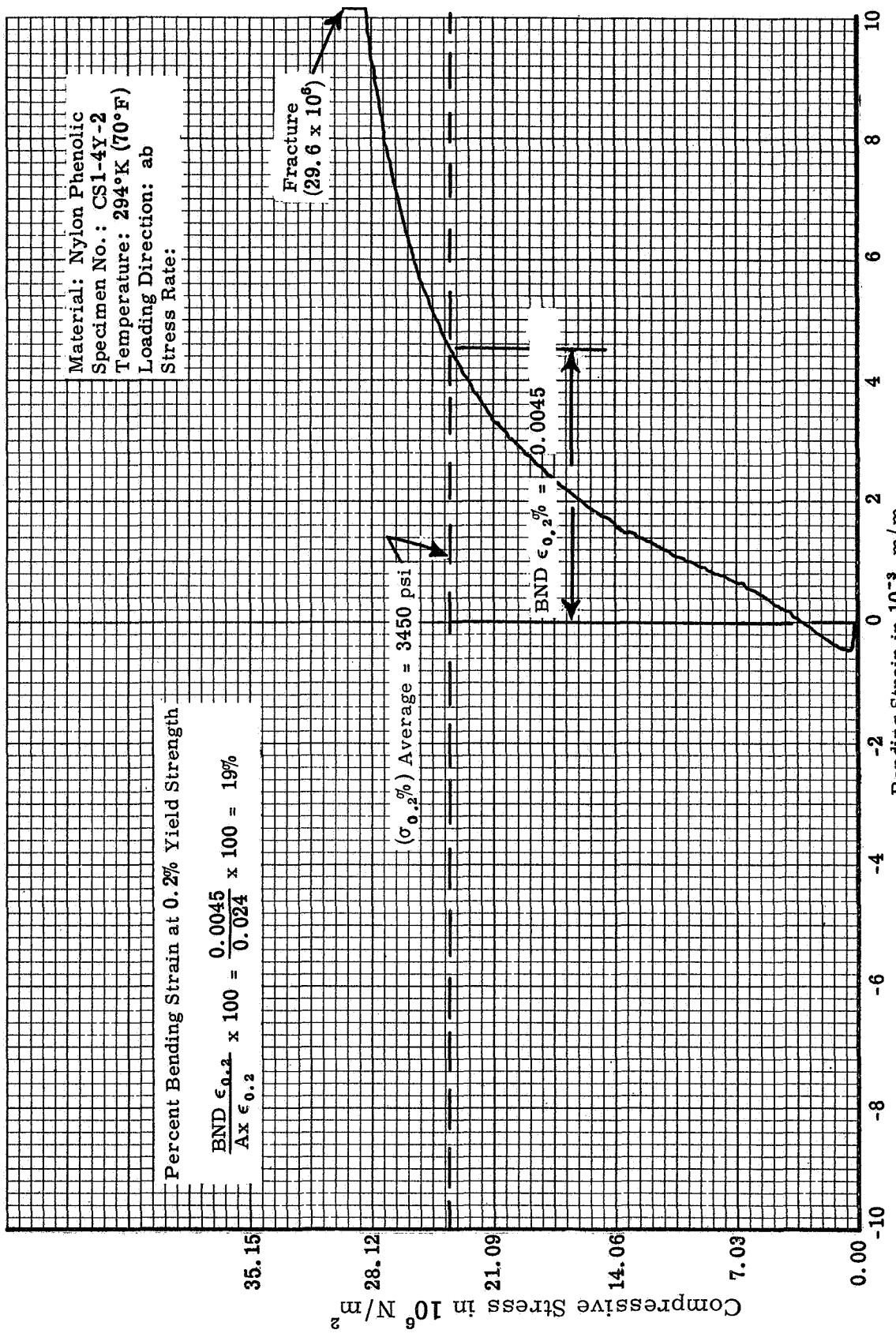

Figure 20. Bending strain versus compressive stress in the ab direction at 294°K (70°F)

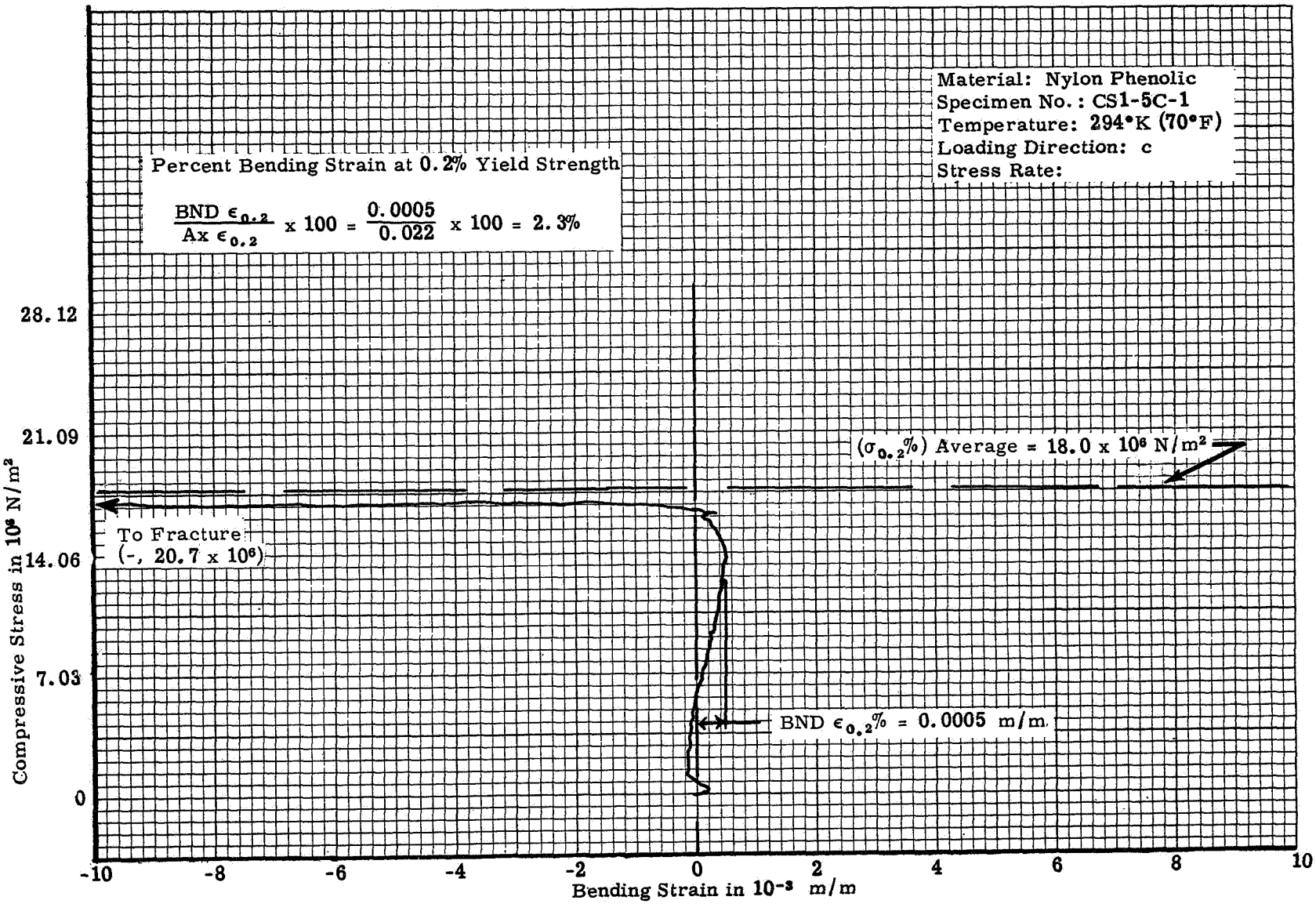

Figure 21. Bending strain versus compressive stress in the c direction at 294°K, specimen no. 1

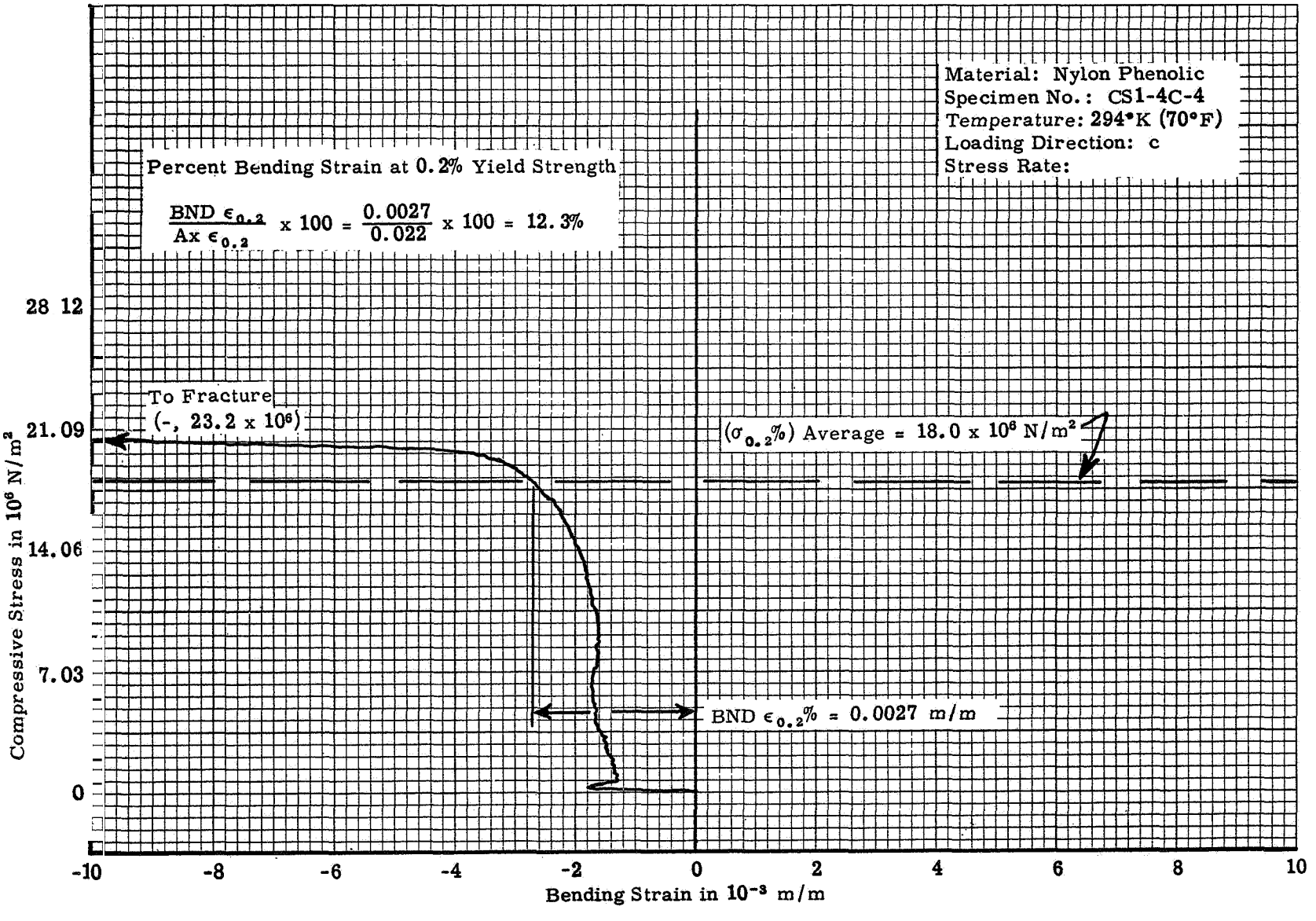

Figure 22. Bending strain versus compressive stress in the c direction at 294°K (70°F), specimen no. 2

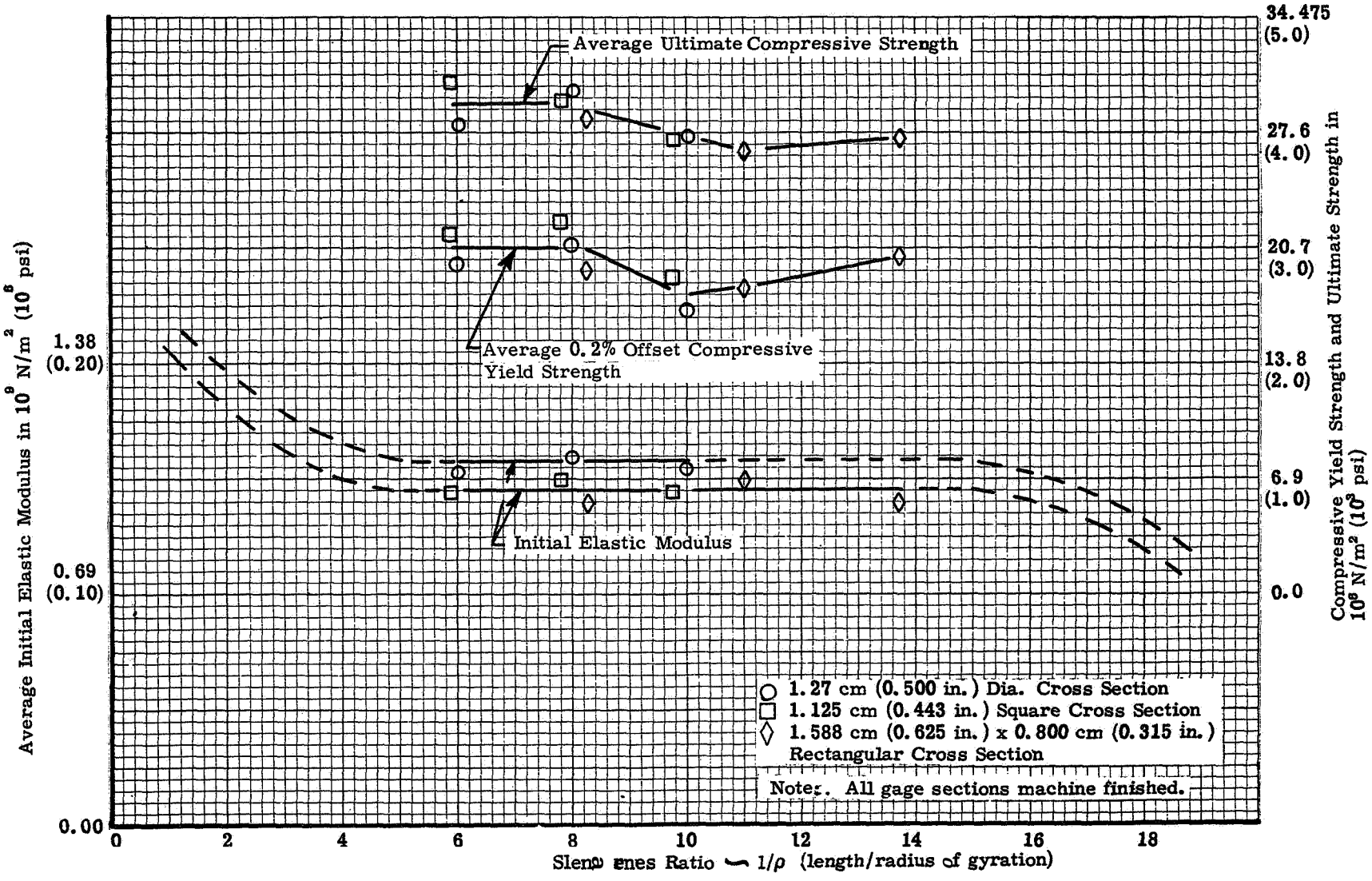

Figure 23. Initial elastic modulus, yield strength, and ultimate compressive strength versus slenderness ratio in the ab direction at 294°K (70°F)

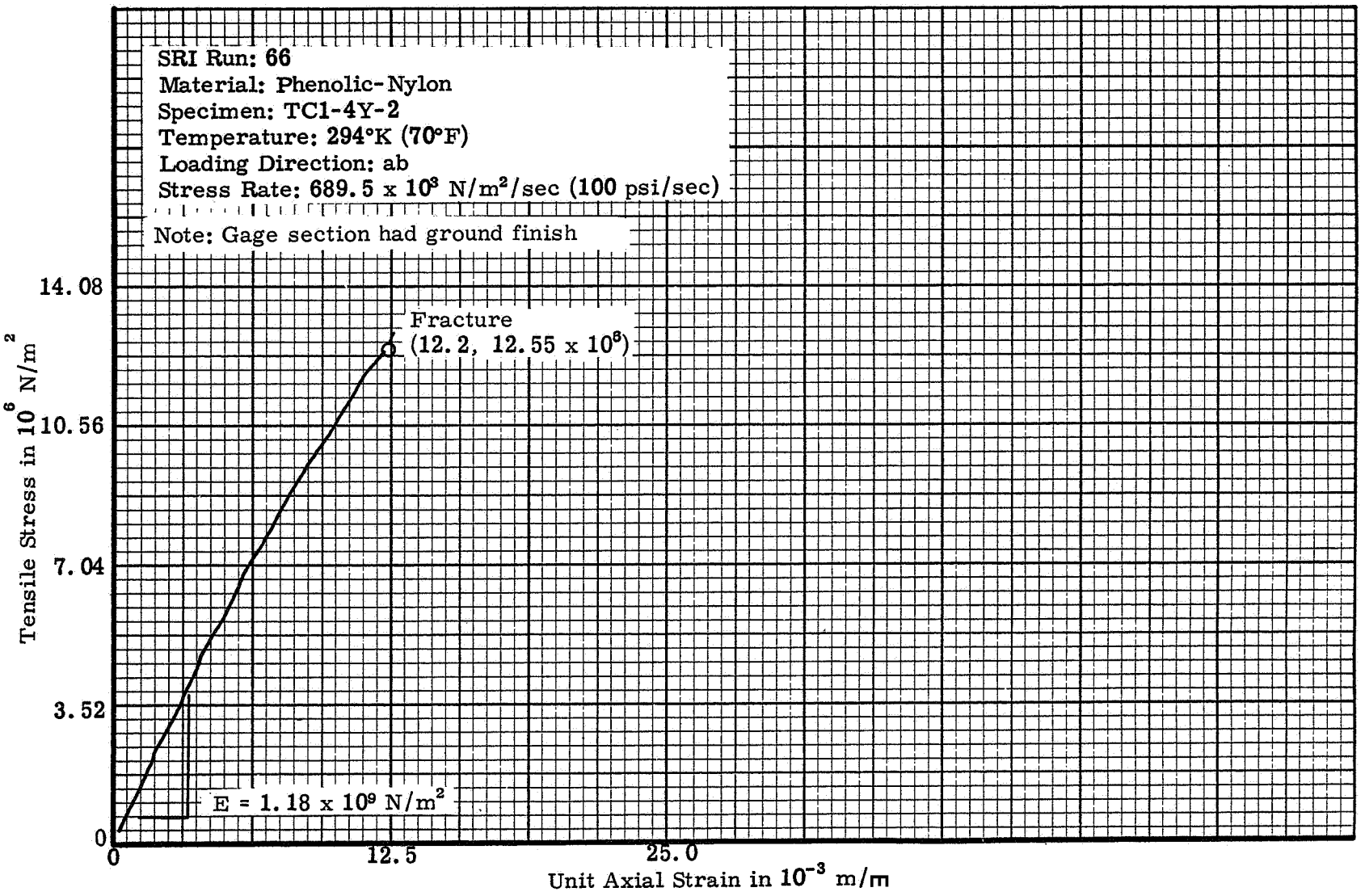

Figure 24. Typical tensile stress-strain curve for 1.27 cm (0.500 in.) diameter cross section in the ab direction at 294°K (70°F)

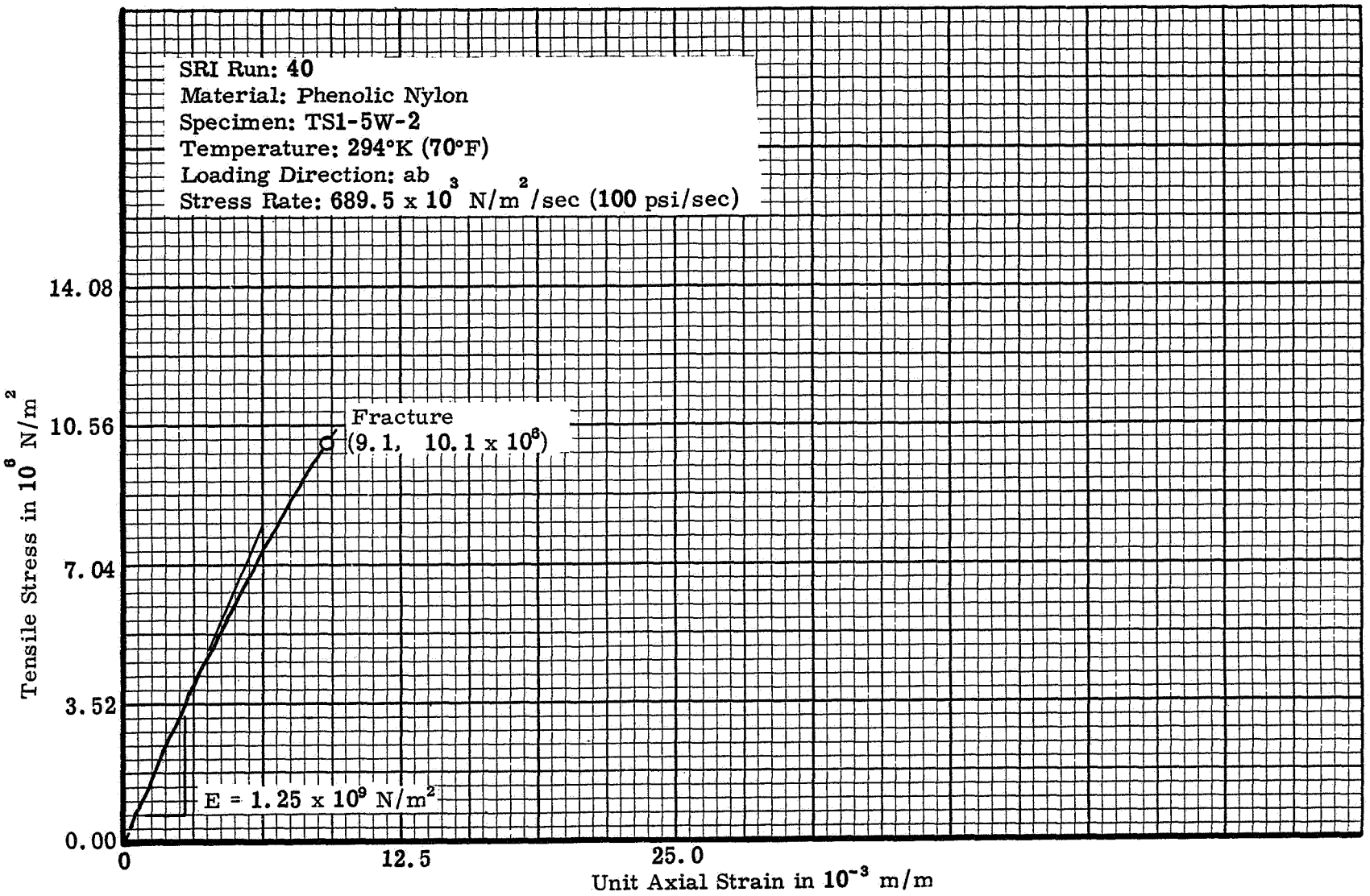

Figure 25. Typical tensile stress-strain curve for 1.125 cm (0.443 in.) square cross section in the ab direction at 294°K (70°F)

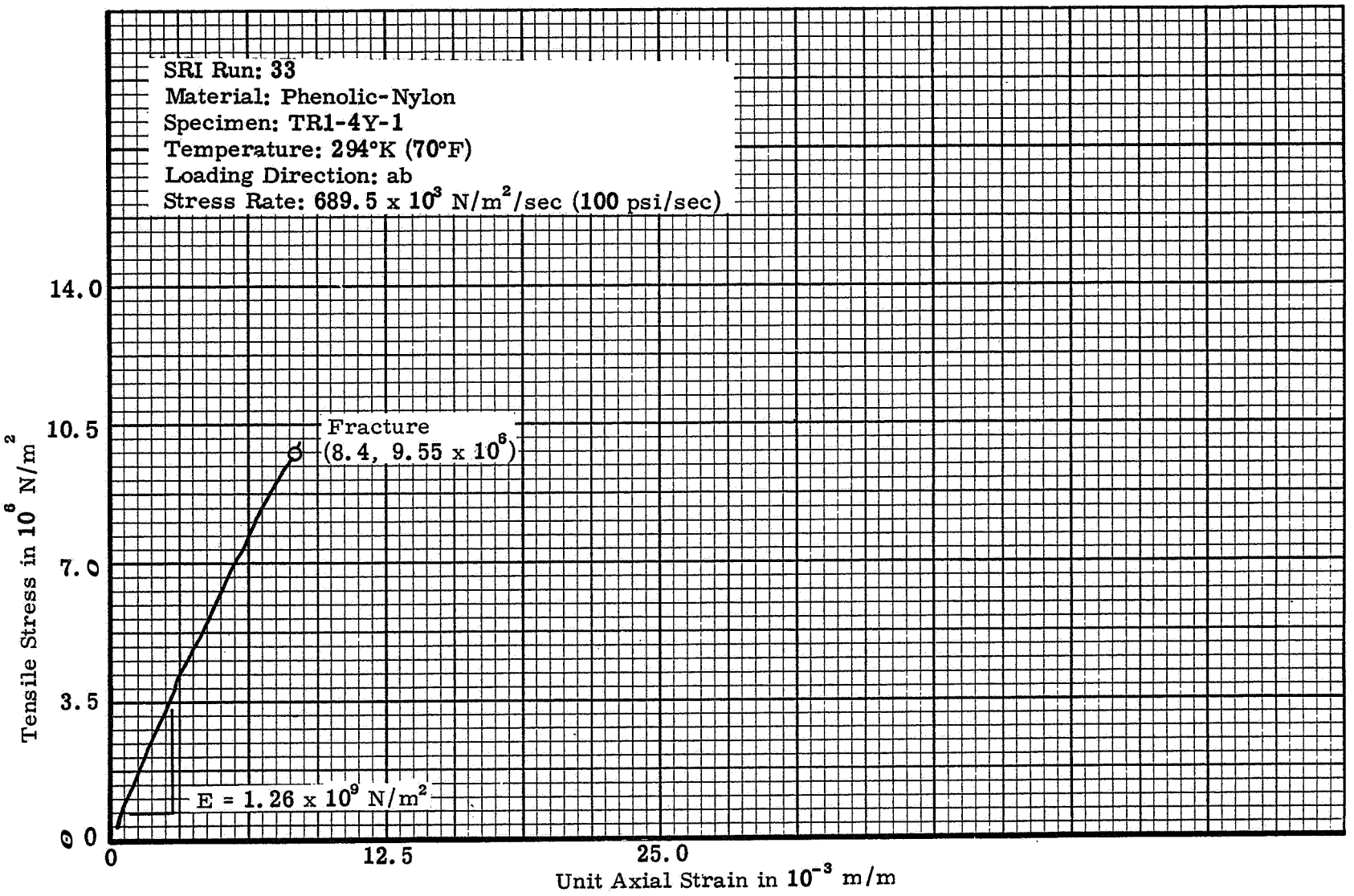

Figure 26. Typical tensile stress-strain curve for 2:1 rectangular cross section 1.588 cm (0.625 in.) x 0.800 cm (0.315 in.) in the ab direction at 294°K (70°F)

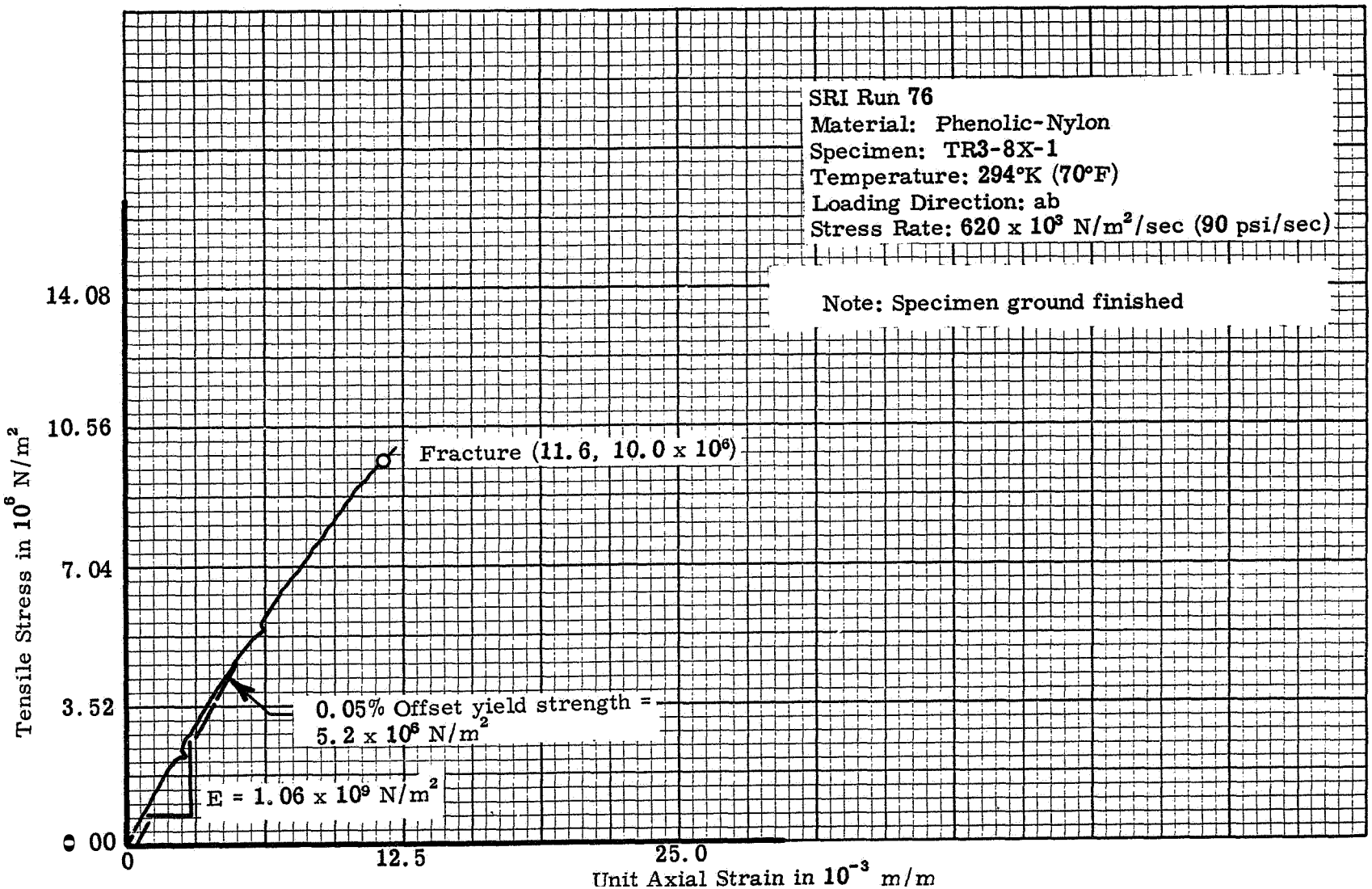

Figure 27. Typical tensile stress-strain curve for 4:1 width-to-thickness ratio (2.260 x 0.559 cm) cross section specimen tested in the ab direction at 294°K (70°F)

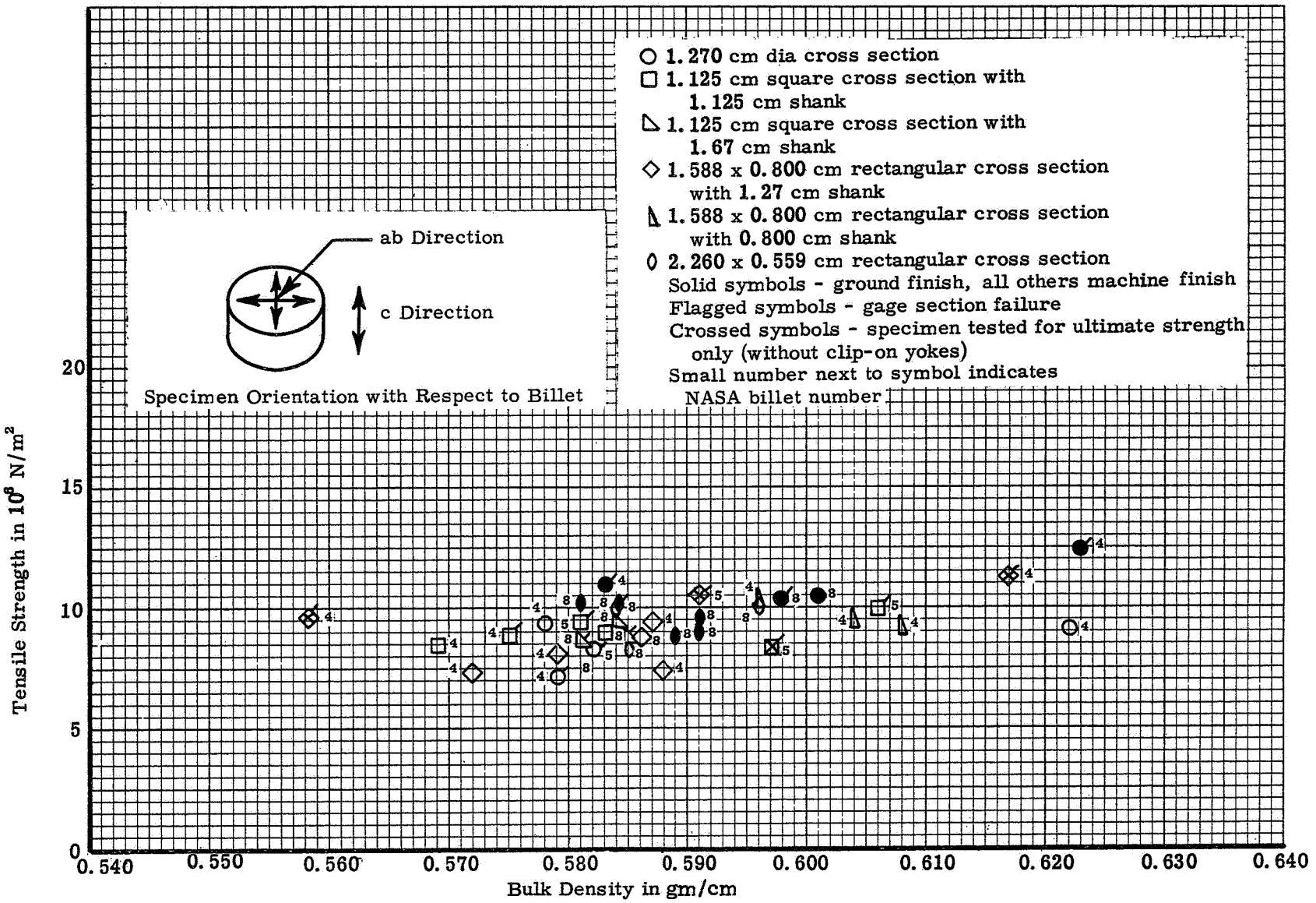

Figure 28. Tension s[illegible]th versus bulk density for various configurations in the ab direction at 294°K (70°F)

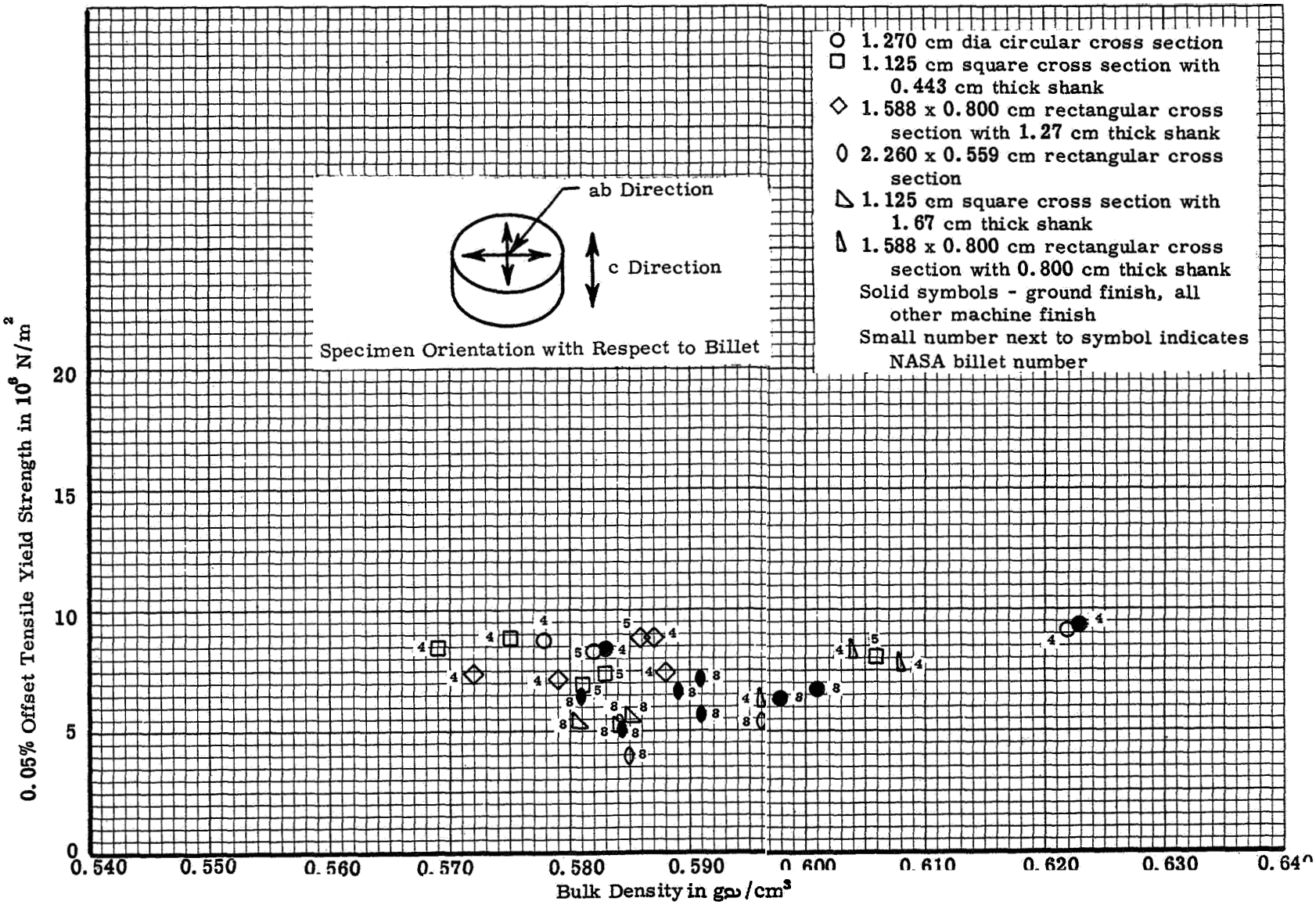

Figure 29. 0.05 offset tensile yield strength versus bulk density for various configurations in the ab direction at 294°K (7)

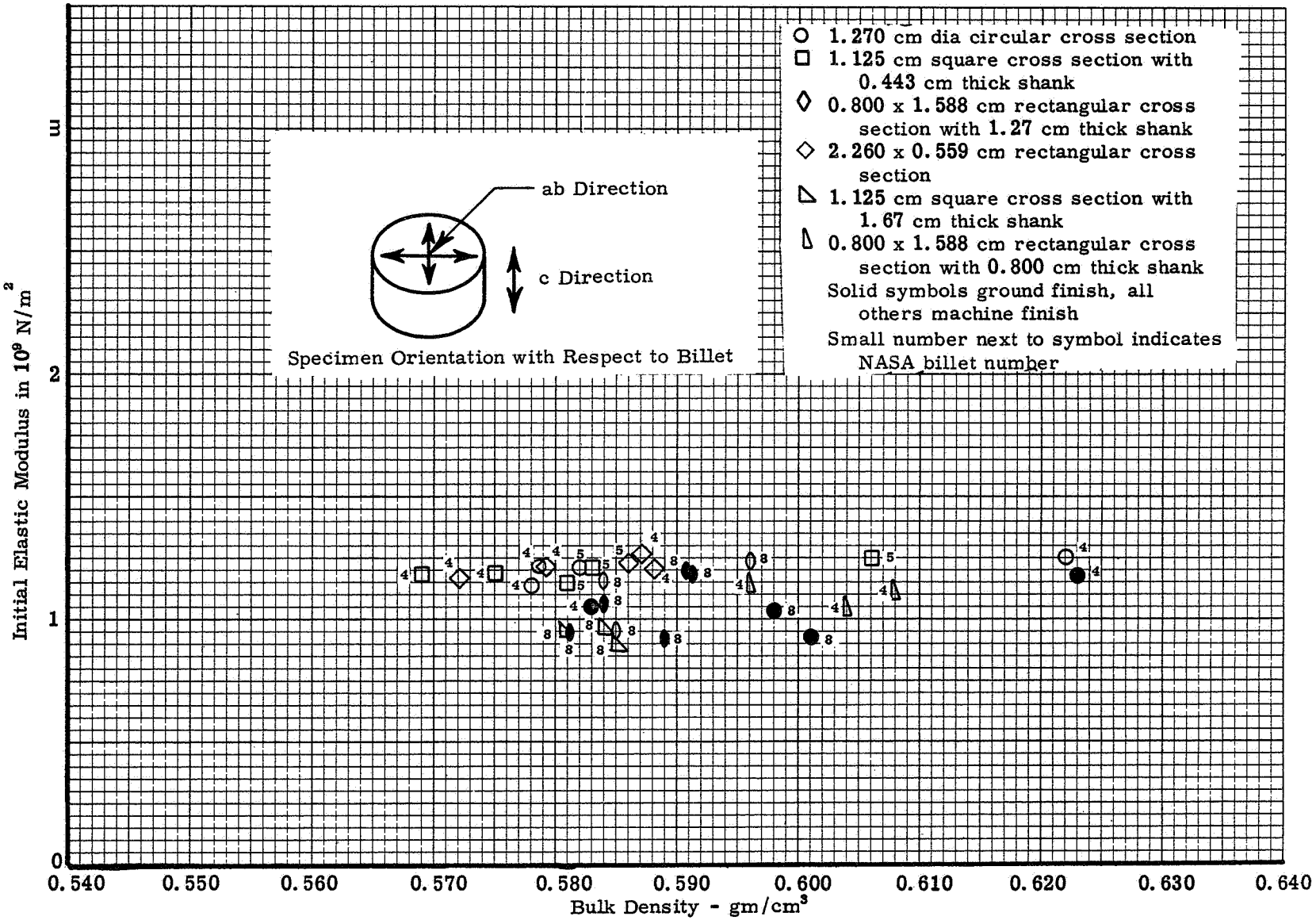

Figure 30. Initial tensile elastic modulus versus bulk density for various configurations in the ab direction at 294°K (70°F)

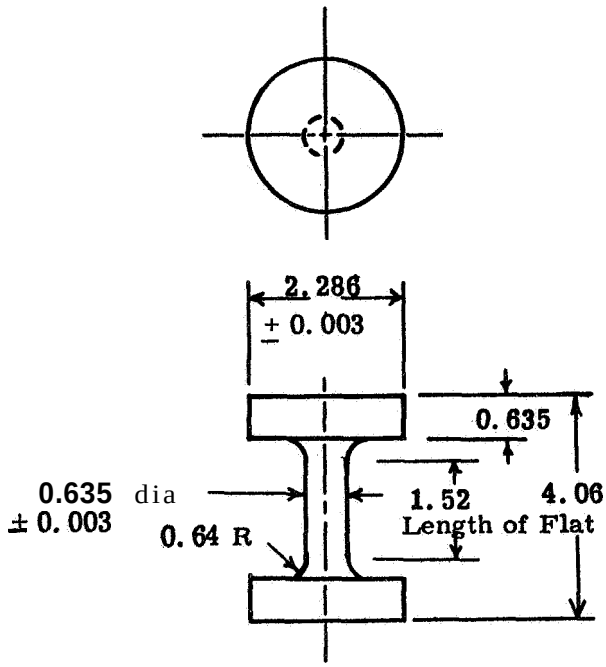

Designation CD2-XX-X

Notes:

1. Dimensions are in centimeters.
2. Dimensional tolerance unless noted: ± 0.013
3. Ends to be perpendicular to ℄ and parallel to each other within 0.003.
4. Do not undercut radii.
5. Surface: Turn to smooth finish.
6. Diameters to be true and concentric to ℄.

Figure 31. Compressive test specimen for testing for volumetric effects of phenolic-nylon in gas bearing compressive facility at 294°K (70°F)

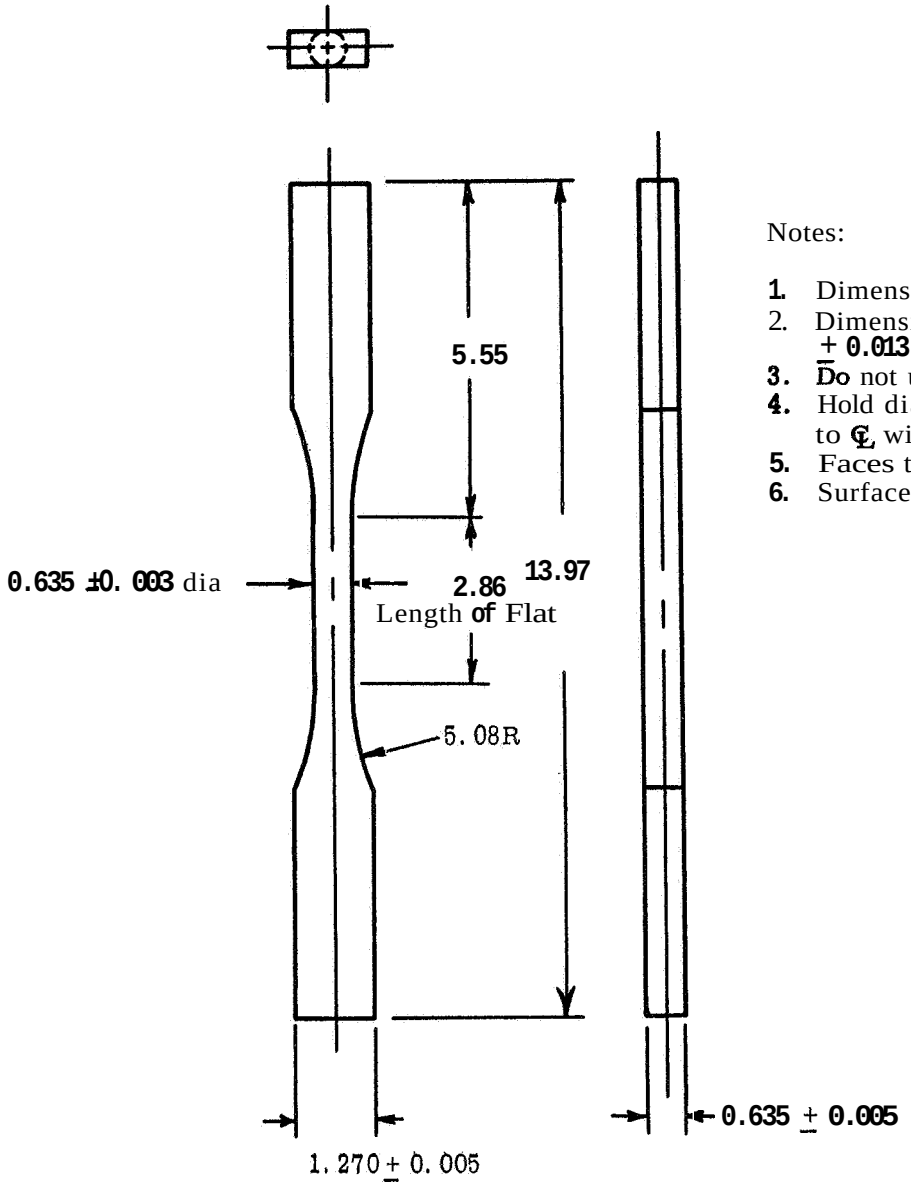

Notes:

1. Dimensions are in centimeters.
2. Dimensional tolerance unless noted: ± 0.013.
3. Do not undercut radii.
4. Hold diameter true and concentric to ℄ within 0.001.
5. Faces to be flat and parallel to ℄.
6. Surface: Grind to smooth finish.

Designation–TC2-XX-X

Figure 32. Tensile test specimen for testing for volumetric effects of phenolic-nylon in Tinius Olsen testing machine at 294°K (70°F)

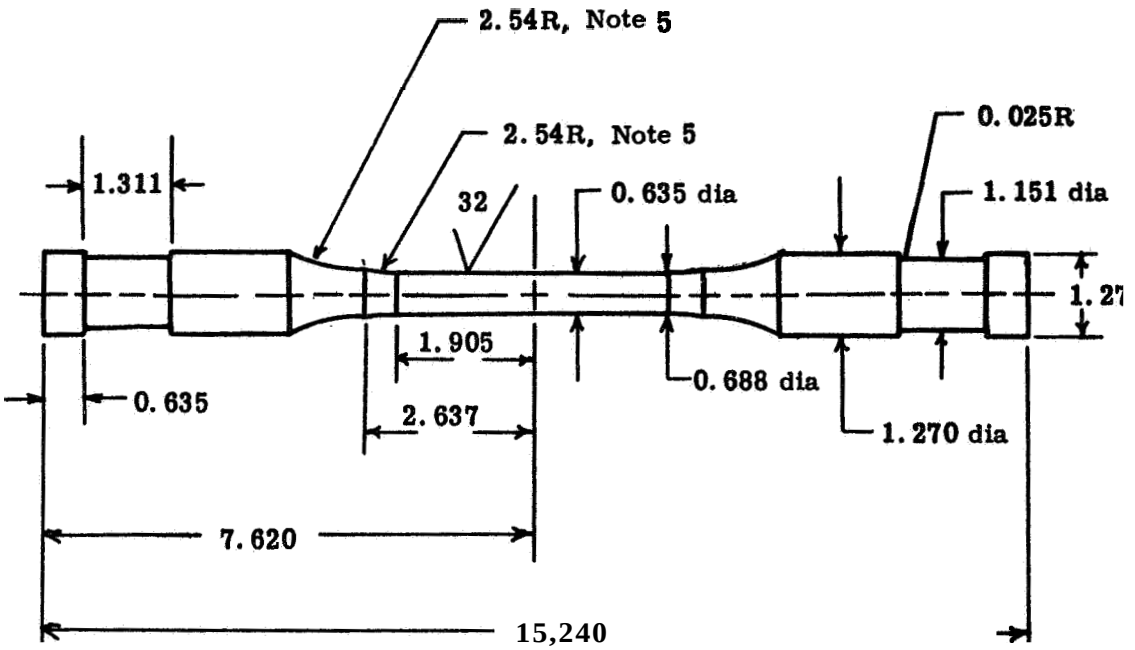

Designation - TC3-XX-X

Notes:

1. Dimensions are in centimeters
2. All diameters must be true and concentric to ± 0.0001.
3. All lengths ± 0.013
4. Both ends must be flat and perpendicular ± 0.0001.
5. Do not undercut at tangent point.

Figure 33. Tensile test specimen for testing for volumetric effects of phenolic-nylon in gas-bearing tensile testing facility at 294°K (70°F)

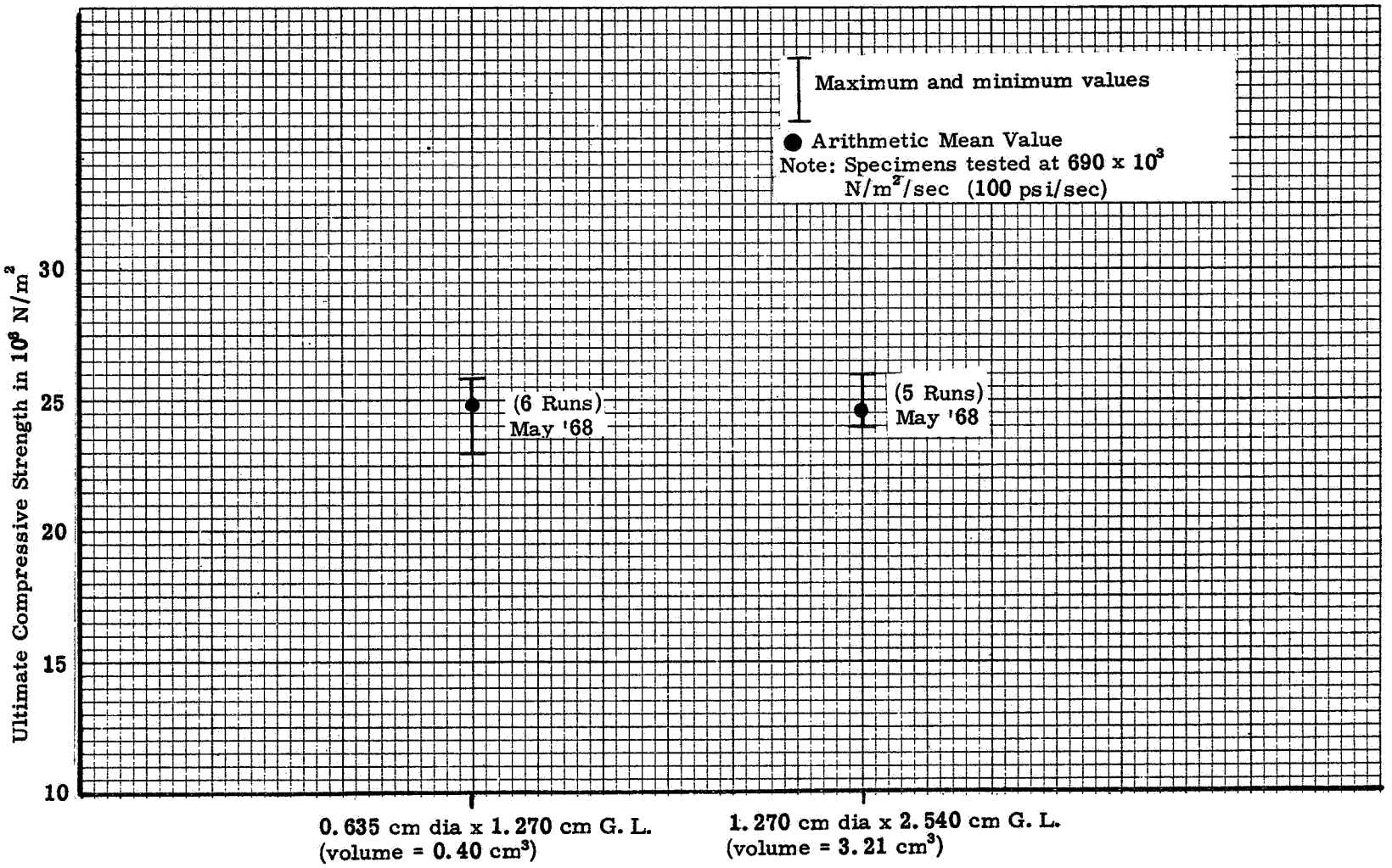

Figure 34. Volumetric effects on compressive ultimate strength for 1.270 cm dia x 2.540 cm gage length vs 0.635 cm dia x 1.270 cm gage length at 294°K (70°F)

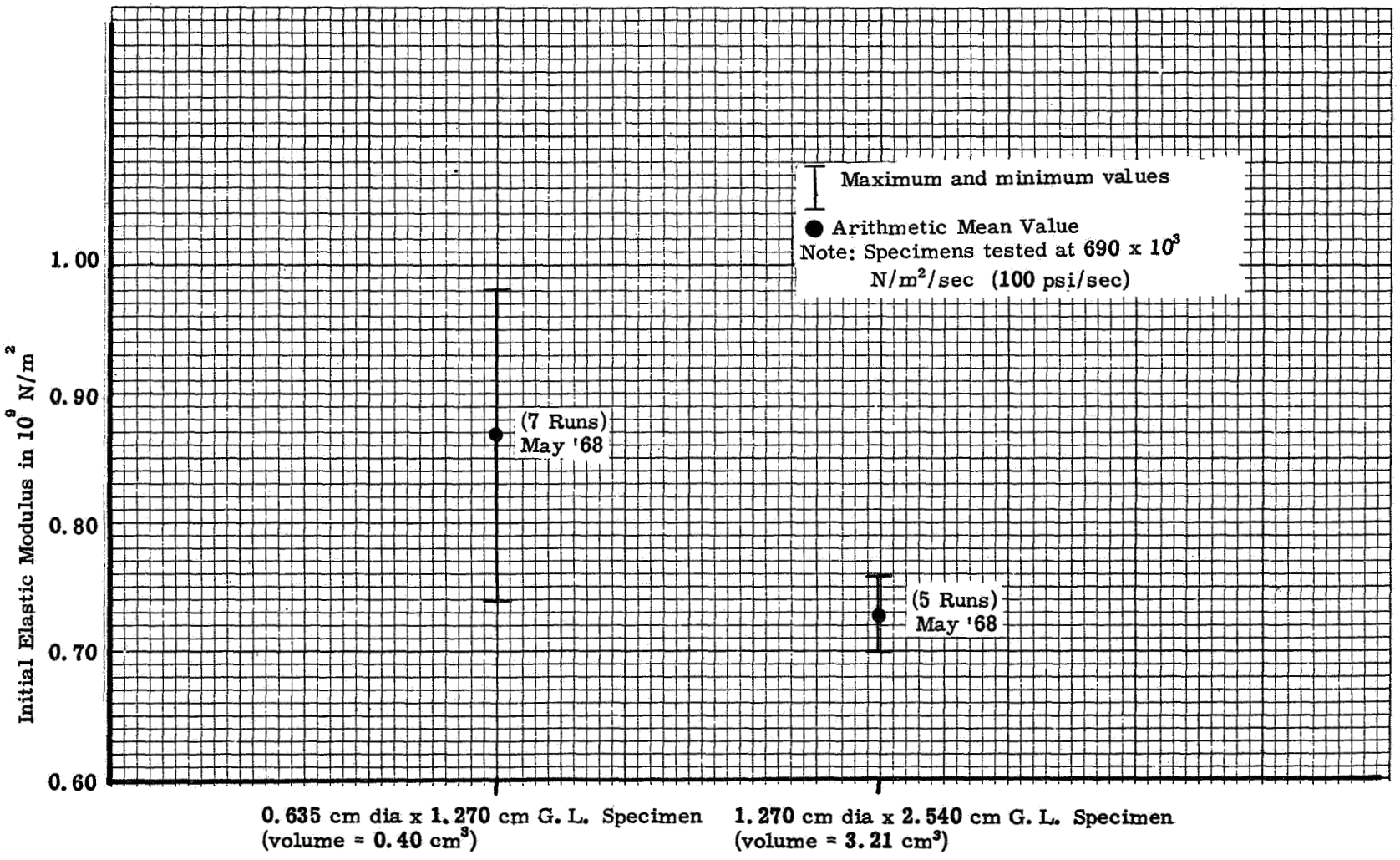

Figure 35. Volumetric effects on compressive elastic modulus for 1.270 cm dia x 2.54 cm gage length vs 0.635 cm dia x 1.270 cm gage length at 294°K (70°F)

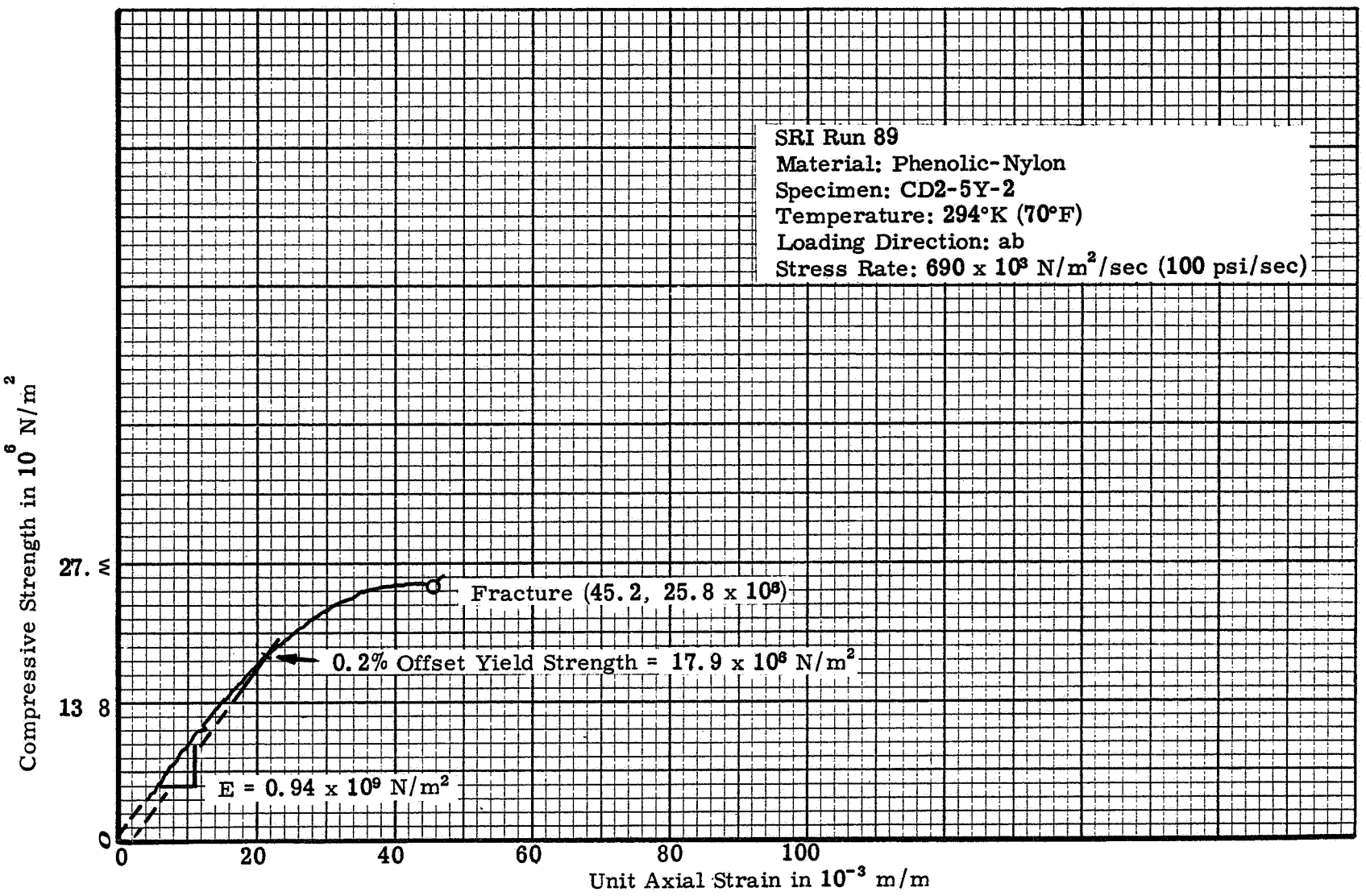

Figure 36. Typical compressive stress-strain curve for 0.635 cm dia x 1.270 cm gage length specimen tested in the ab direction for volumetric effects at 294°K (70°F)

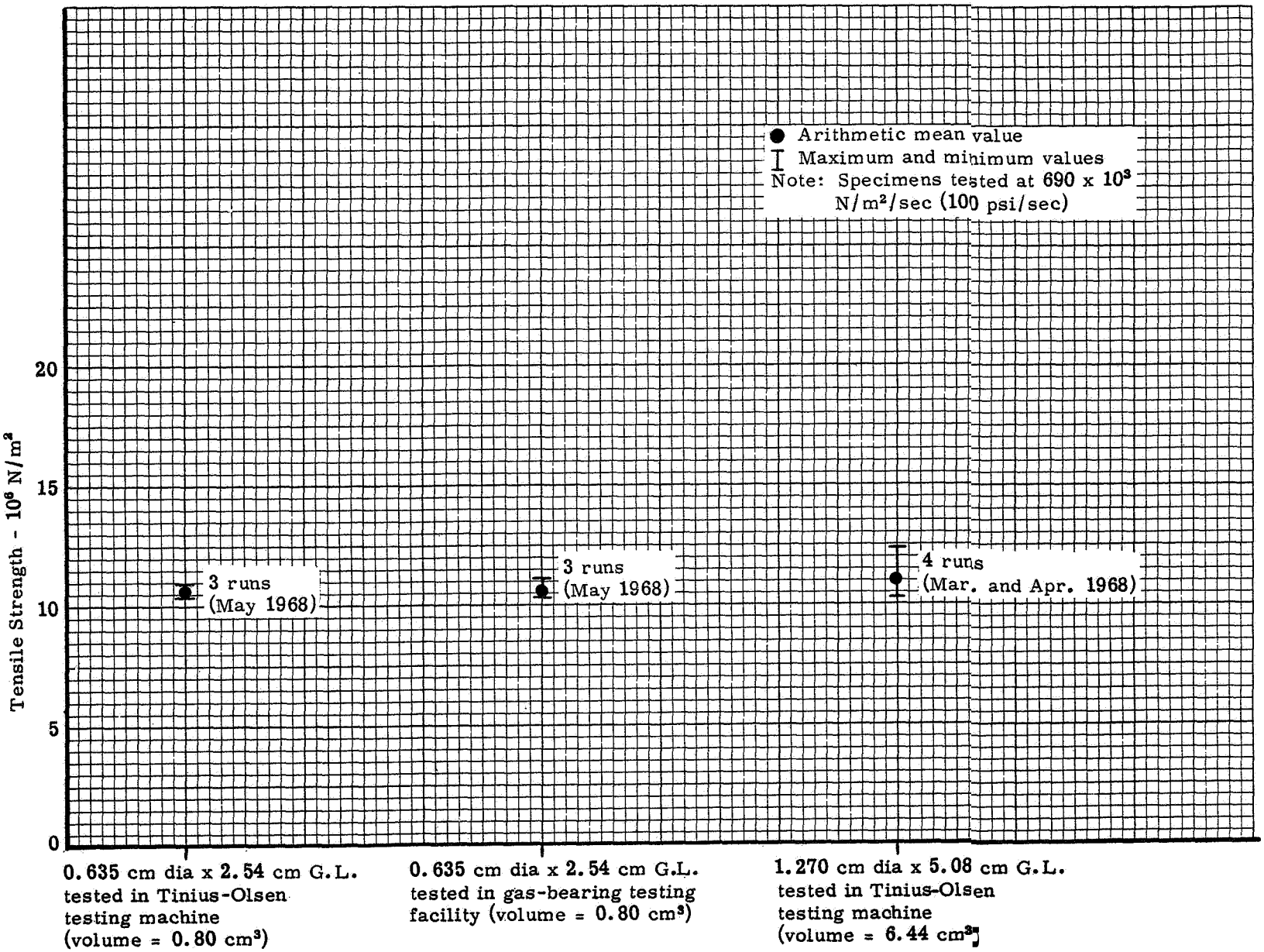

Figure 37. Volumetric effects on tensile strength for 1.270 cm dia x 5.08 cm gage length versus 0.635 cm dia x 2.54 cm gage length at 294°K (70°F) – ground gage section

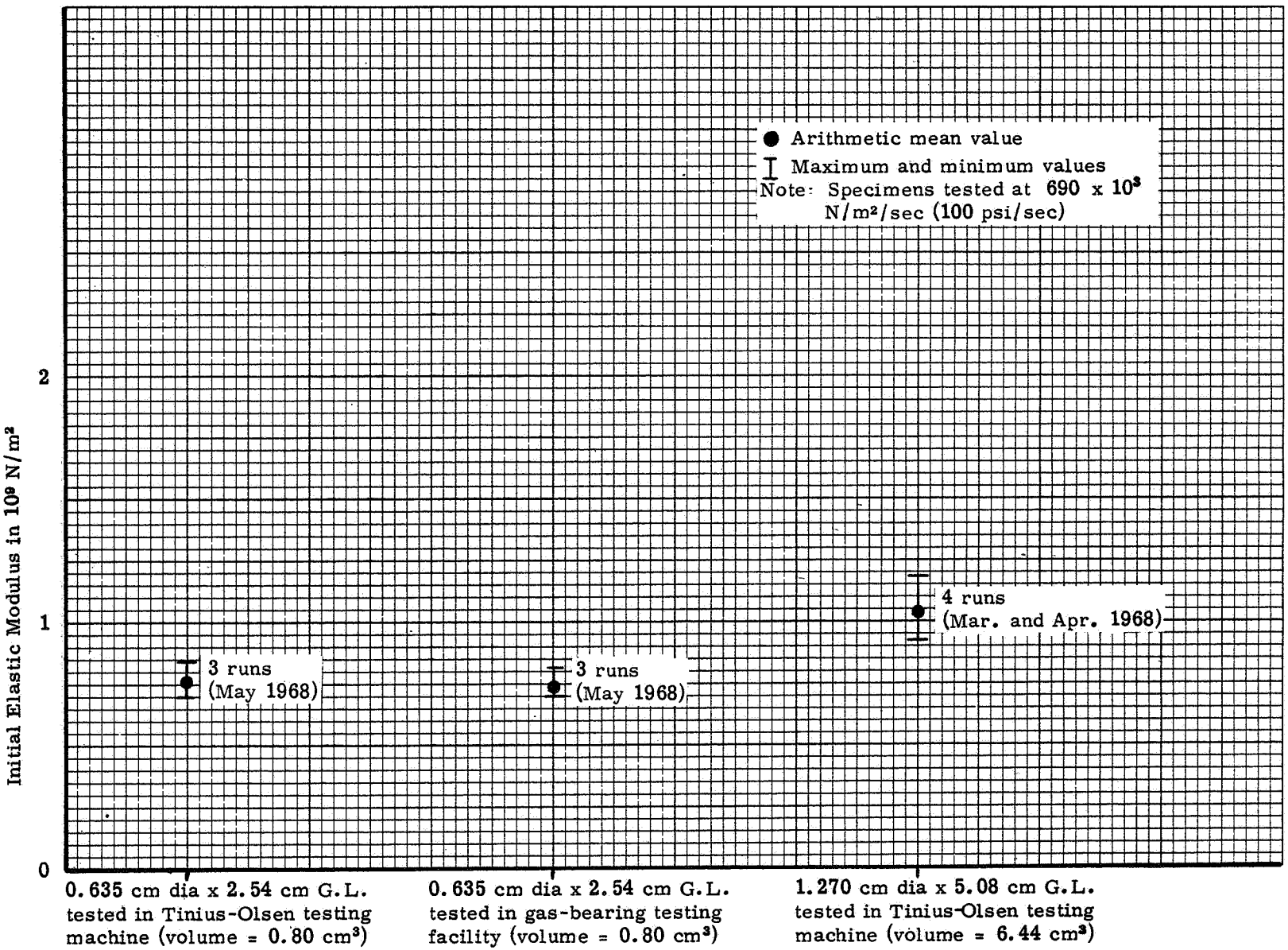

Figure 38. Volumetric effects on tensile elastic modulus for 1.270 cm dia x 5.08 cm gage length versus 0.635 cm dia x 2.54 cm gage length at 294°K (70°F) – ground gage section

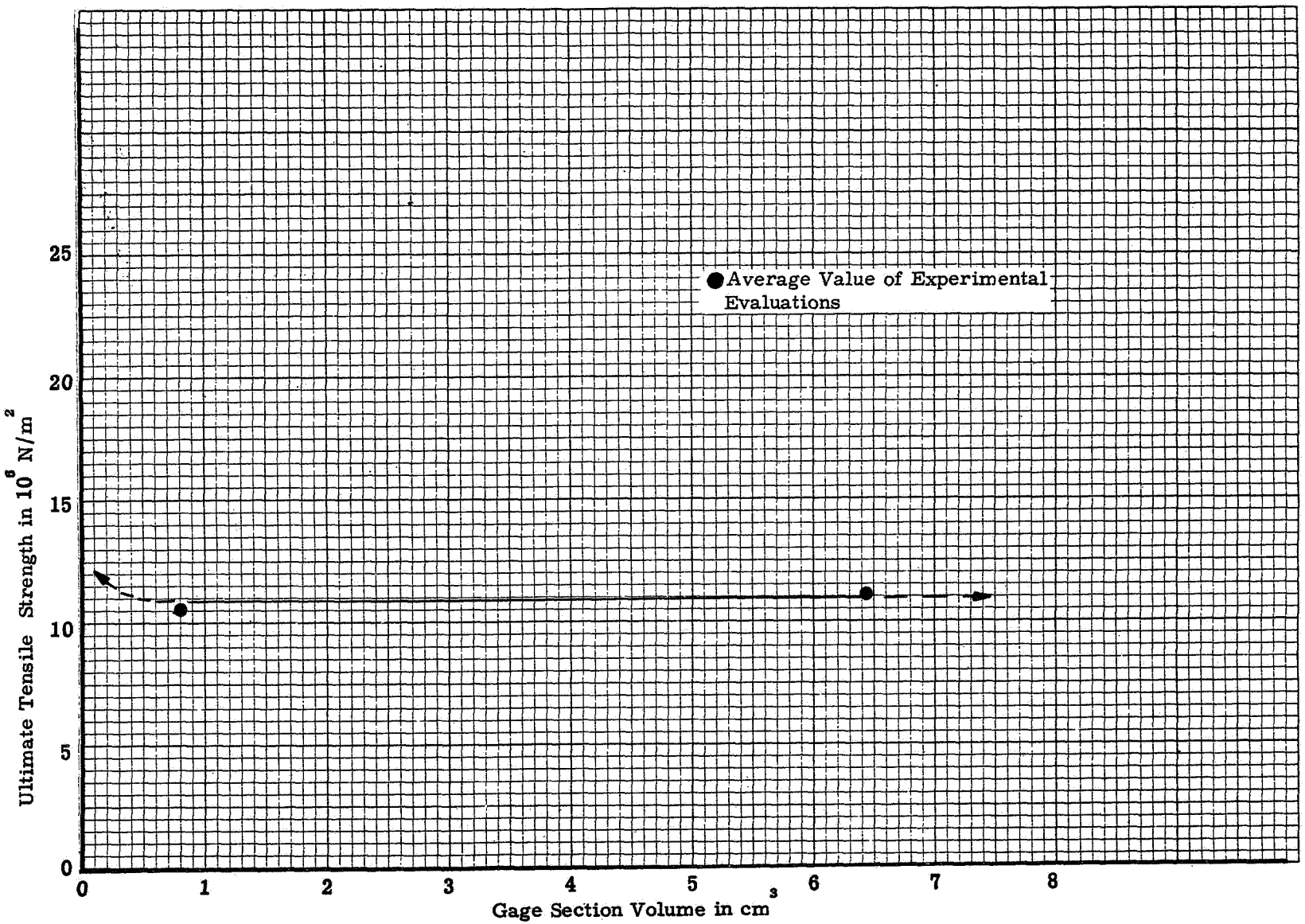

Figure 39. Volumetric effects on tensile ≡tr gᗡ

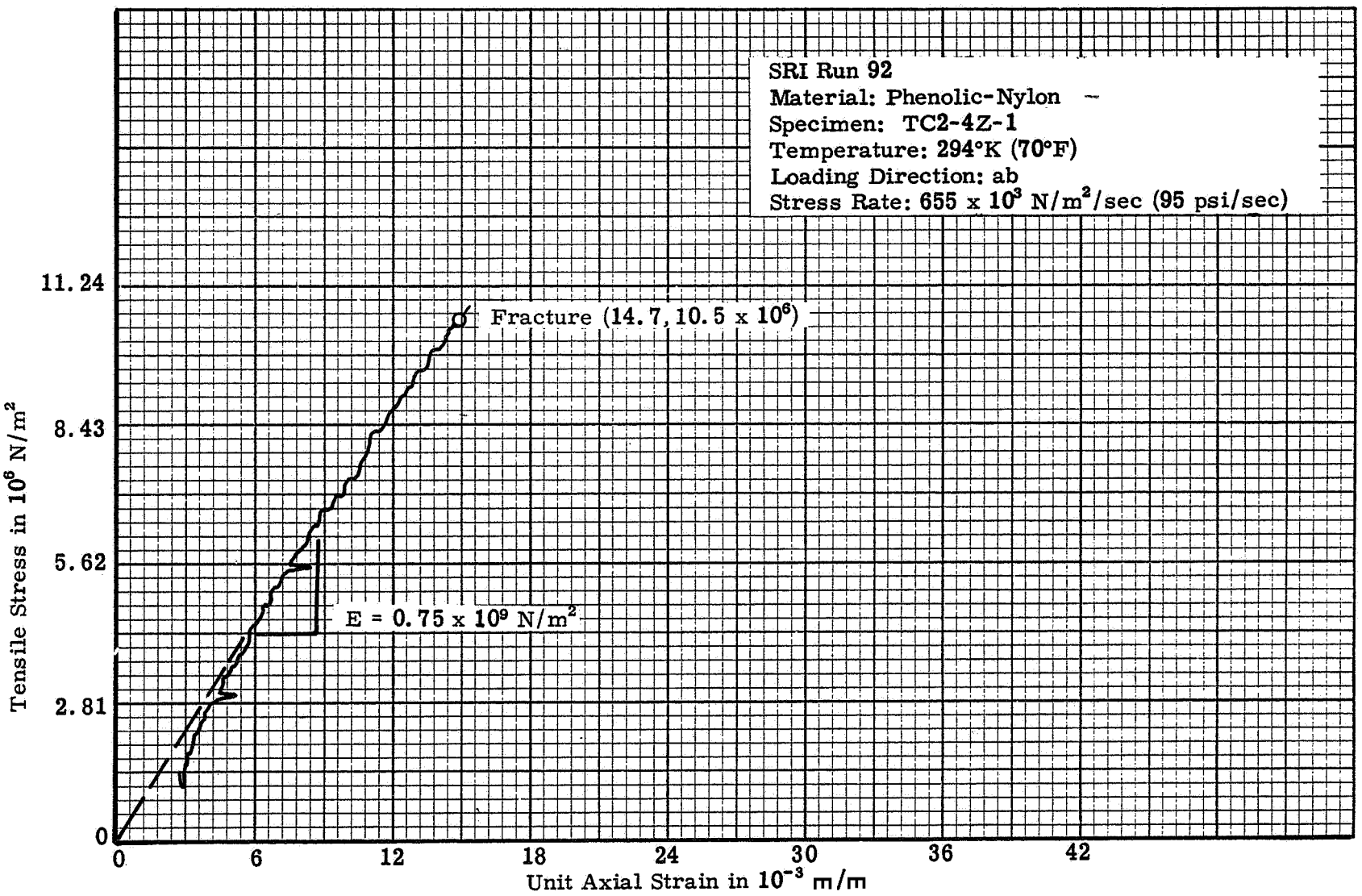

Figure 40. Typical tensile stress-strain curve for 0.635 cm dia x 2.54 cm gage length specimen tested in the Tinius-Olsen testing machine in the ab direction for volumetric effects at 294°K (70°F)

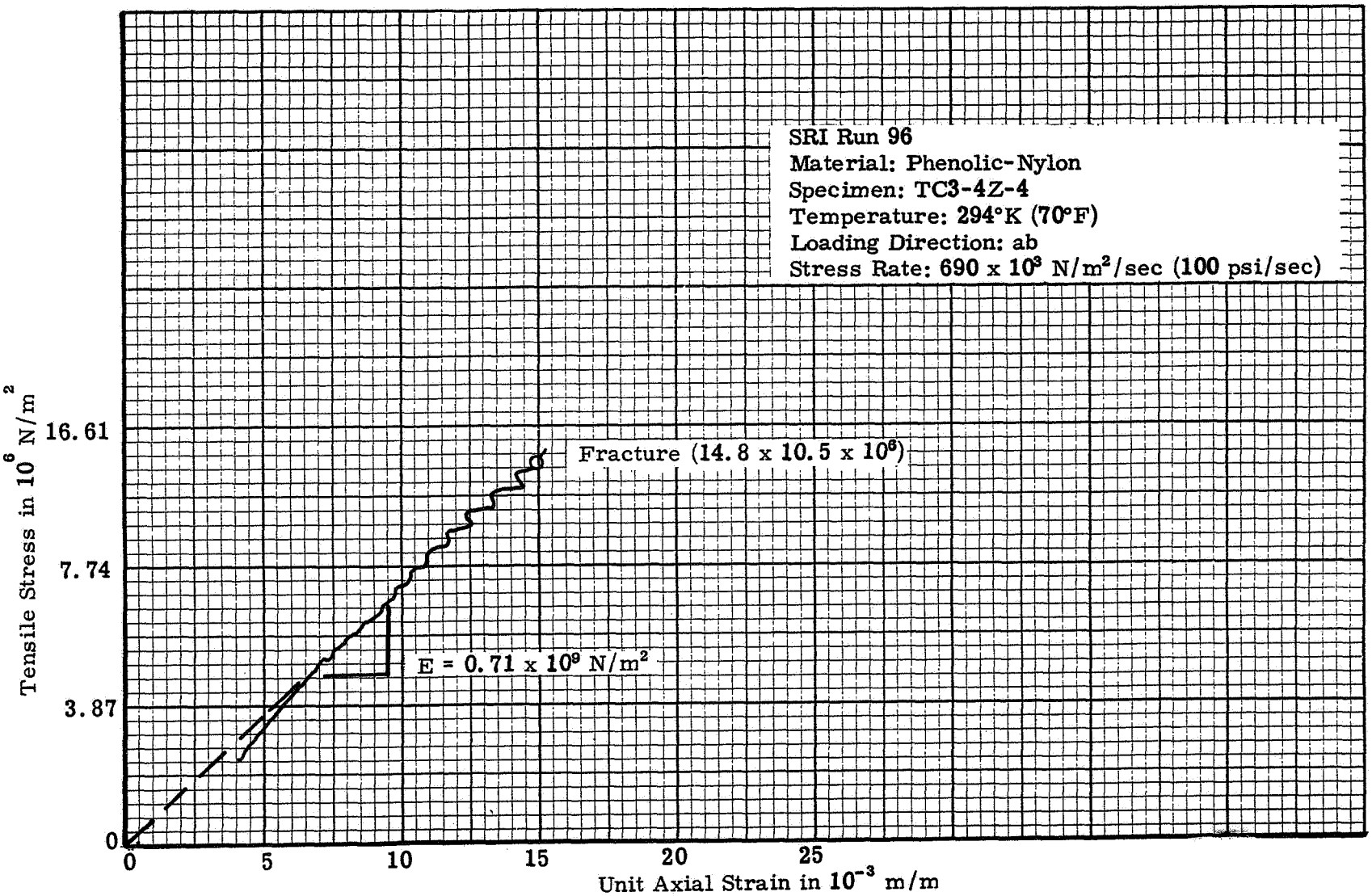

Figure 41. Typical test stress-strain curve for 0.635 dia x 2.54 cm gage length specimen tested in gas-bearing facility in the ab direction for volumetric effects at 294°K (70°F)

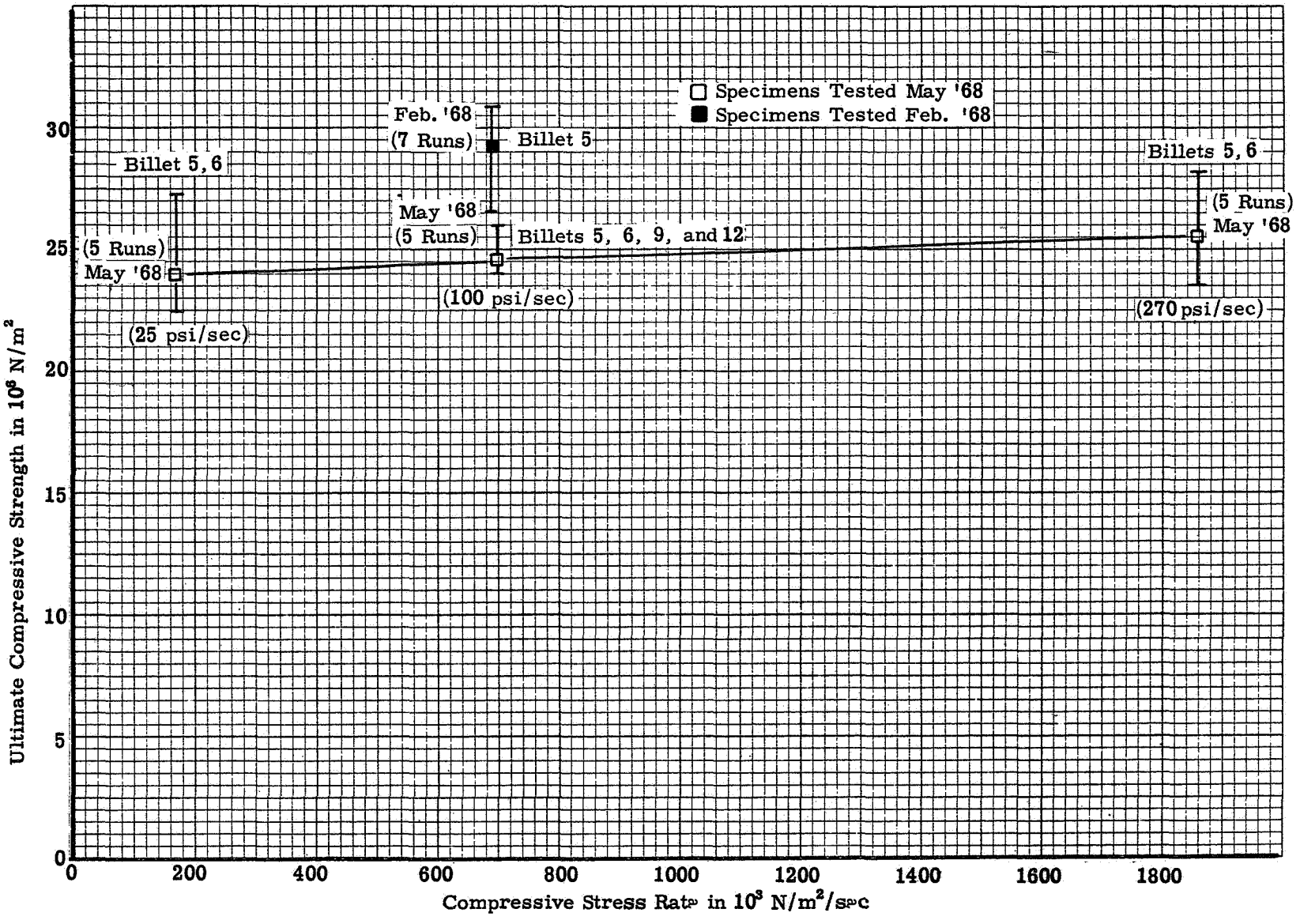

Figure 42. Compressive ultimate strength for stress rates of 172, 690, and 1860 x 10^3 N/m^2/sec for 1.270 cm dia x 2.54 cm gage length specimen tested at 294°K (70°F)

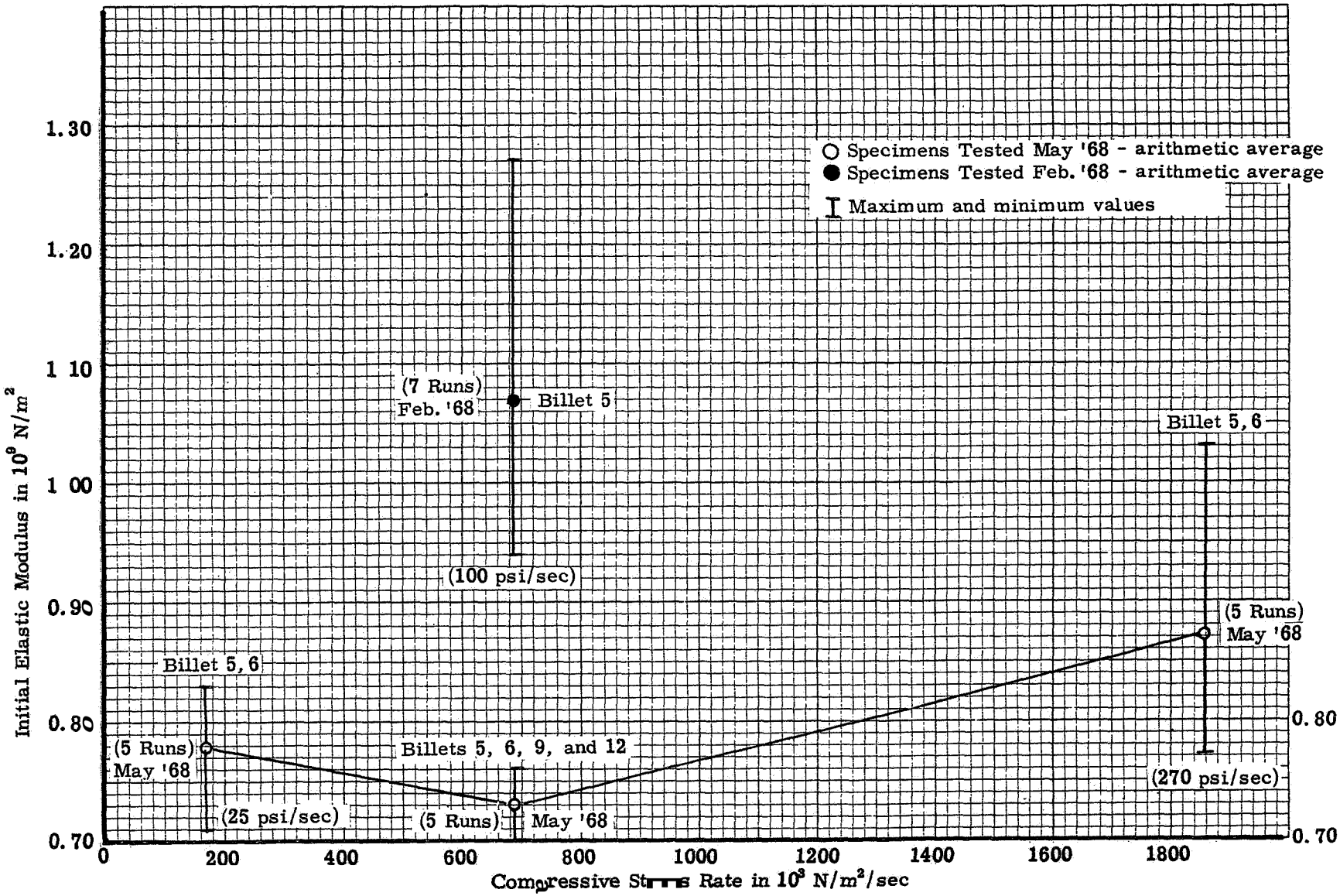

Figure 43. Compressive initial elastic modulus for stress rates of 172, 690, and 1850 x 10^3 N/m^2/sec for 1.270 cm dia x 2.54 cm gage length specimens tested at 294°K (70°F)

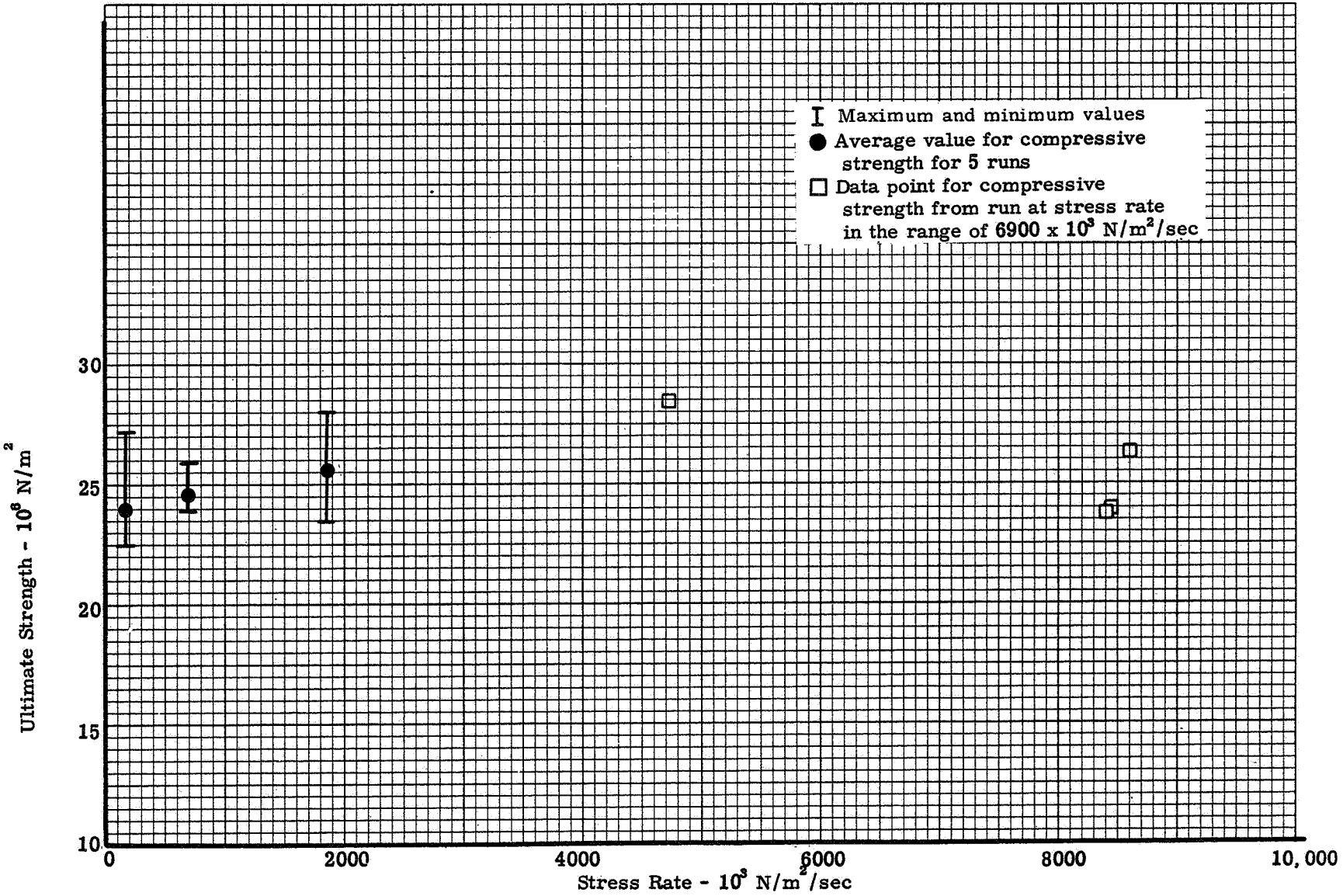

Figure 44. Ultimate strength in compression versus stress rate from 170 x 10^3 to 8600 x 10^3 N/m^2/sec in the ab direction at 294°K (70°F)

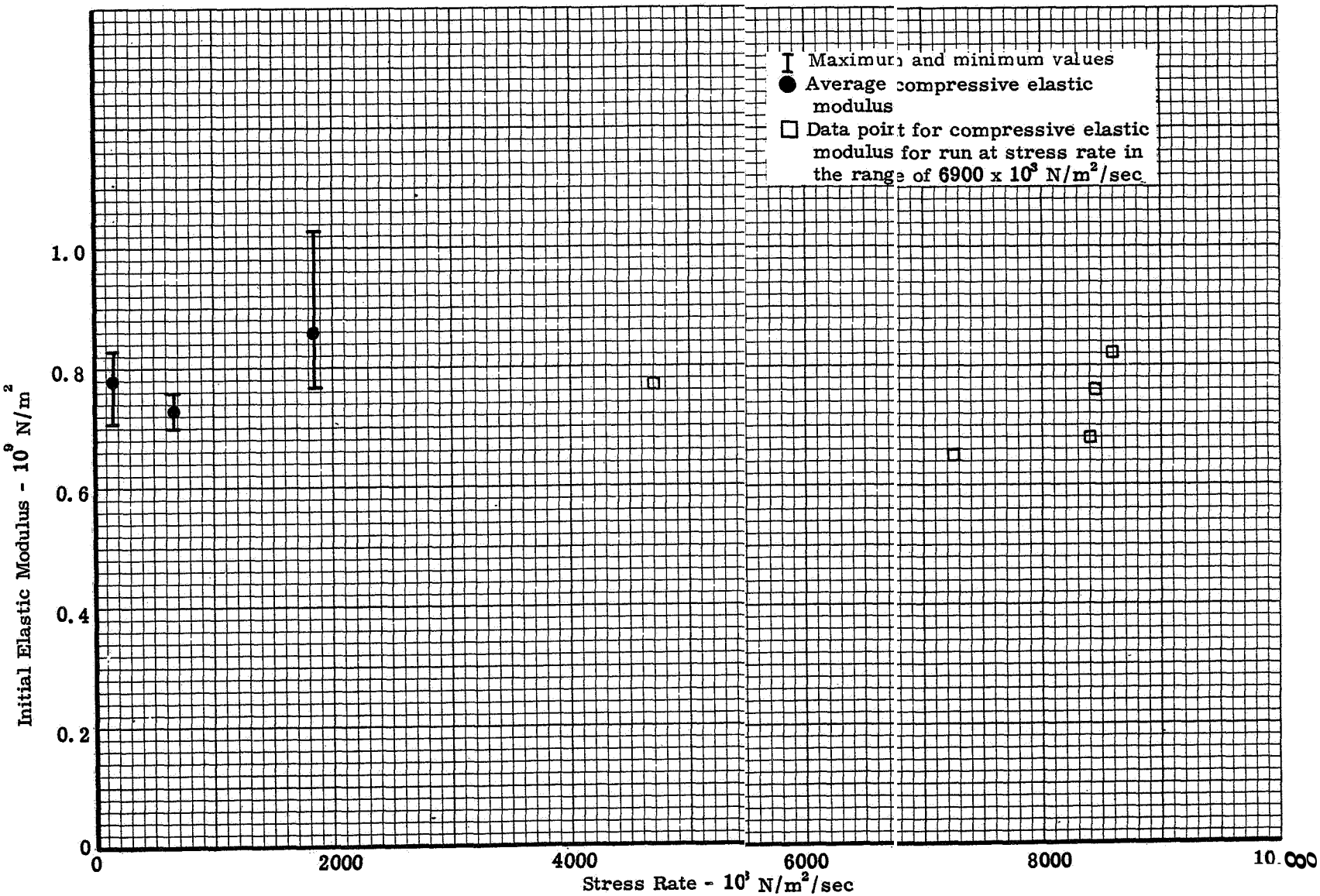

Figure 45. Initial elastic modulus in compression versus stress rate for stress rates from 170×10^3 to 8600×10^3 $N/m^2/sec$ in the ab direction at 294°K (70°F)

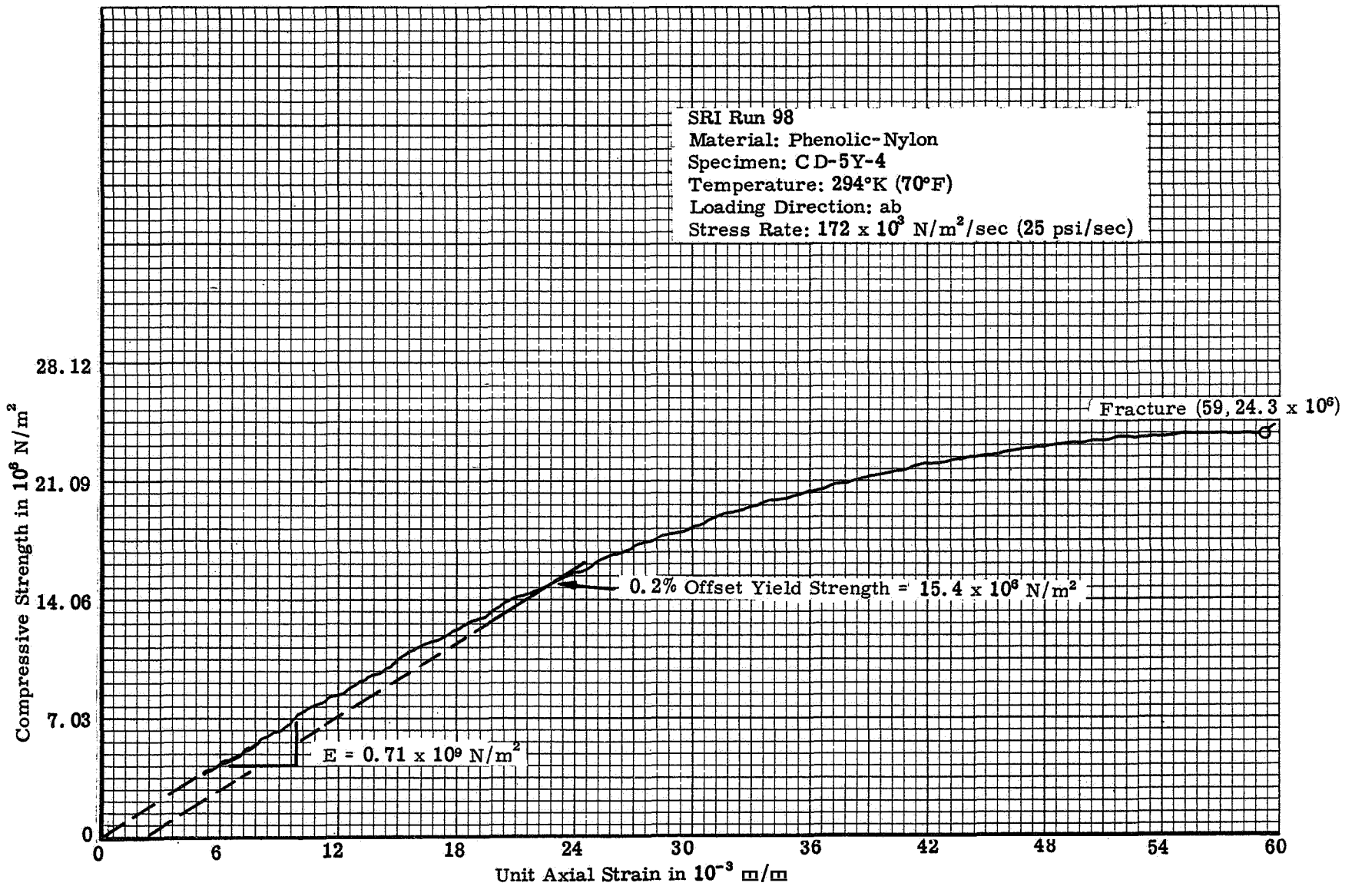

Figure 46. Typical compressive stress-strain curve for 1.270 cm dia x 2.54 gage length specimen tested in the ab direction at 172 x 103 N/m^2/sec for stress rate effects at 294°K (70°F)

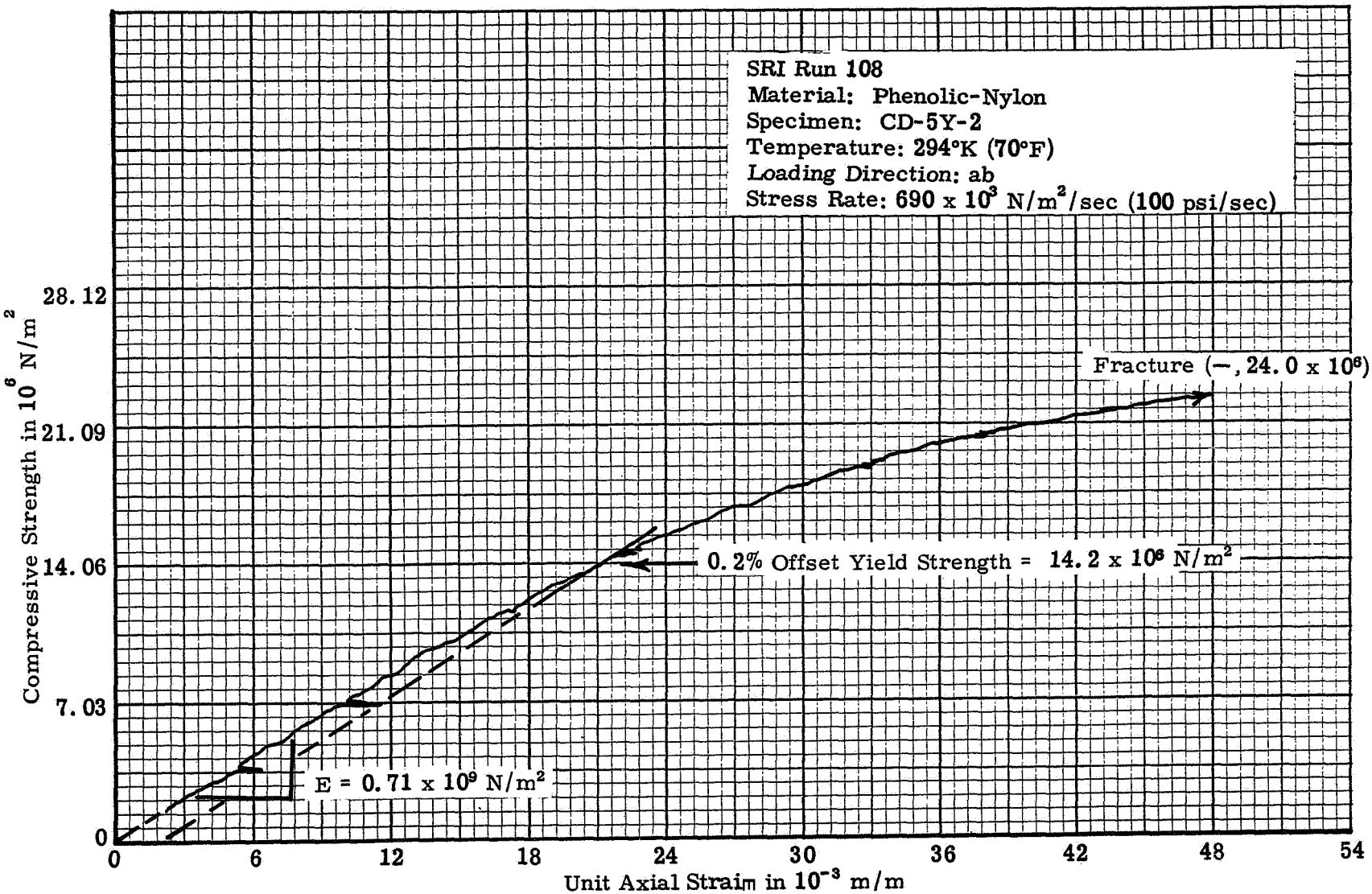

Figure 47. Typical compressive stress-strain curve for 1.270 cm dia x 2.54 cm gage length specimen tested in the ab irection at 690 x 10^3 N/m^2/sec for stress rate effects at 294°K (70°F)

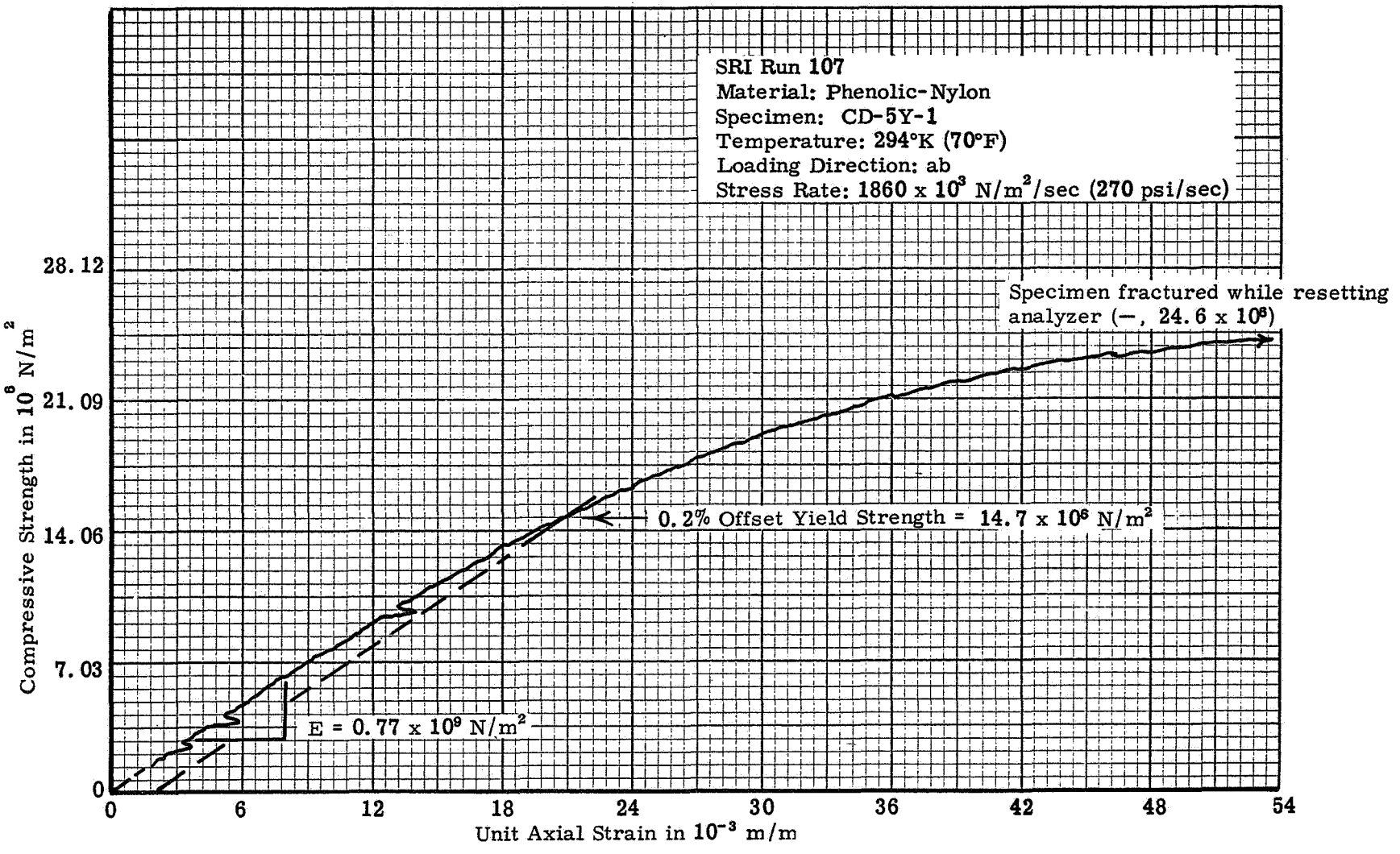

Figure 48. Typical compressive stress-strain curve for 1.270 cm dia x 2.54 cm gage length specimen tested in the ab direction at 1860 x 10^3 N/m^2/sec for stress rate effects at 294°K (70°F)

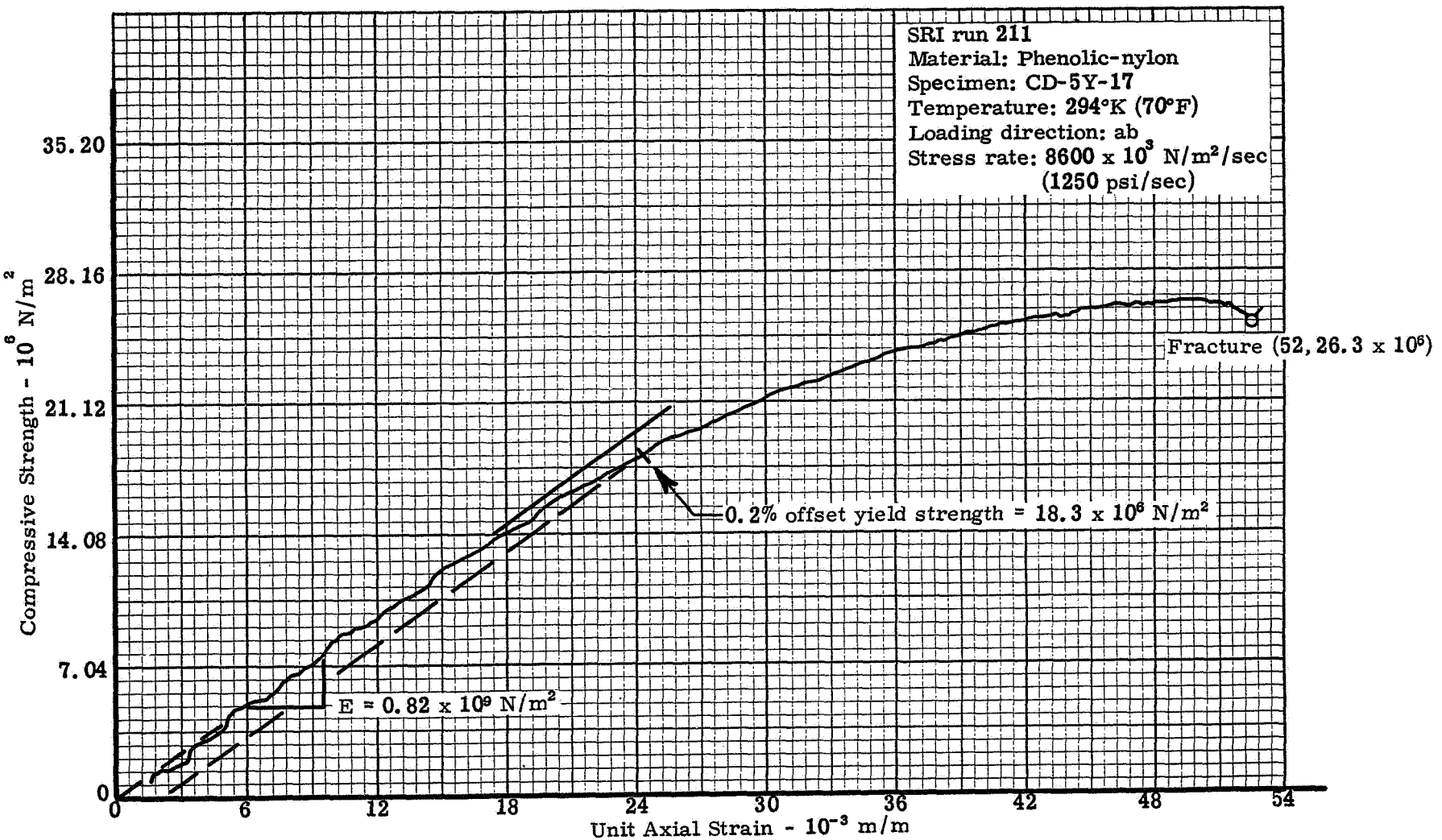

Figure 49. Compressive stress-strain curve for 1.270 cm dia x 2.54 cm gage length specimen tested in ab direction for stress-rate effects in the range of 6900 x 10^3 N/m²/sec (1000 psi/sec) at 294°K (70°F)

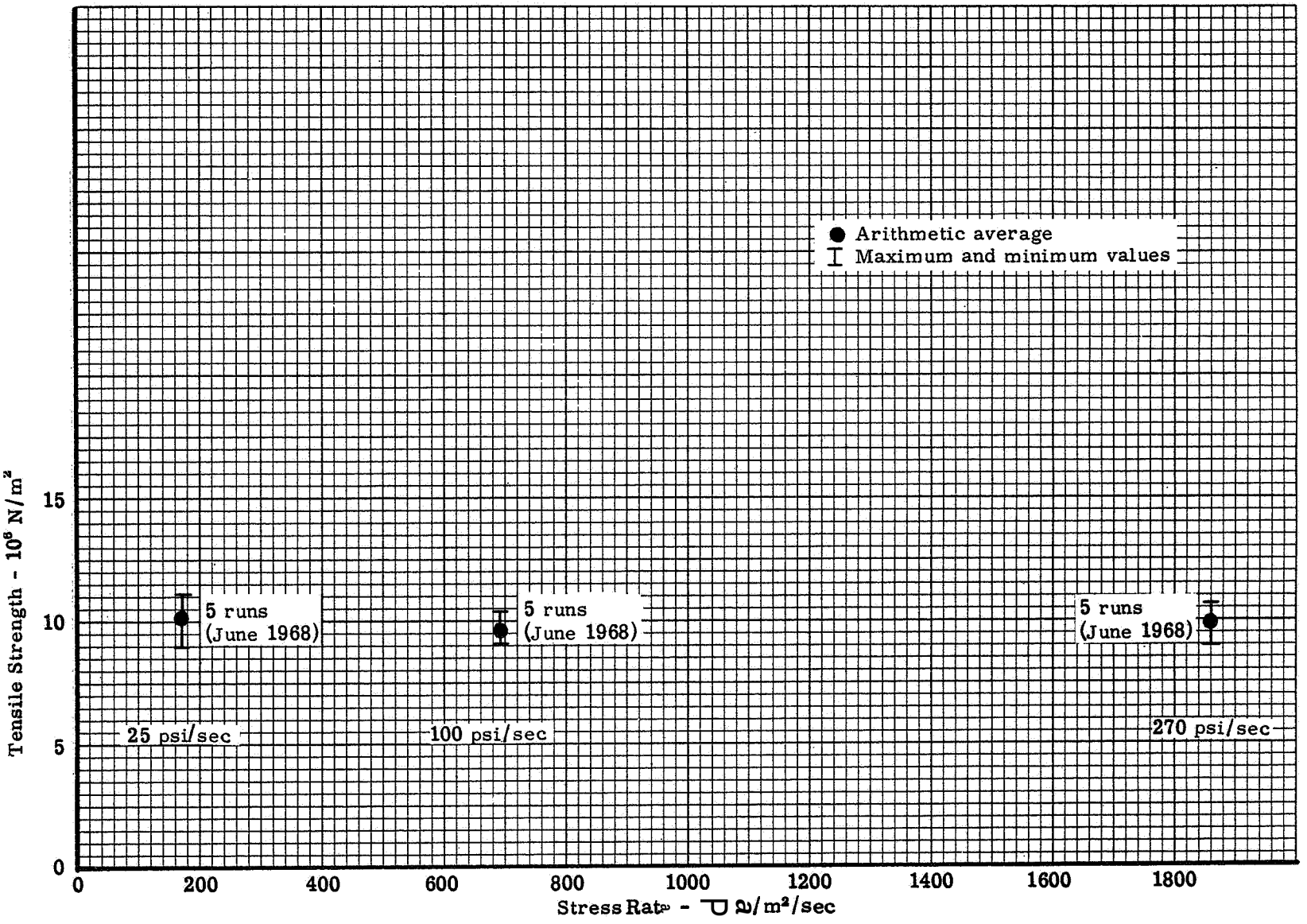

Figure 50. Ultimate tensile strength for stress rates of 172 x 10^3 , 690 x 10^3, and 1860 x 10^3 N/m^2/sec for 1.270 cm dia x 2.54 cm gage length specimen tested at 294°K (70°F)

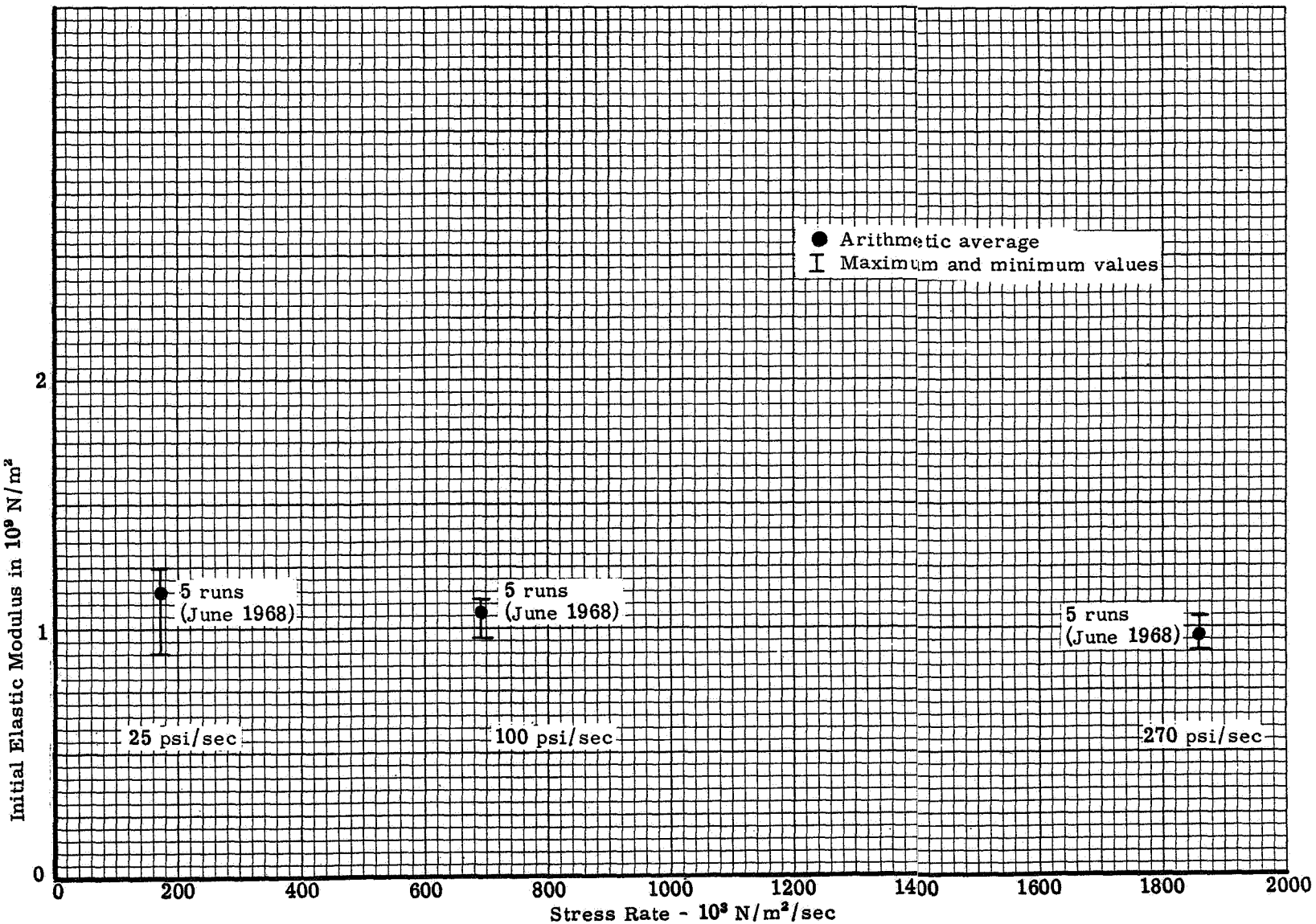

Figure 51. Initial tensile elastic modulus for stress rates of 172 x 10^3, 690 x 10^3 and 1860 x 10^3 N/m^2/sec for 1.270 cm dia x 2.54 cm gage length specimen tested at 294°K (70°F)

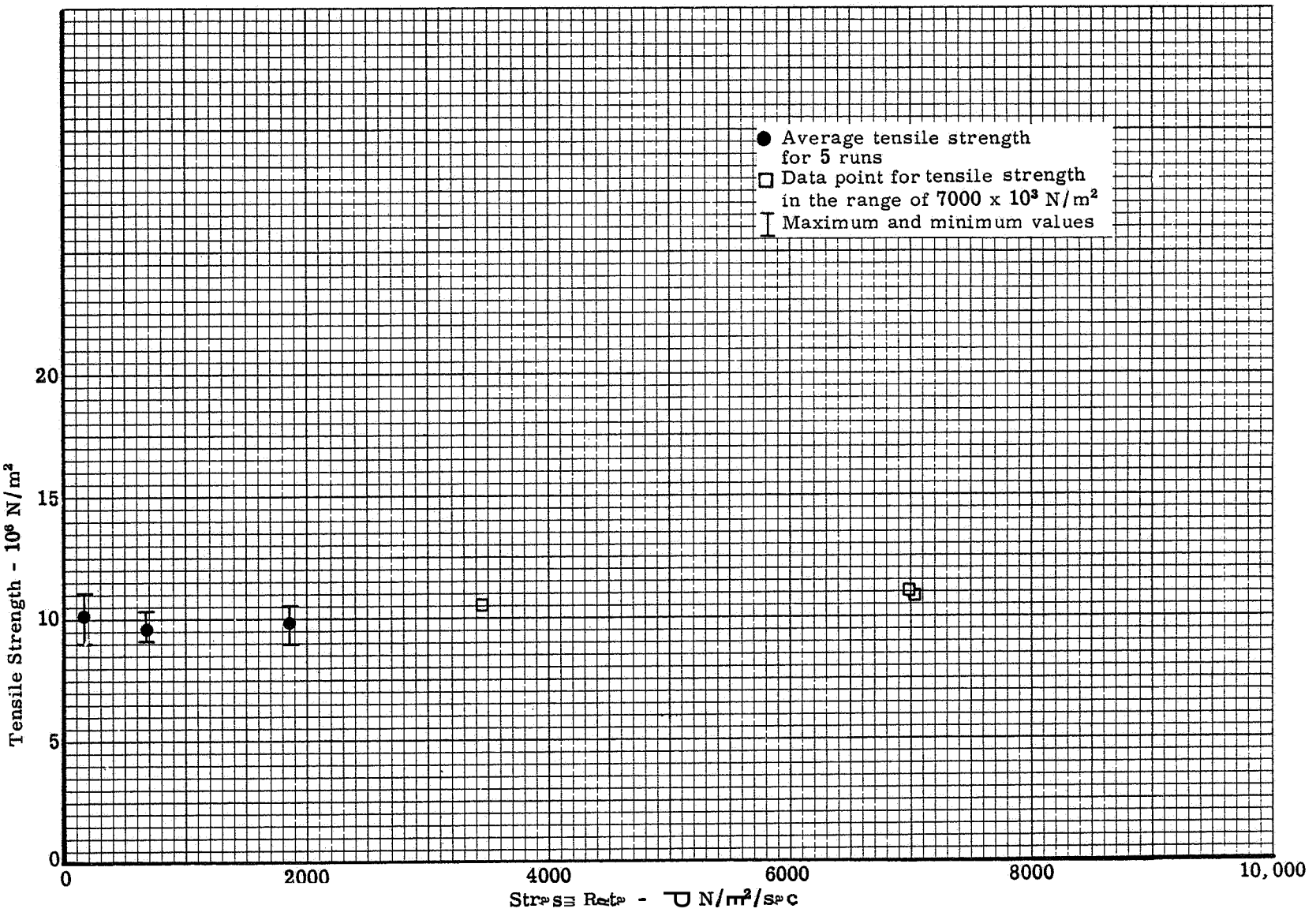

Figure 52. Ultimate strength in tension versus stress rate from 170 x 10^3 to 7000 x 10^3 N/m^2/sec in the ab direction at 294°K (70°F)

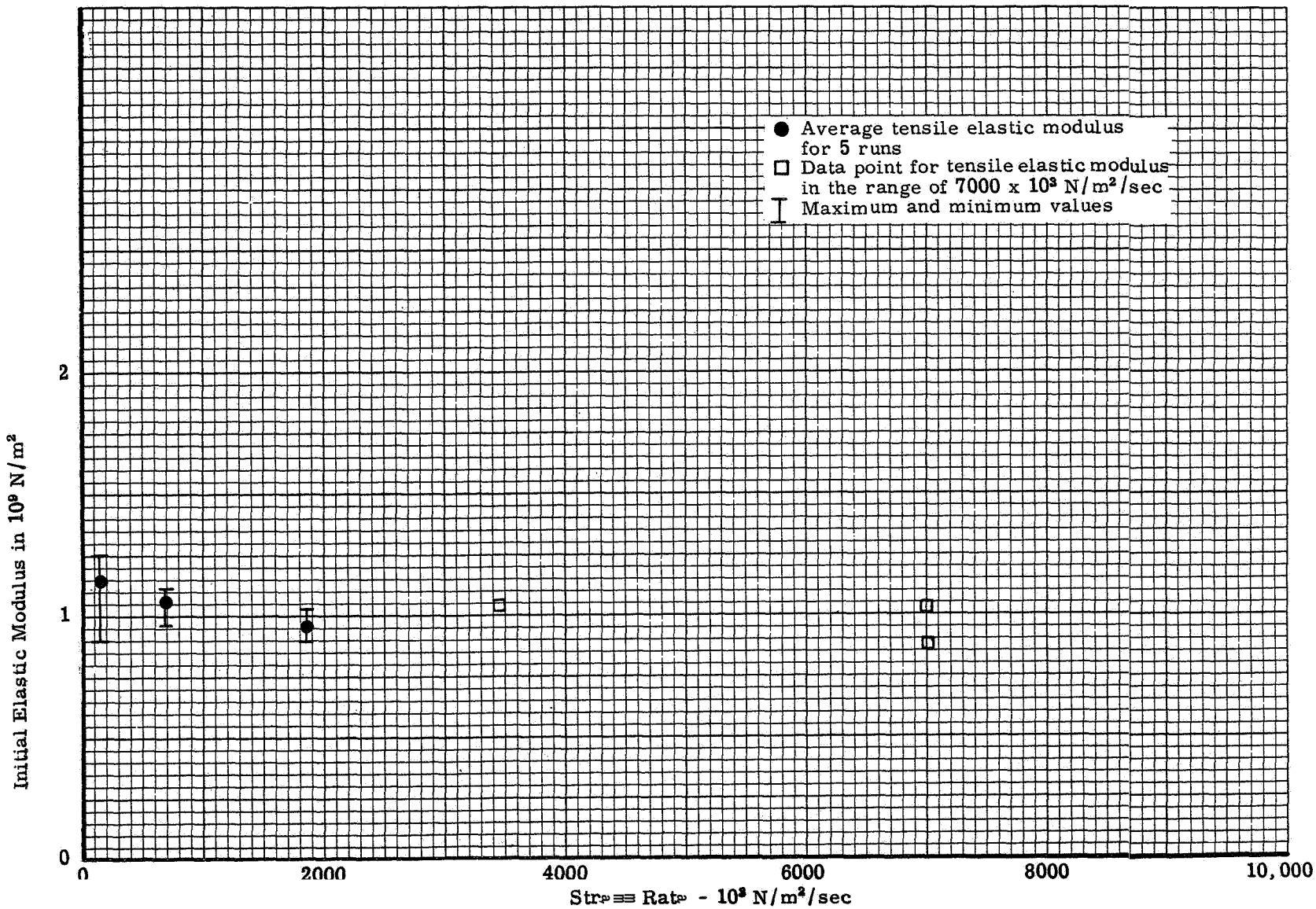

Figure 53. Initial elastic modulus in tension versus stress rate for stress rates from 170 × 10^3 to 7000 x 10^3 N/m²/sec in the ab direction at 294°K (70°F)

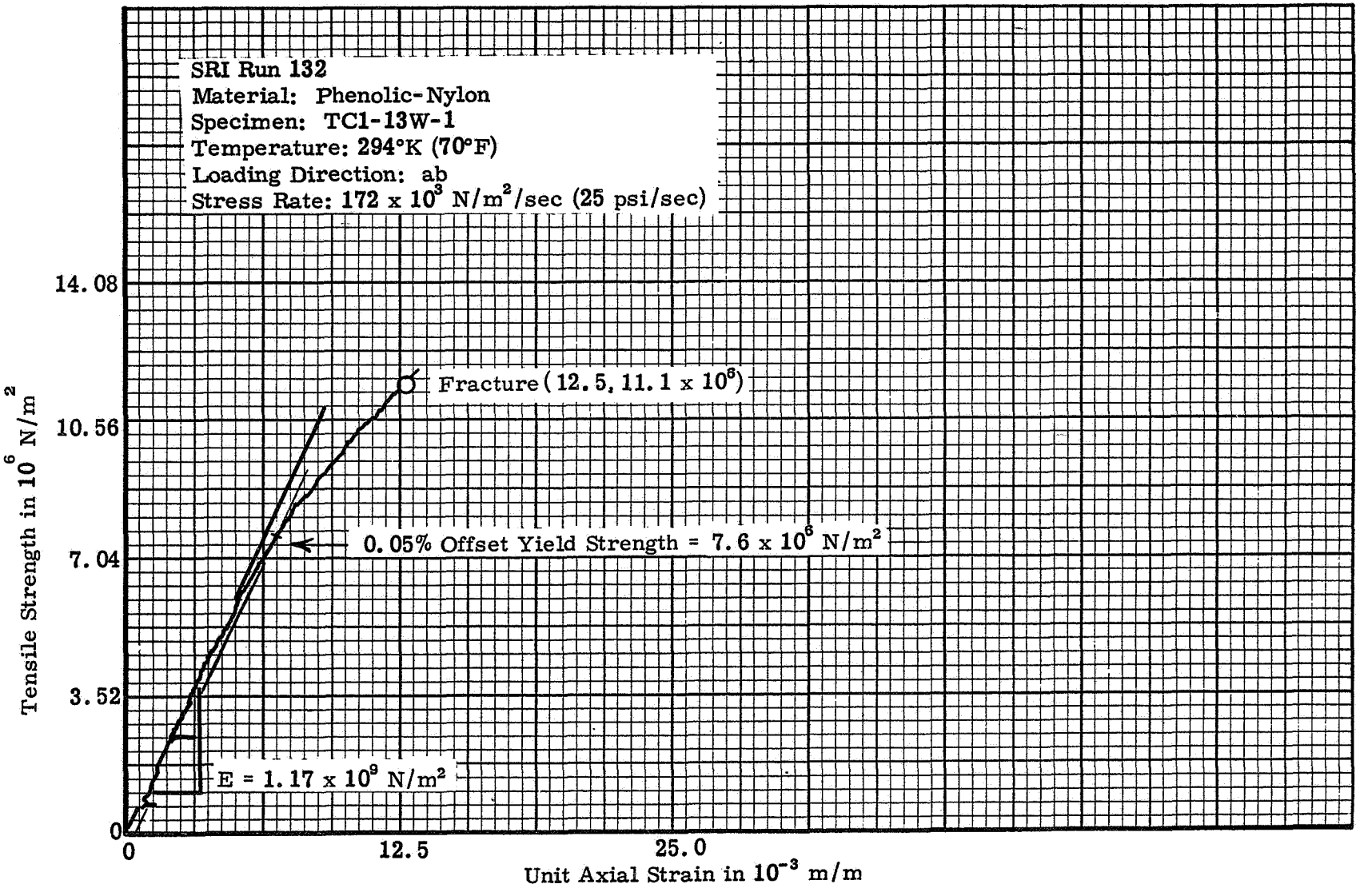

Figure 54. Typical tensile stress-strain curve for 1.270 cm dia x 5.08 cm gage length specimen tested in ab direction at 172 x 10^3 N/m^2/sec for stress rate effects at 294°K (70°F)

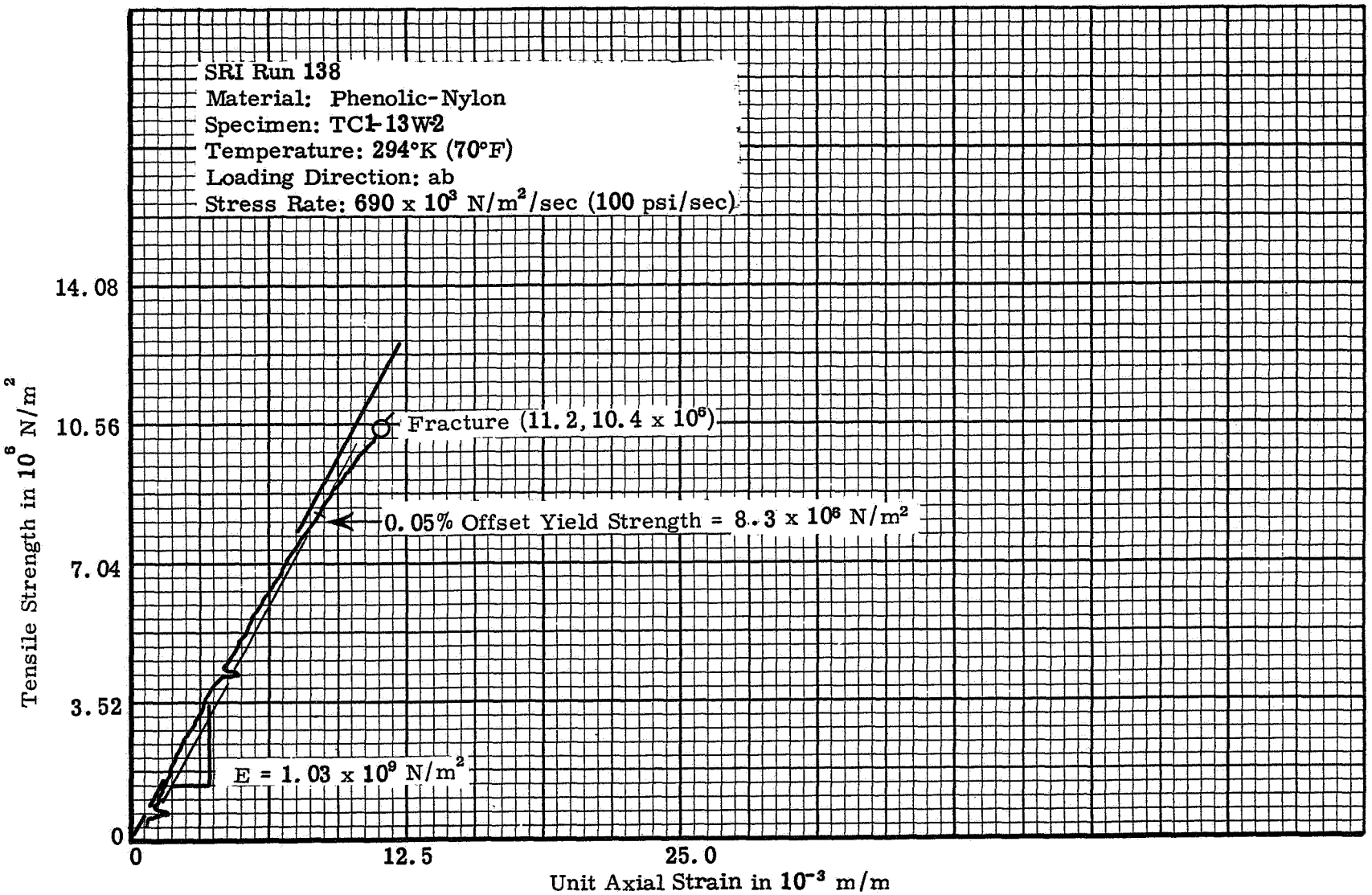

Figure 55. Typical tensile stress-strain curve for 1.270 cm dia x 5.08 cm gage length specimen tested in ab direction at 690 x 10^3 N/m^2/sec for stress rate effects at 294°K (70°F)

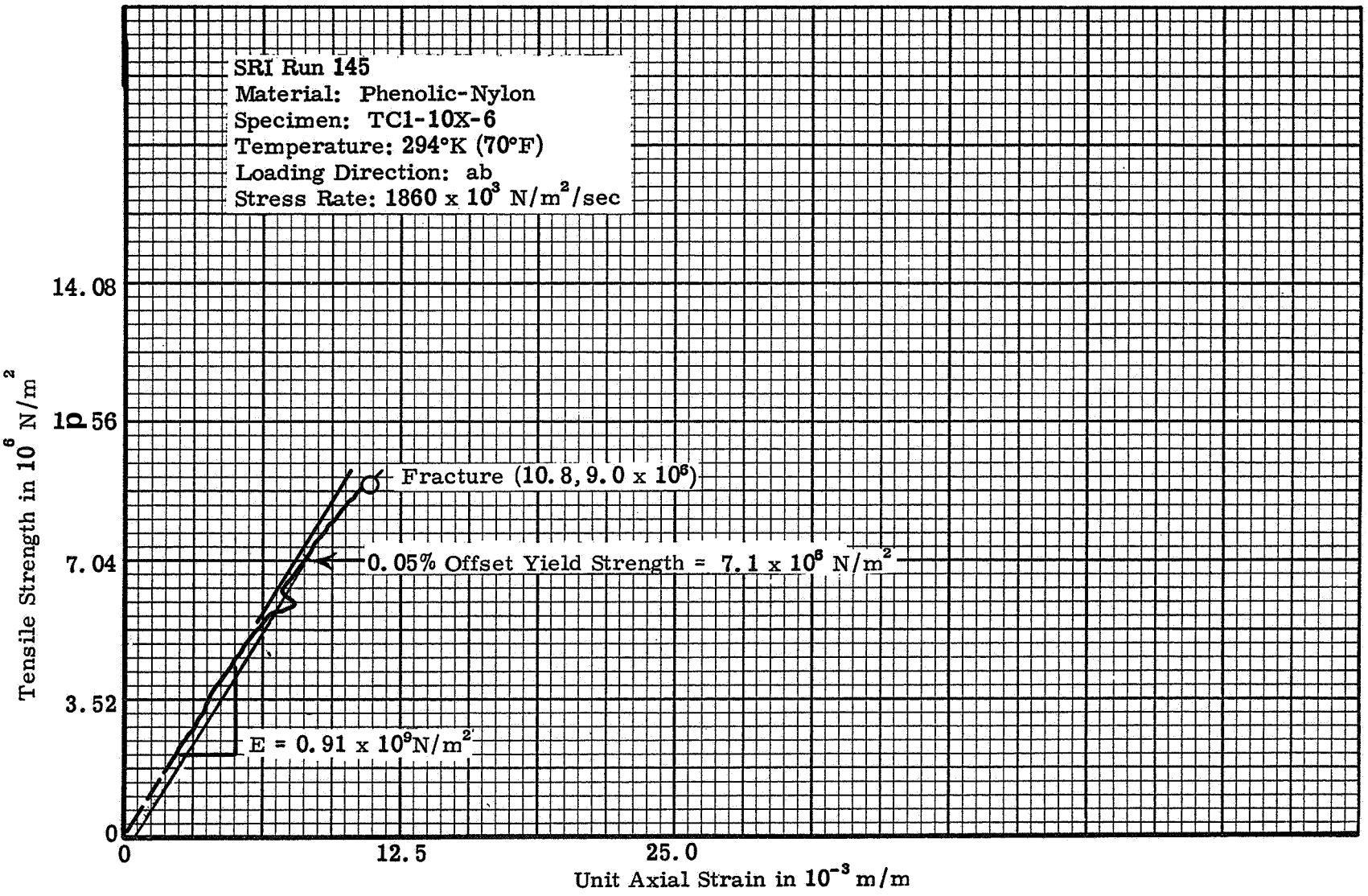

Figure 56. Typical tensile stress-strain curve for 1.270 cm dia x 5.08 cm gage length specimen tested in ab direction at 1860 x 10^3 N/m²/sec for stress rate effects at 294°K (70°F)

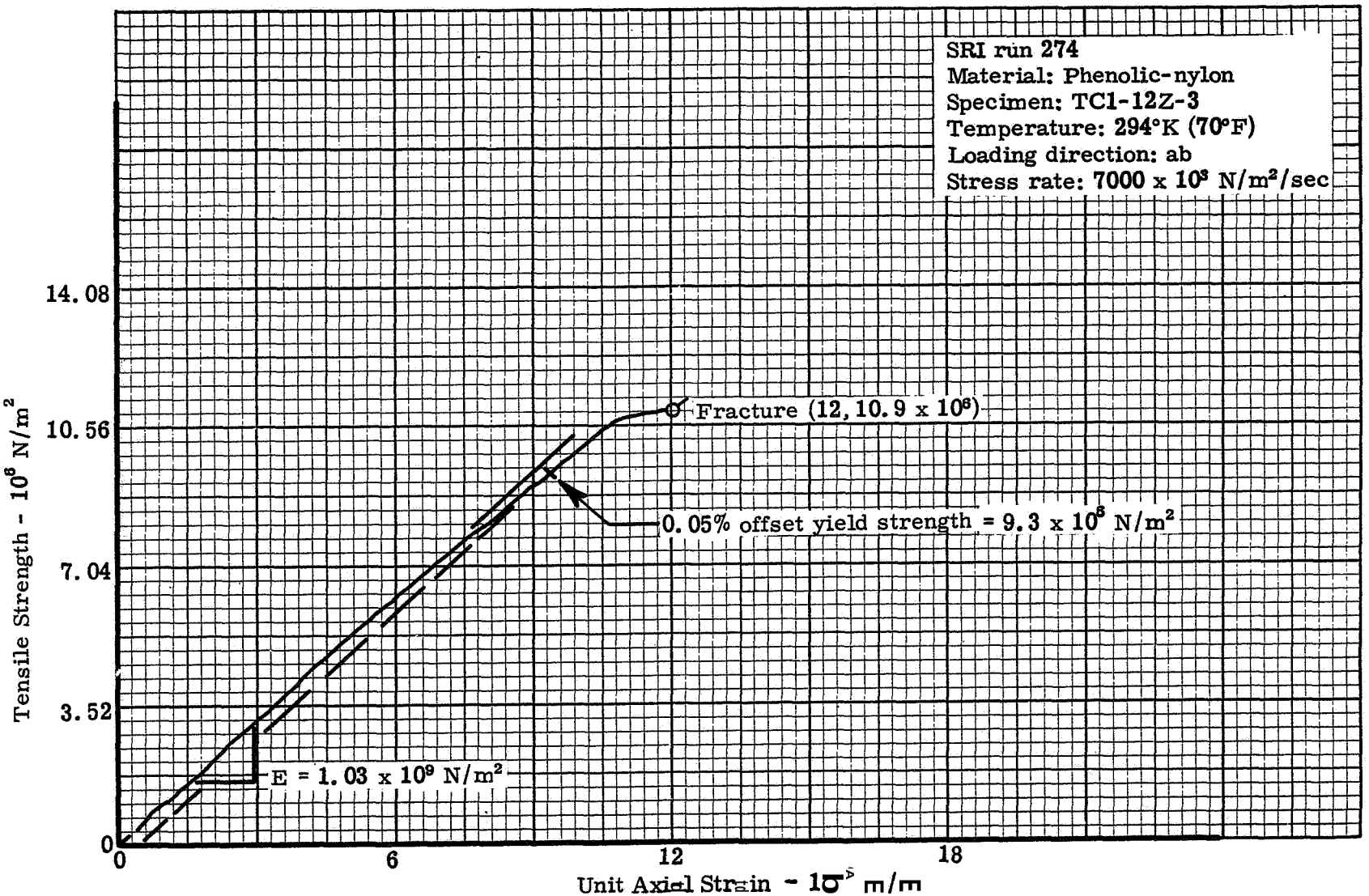

Figure 57. Typical tensile stress-strain curve for 1.270 cm dia x 5.08 cm gage length specimen tested in ab direction at 7000 x 10^3 N/m^2/sec for stress rate effects at 294°K (70°F)

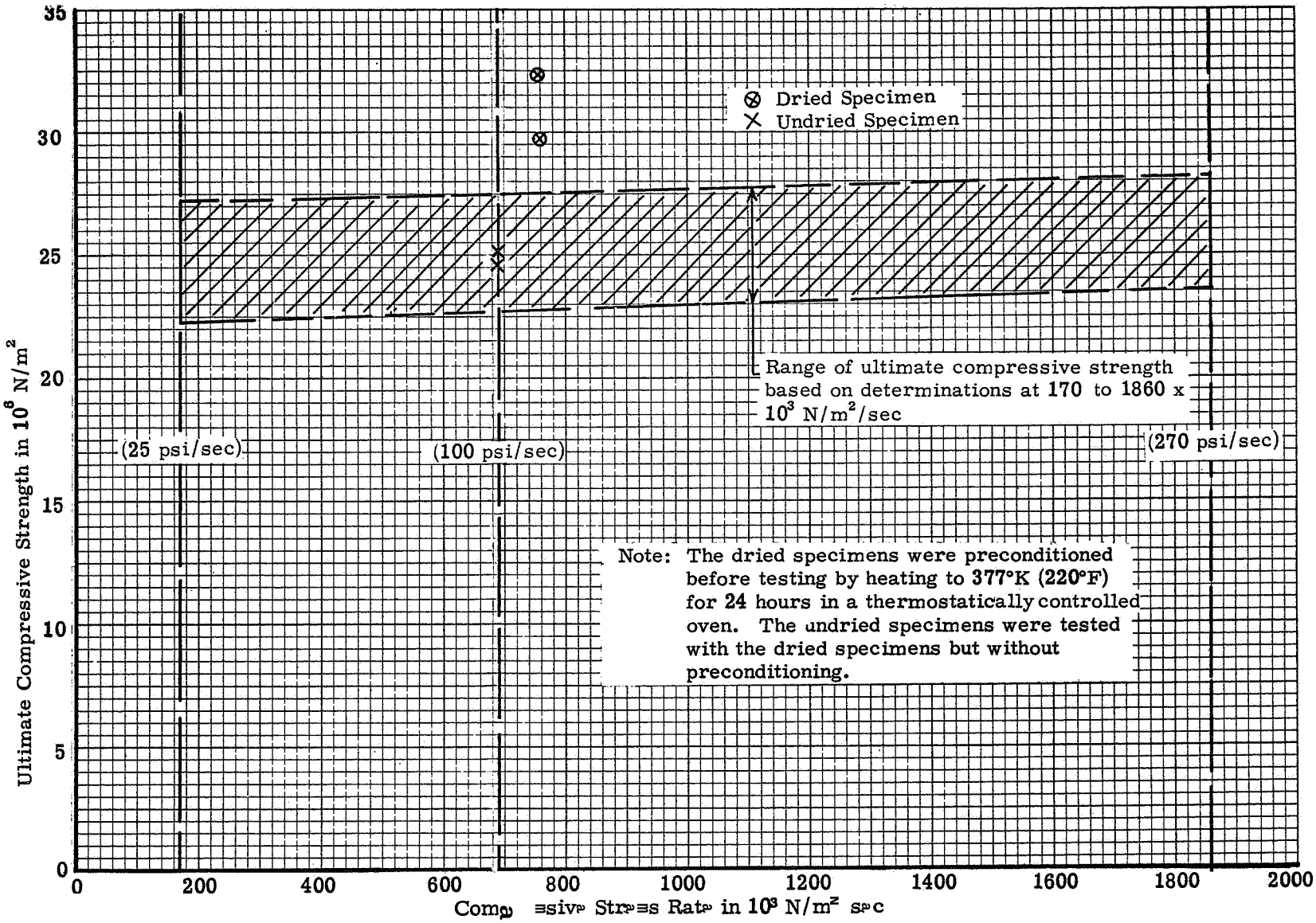

Figure 58. Moisture effects on compressive strength at 294°K (70 F.)

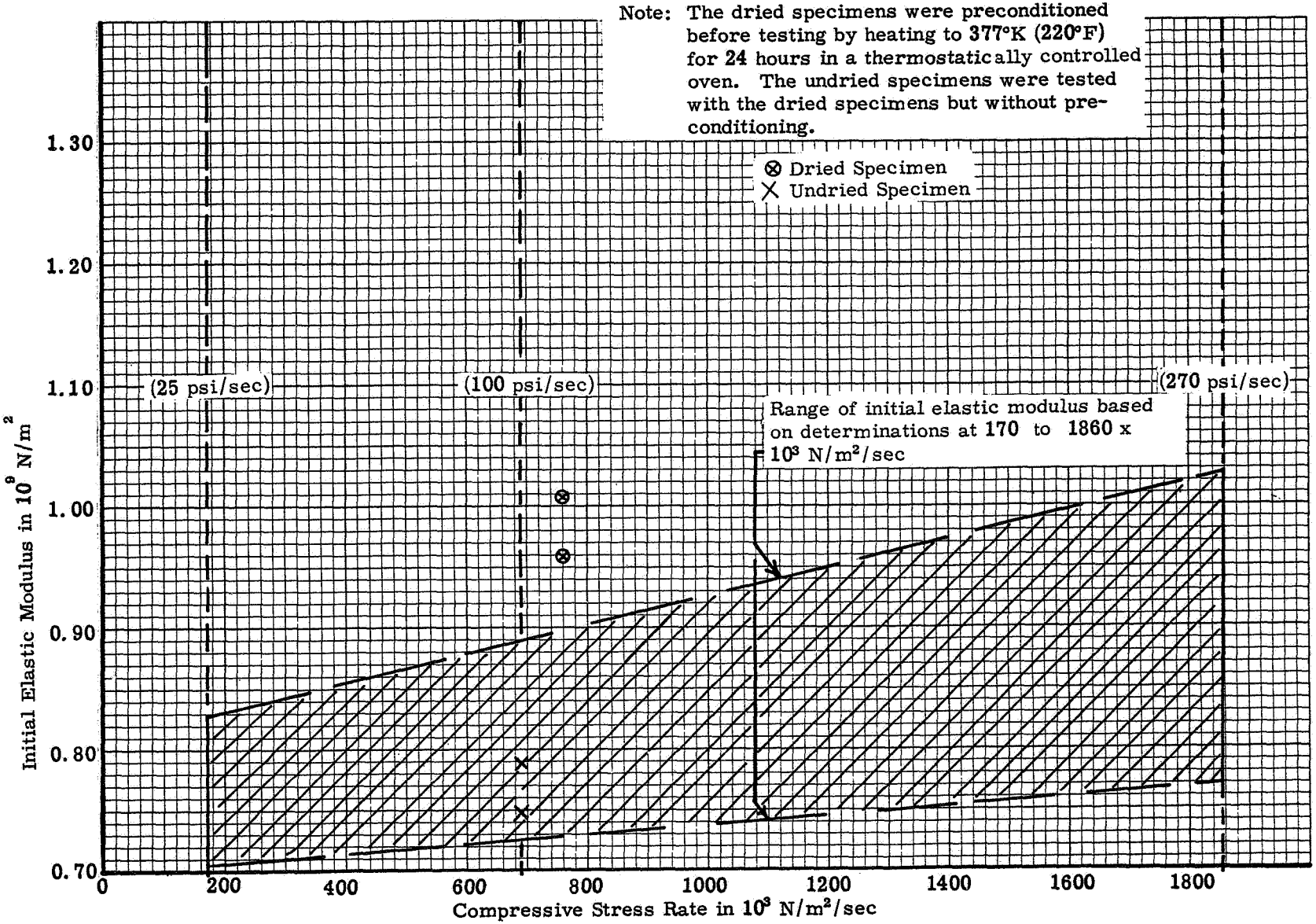

Figure 59. Moisture effects on compressive elastic modulus at 294°K (70°F)

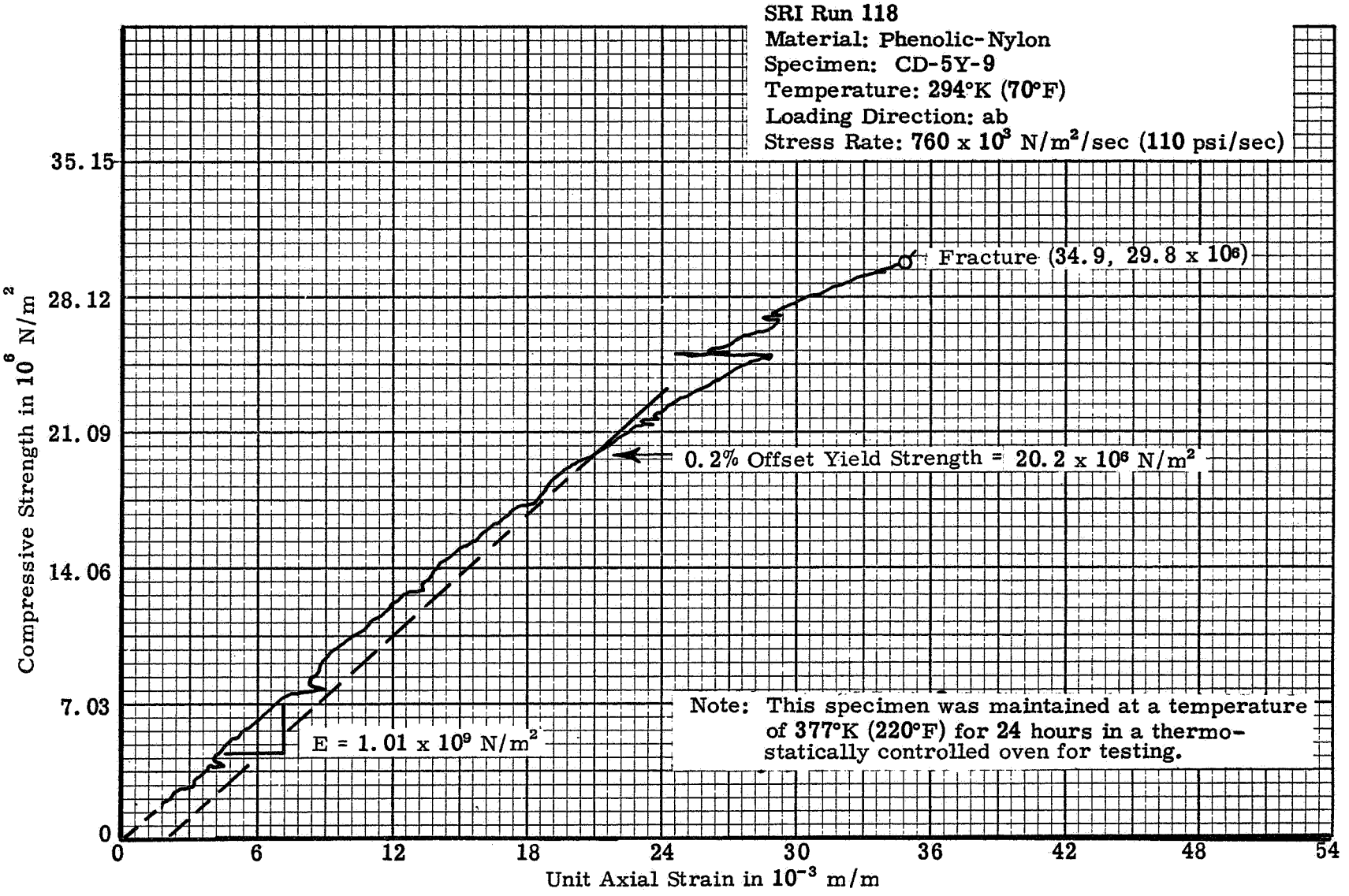

Figure 60. Typical compressive stress-strain curve for 1.270 cm dia x 2.54 cm gage length specimen tested for moisture effects at 294°K (70°F) -- specimen dried before testing

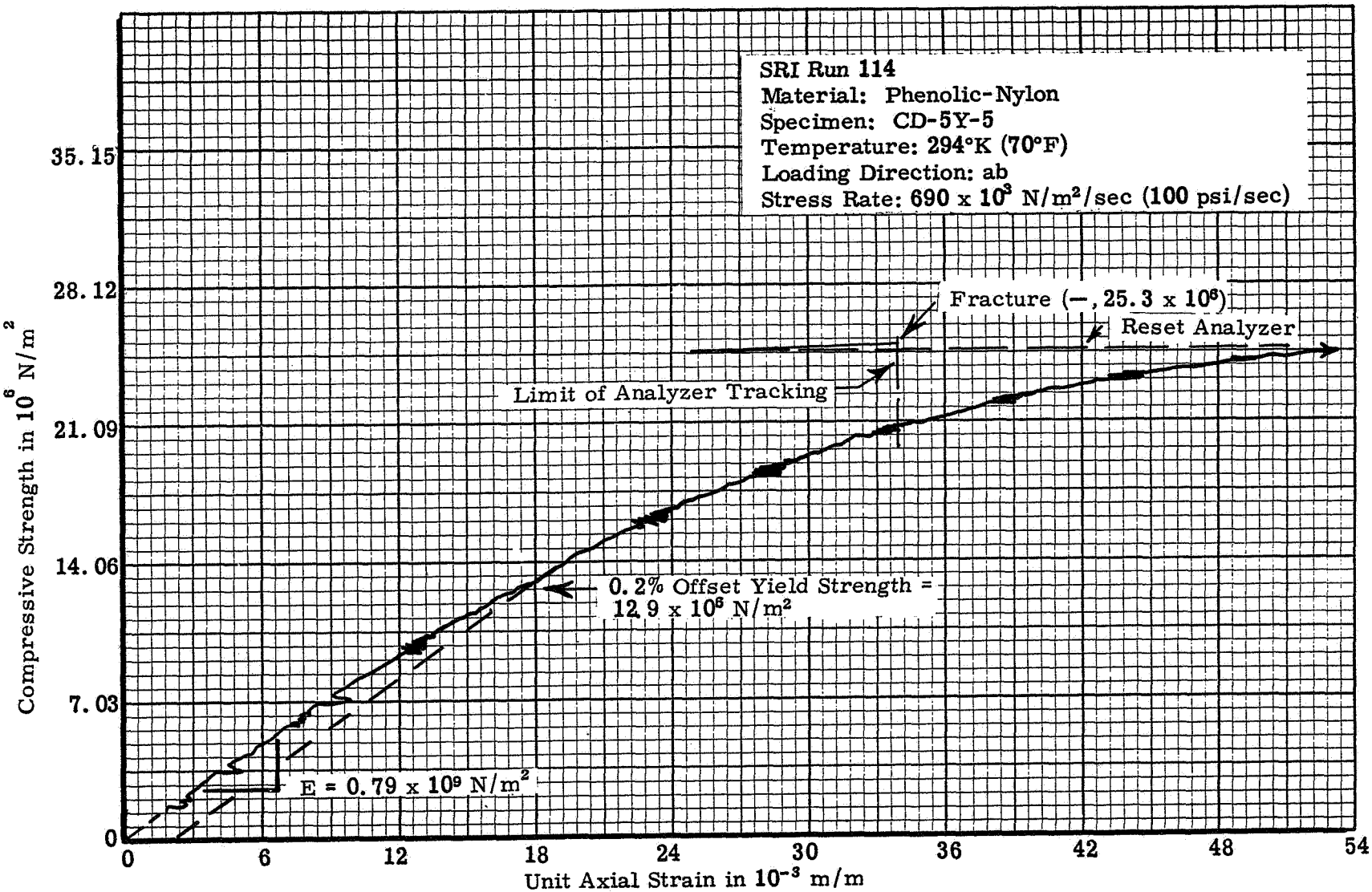

Figure 61. Typical compressive stress-strain curve for 1.270 cm dia x 2.54 cm gage length specimen tested for moisture effects at 294°K (70°F) -- specimen tested without drying

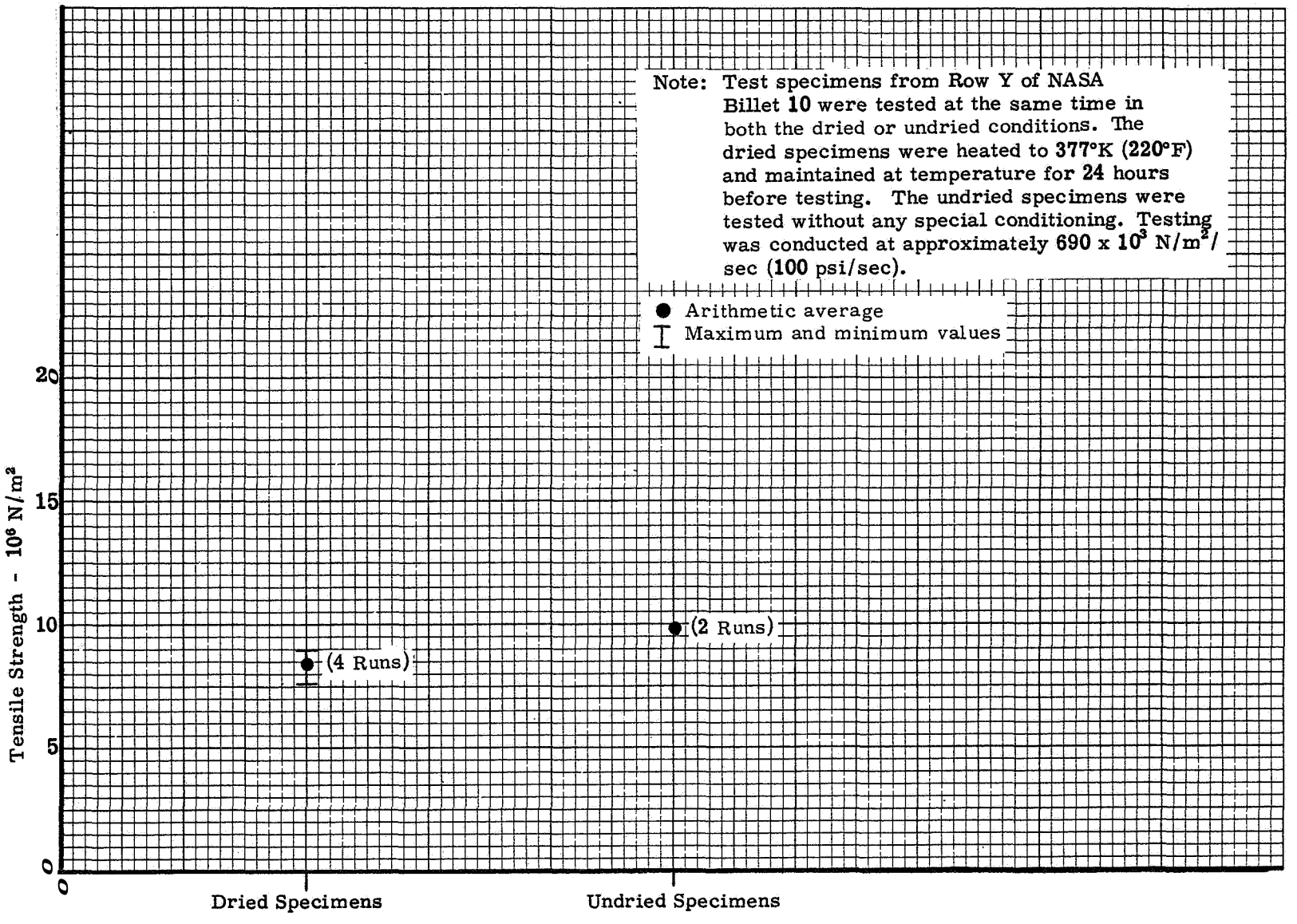

Figure 62. Moisture effects on tensile strength at 294°K (70°F)

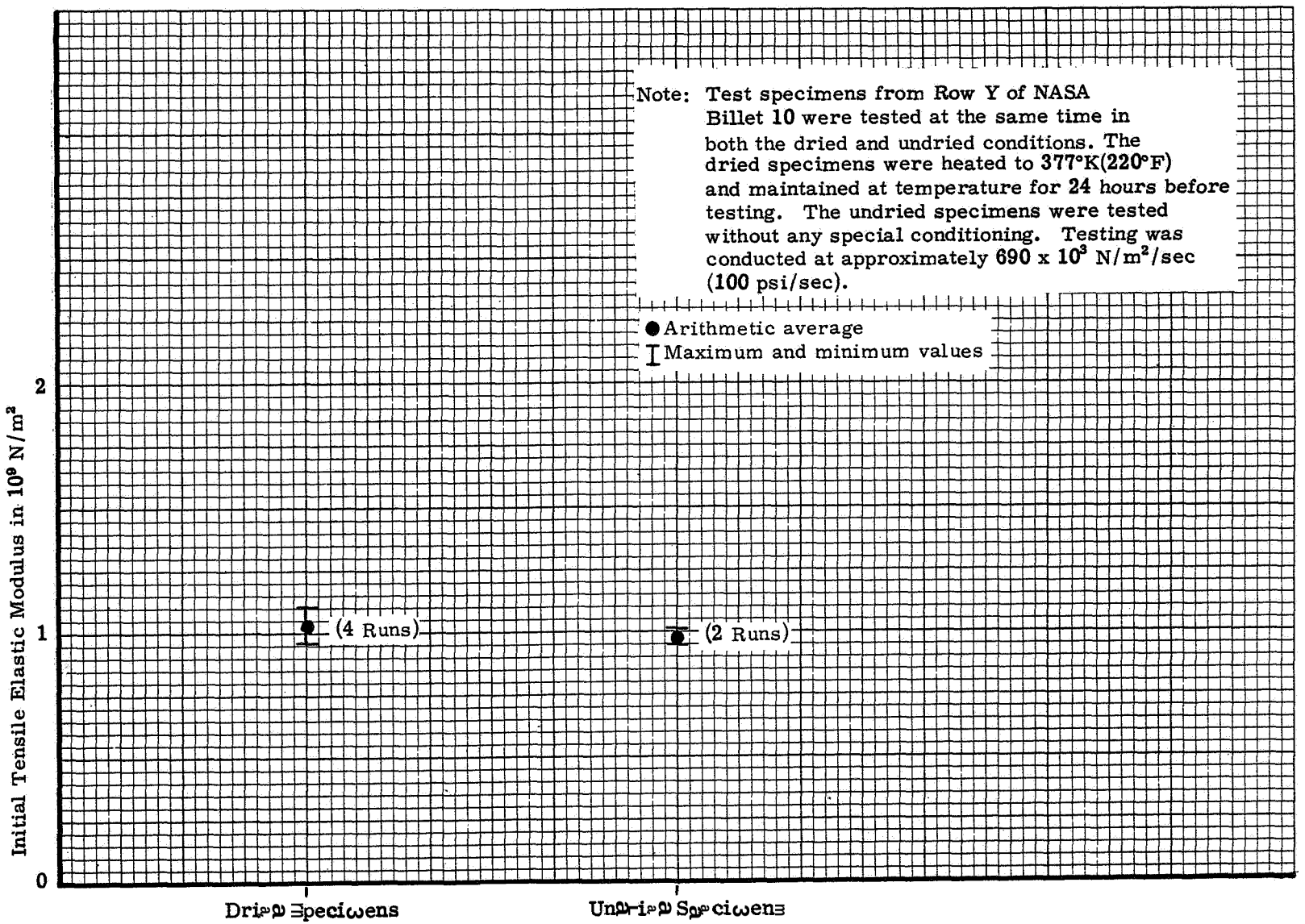

Figure 63. Moisture effects on tensile elastic modulus at 294°K (70°F)

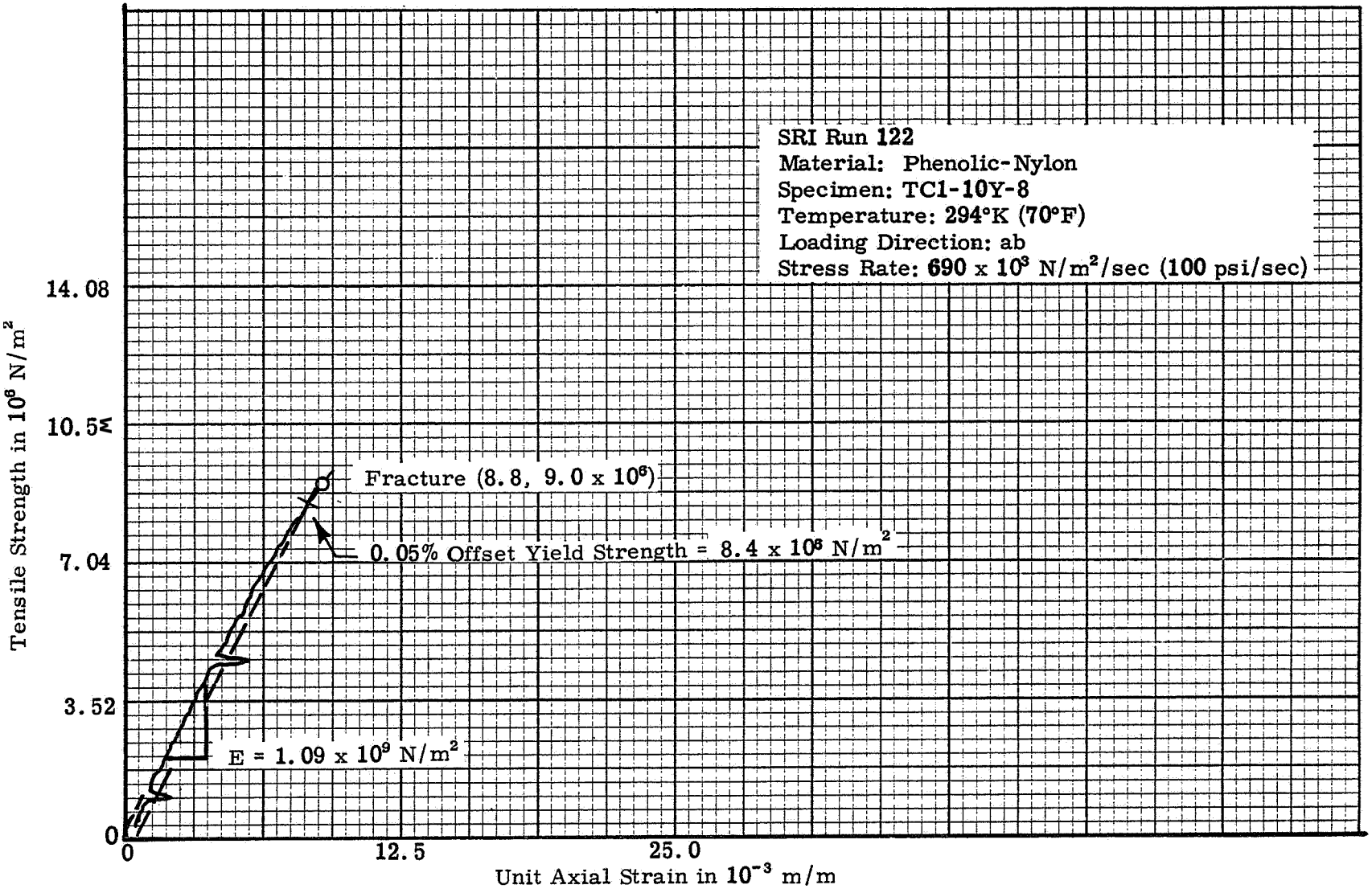

Figure 64. Typical tensile stress-strain curve for 1.270 cm dia x 5.08 cm gage length specimen [illegible] for moisture effects at 294°K (70°F) -- specimen dried before testing

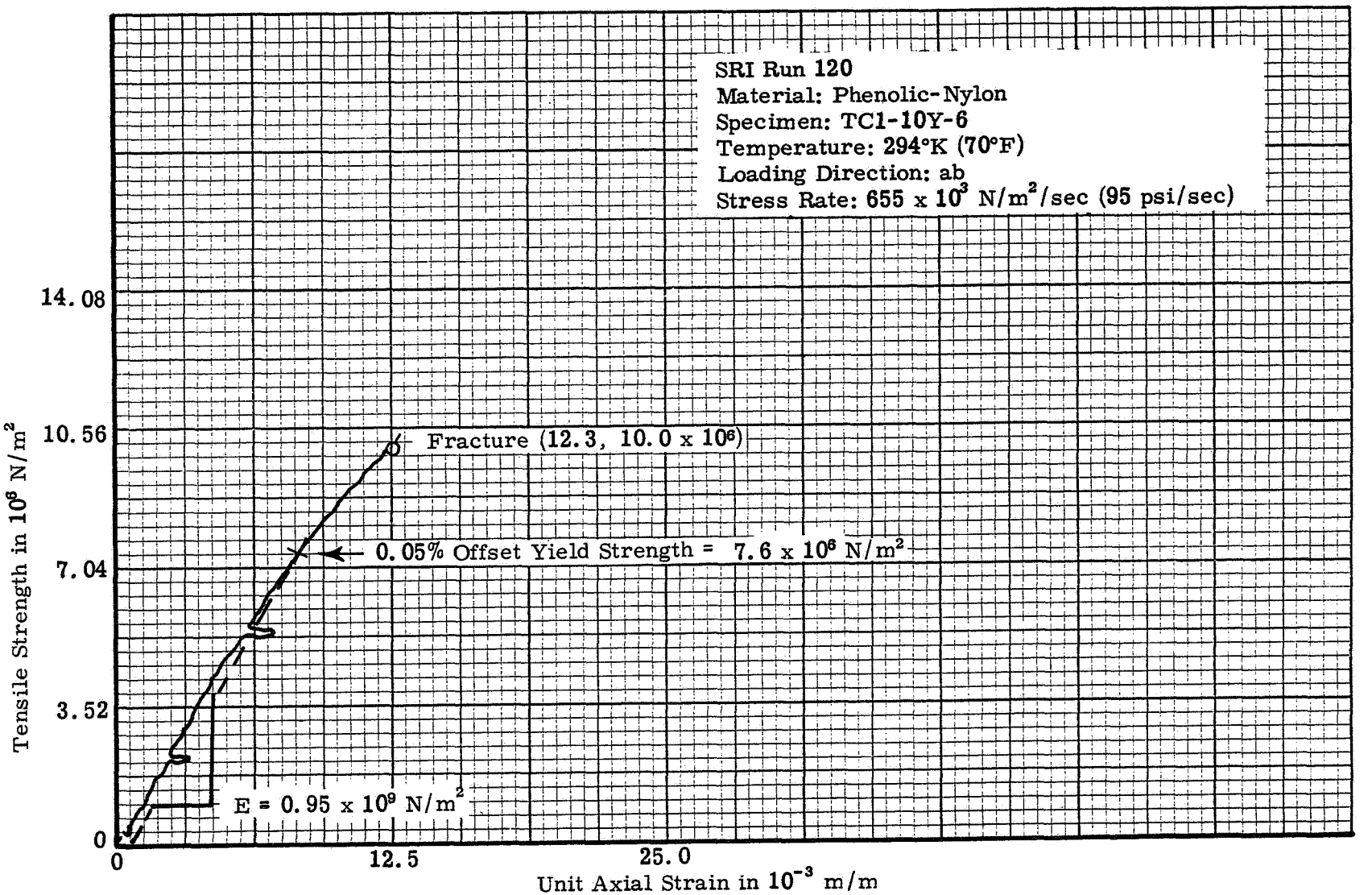

Figure 65. Typical tensile stress-strain curve for 1.270 cm dia x 5.08 cm gage length specimen tested for moisture effects at 294°K (70°F) -- specimen tested without drying

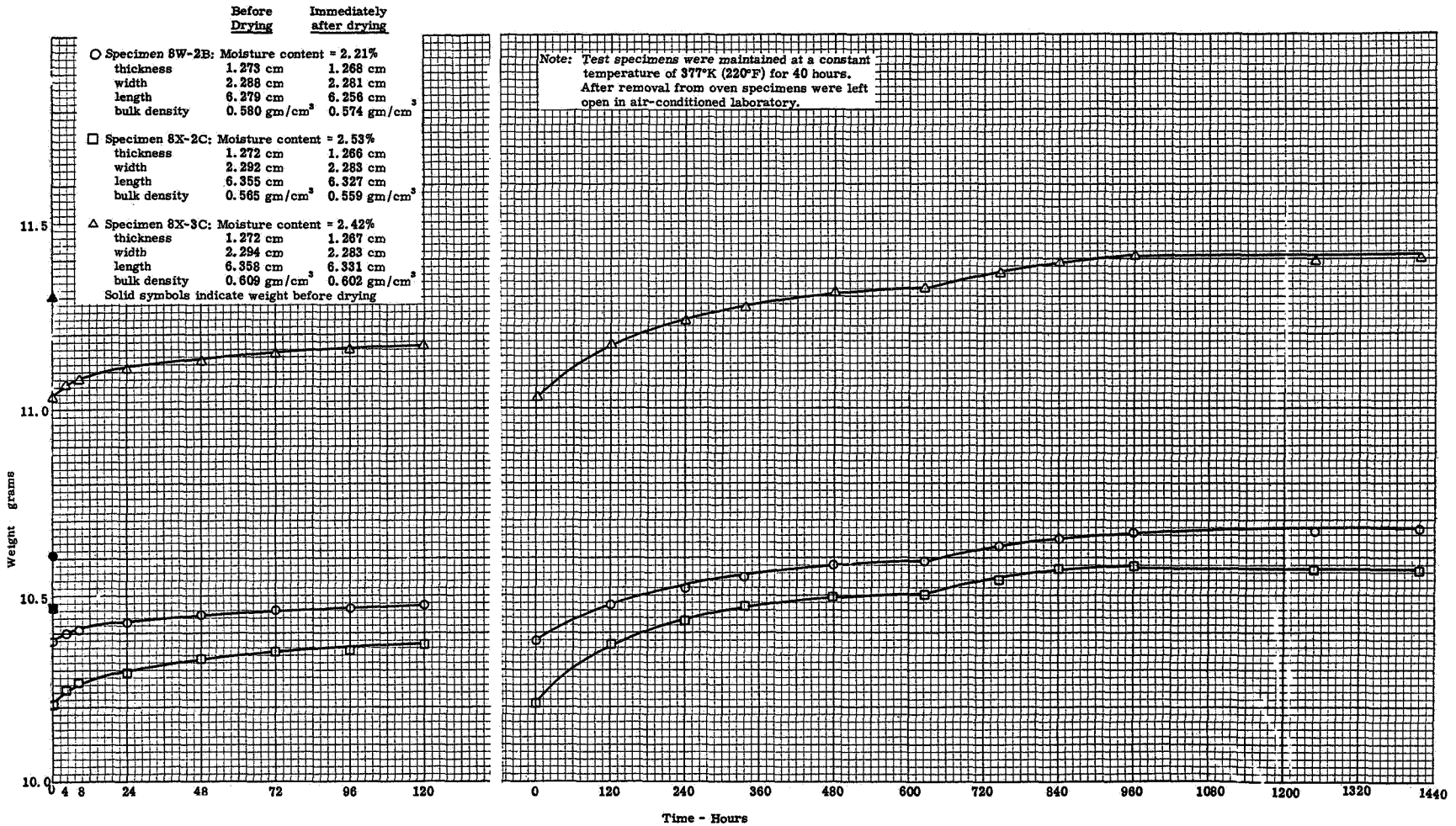

Figure 66. Moisture absorption test

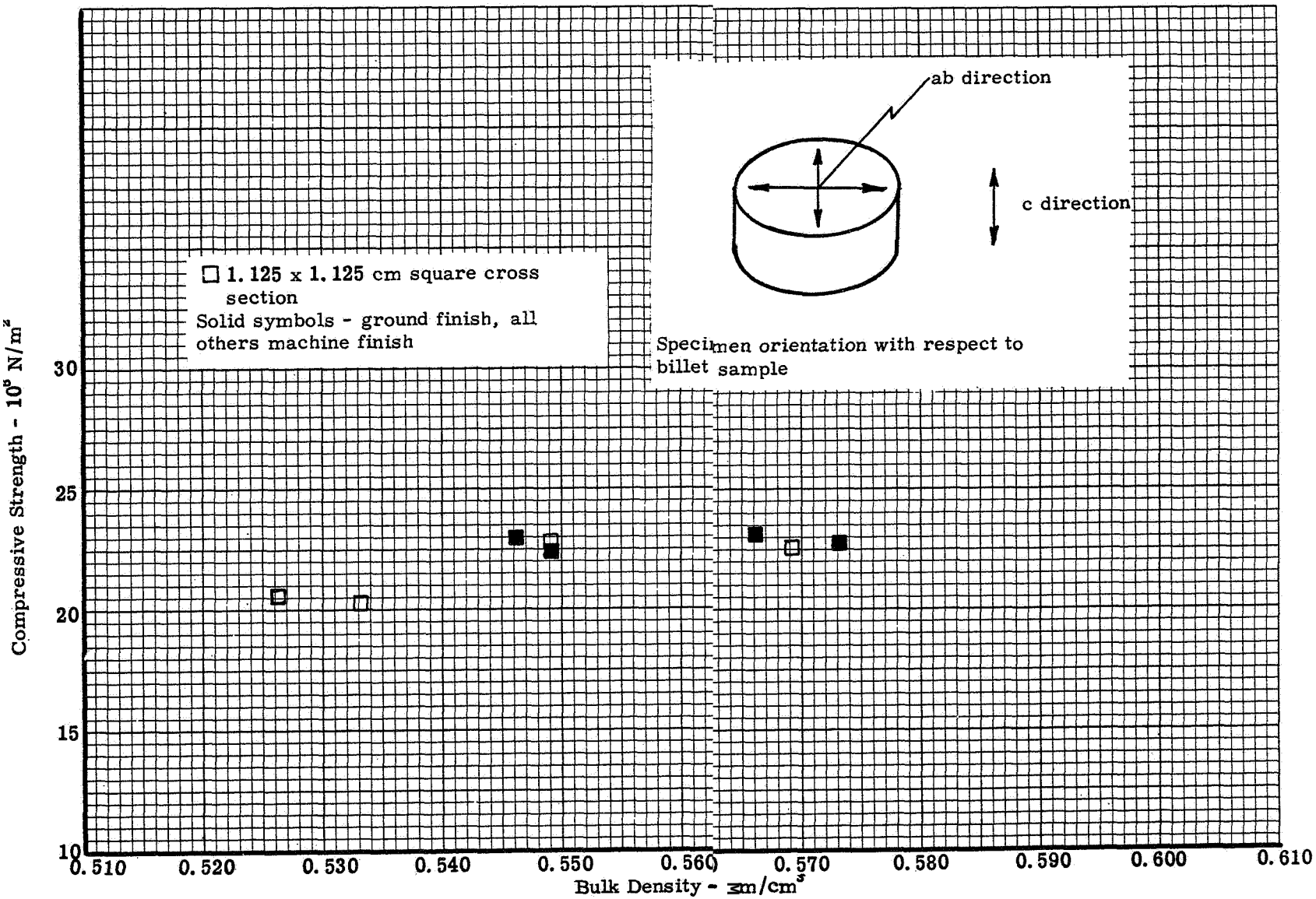

Figure 67. Compressive strength versus bulk density in the c direction

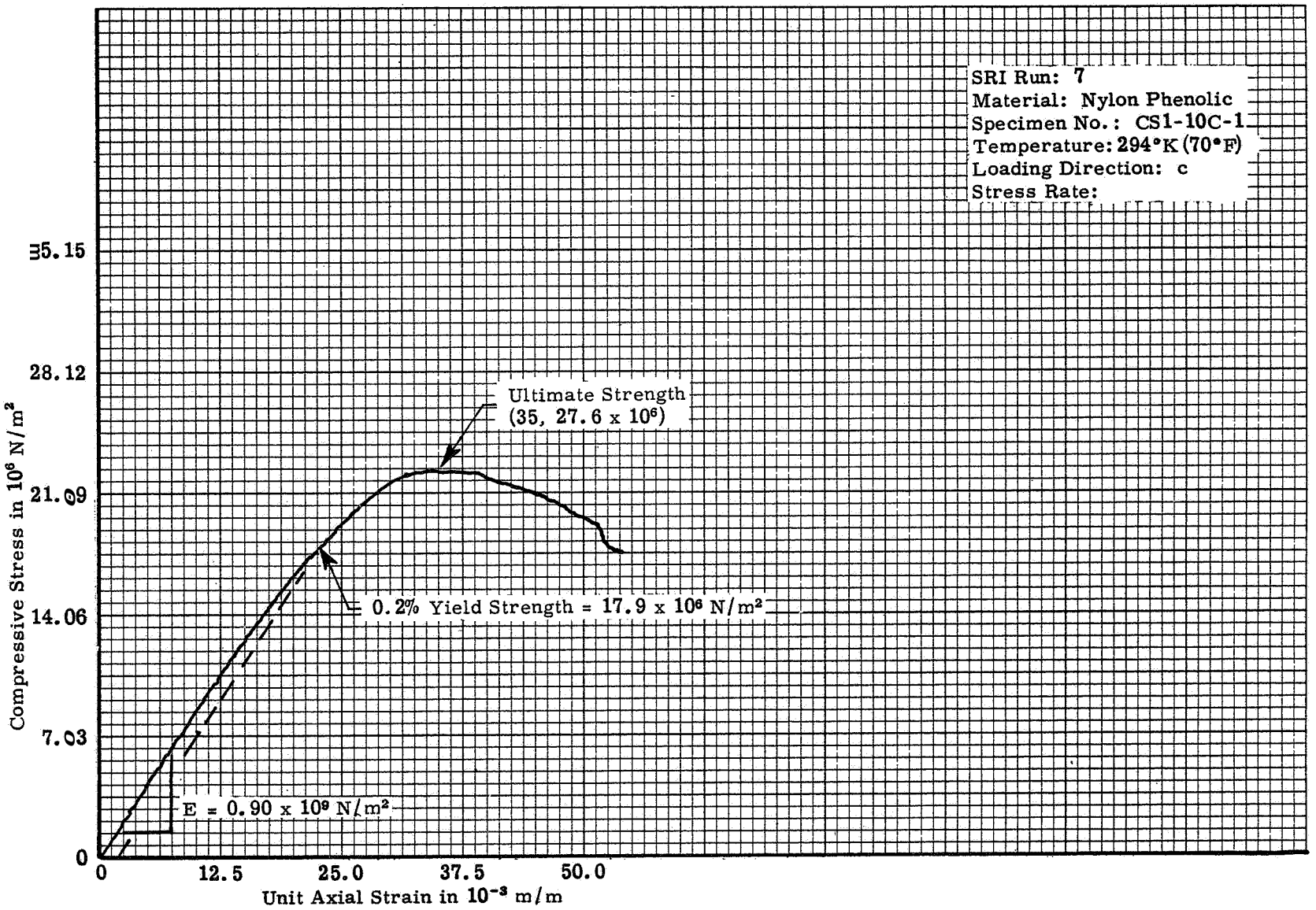

Figure 68. Typical compressive Stress-strain curve for square cross section in the c direction at 294°K (70°F) tested in the Tinius-Olsen apparatus

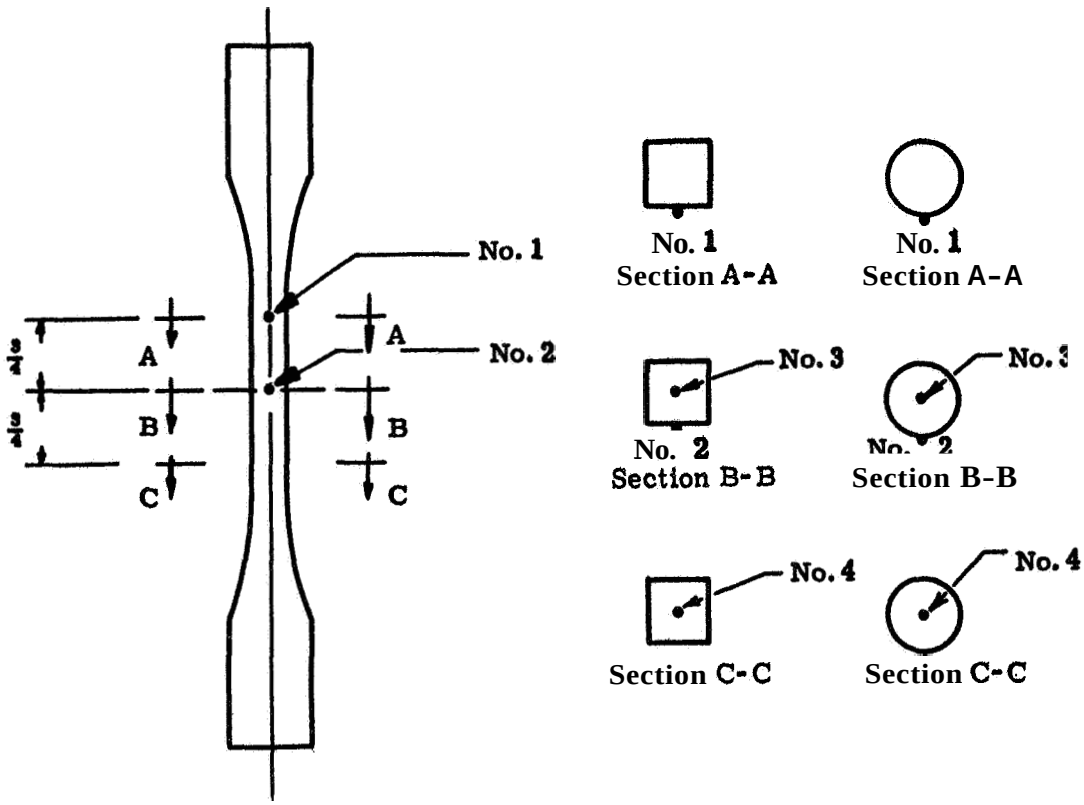

Note: Thermocouple8 Nos. 2 and 3 are actually located $\frac{1}{8}$ inch above and below centerline shown.

Figure 69. Thermocouple locations for determining heat rates and thermal gradients. for 1.125 cm square and 1.270 cm diameter specimens TS1-4Y-1 and TC1-8Y-1

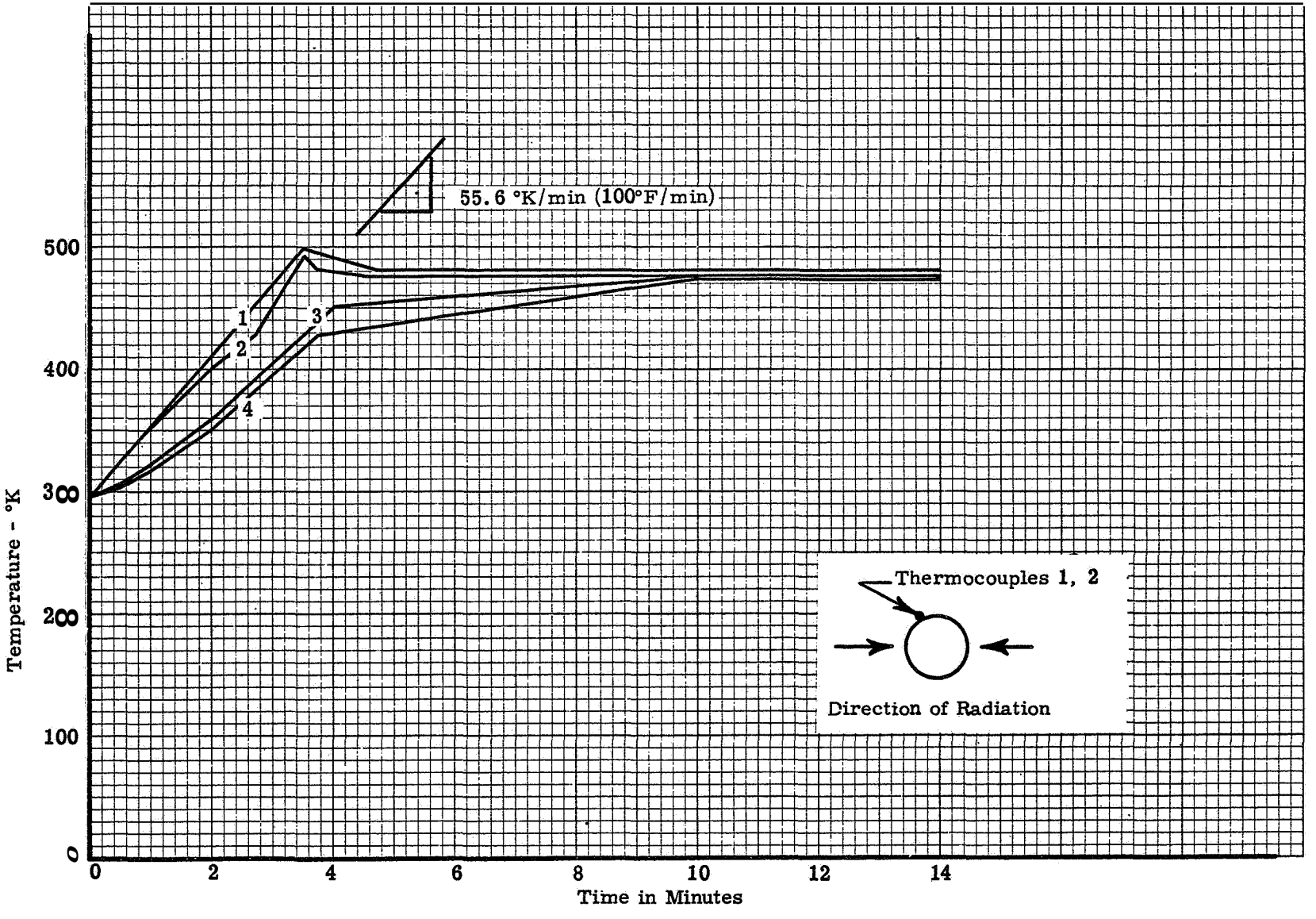

Figure 70. Heating rate for 1.27 cm diameter phenolic-nylon specimen TCI-8Y-1, 477°K determination (400°F)

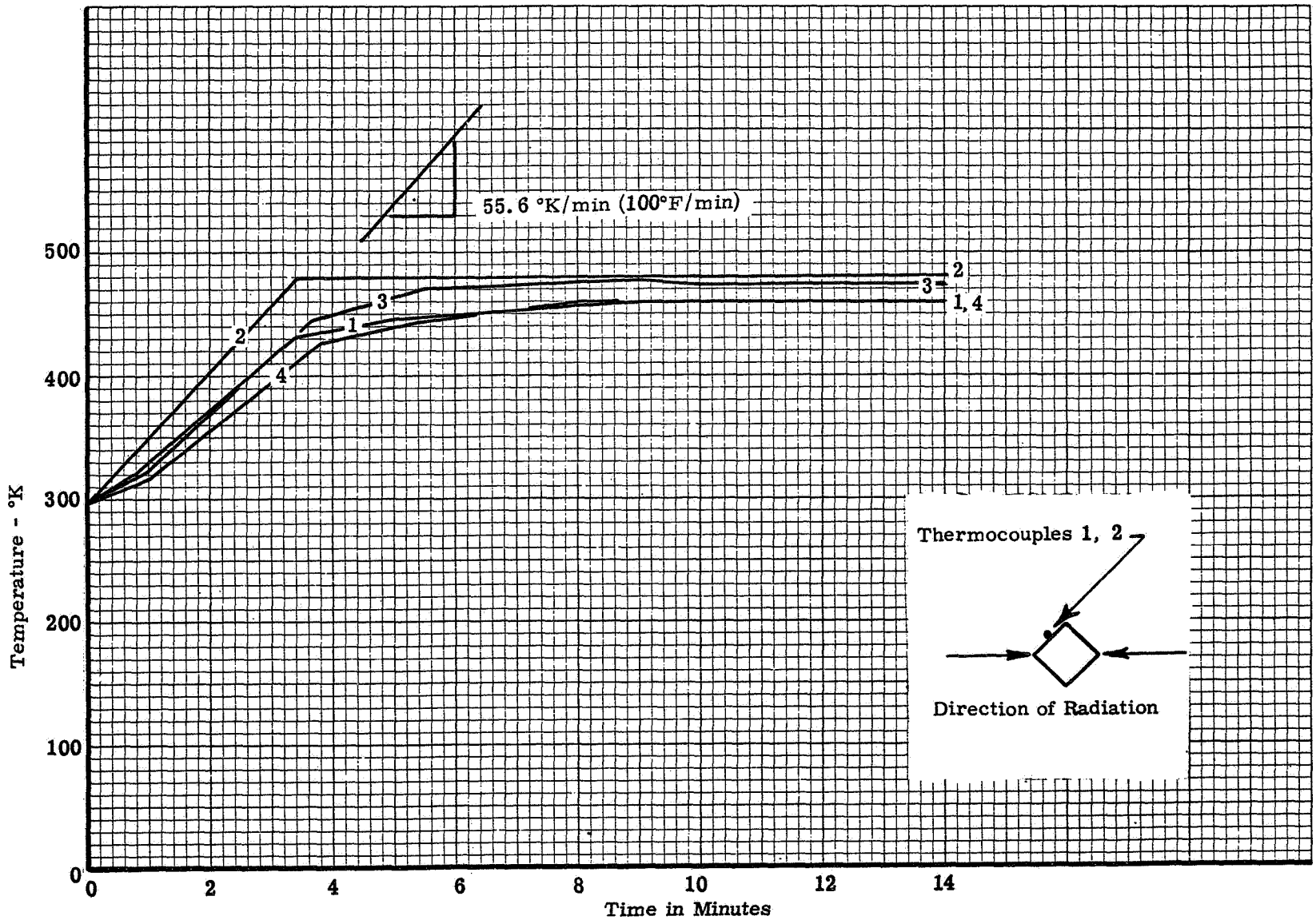

Figure 71. Heating rate for 1.125 cm square phenolic-nylon specimen TS1-4Y-1, 477°K determination (400°F)

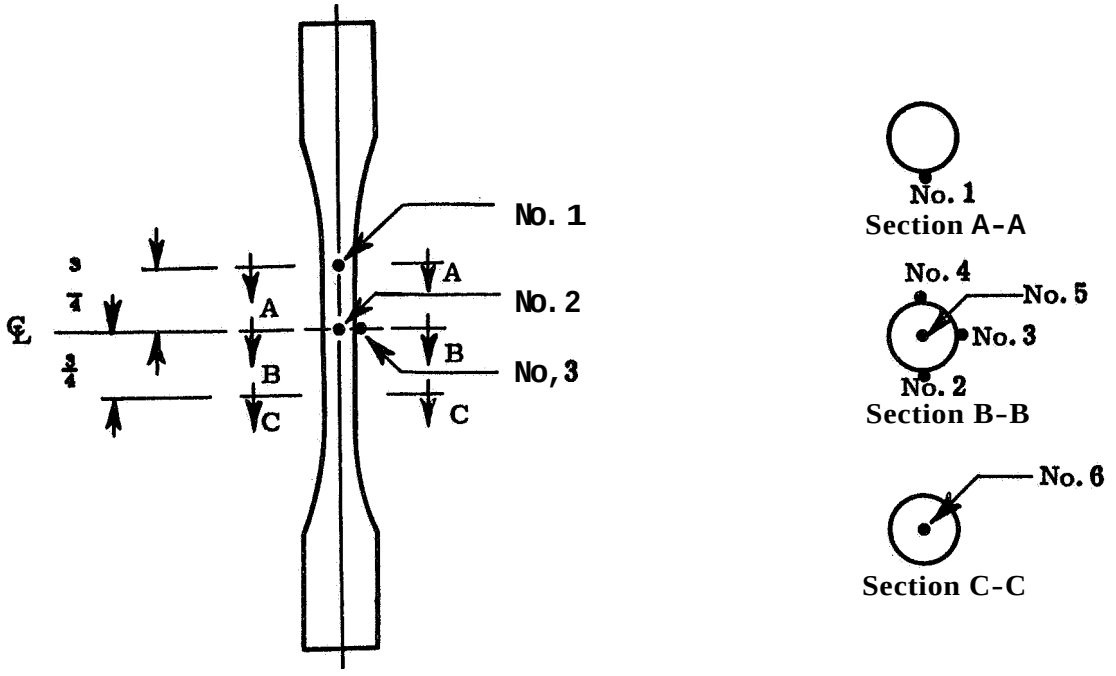

Figure 72. Thermocodple locations for determining heating rates and thermal gradient6 for testing the effects of time at temperature on tensile properties

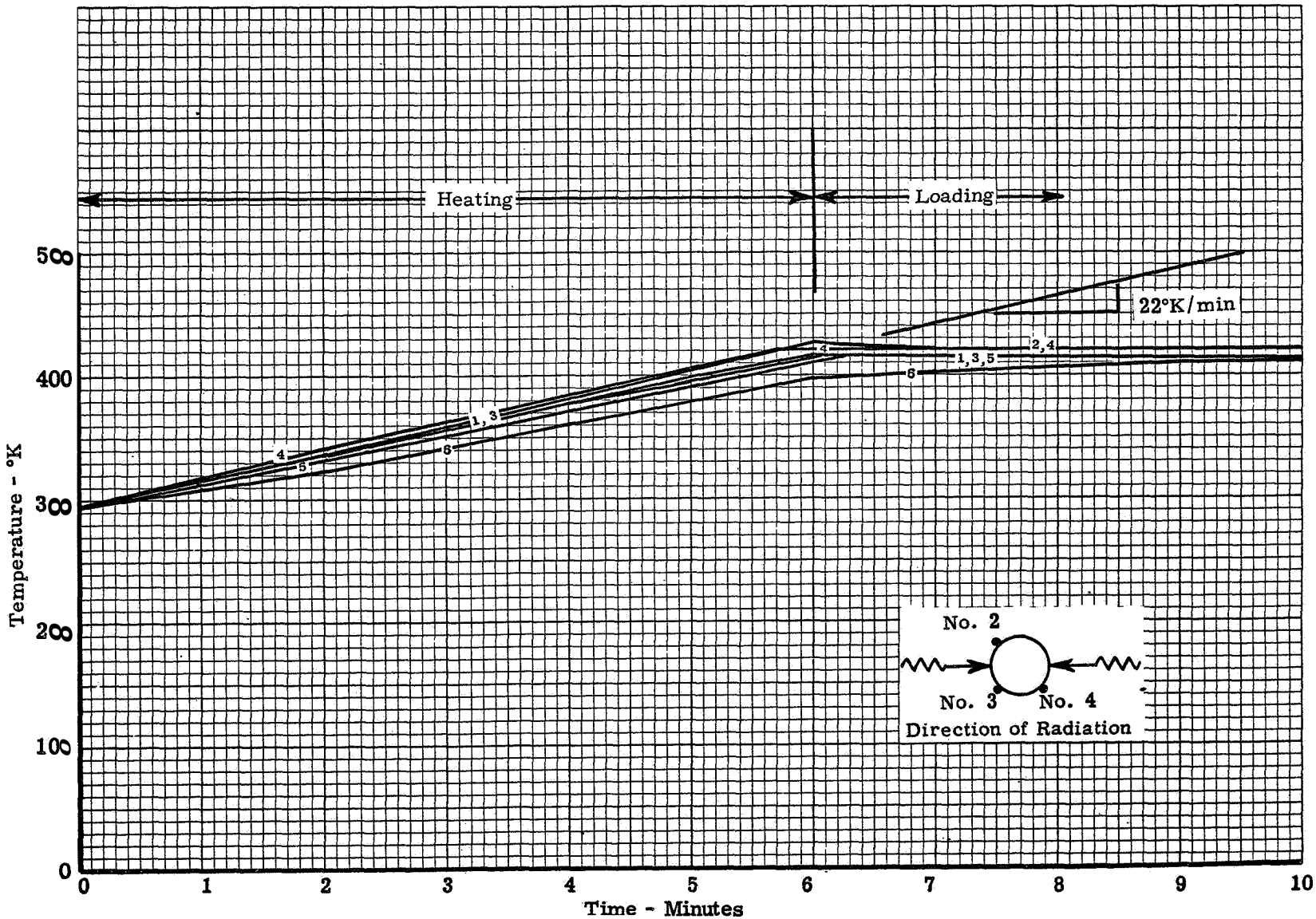

Figure 73. Typical heating curve for 1.27 cm dia x 5.08 cm g[illegible] length [illegible]ecimen [illegible]or determining heat rate effects— 22°K/min to 422°K (40°F/min to 300°F)

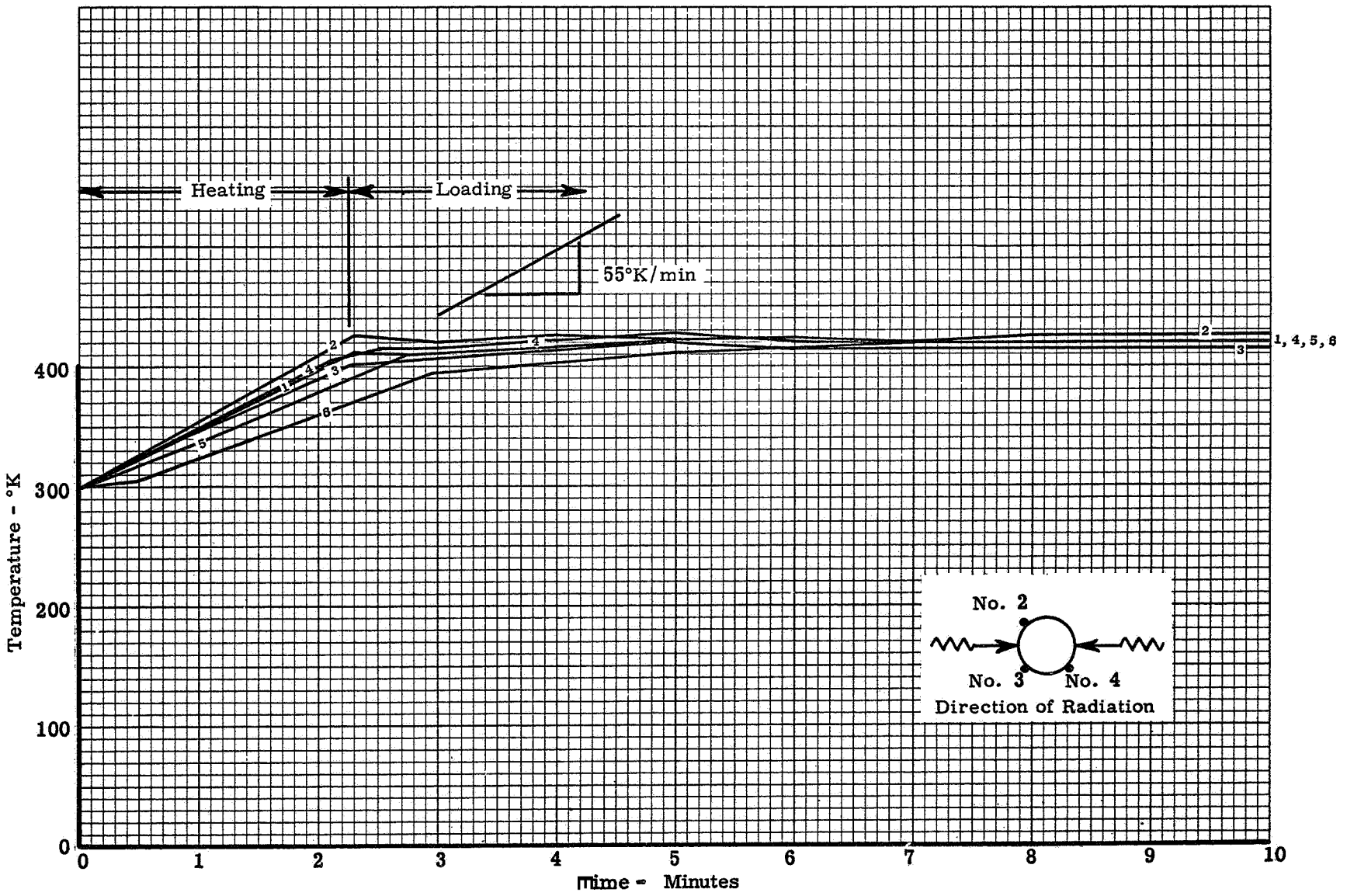

Figure 74 Typical heating curve for 1.27 cm dia x 5.08 cm gage length specimen for determining heat rate effects—55°K/min to 422°K (100°F/min to 300°F)

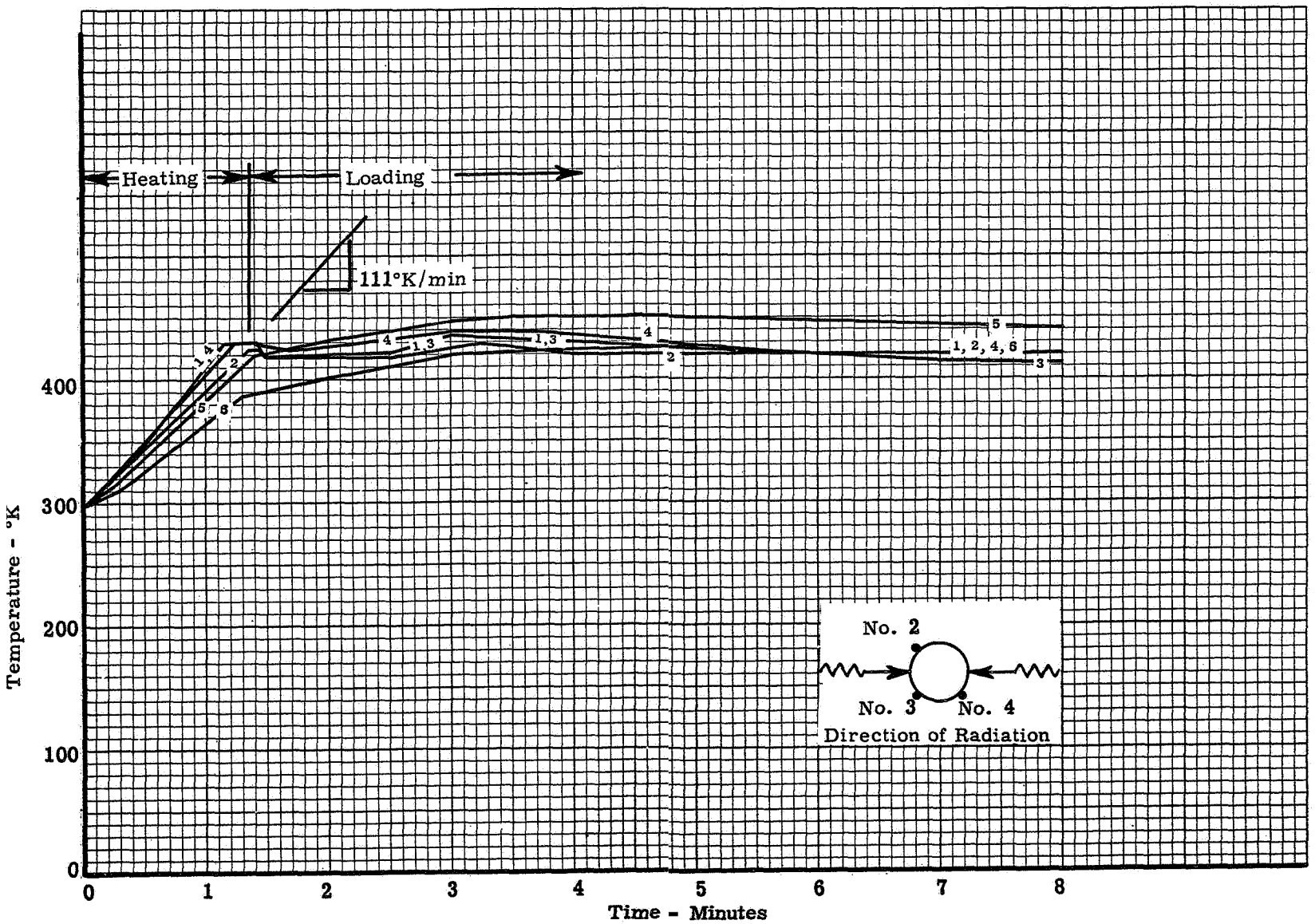

Figure 75. Typical heating curve for 1.27 cm dia x 5.08 cm gage length specimen for determining heat rate effects—111°K/min to 422°K (200°F/min to 300°F)

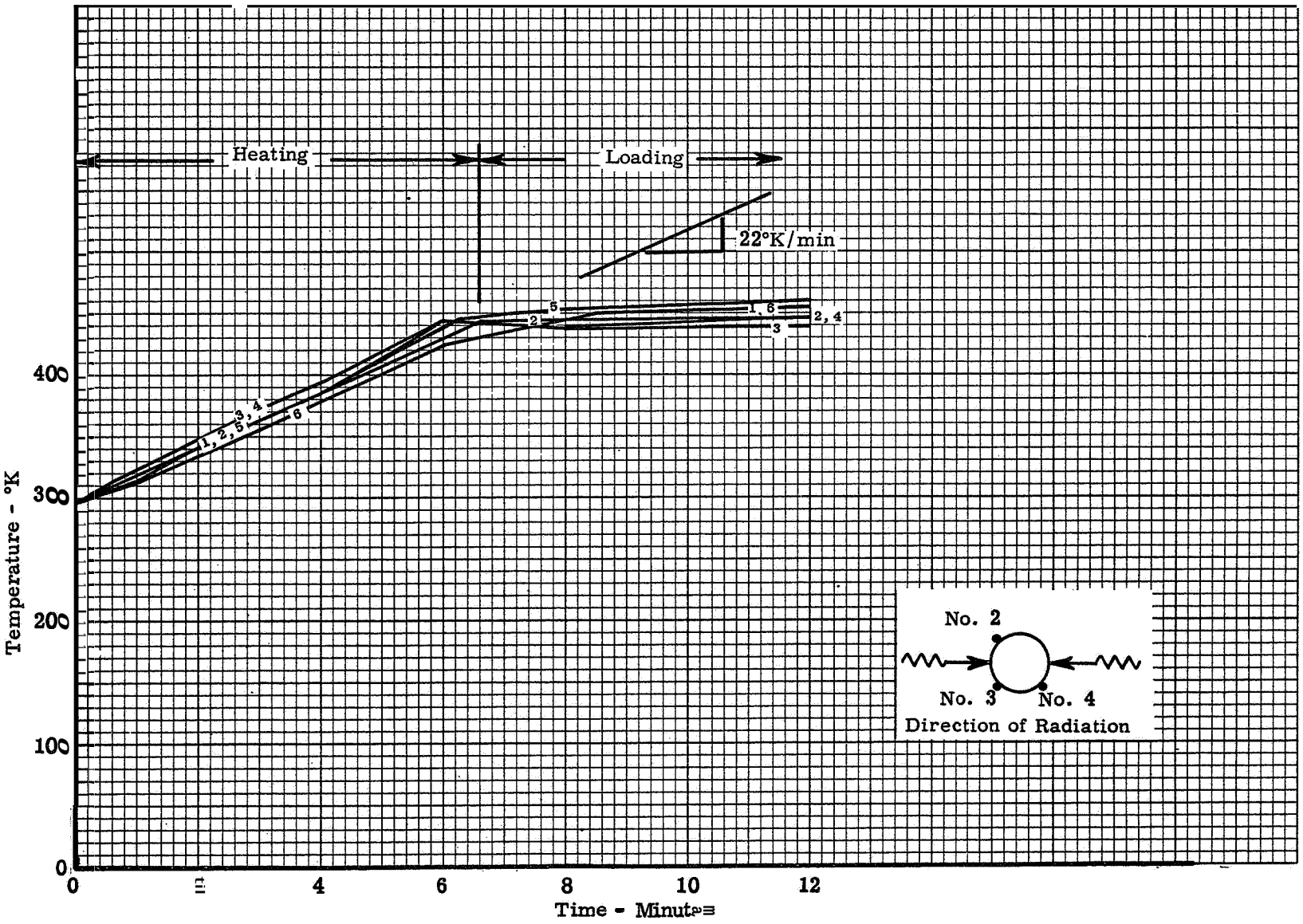

Figure 76. Typical heating curve for 1.27 cm dia x 5.08 cm gage length specimen for determining heat rate effects—22°K/min to 450°K (40°F/min to 350°F)

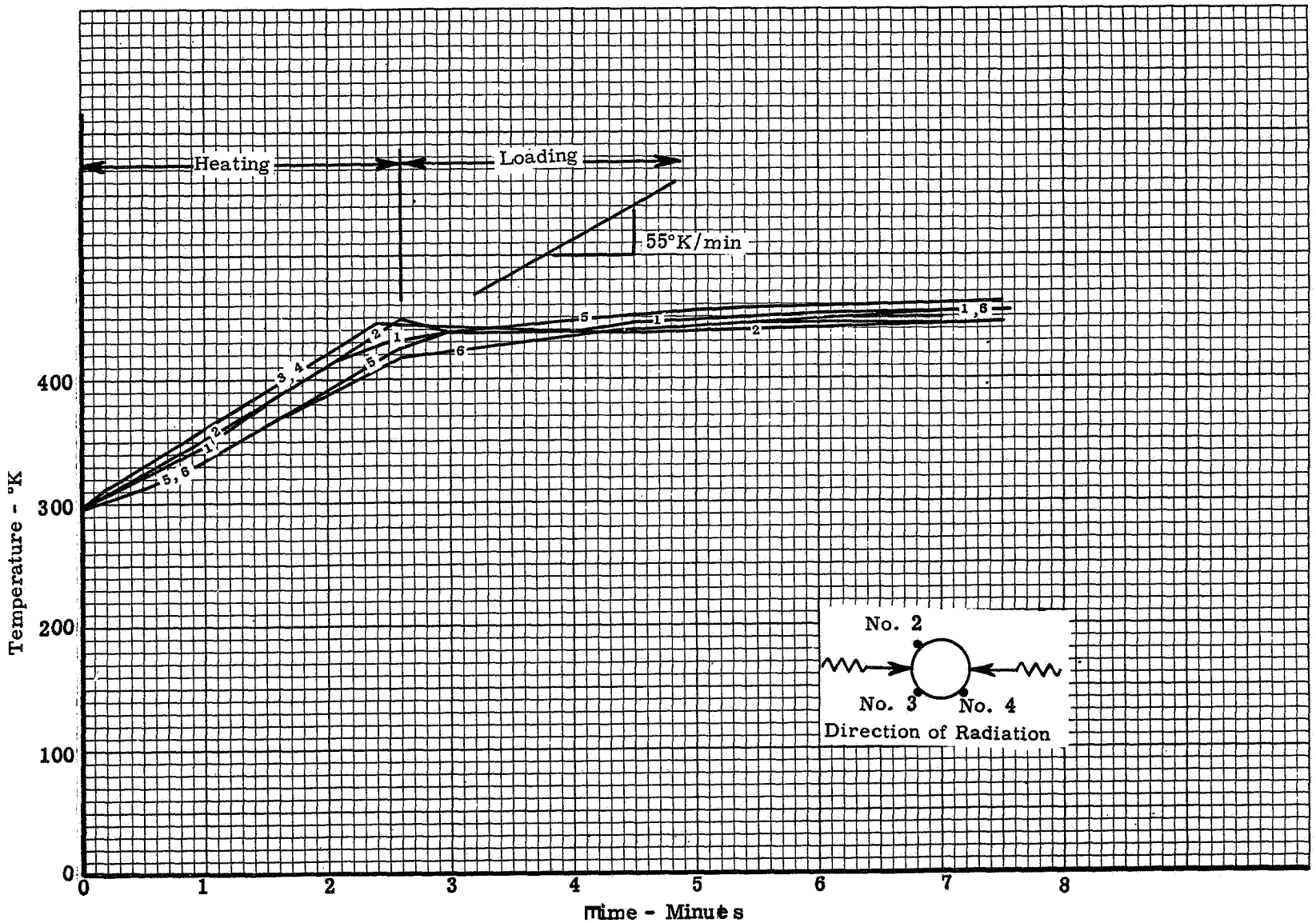

Figure 77. Typical heating curve for 1.27 cm dia x 5 08 cm g4 length specimen Cor determining h t rate effects— 55°K/min to 450°K (100°F/min to 350°F)

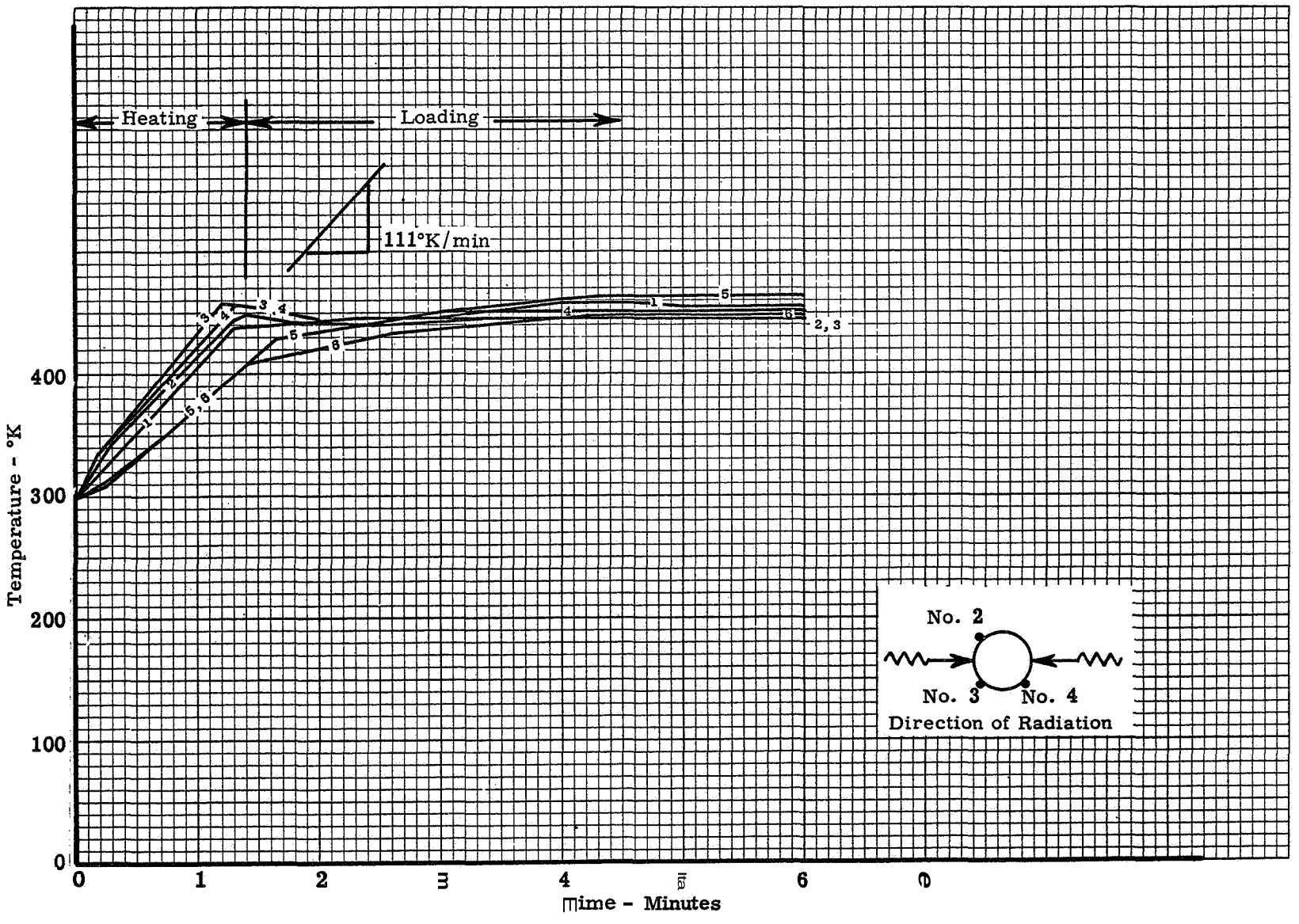

Figure 08. Typical heating curve for 1.27 cm dia x 5.08 cm gage length specimen for determining heat rate effects—111°K/min to 450°K (200°F/min to 350°F)

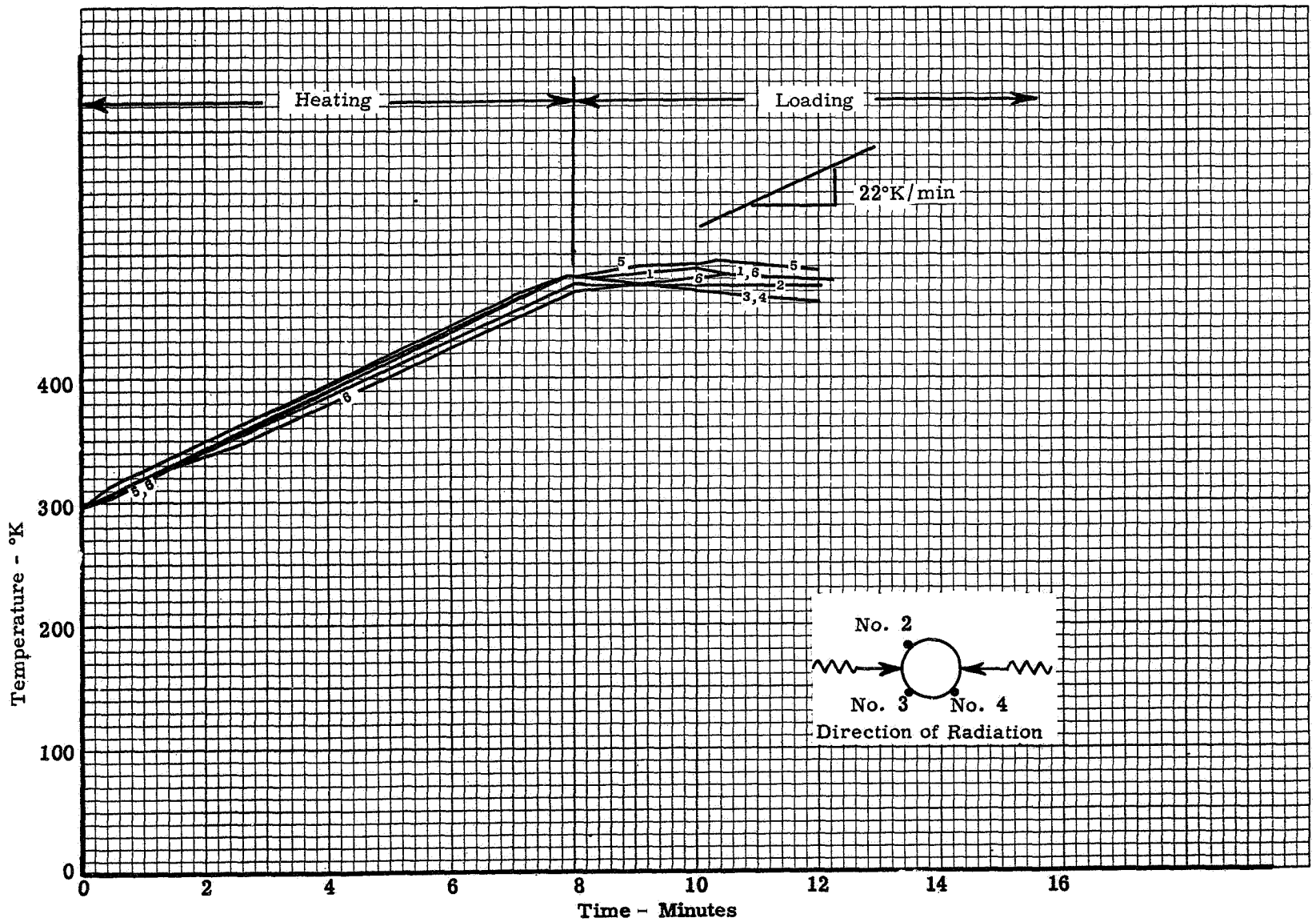

Figure 79. Typical heating curve for 1.27 cm dia x 5.08 cm gage length specimen for determining heat rate effects — 22°K/min to 477°K (40°F/min to 400°F)

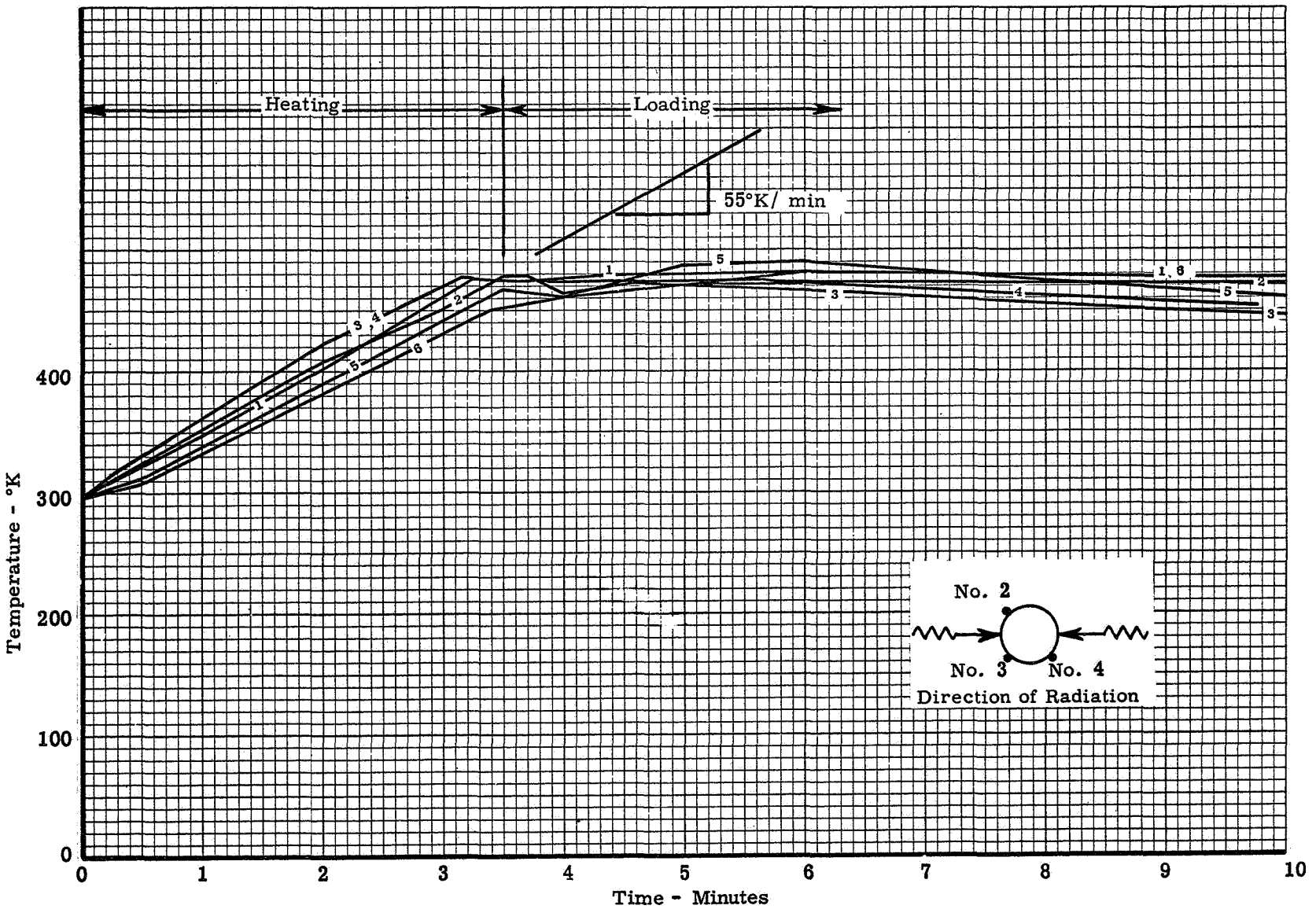

Figure 80. Typical heating curve for 1.27 cm dia x 5 08 cm gage length specimen for determining heat rate effects—55°K/min to 477°K (100°F/min to 400°F)

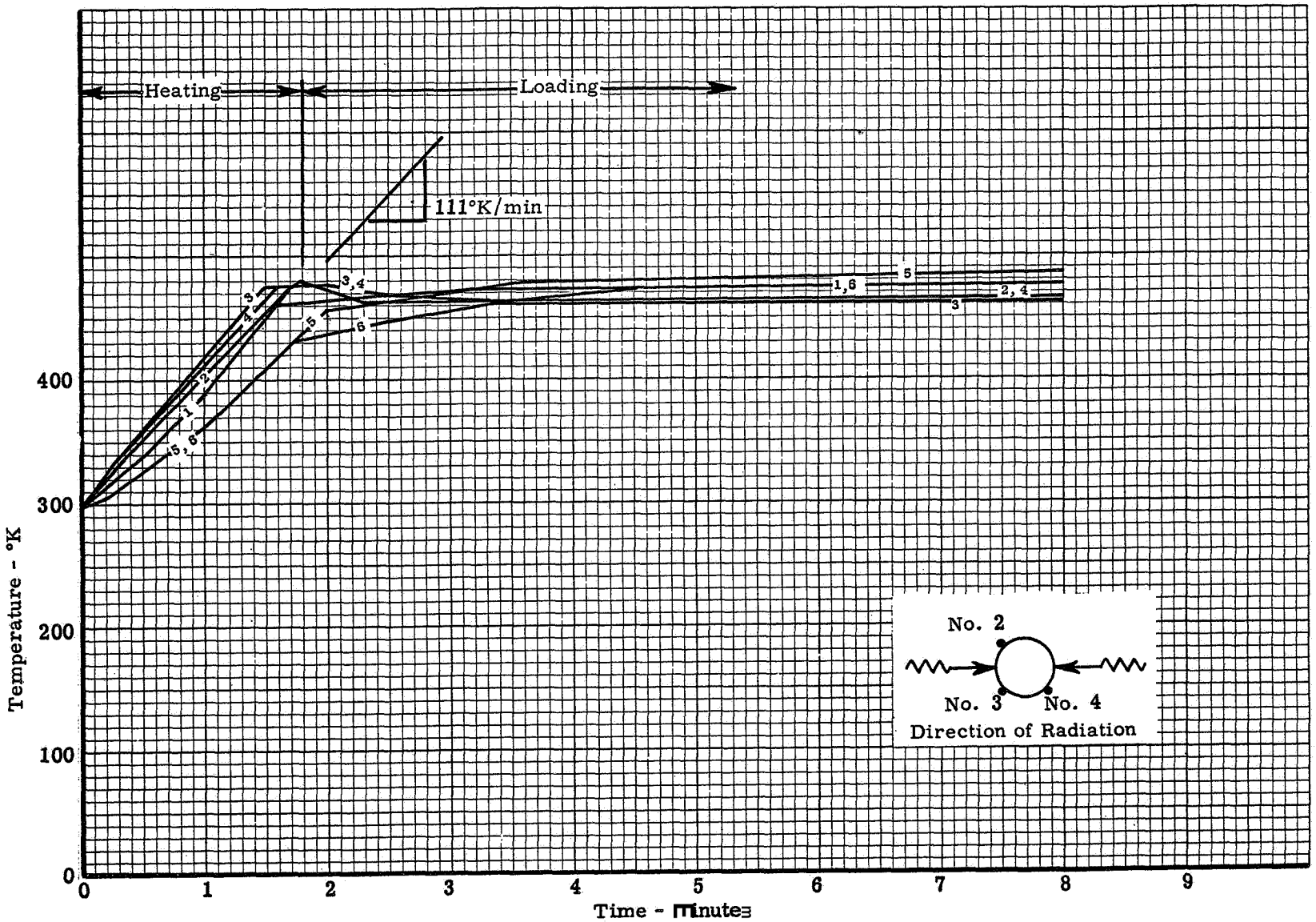

Figure 81. Typical heating curve for 1.27 cm dia x 5.08 cm gage length specimen for determining heat rate effects—111°K/min to 477°K (200°F/min to 400°F)

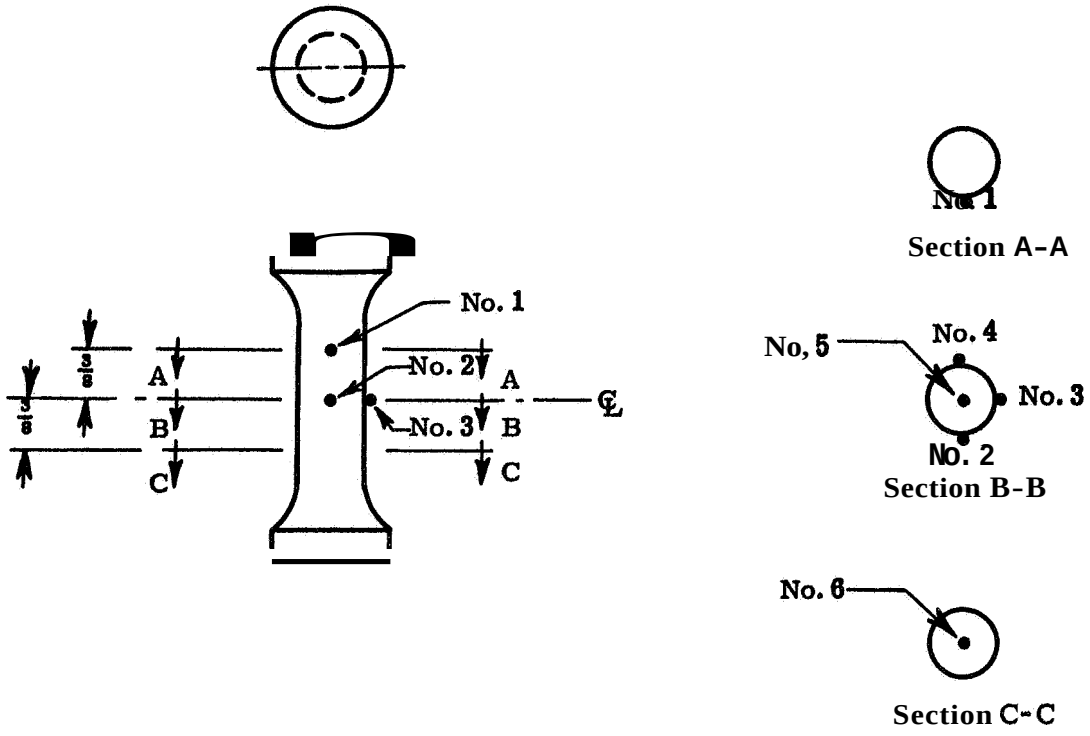

Figure 82. Thermocouple locations for determining heating rates and thermal gradients for compressive determinations

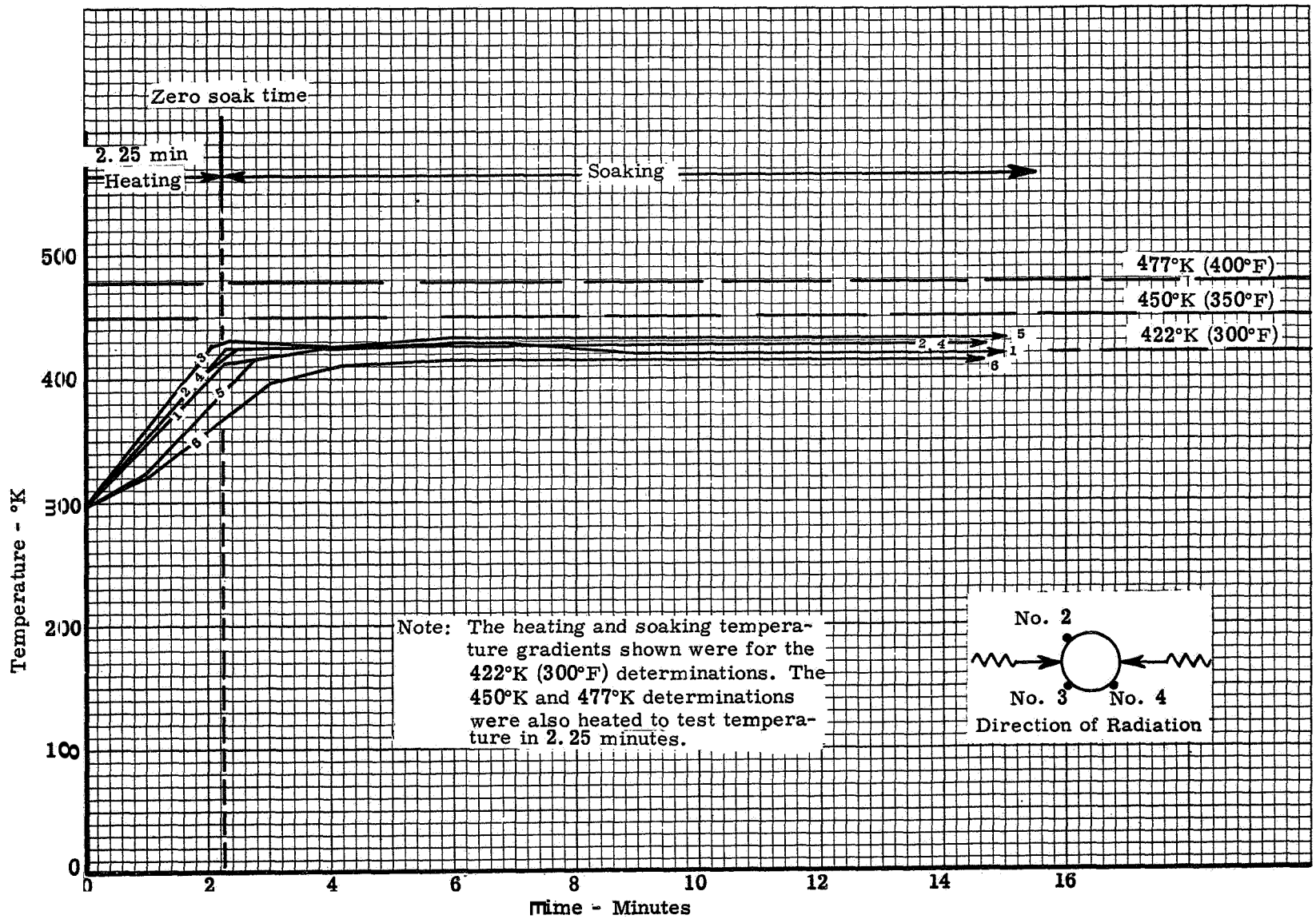

Figure 83 Typical heating and soaking curves for determining effects of time at temperature on compressive properties

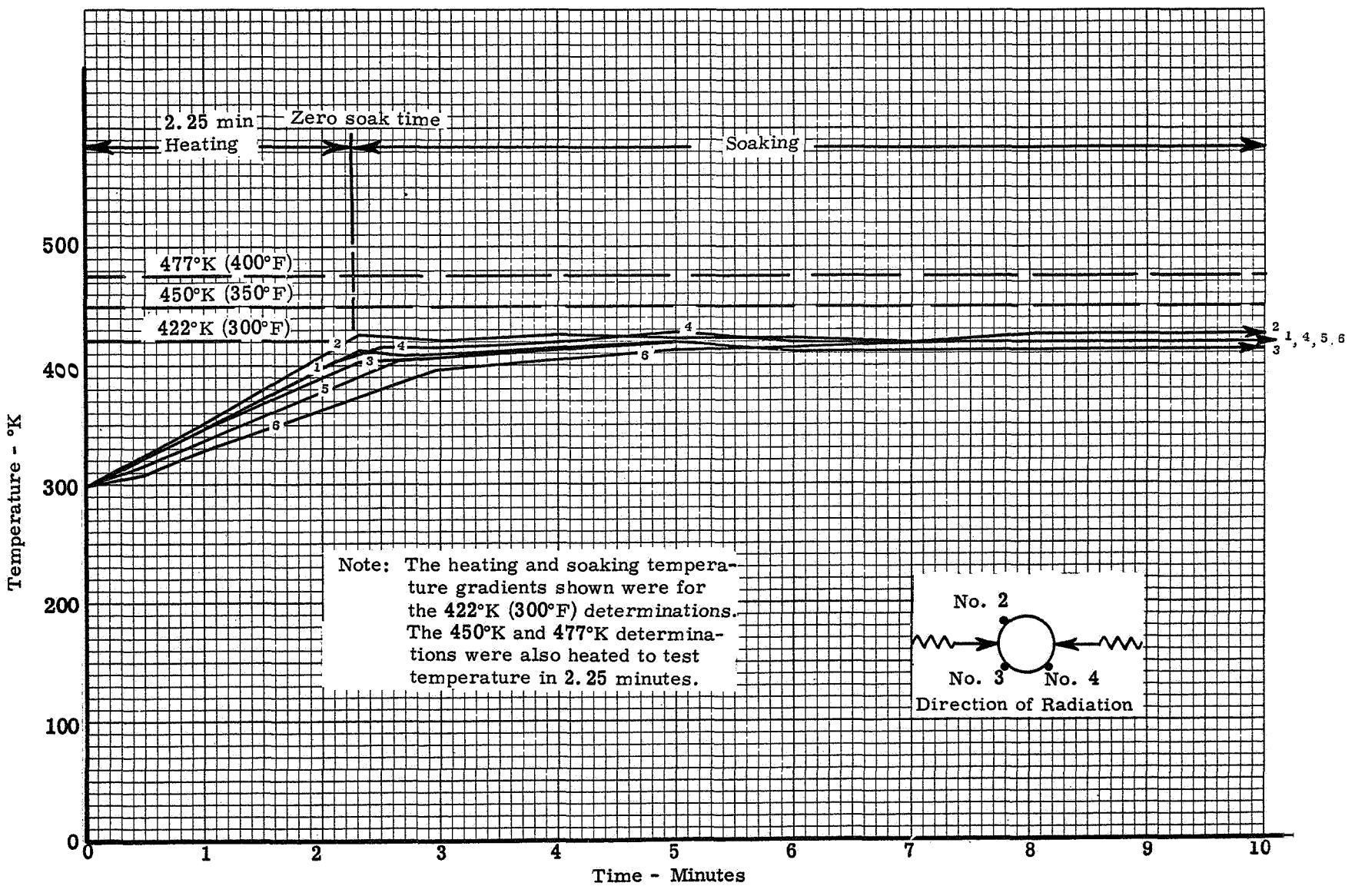

Figure 84. Typical heating and soaking curve for determining effects of time at temperature on tensile properties

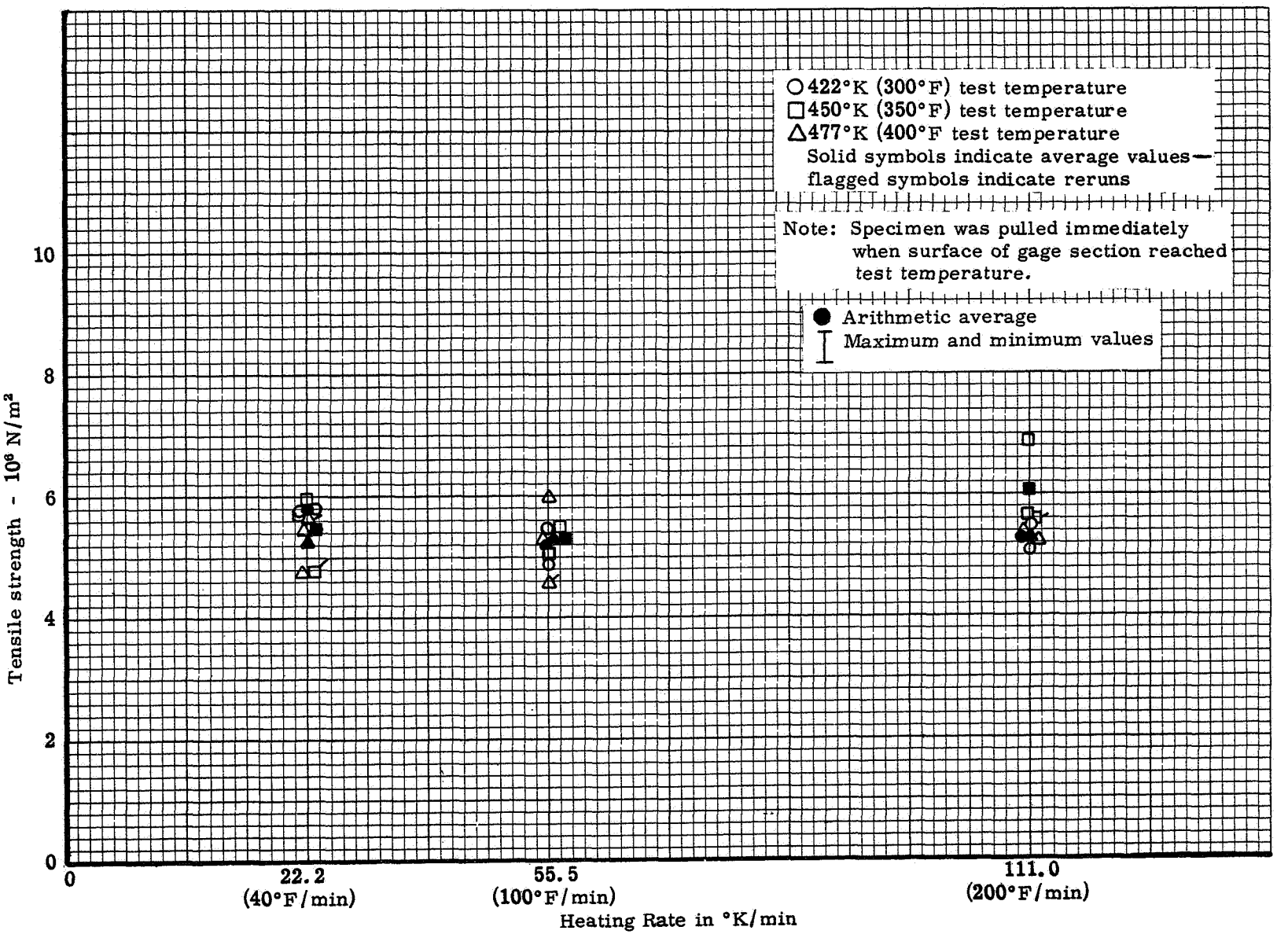

Figure 85. Ultimate strength in tension versus heating rate to test temperatures 422 K, 450°K, and 477°K

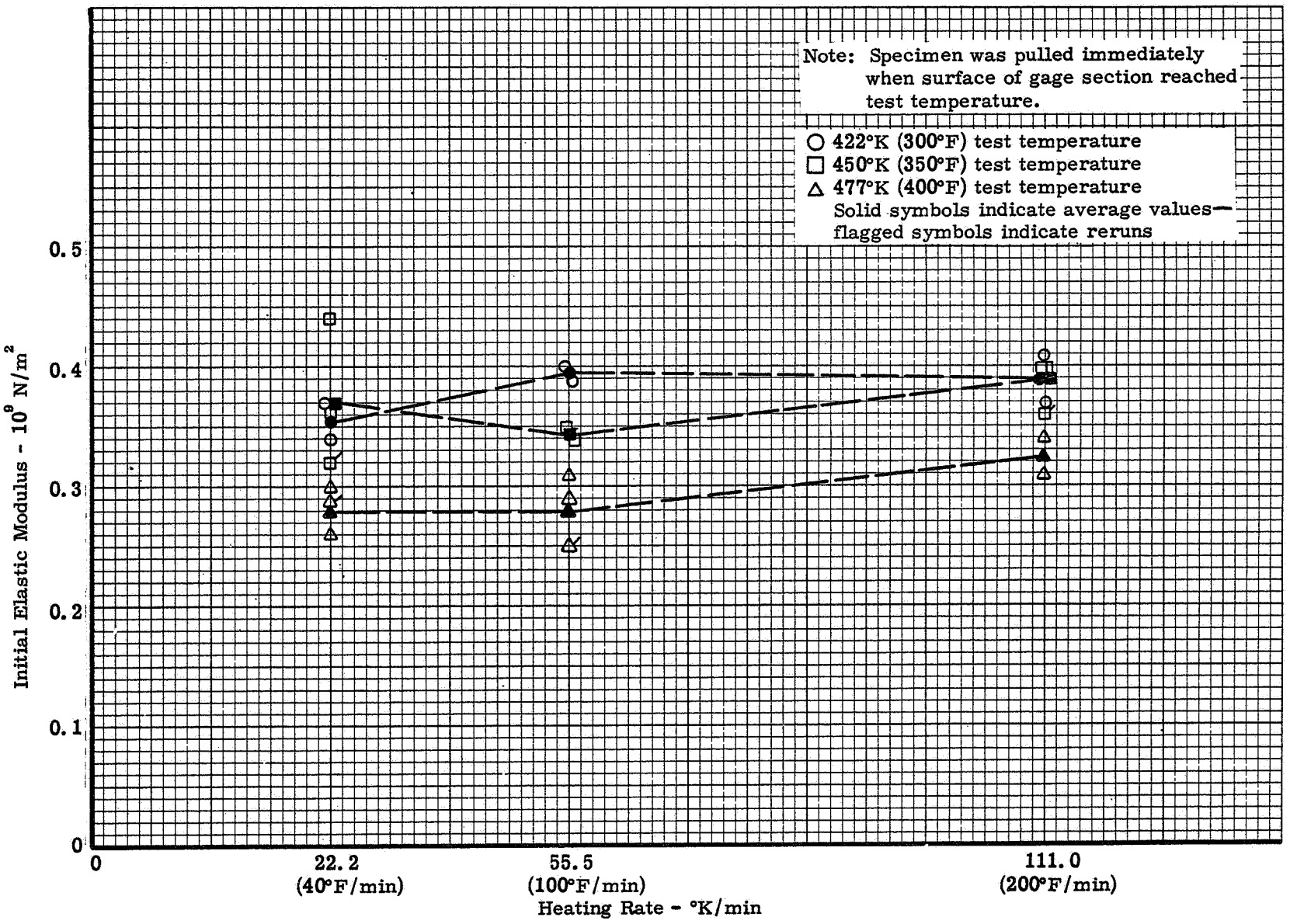

Figure 86. Initial elastic modulus in tension versus heating rate to test temperature= 422°K, 450°K and 477°K

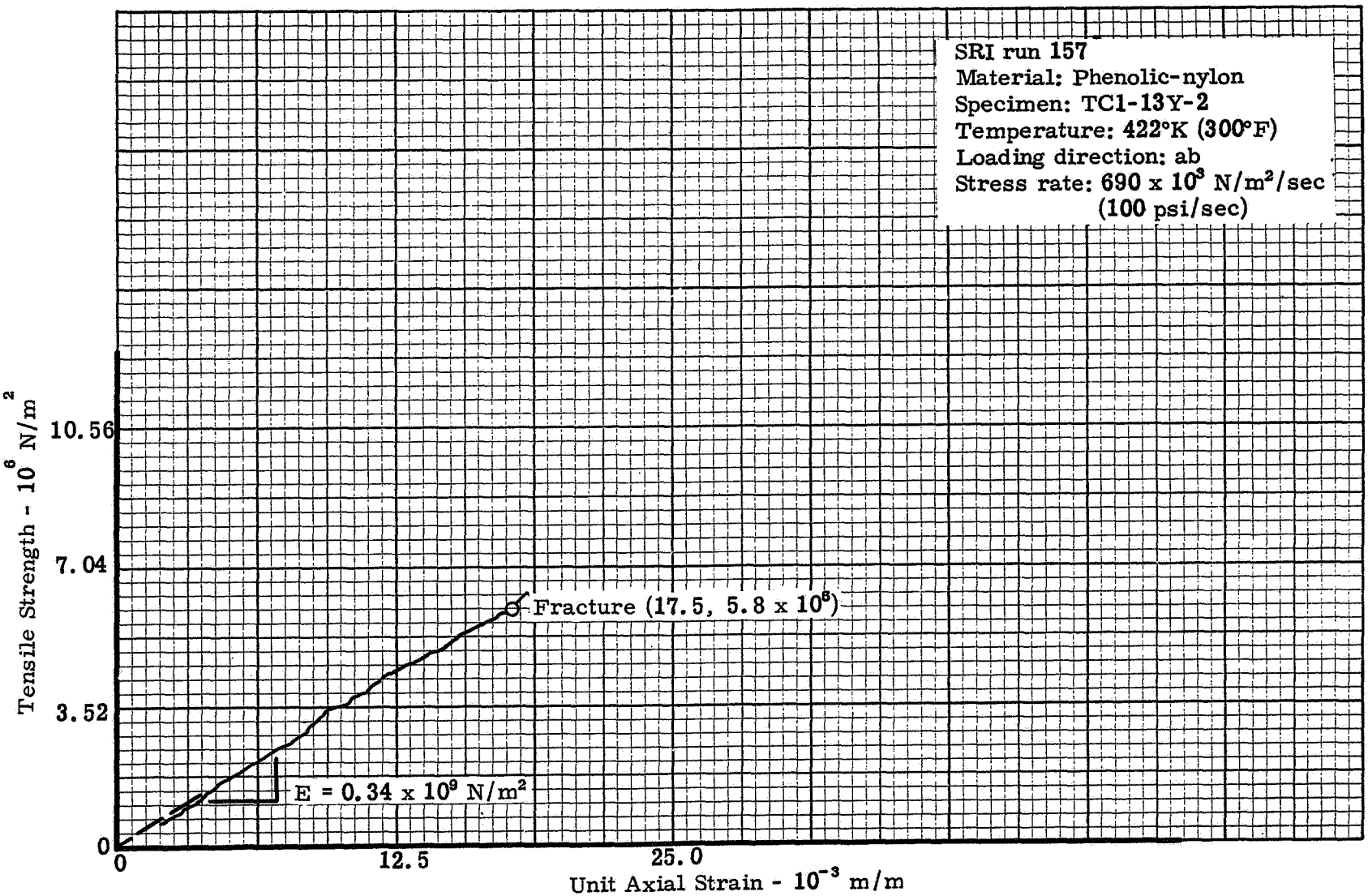

Figure 87. Typical tensile stress-strain curve for 1.270 cm dia x 5.08 cm gage length specimen tested in ab direction for determining heat rate effects - 22°K/min to 422°K (40°F/min to 300°F)

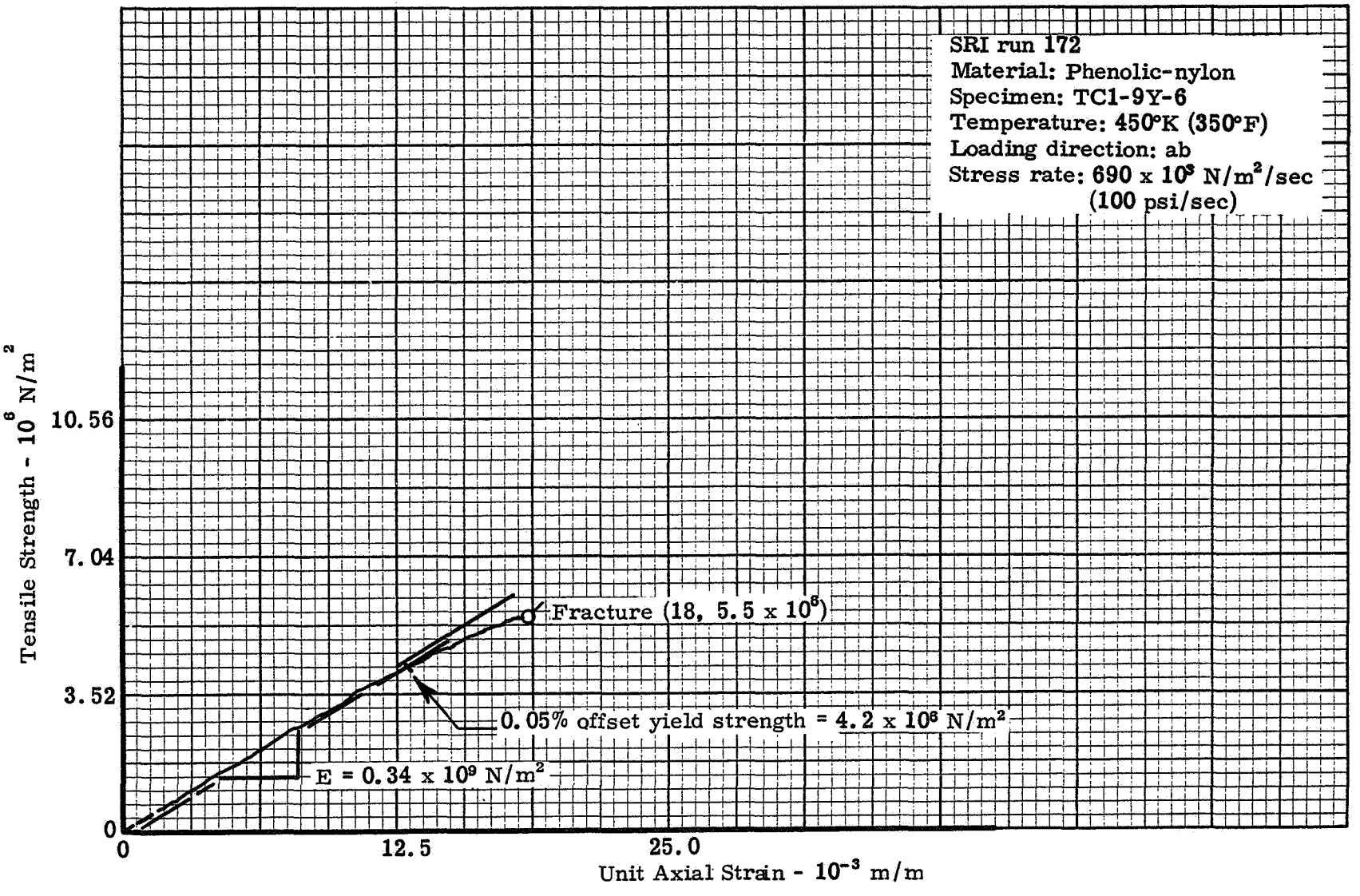

Figure 88. Typical tensile stress-strain curve for 1.270 cm dia x 5.08 cm gage length specimen tested in ab direction for determining heat rate effects - 55°K/min to 450°K (100°F/min to 350°F)

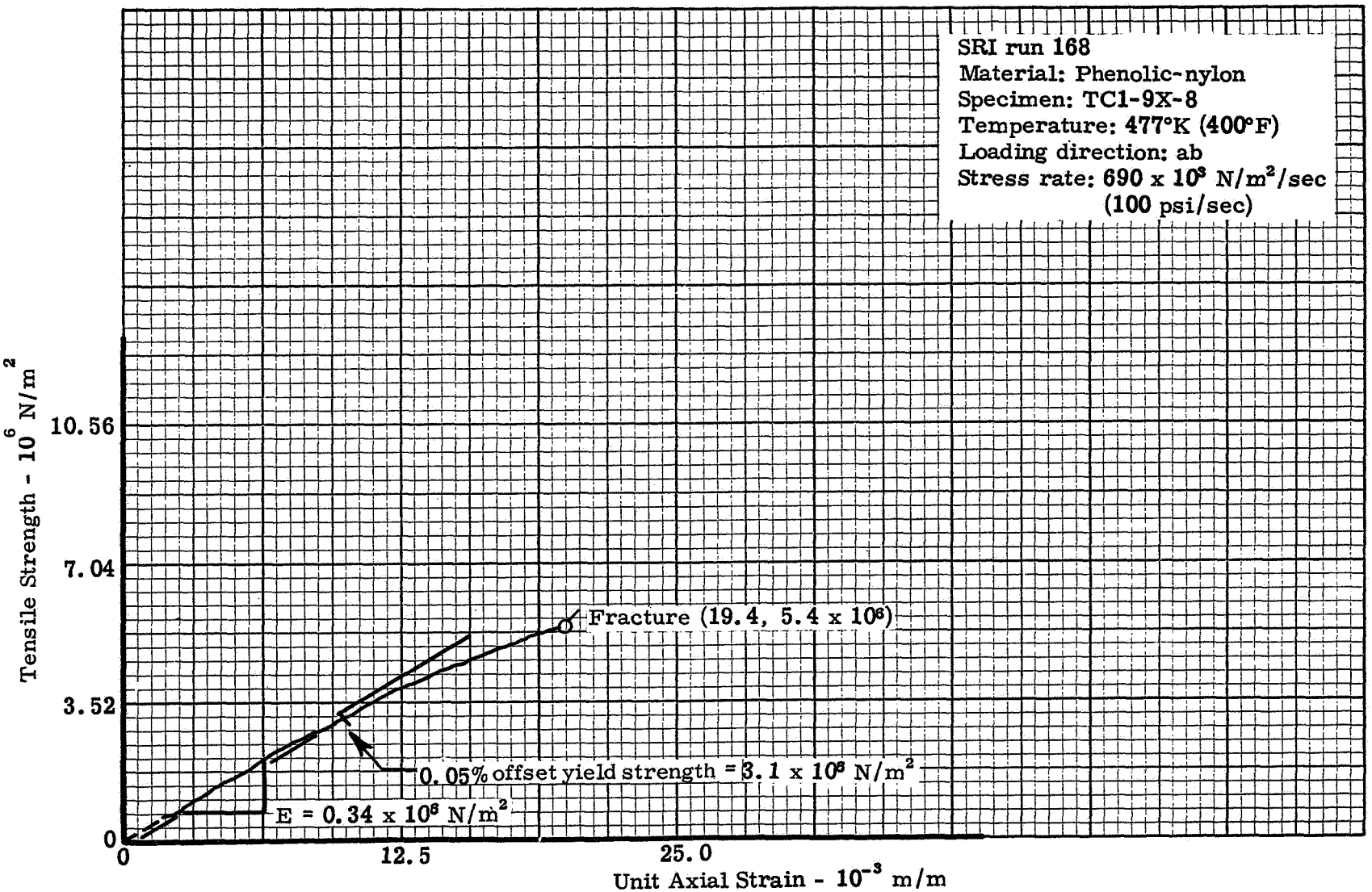

Figure 89. Typical tensile stress-strain curve for 1.270 cm dia x 5.08 cm gage length specimen tested in ab direction for determining heat rate effects - 111°K/min to 477°K (200°F/min to 400°F)

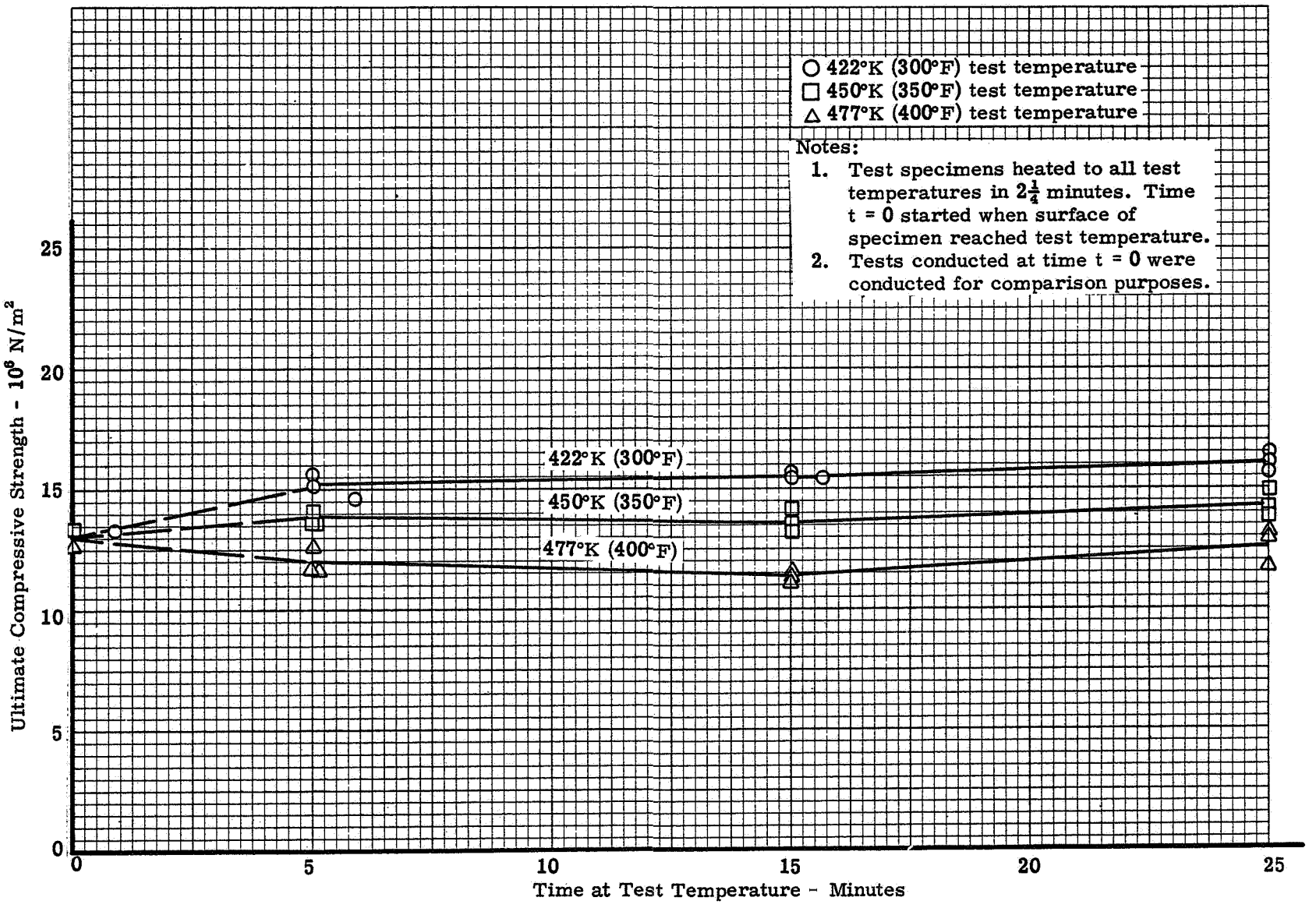

Figure 90 Ultimate strength in compression versus time at temperature for test temperatures 422°K, 450°K and 477°K

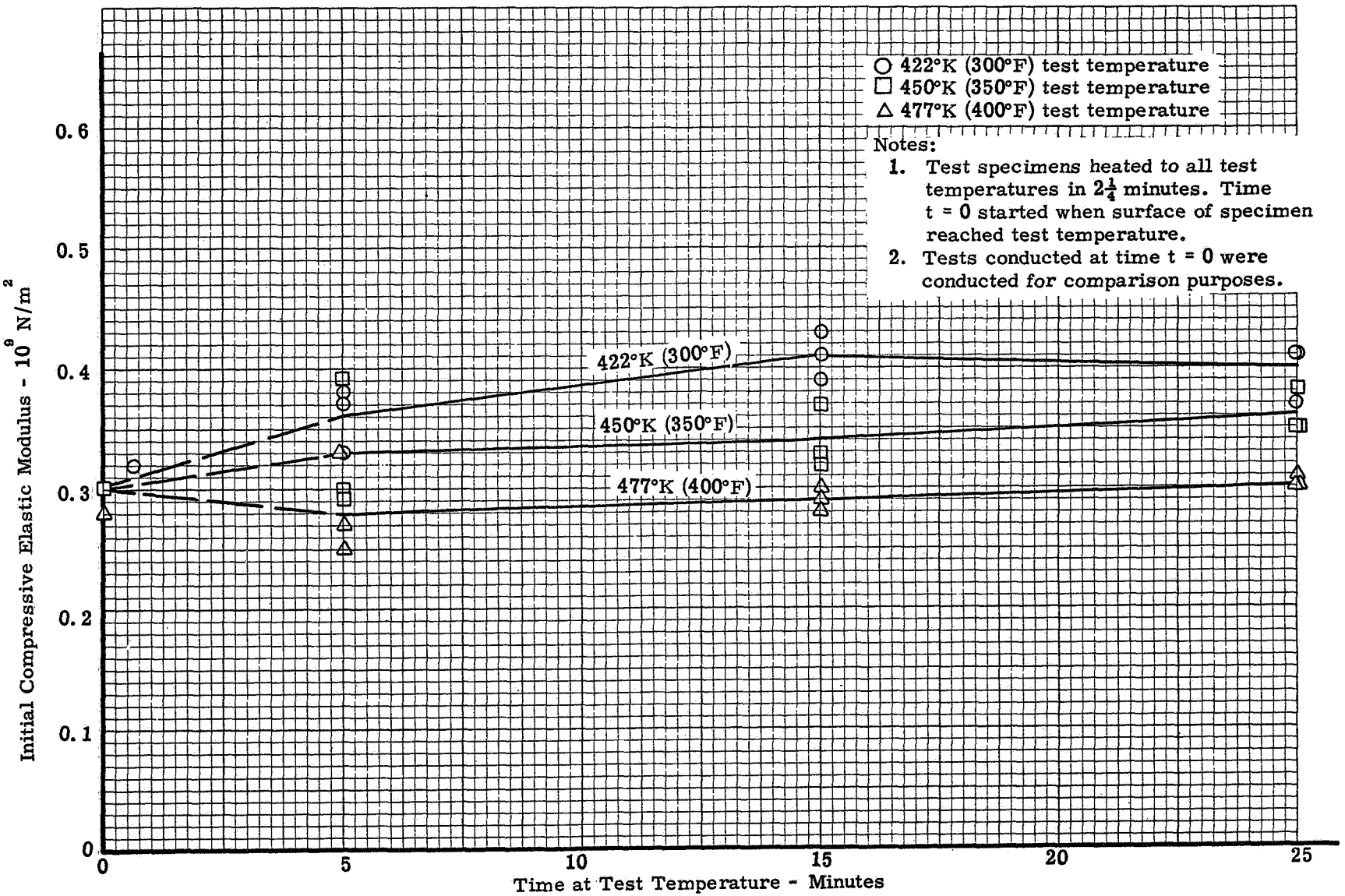

Figure 91. Initial elastic modulus in compression versus time at temperature for test temperatures 422°K, 450°K, and 477°K

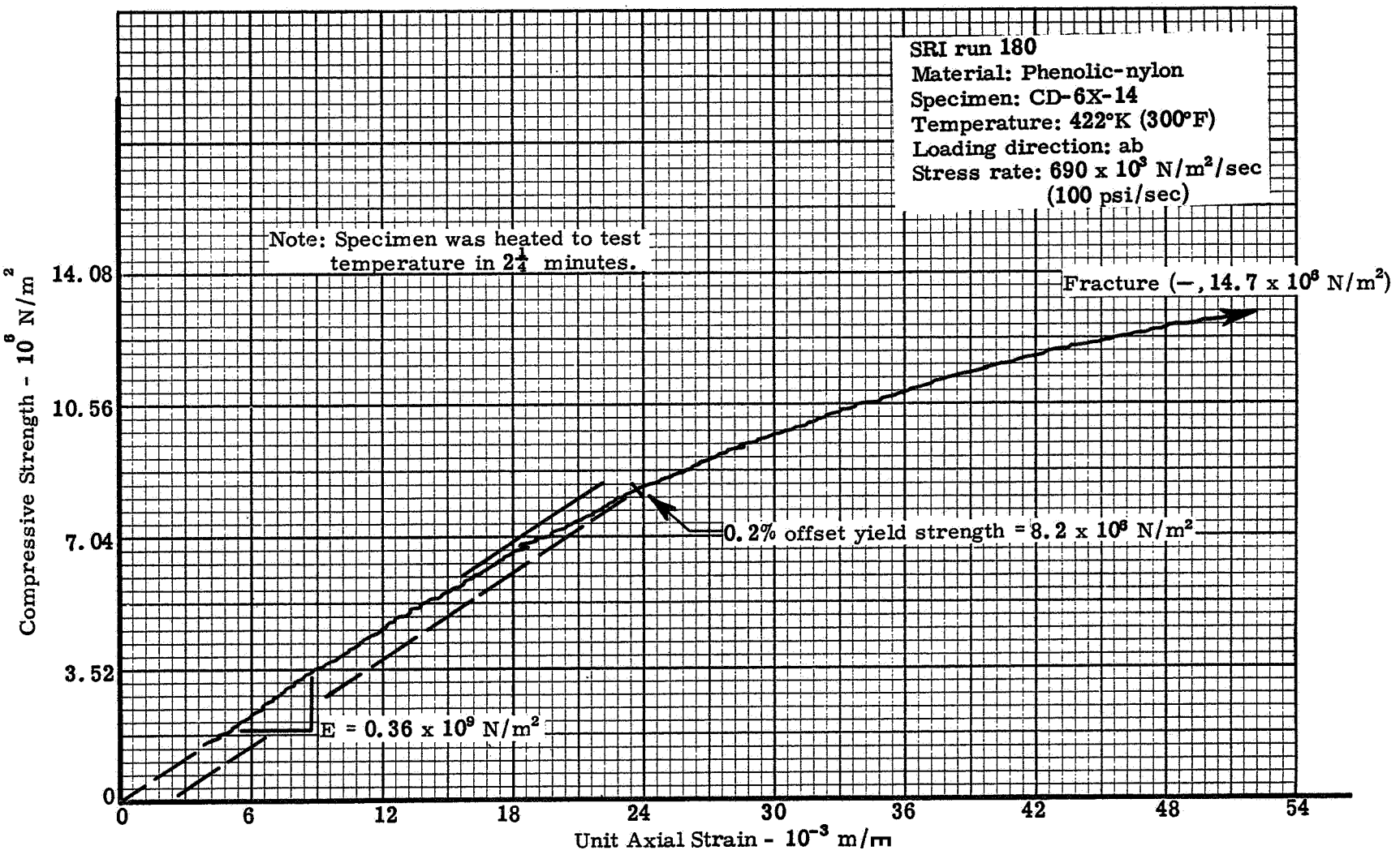

Figure 92. Typical compressive stress-strain curve for 1.270 cm dia x 2.54 cm gage length specimen tested in the ab direction for effects of time at temperature - 422°K for 6.75 minutes

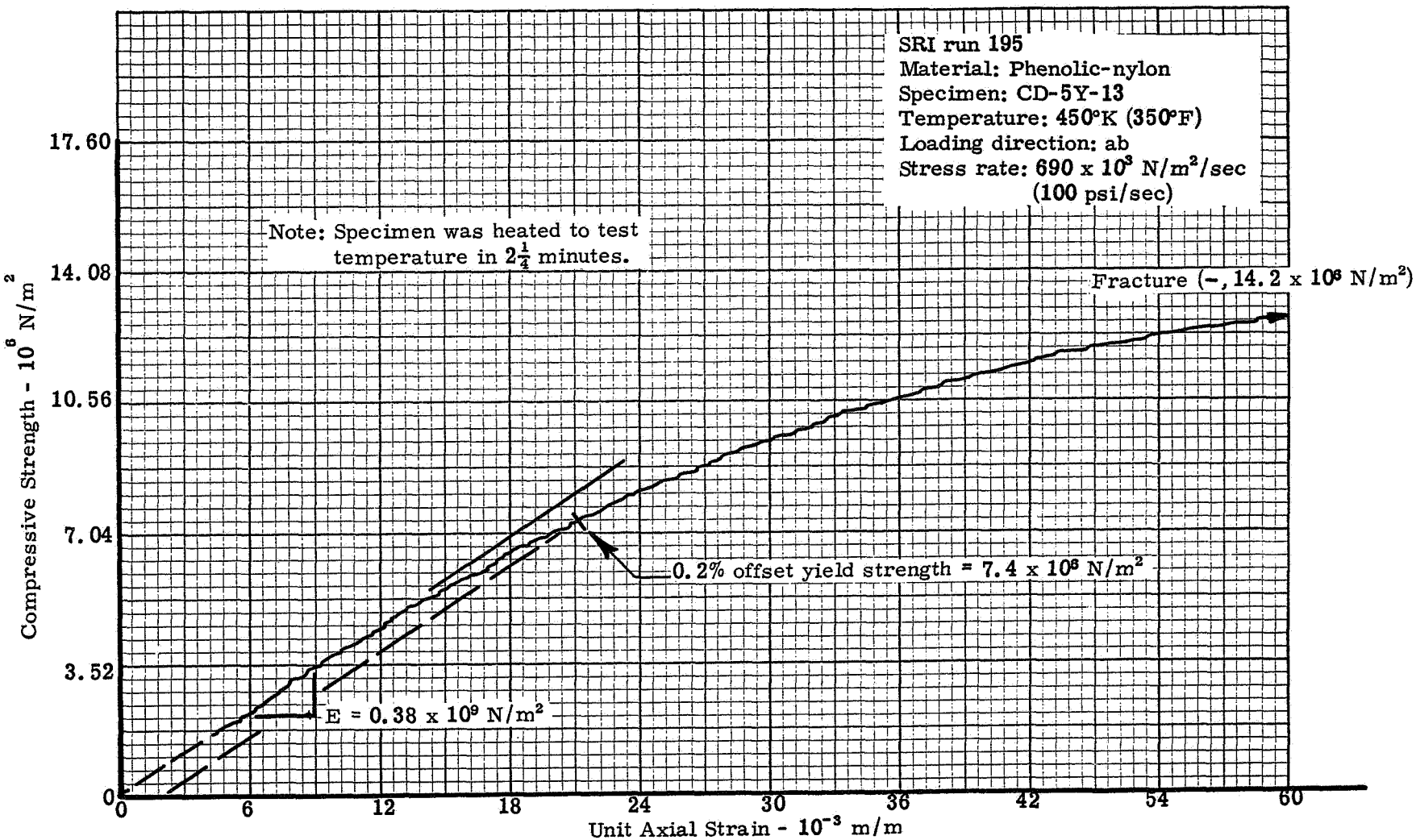

Figure 93. Typical compressive stress-strain curve for 1.270 cm dia x 2.54 cm gage length specimen tested in the ab direction for effects of time at temperature - 450°K for 25 minutes

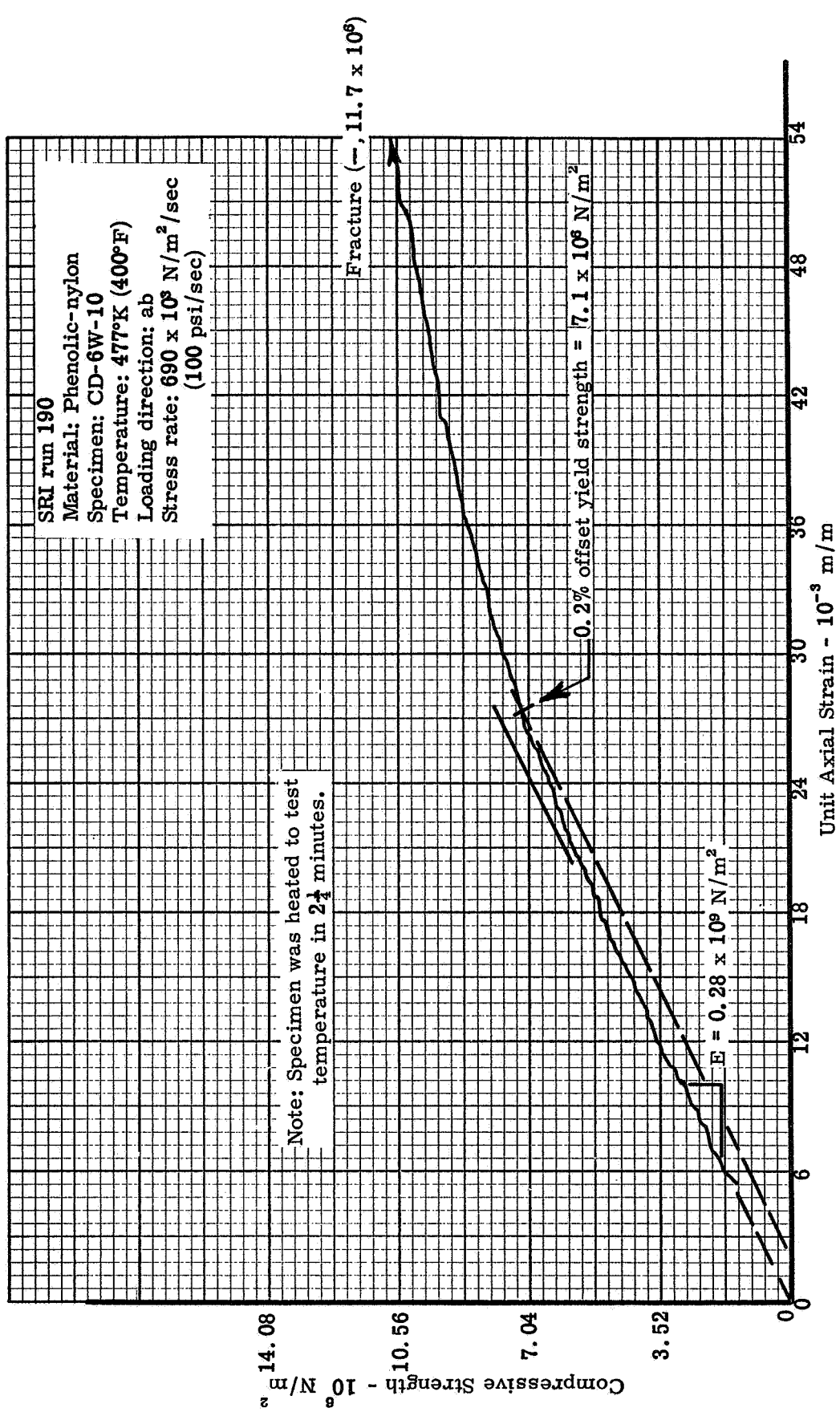

Figure 94. Typical compressive stress-strain curve for 1.270 cm dia x 2.54 cm gage length specimen tested in the ab direction for effects of time at temperature - 477°K for 15 minutes

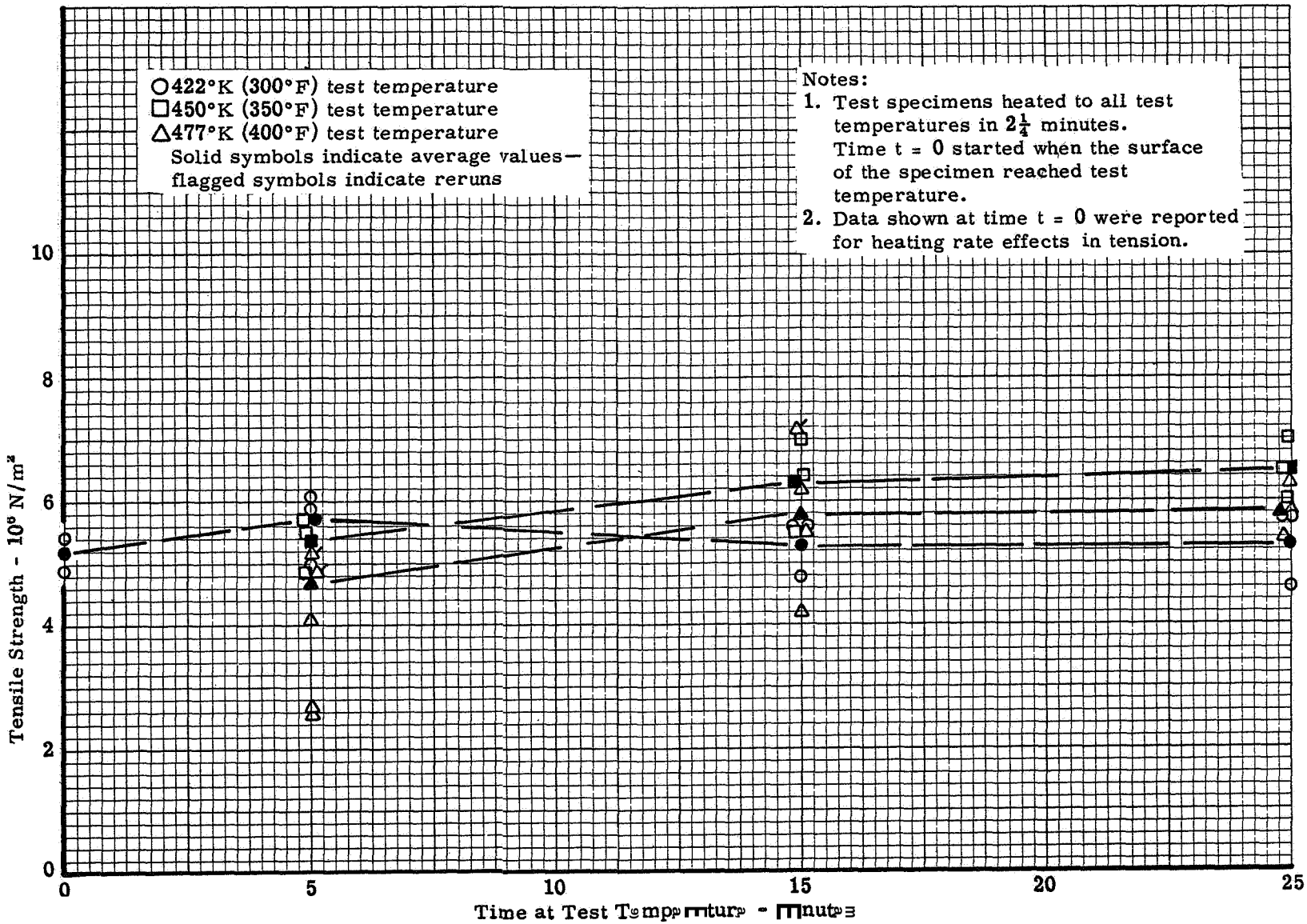

Figure 95. Ultimate strength in tension versus time at temperature for test temperatures 422°K, 450°K, and 477°K

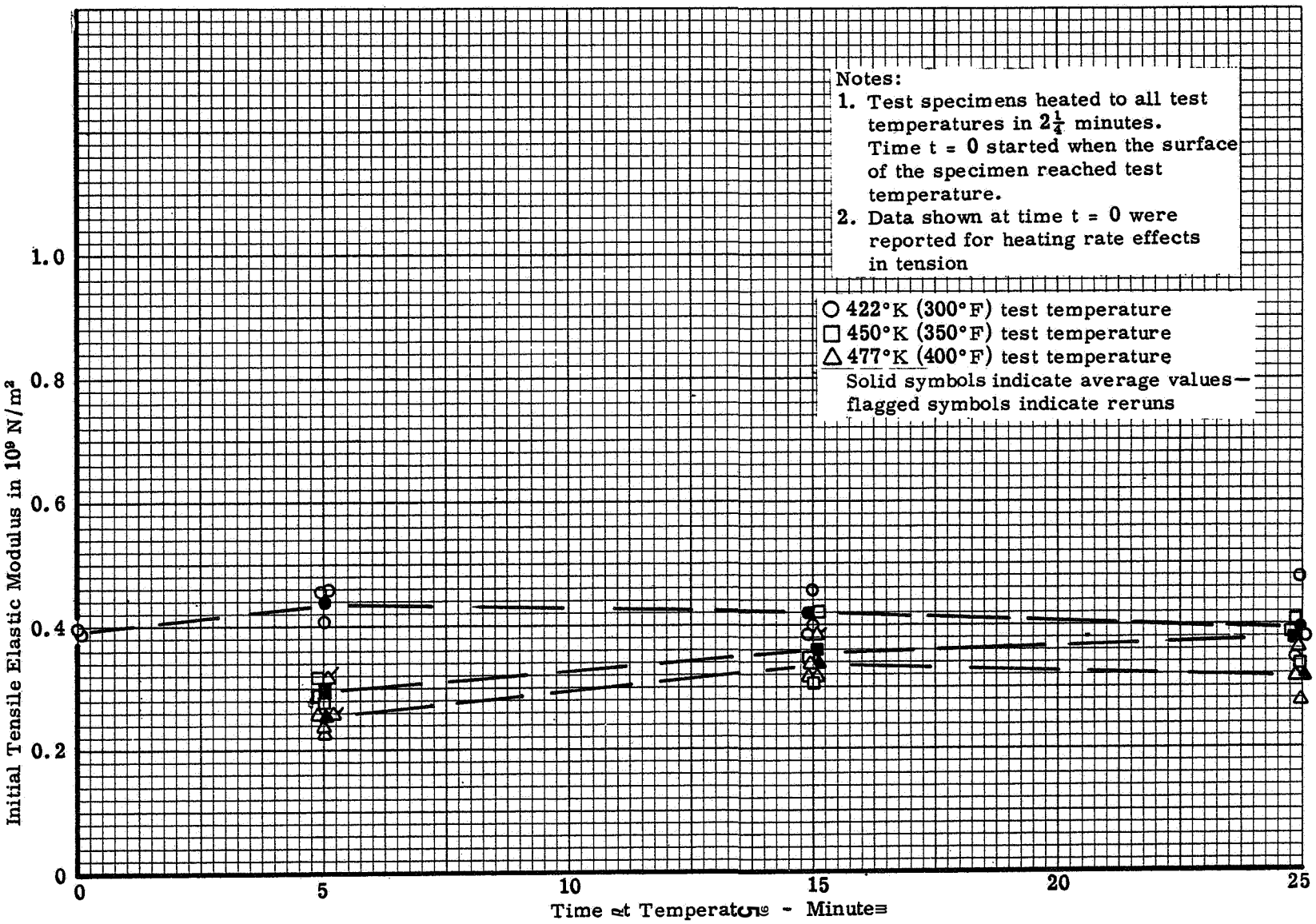

Figure 96. Initial elastic modulus in tension versus time at temperature for test temperatures 422°K, 450°K, and 477°K

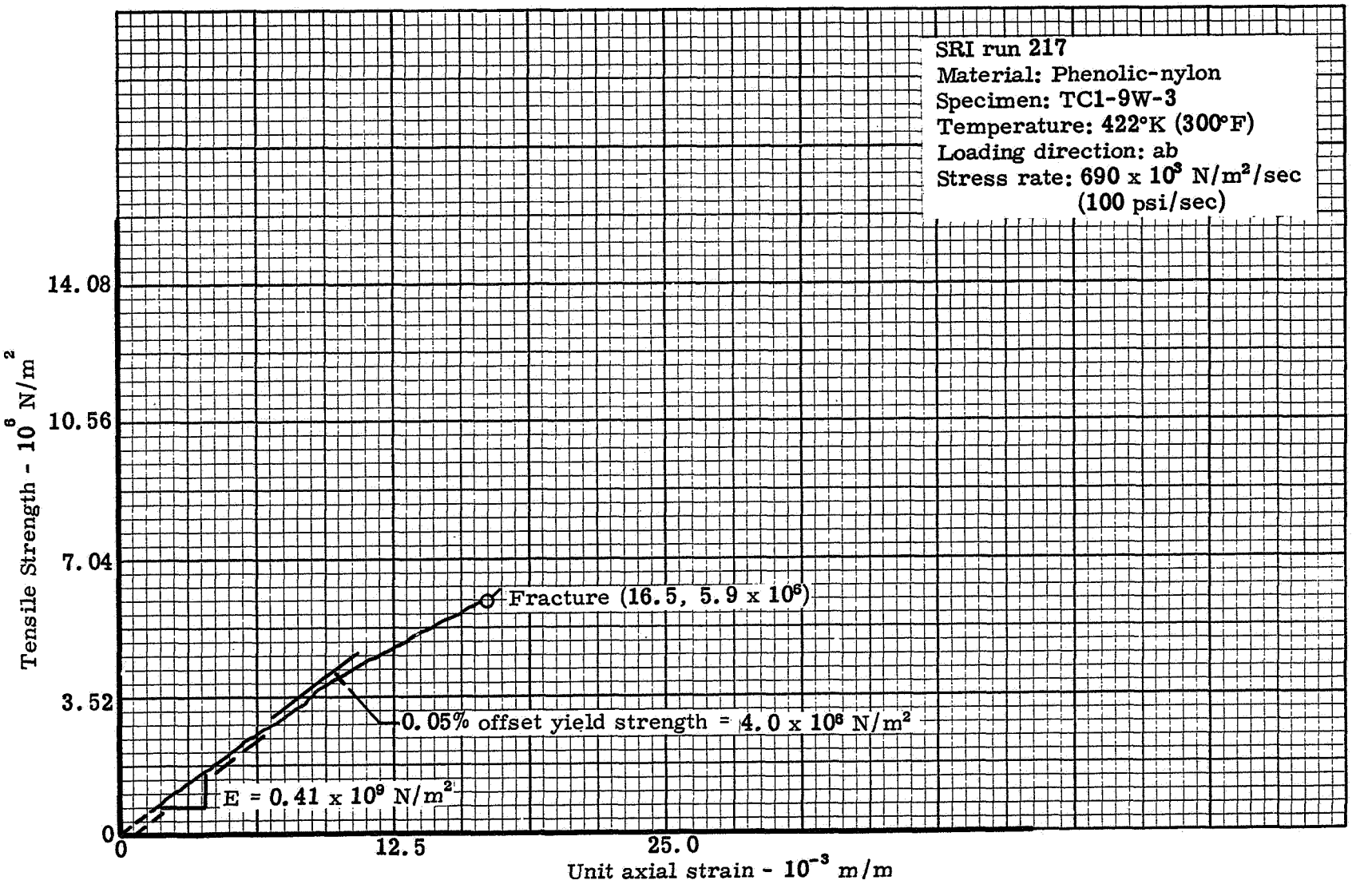

Figure 97. Typical tensile stress-strain curve for 1.270 cm dia x 5.08 cm gage length specimen tested in ab direction for effects of time at temperature - 422°K for 5.0 minutes

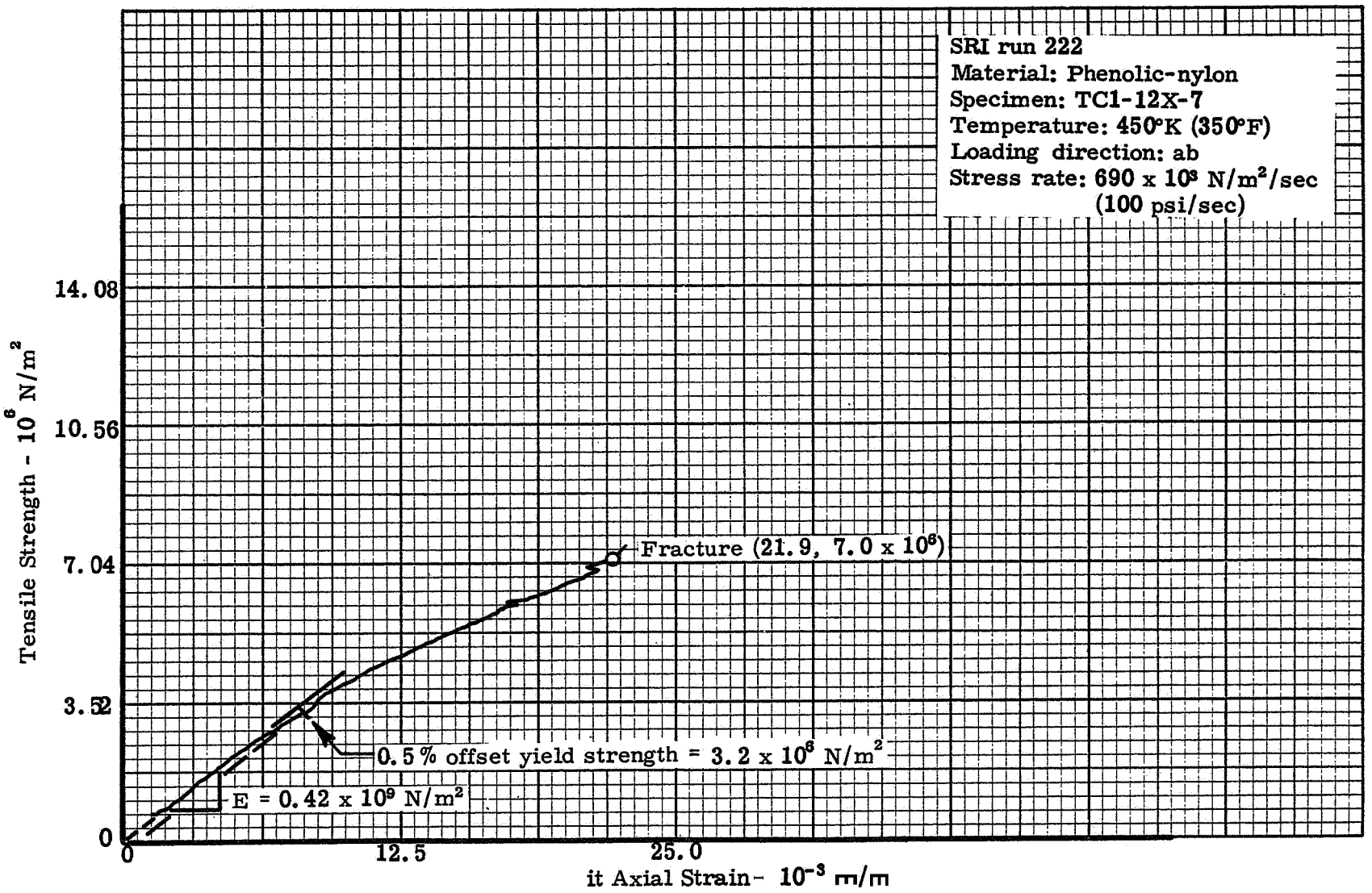

Figure 98. Typical tensile stress-strain curve for 1.270 in. dia x 5.08 cm gage length specimen tested in ab direction for effects of time at temperature - 450°K for 15.0 minutes

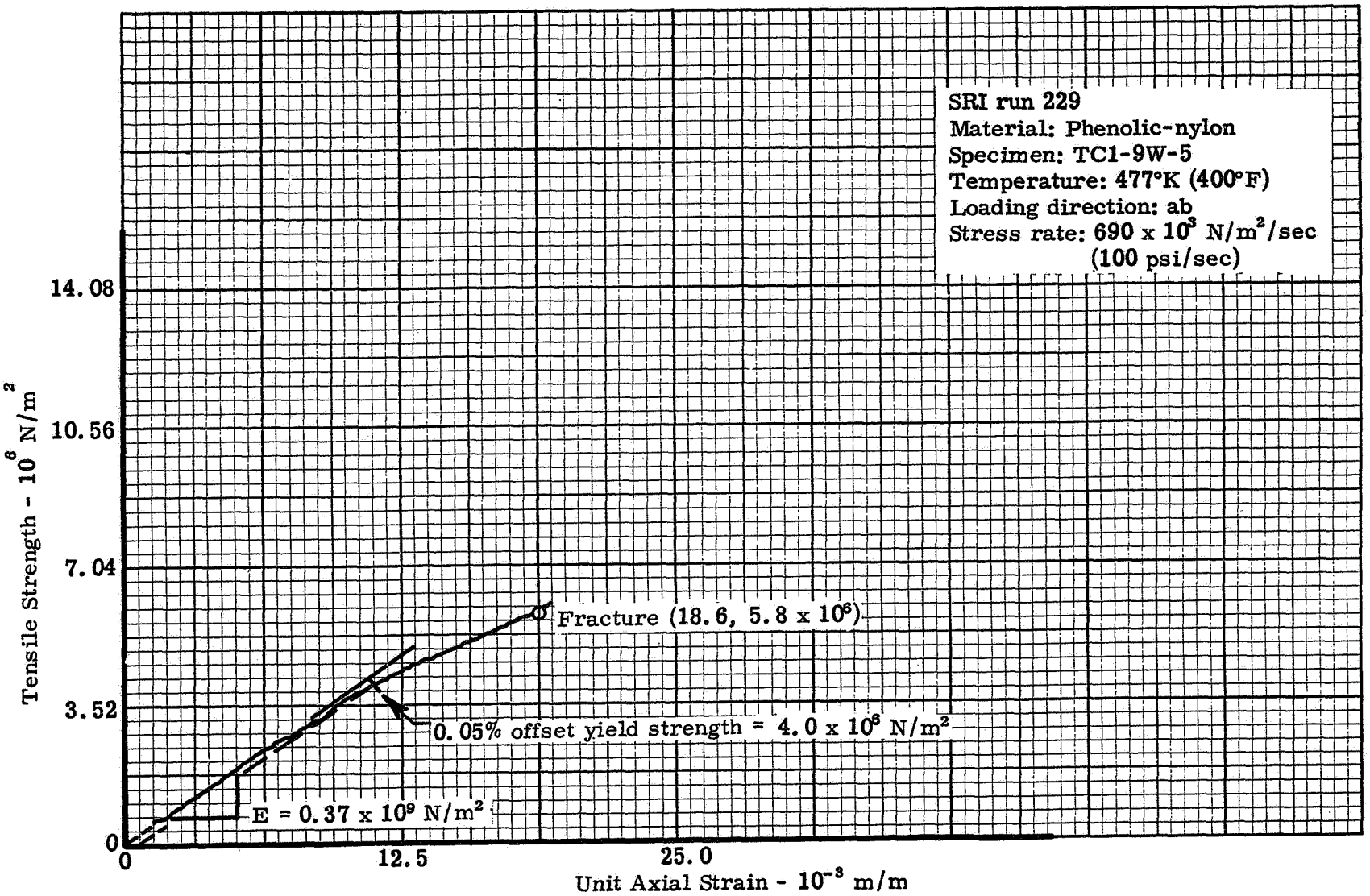

Figure 99. Typical tensile stress-strain curve for 1.270 cm dia x 5.08 cm gage length specimen tested in ab direction for effects of time at temperature - 477°K for 25.0 minutes

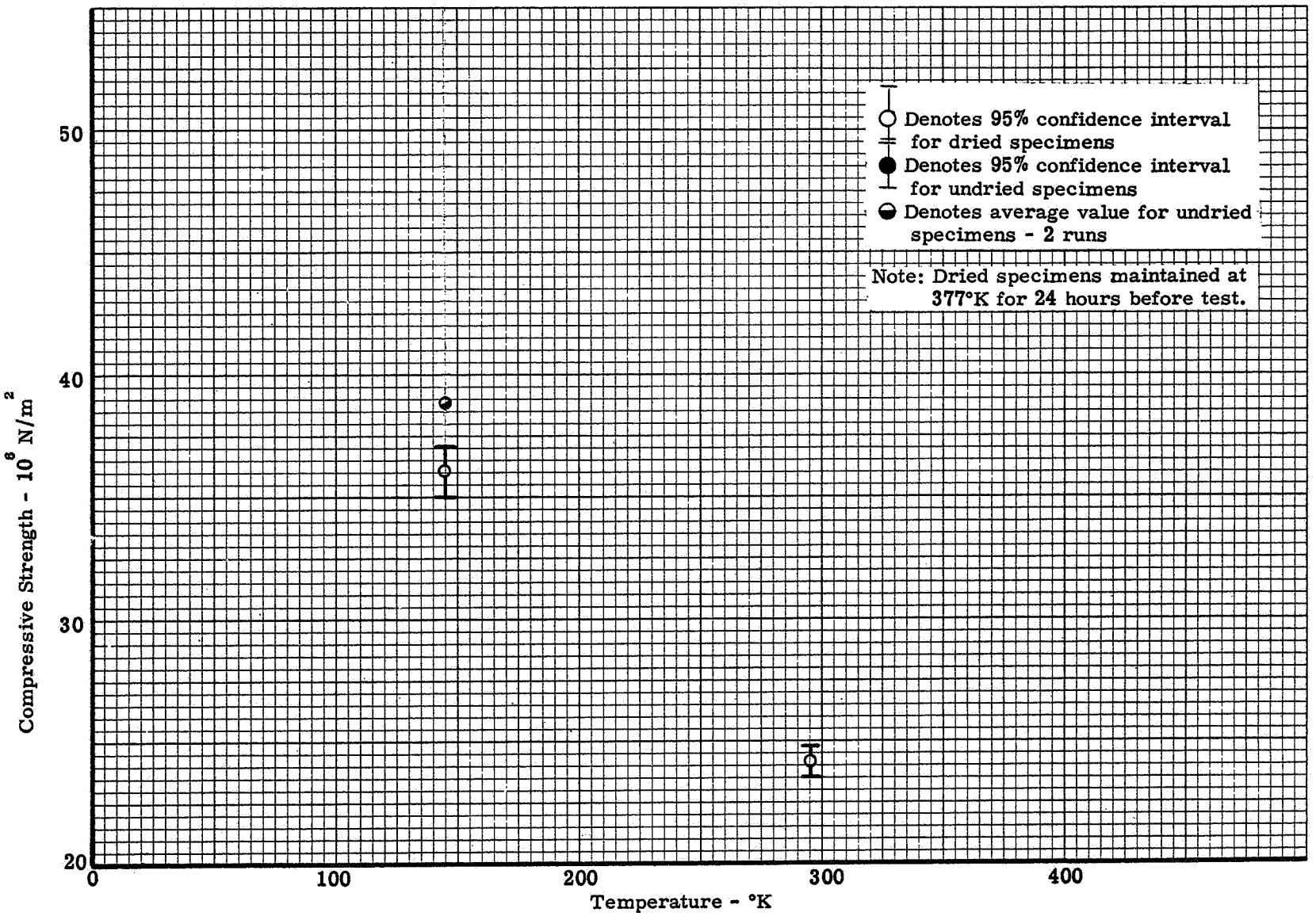

Figure 100. Compressive strength versus temperature evaluated in ab direction at 294°K and 144°K

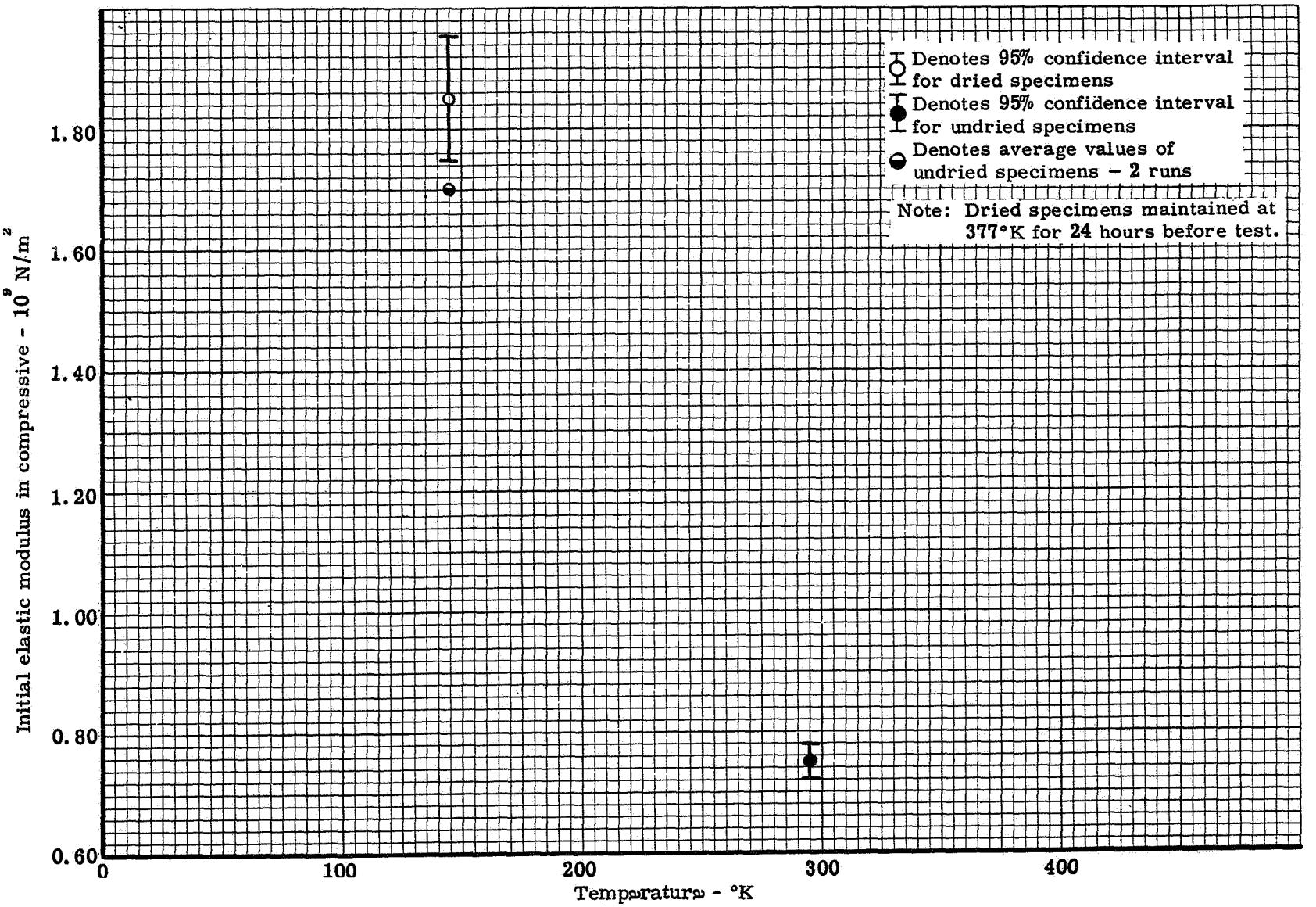

Figure 101. Elastic modulus in compression versus temperature evaluated in ab direction at 294°K and 144°K

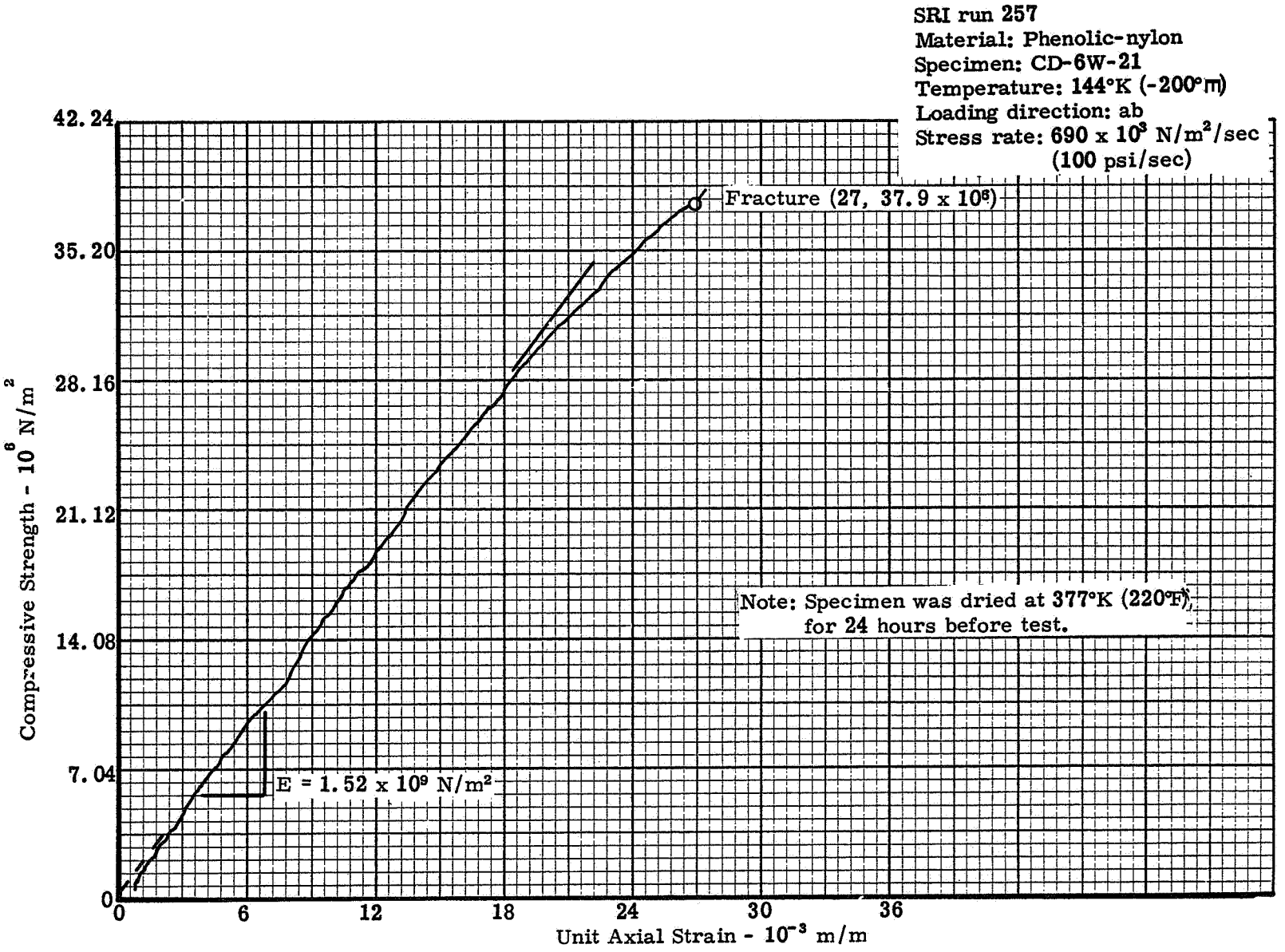

Figure 102. Typical compressive stress-strain curve for 1.270 cm dia x 2.54 cm gage length specimen tested in ab direction at 144°K (-200°F) for data scatter study

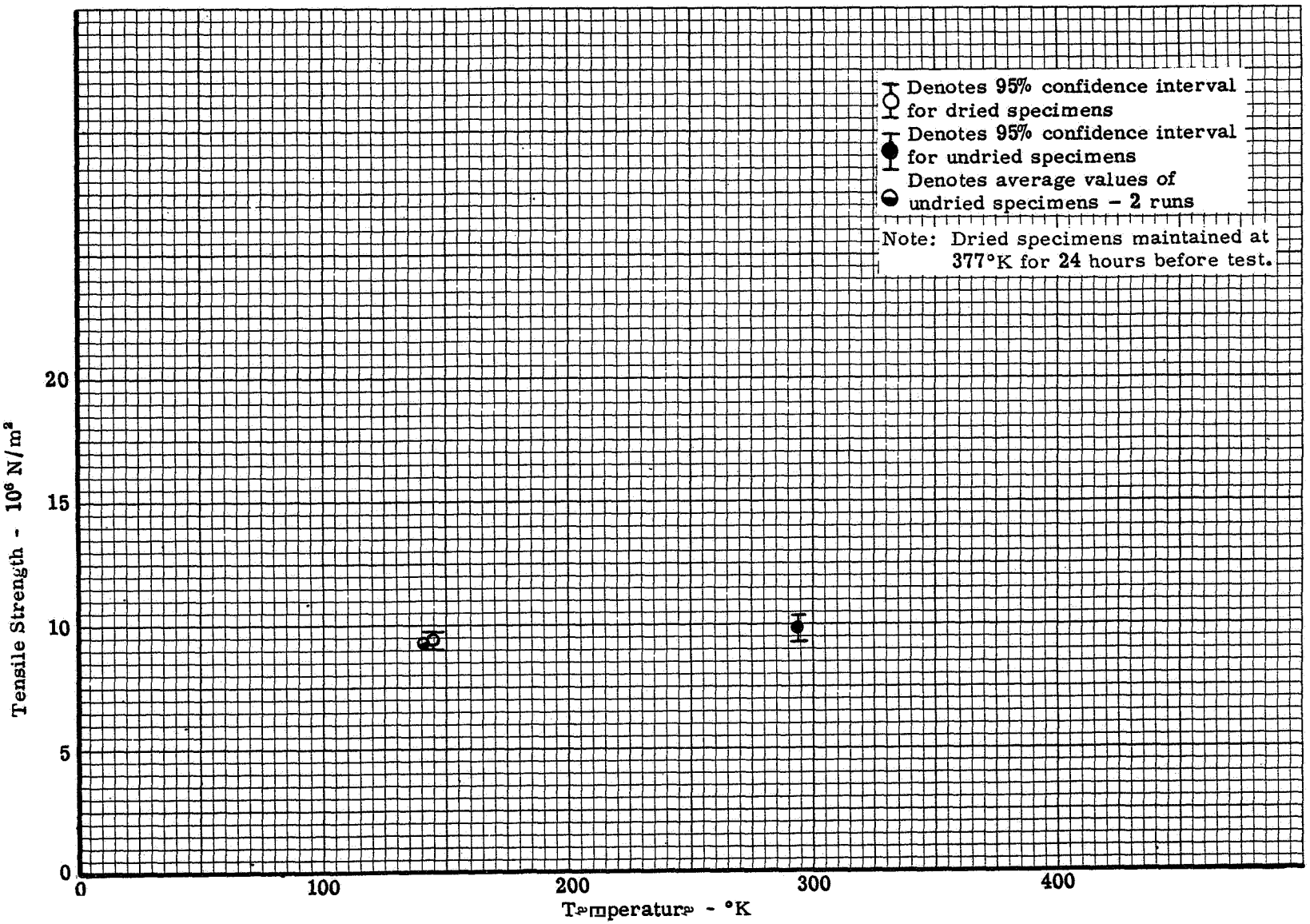

Figure 43 Tensile strength versus temperature evaluated in L direction at 294°K and 144°K

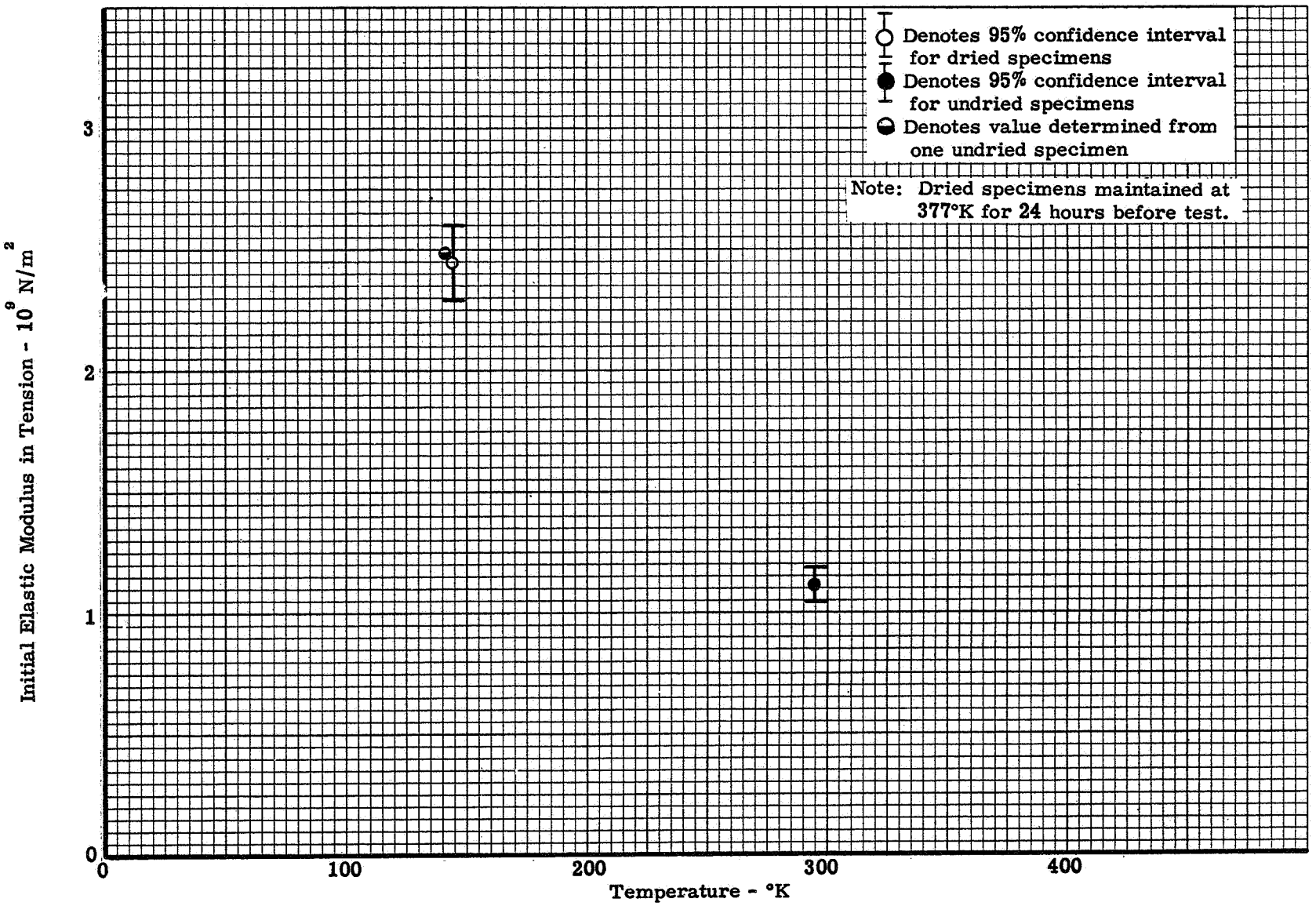

Figure 104. Elastic modulus in tension versus temperature evalued in ⏢ direction at 294°K and 144°K

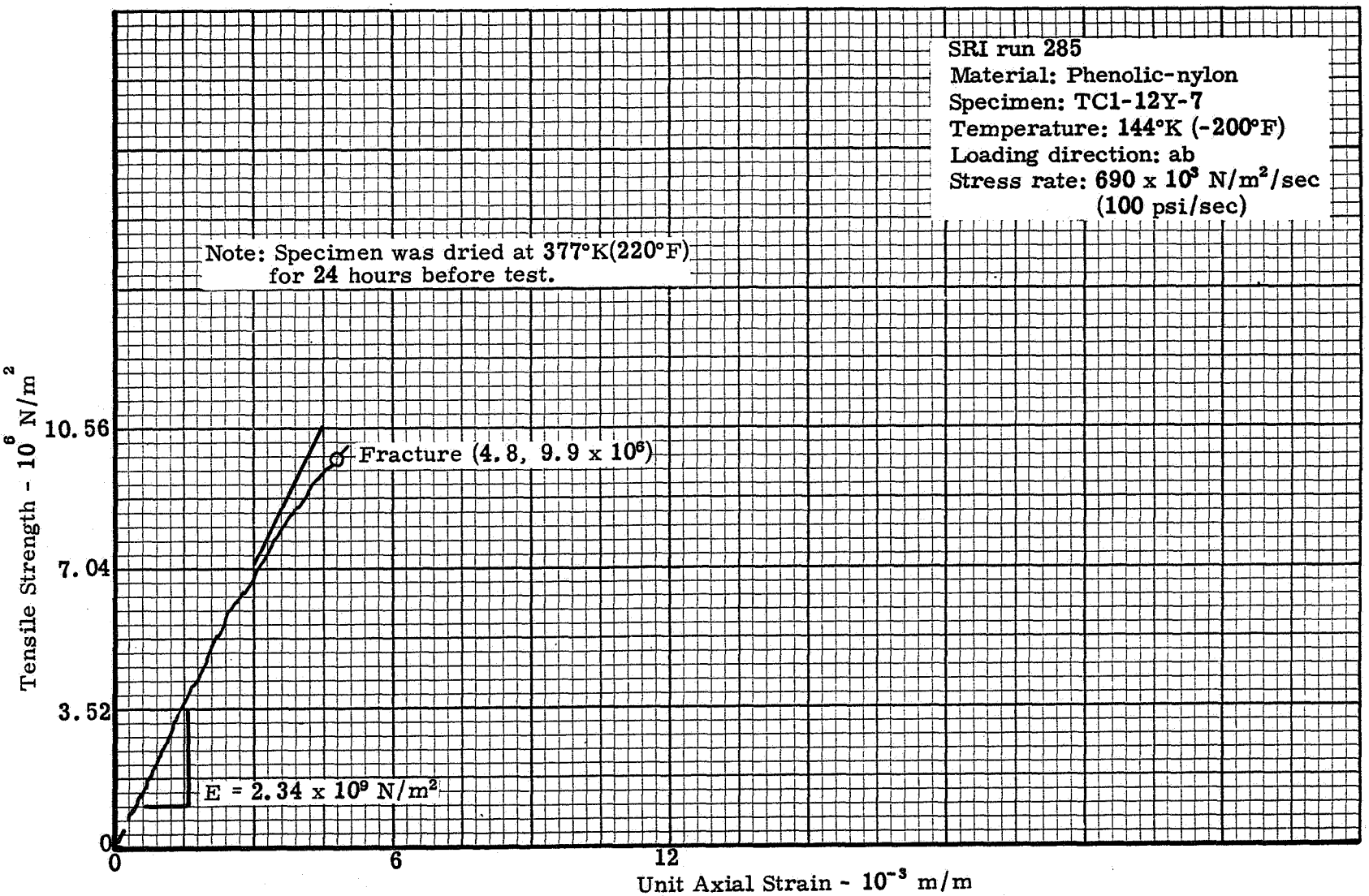

Figure 105 Typical tensile stress-strain curve for 1.270 cm dia x 5.08 cm gage length specimen tested in ab direction at 144°K (-200°F) for data scatter study

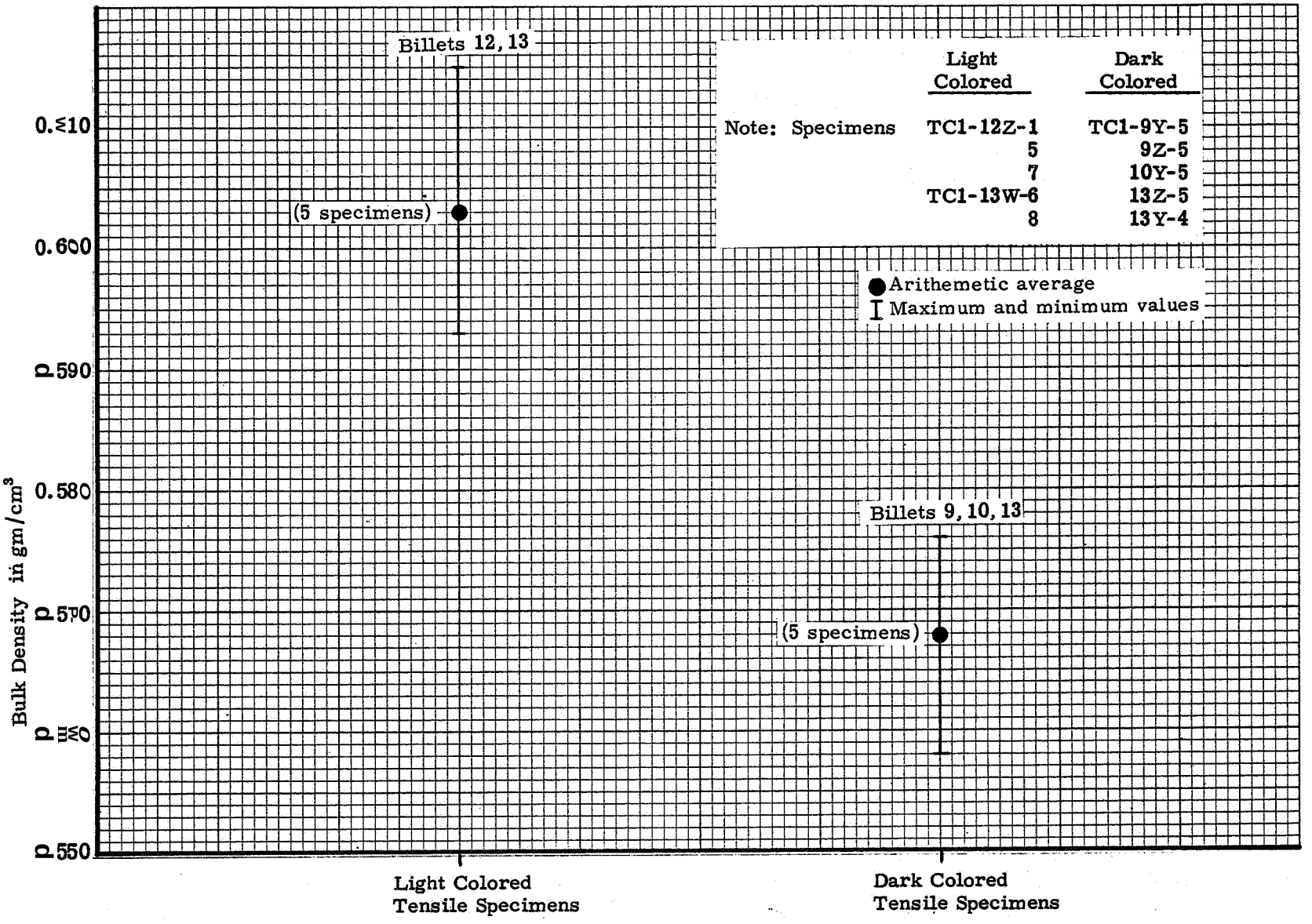

Figure 106. Bulk density variations in light and dark colored areas within phenolic-nylon at 294°K (70°F)

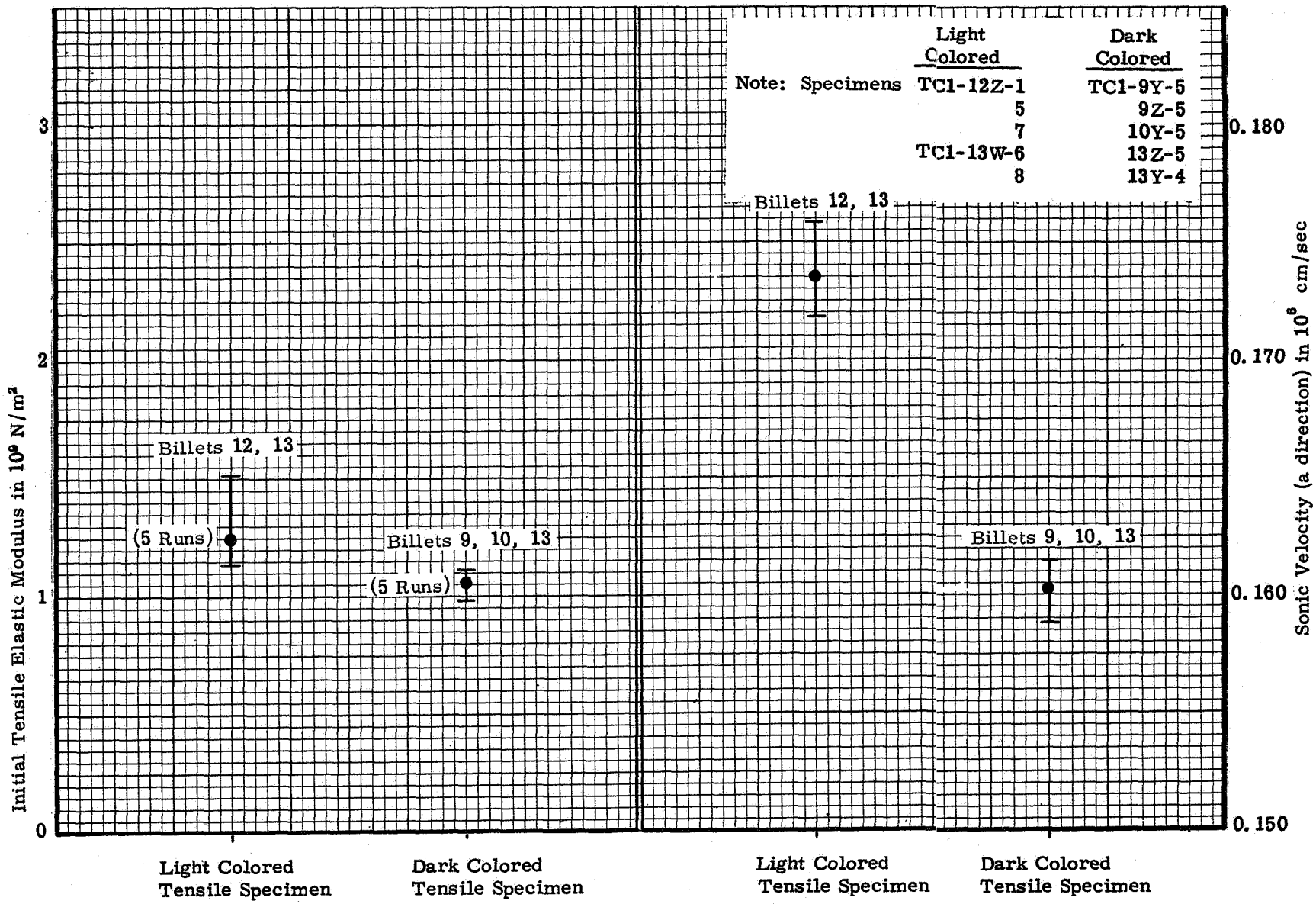

Figure 107. Initial tensile elastic modulus and sonic velocity variations in light and dark colored areas within phenolic-nylon at 294°K (70°F)

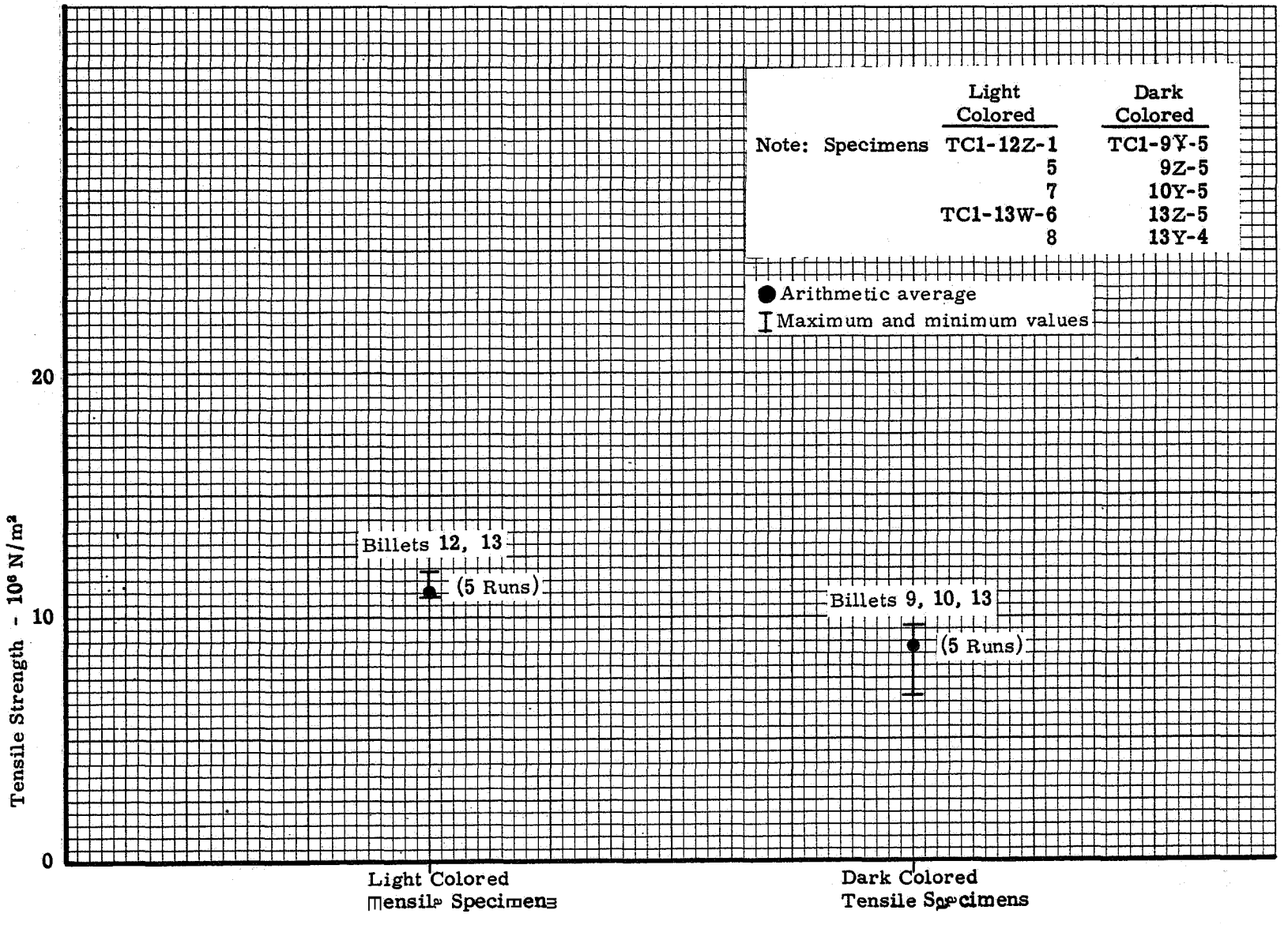

Figure 108. Tensile strength variations in light and dark colored areas within phenolic-nylon at 294°K (70°F)

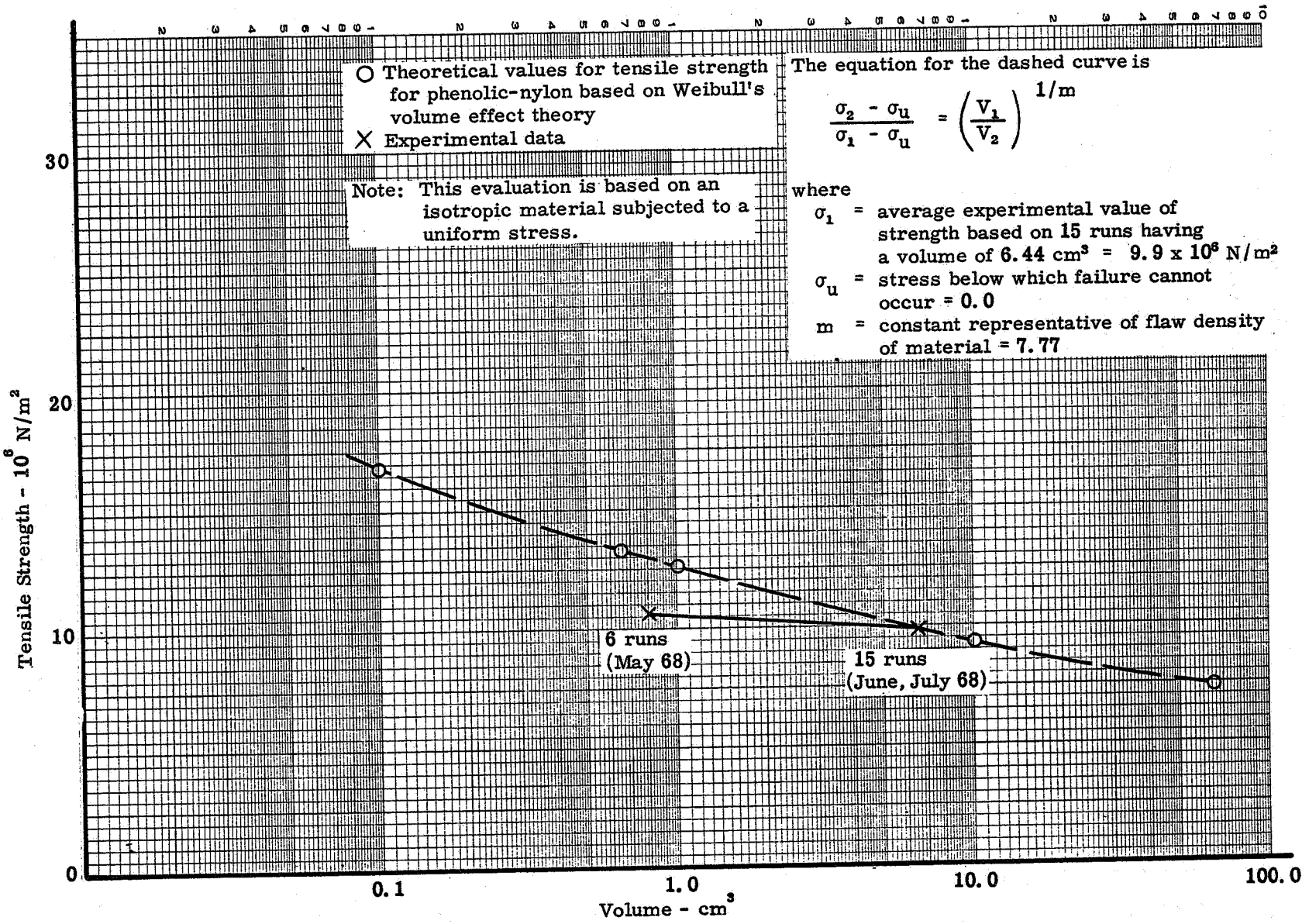

Figure 109. Average ultimate tensile strength versus volume based on Weibull's volume effect theory

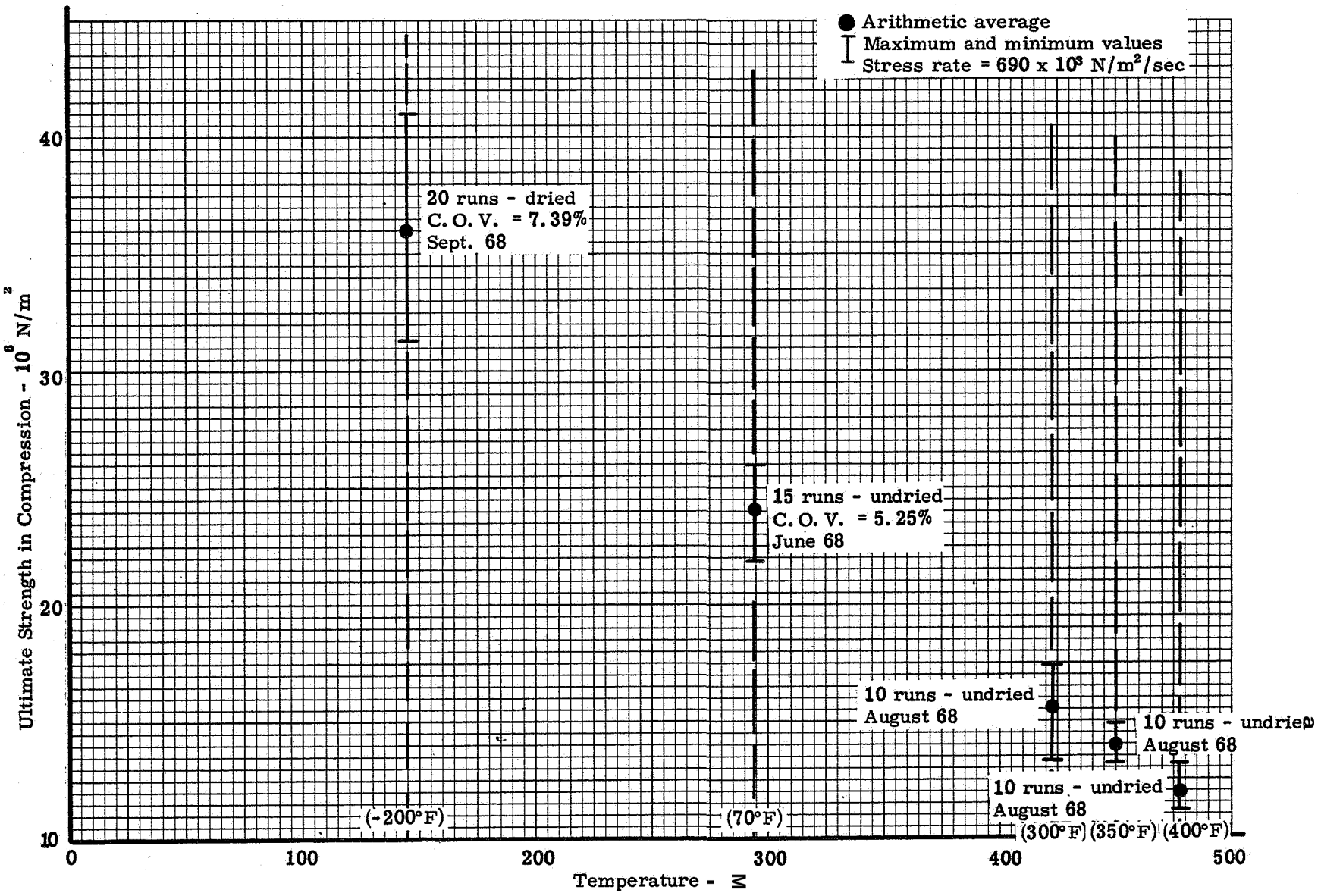

Figure 110. Ultimate strength in compression versus temperature for low-density phenolic-nylon

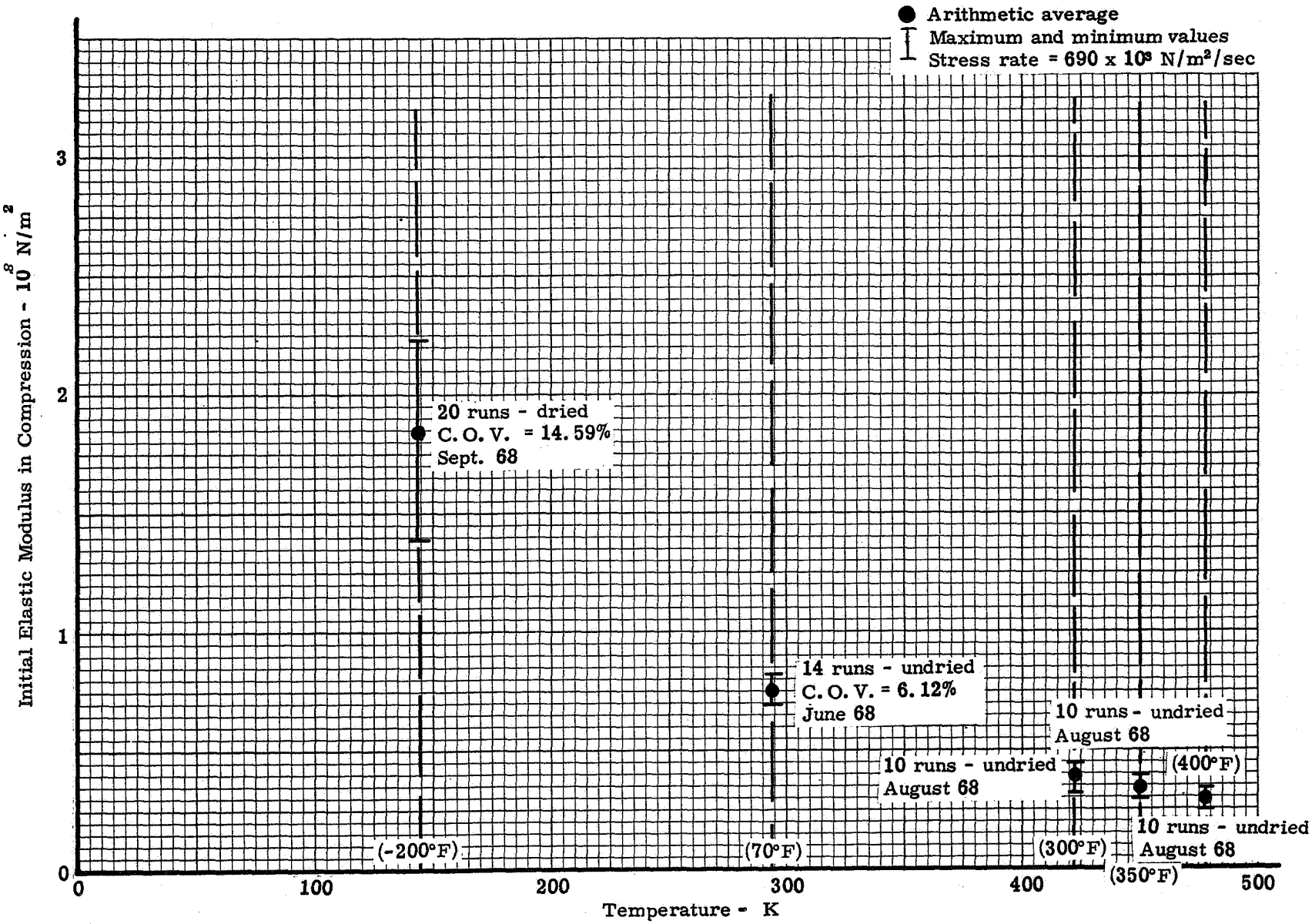

Figure 111. Initial elastic modulus in compression vs temperature for low-density phenolic-nylon

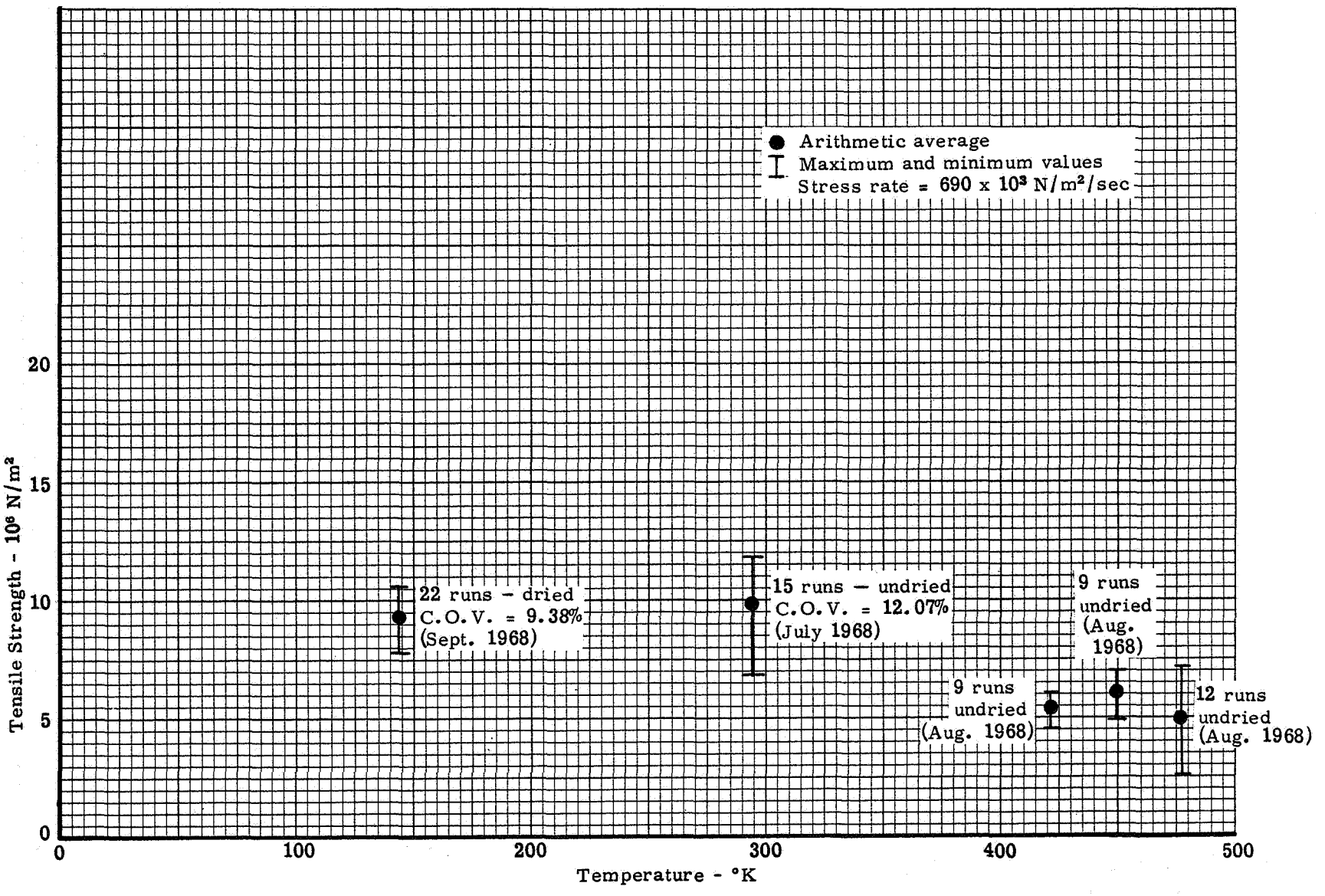

Figure 112. Ultimate strength in tension versus temperature for low-density phenolic-nylon

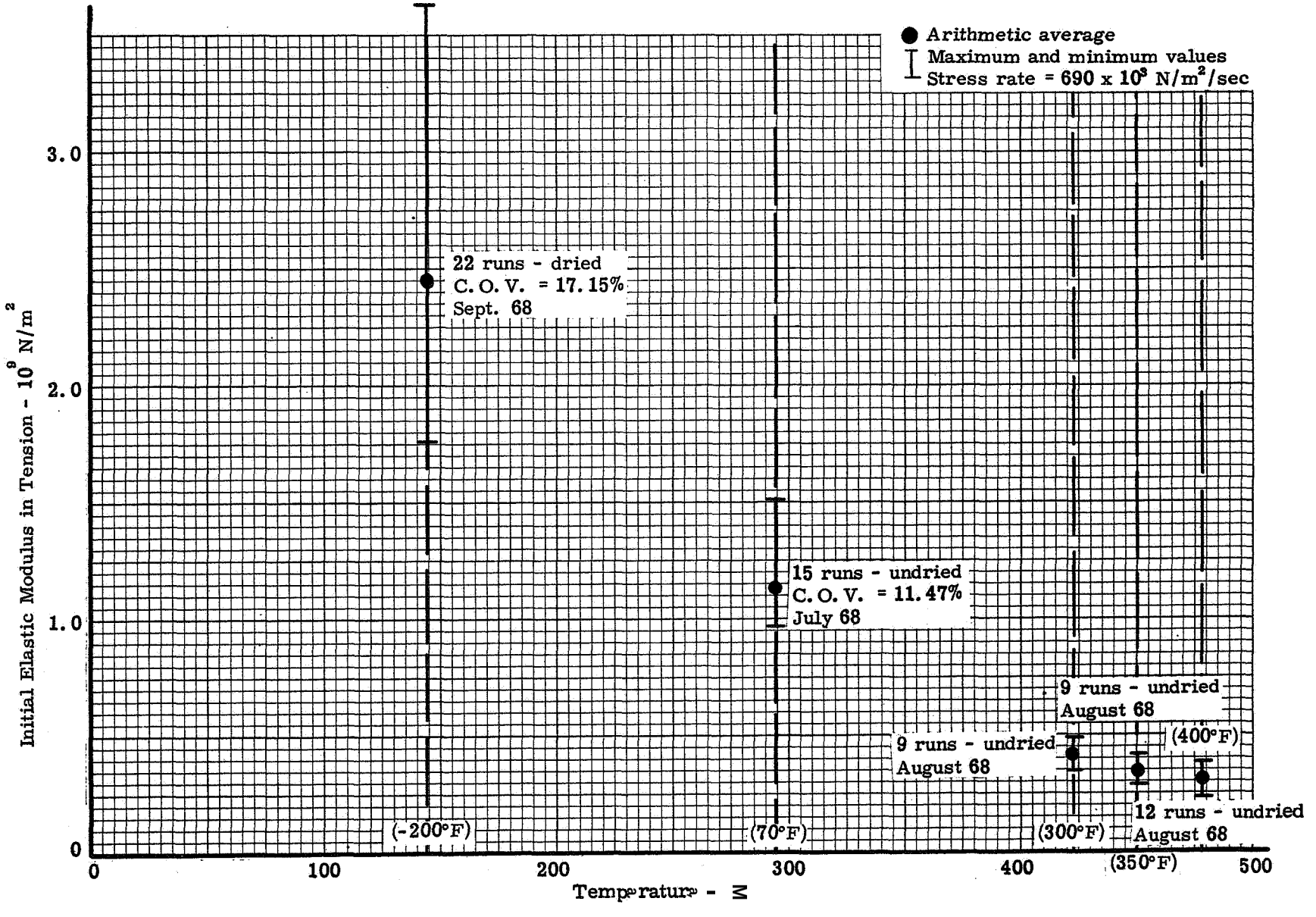

Figure 113. Initial elastic modulus in tension versus temperature for low-density phenolic-nylon

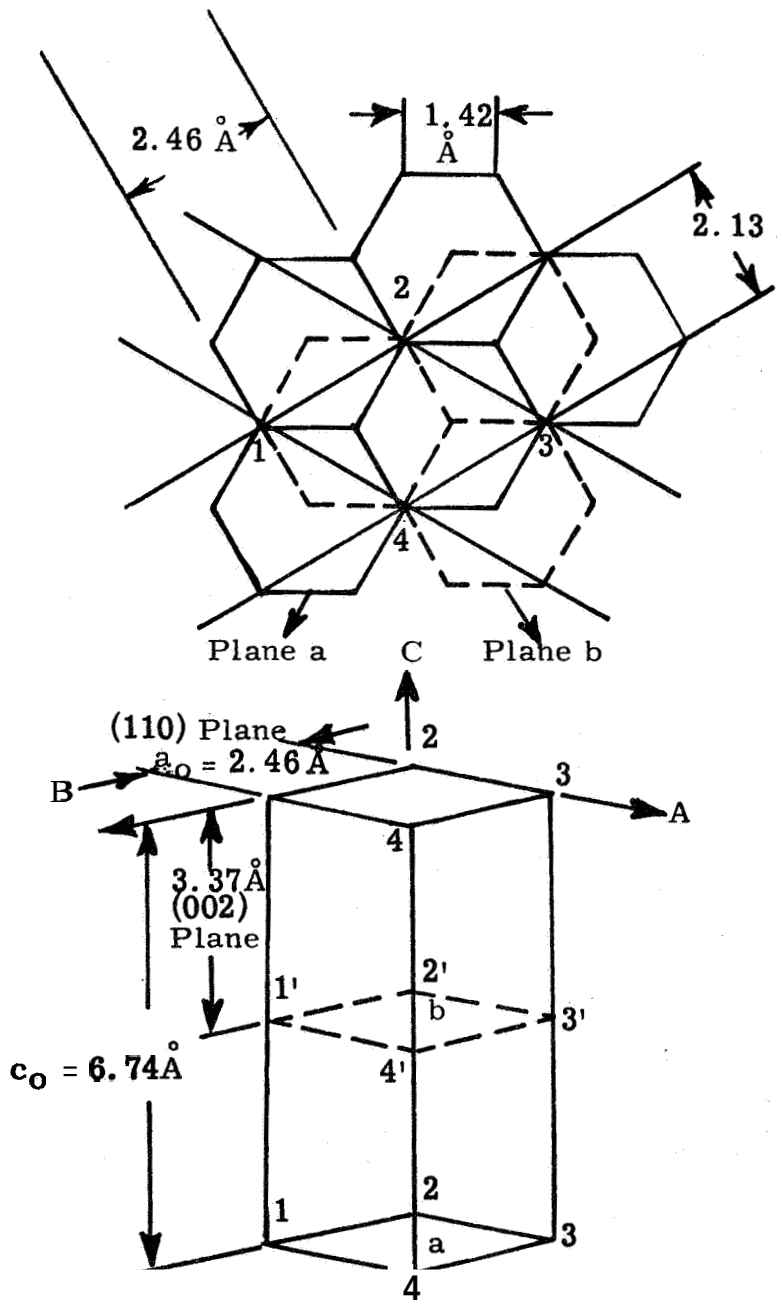

Figure 114. Critical planes for synthetic graphite with a structure in accordance with ASTM Card 12-212

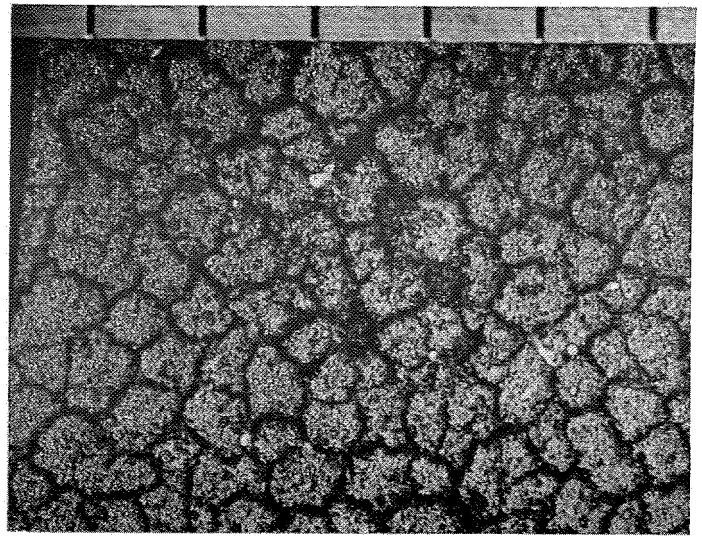

2.27 MW/m^2 arc-jet char
Unheated surface - 6X magnification

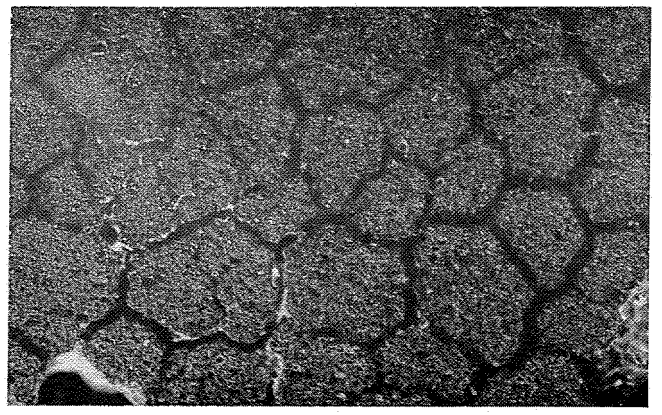

1 13 MW/□^{2} arc-jet char
Unheated surface - 6X magnification

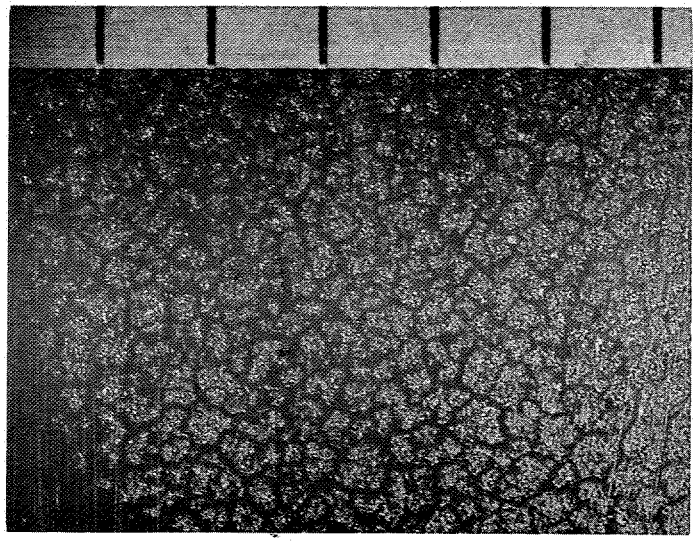

2.27 MW/m^2 arc-jet char
Heated surface - 6X magnification

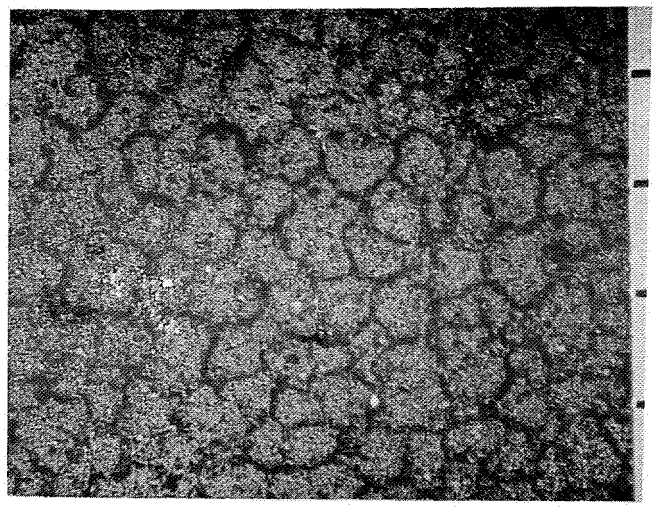

1.13 MW/m^2 arc-jet char
Heated surface - 4X magnification

Figure 115. Pictures of phenolic-nylon arc-jet char

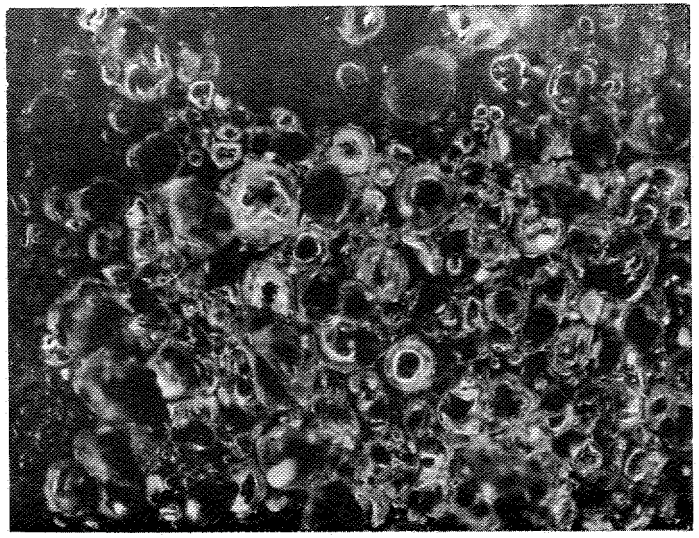

2.27 MW/m² arc-jet char
Unheated surface

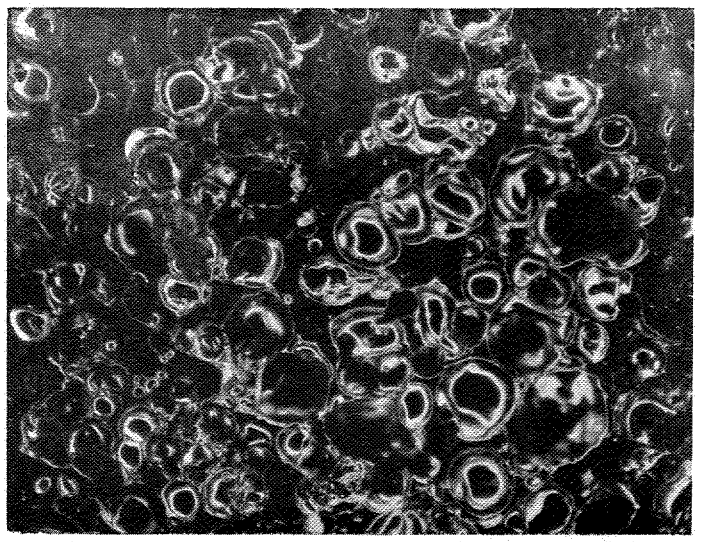

1.13 MW/m² arc-jet char
Unheated surface

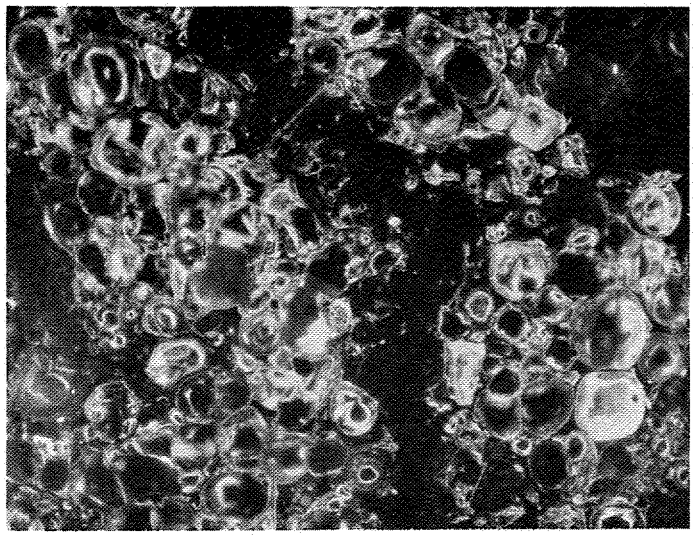

2.27 MW/m² arc-jet char
Heated surface

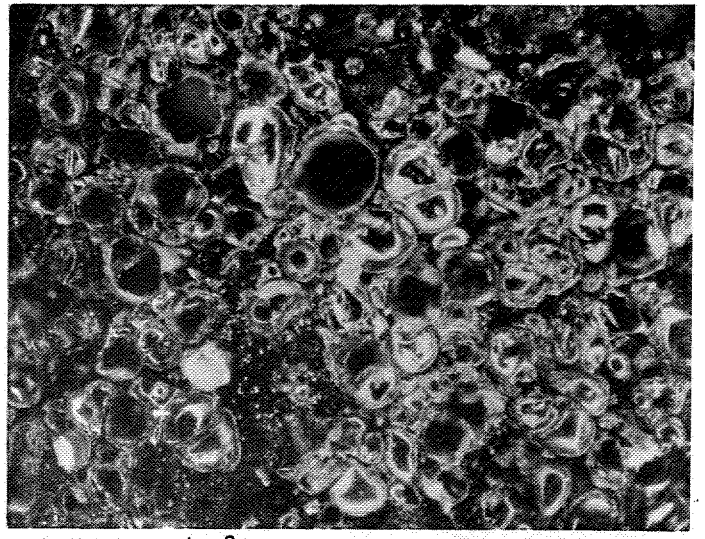

1.13 MW/m² arc-jet char
Heated surface

Figure 116. Photomicrographs at 100X magnification of phenolic-nylon arc-jet char

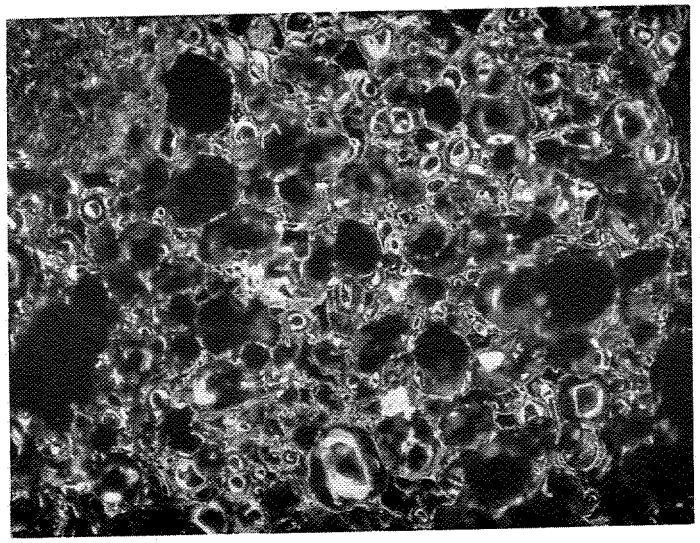

1366°K F■ ace char

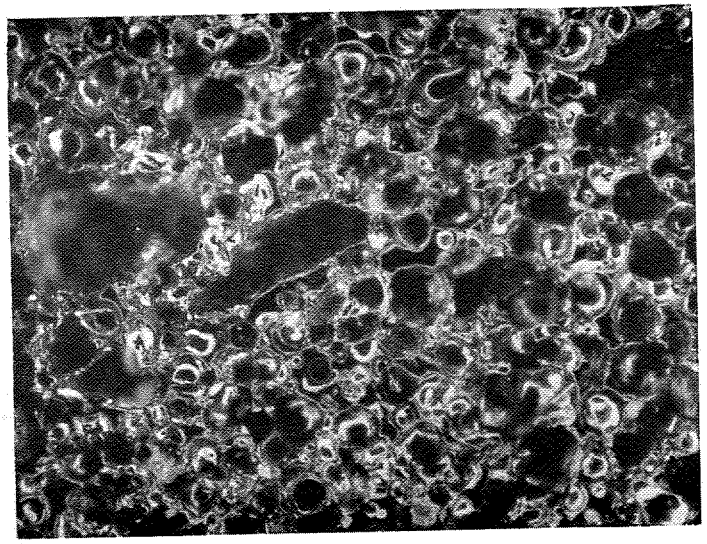

303∃ K F■ ac• char

Figure 117. Photomicrogr phs at 100X magnification o≤ phenolic-nylon furnac• char

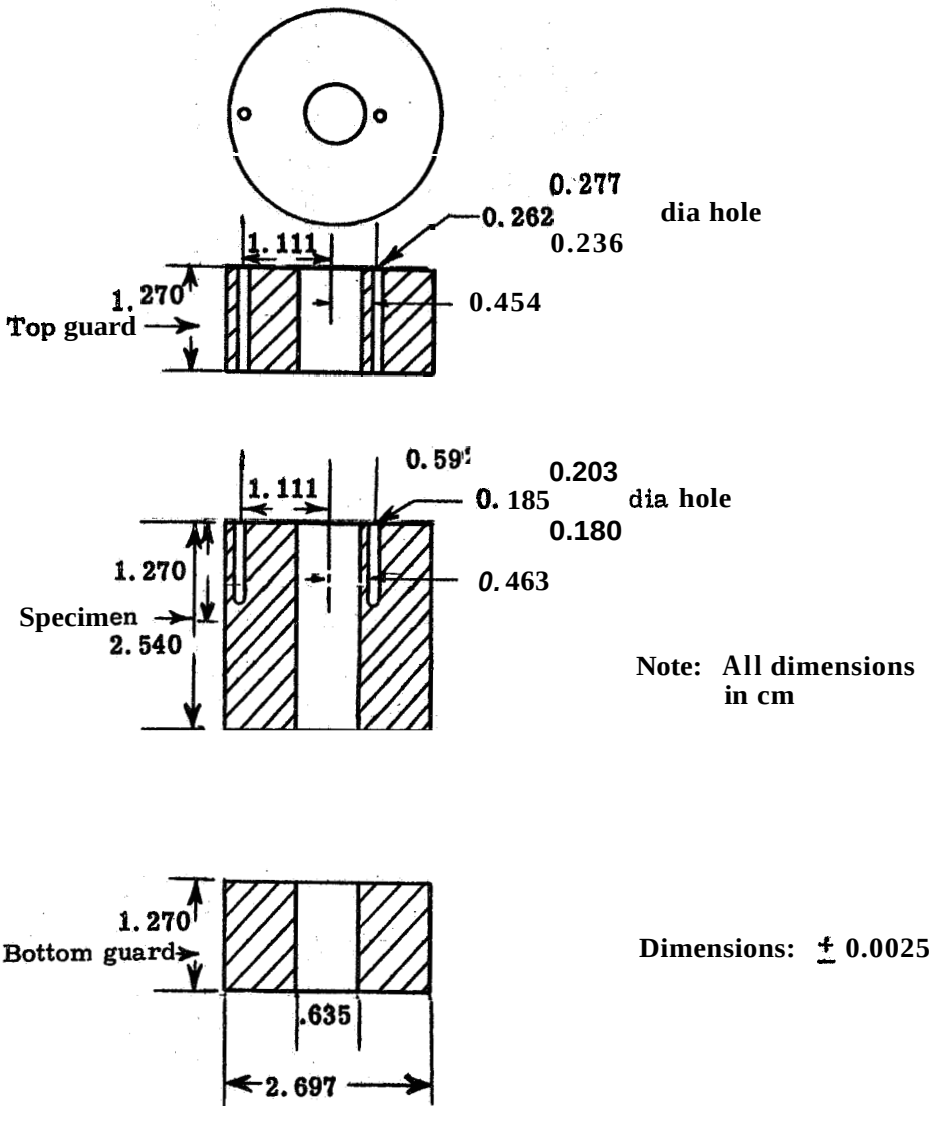

Figure 118. Configuration of the cylindrical thermal conductivity specimen for the radial inflow apparatus

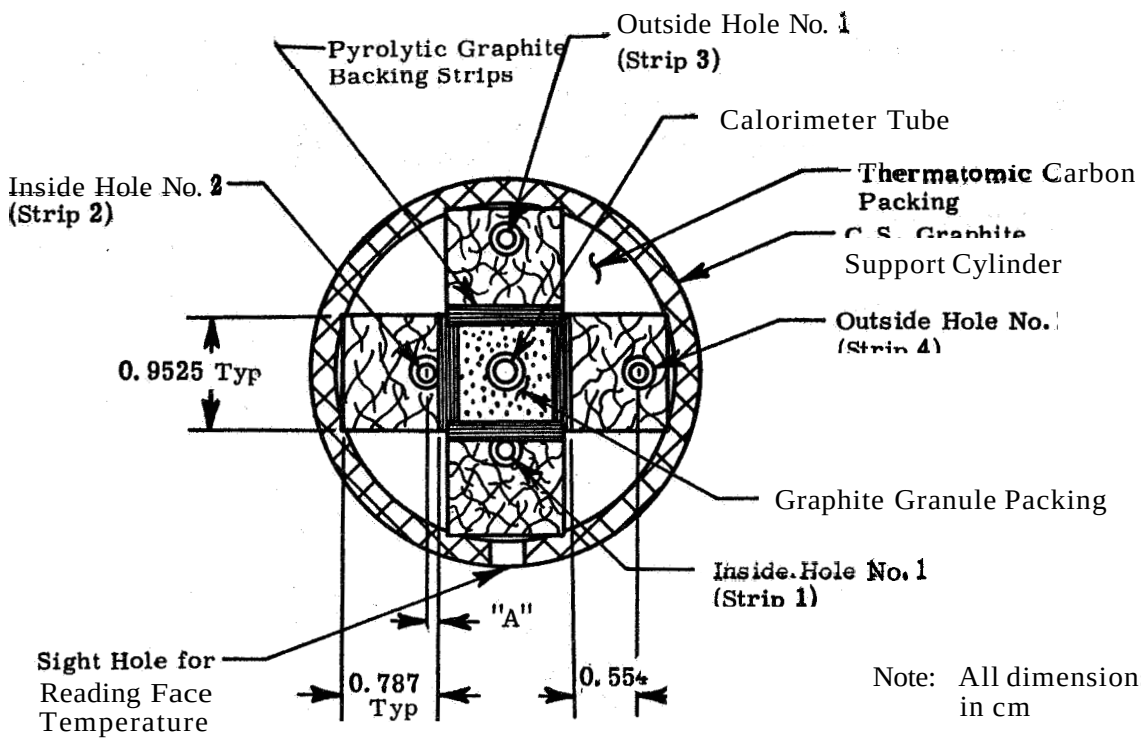

Notes
1. Specimen is 5.08 cm long. Sight hales consist of 0.178 cm dia holes 2.54 cm deep counterbored 0,236 cm dia and 1.27 cm deep
2. "A" dimension 0.0787 cm for some specimens and 0.127 cm for others

Figure 119. Strip specimen configuration for radial inflow apparatus

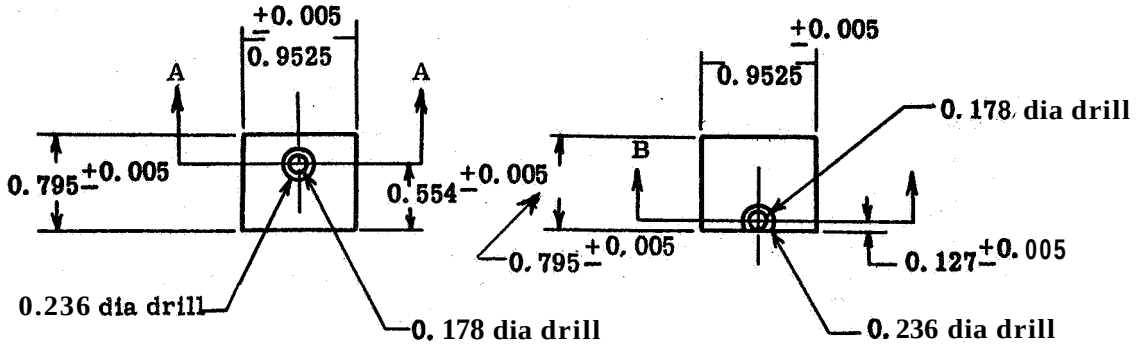

Note: All dimensions in cm

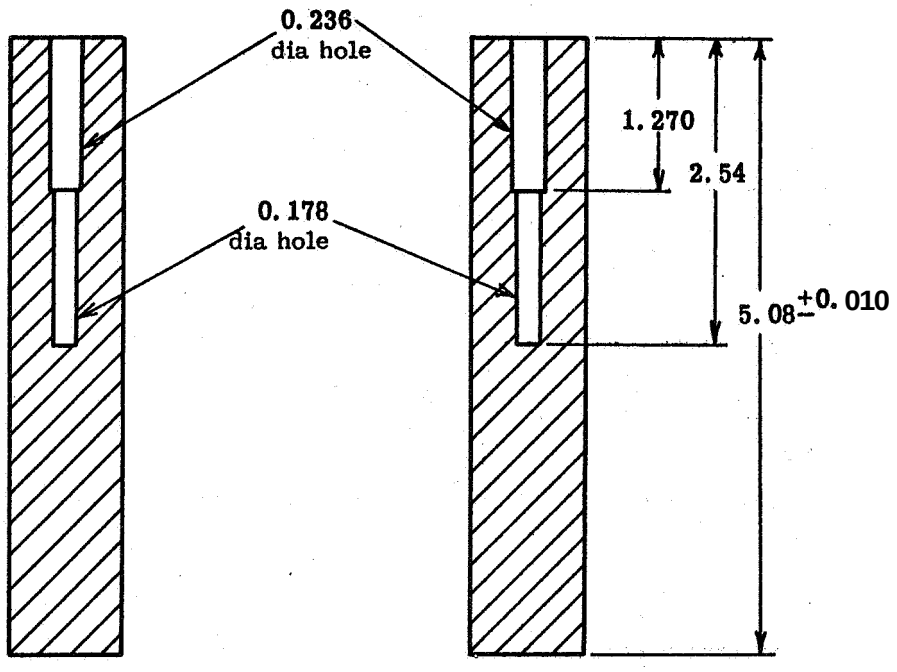

Section A-A

1. Hot Hole Strip
   2 required per specimen

Section B-B

2. Cold Hole Strip
   2 required per specimen

Figure 120. Strip specimen configuration for radial inflow apparatus dimensions of strip used for thermal conductivity measurements

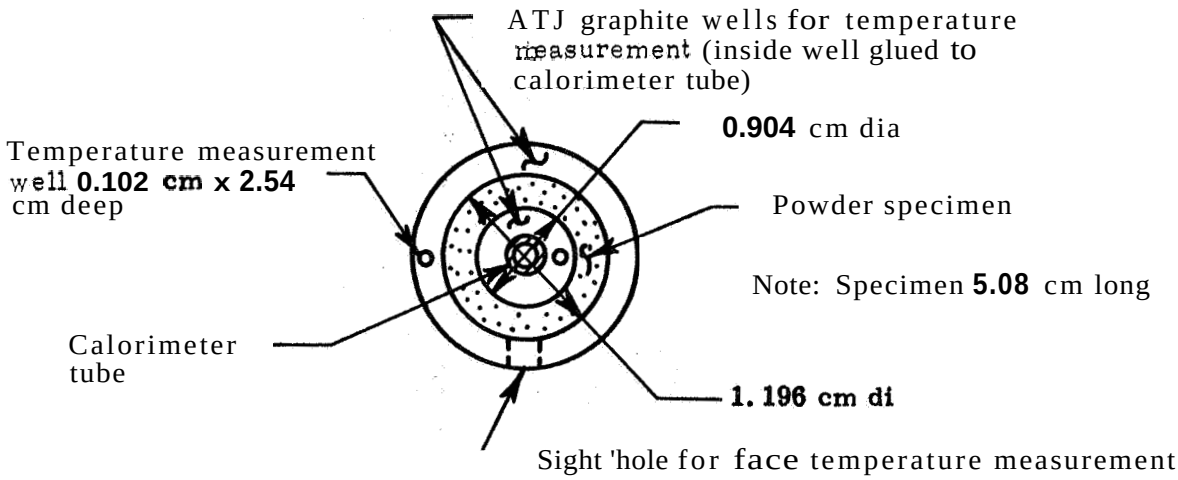

Apparatus A

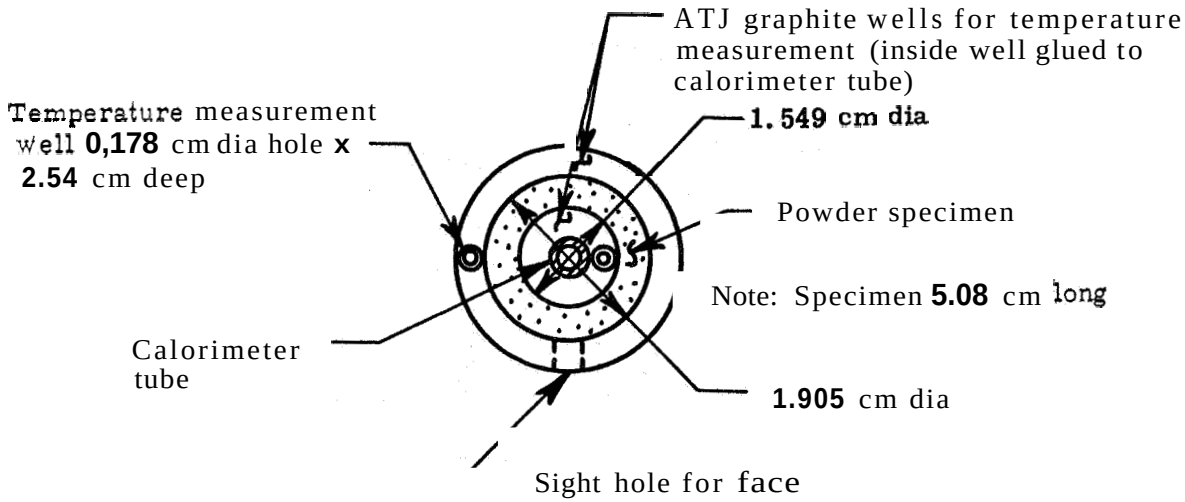

Apparatus B

Note: All dimensions in cm

Figure 121. Apparatuses used to measure thermal conductivity of powders

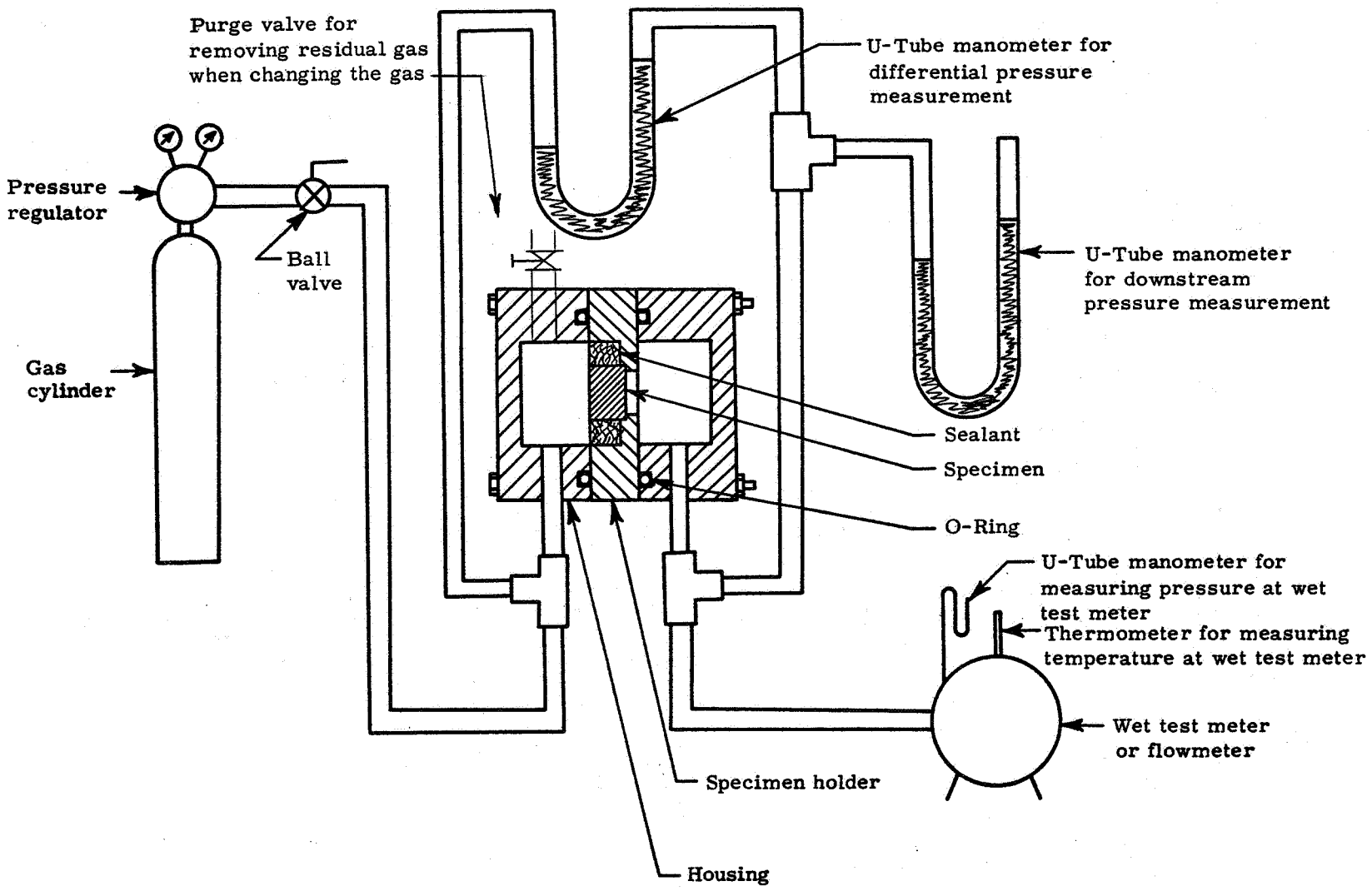

Figure 122. Permeability apparatus

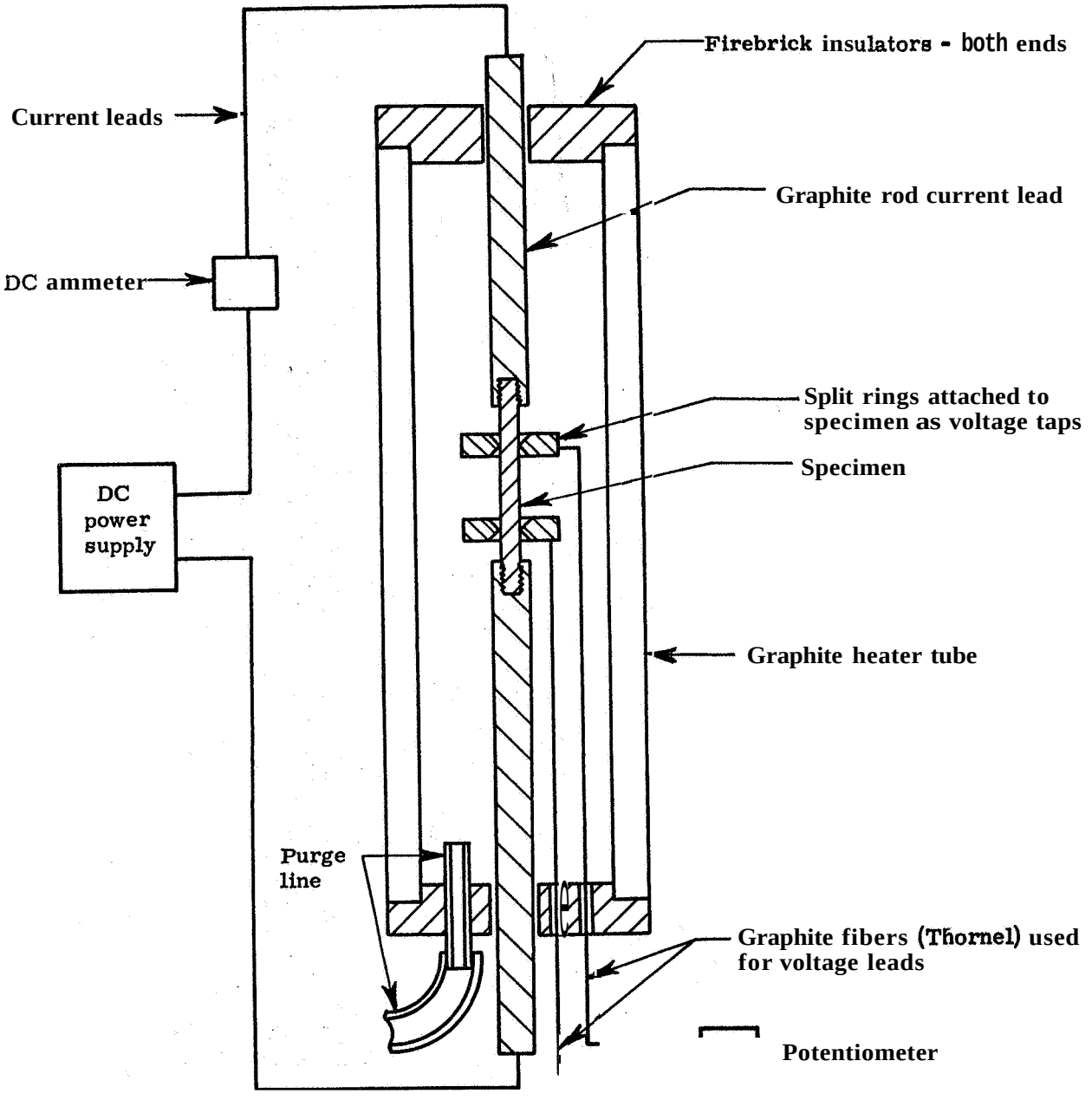

Figure 123. Schematic of apparatus used for high temperature electrical resistivity measurements

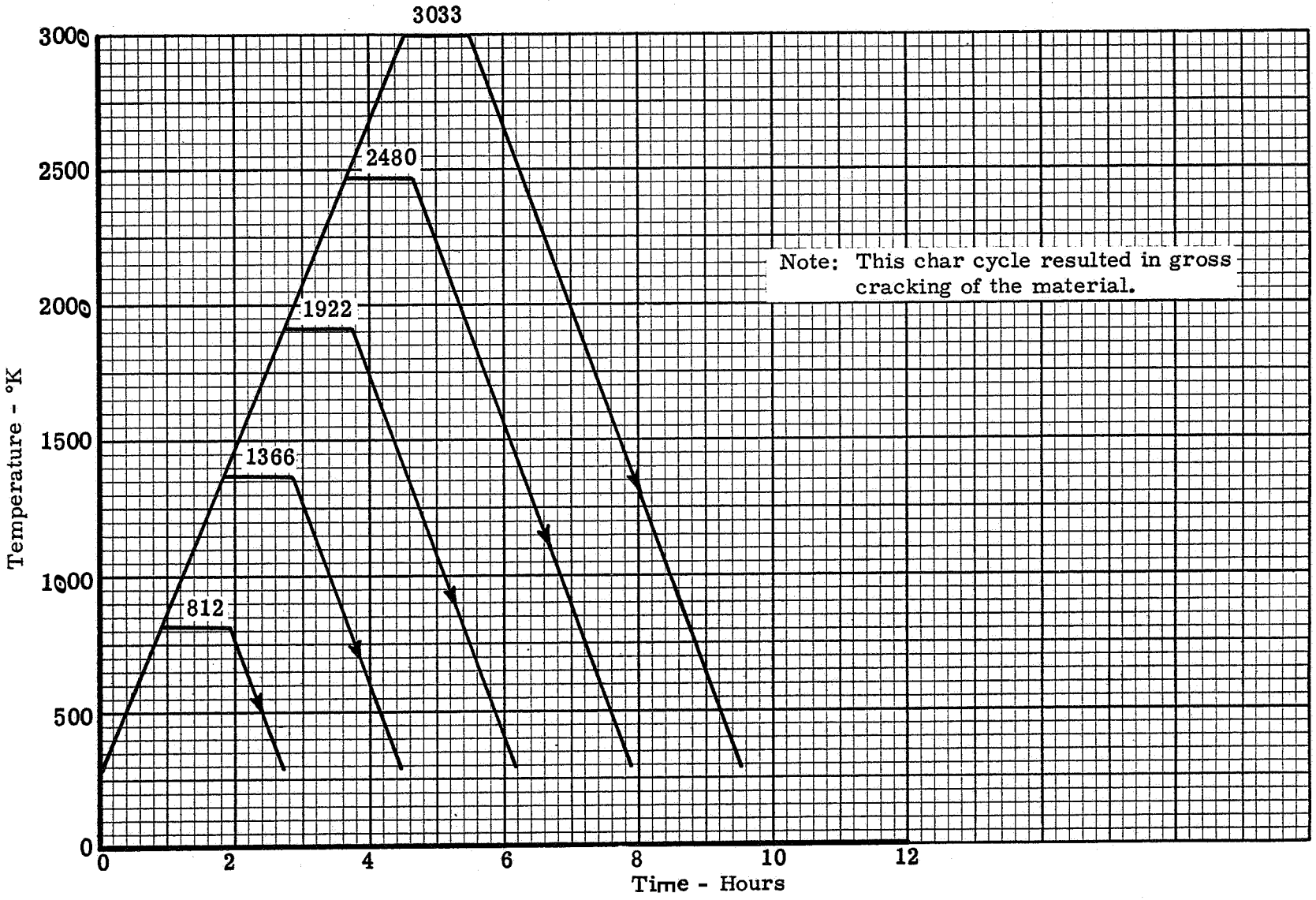

Figure 124. Charring cycles used to prepare phenolic-nylon char specimens used for X-ray diffraction and chemical analysis

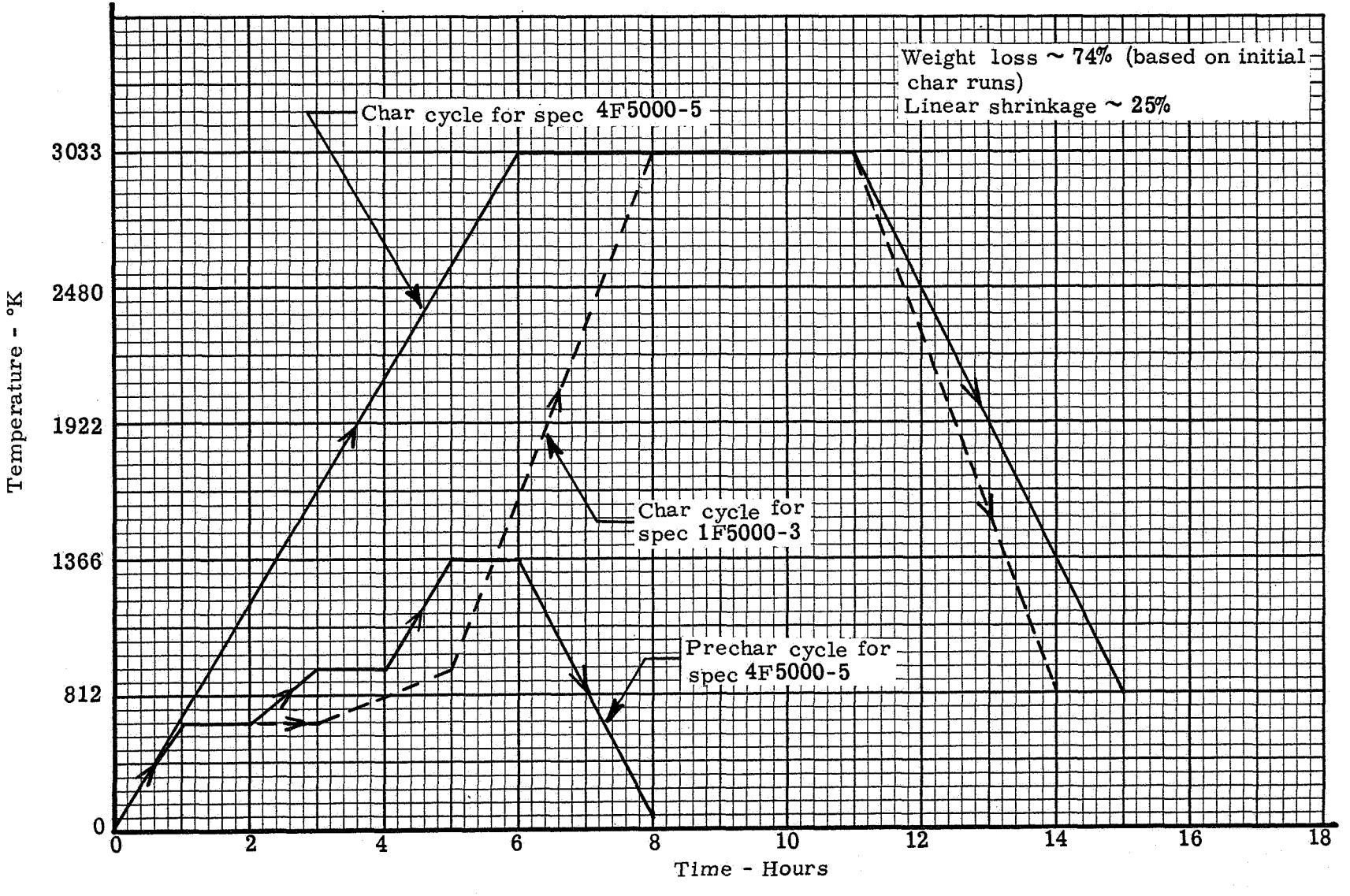

Figure 125. Charring schedules for comparative rod specimens 1F5000-3 and 4F5000-5

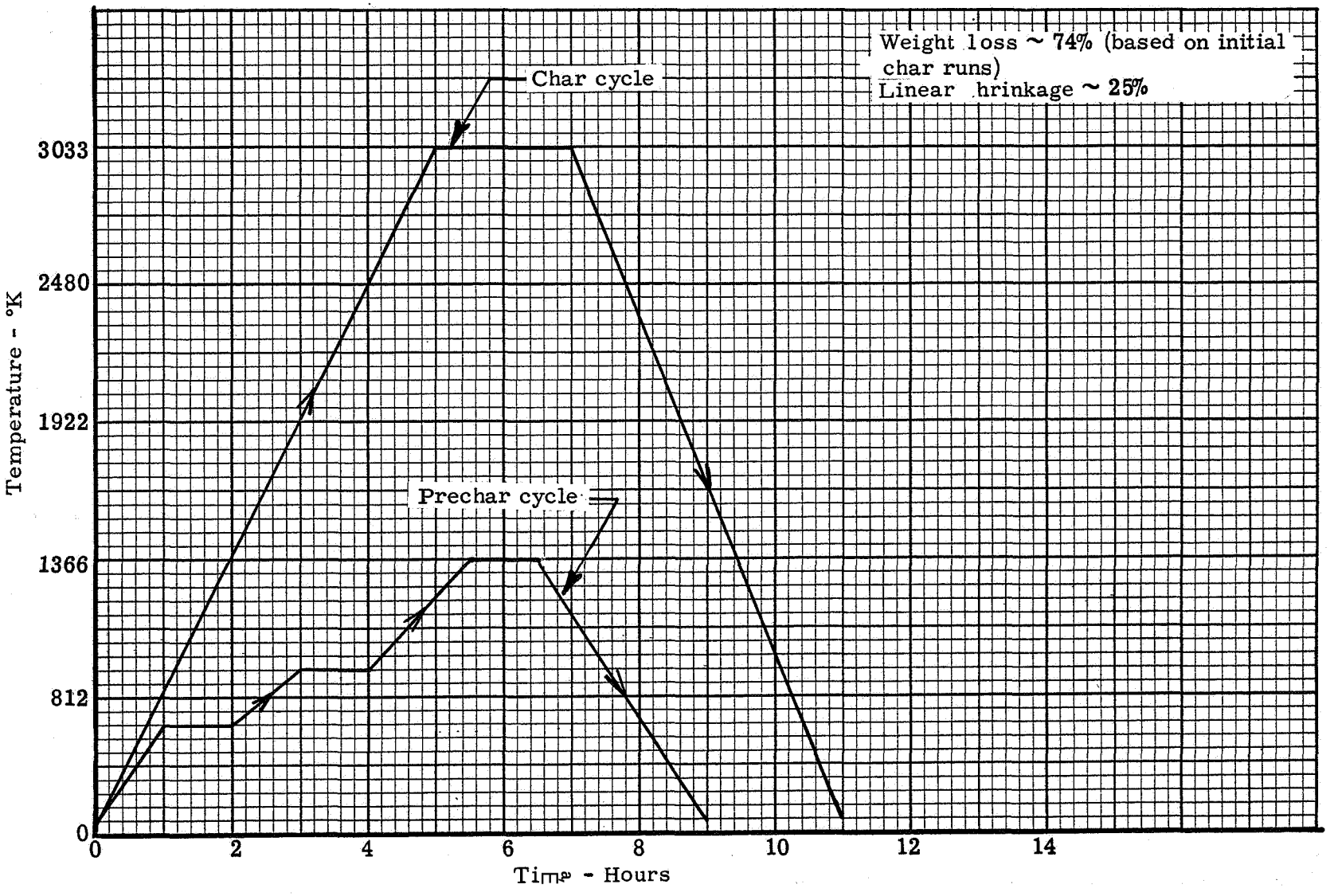

Figure 126. Charring schedule for radial inflow specimen 2F5000-2

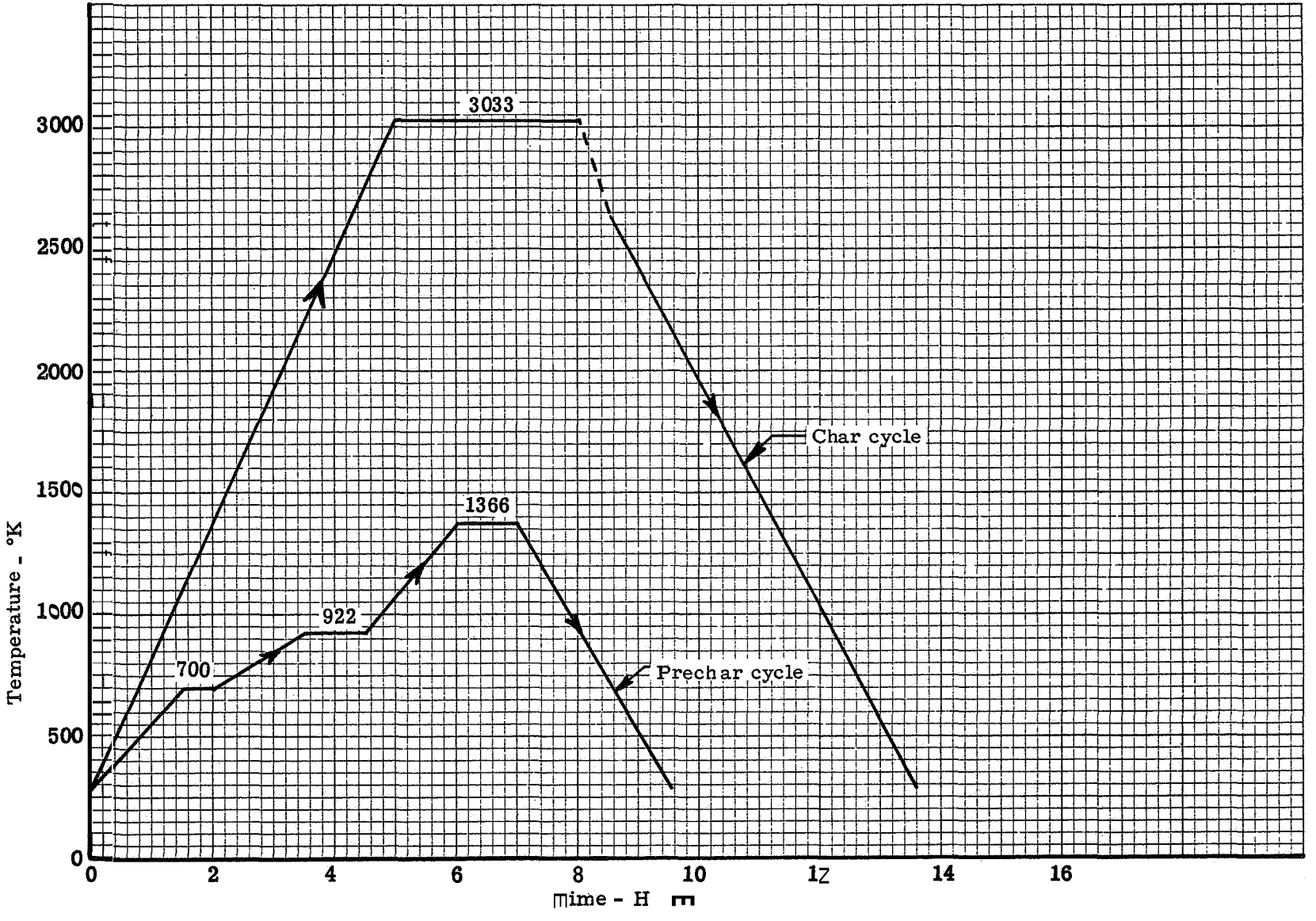

Figure 127. Char cycles used to prepare specimen 3F5000-3

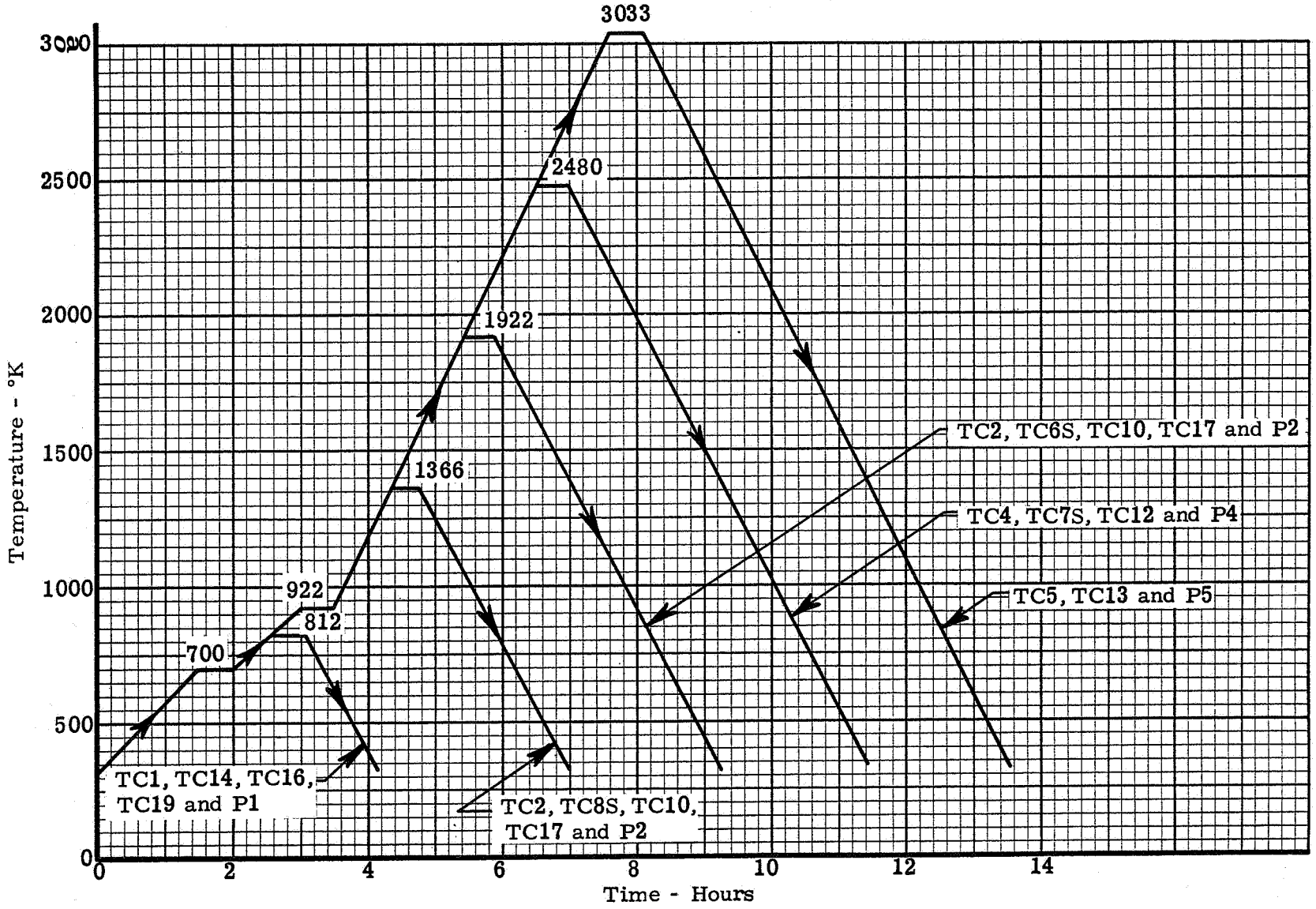

Figure 128. Temperature-time cycles used to prepare phenolic-nylon char, specimens TC1, 2, 3, 4, 5, 6S, 7S, 8S, 10, 11, 12, 13, 14, 16, 17, 19 and P1, 2, 3, 4, 5

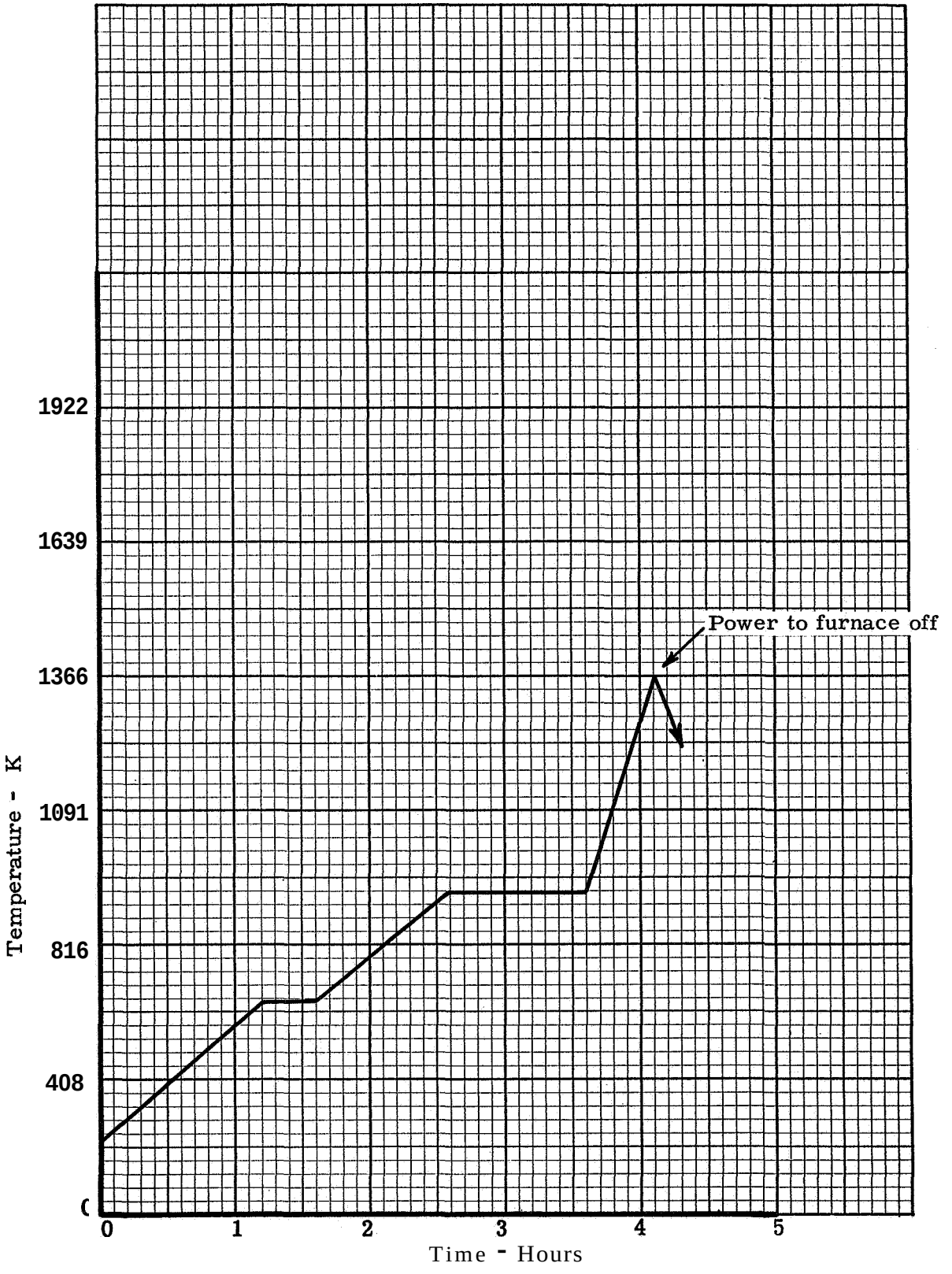

Figure 129. Temperature-time cycle used to prepare phenolic-nylon char specimen 5R

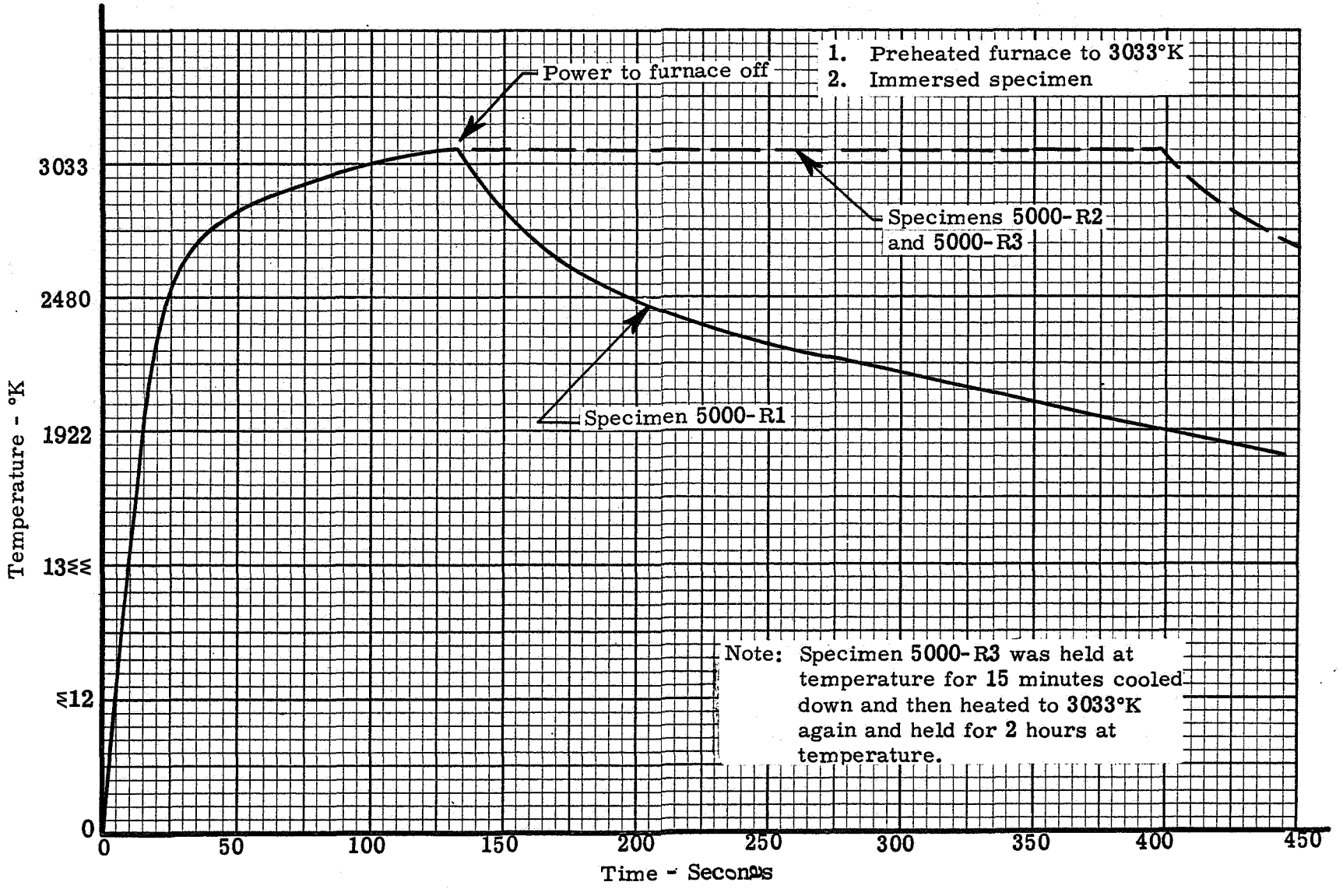

Figure 130 Temperature-time history during charring for specimens 5000-R1, 5000-R2, and 5000-R3

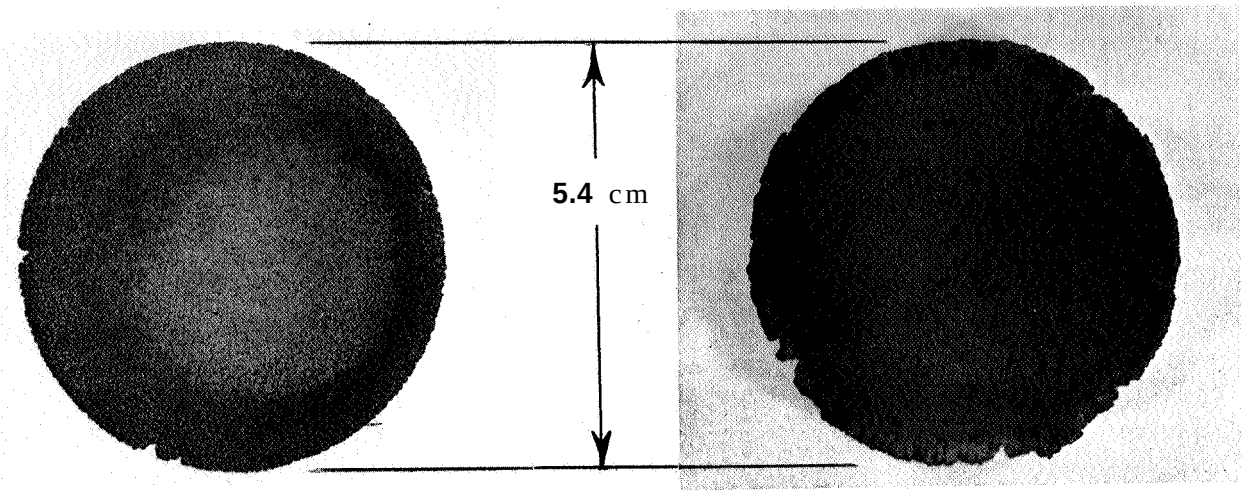

a. Arc-jet char prepared at 2.27 MW/m^2

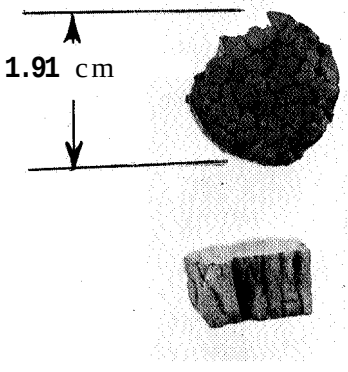

b. Arc-jet char prepared at 1.13 MW/m^2

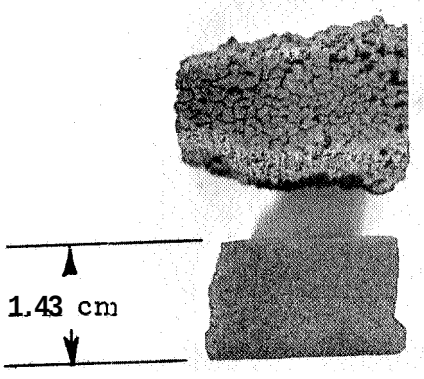

c. Furnace chars

Figure 131. Pictures of arc-jet chars and furnace chars

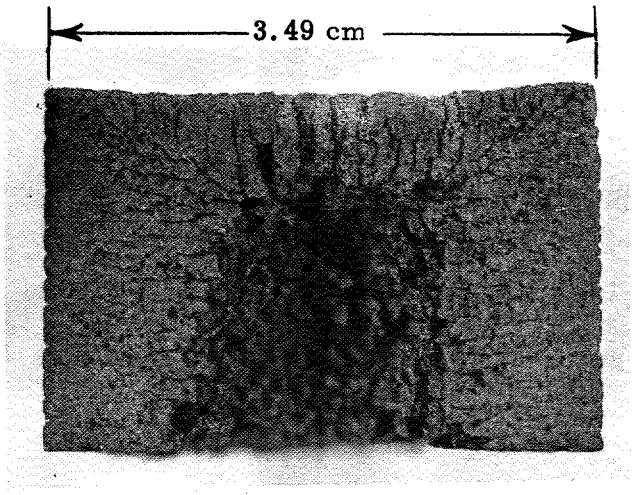

a. Internal view of end section of cylinder charred at rapid heating rate

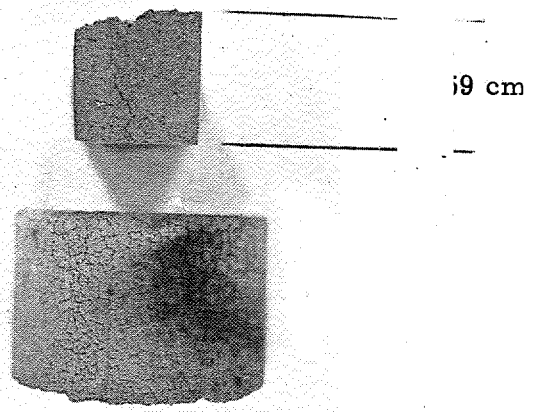

b. Heated surface of cylinder charred at rapid heating rate

a. Closeup view of heated surface

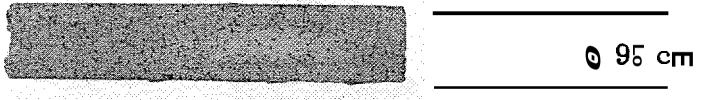

b. Full view

c. Strip from radial inflow thermal conductivity specimen 5000-R2

Figure 132 Pictures of phenolic-nylon charred in furnace at rapid heating rate

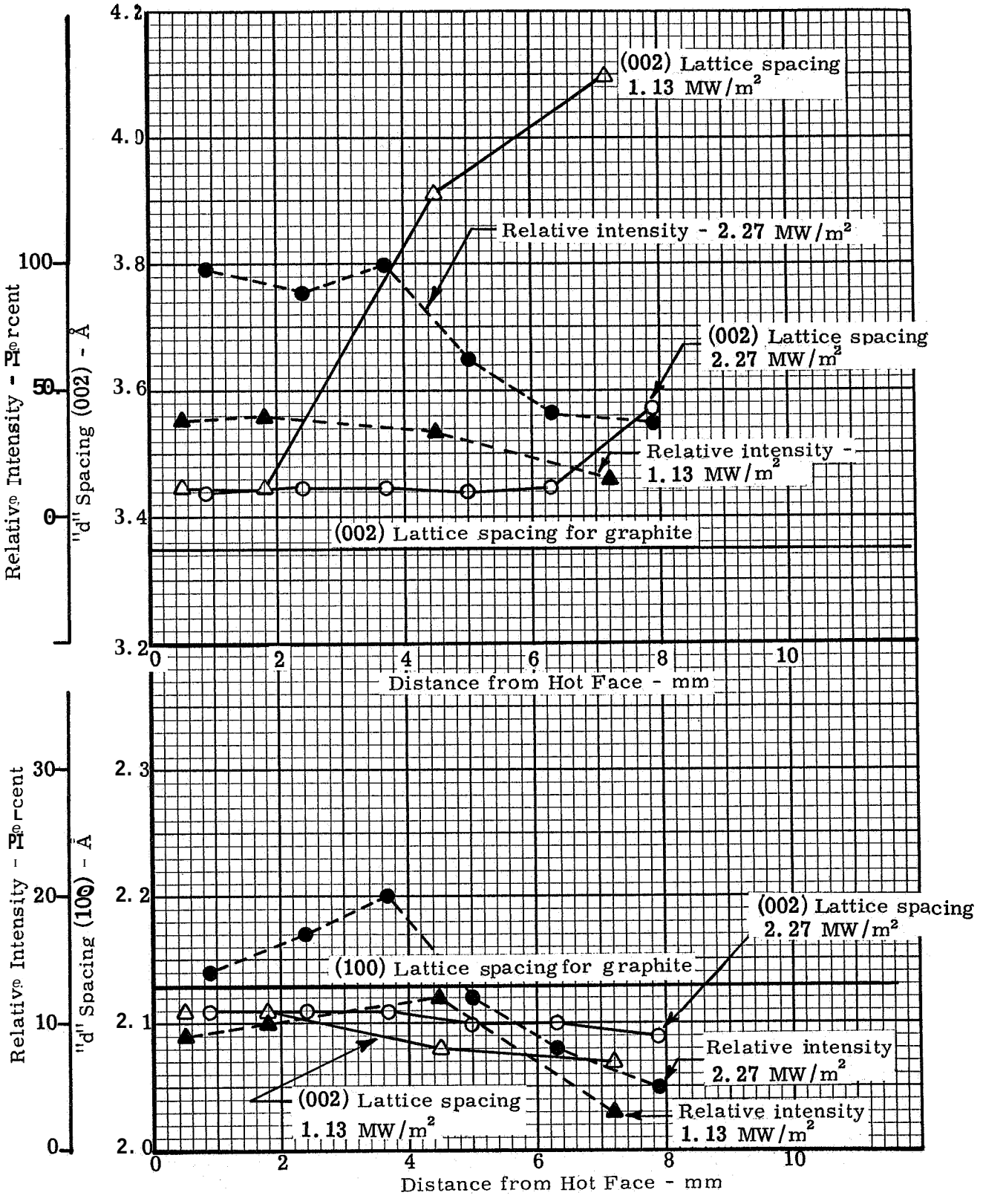

Figure 133. Results of X-ray diffraction studies on Arc-jet Chars

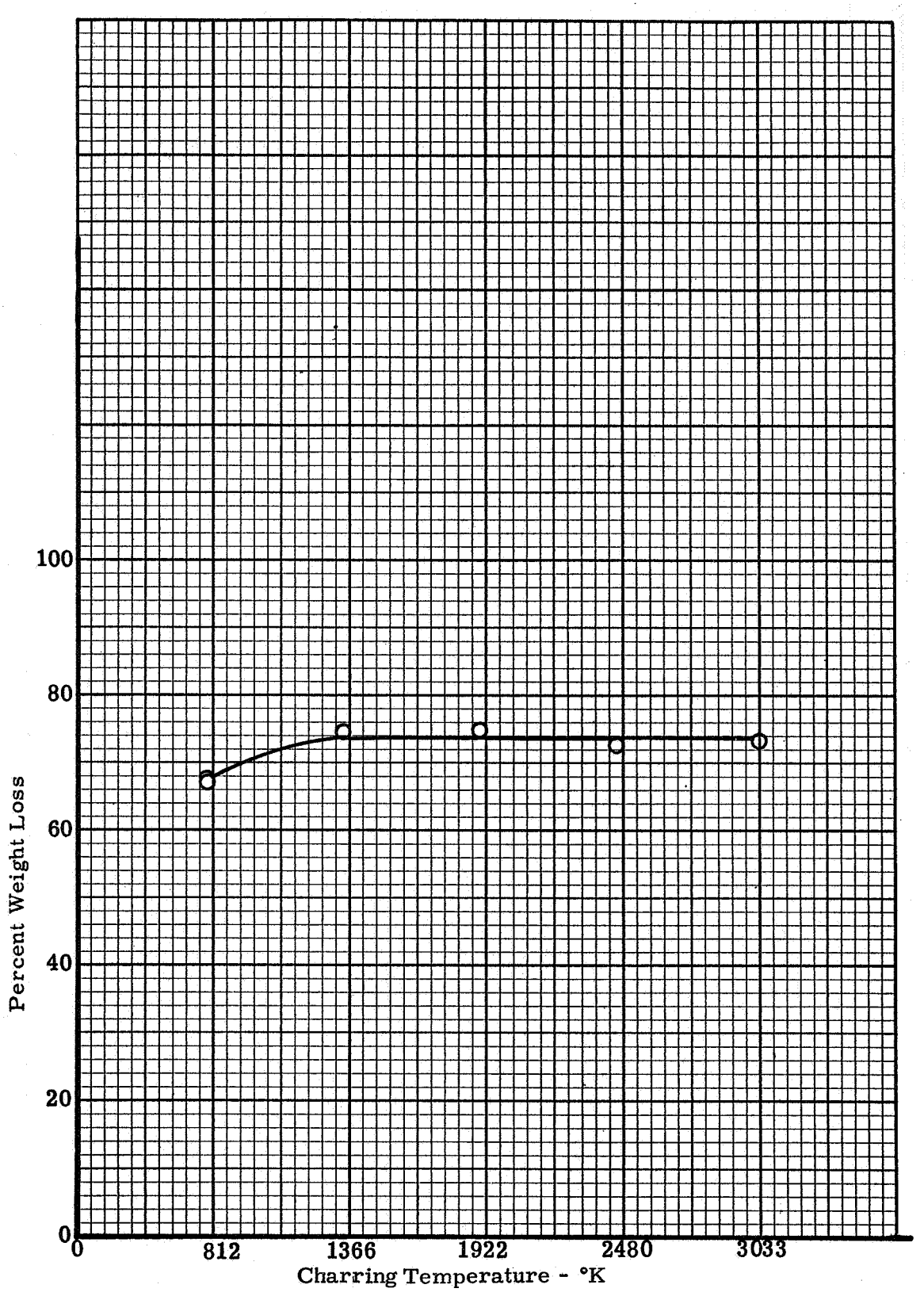

Figure 134. Percent weight loss versus eharring temperature for specimens used for characterization measurements

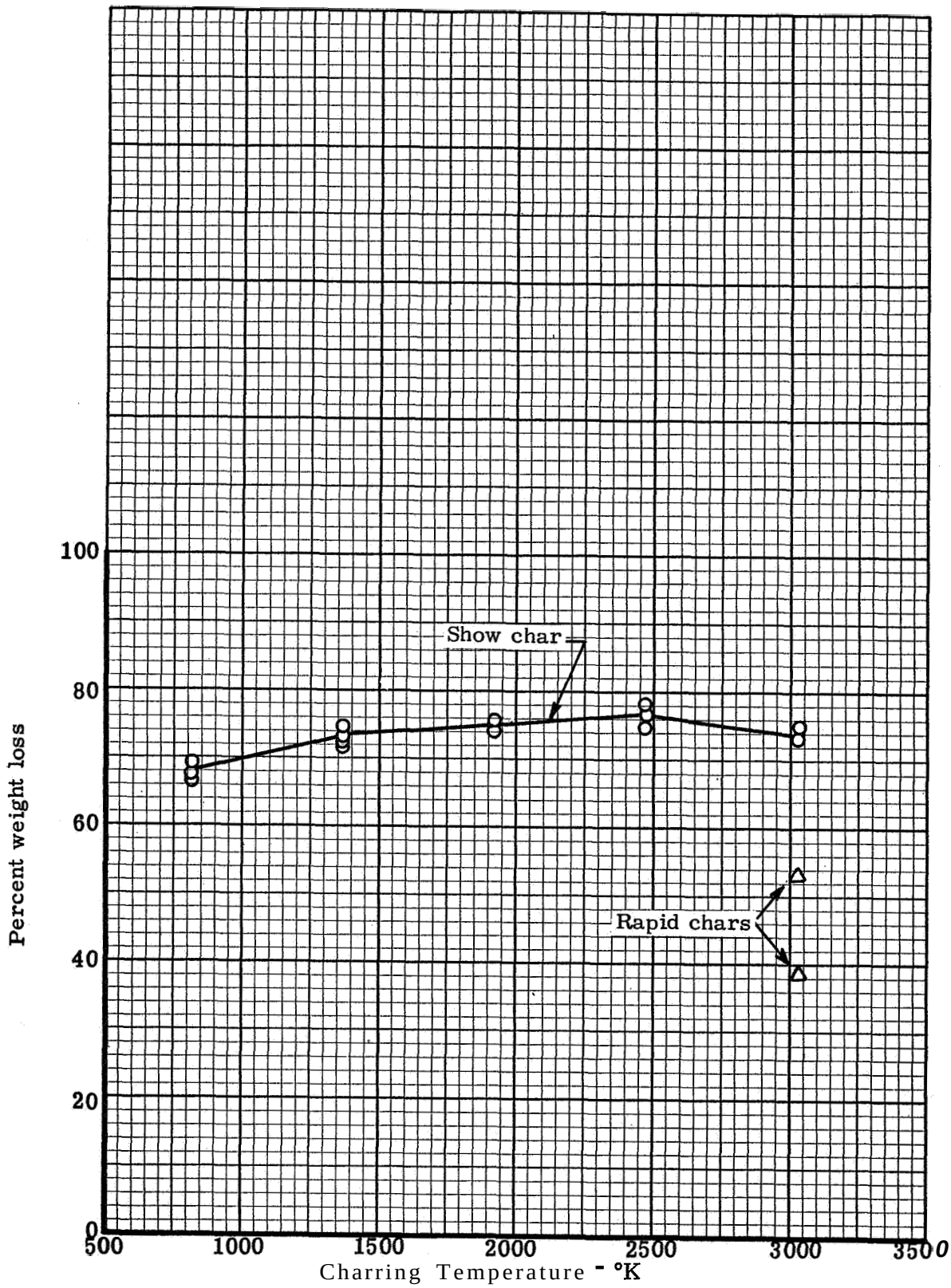

Figure 135. Percent weight loss versus charring temperature

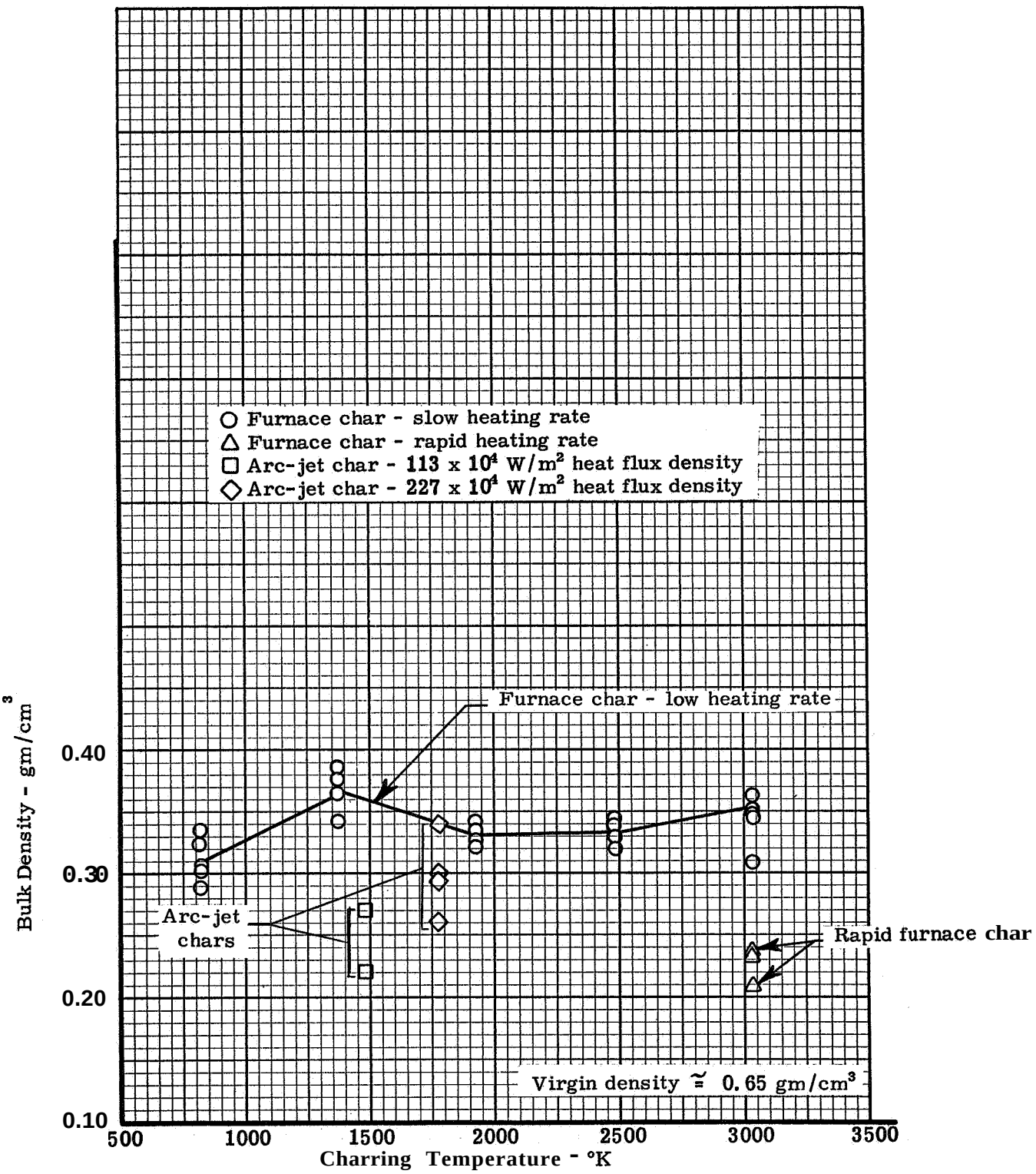

Figure 136. Bulk density of phenolic-nylon char versus charring temperature

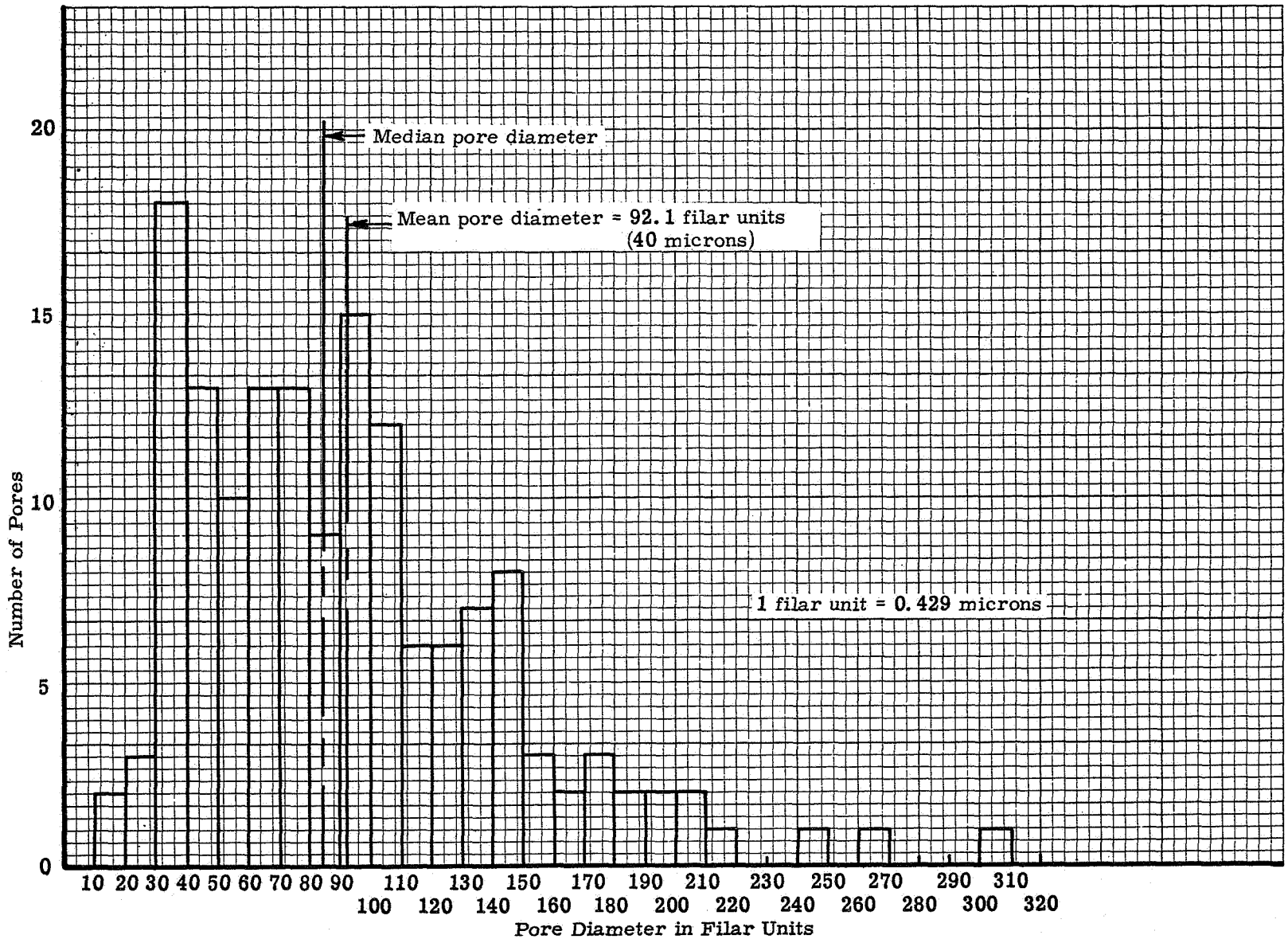

Figure 137. Pore diameter histogram for heated surface of phenolic-nylon arc-jet char (1.13 MW/m^2)

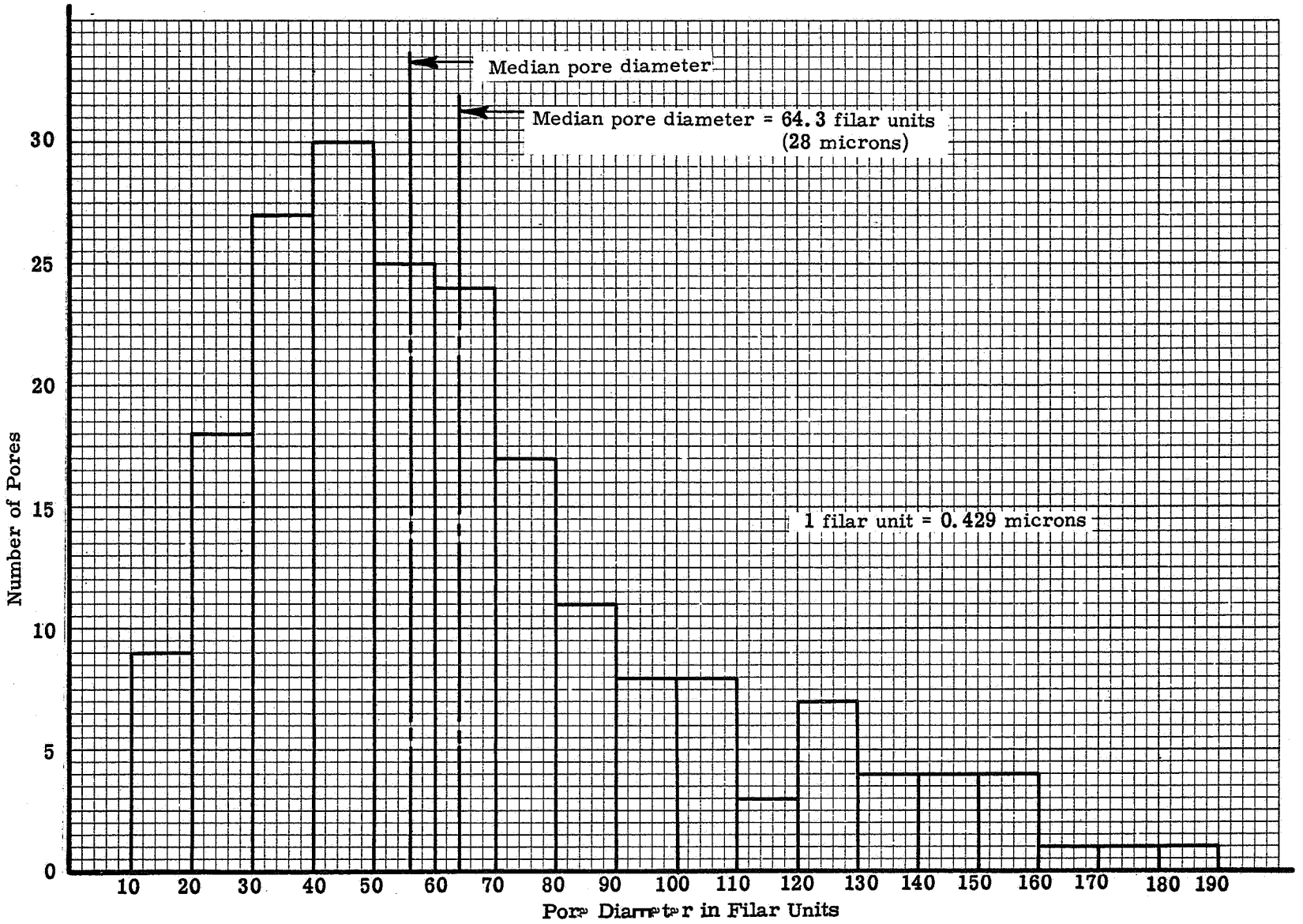

Figure 138. Pore diameter histogram for unheated surface of phenolic nylon arc-jet char (1.13 MW/m²)

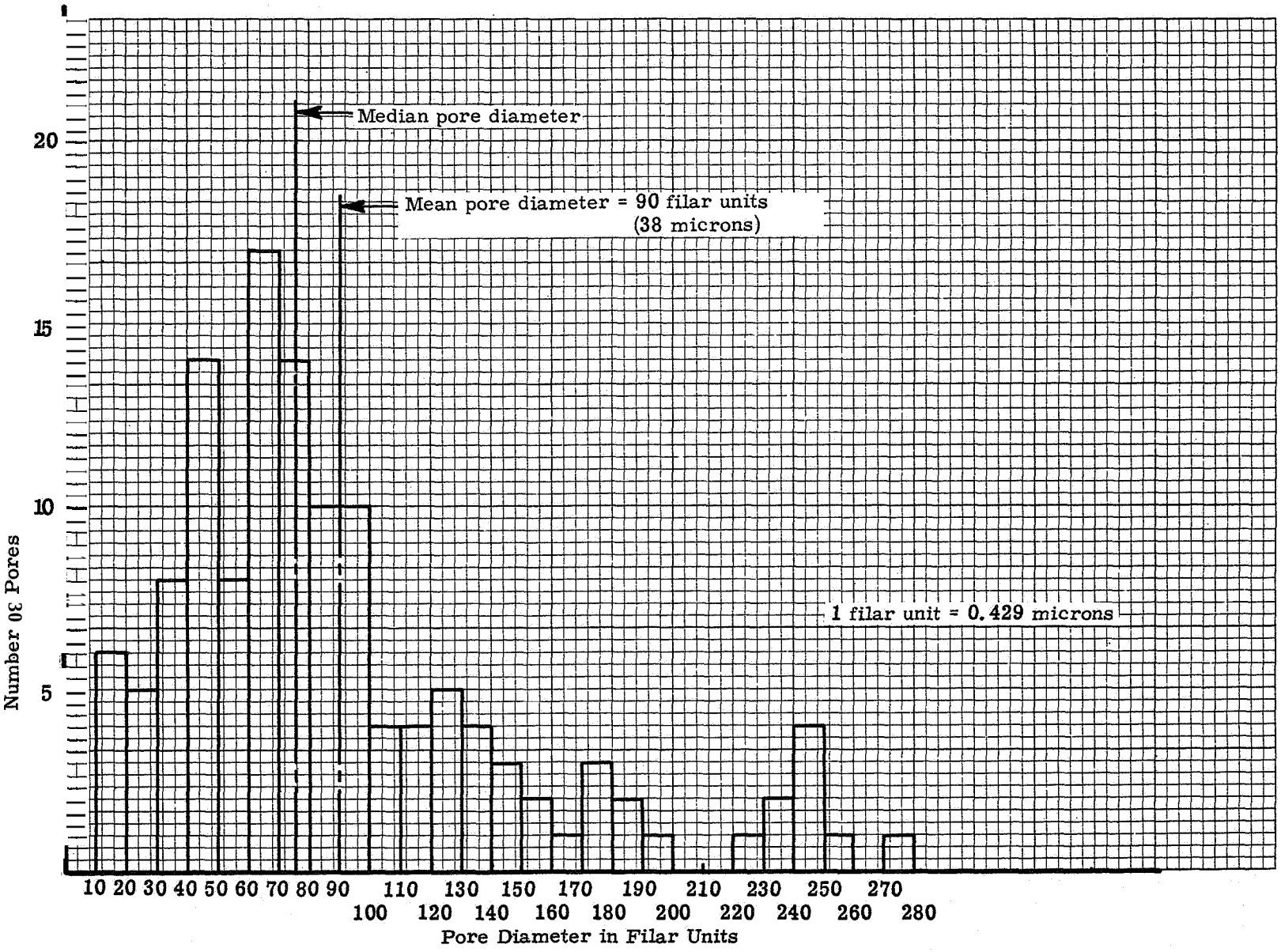

Figure 139. Pore diameter histogram for heated surface of phenolic-nylon arc-jet char (2.27 MW/m^2)

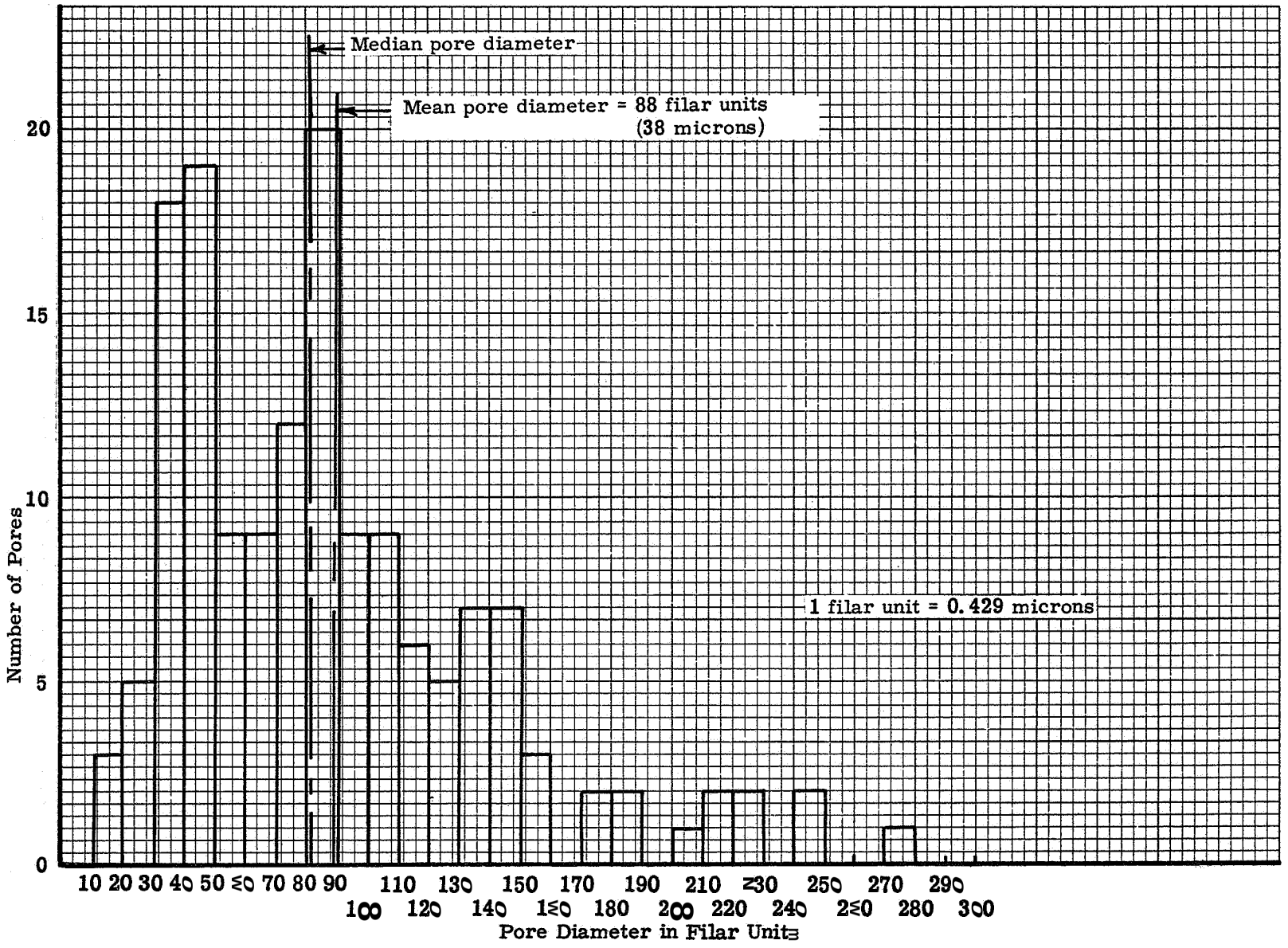

Figure 140. Pore diameter histogram for unheated surface of phenolic-nylon arc-jet char (2.27 MW/m^2)

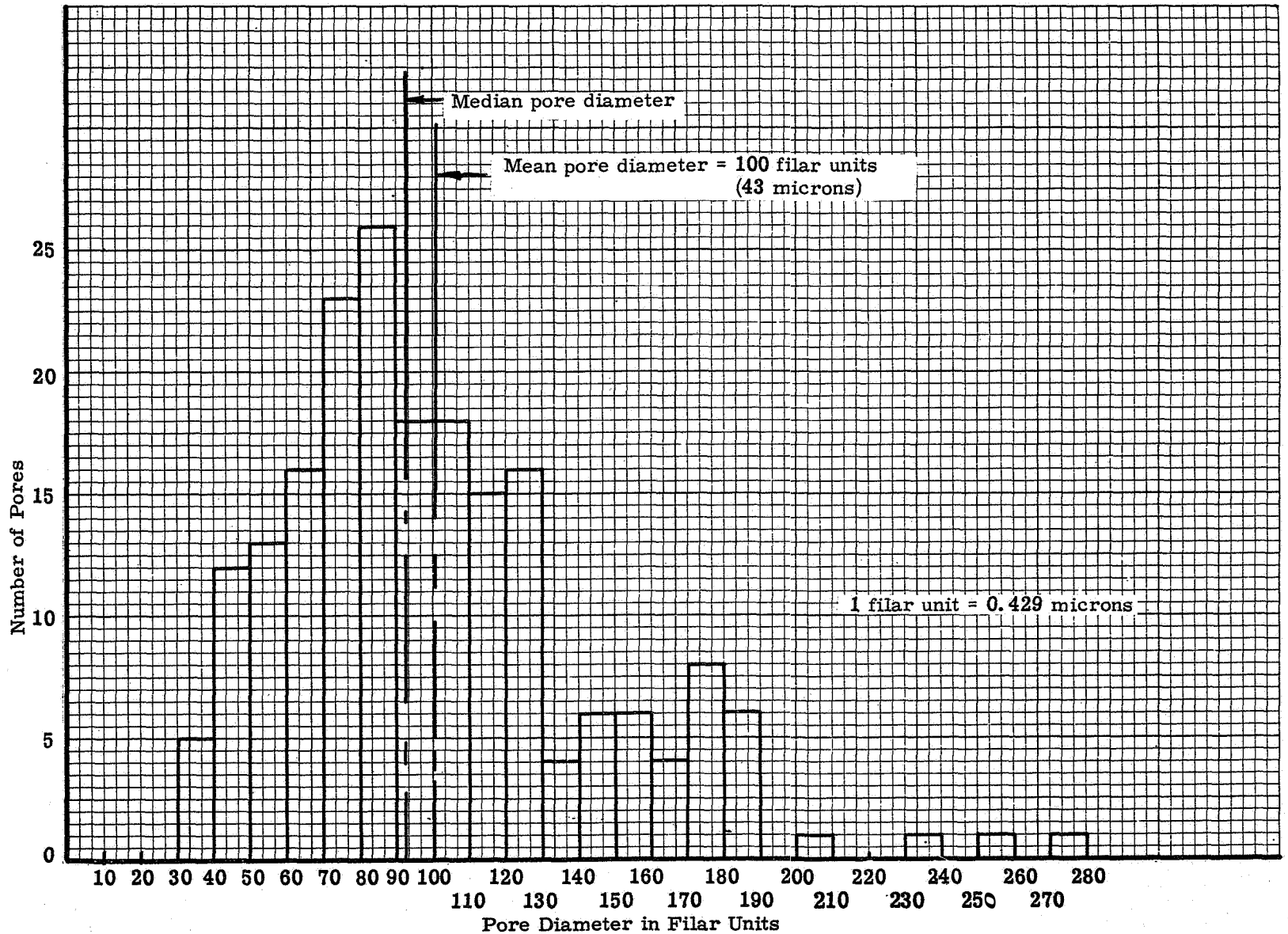

Figure 141. Pore diameter histogram for phenolic-nylon, furnace charred at 1366°K

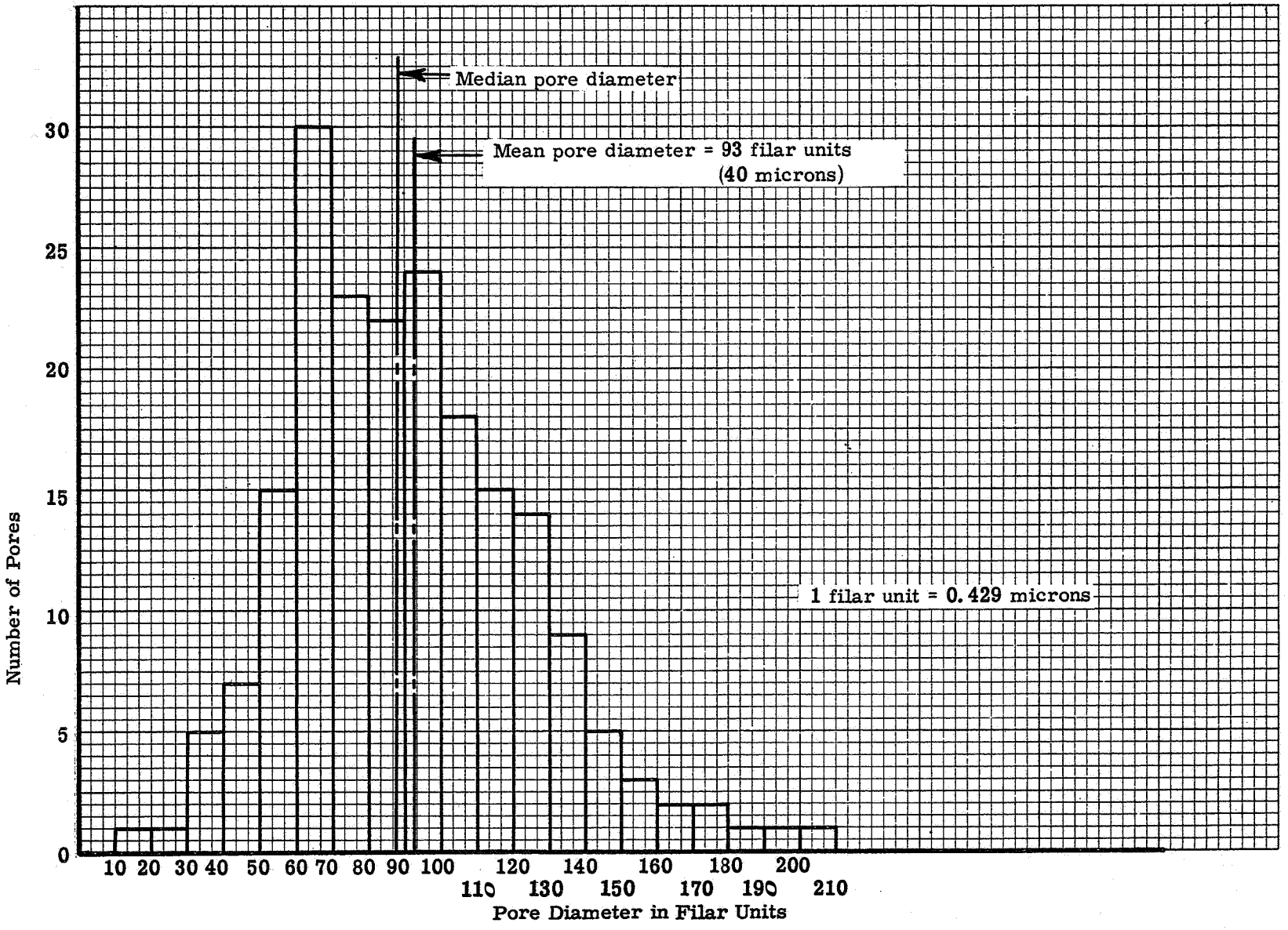

Figure 142. Pore diameter histogram for [illegible]lic nylon, f [illegible] ch[illegible] red [illegible]t 3033°K

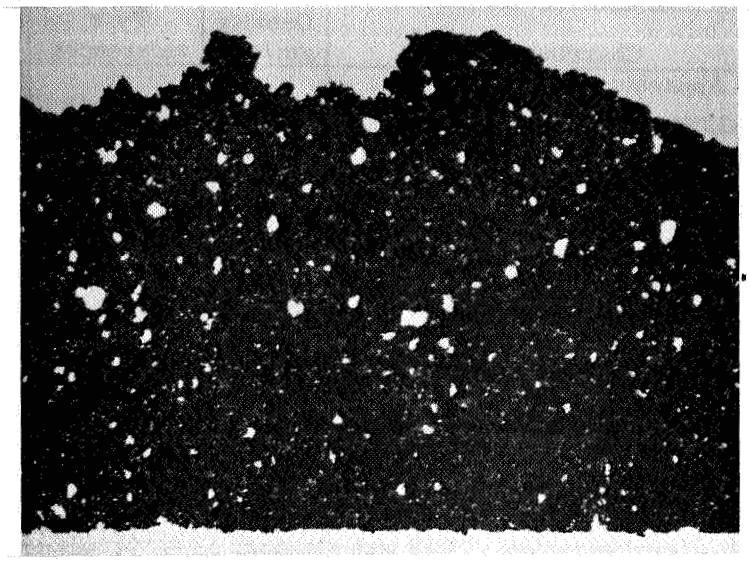

0.100 cm
0.039 in.

a. 0.0254 cm (0.010 in.) thick
measured transmittance = 2.5%
measured area fraction of holes = 5.06%
using point count technique

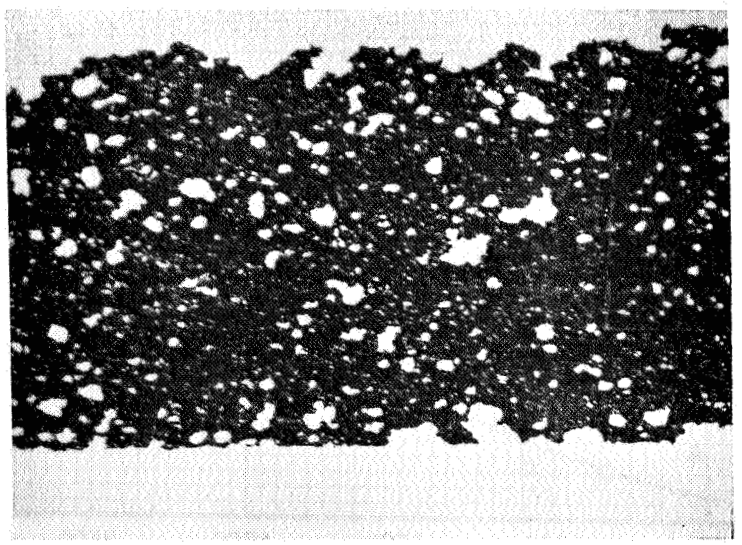

0.100 cm
0.039 in.

b. 0.0127 cm (0.005 in.) thick
measured transmittance = 11.4%
measured area fraction of holes = 12.5% to 16.8%
using point count technique

Figure 143. Pictures at about 10X magnification of phenolic-nylon char ground to various thicknesses

Symbol	Spec.	Charring history	Density gm/cm³	Type references	Environment for measurements
Comparative Rod Apparatus					
●	TC19	812°K for 30 minutes	0,289	Teflon	Air
A	TC16	816°K for 30 minutes	0.302	Pyroceram	Nitrogen
Radial Inflow Apparatus					
O	TC14	812°K for 30 minutes	0.323		Argon purge
	TC1	812°K for 30 minutes	0.303		Argon purge
◇	TC19	812°K for 30 minutes	0.311		First point in helium purge. Others in argon purge.

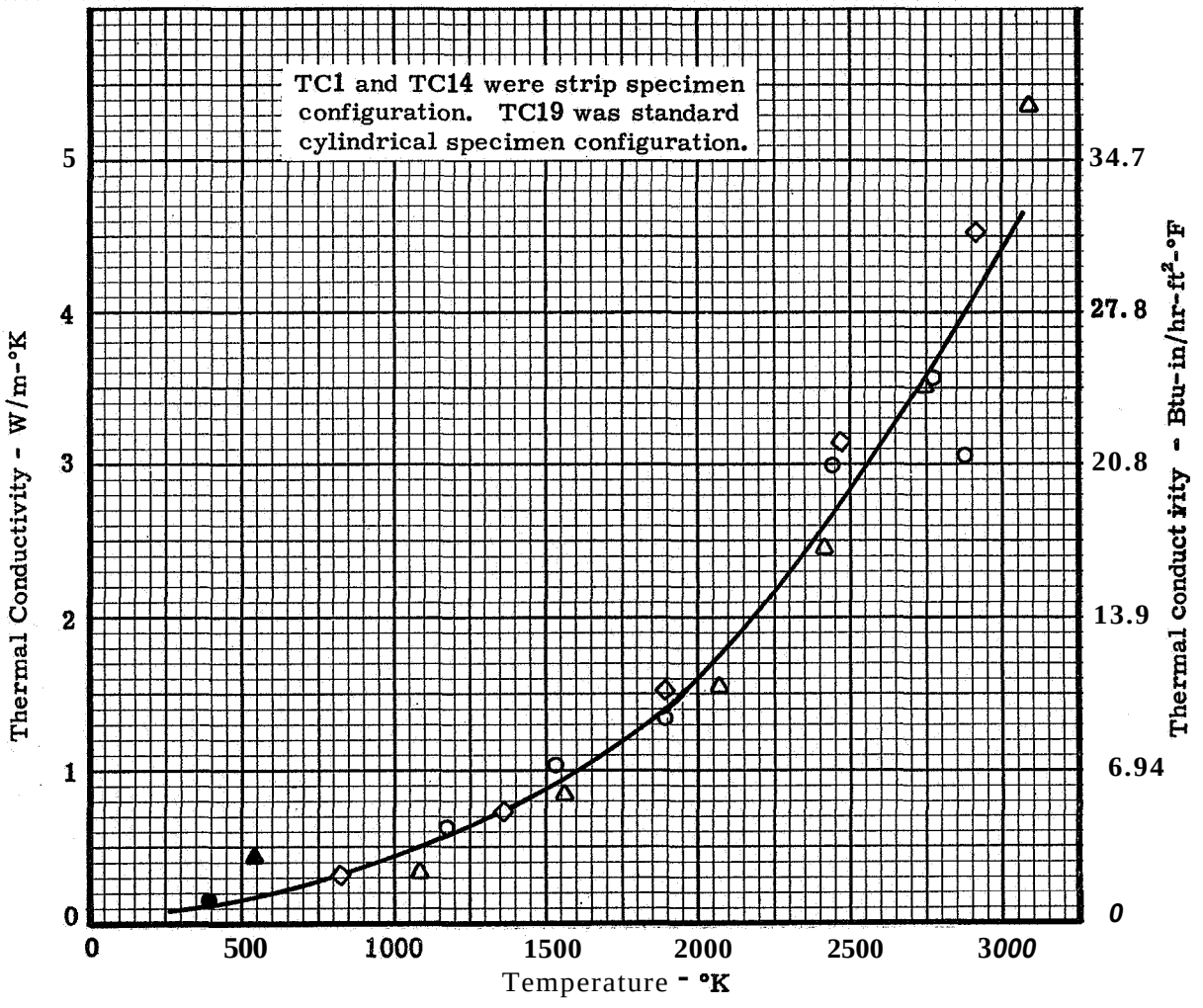

Figure 144. The thermal conductivity of phenolic-nylon furnace charred at low heating rate to 812°K - measured in argon

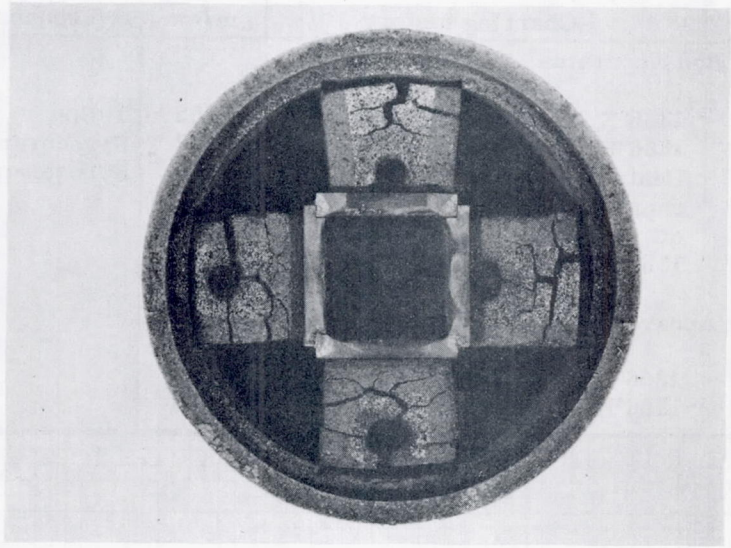

a. Specimen TC14 (precharred at 812°K for 30 minutes)

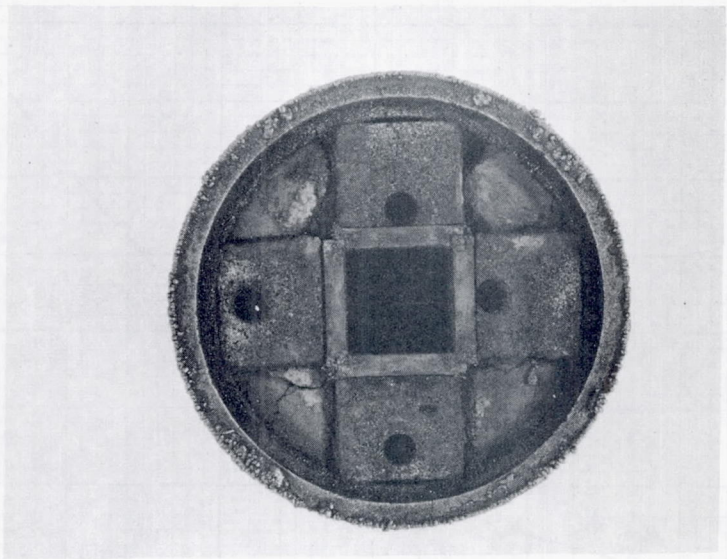

b. Specimen TC10 (precharred at 1366°K for 30 minutes)

Figure 145. Pictures of phenolic-nylon char specimens after exposure to 3033°K during thermal conductivity evaluation in radial inflow apparatus

Symbol	Spec.	Charring history	Density, gm/cm³	Type references	Environment for measurements
Comparative Rod Apparatus					
●	TC8S	1366°K for 30 minutes	0.365	Teflon	Nitrogen
A	TC17	1366°K for 30 minutes	0.377	Pyroceram	Nitrogen
×	5R	Heated slowly to 1022°K, then rapidly to 1366°K. Power turned off immediately after reaching 1366°K	0.342	Pyroceram	Nitrogen
Radial Inflow Apparatus					
○	TC10	1366°K for 30 minutes	0.377		Argon purge
△	TC2	1366°K for 30 minutes	0.363		Helium purge

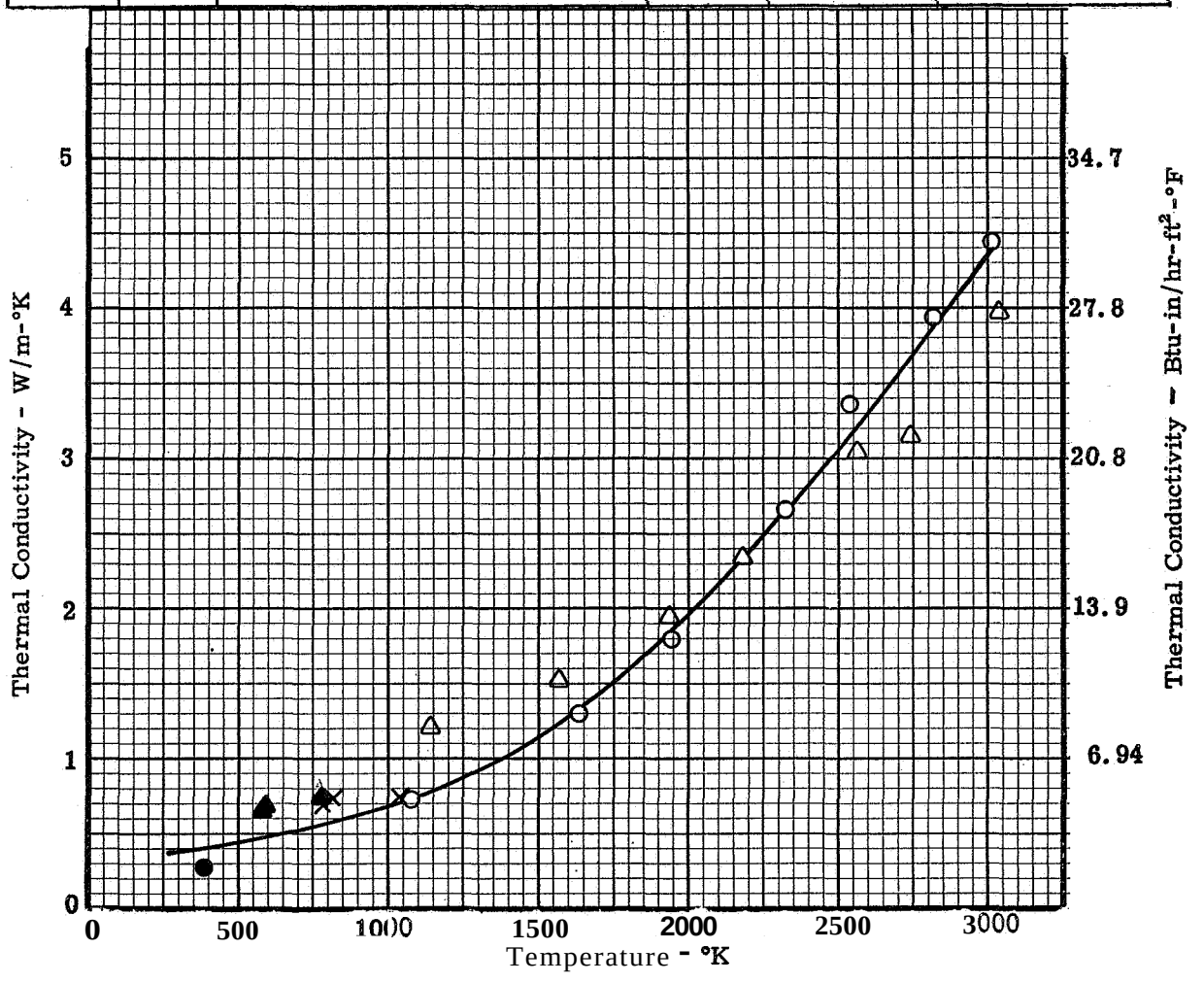

Figure 146. The thermal conductivity of phenolic-nylon furnace charred at low heating rate to 1366°K

Symbol	Spec.	Charring history	Density gm/cm³	Type references	Environment for measurements
Comparative Rod Apparatus					
●	TC6S	1922°K for 30 minutes	0.321	Teflon	Air
▲	TC6S	1922°K for 30 minutes	8.321	Pyrex	Nitrogen
■	TC6S	1922°K for 30 minutes	0.321	Pyroceram	Nitrogen
Radial Inflow Apparatus					
⊙	TC3	1922°K for 30 minutes	0.335		Argon purge
△	TC11	1922°K for 30 minutes	0.341		Argon purge

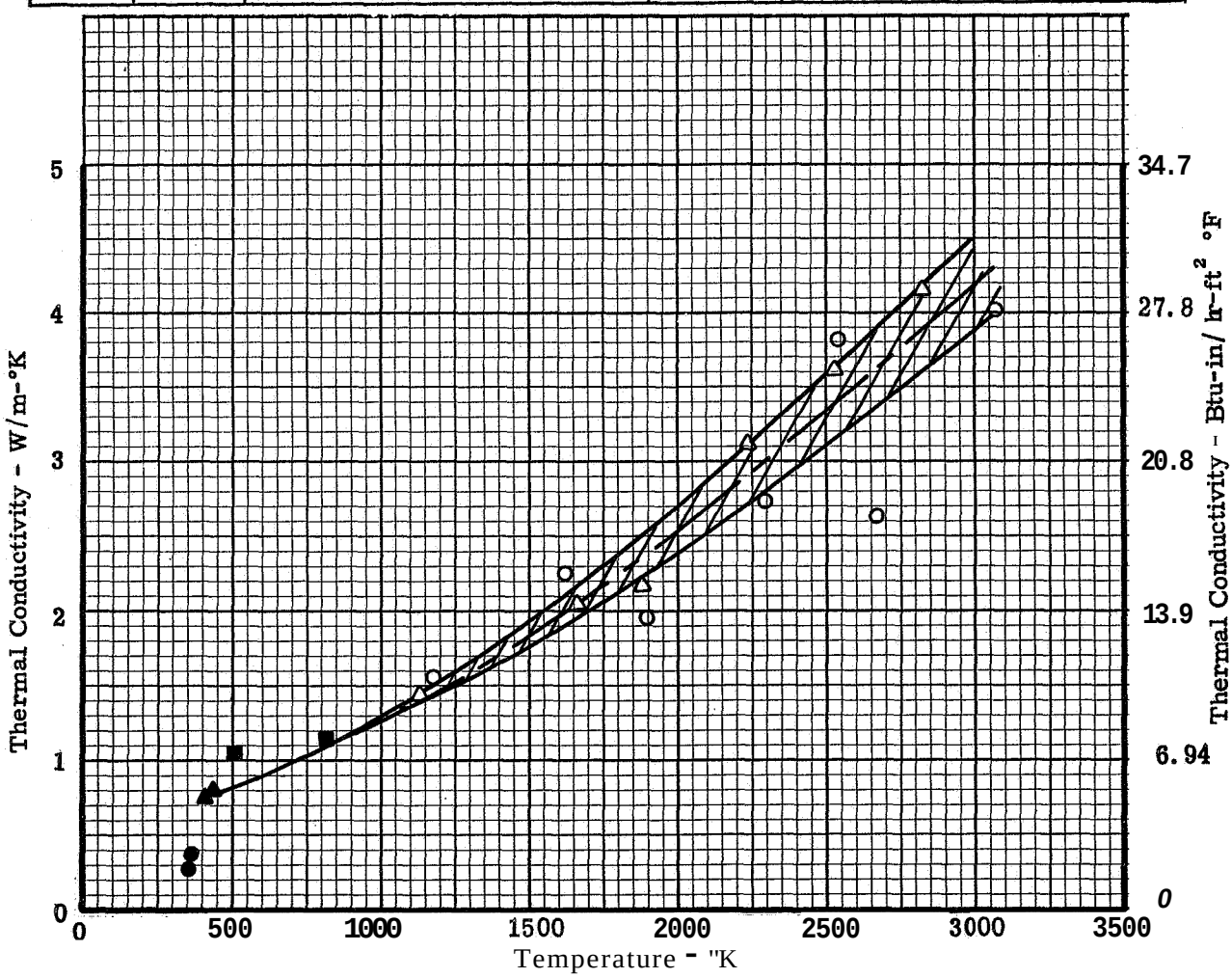

Figure 147. The thermal conductivity of phenolic-nylon furnace charred at low heating rate to 1922°K - measured in argon

			Density, gm/cm	Type references	Environment for measurements
					Nitrogen
○	TC4	2480°K for 30 minutes	0.339		Argon purge
△	TC12	2480°K for 30 minutes	0.344		Argon purge. Ran t 2247°K face
⩚	TC12	2480°K for 30 minutes	0.344		Argon purge, rerun

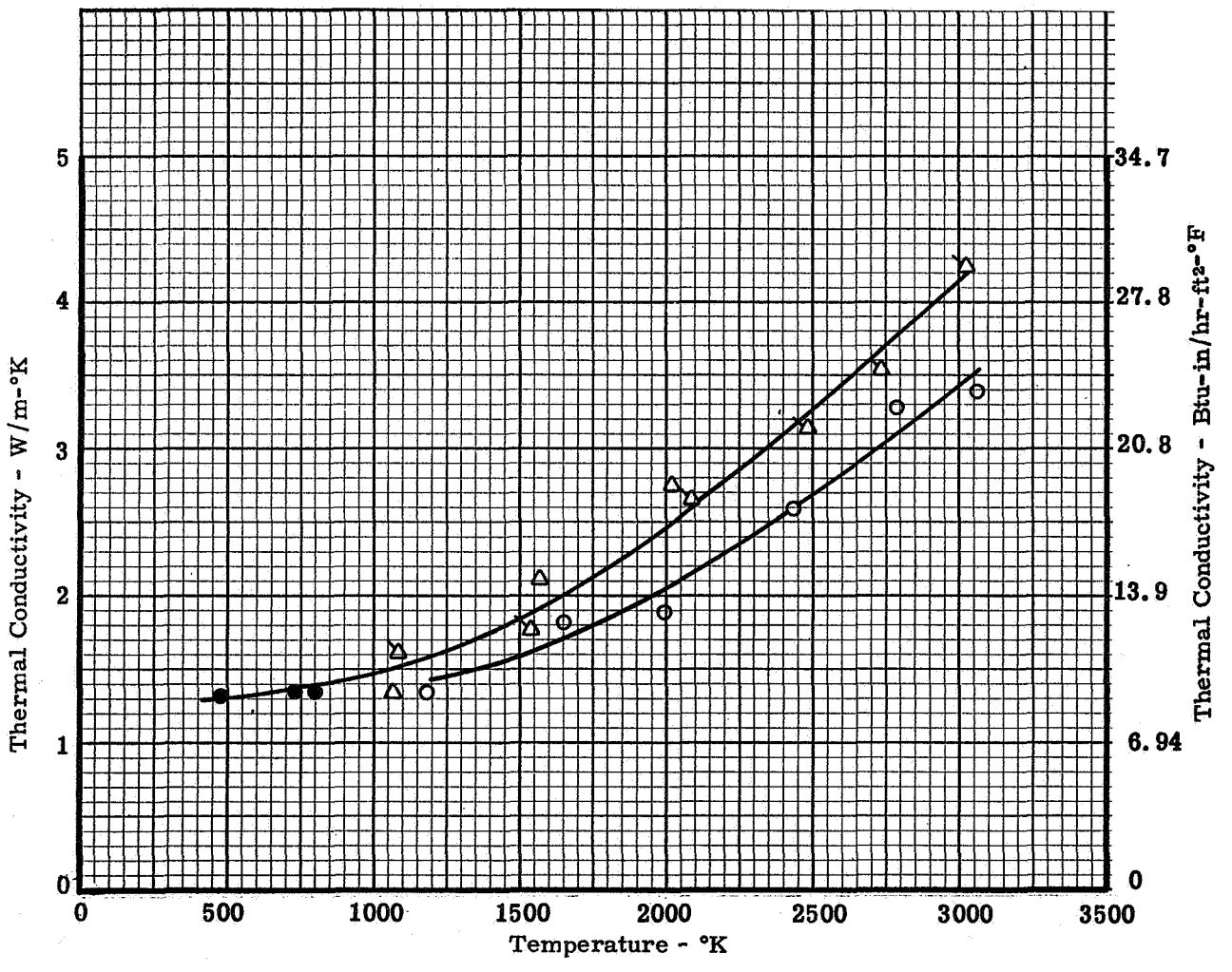

Figure 148. The thermal conductivity of phenolic-nylon furnace charred at low heating rate to 2480°K - measured in argon

Symbol	Spec.	Charring history	Density, gm/cm³	Type references	Environment for measurements
Comparative Rod Apparatus					
●	1F5000-3	3033°K for 180 minutes	0.347	Pyroceram	Nitrogen
A	4F5000-5	3033°K for 300 minutes	0.353	Pyroceram	Nitrogen
Radial Inflow Apparatus					
○	TC5	3033°K for 30 minutes	0.349		Argon purge, Run 3
△	2F5000-2	3033°K for 120 minutes	0.353		Argon purge, Run 2
⊗	TC13	3033°K for 30 minutes	0.351		Argon purge, 4 to 7 percent impregnation with thermatomic carbon

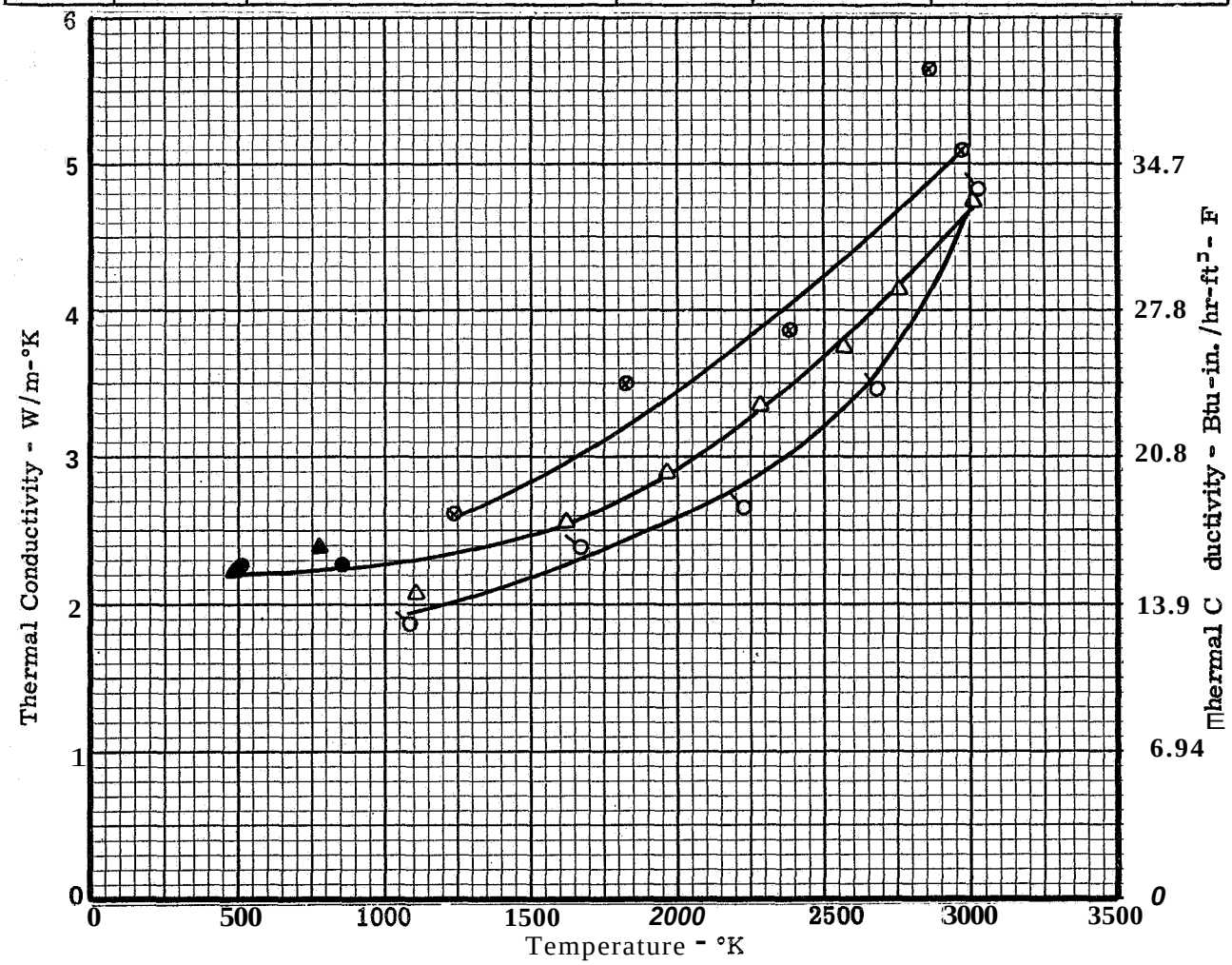

Figure 149. The thermal conductivity of phenolic-nylon furnace charred at low heating rate to 3033°K - measured in argon

Symbol	Spec.	Charring history	Density gm/cm³	Type references	Environment for measurements
Comparative Rod Apparatus					
●	1F5000-3	3033°K for 180 minutes	0.347	Pyroceram	Helium purge
▲	4F5000-5	3033°K for 300 minutes	0.353	Pyroceram	Helium purge
Radial Inflow Apparatus					
○	2F5000-2	3033°K for 120 minutes	0.353		Helium purge
△	3F5000-3	3033°K for 180 minutes	0.383		Helium purge

Specimen	Mean temp. level °K	ΔT/ΔX during measurement °K/cm	Gage length cm	Hot face temp. °K	Cold face temp. °K
2F5000-2	2091	1000	0.475	2329	1854
2F5000-2	2955	850	0.475	3157	2753
3F5000-3	2054	362	0.475	2140	1968
3F5000-3	3101	541	0.475	3229	2973

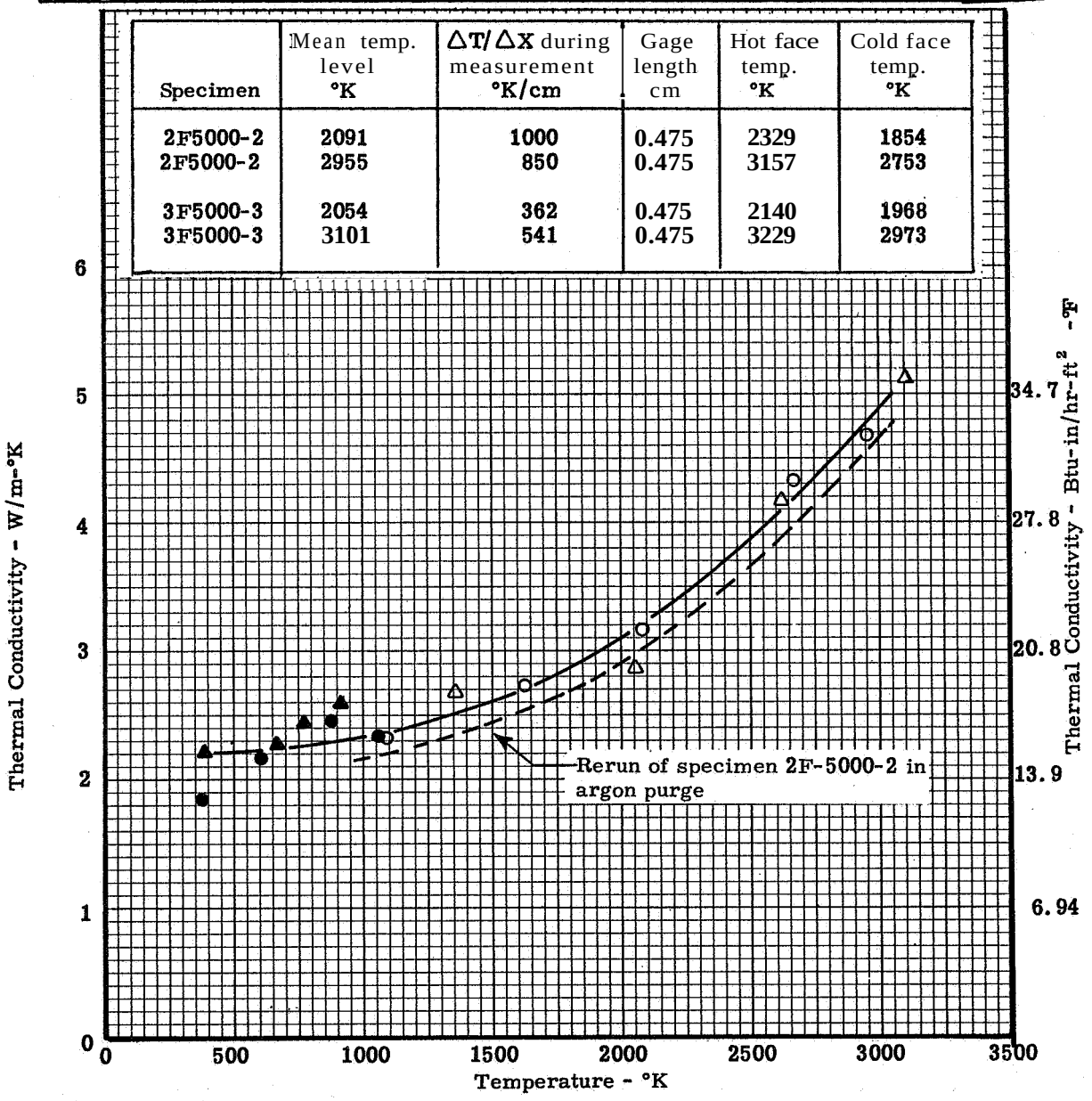

Figure 150. The thermal conductivity of phenolic–nylon charred at low heating rate to 3033°K–measured in helium

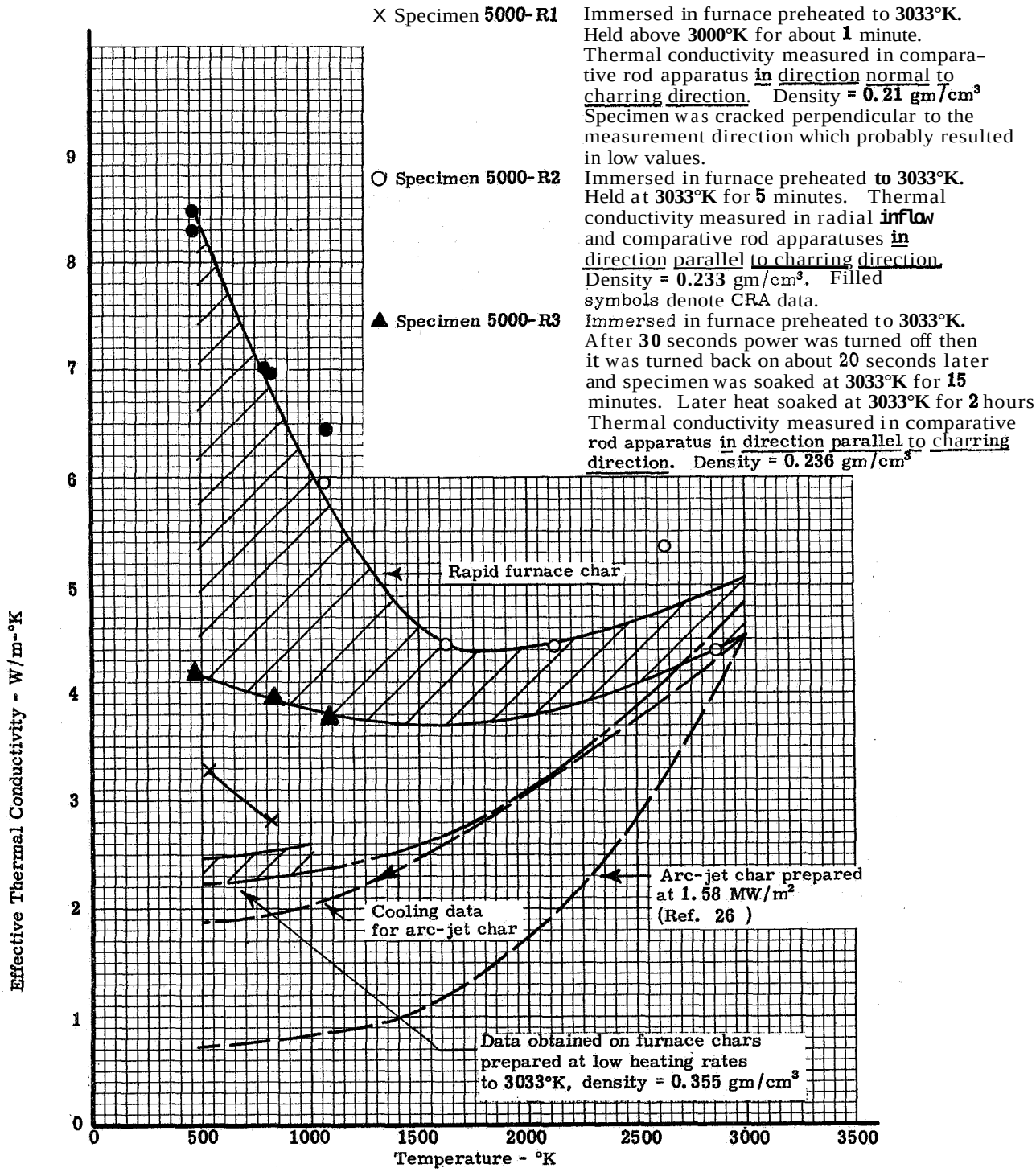

Figure 151. The thermal conductivity of chars prepared in the furnace at rapid heating rates (cold wall heat flux ≅ 4.9 MW/m²)

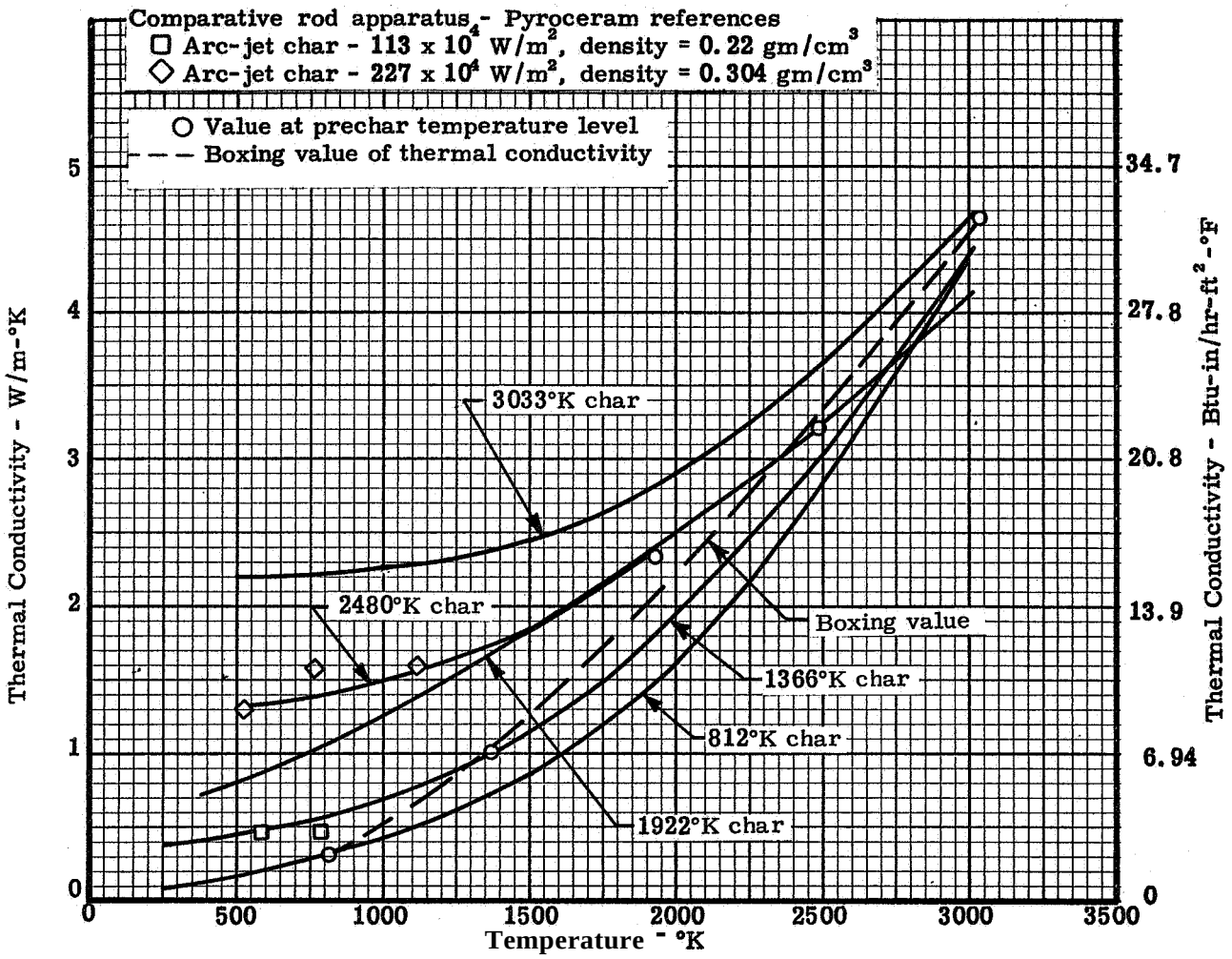

Figure 152. Summary of effects of charring temperature level on thermal conductivity of char prepared in furnace at low heating rate

Symbol	Specimen	Bulk density gm/cm³	Environment
O	Thermatomic carbon	----	Helium purge
Δ	ATJ powder - specimen 1	0.95	Helium purge
a	ATJ powder - specimen 2	1.13	Helium purge after two evacuations and backfill with helium
◇	ATJ powder - specimen 3	1.13	" "
●	Powder from phenolic-nylon charred at 3033°K specimen 1	1.05	Helium purge
■	Powder from phenolic-nylon charred at 3033°K specimen 2	0.975	Helium purge

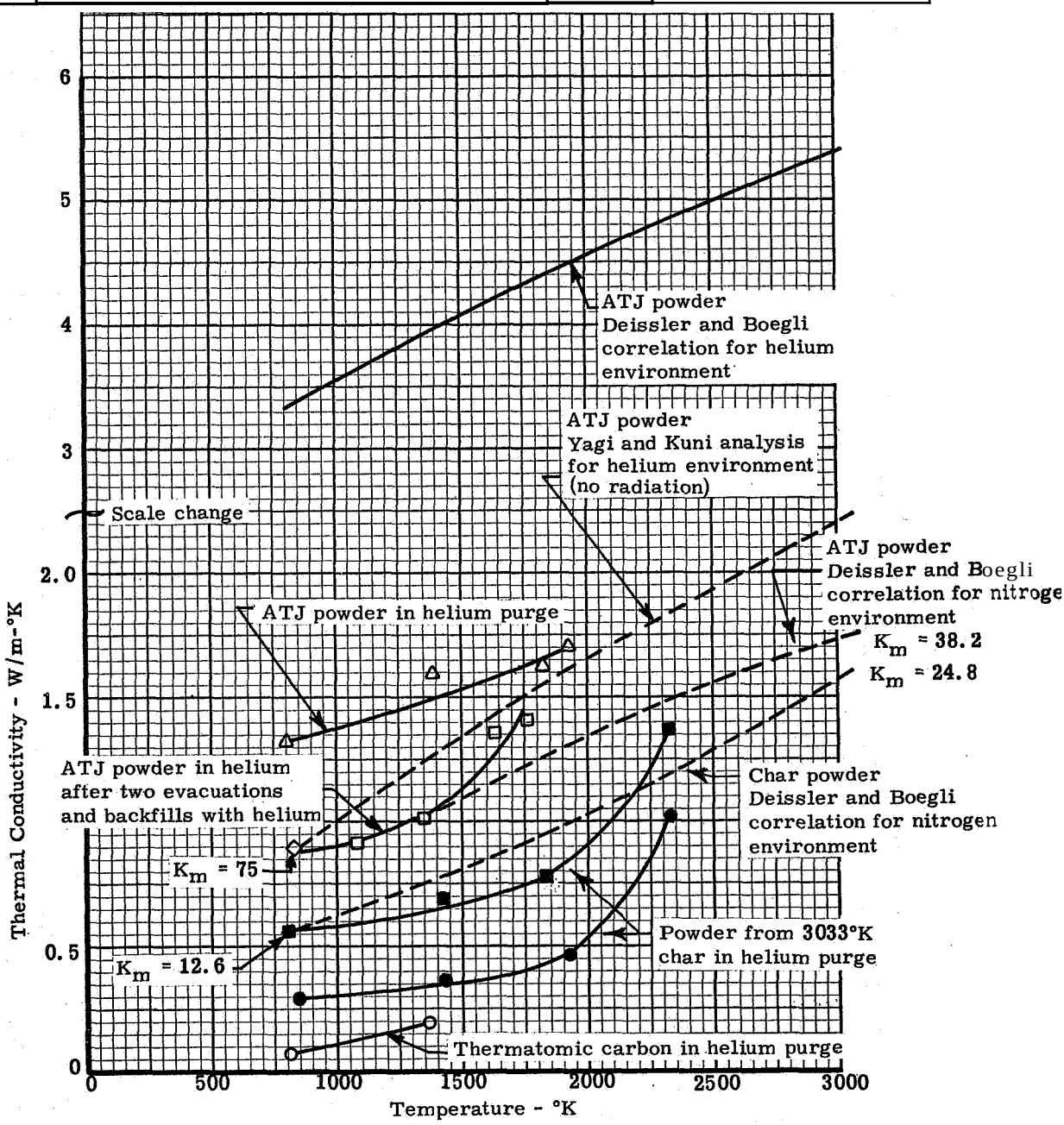

Figure 153. Results of measurements of thermal conductivity of thermatomic carbon, ATJ powder and powder from 3033°K phenolic-nylon char

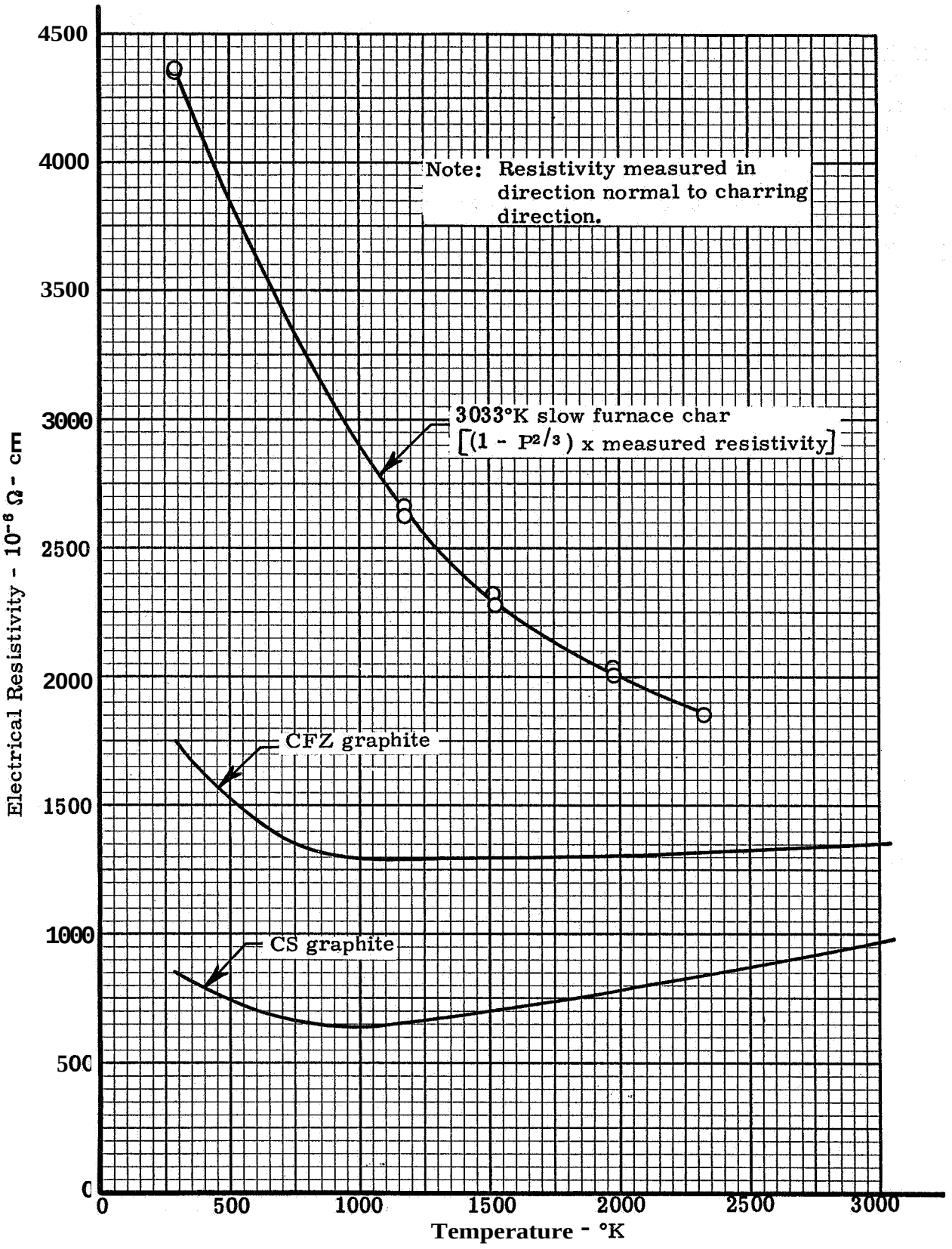

Figure 154. Electrical resistivity of phenolic-nylon charred at low heating rate to 3033°K (3 hours at temperature)

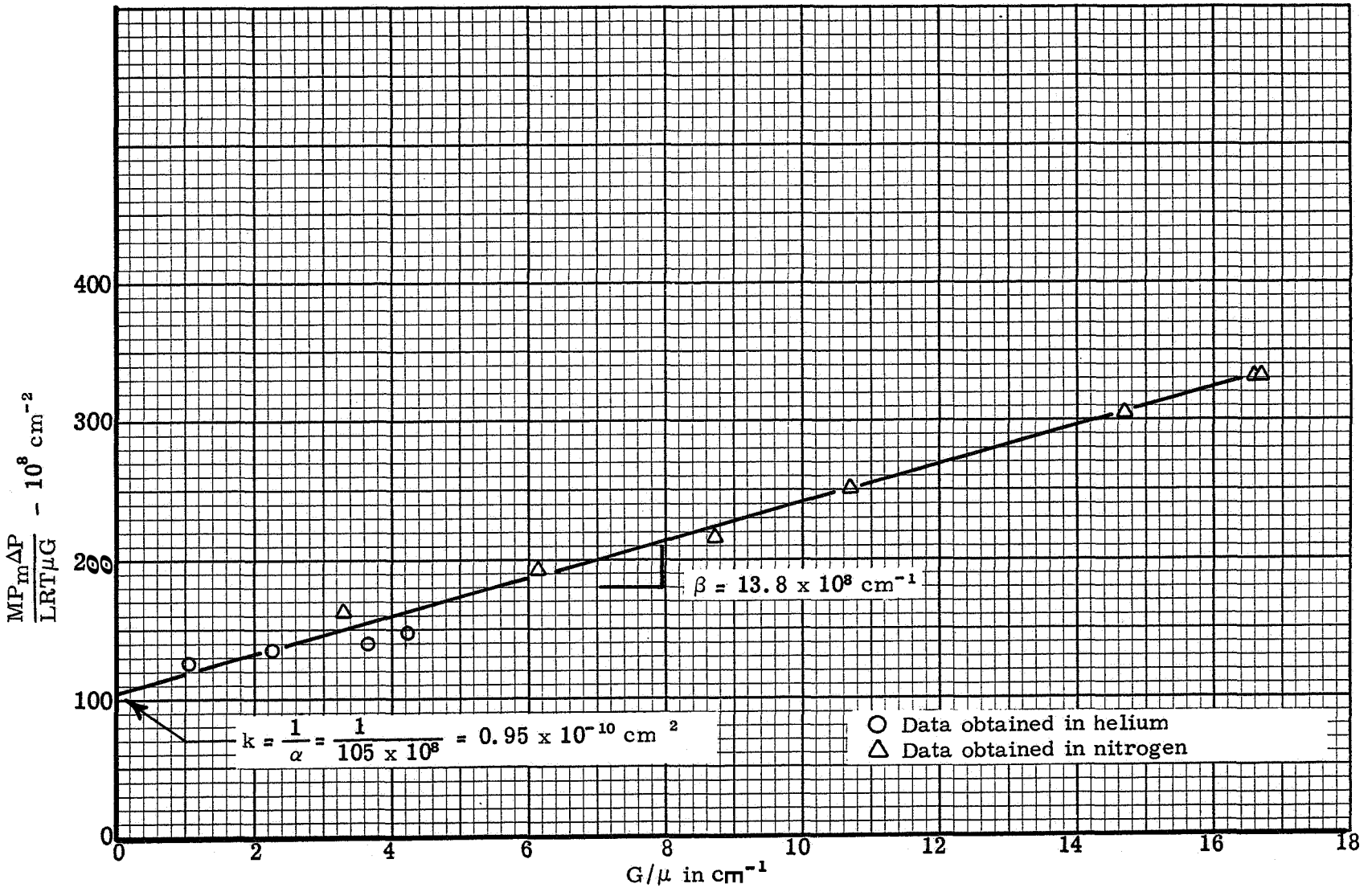

Figure 155. Cornell-Katz permeability correlation for phenolic-nylon charred in furnace at low heating rate to 812°K (30 minutes at temperature)(specimen P1)

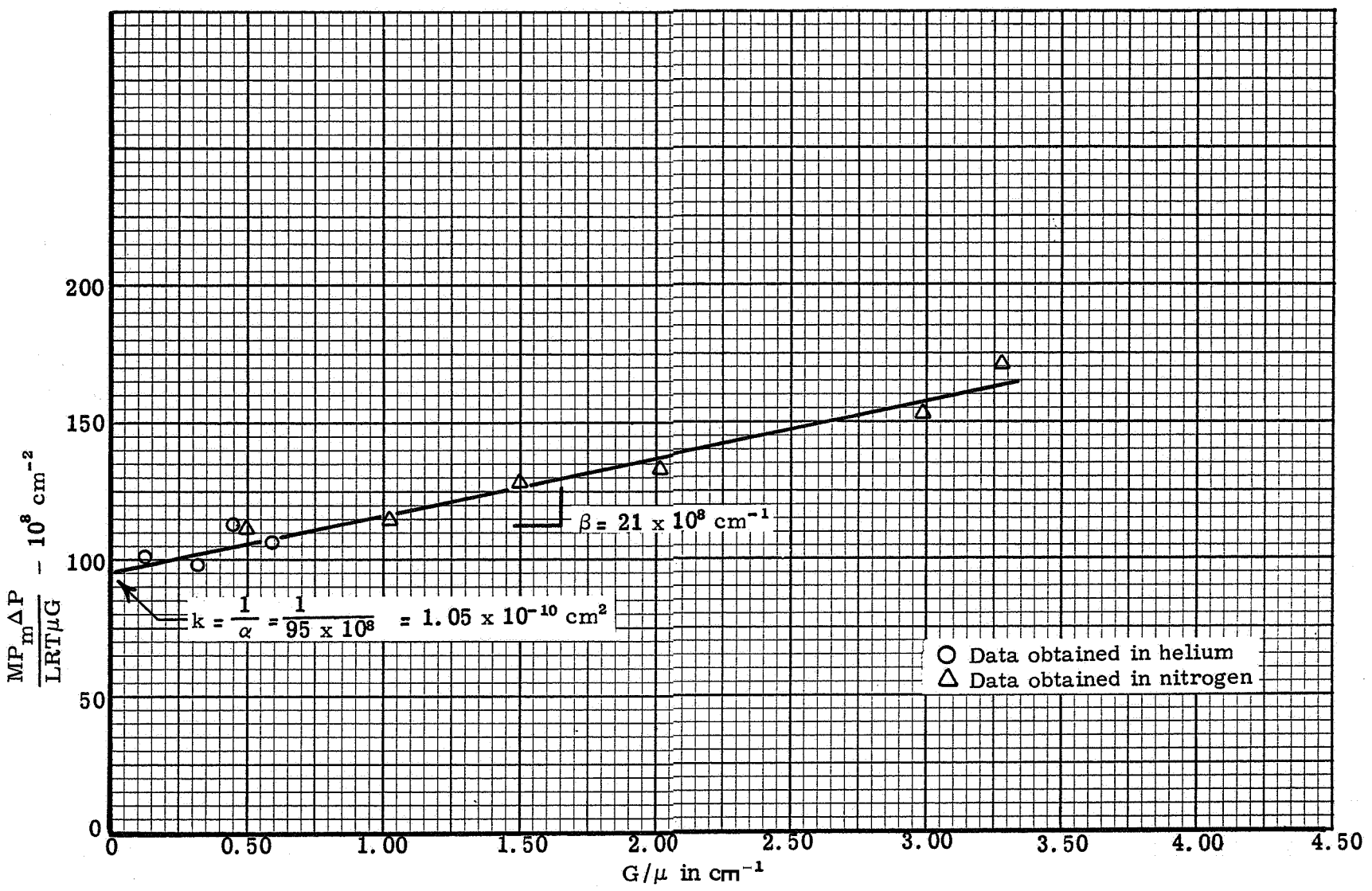

Figure 156. Cornell-Katz permeability correlation for phenolic-nylon charred in furnace at 1 heating rate to 1366°K (30 minutes at temperature)(specimen P2)

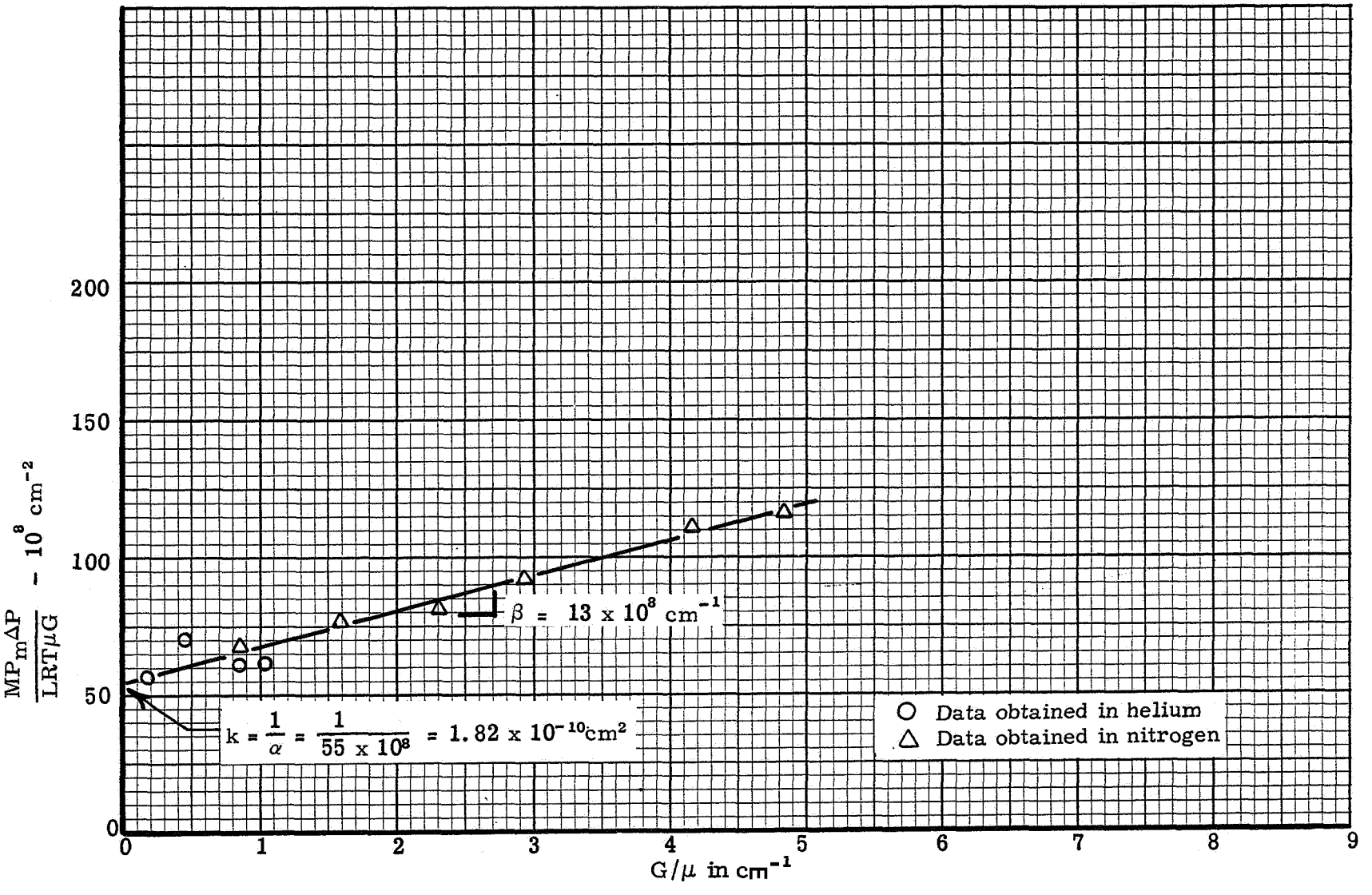

Figure 157. Cornell-Katz permeability correlation for phenolic-nylon charred in furnace at low heating rate to 1922°K (30 minutes at temperature)(specimen P3)

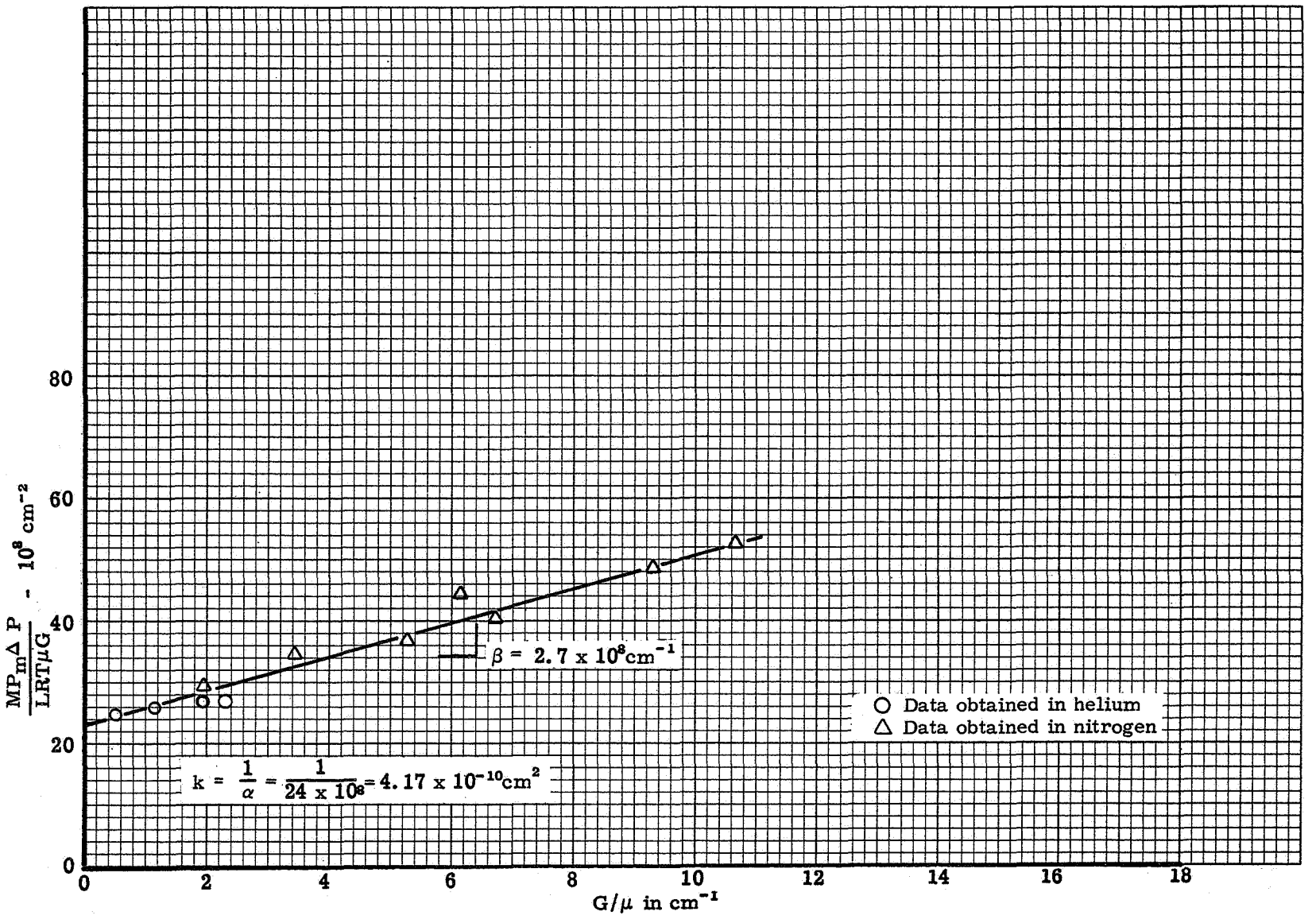

Figure 158. Cornell-Katz permeability correlation for phenolic-nylon charred in furnace at Δw heating rate to 2480°K (30 minutes at temperature)(specimen P4)

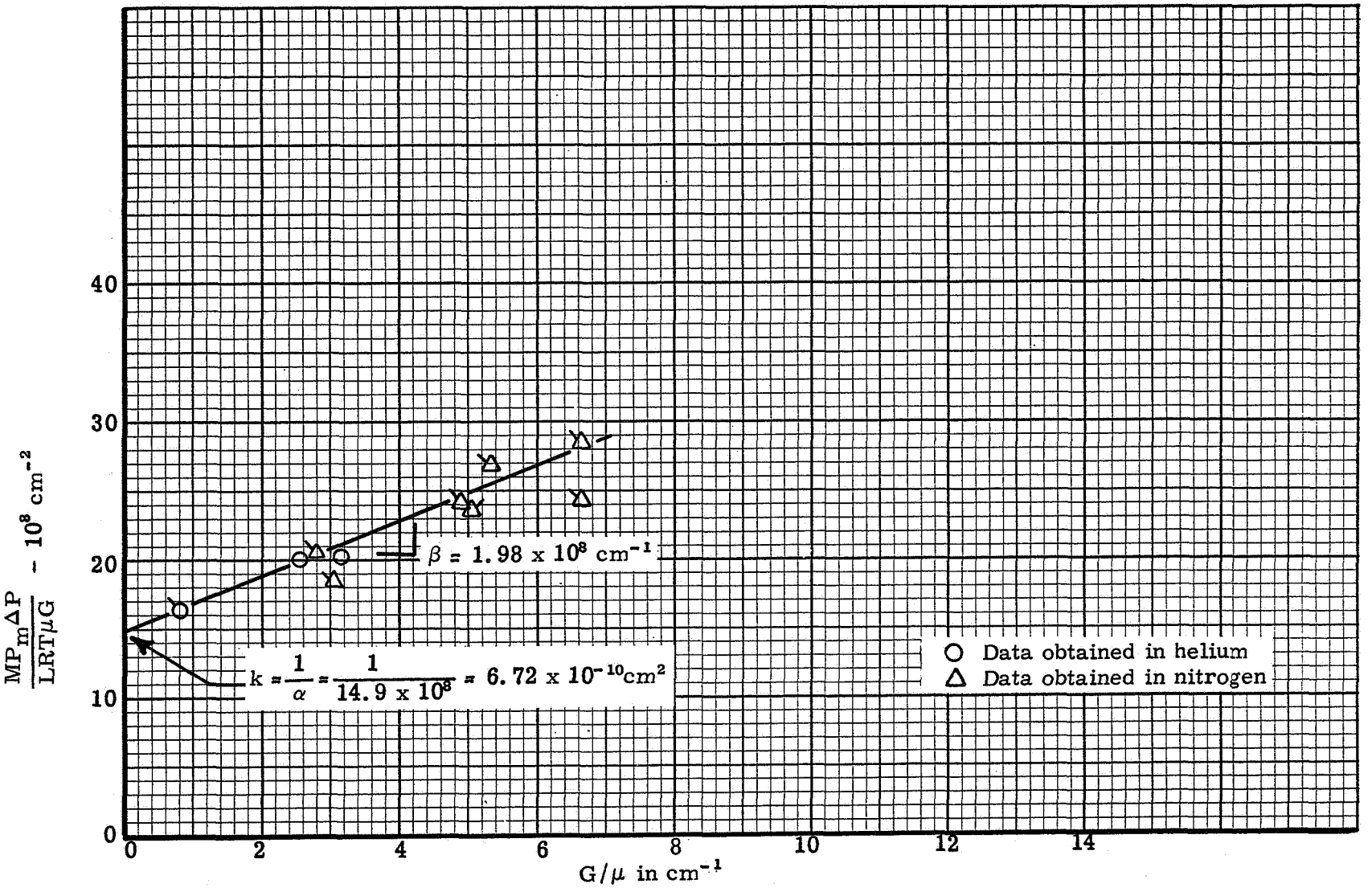

Figure 159. Cornell-Katz permeability correlation for phenolic-nylon charred in furnace at low heating rate to 3033°K (30 minutes at temperature)(specimen P5)

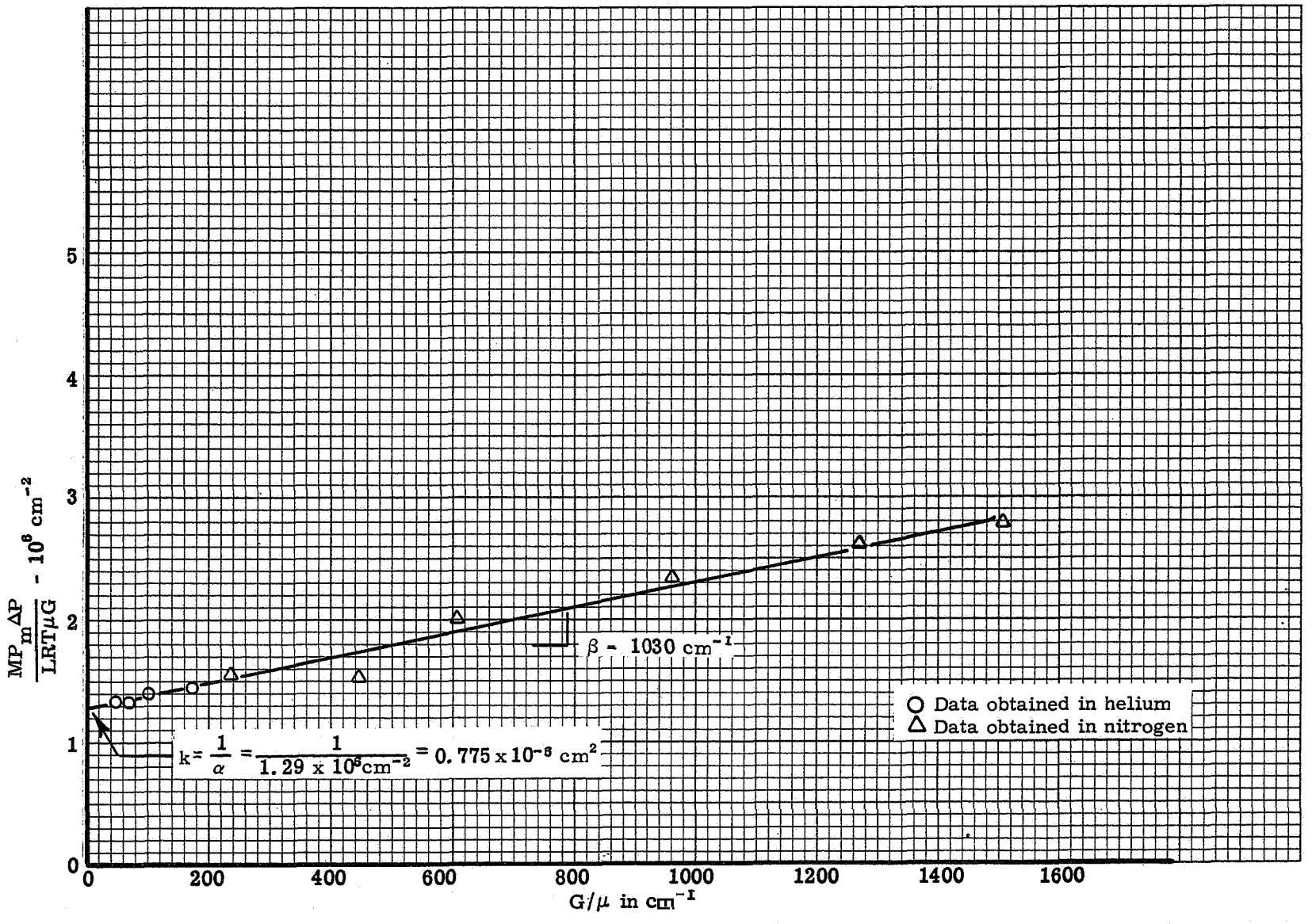

Figure 160. Cornell-Katz permeability correlation for phenolic-nylon charred at rapid rate in furnace to 3033°K (specimen 5000-R3)(measurements made in charring direction)

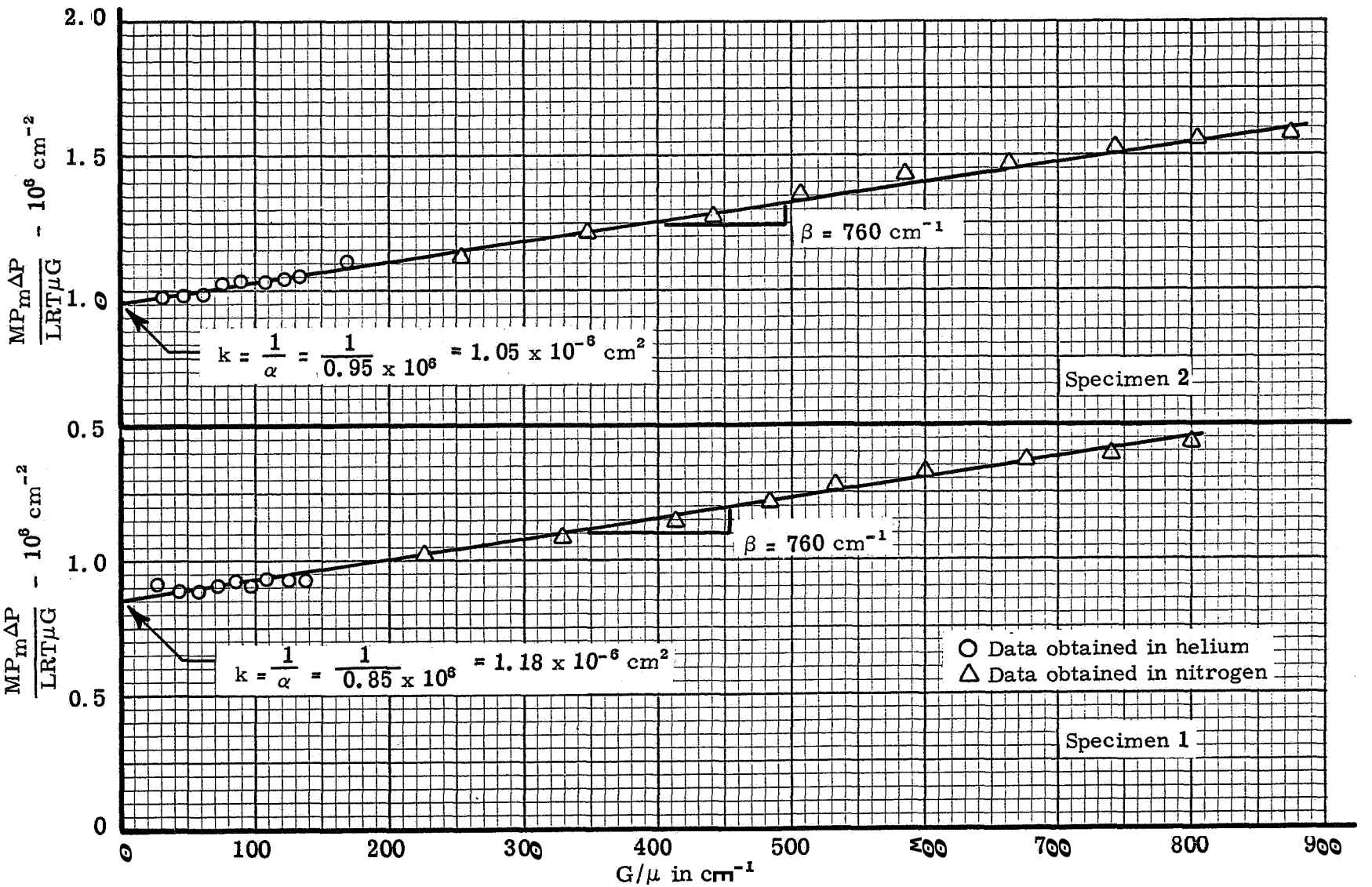

Figure 16 1. Cornell-Katz permeability correlation for phenolic-nylon charred in arc-jet at 227×10^4 W/m^2 (measurements made in charring direction)

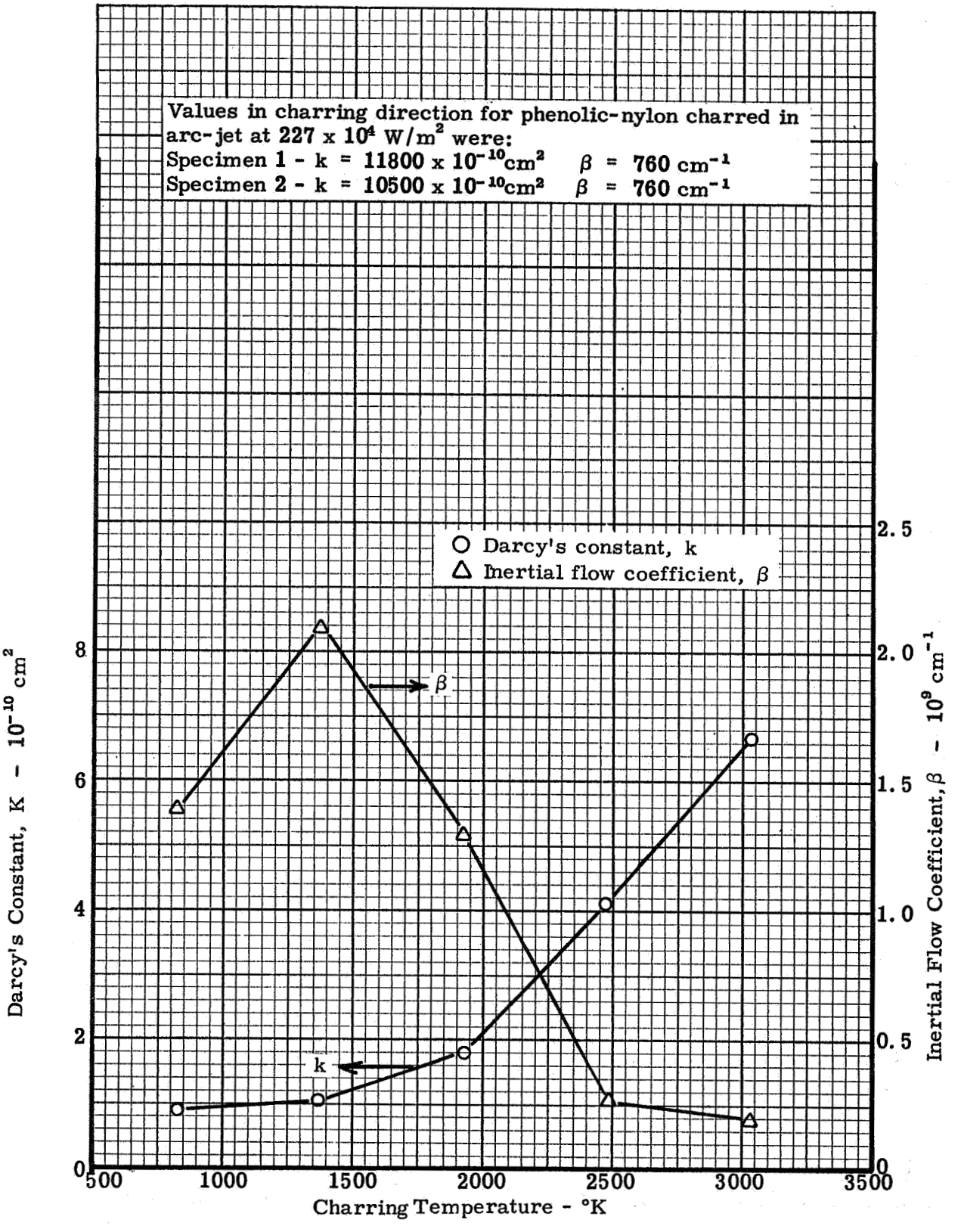

Figure 162. Permeability coefficients versus charring temperature for phenolic-nylon charred in furnace at low heating rate

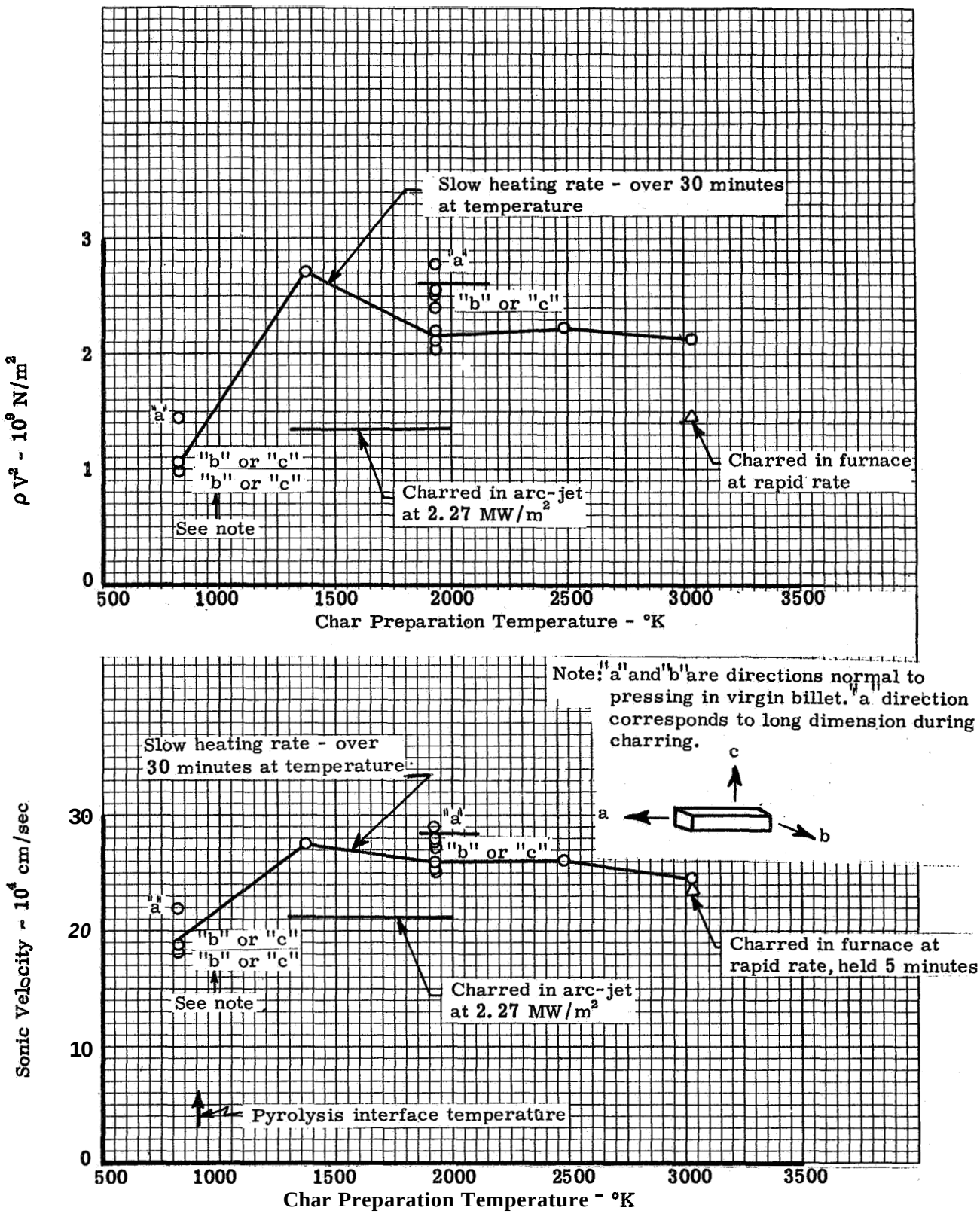

Figure 163. Effects of char history on sonic velocity of char

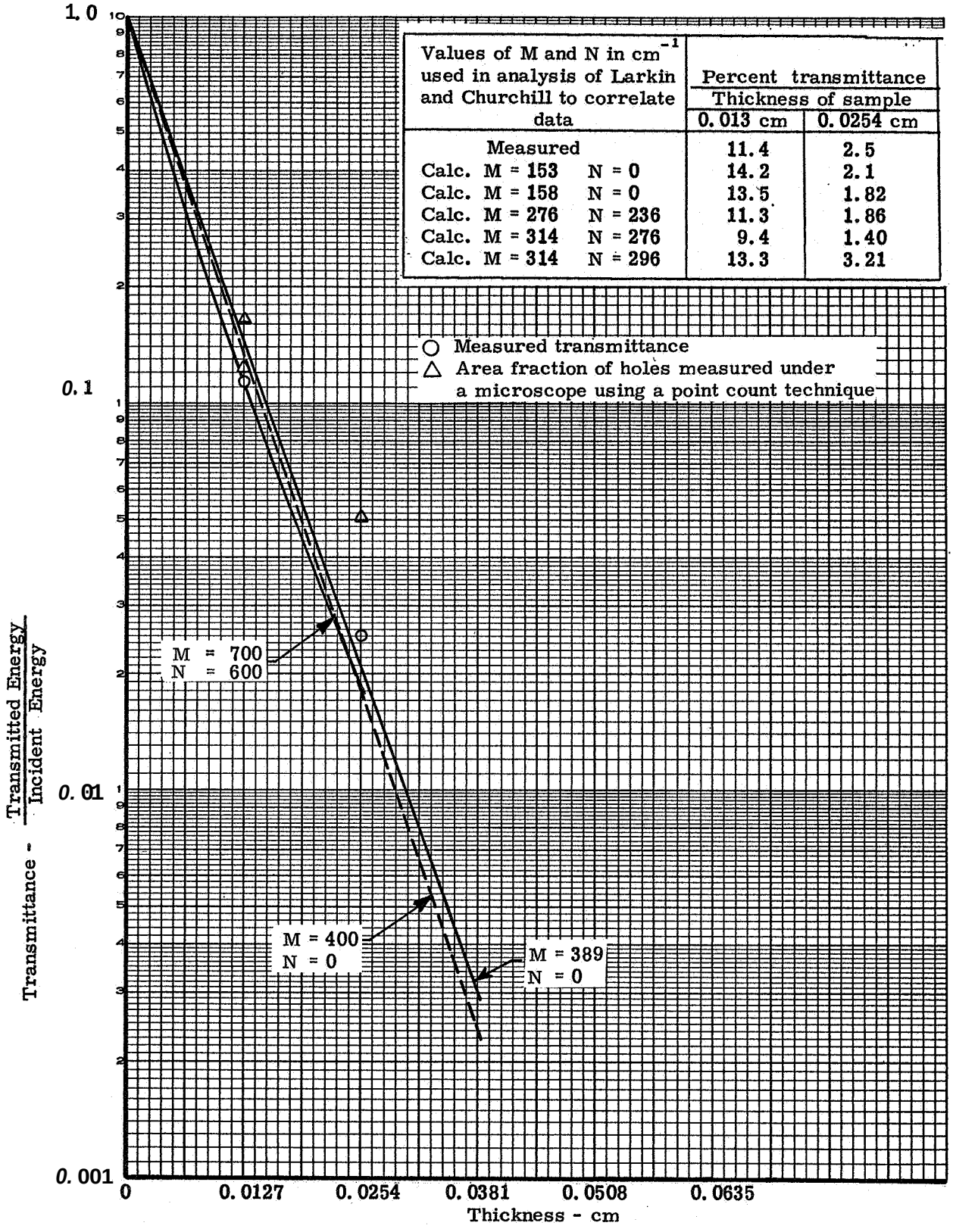

Figure 164. Transmittance at 294°K of phenolic-nylon charred at 3033°K for 30 minutes

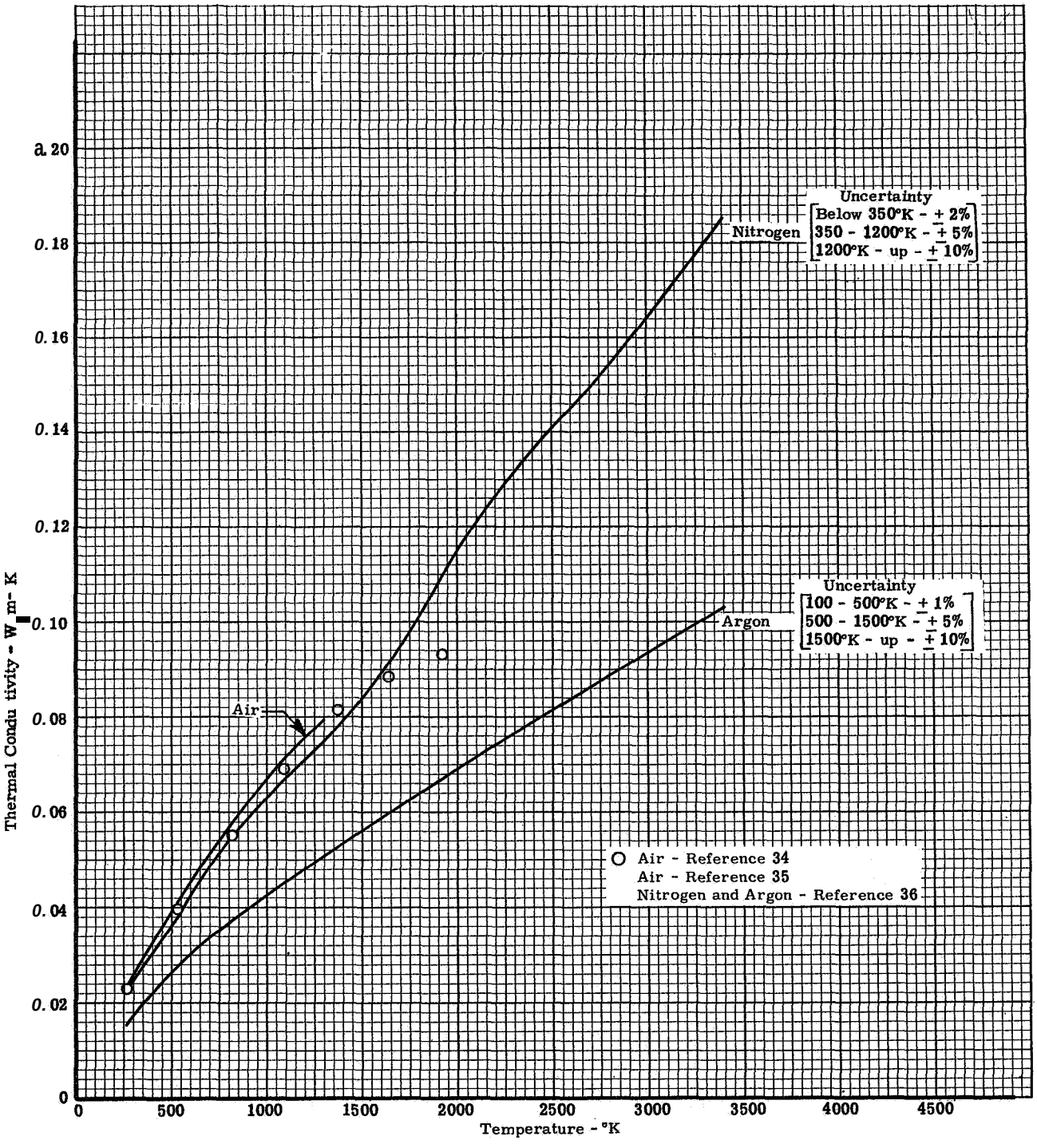

Figure 166. The thermal conductivities of gaseous argon and nitrogen at a pressure of 1 atmosphere

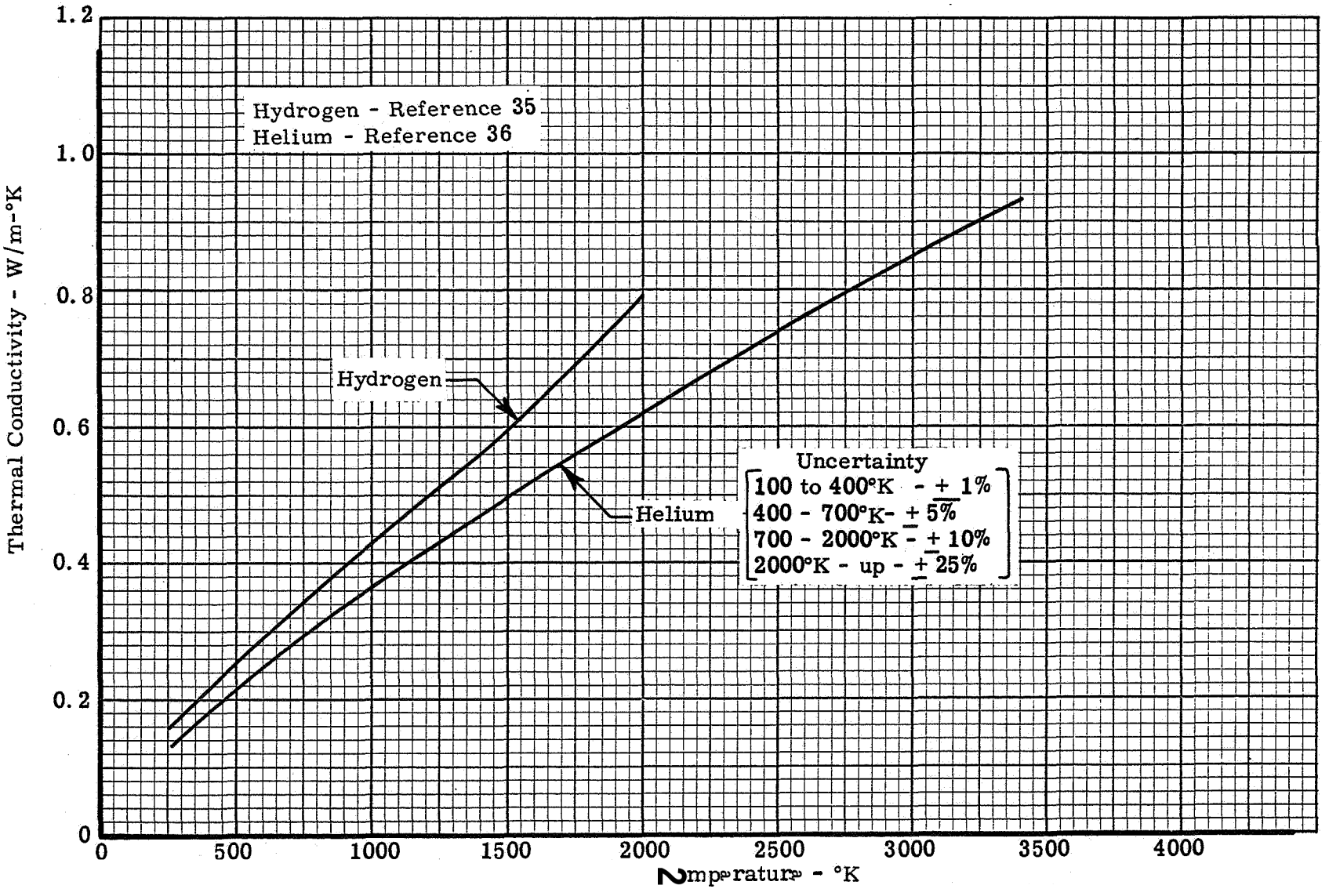

Figure 166. The thermal conductivity of gaseous helium and hydrogen at a pressure of 1 atmosphere

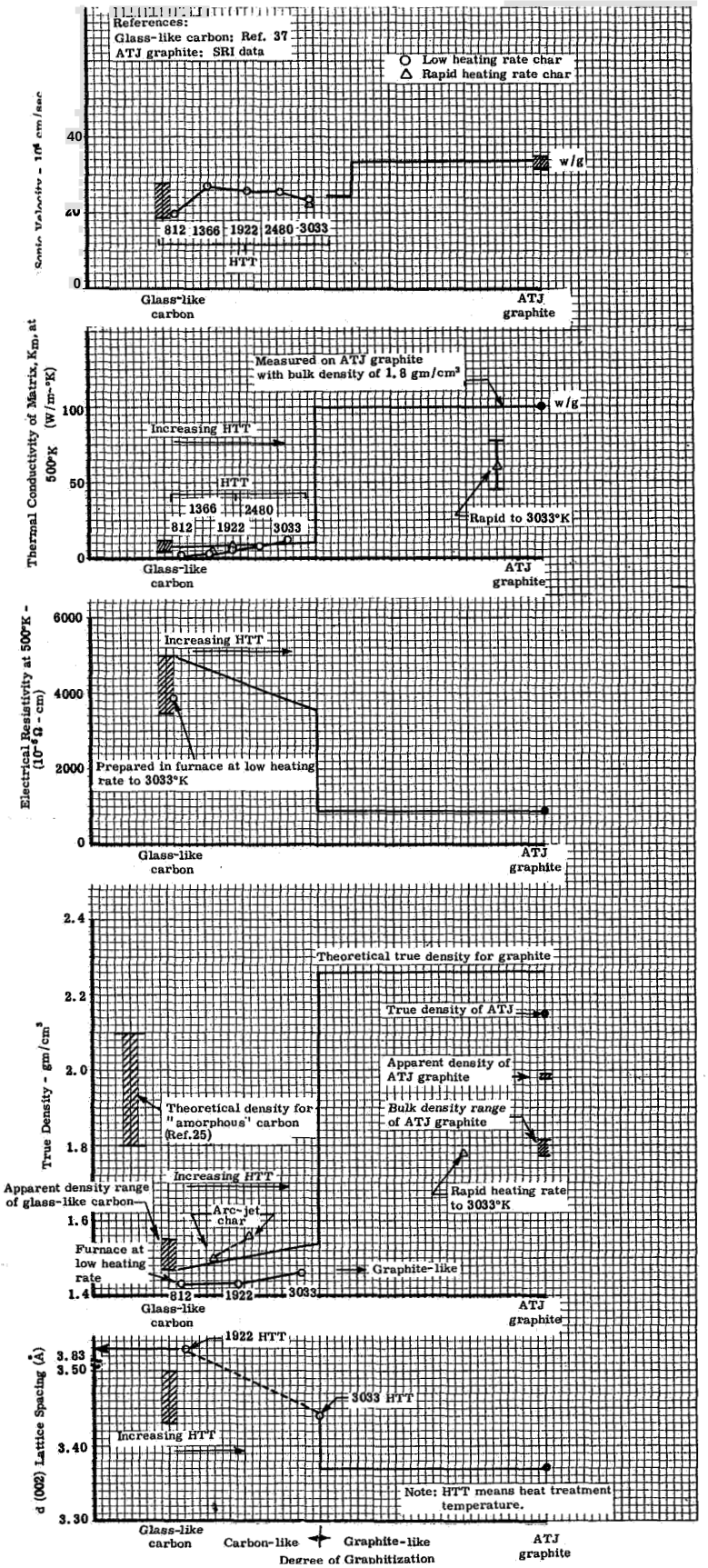

Figure 167. Relation of properties measured to properties of glass-like carbon (nongraphitized) and ATJ graphite

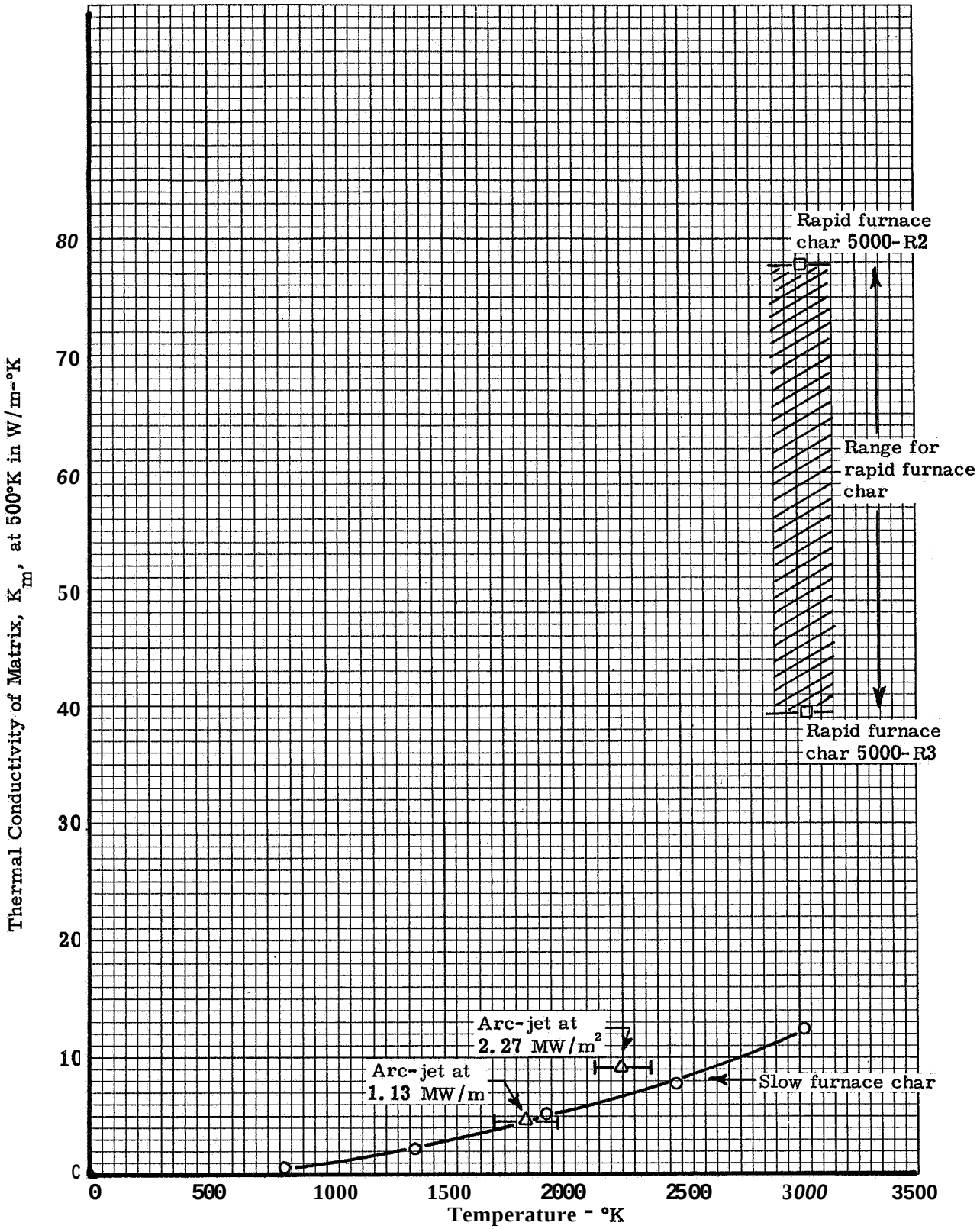

Figure 168. Effects of precharring temperature level on thermal conductivity of matrix at 500°K

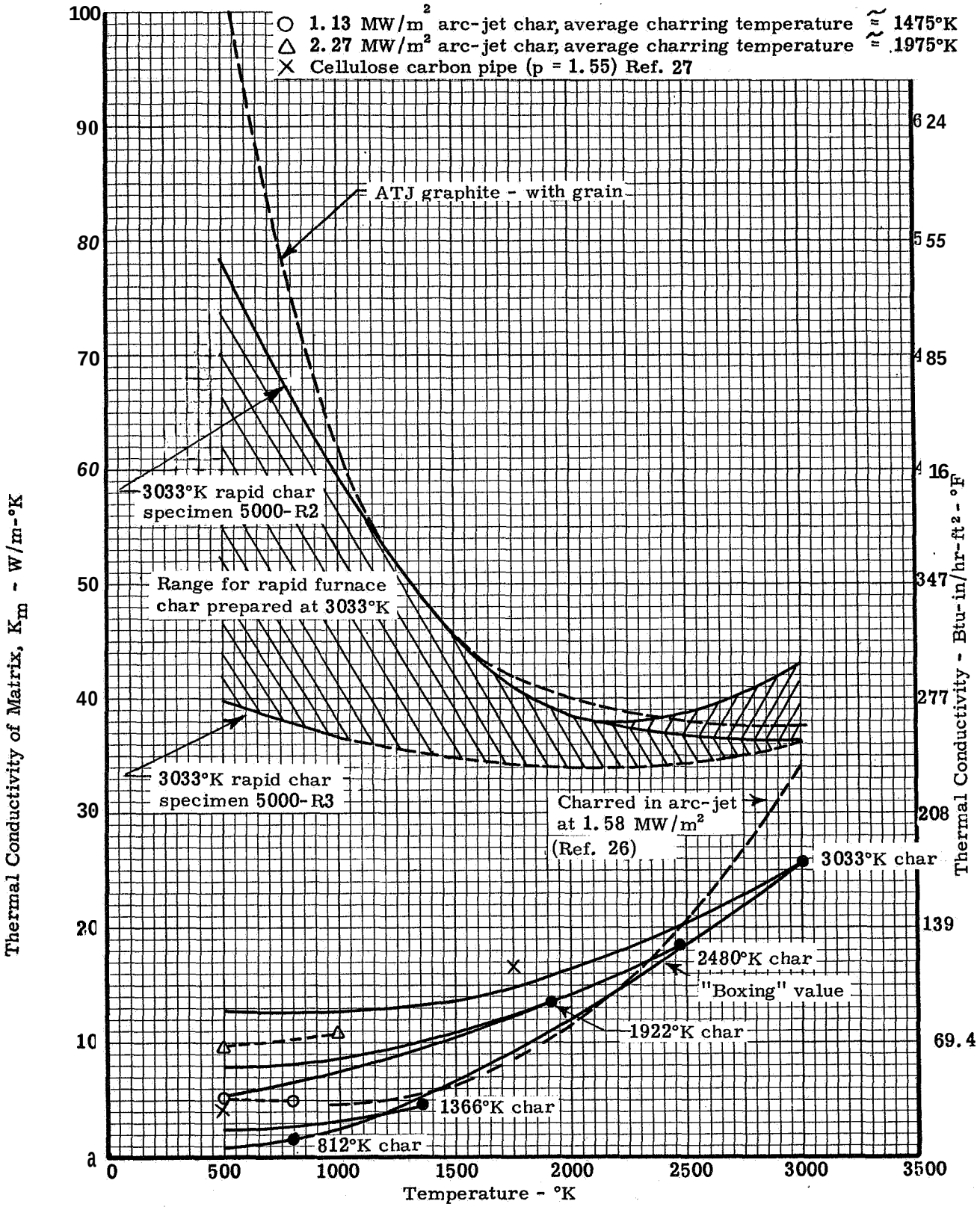

Figure 169. Results of reductions of matrix (solid) thermal conductivity from effective thermal conductivity measurements using $4P^{2/3}\phi\sigma T_m^3$ as the radiant contribution – neglecting transparency effects

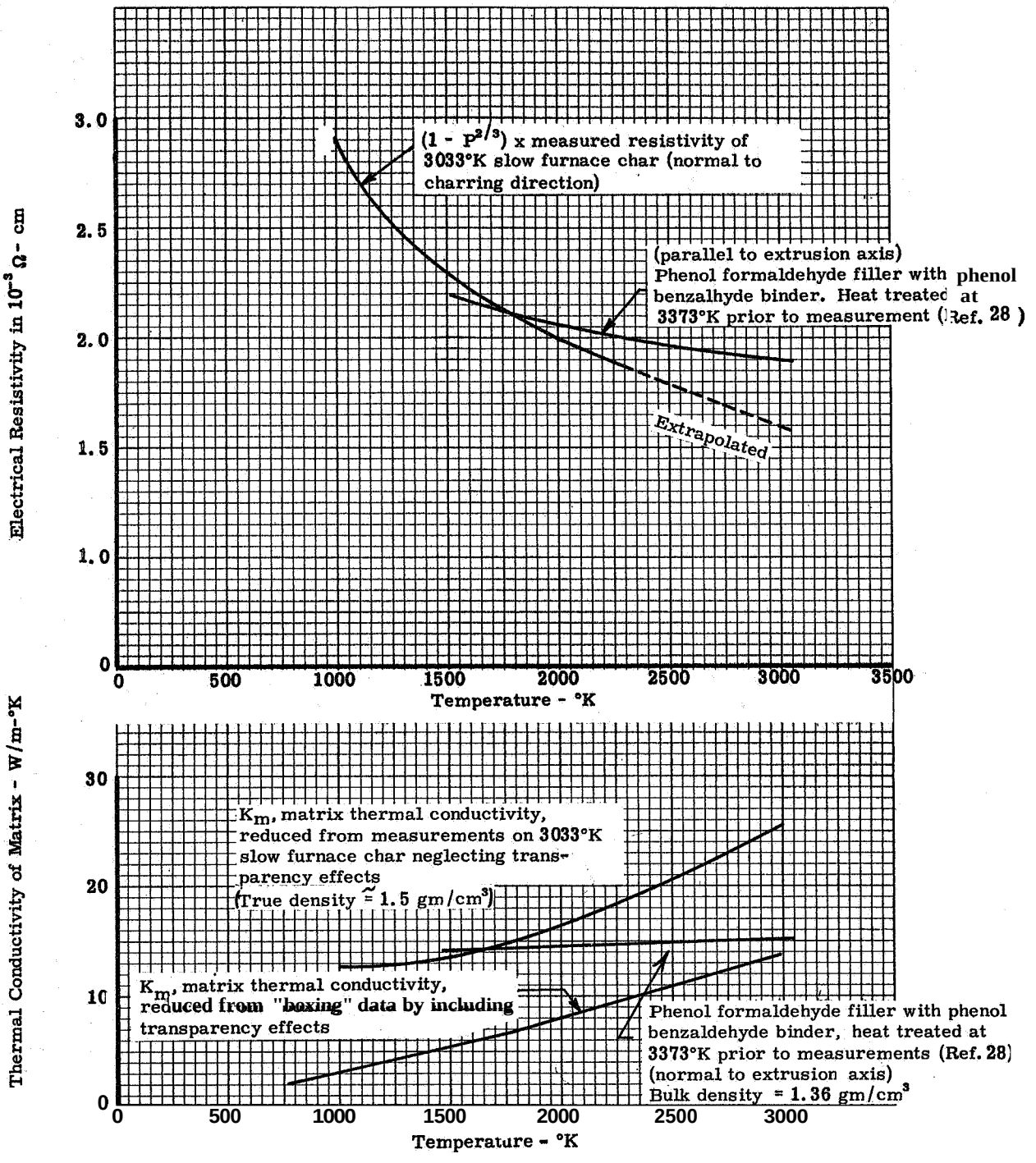

Figure 170. Comparison of values of K_m(matrix) reduced from measurements (neglecting transparency effects) with data on another carbon-like material

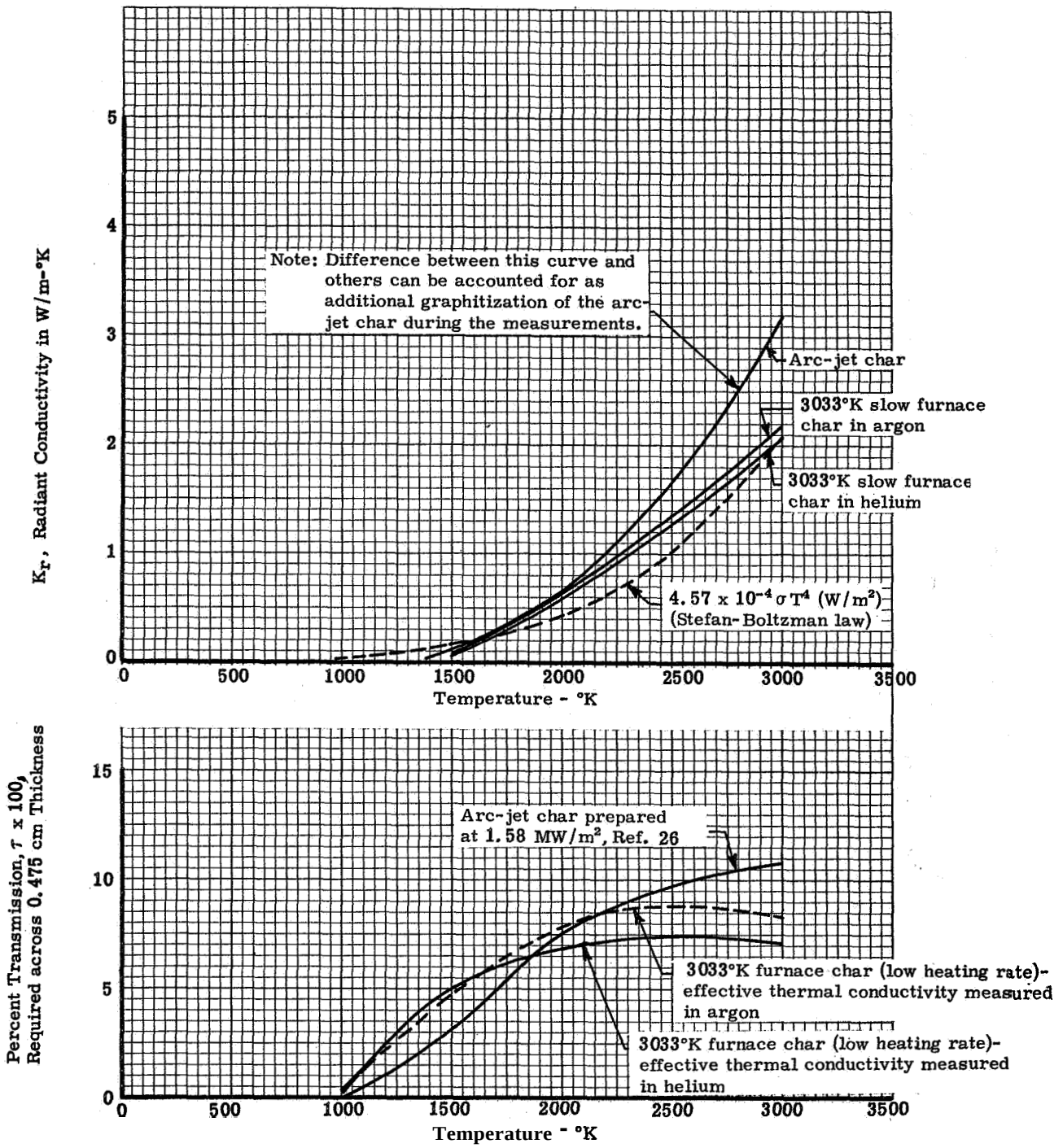

Figure 171. Percent transmission and "radiant" conductivity required through phenolic-nylon char if the thermal conductivity of the matrix (solid) remains constant at the value which it has at 500°K

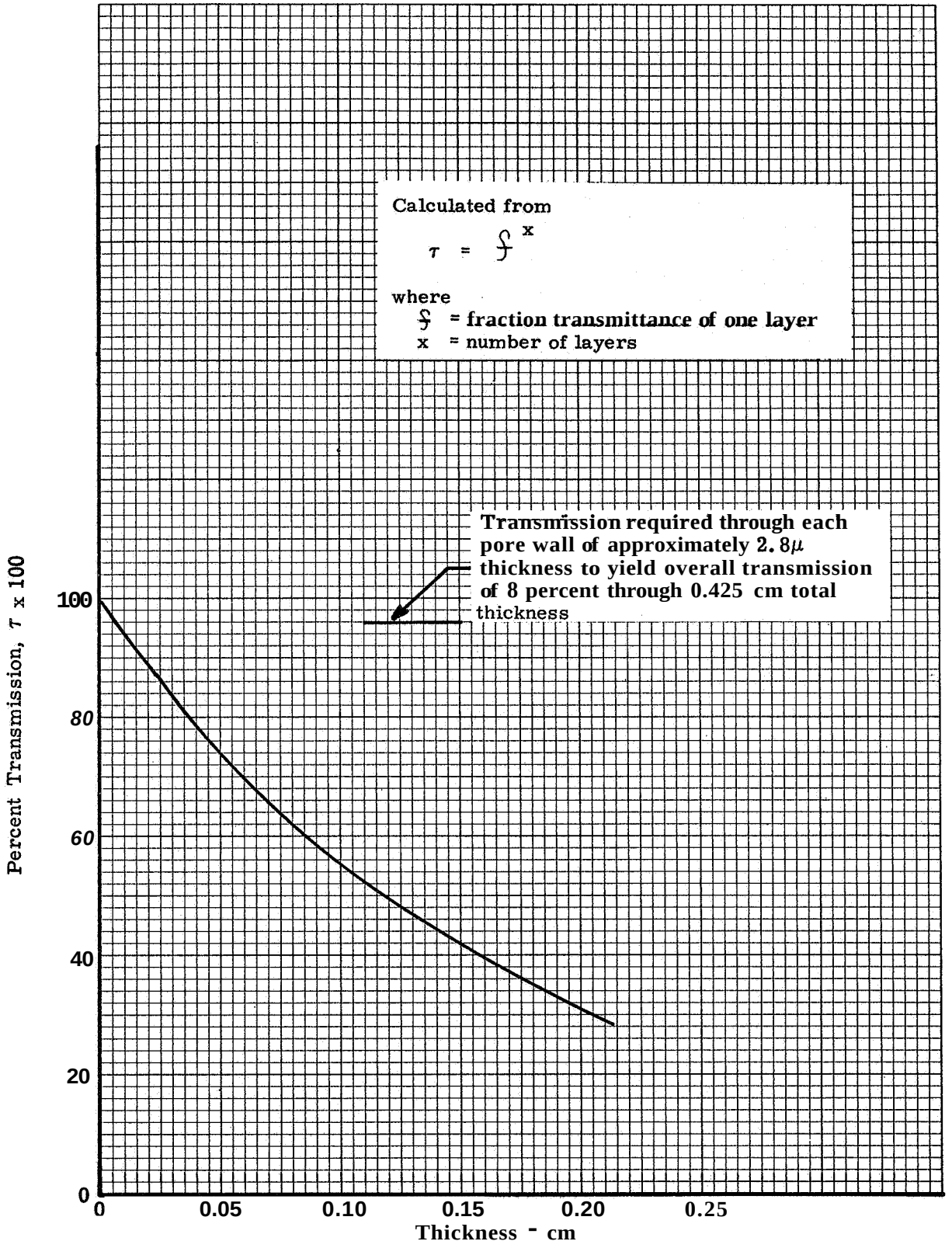

Figure 172. Percent transmission required at 3000°K, as a function of layer thickness, to give 8 percent transmission through a thickness of 0.425 cm

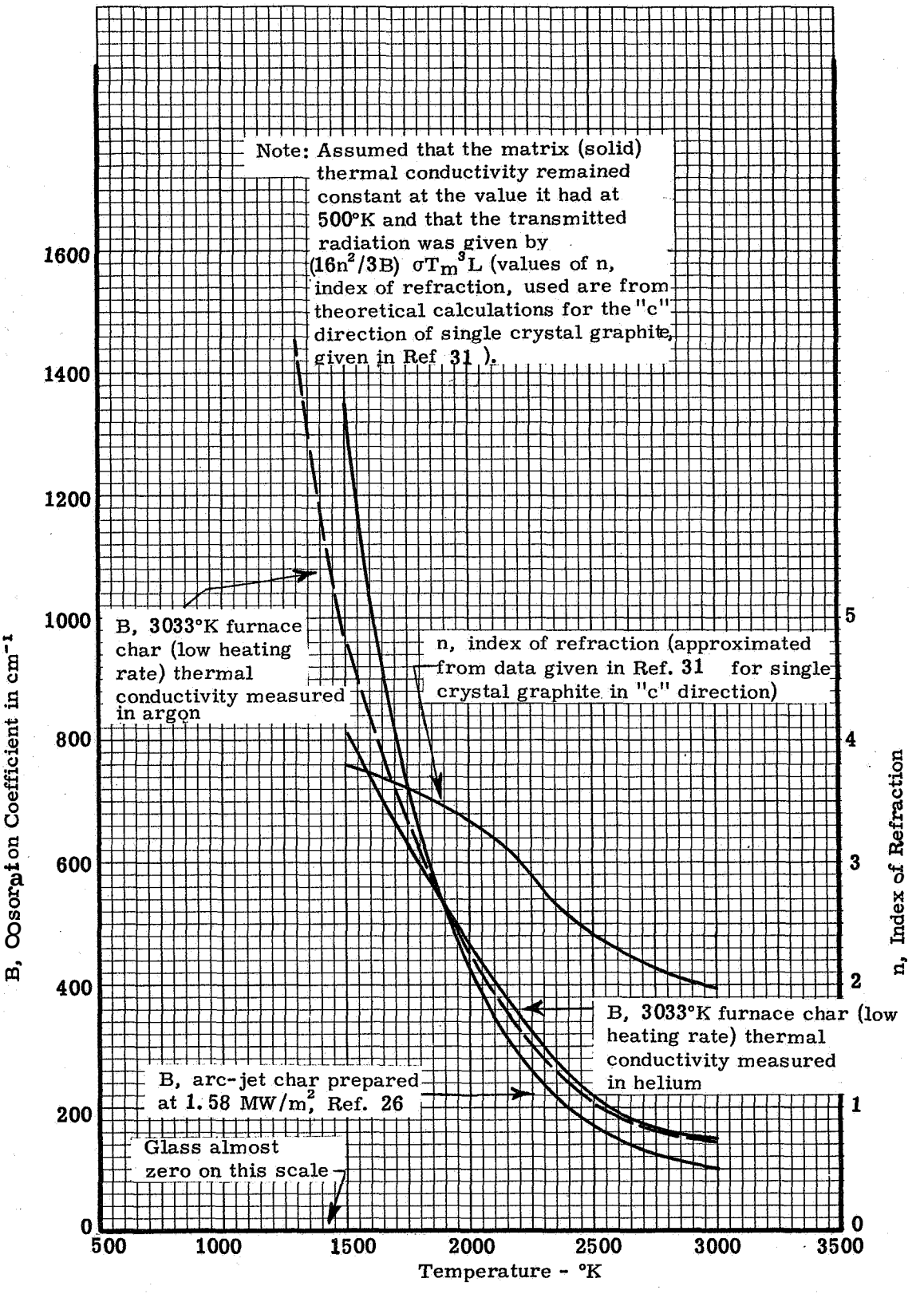

Figure 173. Approximate values required for absorption coefficient of char of 0.425 cm thickness if high temperature conductivity is primarily a radiation phenomena

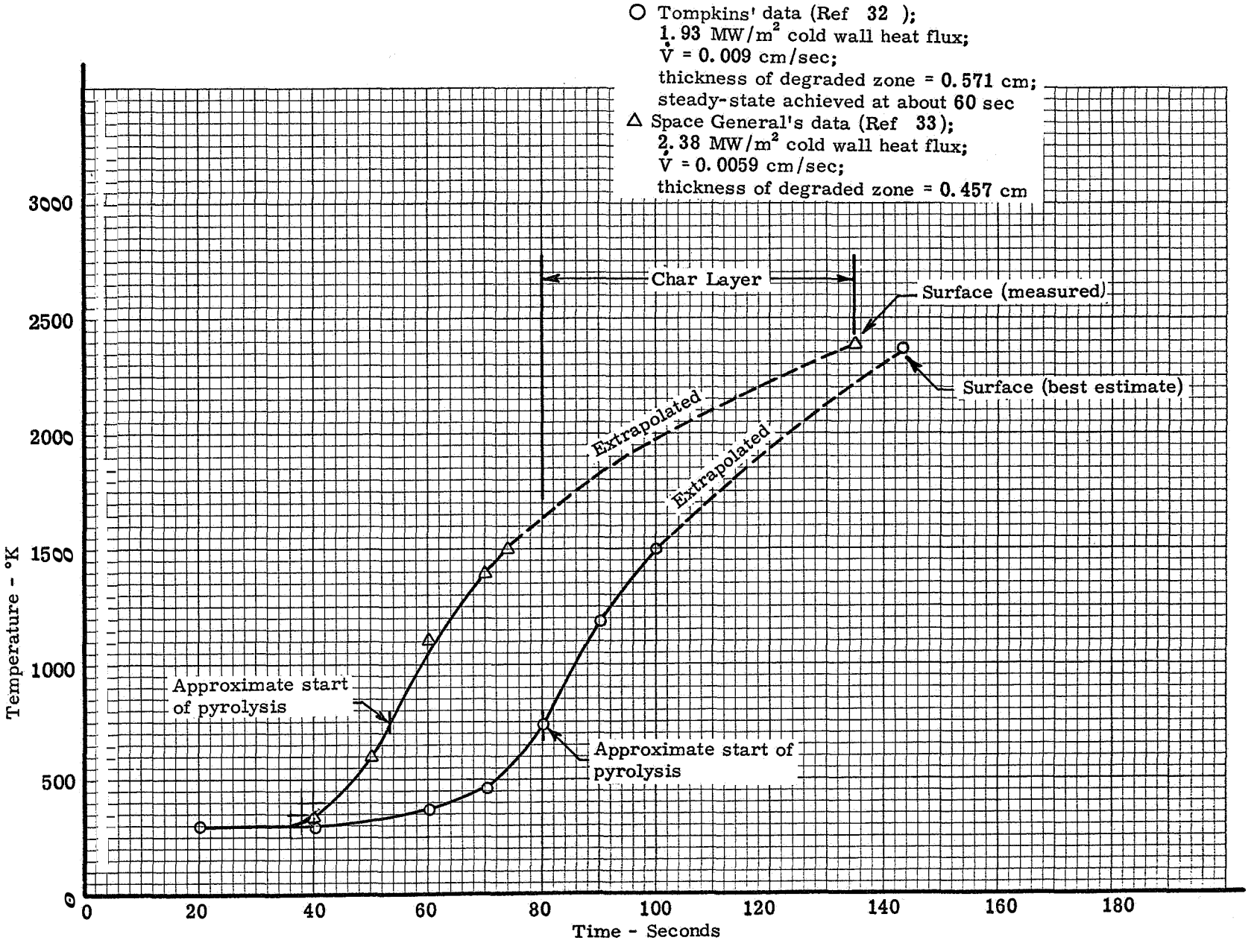

Figure 174. Temperature-time curves from ablation testing of low-density phenolic-nylon by other laboratories

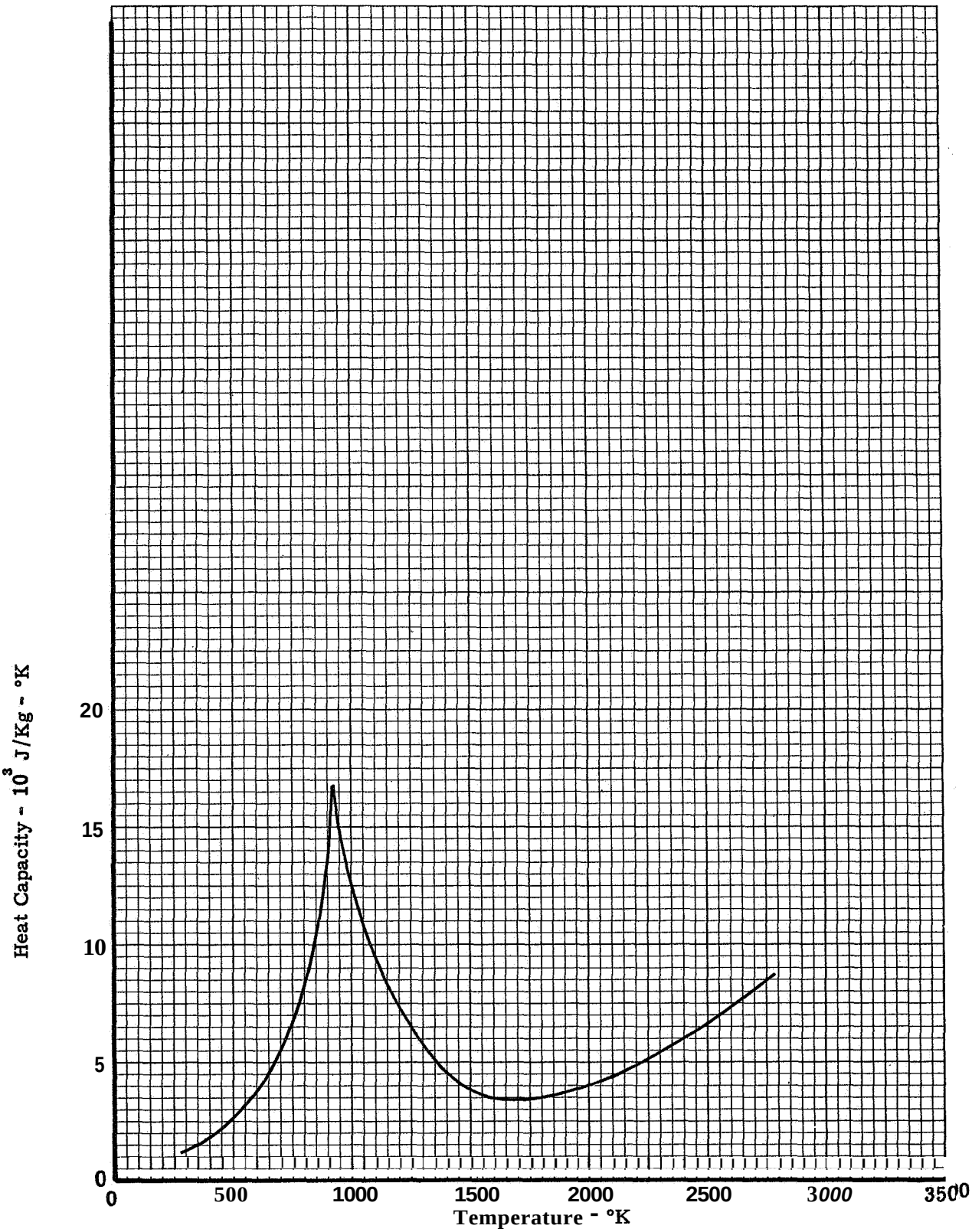

Figure 175. Heat capacity of gaseous products of phenolic-nylon pyrolysis (includes heats of reactions as gas composition changes as a function of temperature level) - taken from Reference [1]

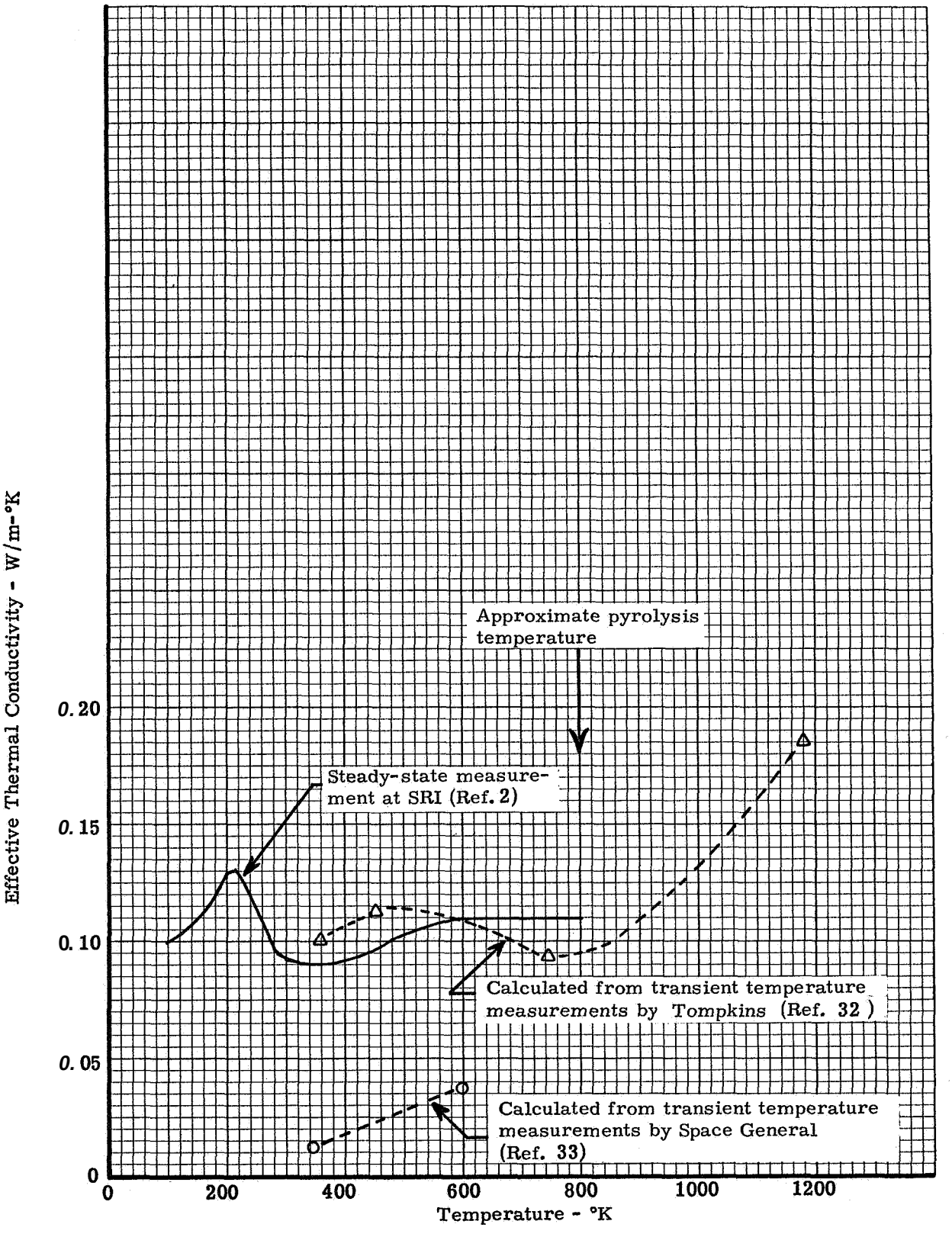

Figure 176 Comparison of thermal conductivity of virgin phenolic-nylon withvalues obtained from data reductions of transient temperature measurements made during simulated ablation tests at other laboratories

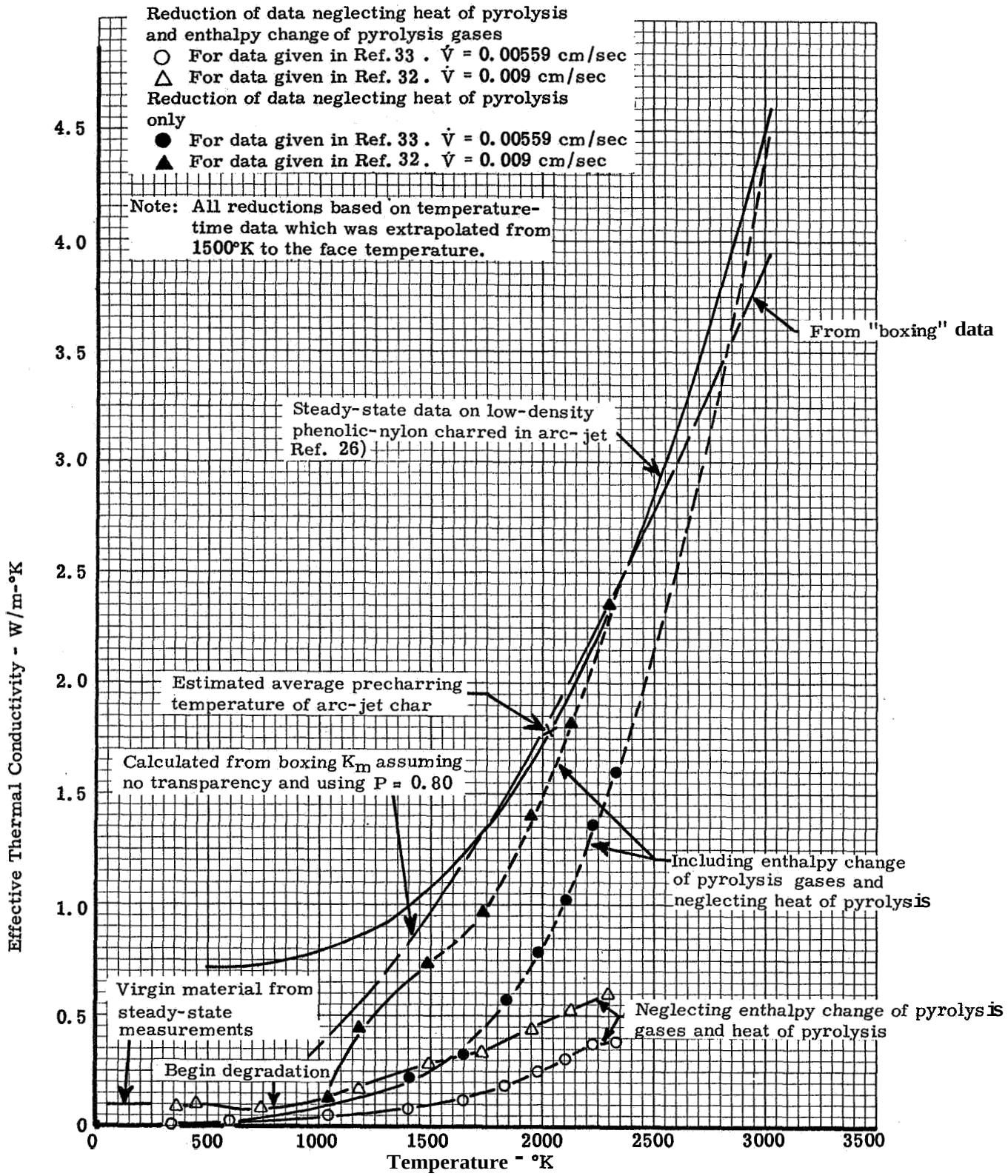

Figure 177. Results of reduction of thermal conductivity values from temperature-time data on low-density phenolic-nylon during simulated ablation tests

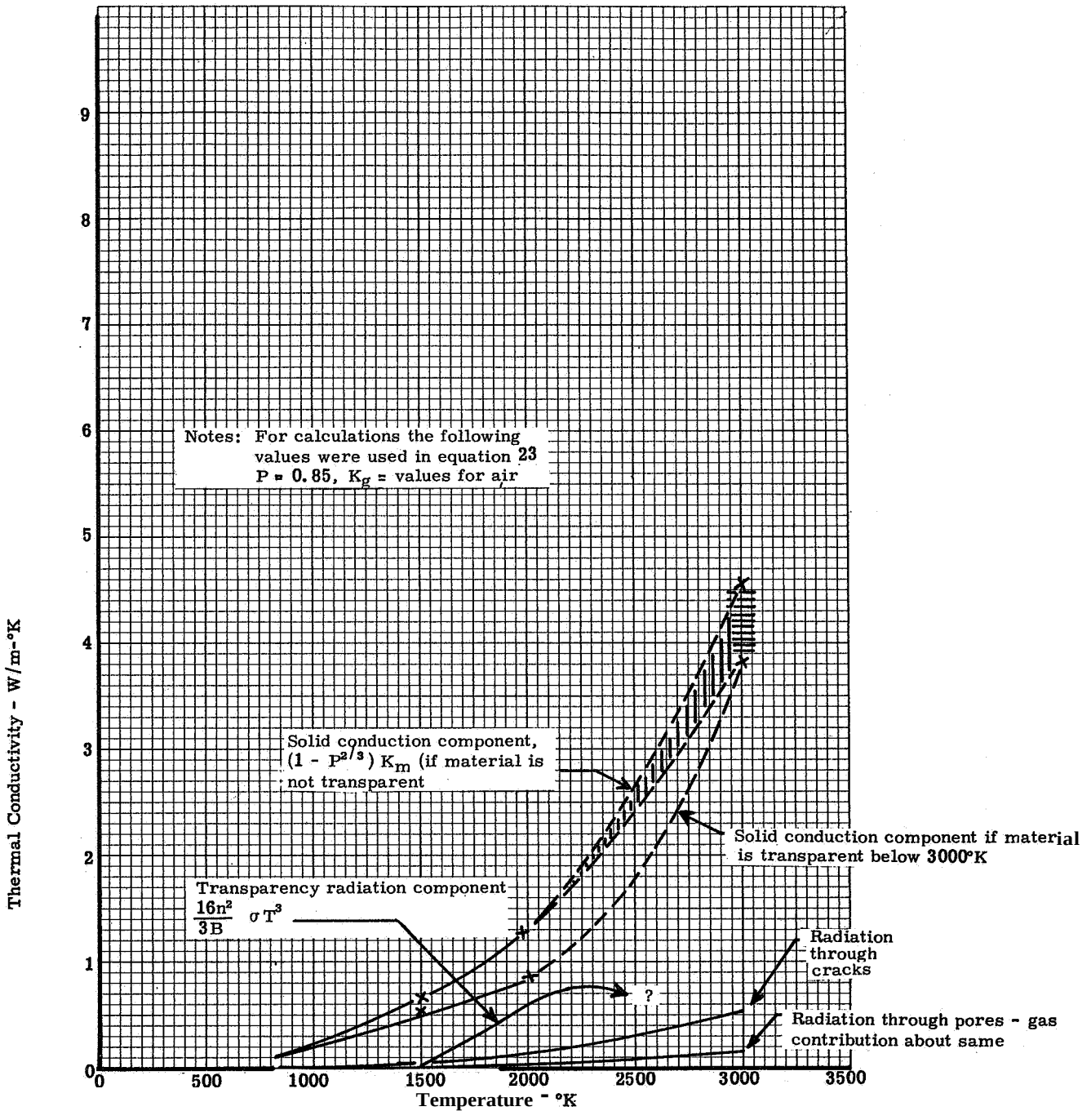

Figure 178. Estimates of various contributions to overall thermal conductivity of flight char 0.152 cm thick

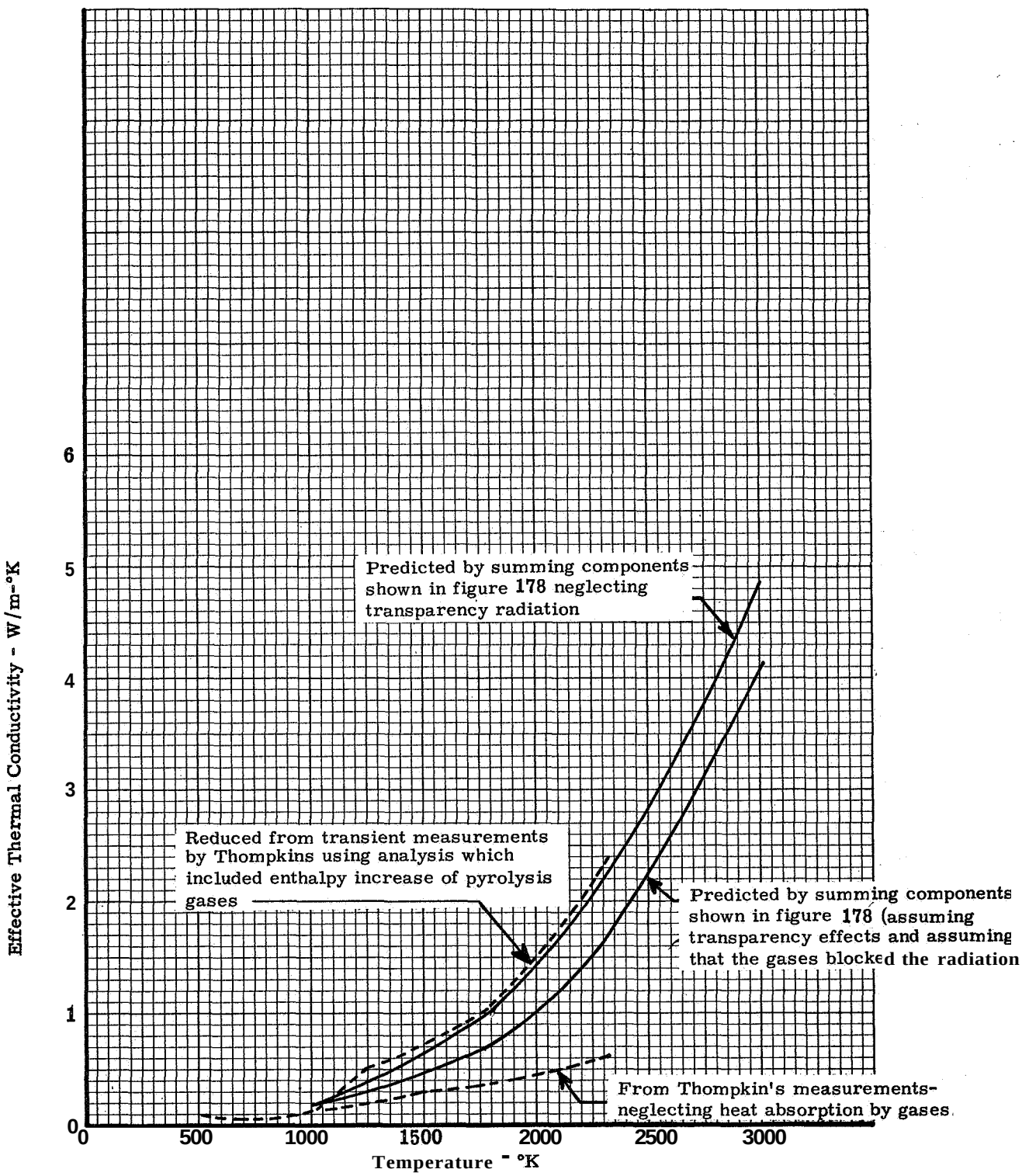

Figure 179. Estimates of effective thermal conductivity of low-density phenolic-nylon char during active ablation

TABLE 1

COMPRESSIVE SPECIMEN CONFIGURATION STUDY AT 294°K

Temperature °K	Direction of interest	Cross section configuration	Cross section volume cm^3	Cross section $1/\rho$ [4]	Specimen	Bulk density gm/cm^3	Stress rate in 10^3 $N/m^2/sec$	Initial elastic modulus in 10^9 N/m^2	0.2% yield strength in 10^6 N/m^2	Ultimate strength in 10^6 N/m^2
294	ab	Circular (1.270 cm dia)	3.21	8.0	CC1-4W-1	0.549	690	0.96	21.1	27.9
					2	0.577	827	1.08	20.1	30.5
					4Y-1	0.585	827	1.09	21.1	30.6
					2	0.584	758	1.15	19.2	30.0
					5W-2	0.569	620	1.12	19.7	30.0
					3	0.582	758	1.05	23.6	31.4
					Average	0.574		1.08	20.8	30.0
294	b	Circular (1.270 cm dia)	3.21	8.0	CD-5X-1[3]	0.570	690	0.94	23.4	28.1
					2[3]	0.557	690	1.05	17.7	26.6
					3[3]	0.597	690	1.08	21.9	30.8
					4[1,3]	0.603	690	1.03	25.9	30.8
					5[1,3]	0.601	690	1.12	23.8	30.4
					6[3]	0.600	690	1.27	17.6	29.7
					7[1,3]	0.598	690	1.02	20.4	29.9
					Average	0.590		1.07	21.5	29.4
294	4	Square (1.125 cm)	3.21	7.8	CS1-4W-1[2]	0.530	517-690	---	---	25.3
					2	0.542	Not run			
					CS1-4X-1[2]	0.571	517-690	---	---	26.2
					CS1-4Y-1	0.555	586	1.03	18.7	27.8
					2[2]	0.569	517-690	---	---	29.5
					3	0.573	586	1.13	21.6	31.0
					CS1-5W-1[1]	0.578	690	1.08	23.6	30.5
					2	0.587	Broken during machining			
					3	0.594	758	1.12	22.4	30.7
					CS1-8W-1	0.597	758	1.15	25.8	33.8
					CS1-10W-1	0.608	552	1.10	22.1	31.4
					Average	0.573		1.10	22.4	29.6
294	4	Rectangular 2:1 width-to-thickness (1.588 cm x 0.800 cm)	3.21	11.0	CR1-4W-1	0.514	586	1.03	11.7	23.2
					2	0.548	Not tested			
					3	0.574	Not tested			
					CR1-4X-1	0.562	690	0.98	19.5	25.3
					2	0.569	518	1.01	18.2	25.2
					CR1-4Y-1	0.564	827	1.15	20.5	29.5
					2	0.588	690	1.02	21.0	28.9
					Average	0.556		1.04	18.3	26.6

Notes:
1. Gage section ground finished, all others machine finished.
2. Specimen tested for gage section bending and ultimate strength only.
3. Specimen tested in gas-bearing compressive facility, all others tested in Tinius-Olsen apparatus.
4. Slenderness ratio defined as length divided by radius of gyration.

Specimen identification

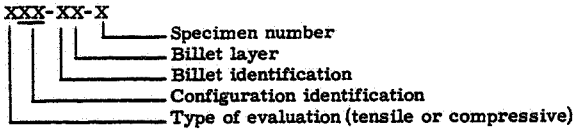

TABLE 2

COMPRESSIVE SLENDERNESS RATIO EVALUATIONS AT 294°K

Temperature (°K)	Direction of interest	Cross section configuration	Gage section volume cm^3	Cross section l/ρ [1]	Specimen	Bulk density gm/cm^3	Stress rate in 10^3 $N/m^2/sec$	Initial elastic modulus in 10^9 N/m^2	0.2% yield strength in 10^8 N/m^2	Ultimate strength in 10^8 N/m^2
RT	a	Experimental Circular (1.27 cm diameter)	2.409	6.0	CCE2-4X-1	0.585	690	1.01	19.0	28.2
					2	0.588	690	1.25	17.6	28.2
					3	0.589	759	0.89	23.2	28.3
					Average	0.587		1.05	19.9	28.2
			4.032	10.0	CCE3-4X-1	0.557	690	1.10	15.4	26.9
					2	0.580	827	1.07	18.5	27.8
					3	0.592	Not run			
					Average	0.576		1.08	17.0	27.3
RT	b	Experimental Square (1.125 cm)	2.409	5.85	CSE2-4X-1	0.593	Not run			
					2	0.599	793	0.98	21.4	30.3
					3	0.595	793	1.06	21.6	31.0
					Average	0.596		1.02	21.5	30.6
			4.032	9.73	CSE3-4X-1	0.560	Not run			
					2	0.549	620	0.97	19.4	27.4
					3	0.579	690	1.01	18.6	26.9
					Average	0.563		0.99	19.0	27.2
RT	a	Experimental Rectangular 2:1 width-to-thickness ratio (1.588 cm x 0.800 cm)	2.409	8.32	CRE2-4X-1	0.565	Not run			
					2	0.561	690	0.92	20.3	27.4
					3	0.595	655	1.07	18.5	29.4
					Average	0.574		0.99	19.4	28.4
			4.032	13.7	CRE3-4X-1	0.568	Not run			
					2	0.582	759	0.99	21.0	27.8
					3	0.540	827	0.99	19.6	26.6
					Average	0.563		0.99	20.3	27.2

Note: 1. Sle ρ s ratio defined as length divided by radius of gyration.

TABLE 3

TENSILE SPECIMEN CONFIGURATION STUDY AT 294°K

Temperature °K	Direction of interest	Cross section configuration	Cross section volume cm³	Specimen	Bulk density gm/cm³	Stress rate in 10^3 N/m²/sec	Initial elastic modulus in 10^9 N/m²	0.05% yield strength in 10^8 N/m²	Ultimate strength in 10^8 N/m²	Fracture location
294	ah	Circular (1.270 cm dia)	0.44	TC1-4W-1	0.579	690	1.21	>7.2	7.2	Gage section and radius
				-2[1]	0.583	690	1.05	8.3	11.0	Gage section
				-3	0.578	690	1.14	8.8	9.3	Grip
				TC1-4Y-1	0.822	690	1.26	9.1	9.1	Tangent
				-2[1]	0.623	090	1.18	9.3	12.5	Gage section
				-3	---	Broken during machining				
				TC1-5W-1	0.502	090	1.22	8.3	8.3	Gage section
				TC1-5X-1	0.570	Broken during machining				
				TC1-8Y-3[1]	0.001	518	0.93	8.7	10.5	Tangent
				-4[1]	0.598	587	1.03	6.3	10.4	Gage section
				Average	0.593	---	1.13	8.0	9.8	
294	ah	Square (1.125 cm) with 1.125 cm thick shank	8.44	TS1-4W-1	0.589	090	1.18	8.5	9.5	Tangent
				-2	0.575	090	1.18	8.9	8.9	Gage section
				TS1-4Y-1	0.611	Heat rate specimen				
				-2	0.589	Not run				
				TS1-5W-1	0.583	890	1.21	7.3	9.0	Radius
				-2	0.608	690	1.25	8.0	10.0	Gage section
				-3	0.597	Not run				
				TS1-5X-1	0.581	890	1.15	8.8	9.4	Gage section
				-2	0.587	Not run				
				-3	0.587	Not run				
				-4'	0.597	090	---		8.4	Gage section
				Average	0.589	---	1.19	7.9	9.0	
294	ab	Square (1.125 cm) with 1.07 cm thick shank	0.44	TS3-8X-3	0.581	690	0.94	5.4	8.8	Gage section
				TS3-8Y-1	0.584	021	0.98	5.1	9.4	Gage section
				TS3-8Y-2	0.585	658	0.90	5.8	8.8	Gage section
				Average	0.583	---	0.93	5.4	8.9	
294	ab	Rectangular 2:1 width-to-thickness ratio (1.588 x 0.800 cm) with 1.27 cm thick shank	8.40	TR1-4W-1[2]	0.558	690	---	---	9.8	Gage section
				-2	0.572	890	1.17	7.4	7.4	Tangent
				TR1-4X-1	0.879	090	1.22	7.2	8.1	Tangent
				-2	0.588	690	1.21	7.4	7.4	Tangent
				-3	0.580	Not run				
				TR1-4Y-1	0.507	690	1.26	8.8	9.5	Tangent
				-2[2]	0.617	890	---	---	11.3	Gage section
				TR1-5W-1[3]	0.591	090	---	---	10.5	Grip and gage section
				-2	0.588	090	1.23	8.8	8.8	Tangent
				TR1-5X-1	0.580	Not run				
				-2	0.597	Broken in handing				
				Average	0.585	---	1.22	7.8	9.1	
294	ab	Rectangular 2:1 width-to-thickness ratio (1.588 x 0.800 cm) with 0.800 cm thick shank	8.40	TR4-4Z-1	0.598	890	1.15	5.3	10.3	Grip
				-2	0.008	050	1.11	7.7	8.2	Tangent
				-3	0.604	690	1.05	8.4	9.5	Gage section
				Average	0.000	---	1.10	7.5	9.7	
294	ah	Rectangular 4:1 width-to-thickness ratio (2.200 x 0.559 cm)	6.42	TR3-8W-1	0.585	090	0.95	4.0	8.3	Gage section
				-2	0.584	090	1.17	5.2	10.0	Tangent
				-3[1]	0.591	690	1.10	7.2	9.0	Tangent
				-4'	0.591	690	1.20	5.0	9.0	Tangent
				-5	0.593	Broken in shop				
				-8	0.590	690	1.24	5.3	10.1	Tangent
				TR3-8X-1[2]	0.584	621	1.06	5.2	10.1	Gage section
				-2'	0.581	621	0.95	0.5	10.2	Tangent
				-3[1]	0.589	621	0.92	0.7	8.9	Tangent
				Average	0.588	---	1.08	5.7	9.5	

1. Specimen gage section ground finished. all others machine finished.
2. Specimen ran without yokes to test for pressure effects incurred by yokes.
3. Evaluation used in volume effect study, see Table 5.

TABLE 4

VOLUME EFFECT STUDY IN COMPRESSION AT 294°K

Temperature °K	Direction of interest	Cross section configuration	Cross section volume cm^3	Cross section l/ρ [1]	Specimen	Bulk density gm/cm^3	Stress rate in 10^3 $N/m^2/sec$	Initial elastic modulus in 10^9 N/m^2	0.2% yield strength in 10^6 N/m^2	Ultimate strength in 10^6 N/m^2	Testing apparatus
294	4	Circular (0.635 cm dia)	0.40	8.0	CD2-5Y-1	0.614	172	0.77	20.4	28.9	Gas-bearing
					2	0.622	690	0.94	17.9	25.8	Gas-bearing
					3	0.629	Broken in Shop				
					4	0.553	Broken in Shop				
					5	0.561	Broken in Shop				
					6	0.537	655	0.90	16.0	23.3	Gas-bearing
					7	0.530	690	0.74	14.2	23.0	Gas-bearing
					8	0.592	690	0.91	15.9	24.2	Gas-bearing
					9	0.583	690	0.86	16.3	24.0	Gas-bearing
					10	0.586	690	0.98	15.2	25.4	Gas-bearing
					Average	0.581		0.87	16.6	24.9	

Notes: 1. Slenderness ratio defined as length divided by radius of gyration.
2. See Note 2 of Table 6 for 3.21 cm^3 evaluations.

TABLE 5

VOLUME EFFECT STUDY IN TENSION AT 294°K

Temperature °K	Direction of interest	Cross section configuration	Cross section volume cm^3	Specimen	Bulk density gm/cm^3	Stress rate in 10^3 $N/m^2/sec$	Initial elastic modulus in 10^9 N/m^2	Poisson's Ratio	0.05% yield strength in 10^8 N/m^2	Ultimate strength in 10^6 N/m^2	Fracture location	Testing apparatus
294	ab	Circular (0.635 cm dia)	0.80	TC2-4Z-1	0.551	655	0.75	----	---[1]	10.5	Gage Section	Tinius Olsen
				2	0.567	586	0.70	----	---[1]	10.9	Gage Section	Tinius Olsen
				3	0.609	620	0.84	----	---[1]	10.7	Gage Section	Tinius Olsen
				Average	0.576		0.76			10.7		
294	ab	Circular (0.635 cm dia) Std. SRI configuration	0.80	TC3-4Z-1	0.611	690	0.81	0.25	---[1]	11.2	Gage Section	Gas-bearing
				2	-----	Broken in Shop						
				3	0.572	690	0.70	0.23	---[1]	10.5	Gage Section	Gas-bearing
				4	0.563	690	0.71	0.25	---[1]	10.5	Gage Section	Gas-bearing
				Average	0.582		1.02	0.25		10.7		

Notes: 1. Insufficient strain to failure to determine 0.05% offset yield strength.
2. All gage sections ground finished.
3. See Note 3 of Table 3 for 6.44 cm^3 evaluations used in this study.

TABLE 6

STRESS-RATE EFFECTS IN COMPRESSION FOR STRESS RATES IN THE RANGE OF 170 x 10^3 TO 8600 x 10^3 N/m^2/sec AT 294°K

Temperature	Direction	Cross section	Cross section volume	Cross section	Specimen	Bulk density gm/cm^3	Stress rate in 10^3 N/m^2/sec	elastic modulus in 10^9 N/m^2	yield strength in 10^6 N/m^2	Ultimate strength in 10^6 N/m^2
294	b	Circular (1.270 cm dia)	3 21	≤ 0	CD-5Y-4	0.562	172	0.71	15.4	24.3
					6W-4	0.536	172	0.77	11.9	23.1
					6W-9	0.621	172	0.78	--- [1]	27.3
					6X-4	0.547	172	0.83	12.7	22.5
					6X-8	0.603	172	0.81	9.6	23.2
					Average	0.574	---	0.78	12.4	24.1
294	b	Circular (1.270 cm dia)	3 21	≤ 0	CD-5Y-2 [2]	0.614	690	0.71	14.2	24.0
					6W-3 [2]	0.590	690	0.75	12.7	24.0
					9W-1 [2]	0.575	690	0.70	12.7	24.0
					9W-2 [2]	0.570	690	----	----	25.1
					12W-2 [2]	0.566	690	0.76	16.1	26.0
					Average	0.583		0.73	13.9	24.6
21	b	Circular (1.270 cm dia)	3 21	8.0	CD-5Y-1	0.575	1860	0.77	14.7	24.6
					6W-1	0.558	1860	0.77	14.0	24.6
					6W-2	0.576	1860	0.85	12.7	23.7 (second run)
					6X-1	0.556	1860	1.03	15.4	28.2
					6X-2	0.578	1860	0.93	17.5	27.4
					Average	0.569		0.87	14.9	25.7
294	4	Circular (1.270 cm dia)	3. 2	8.0	CD-5X-10	-----	4720	0.77	18.8	28.5
					6X- 9	0.592	7230	0.65	14.8	----
					6W-20	0.599	8400	0.68	16.6	23.8
					19	0.569	8450	0.76	17.9	24.0
					5Y-17	0.569	8600	0.82	18.3	26.3
					Average	0.582		0.74	17.3	25.6

Note:

1. Specimen cracked at 0.07%.
2. Evaluation used in volume effect study, see Table 4.
3. Slenderness ratio defined as length divided by radius of gyration.
4. Compressive stress rate tests were conducted in our gas-bearing facility.

TABLE 7

STRESS-RATE EFFECTS IN TENSION FOR STRESS RATES IN THE RANGE OF 170×10^3 TO 7000×10^3 N/m^2/sec AT 294°K

Temperature °K	Direction of interest	Cross section configuration	Cross section volume cm^3	Specimen	Bulk density gm/cm^3	Stress rate in 10^3 N/m^2/sec	Initial elastic modulus in 10^9 N/m^2	0.05% yield strength in 10^6 N/m^2	Ultimate strength in 10^6 N/m^2	Fracture location
294	ab	Circular (1.270 cm dia)	6.44	TC1-6Y-6	0.586	172	1.16	4.7	10.6	Gage Length
				13W-1	0.602	172	1.17	7.6	11.1	Gage Length
				13W-7	0.597	172	1.24	4.8	10.1	Gage Length
				13X-6	0.566	172	1.25	4.0	9.0	Gage Length
				13X-7	0.567	172	0.91	3.8	10.2	Tangent
				Average	0.584		1.15	5.0	10.2	
294	⊥	Circular (1.270 cm dia)	6.4	TC1-10X-1	0.577	620	1.10	4.4	9.1	Gage Length
				2	0.576	620	1.12	4.6	9.5	Gage Length
				4	0.575	690	0.97	3.8	9.0	Gage Length
				13W-2	0.575	690	1.03	8.3	10.4	Gage Length
				13X-8	0.570	620	1.12	4.2	10.1	Gage Length
				Average	0.575		1.07	5.1	9.6	
294	⊥	Circular (1.270 cm dia)	≤ 44	TC1-6Y-7	0.589	1860	1.02	8.2	10.6	Gage Length
				8	0.582	2000	0.90	---	10.2	Gage Length
				10X-6	0.573	1860	0.91	7.1	9.0	Gage Length
				10Z-2	0.580	1860	1.03	4.5	9.1	Gage Length
				10Z-7	0.571	1860	0.92	8.7	9.9	Tangent
				Average	0.579		0.96	7.1	9.8	
294	ab	Circular (1.270 cm dia)	6.44	TC1-12W-8	0.579	3450	1.05	6.5	10.7	Gage Length
294	ab	Circular (1.270 cm dia)	6.44	TC1-6Y-3	0.591	7000	0.89	6.4	11.1	Gage Length
				12Z-3	0.611	7000	1.03	9.3	10.9	Gage Length
				Average	0.601		0.96	7.8	11.0	

TABLE 8

MOISTURE EFFECT STUDY IN COMPRESSION AT 294°K

Temperature °K	Direction of interest	Cross section configuration	Cross section volume cm^3	Cross section l/ρ [1]	Specimen	Bulk density gm/cm^3	Stress rate in 10^3 $N/m^2/sec$	Initial elastic modulus in 10^9 N/m^2	0.2% yield strength in 10^8 N/m^2	Ultimate strength in 10^8 N/m^2	Moisture content %
Specimens dried at 377°K (220°F) for 24 hours in a thermostatically controlled oven before testing											
294	ab	Circular (1.270 cm dia)	3.21	8.0	CD-5Y-8	0.634	760	0.96	----	32.5	2.39
					9	0.625	760	1.01	20.2	29.8	2.37
Specimens tested without drying											
294	ab	Circular (1.270 cm dia)	3.21	8.0	CD-5Y-5	0.627	690	0.79	12.9	25.3	----
					6	0.627	690	0.75	15.4	24.7	----

Note: 1. Slenderness ratio defined as length divided by radius of gyration.

TABLE 9

MOISTURE EFFECT STUDY IN TENSION AT 294°K

Temperature °K	Direction of interest	Cross section configuration	Cross section volume cm^3	Specimen	Bulk density gm/cm^3	Stress rate in 10^3 $N/m^2/sec$	Initial elastic modulus in 10^9 N/m^2	0.05% yield strength in 10^6 N/m^2	Ultimate strength in 10^6 N/m^2	Moisture content %	Fracture location
Specimens dried at 377°K (220°F) for 24 hours in a thermostatically controlled oven before testing											
294	b	Circular (1.270 cm dia)		TC1-10Y-7	0.564	690	0.96	7.2	8.6	2.97	Gage Section
				8	0.552	690	1.09	8.4	9.0	2.96	Gage Section
Specimens [illegible] t 377°K (220°F) for 42 ho [illegible] in a thermostatically controlled oven before testing											
294	ab	Circular (1.270 cm dia)	6.4	TC1-10Y-2	0.566	655	[illegible] 10	7.2	8.3	3.38	Gage Section
				4	0.575	690	0 97	6.9	7.7	3.38	Tangent
Specimens tested without drying											
294	ab	Circular (1.270 cm dia)		TC1-10Y-3	0.573	655	[illegible] 01	5.9	9.6	----	Radius
				6	0.573	655	0 95	7.6	10.0	----	Gage Section

TABLE 10

VARIATIONS IN BULK DENSITY CAUSED BY MOISTURE ABSORBED FROM ATMOSPHERE

Specimen	Bulk density before drying		Bulk density 2 hrs after drying		Bulk density 72 hrs after drying	
	gm/cm^3	% Diff.	gm/cm^3	% Diff.	gm/cm^3	% Diff.
8W-1	0.5914	---	0.5849	-1.10	0.5881	- 0.56
8W-2A	0.5731	---	0.5677	-0.95	0.5702	- 0.51
8W-2B	0.5800	---	0.5747	-0.92	0.5773	- 0.47
8W-2C	0.5818	---	0.5744	-1.2%	0.5774	- 0.76
8W-4A	0.5979	---	0.5917	-1.04	0.5959	- 0.34
8W-4B	0.6047	---	0.5990	-0.95	0.6027	- 0.34
8X-1A	0.5815	---	0.5750	-1.12	0.5777	- 0.71
8X-1B	0.5960	---	0.5897	-1.06	0.5928	- 0.54
8X-2A	0.5667	---	0.5607	-1.06	0.5647	- 0.36
8X-2B	0.5699	---	0.5631	-1.20	0.5680	- 0.34
8X-2C	0.5652	---	0.5589	-1.12	0.5642	- 0.18
8X-3B	0.5958		0.5865	-1.57	0.5947	- 0.19
8X-3C	0.6088	---	0.6031	-0.94	0.6076	- 0.20
Average	0.5856	---	0,5792	-1.10	0.5832	- 0.42

Note: Specimens from NASA Billet 8 were machined to a blank size of 1.270 x 2.286 x 6.350 cm and dryed in a thermostatic-controlled oven for 24 hours at 377°K. Bulk density was measured before drying, 2 hours after drying, and 72 hours after drying. After removal from the oven, specimens were exposed to the environment of the laboratory with no special environmental controls being used.

TABLE 11

COMPRESSIVE EVALUATION IN THE "c" DIRECTION

Temperature °K	Direction of interest	Cross section configuration	Cross section volume cm^3	Cross section $1/\rho$ s	Specimen	Bulk density gm/cm^3	Stress rate in 10^8 $N/m^2/sec$	Initial elastic modulus in 10^9 N/m^2	0.2% yield strength in $10^8 N/m^2$	Ultimate strength in 10^8 N/m^2
294	c	Square (1.125 cm)	2.21	7.8	CS1-4C-1[2]	0.533	517-690	----	----	20.4
					4[1,2]	0.566	517-690	----	----	23.2
					5C-1[2]	0.526	517-690	----	----	20.7
					4[1,2]	0.573	517-690	----	----	22.9
					8C-1	0.549	517	0.93	18.8	22.8
					4[1,2]	0.549	517-690	----	----	22.5
					10C-1	0.569	552	0.86	17.9	22.5
					4[1]	0.546	517	0.84	17.2	23.0
					Average	0.551		0.88	18.0	22.3

Notes: 1. Gage section ground finished, all others machine finished.
2. Specimen tested for gage section bending and ultimate strength.
3. Slenderness ratio defined as length divided by radius of gyration.

TABLE 12

SONIC VELOCITY MEASUREMENTS IN THE "c" DIRECTION ON NASA BILLET 13

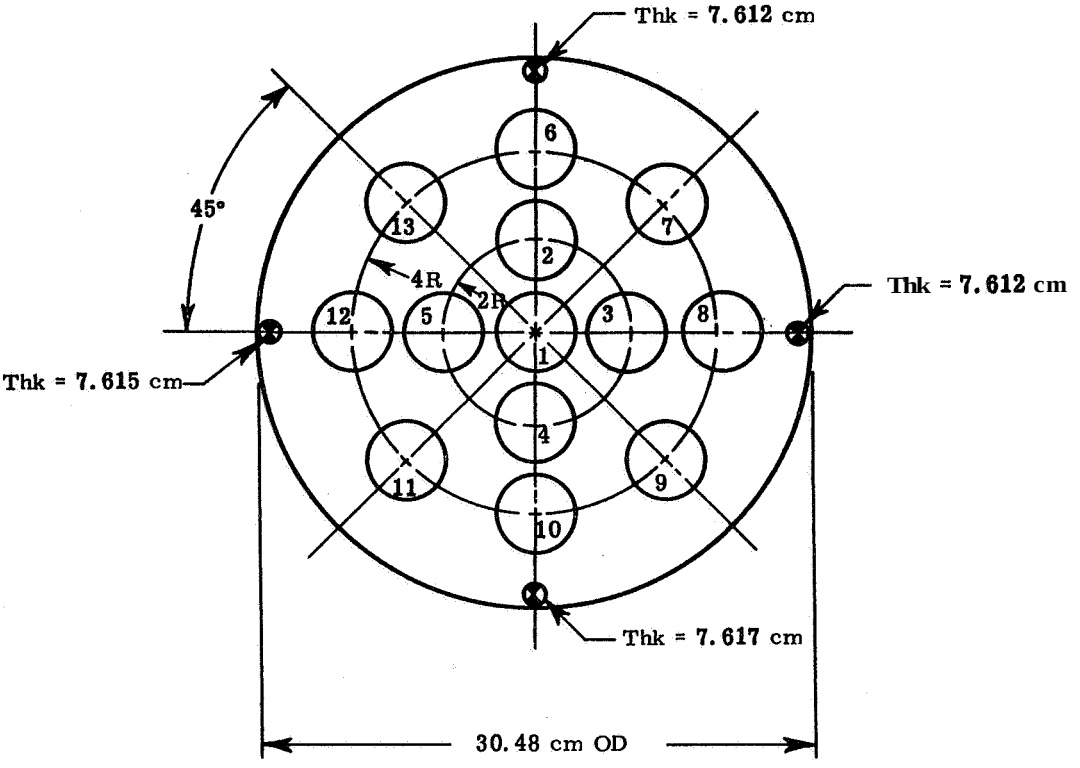

Location	Delay in μ sec	Sonic velocity in 10 cm/sec
1	48.20	0.158
2	47.59	0.160
3	47.75	0.160
4	47.15	0.162
5	47.25	0.161
6	47.45	0.161
7	46.78	0.163
8	47.15	0.162
9	47.73	0.160
10	47.00	0.162
11	46.75	0.163
12	46.35	0.164
13	46.75	0.163

Note: Tests were conducted utilizing the longitudinal motion at a frequency of 1 MHz. Velocities were calculated based on an average billet thickness of 7.614 cm.

TABLE 13

SONIC VELOCITY MEASUREMENTS ON FAILED TENSILE SPECIMENS

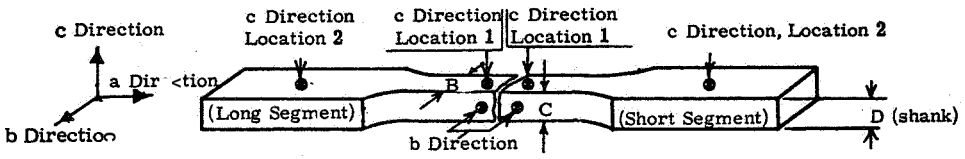

Specimen	Dimensions B cm	Dimensions C cm	Dimensions D cm	Delays b direction in μsec	Delays c direction location 1 in μsec	Delays c direction location 2 in μsec	Velocities b direction 10^6 cm/sec	Velocities c direction location 1 10^6 cm/sec	Velocities c direction location 2 10^6 cm/sec	Density gm/cm³	Experimental tensile elastic modulus in a direction in 10^9 N/m²
TS1-4W-2(L)	1.2743	1.2652	1.2733	6.950	7.143	7.435	0.1833	0.1771	0.1712	0.579	1.05
TS1-4Y-2(L)	1.2710	1.2670	1.2715	6.520	6.934	7.363	0.1949	0.1827	0.1726	0.623	1.18
TS1-4Y-2(S)	1.2672	1.2654	1.2756	6.343	6.862	7.162	0.1997	0.1844	0.1781		
TC1-5W-1(L)	1.2817	1.2776	1.2756	6.823	7.250	7.192	0.1878	0.1762	0.1773	0.582	1.22
TC1-5W-1(S)	1.2771	1.2761	1.2779	6.790	7.217	7.091	0.1880	0.1768	0.1802		
TC1-8Y-4(L)	1.2398	1.2382	1.2743	6.670	7.122	7.341	0.1858	0.1738	0.1735	0.598	1.03
TC1-8Y-4(S)	1.2377	1.2390	1.2761	6.779	7.321	7.222	0.1825	0.1692	0.1766		
TS1-4W-2(L)	1.1290	1.1328	1.1280	5.888	6.419	6.374	0.1917	0.1765	0.1769	0.575	1.18
TS1-4W-2(S)	1.1303	1.1331	1.1316	6.130	6.423	6.592	0.1843	0.1764	0.1716		
TS1-5W-2(L)	1.1364	1.1285	1.1285	5.878	6.325	6.233	0.1933	0.1784	0.1810	0.606	1.25
TS1-5W-2(S)	Curved	1.1290	1.1298	-----	6.377	6.460	----	0.1770	0.1748		
TS1-5X-1(L)	1.1333	1.1339	1.1034	6.023	6.389	6.462	0.1881	0.1774	0.1707	0.583	1.15
TS1-5X-1(S)	1.1377	1.1377	1.1309	6.017	6.449	6.315	0.1890	0.1764	0.1790		
										Average	1.15

Notes: 1. Suffix "L" and "S" on specimen number, indicates long and short segments of failed specimen.
2. Tests were conducted utilizing the longitudinal wave motion at a frequency of 1MHz.

TABLE 14

HEATING RATE EFFECTS IN TENSION FOR HEATING RATES FROM 22°K/min to 111°K/min

Temperature °K	Direction of interest	Cross section configuration	Cross section volume cm^3	Heating rate °K/min	Specimen	Bulk density gm/cm^3	Stress rate in 10^9 $N/m^2/sec$	Initial elastic modulus in 10^9 N/m^2	strength in 10^8 N/m^2	Ultimate strength in 10^8 N/m^2	Fracture location
							Experimental run				
422	ab	Circular (1.270 cm dia)	3.21	--	TC1-10Z-3	0.582	690	0.37	4.8	5.8	Gage section
				22	13Y-1	0.579	690	0.34	5.8	5.8	Tangent
				22	2	0.575		0.35	5.3	5.8	Gage section
					Average	0.579					
				55.5	TC1-9Y-2	0.558	690	0.40	3.9	4.9	Gage section
				55.5	3	0.568	690	0.39	3.7	5.5	Gage section
					Average	0.563		0.39	3.8	5.2	
				111	TC1-13X-3	0.576	690	0.37	5.5	5.5	Gage section
				111	13Y-7	0.567	690	0.41	5.1	5.8	Gage section
					Average	0.571		0.39	5.3	5.6	
450	ab	Circular (1.270 cm dia)	3.21	22	TC1-12X-5	0.606	690	0.44	3.0	6.0	Gage section
				22	13X-1	0.576	690	0.36	4.8	5.8	Gage section
				22	9Y-1 [1]	0.539	690	0.32	4.4	4.8	Gage section
					Average	0.574		0.37	4.1	5.5	
				55.5	TC1-9Y-4	0.567	690	0.35	4.1	5.1	Gage section
				55.5	6	0.566	690	0.34	4.2	5.5	Tangent
					Average	0.566		0.34	4.1	5.3	
				111	TC1-9W-1	0.575	690	0.40	4.0	5.7	Gage section
				111	12X-6	0.602	690	0.40	4.4	6.9	Gage section
				111	9X-4 [1]	0.567	690	0.36	3.9	5.6	Gage section
					Average	0.581		0.39	4.1	6.1	
477	ab	Circular (1.270 cm dia)	3.21	22	TC1-9X-5	0.565	690	0.30	2.9	5.5	Gage section
				22	6	0.565	690	0.26	3.2	4.8	Gage section
				22	2 [1]	0.565	690	0.29	3.2	5.6	Gage section
					Average	0.565		0.28	3.1	5.3	
				55.5	TC1-9X-1	0.551	690	0.28	3.8	6.0	Gage section
				55.5	9Y-7	0.562	690	0.31	2.3	5.3	Gage section
				55.5	9W-2 [1]	0.585	690	0.25	2.8	4.6	Gage section
					Average	0.566		0.28	3.0	5.3	
				111	TC1-9X-7	0.566	690	0.31	3.9	5.3	Gage section
				111	8	0.567	690	0.34	3.1	5.4	Gage section
					Average	0.566		0.32	3.5	5.3	

1. Rerun to further verify test results.

TABLE 15

EFFECTS OF TIME AT TEMPERATURE IN COMPRESSION FOR TEST TEMPERATURES FROM 422°K TO 477°K

Temperature °K	Direction of interest	Cross section configuration	Cross section volume cm^3	Cross section l/ρ [1]	Time at temperature min	Specimen	Bulk density gm/cm^3	Stress rate in 10^3 $N/m^2/sec$	Initial elastic modulus in 10^9 N/m^2	0.2% yield strength in 10^6 N/m^2	Ultimate strength in 10^6 N/m^2
422	ab	Circular (1.270 cm dia)	3.21	8.0	1.75	CD-6X-13	0.586	690	0.32	7.7	13.4
					5.00	5Y-16	0.620	690	0.37	9.0	15.7
					5.00	19	0.630	690	0.33	7.4	15.1
					6.75	6X-14	0.586	690	0.38	8.3	14.7
						Average	0.612		0.36	8.2	15.2
					15.00	CD-6X-10	0.584	690	0.41	8.6	15.5
					15.00	11	0.549	690	0.43	8.4	15.6
					16.75	18	0.587	690	0.39	9.9	15.5
						Average	0.573		0.41	9.0	15.5
					25.00	CD-6W-15	0.558	690	0.41	9.7	16.5
						17	0.611	690	0.41	9.3	16.1
						6X-16	0.594	690	0.37	9.0	15.7
						Average	0.588		0.40	9.3	16.1
450	ab	Circular (1.270 cm dia)	3 [2]	8.0	0	CD-6W-14	0.596	690	0.30	6.9	13.4
					5.00	12	0.612	690	0.39	6.5	14.2
						16	0.612	690	0.30	7.3	13.7
						CD-5Y-15	0.632	690	0.29	8.0	13.7
						Average	0.619		0.33	7.3	13.9
					15.00	CD-6X-12	0.601	690	0.33	6.7	13.2
						15	0.562	690	0.32	7.9	13.6
						33	0.548	690	0.37	9.0	14.2
						Average	0.570		0.34	7.9	13.7
					25.00	CD-6W-13	0.618	690	0.35	7.6	13.8
						5Y-13	0.604	690	0.38	7.4	14.2
						14	0.599	690	0.35	9.7	14.8
						Average	0.607		0.36	8.2	14.3
477	ab	Circular (1.270 cm dia)	3.2	8.0	0	CD-6X-26	0.586	690	0.28	7.2	12.6
					5.00	6W-30	0.586	690	0.27	5.7	11.6
						6X-34	0.551	690	0.33	5.2	11.6
						5Y-12	0.623	690	0.25	6.3	12.7
						Average	0.587		0.28	5.7	12.0
					15.00	CD-6W-10	0.597	690	0.28	7.1	11.7
						6X - 5	0.602	690	0.29	5.5	11.4
						24	0.586	690	0.30	6.0	11.2
						Average	0.595		0.29	6.2	11.4
					25.00	CD-6X-20	0.588	690	0.30	6.8	11.6
						5Y-11	0.628	690	0.30	7.0	13.2
						18	0.593	690	0.31	---	13.0
						Average	0.603		0.30	6.9	12.6

Notes
1. Slenderness ratio defined as length divided by radius of gyration.
2. All test specimens were heated to test temperatures in 2½ minutes. Time t = 0 started when the surface of specimen reached test temperature.

TABLE 16

EFFECTS OF TIME AT TEMPERATURE IN TENSION FOR TEST TEMPERATURES FROM 422°K TO 477°K

Temperature °K	Direction of interest	Cross section configuration	Cross section volume cm^3	Time at temperature min	Specimen	Bulk density gm/cm^3	Stress rate in 10^3 $N/m^2/sec$	Initial elastic modulus in 10^9 N/m^2	0.05% yield strength in 10^8 N/m^2	Ultimate strength in 10^8 N/m^2	Fracture location
422	ab	Circular (1.270 cm dia)	3.21	5.0	TC1-9W-3	0.587	690	0.41	4.0	5.9	Tangent
					7	0.586	690	0.46	4.6	6.1	Tangent
					10W-4	0.610	690	0.46	4.4	5.0	Gage section
					Average	0.594		0.44	4.3	5.7	
				15.0	TC1-9Z-3	0.571	690	0.40	4.1	5.6	Gage section
					10W-3	0.610	690	0.46	4.5	4.8	Tangent
					12W-2	0.597	690	0.39	4.5	5.6	Gage section
					Average	0.593		0.42	4.4	5.3	
				25.0	TC-9Z-5	0.583	690	0.38	---	5.7	Tangent
					10W-1	0.607	690	0.48	3.9	4.6	Radius
					12W-3	0.606	690	0.35	4.7	5.7	Gage section
					Average	0.599		0.40	4.3	5.3	
450	ab	Circular (1.270 cm dia)	3.21	5.0	TC1-9W-8	0.582	690	0.29	3.2	5.7	Gage section
					10X-8	0.554	690	0.32	---	4.9	Gage section
					12Y-3	0.595	690	0.28	---	5.5	Tangent
					Average	0.577		0.30	3.2	5.4	
				15.0	TC1-12X-7	0.596	690	0.42	3.2	7.0	Gage section
					13Y-3	0.574	690	0.31	---	6.4	Gage section
					8	0.565	690	0.35	3.4	5.5	Gage section
					Average	0.578		0.36	3.3	6.3	
				25.0	TC1-9W-4	0.590	690	0.34	---	6.5	Tangent
					12W-1	0.580	690	0.41	2.9	6.0	Gage section
					12Y-4	0.600	690	0.39	4.3	7.0	Gage section
					Average	0.590		0.38	3.6	6.5	
477	ab	Circular (1.270 cm dia)	3.21	5.0	TC1-9W-6	0.585	690	0.26	3.1	4.1	Gage section
					10W-2	0.609	690	0.24	---	2.6	Tangent
					12W-4	0.607	690	0.23	2.7	2.7	Gage section
					12Y-1	0.583	690	0.26	---	4.9	Radius
					5	0.600	690	0.32	3.2	5.2	Gage section
					Average	0.597		0.26	3.0	3.9	
				15.0	TC1-9Z-4	0.581	690	0.34	3.2	4.2	Tangent
					12X-1	0.577	690	0.32	3.2	7.2	Gage section
					12Y-2	0.589	690	0.32	4.3	6.2	Gage section
					8	0.597	690	0.39	---	5.5	Gage section
					Average	0.586		0.34	3.6	5.8	
				25.0	TC1-9W-5	0.588	690	0.37	4.0	5.8	Gage section
					12X-4	0.606	690	0.32	2.6	6.3	Tangent
					8	0.581	690	0.28	2.9	5.4	Gage section
					Average	0.592		0.32	3.2	5.8	

Note: All test specimens were heated to test temperature in $2\frac{1}{4}$ minutes. Time t = 0 started when the surface of the specimen reached test temperature.

TABLE 17

THE STATISTICAL CORRELATION OF THE MECHANICAL PROPERTY DATA

Property	Temperature °K	No. of evaluations	Average value[1]	Standard deviation[1]	Coefficient of variation %	Maximum percentage of error at 95% confidence level %
Ultimate strength in compression	294	15	24.2	1.3	5.25	2.4
	144	20	36.2	2.7	7.39	2.9
Elastic modulus in compression	294	14	0.75	0.05	6.12	3.0
	144	20	1.85	0.27	14.59	5.6
Ultimate strength in tension	294	15	9.90	1.2	12.07	5.5
	144	22	9.40	0.9	9.38	3.4
Elastic modulus in tension	294	15	1.12	0.13	11.47	5.3
	144	22	2.45	0.42	17.15	6.3

Note:

1. The values for ultimate strength are in 10^6 N/m^2 and elastic moduli are in 10^9 N/m^2.

TABLE 18

PROPERTIES OF LOW-DENSITY PHENOLIC-NYLON IN COMPRESSION AT 294°K and 144°K

Temperature °K	Direction of interest	Cross section configuration	Cross section volume cm^3	Cross section l/ρ	Specimen	Bulk density gm/cm^3	Stress rate 10^3 $N/m^2/sec$	Initial elastic modulus in 10^9 N/m^2	0.2% yield strength in 10^6 N/m^2	Ultimate strength in 10^6 N/m^2
294	ab	Circular (1.270 cm dia)	3.21	8.0	CD-5Y-3	0.603	690	0.74	14.3	23.7
					7	0.597	690	0.82	14.1	25.4
					6W-6	0.606	690	0.82	12.7	24.8
					7	0.570	690	0.70	15.6	24.1
					8	0.607	690	0.82	12.8	25.8
					11	0.541	655	0.70	13.6	21.8
					6X-6	0.595	690	0.70	11.3	22.1
					7	0.572	690	0.72	14.2	22.6
					5Y-2[1]	0.614	690	0.71	14.2	24.0
					6W-3[1]	0.590	690	0.75	12.7	24.0
					9W-1[1]	0.575	690	0.70	12.7	24.0
					9W-2[1]	0.570	690	----	----	25.1
					12W-2[1]	0.566	690	0.76	16.1	26.0
					5Y-5[2]	0.627	690	0.79	12.9	25.3
					6[2]	0.627	690	0.75	15.4	24.7
					Average	0.591		0.75	13.8	24.2
	ab	Circular (1.270 cm dia)	3.2	8.0	CD-6W-32	0.591	1030	1.63	----	40.8
					34	0.544	690	1.76	----	36.8
					Average	0.573		1.70		38.8
	ab	Circular (1.270 cm dia)	3.2	8.0	CD-5Y-20[3]	0.606	690	2.06	----	41.4
					21[3]	0.606	690	1.81	----	39.1
					22[3]	0.578	690	2.16	----	39.6
					6W-21[3]	0.608	690	1.52	----	37.9
					23[3]	0.578	690	1.45	----	36.2
					24[3]	0.594	690	1.66	----	38.3
					26[3]	0.602	690	1.66	----	39.3
					27[3]	0.562	690	1.38	----	33.4
					31[3]	0.564	690	1.90	----	37.6
					6X-19[3]	0.565	690	2.14	----	34.9
					21[3]	0.578	690	2.06	----	31.3
					22[3]	0.588	690	2.14	----	34.5
					23[3]	0.567	690	2.02	----	36.2
					25[3]	0.578	690	1.89	----	32.6
					27[3]	0.561	690	1.46	----	36.2
					28[3]	0.581	690	2.11	----	33.1
					29[3]	0.574	690	1.59	----	33.8
					30[3]	0.576	690	1.78	----	36.8
					32[3]	0.574	690	1.93	----	33.8
					12W-1[3]	0.566	690	2.23	----	36.6
					Average	0.580		1.85		36.1

Notes:

1. Run previously reported for Phase I test conditions to determine stress-rate effects.
2. Run previously reported for comparing properties of undried specimen with dried specimen —specimens noted were undried.
3. Specimens noted dried at 377°K (220°F) for 24 hours before test —all others tested without any preconditioning of moisture content.
4. Slenderness ratio defined as length divided by radius of gyration.

TABLE 19

PROPERTIES OF LOW-DENSITY PHENOLIC-NYLON IN TENSION AT 294°K AND 144°K

Temper °K	Direction	Cross section configuration	Cross section volume cm^3	Specimen	Bulk density gm/cm^3	Stress rate in 10^3 $N/m^2/sec$	Initial elastic modulus in 10^9 N/m^2	0.05% yield strength in 10^6 N/m^2	Ultimate strength in 10^6 N/m^2	Specimen color	Fracture location
294		Circular (1.270 cm dia)	6.44	TC1-12Z-1 [1]	0.599	690	1.22	8.5	11.0	Light	Gage length
				5 [1]	0.615	690	1.21	8.7	11.8	Light	Gage length
				7 [1]	0.610	690	1.52	4.8	10.9	Light	Gage length
				13W-6 [1]	0.596	655	1.15	5.4	10.9	Light	Gage length
				8 [1]	0.593	690	1.14	7.0	10.9	Light	Gage length
				Average	0.603		1.25	6.9	11.1		
94		Circular (1.270 cm dia)	6.44	TC1-9Y-5 [1]	0.567	620	1.12	4.8	9.2	Dark	Gage length
				9Z-2 [1]	0.558	585	0.98	4.3	6.9	Dark	Gage length
				10Y-5 [1]	0.576	655	1.06	3.9	9.7	Dark	Gage length
				13X-5 [1]	0.566	620	1.04	6.9	9.5	Dark	Gage length
				13Y-4 [1]	0.571	620	1.11	4.9	9.2	Dark	Gage length
				Average	0.568		1.06	5.0	8.9		
94		Circular (1.270 cm dia)	6.44	TC1-10X-1 [2]	0.577	620	1.10	4.4	9.1	Specimens selected randomly	Gage length
				2 [2]	0.576	620	1.12	4.6	9.5		Gage length
				4 [2]	0.575	690	0.97	3.8	9.0		Gage length
				13W-2 [2]	0.575	690	1.03	8.3	10.4		Gage length
				13X-8 [2]	0.570	620	1.12	4.2	10.1		Gage length
				Average	0.575		1.07	5.1	9.6		
		Circular (1.270 cm dia)	6.44	TC1-10X-7	0.567	690	----	---	9.5		Gage length
				10Z-8	0.556	690	2.48	---	8.9		Gage length
				Average	0.561		2.48		9.2		
		Circular (1.270 cm dia)	6.44	TC1-6Y-1 [3]	0.594	690	2.73	---	10.0	Specimens selected randomly	Gage length
				2 [3]	0.595	690	2.03	---	9.3		Gage length
				4 [3]	0.588	690	2.44	---	9.3		Gage length
				5 [3]	0.589	690	1.76	---	9.0		Gage length
				9Z-6 [3]	0.578	690	2.50	---	7.8		Gage length
				7 [3]	0.570	690	2.15	---	8.3		Gage length
				8 [3]	0.571	690	2.34	---	8.1		Gage length
				10W-7 [3]	0.597	690	2.85	---	10.3		Gage length
				8 [3]	0.577	690	2.28	---	9.2		Gage length
				10Z-1 [3]	0.570	690	1.87	---	9.0		Gage length
				4 [3]	0.584	690	2.28	---	8.7		Gage length
				6 [3]	0.578	690	2.52	---	9.1		Gage length
				12W-5 [3]	0.605	690	2.15	---	10.2		Gage length
				6 [3]	0.604	690	2.58	---	10.4		Gage length
				7 [3]	0.598	690	3.28	---	10.3		Gage length
				12Y-7 [3]	0.602	690	2.34	---	9.9		Gage length
				12Z-2 [3]	0.607	690	2.58	---	10.2		Gage length
				8 [3]	0.605	690	2.58	---	8.4		Gage length
				13W-3 [3]	0.602	690	3.63	---	10.6		Gage length
				4 [3]	0.597	690	2.23	---	10.7		Gage length
				5 [3]	0.596	690	2.28	---	10.2		Gage length
				13Y-6 [3]	0.569	690	2.52	---	8.6		Gage length
				Average	0.590		2.45		9.4		

1. Specimen carefully selected from light and dark areas of billet.
2. Run previously reported for Phase I test conditions to determine stress-rate effects.
3. Specimens noted dried at 377°K (220°F) for 24 hours before test—all others tested without any preconditioning.

TABLE 20

RESULTS OF SONIC AND MECHANICAL TESTS ON LIGHT AND DARK COLORED TEST SPECIMENS

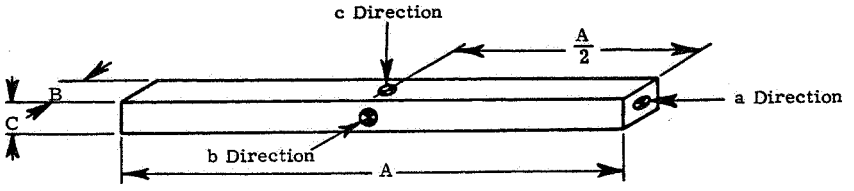

Specimen	Dimensions A cm	B cm	C cm	Delays a direction μ sec	b direction μ sec	c direction μ sec	Velocities a direction 10^6 cm/sec	b direction 10^6 cm/sec	c direction 10^6 cm/sec	Density (gm/cm³)	elastic modulus in a irection (in 10^9 N/m²)	Specimen color
TC1-9X-3	22.233	2.2860	1.2730	137.250	13.420	7.910	0.1619	0.1703	0.1609	0.564	Not Tested	Dark
TC1-9Y-5	22.230	2.2878	1.2715	138.950	13.356	7.784	0.1599	0.1712	0.1633	0.567	1.12	Dark
TC1-9Z-2	22.230	2.2837	1.2703	139.900	13.204	7.732	0.1589	0.1730	0.1643	0.558	0.98	Dark
TC1-10Y-5	22.225	2.2873	1.2703	138.600	13.204	7.822	0.1604	0.1732	0.1624	0.576	1.06	Dark
TC1-10Z-5	22.233	2.2888	1.2690	136.650	12.890	7.646	0.1627	0.1776	0.1660	0.583	Not Tested	Dark
TC1-10Z-6	22.235	2.2860	1.2697	135.200	12.838	7.594	0.1645	0.1781	0.1672	0.578	Not Tested	Dark
TC1-12Z-1	22.233	2.2868	1.2705	129.350	12.488	6.988	0.1719	0.1831	0.1818	0.599	1.22	Light
TC1-12Z-5	22.238	2.2875	1.2720	128.100	12.446	7.030	0.1736	0.1838	0.1809	0.615	1.21	Light
TC1-12Z-7	22.238	2.2870	1.2733	126.450	12.256	7.162	0.1759	0.1866	0.1778	0.610	1.52	Light
TC1-13W-5	22.240	2.2878	1.2708	129.700	12.524	7.158	0.1715	0.1827	0.1775	0.596	Not Tested	Light
TC1-13W-6	22.238	2.2880	1.2692	128.150	12.520	7.018	0.1735	0.1827	0.1808	0.596	1.15	Light
TC1-13W-8	22.233	2.2852	1.2710	128.500	12.484	7.124	0.1730	0.1830	0.1784	0.593	1.14	Light
TC1-13X-5	22.233	2.2873	1.2700	137.700	13.484	7.748	0.1615	0.1696	0.1639	0.566	1.04	Dark
TC1-13Y-4	22.233	2.2863	1.2692	137.800	13.280	7.660	0.1613	0.1722	0.1657	0.571	1.11	Dark
TC1-13Y-6	22.233	2.2875	1.3332	137.750	13.278	7.718	0.1614	0.1723	0.1727	0.569	Not Tested	Dark

Notes: 1. For the purpose of calculations based on Sonic velocity, Poisson's ratio was measured for phenolic-nylon as shown:

Specimen TC3-4Z-1: $\mu = 0.25$
Specimen TC3-4Z-3: $\mu = 0.23$
Specimen TC3-4Z-4: $\mu = 0.25$

2. Tests were conducted utilizing the longitudinal wave motion at a frequency of 0.2 MHz in the a direction; 1MHz in the b and c directions.
3. Experimental elastic modulus was determined at a stress rate of 690 x 10^3 N/m²/sec (100 psi/sec).

TABLE 21

THICKNESSES OF THE VARIOUS SAMPLES REMOVED
FROM THE ARC-JET CHARS FOR THE CHARACTERIZATION STUDIES

Material	Sample		Thickness mm	Average distance from hot surface mm
2.27 MW/m² char	200-1		1.80	0.9
2.27 MW/m² char	200-2		1.28	2.4
2.27 MW/m² char	200-3		1.28	3.7
2.27 MW/m² char	200-4		1.28	5.0
2.27 MW/m² char	200-5		1.28	6.3
2.27 MW/m² char	200-6		2.00	7.9
		Total	8.92	
1.13 MW/m² char	100-1		0.94	0.5
1.13 MW/m² char	100-2		2.68	1.8
1.13 MW/m² char	100-3		2.68	4.5
1.13 MW/m² char	100-4		2.68	7.2
		Total	8.98	

TABLE 22

CHEMICAL ANALYSIS OF PHENOLIC-NYLON CHAR

Sample No.	Average distance from hot surface (mm)	Carbon (%)	Hydrogen (%)	Nitrogen (%)	Unidentified balance (%)	Remarks
100-1	0.5	78.81	0.3	0.4	20.49	113 x 10^4 W/m^2 arc-jet char - suspect measurement
100-1	0.5	98.60	0.4	1.16	None	113 x 10^4 W/m^2 arc-jet char - (rerun on extra material using oxidizing aid) found traces of Mg, Si, and Ca in about equal concentrations
100-2	1.8	90.14	0.4	0.5	8.96	113 x 10^4 W/m^2 arc-jet char
100-3	4.5	90.24	0.4	0.9	8.46	113 x 10^4 W/m^2 arc-jet char
100-4	7.2	91.22	0.8	1.1	6.88	113 x 10^4 W/m^2 arc-jet char
200-1	0.9	76.22	0.3	0.3	23.18	227 x 10^4 W/m^2 arc-jet char - suspect measurement
200-1	0.9	98.40	0.3	NF	1.30	227 x 10^4 W/m^2 arc-jet char - (rerun on extra material using oxidizing aid) - found traces of Mg, Si and Ca. Mg and Si in about equal concentrations, Ca lowest concentration.
200-2	2.4	98.85	0.4	0.2	5.55	227 x 10^4 W/m^2 arc-jet char
200-3	3.7	93.35	0.4	0.3	5.95	227 x 10^4 W/m^2 arc-jet char
200-4	5.0	93.66	0.5	0.2	5.64	227 x 10^4 W/m^2 arc-jet char
200-5	6.3	98.36	1.03	0.4	0.21	227 x 10^4 W/m^2 arc-jet char
200-6	7.9	94.55	2.66	0.5	2.29	227 x 10^4 W/m^2 arc-jet char
812°K Furnace Char	---	81.20	2.89	1.87	14.04	Held at temperature 1 hour during charring.
1366°K Furnace Char	---	84.40	1.37	1.46	12.77	" "
3033°K Furnace Char	---	83 ≤5	0.30	<0.10	16.05	" "
3033°K Furnace Char	---	99.≤9	0.5	<0.20	0.00	" "

TABLE 23

X-RAY DATA FOR PHENOLIC-NYLON CHAR

Specimen	Average distance from hot surface (mm)	"d" spacing (002)	Relative intensity	"d" spacing (100)	Relative intensity	"d" spacing (004)	Relative intensity	Remarks
200-1	0.9	3.44	98	2.11	14	1.72	3	NASA arc-jet char 227×10^4 W/m² Heat flux density
200-2	2.4	3.45	89	2.11	16	1.72	3	" "
200-3	3.7	3.45	100	2.11	20	1.72	3	" "
200-4	5.0	3.44	63	2.10	12	too faint to read		" "
200-5	6.3	3.45	41	2.10	8	absent		" "
200-6	7.9	3.75	37	2.09	5	absent		" "
100-1	0.5	3.44	38	2.10	9	absent		NASA arc-jet char 113×10^4 W/m² Heat flux density
100-2	1.8	3.44	40	2.10	10	absent		" "
100-3	4.5	3.91	34	2.08	12	absent		" "
100-4	7.2	4.10	15	2.07	3	absent		" "
ASTM Card 13-148 (graphite)		3.35		2.13		1.68		
1922°K Furnace Char		3.83	26	2.09	8	absent		Furnace char
3033°K Furnace Char		3.44	53	2.11	10	too faint to read		Furnace char

TABLE 24

SUMMARY OF BULK AND TRUE DENSITY MEASUREMENTS ON PHENOLIC-NYLON CHAR

Sample No.	Bulk density (gm/cm^3)	Remarks
Arc-jet 1	0.22	Charred in arc-jet at 113×10^4 W/m^2 - density determined by weighing and measuring sample
100-A	0.273[1]	Charred in arc-jet at 113×10^4 W/m^2 - density determined by weighing and measuring sample
Average	0.247	
Arc-jet 2	0.304[1]	Charred in arc-jet at 227×10^4 W/m^2 - density determined by weighing and measuring sample
200-A	0.26 [1]	Charred in arc-jet at 227×10^4 W/m^2 - density determined by paraffin coating sample
1	0.295	Charred in arc-jet at 227×10^4 W/m^2 - density determined by weighing and measuring sample
200-B	0.30	Charred in arc-jet at 227×10^4 W/m^2 - density determined by liquid absorption technique
	0.34	Charred in arc-jet at 227 x Id W/m^2 - density determined by weighing and measuring sample
Average	0.30	
	True density (gm/cm^3)	
1	1.5892	Charred in arc-jet at 113×10^4 W/m^2
2	1.651'	
3	1.489'	
4	1.505[3]	
Average	1.559	
1	1.508[2]	Charred in arc-jet at 227×10^4 W/m^2
2	1.561[2]	" " "
3	1 487'	" "
4	1 524[3]	" "
5	1.4593	" "
6	1.467'	" "
Average	1.502	
	1.429[3]	Charred in furnace to 812°K
	1.441[3]	" "
Average	1.435	
	1 433'	Charred in furnace to 1922°K
	1.455'	Charred in furnace to 3033°K
	1.466'	" "
Average	1.461	
	1.780'	Charred in furnace to 3033°K at rapid rate

Notes:
1. Considered best measurement from standpoint of sample quality.
2. Samples ground to 100 mesh screen.
3. Samples ground to 325 mesh screen (44 microns).
4. Added wetting agent (Tergitol TNN, non-ionic detergent (product of Union Carbide) to make material sink.
5. Uncertainty in true density measurements estimated to be ± 5%.

TABLE 25

WEIGHT 'LOSSOF SPECIMENS DURING CHARRING

Specimen	Char history	Percent weight loss	Density of char, (gm/cm)
TC19	Charred at slow rate to 812°K	67.6	0.289
TC16	" "	67.5	0.302
TC14	" "	67.1	0.323
TC1	" "	69.2	0.303
TC8S	" " 1366°K	74.9	0.365
TC17	" "	75.1	0.377
5R	Charred at slow rate to 922°K - rapid rate to 1366°K	73.4	0.342
TC10	Charred at slow rate to 1366°K	72.3	0.377
TC2	" "	74.4	0.363
TC6S	" " 1922°K	75.8	0.321
TC3	" "	75.6	0,335
TC11	" "	73.9	0.341
TC7S	" " 2400°K	78.1	0.330
TC4	" "	74.6	0.339
TC12	" "	74.2	0.344
1F5000-3	" " 3033°K	----	0.347
4F5000-5	" "	----	0.353
TC5	" "	74.9	0.349
2F-5000-2	" "	----	0.353
TC13	" "	73.2	0.351
5000R1	Charred at rapid rate to 3033°K	----	0.210
5000R2	" "	53.4	0.233
5000R3	" "	38.7	0.236
3F5000-3	Charred at slow rate to 3033°K	----	0.363
P1	" " 812°K	67.0	0.337
P2	" " 1366°K	71.8	0.387
P3	" " 1922°K	74.1	0.327
P4	" " 2480°K	76.5	0.320
P5	" " 3033°K	73.1	0.310

TABLE 26

RESULTS OF LIQUID ABSORPTION MEASUREMENTS ON PHENOLIC-NYLON CHARRED IN ARC-JET AT 2.27 MW/m^2

WA = 213 percent

ρ_B = 0.30 gm/cm^3

ρ_A = 0.82 gm/cm^3

P_O = 64 percent

P_T = 80 percent (based on specimen true density of 1.5 gm/cm^3)

P_T = 83 percent (based on specimen true density of 1.8 gm/cm^3)

TABLE 27

SUMMARY OF RESULTS OF MEASUREMENTS MADE TO CHARACTERIZE PHENOLIC-NYLON CHAR

Material description	Bulk density (gm/cm^3)	True density (gm/cm^3)	Porosity (%)	"d" lattice spacing (002) (A)	Relative intensity (%)	Carbon (%)	Hydrogen (%)	Nitrogen (%)	Mean pore size (microns)	
1.13 MW/m^2 arc-jet char - 0 to 1.8 mm below surface	0.25	1.56	82/87	3.44	8 [illegible] 40	90.1/ 98.6[3]	0.3/0.4[2]	0.4/1.2[2]	40	Spectrograph also indicated presence of Mg, Si and Ca in about equal concentrations
1.13 MW/m^2 arc-jet char - 4.5 to 7.2 mm below surface	0.25	1.56	82/87	3.91/4.10	34/15	90.2/ 91.2	0.4/0.8	0.9/1.1	28	
2.27 MW/m^2 arc-jet char - 0 to 3.7 mm below surface	0.29	1.50	80/83	3.44/3.45	89/100	93.4/ 98.4[2]	0[2]/0.4	0.2/0.3[2]	38	Spectrograph also indicated presence of Mn, Mg, Si, and Ca. Mn in highest concentration, Ca in lowest concentration.
2.27 MW/m^2 arc-jet char - 5.0 to 7.9 mm below surface	0.29	1.50	80/83	3.44/3.45	89/100	93.7/ 98.4	0.5/2.66	0.2/0.5	38	
812°K furnace char, low heating rate in helium held 30 minutes at temperature	0.304	1.44	79			81.2	2.89	1.87		
1366°K furnace char, low heating rate in helium, held 1 hr at temperature	0.374		74			84.4	1.37	1.46		
1922°K furnace char, low heating rate in helium, held 1 hr at temperature	0.331	1.43	77	3.83	26					
3033°K furnace char, low heating rate in helium, held 1 hr at temperature	0.347	1.46	76	3.44	53	83.65[1]/ 99.69	0.3/0.5	<0.1 / <0.2	40	

Notes: 1. Suspect incomplete oxidation of sample.
2. Used better procedure to obtain more reliable measurement.
3. Slashes give range of values where two or more measurements w [illegible] m <e.

TABLE 28

SUMMARY OF CONDITIONS UNDER WHICH CHAR SPECIMENS WERE PREPARED

Studying	Heating rate	Temp. level (°K)	Time at max. temp. (min)	Thermal conductivity measured to (°K)
1. Effect of charring temperature	Low (see figure 128)	812	30	550 CRA 3033 RIA
	" "	1366	30	800 CRA 3033 RIA
	" "	1922	30	800 CRA 3033 RIA
	" "	2480	30	800 CRA 3033 RIA
	" "	3033	30	3033 RIA
2. Effect of time at temperature	Low (see figure 128)	3033	30	3033 RIA
	Low (see figure 126)	3033	120	3033 RIA
	Low (see figure 127)	3033	180	3033 RIA
	Low (see figure 125)	3033	180	850 CRA
	Low (see figure 125)	3033	300	850 CRA
	Low (see figure 128)	1366	30	3033 RIA
	Low (see figure 129)	1366	less than 1 minute	1050 CRA
3. Effect of heating rate combined with time at temperature	High (see figure 130)	3033	less than 1 minute	800 CRA
	" "	3033	5	1090 CRA
	" "	3033	5	3033 RIA
	" "	3033	15, 120	1090 CRA
	High (1.13 MW/m2 in arc-jet)	gradient	5	800 CRA
	High (2.27 MW/m^2 in arc-jet)	gradient	between 2 and 3	1100 CRA

Notes: RIA - thermal conductivity measured in radial inflow apparatus
CRA - thermal conductivity measured in comparative rod apparatus

TABLE 29

THE THERMAL CONDUCTIVITY OF PHENOLIC-NYLON CHARRED AT 812°K FOR 30 MINUTES—
MEASURED IN COMPARATIVE ROD APPARATUS WITH TEFLON REFERENCES

Specimen and time	Mean temperature of specimen °K	Thermal conductivity of specimen K_S W/m-°K	ΔT through specimen °K	Mean temperature of lower reference °K	Thermal conductivity of lower reference K_1 W/m-°K	ΔT through lower reference ΔT_1 °K	Mean temperature of upper reference °K	Thermal conductivity of upper reference K_2 W/m-°K	ΔT through upper reference ΔT_2 °K
Specimen TC-19 Run 4985-68 Density = 0.2886 gm/cm^3 Initial thickness = 2.5375 cm Final thickness = 2.5354 cm Initial weight = 2.0564 gm Final weight = 2.0818 gm									
8:00 am	389	0.137	53.4	338	0.219	26.2	454	0.229	38.4
11:00 am	393	0.113	47.8	343	0.217	28.4	442	0.217	21.8

Notes:

1. All measurements made in air. Apparatus was not evacuated prior to determination.
2. Thermal conductivity (k_S) of specimen calculated from following equation

$$k_S = \left[\frac{k_1 \Delta T_1}{l_1} + \frac{k_2 \Delta T_2}{l_2} \right] \frac{l_S}{2 \Delta T_S}$$

where subscripts 1, 2, and s refer to top reference, bottom reference, and specimen, respectively.

3. Gage lengths: l_S = 1.9126 cm, l_1 = 1.905 cm, l_2 = 1.905 cm

TABLE 30

THE THERMAL CONDUCTIVITY OF PHENOLIC-NYLON CHARRED AT 812°K FOR 30 MINUTES — MEASURED IN COMPARATIVE ROD APPARATUS WITH PYROCERAM REFERENCES

Specimen and time	Mean temperature of specimen °K	Thermal conductivity of specimen K_S W/m-°K	ΔT through specimen °K	Mean temperature of lower reference °K	Thermal conductivity of lower reference K_1 W/m-°K	ΔT through lower reference ΔT_1 °K	Mean temperature of upper reference °K	Thermal conductivity of upper reference K_2 W/m-°K	ΔT through upper reference ΔT_2 °K
Specimen TC-16 Run 4985-60 Density = 0.302 gm/cm^3 Initial thickness = 2.5384 cm Final thickness[4] = 0.6634 cm Initial weight = 2.1240 gm Final weight = 0.5825 gm									
2:15 pm	549	0.44	215	380	3 71	17.8	015	3.22	38.0

Notes:

1. All measurements made with nitrogen purge. Apparatus was not evacuated prior to determination.
2. Thermal conductivity (k_S) of specimen calculated from following equation

$$k_S = \left[\frac{k_1 \Delta T_1}{l_1} + \frac{k_2 \Delta T_2}{l_2} \right] \frac{l_S}{2 \Delta T_S}$$

where subscripts 1, 2, and s refer to top reference, bottom reference, and specimen, respectively.

3. Gage lengths: l_S = 1.905 cm, l_1 = 1.892 cm, l_2 = 1.887 cm
4. Specimen deteriorated.

TABLE 31

THE THERMAL CONDUCTIVITY OF PHENOLIC-NYLON CHARRED AT 812°K FOR 30 MINUTES—
STRIP SPECIMEN CONFIGURATION IN RADIAL INFLOW APPARATUS - ARGON PURGE

Specimen and run no.	Time	Outer face temp. °K	Outside hole temperature K No. 1		Inside hole temperature K No. 1	No. 2	Specimen ΔT °K	Heat to calorimeter watts	Mean temperature °K	Thermal conductivity watts/meter-°K
Specimen TC-1										
Run 4985-47-5	9:30							8.35		
Density[4]	11:00							9.48		
0.314 gm/cm³								10.40		
0.292 " "								9.25		
Average 0.303 " "	Avg.	1305	12M	1221	944	973	255.5	9.37	1088	0.32
	12:50							24.7		
								23.8		
								23.8		
								24.5		
	Avg.	1822	1703	1615	1447	1425	253	24.2	1553	0.84
	2:10							45.0		
								44.3		
								43.6		
								47.3		
	Avg.	2339	2075	2069	1814	1814	258	45.1	2064	1.54
								61.5		
								59.1		
								56.0		
								51.0		
	Avg.	2630	2350	2298	2089	2091	209	58.4	2401	2.46
								81.0		
								82.2		
								82.4		
								80.5		
	Avg.	2955	2629	2623	2425	2423	202	81.5	2140	3.58
								119.0		
								125.5		
								125.5		
								121.5		
	Avg.	3311	2854	2842	2646	2644	203	124.4	3095	5.40

Notes:

1. Inside and outside hole temperatures below 1500°K are true temperatures as measured with thermocouples. All other inside and outside hole temperatures are observed optical temperatures, not true temperatures.
2. Mean temperature below 1500°K calculated as the average of thermocouple readings—
3. Mean temperature above 1500°K = T_{OF} - 1.065 AT; T_{OF} - outer face temperature

$$k = \frac{tQ}{A\Delta T}$$

where

k = thermal conductivity
t = distance between outside and inside hole = 0.421 cm
Q = heat to calorimeter gage section
A = area of specimen = 4.839 cm² (total for 4 strips)
AT = temperature drop from outside to inside hole

4. Densities are those of some pieces charred at the same time as the specimen.

TABLE 32

THE THERMAL CONDUCTIVITY OF PHENOLIC–NYLON CHARRED AT 812°K FOR 30 MINUTES – STRIP SPECIMEN CONFIGURATION IN RADIAL INFLOW APPARATUS - ARGON PURGE

Specimen and run no.	Time	Outer face temp. °K	Outside hole temperature °K No. 1		Inside hole temperature °K No. 1		Specimen AT °K	Heat to calorimeter watts	Mean temperature °K	Thermal conductivity watts/meter-°K
Specimen TC-14	On									
Run 4985-29-104	10:30									
Run 4985-29-io	12:30	1395	1280	1281	1086	1050		15.5		
			1278	1280	1086	1049		15.5		
Strip 1 = 0.314 gm/cm³			1275	1278	1086	1048		14.9		
2 = 0.327 " "			1283	1283	1071	1045		14.7		
3 = 0.330 " "			1285	1284	1072	1046		----		
4 = 0.319 " "		1395	1284	1283	1071	1045		----		
Average 0.323 " "	Avg.	1395	1281	1282	1079	1045	219.5	15.2	1172	0.61
		1744	1586	1658	1392	1439		25.5		
	1:35		1647	1658	1439	1442		23.7		
			1647	1656	1431	1439		22.8		
			1656	1650	1467	1439		24.9		
		1744	1661	1656	1471	1439		----		
	Avg.	1774	1639	1656	1440	1440	207.5	24.3	1523	1.03
		2145	1989	2000	1761	1758		36.6		
			2000	2011	1772	1761		37.5		
	2:45		1997	2006	1768	1756		34.9		
			2000	2000	1775	1758		36.1		
		2145	2000	2006	1768	1761		----		
	Avg.	2145	1997	2005	1769	1758	237.5	38.3	1892	1.35
		2645	2492	2492	2311	230C		65.9		
			2495	2489	2311	2308		65.7		
	4:0(		2492	2492	2311	230(		60.4		
			2495	2492	2311	2304		59.5		
		2645	2495	2489	2311	2308		----		
	Avg.	2645	2494	2491	2311	2308	185.5	63.0	2447	3.00
		2978	2722	2744	2522	2534		90.6		
	5:0(		2725	2750	2517	2534		83.8		
			2728	2744	2522	2534		78.8		
		2978	2728	2750	2528	2534		85.6		
	Avg.	2978	2726	2747	2522	2534	208.5	84.7	2756	3.58
		3172	2934	2950	2645	2667		114.9		
			2934	2956	2645	2667		97 3		
	6:0(		2939	2950	2645	2672		97 0		
		3172	2934	2950	2645	2667		92.0		
	Avg.	3172	2935	2952	2645	2668	287	100.2	2866	3.08

Notes:

1. Inside and outside hole temperatures below 1500°K are true temperatureas as measured with thermocouples. All other inside and outside hole temperatures are observed optical temperatures. not true temperatures.
2. *Mean* temperature below 1500°K calculated as the average of thermocouples readings.
3. Mean temperature above 1500°K = T_{OF} - 1.065ΔT; T_{OF} - outer face temperature

$$k = \frac{tQ}{A\Delta T}$$

where

- k = thermal conductivity
- t = distance between outside and inside hole = 0.427 cm
- Q = heat to calorimeter gage section
- A = area of specimen = 4.839 cm² (total for 4 strips)
- A T = temperature drop from outside hole

TABLE 33

THE THERMAL CONDUCTIVITY OF PHENOLIC–NYLON CHARRED AT 812°K FOR 30 MINUTES–CYLINDRICAL SPECIMEN CONFIGURATION IN RADIAL INFLOW APPARATUS

Specimen and run no.	Time	Outer face temp. °K	Outside hole temp. °K	Inside hole temp. °K	Specimen A T °K	Heat to calorimeter watts	Mean temperature °K	Thermal conductivity $\frac{W}{m-°K}$
specimen TC19 Run 5053-45-5 Density = 0.311 gm/cm³						9.02 8.80 8.35 8.57 8.12		
	12:15	----	937	714	223	8.57	826	0.30
						15.5 15.5 15.1 14.6		
	2:00	1493	1397	1228	169	15.2	1356	0.71
						46.9 45.5 46.9 45.9		
	3:30	2094	1851	1610	241	46.3	1899	1.51
						89.0 132.7 81.5 81.5		
	4:45	2637	2242	2034	208	83.7	2469	3.17
						138.9 141.0 139.7 140.2		
	5:45	3100	2624	2381	243	140.0	2904	4.54

Notes:

1. Mean temperature below 1500°K calculated as the average of thermocouple readings.
2. Mean temperature above 1500°K = T_{OF} - 0.808 AT; T_{OF} - outer face temperature.
3. $K = \left(\frac{\ln (R_o/R_i)}{2\pi L}\right) \frac{Q}{AT}$

where

K = thermal conductivity
R_o = outside radius = 1.111 cm
R_i = inside radius = 0.592 cm
Q = heat to calorimeter
A T = temperature drop from hot to cold hole on the outside and inside radius respectively
L = gage length of calorimeter = 1.270 cm

4. Specimen was cracked upon removal from furnace.
5. First point taken with helium purge. Argon purge used for all other data points.

TABLE 34

THE THERMAL CONDUCTIVITY OF PHENOLIC-NYLON CHARRED AT 1366°K LESS THAN ONE MINUTE— MEASURED IN COMPARATIVE ROD APPARATUS WITH PYROCERAM REFERENCES

Specimen and time	Mean temperature of specimen °K	Thermal conductivity of specimen K_S W/m-°K	ΔT through specimen °K	Mean temperature of lower reference °K	Thermal conductivity of lower reference K_1 W/m-°K	ΔT through lower reference ΔT_1 °K	Mean temperature of upper reference °K	Thermal conductivity of upper reference K_2 W/m-°K	ΔT through upper reference ΔT_2 °K
Specimen 5R									
Run 4985-62									
Density = 0.3417 gm/cm³									
Initial thickness = 1.2616 cm									
Final thickness = 1.2611 cm									
Initial weight = 1.2705 gm									
Final weight = 1.1840 gm									
9:45 pm	784	0.71	148.3	613	3.32	70.2	960	3.00	89.9
8:30 am	801	0.73	149.4	625	3.31	75.9	979	2.98	90.4
3:25 pm	1049	0.75	87.8	946	3.01	46.7	1159	2.84	61.6
3:45 pm	1049	0.73	77.9	958	3.00	40.4	1144	2.85	52.3

Notes:

1. All measurements made with nitrogen purge. Apparatus was not evacuated prior to determination.
2. Thermal conductivity (k_S) of specimen calculated from following equation

$$k_S = \left[\frac{k_1 \Delta T_1}{l_1} + \frac{k_2 \Delta T_2}{l_2} \right] \frac{l_S}{2 \Delta T_S}$$

where 1, 2, and s refer to top reference, bottom reference, and specimen, respectively.

3 Gage lengths: l_S = 0.7899 cm, l_1 = 1.8872 cm, l_2 = 1.8847 cm

TABLE 35

THE THERMAL CONDUCTIVITY OF PHENOLIC-NYLON CHARRED AT 1366°K FOR 30 MINUTES—
MEASURED IN COMPARATIVE ROD APPARATUS WITH TEFLON REFERENCES

Specimen and time	Mean temperature of specimen °K	Thermal conductivity of specimen K_S W/m-°K	ΔT through specimen °K	Mean temperature of lower reference °K	Thermal conductivity of lower reference K_1 W/m-°K	ΔT through lower reference ΔT_1 °K	Mean temperature of upper reference °K	Thermal conductivity of upper reference K_2 W/m-°K	ΔT through upper reference ΔT_2 °K
Specimen TC-8S Run 4985-67 Density = 0.365 gm/cm^3 Initial thickness = 2.3216 cm Final thickness = 2.3223 cm Initial weight = 2.3477 gm Final weight = 2.4470 gm									
11:00 pm	374	0.274	24.1	340	0.219	29.4	413	0.223	37.8
1:20 am	380	0.274	23.5	345	0.219	31.0	418	0.223	35.1

Notes:

1. All measurements made with nitrogen purge. Apparatus was evacuated three times prior to determinations.
2. Thermal conductivity (k_S) of specimen calculated from following equation

$$k_S = \left[\frac{k_1 \Delta T_1}{l_1} + \frac{k_2 \Delta T_2}{l_2} \right] \frac{l_S}{2 \Delta T_S}$$

   where subscripts 1, 2, and s refer to top reference, bottom reference, and specimen, respectively.
3. Gage lengths: l_S = 1.6866 cm, l_1 = 1.905 cm, l_2 = 1.905 cm

TABLE 3

THE THERMAL CONDUCTIVITY OF PHENOLIC-NYLON CHARRED AT 1366°K FOR 30 MINUTES—
MEASURED IN COMPARATIVE ROD APPARATUS WITH PYROCERAM REFERENCES

Specimen and time	Mean temperature of specimen °K	Thermal conductivity of specimen K_S W/m-°K	ΔT through specimen °K	Mean temperature of lower reference °K	Thermal conductivity of lower reference K_1 W/m-°K	ΔT through lower reference ΔT_1 °K	Mean temperature of upper reference °K	Thermal conductivity of upper reference K_2 W/m-°K	ΔT through upper reference ΔT_2 °K
Specimen TC-17 Run 4985-61 Density = 0.377 gm/cm^3 Initial thickness = 2.260 cm Final thickness = 1.992 cm Initial weight = 2.3566 gm Final weight = 1.8665 gm									
10:50 am	596	0.69	201	431	3.58	39.1	789	3.14	58.9
4:45 pm	573	0.66	166	433	3.58	36.0	716	3.21	39.6
9:10 am	781	0.73	109.5	688	3.24	27.0	874	3.07	32.0

Notes:

1. All measurements made with nitrogen purge. Apparatus was not evacuated prior to determination.
2. Thermal conductivity (k_S) of specimen calculated from following equation

$$k_S = \left[\frac{k_1 \Delta T_1}{l_1} + \frac{k_2 \Delta T_2}{l_2}\right] \frac{l_S}{2\Delta T_S}$$

where subscripts 1, 2, and s refer to top reference, bottom reference, and specimen, respectively.

3. Gage lengths: l_S = 1.6256 cm, l_1 = 1.905 cm, l_2 = 1.905 cm

TABLE 37

THE THERMAL CONDUCTIVITY OF PHENOLIC-NYLON CHARRED AT 1366°K FOR 30 MINUTES—
STRIP SPECIMEN CONFIGURATION IN RADIAL INFLOW APPARATUS - HELIUM PURGE

Specimen and run no.	Time	Outer face temp. °K	Outside hole temperature No. 1	Outside hole temperature No. 2	Inside hole temperature °K	Inside hole temperature No. 2	SpΔTmen °K	Heat to calorimeter watts	Mean emperature °K	Thermal conductivity watts/meter-°K
Specimen TC-2	On							33.9		
Run 4985-29-13	9:00	1350	1261	1258	1024	1036		39.9		
Density	10:30		1269	1267	1032	1042		30.9		
Strip 1 = 0.366 gm/cm³			1270	1267	1031	1042		31.9		
2 = 0.364 " "			1265	1261	1022	1028		39.7		
3 = 0.365 " "			1264	1260	1021	1027		30.2		
4 = 0.358 " "		1350	1263	1258	1020	1027		33.1		
Average 0.363 " "	Avg.	1350	1266	1262	1025	1034	34.5	32.2	1147	1.21
		1800	1689	1683	1467	1461		40.7		
			1678	1683	1461	1450		35.2		
	12:30		1689	1889	1456	1461		38.9		
			1683	1689	1456	1456		41.3		
		1800	1683	1683	1461	1456				
	Avg.	1800	1684	1685	1460	1457	226	38.9	1559	1.52
		2161	1900	1889	1672	1667		53.6		
			1889	1883	1661	1661		51.9		
	1:40		1895	1889	1667	1667		46.9		
			1889	1883	1661	1861		46.9		
			----	---	----	----		49.2		
		2167	----					47.8		
	Avg.	2167	1893	1886	1661	1664	224	49.5	1928	1.95
		2450	2289	2284	2033	2039		68.6		
			2284	2284	2033	2033		64.2		
	2:50		2289	2288	2036	2033		62.7		
			2289	2284	2033	2033		70.6		
			----	...	----			----		
		2450	.....							
	Avg.	2450	2288	2285	2034	2035	252	66.5	2182	2.33
		2828	2617	2611	2366	2366		90.6		
			2617	2614	2366	2366		80.0		
	4:00		2622	2611	2310	2366		81.8		
		2828	2611	2617	2366	237C		90.3		
	Avg.	2828	2618	2613	2367	2361	248.5	85.6	2563	3.04
		3050	2834	2822	2545	2539		109.3		
			2839	2822	2545	2534		90.3		
	5:00		2834	2828	2542	2536		106.7		
		3050	2836	2822	2545	2534		108.2		
	Avg.	3050	2836	2824	2544	2536	290	103.5	2741	3.15
		3334	2945	2939	2678	2667		126.3		
			2945	2945	2612	267(		117 8		
	5:30		2950	2950	2667	2667		121 1		
		3334	2945	2945	2612	2667		130.4		
	Avg.	3334	2946	2945	2672	266(	275.5	123.9	3041	3.97

Notes:

1. Inside and outside hole temperatures below 1500°K are true temperatures as measured with thermocouples. All other inside and outside hole temperatures are observed optical temperatures, not true temperatures.
2. Mean temperature below 1500°K calculated as the average of thermocouples readings.
3. Mean temperature above 1500°K = T_{OF} - 1 065ΔT; T_{OF} - outer face temperature

$$k = \frac{tQ}{A\Delta T}$$

where

k = thermal conductivity
t = distance between outside and inside hole = 0.427 cm
Q = heat to calorimeter gage section
A = area of specimen = 4.839 cm (total for 4 strips)
AT = temperature drop from outside hole

TABLE 38

THE THERMAL CONDUCTNITY OF PHENOLIC-NYLON CHARRED AT 1366°K FOR 30 MINUTES – STRIP SPECIMEN CONFIGURATION IN RADIAL INFLOW APPARATUS - ARGON PURGE

Specimen and runno.		Outer face temp. °K	Outside hole temperature No. 1	Outside hole temperature No. 2	Inside hole temperature No. 1	Inside hole temperature No. 2	Specimen AT °K	Heat to calorimeter watts	Mean temperature °K	Thermal conductivity watts/meter-°K
Specimen TC-10										
Run 4985-40-5	8:30							18.5		
Density:								18.5		
trip 1 = 0.379 gm/cm³								18.1		
2 = 0.375 " "								17.8		
3 = 0.383 " "	Avg.	1289	1173	1179	962	940	225	18.2	1064	0.71
4 = 0.370 " "										
Average 0.377 " "	12:45							32.4		
								31.5		
								33.8		
								34.3		
	Avg.	1872	1668	1705	1450	1473	225	33.0	1632	1.29
	2:45							47 8		
								48.5		
								47 6		
								48.0		
	Avg.	2191	1966	1966	1721	1738	236.5	48.0	1939	1.79
	4:30							76.2		
								76.4		
								76.6		
								75.9		
	Avg.	2583	2290	2278	2034	2028	253	76.3	2314	2.66
	6:00							94.0		
								92.3		
								95.2		
								95.5		
	Avg.	2805	2455	2464	2200	2223	248	94.3	2541	3.35
	7:20							121.5		
								121.0		
								120.7		
								125.0		
	Avg.	3111	2765	2762	2486	2493	274	122.1	2819	3.93
	8:05							145.6		
								147.3		
								149.4		
								142.2		
	Avg.	3311	2850	2850	2558	2561	290.5	146.1	3002	4.44

Notes:

1. Inside and outside hole temperatures below 15WK are true temperatures as measured with thermocouples. All other inside and outside hole temperatures are observed optical temperatures, not true temperatures.
2. Mean temperature below 1500°K calculated as the average of thermocouples readings.
3. Mean temperature above 1500°K = T_{OF} - 1.065 AT; T_{OF} - outer face temperature

$$k = \frac{tQ}{A\Delta T}$$

where

k = thermal conductivity
t = distance between outside and inside hole = 0.427 cm
Q = heat to calorimeter gage section
A = area of specimen = 4.839 cm (total for 4 strips)
AT = temperature drop from outside hole

TABLE 39

THE THERMAL CONDUCTIVITY OF PHENOLIC-NYLON CHARRED AT 1922°K FOR 30 MINUTES—MEASURED IN COMPARATIVE ROD APPARATUS WITH TEFLON REFERENCES

Specimen and time	Mean temperature of specimen °K	Thermal conductivity of specimen K_S W/m-°K	ΔT through specimen °K	Mean temperature of lower reference °K	Thermal conductivity of lower reference K_1 W/m-°K	ΔT through lower reference ΔT_1 °K	Mean temperature of upper reference °K	Thermal conductivity of upper reference K_2 W/m-°K	ΔT through upper reference ΔT_2 °K
Specimen TC-6S Run 4985-69 Density = 0.321 gm/cm³ Initial thickness = 2.5918 cm Final thickness = 2.6556 cm Initial weight = 2.4390 gm Final weight = 2.4386 gm									
8:10 am	359	0.245	19.2	330	0.219	24.9	396	0.223	38.3
3:00 pm	377	0.343	22.4	340	0.219	34.1	413	0.223	31.8
12:20 pm	361	0.373	19.3	332	0.219	27.0	396	0.223	34.4

Notes:

1. All measurements made in air. Apparatus was not evacuated prior to determination.
2. Thermal conductivity (k_S) of specimen calculated from following equation

$$k_S = \left[\frac{k_1 \Delta T_1}{l_1} + \frac{k_2 \Delta T_2}{l_2}\right] \frac{l_S}{2 \Delta T_S}$$

where subscripts 1, 2, and s refer to top reference, bottom reference, and specimen, respectively.

3. Gage lengths: l_S = 2.0193 cm, l_1 = 1.905 cm, l_2 = 1.905 cm

TABLE 40

THE THERMAL CONDUCTIVITY OF PHENOLIC-NYLON CHARRED AT 1922°K FOR 30 MINUTES—
MEASURED IN COMPARATIVE ROD APPARATUS WITH PYREX REFERENCES

Specimen and time	Mean temperature of specimen °K	Thermal conductivity of specimen K_S W/m-°K	ΔT through specimen °K	Mean temperature of lower reference °K	Thermal conductivity of lower reference K_1 W/m-°K	ΔT through lower reference ΔT_1 °K	Mean temperature of upper reference °K	Thermal conductivity of upper reference K_2 W/m-°K	ΔT through upper reference ΔT_2 °K
Specimen TC-6S Run 4985-70 Density = 0.321 gm/cm^3 Initial thickness = 2.6556 cm Final thickness = 2.6556 cm Initial weight = 2.4386 gm Final weight = 2.4386 gm									
8:10 am	411	0.74	57.4	353	1.1≤	30.1	468	1.30	26.4
12:30	448	0.78	72.1	373	1.2o	41.3	519	1.36	31.9

Notes:

1. All measurements made in nitrogen purge. Apparatus was not evacuated prior to determination.
2. Thermal conductivity (k_S) of specimen calculated from following equation

$$k_S = \left[\frac{k_1 \Delta T_1}{l_1} + \frac{k_2 \Delta T_2}{l_2} \right] \frac{l_S}{2 \Delta T_S}$$

   where subscripts 1, 2, and s refer to top reference, bottom reference, and specimen, respectively.
3. Gage lengths: l_S = 2.0193 cm, l_1 = 1.455 cm, l_2 = 1.895 cm

TABLE 41

THE THERMAL CONDUCTIVITY OF PHENOLIC-NYLON CHARRED AT 1922°K FOR 30 MINUTES—
MEASURED IN COMPARATIVE ROD APPARATUS WITH PYROCERAM REFERENCES

Specimen and time	Mean temperature of specimen °K	Thermal conductivity of specimen K_S W/m-°K	ΔT through specimen °K	Mean temperature of lower reference °K	Thermal conductivity of lower reference K_1 W/m-°K	ΔT through lower reference ΔT_1 °K	Mean temperature of upper reference °K	Thermal conductivity of upper reference K_2 W/m-°K	ΔT through upper reference ΔT_2 °K
Specimen TC-6S Run 4985-63 Density = 0.321 gm/cm^3 Initial thickness = 2.7196 cm Final thickness = 2.5918 cm Initial weight = 2.4137 gm Final weight = 2.4390 gm									
8:40 pm	503	1.01	118.7	402	3.64	29.7	604	3.03	35.1
12:30 pm	806	1.02	119.3	705	3.23	34.4	916	3.03	45.4
1:45 pm	821	1.03	116.9	721	3.21	35.9	929	3.03	43.2

Notes:

1. All measurements made in nitrogen purge. Apparatus was evacuated three times prior to determination.
2. Thermal conductivity (k_S) of specimen calculated from following equation

$$k_S = \left[\frac{k_1 \Delta T_1}{l_1} + \frac{k_2 \Delta T_2}{l_2}\right] \frac{l_S}{2 \Delta T_S}$$

where subscripts 1, 2, and s refer to top reference, bottom reference, and specimen, respectively.

3. Gage lengths: l_S = 2.0193 cm, l_1 = 1.887 cm, l_2 = 1.885 cm

TABLE 42

THE THERMAL CONDUCTIVITY OF PHENOLIC-NYLON CHARRED AT 1922°K FOR 30 MINUTES– STRIP SPECIMEN CONFIGURATION IN RADIAL INFLOW APPARATUS - ARGON PURGE

Specimen and run no.	Time	Outer face temp. °K	Outside hole temperature °K No. 1	Outside hole temperature °K No. 2	Inside hole temperature °K No. 1	Inside hole temperature °K No. 2	Specimen ΔT °K	Heat to calorimeter watts	Mean temperature °K	Thermal conductivity watts/meter-°K
pecimen TC-3	On									
un 4985-17-29	8:00							23.6		
ensity								22.8		
trip 1 = 0.337 gm/c								19.0		
2 = 0.332 " "								16.7		
3 = 0.336 " "	4vg.	1319	1238	1239	1126	1120	115.5	20.5	1181	1.56
4 = 0.335 " "										
verage 0.335 " "	11:00							33.7		
								29.6		
								27.0		
								26.7		
	Avg.	1733	1630	1631	1515	1519	113.5	29.3	1612	2.28
	12:30							41.6		
								35.2		
								33.7		
								34.9		
	Avg.	2066	1924	1925	1761	1760	164	36.4	1891	1.96
	1:30							59.2		
								56.5		
								45.7		
								48.1		
	Avg.	2478	2332	2335	2164	2165	169	52.4	2298	2.73
	2:30							80.0		
								76.2		
								63.0		
								58.3		
	Avg.	2711	2516	2509	2349	2356	160	69.4	2541	3.82
	3:30							93.8		
								60.6		
								75.9		
								78.6		
	Avg.	2944	2702	2782	2504	2508	276	02.3	2666	2.63
	4:30							124.2		
								119.5		
								95.0		
								95.2		
	Avg.	3322	2903	2939	2685	2696	230.5	108.7	3077	4.16

Notes:

1. Inside and outside hole temperatures below 1500°K are true temperatures as measured with thermocouples. All other inside and outside hole temperature are observed optical temperatures, not true temperatures.
2. Mean temperature below 1500°K calculated as the average of thermocouple readings.
3. Mean temperature above 1500°K = T_{OF} - 1.065 ΔT; T_{OF} - outer face temperature

$$k = \frac{tQ}{A\Delta T}$$

where

k = thermal. conductivity
t = distance between outside and inside hole = 0.427 cm
Q = heat to calorimeter gage section
A = area of specimen = 4.839 cm² (total for 4 strips)
AT = temperature drop from outside to inside hole

TABLE 43

THE THERMAL CONDUCTIVITY OF PHENOLIC-NYMN CHARRED AT 1922°K FOR 30 MINUTES—
STRIP SPECIMEN CONFIGURATION IN RADIAL INFLOW APPARATUS - ARGON PURGE

Specimen and run no.	Time	Outer face temp. °K	Outside hole temperature No. 1	Outside hole temperature No. 2	Inside hole temperature No. 1	Inside hole temperature No. 2	Specimen AT °K	Heat to calorimeter watts	Mean temperature °K	Thermal conductivity watts/meter-°K
Specimen TC-11	On									
Run 4985-44-5	8:45									
Density	10:45									
Strip 1 = 0.350 gm/										
2 = 0.343 "										
3 = 0.328 "	Avg.	1316	1229	1231	1052	1025	191.5	30.3 31.9 29.6 33.3 31.3	1134	1.44
4 = 0.341 "										
Average 0.341 "	12:30							53.2 53.4 52.4 53.2		
	Avg.	1900	1664	1666	1441	1437	226	53.1	1659	2.07
	2:00							64.1 63.7 65.6 65.8		
	Avg.	2158	1902	1912	1646	1646	261	64.8	1880	2.19
	3:30							94.5 95.7 95.0 98.9		
	Avg.	2528	2208	2232	1948	1951	270.5	96.0	2240	3.13
	5:00							110.0 107.1 114.8 116.8		
	Avg.	2816	2533	2529	2258	2257	273.5	112.2	2525	3.62
	7:00							138.8 134.3 137.3 139.6		
	Avg.	3130	2786	2762	2490	2479	289.5	137.5	2822	4.19

Notes:

1. Inside and outside hole temperatures below 1500°K are true temperatures as measured with thermocouples. All other inside and outside hole temperatures are observed optical temperatures, not true temperatures.
2. Mean temperature below 1500°K calculated as the average of thermocouple readings.
3. Mean temperature above 1500°K = T_{OF} - 1.065 AT; T_{OF} - outer face temperature

$$k = \frac{tQ}{A\Delta T}$$

where

- k = thermal conductivity
- t = distance between outside and inside hole = 0.427 cm
- Q = heat to calorimeter gage section
- A = area of specimen = 4.839 cm^2 (total for 4 strips)
- AT = temperature drop from outside hole

TABLE 44

THE THERMAL CONDUCTIVITY OF PHENOLIC-NYLON CHARRED AT 2480°K FOR 30 MINUTES—MEASURED IN COMPARATIVE ROD APPARATUS WITH PYROCERAM REFERENCES

Specimen and time	Mean temperature of specimen °K	Thermal conductivity of specimen K_S W/m-°K	ΔT through specimen °K	Mean temperature of lower reference °K	Thermal conductivity of lower reference K_1 W/m-°K	ΔT through lower reference ΔT_1 °K	Mean temperature of upper reference °K	Thermal conductivity of upper reference K_2 W/m-°K
Specimen TC-7S Run 4985-65 Density = 0.330 gm/cm^3 Initial thickness = 2.245 cm Final thickness = 2.2443 cm Initial weight = 2.0528 gm Final weight = 2.0637 gm								
9:15 pm	493	1.32	82.2	408	3.63	33.7	573	3.37
11:10 am	746	1.36	57.1	684	3.25	29.0	803	3.14
2:45 pm	800	1.35	61.4	735	3.20	28.5	863	3.08

Notes:

1. All measurements made in nitrogen purge. Apparatus was evacuated three times prior to determination.
2. Thermal conductivity (k_S) of specimen calculated from following equation

$$k_S = \left[\frac{k_1 \Delta T_1}{l_1} + \frac{k_2 \Delta T_2}{l_2}\right] \frac{l_S}{2 \Delta T_S}$$

where subscripts 1, 2, and s refer to top reference, bottom reference, and specimen, respectively.

3. Gage lengths: l_S = 1.590 cm, l_1 = 1.887 cm, l_2 = 1.885 cm

TABLE 45

THE THERMAL CONDUCTIVITY OF PHENOLIC-NYLON CHARRED AT 2480°K FOR 30 MINUTES–
STRIP SPECIMEN CONFIGURATION IN RADIAL INFLOW APPARATUS - ARGON PURGE

Specimen and run no.	Time	Outer face temp. °K	Outside hole temperature °K No. 1	Outside hole temperature °K No. 2	Inside hole temperature °K No. 1	Inside hole temperature °K	Specimen AT °K	Heat to calorimeter watts	Mean temperature °K	Thermal conductivity watts/meter-°K
	On									
	9:30							13.8		
	11,00							14.3		
Strip 1 = 0.344 gm/cm								15.2		
2 = 0.336 " "								14.9		
3 = 0.336 " "	Avg.	1319	1220	1229	1137	[illegible]	96	14.6	1177	1.34
4 = 0.339 " "										
Average 0.339 " "	12:30							23.7		
								23.7		
								23.2		
								24.4		
	Avg.	1769	1659	1674	15[illegible]	1541	115.5	23.8	1646	1.82
	1:45							27.9		
								30.4		
								31.8		
								29.9		
	Avg.	2130	1920	1942	1796	1786	140	30.0	1981	1.89
	2:55							50.0		
								50.3		
								49.3		
								49.1		
	Avg.	2605	2413	2444	2261	2259	168.5	49.7	2426	2.60
	4:00							78.8		
								76.0		
								76.5		
								15.2		
	Avg.	3005	2771	2792	2591	2562	205	76.6	2787	3.30
	4:45							95.2		
								98.1		
								97.0		
								102.0		
	Avg.	3322	2939	2949	2704	2675	254.5	98.1	3051	3.40

Notes:

1. Inside and outside hole temperatures below 1500°K are true temperatures as measured with thermocouples. All other inside and outside hole temperatures are observed optical temperatures, not true temperatures.
2. Mean temperature below 1500°K calculated as the average of thermocouple readings.
3. Mean temperature above 1500°K = T_{OF} - 1.065 AT; T_{OF} = outer face temperature

$$k = \frac{tQ}{A\Delta T}$$

where

k = thermal conductivity
t = distance between outside and inside hole = 0.427 cm
Q = heat to calorimeter gage section
A = area of specimen = 4.839 cm² (total for 4 strips)
AT = temperature drop from outside hole

TABLE 46

THE THERMAL CONDUCTIVITY OF PHENOLIC-NYLON CHARRED AT 2480°K FOR 30 MINUTES—
STRIP SPECIMEN CONFIGURATION IN RADIAL INFLOW APPARATUS - ARGON PURGE

Specimen and runno.	Time	Outer face temp. °K	Outside hole temperature °K		Inside hole temperature °K		Specimen AT °K	Heat to calorimeter watts	Mean temperature °K	Thermal conductivity watts meter-°K
			No. 1	No. 2	No. 1	No. 2				
Specimen TC-12	On							28.0		
Run 4985-31-5	9:15							28.2		
Density	10:50							26.2		
Strip 1 = 0.363 gm/cm³								26.6		
2 = 0.348 " "										
3 = 0.334 " "	Avg.	1228	1142	1155	977	965	177.5	27.3	1060	1.36
4 = 0.331										
Average 0.344	12:30							51.8		
Run 1								52.3		
								51.1		
								51.6		
	Avg.	1797	1646	1655	1432	1436	216.5	51.7	1566	2.11
	2:10							69.7		
								74.5		
								70.9		
								74.2		
	Avg.	2247	2020	2021	1791	1791	229.5	72.3	2003	2.78

Notes:

1. Inside and outside hole temperatures below 1500°K are true temperatures as measured with thermocouples, All other inside and outside hole temperatures are observed optical temperatures, not true temperatures,
2. Mean temperature below 1500°K calculated as the average of thermocouple readings.
3. Mean temperature above 1500°K = T_{OF} - 1,065 AT; T_{OF} - outer face temperature

$$k = \frac{tQ}{A\Delta T}$$

where

- k = thermal conductivity
- t = distance between outside and inside hole = 0.427 cm
- Q = heat to calorimeter gage section
- A = area of specimen = 4.839 cm² (total for 4 strips)
- AT = temperature drop from outside hole

TABLE 47

THE THERMAL CONDUCTIVITY OF PHENOLIC–NYLON CHARRED AT 2480°K FOR 30 MINUTES—STRIP SPECIMEN CONFIGURATIONS IN RADIAL INFLOW APPARATUS - ARGON PURGE

Specimen and run no.	Time	Outer face temp. °K	Outside hole temperature °K No. 1	Outside hole temperature °K No. 2	Inside hole temperature No. 1	Inside hole temperature No. 2	Specimen AT °K	Heat to calorimeter watts	Mean temperature °K	Thermal conductivity watts/meter-°K
pecimen TC-12	On									
un 4985-33-5	8:15							26.5		
ensity	9:30							25.8		
trip 1 = 0.363 gm/								25.8		
2 = 0.348 "								27.0		
3 = 0.334 "	Avg.	1228	1151	1171	1014	1020	144	26.3	1089	1.61
4 = 0.331 "										
verage 0.344 "	10:45							40.8		
un 2								41.0		
								40.8		
								40.8		
	Avg.	1747	1614	1619	1421	1410	201	40.9	1533	1.79
	12:45							60.3		
								60.0		
								59.8		
								61.9		
	Avg.	2305	2046	2052	1851	1846	200	60.5	2092	2.67
	1:45							86.8		
								85.4		
								86.1		
								84.9		
	Avg.	2739	2501	2490	225[illegible]	2255	240.5	85.8	2483	3.15
	2:45							106.3		
								101.9		
								100.0		
								104.4		
	Avg.	3005	2735	2729	247[illegible]	2477	255.5	103.2	2733	3.56
	3:30							138.[illegible]		
								136.3		
								134.8		
								141.6		
	Avg.	3311	2979	2967	2694	2686	283	137.8	3010	4.29

Notes:

1. inside and outside hole temperatures below 1500°K are true temperatures as measured with thermocouples. All other inside and outside hole temperatures are observed optical temperatures, not true temperatures.
2. Mean temperature below 1500°K calculated as the average of thermocouple readings.
3. Mean temperature above 1500°K = T_{OF} - 1.065 AT; T_{OF} - outer face temperature

$$k = \frac{tQ}{A\Delta T}$$

where

k = thermal conductivity
t = distance between outside and inside hole = 0.427 cm
Q = heat to calorimeter gage section
A = area of specimen = 4.839 cm^2 (total for 4 strips)
A T = temperature drop from outside hole

TABLE 48

THE THERMAL CONDUCTIVITY OF PHENOLIC-NYLON CHARRED AT 3033°K FOR 180 MINUTES—
MEASURED IN COMPARATIVE ROD APPARATUS WITH PYROCERAM REFERENCES

Specimen and time	Mean temperature of specimen °K	Thermal conductivity of specimen K_S W/m-°K	ΔT through specimen °K	Mean temperature of lower reference °K	Thermal conductivity of lower reference K_1 W/m-°K	ΔT through lower reference ΔT_1 °K	Mean temperature of upper reference °K	Thermal conductivity of upper reference K_2 W/m-°K	ΔT through upper reference ΔT_2 °K
Specimen 1F-5000-3 Run 4985-64 Density = 0.347 gm/cm³ Initial thickness = 2.3980 cm Final thickness = 2.4005 cm Initial weight = 2.3086 gm Final weight = 2.3086 gm									
8:10 am	502	2.28	68.2	425	3.59	42.2	583	3.36	53.8
5:45 pm	859	2.28	62.0	504	3.15	47.4	934	3.02	50.7
7:30 pm	861	2.29	60.8	786	3.15	47.6	936	3.02	48.9
9:50 am	500	2.23	66.9	424	3.60	41.6	578	3.36	51.1

Notes:

1. All measurements made with nitrogen purge. Apparatus was evacuated twice prior to determination.
2. Thermal conductivity (k_S) of specimen calculated from following equation

$$k_S = \left[\frac{k_1 \Delta T_1}{l_1} + \frac{k_2 \Delta T_2}{l_2} \right] \frac{l_S}{2 \Delta T_S}$$

where subcripts 1, 2, and s refer to top reference, bottom reference, and specimen, respectively.

3. Gage lengths: l_S = 1.7627 cm, l_1 = 1.887 cm, l_2 = 1.885 cm

TABLE 49

THE THERMAL CONDUCTIVITY OF PHENOLIC-NYLON CHARRED AT 3033°K FOR 180 MINUTES—
MEASURED IN COMPARATIVE ROD APPARATUS WITH PYROCERAM REFERENCES

Specimen and time	Mean temperature of specimen °K	Thermal conductivity of specimen K_S W/m-°K	ΔT through specimen °K	Mean temperature of lower reference °K	Thermal conductivity of lower reference K_1 W/m-°K	ΔT through lower reference ΔT_1 °K	Mean temperature of upper reference °K	Thermal conductivity of upper reference K_2 W/m-°K	ΔT through upper reference ΔT_2 °K
Specimen 1F-5000-3 Run 1 Density = 0.347 gm/cm^3 Initial weight = 2.2962 gm Final weight = 2.3086 gm Initial length = 2.401 cm Final length = 2.401 cm									
11:50	363	1.86	25.9	336	3.83	13.4	391	3.66	14.3
2:30	603	2.19	49.3	546	3.40	34.1	661	3.27	35.2
7:45	893	2.48	44.6	839	3.10	36.8	951	3.01	40.9
1:15	1066	2.34	30.9	1029	2.94	24.1	1107	2.88	29.2

Notes:

1. All measurements made with helium purge. Apparatus was not evacuated prior to determination.
2. Thermal conductivity (k_S) of specimen calculated from following equation

$$k_S = \left[\frac{k_1 \Delta T_1}{l_1} + \frac{k_2 \Delta T_2}{l_2}\right] \frac{l_S}{2 \Delta T_S}$$

where subscripts 1, 2, and s refer to top reference, bottom reference, and specimen, respectively.

3. Gage lengths: l_S = 1.763 cm, l_1 = 1.887 cm, l_2 = 1.885 cm

TABLE 50

THE THERMAL CONDUCTIVITY OF PHENOLIC-NYLON CHARRED AT 3033°K FOR 300 MINUTES-MEASURED IN COMPARATIVE ROD APPARATUS WITH PYROCERAM REFERENCES

Specimen and time	Mean temperature of specimen °K	Thermal conductivity of specimen K_S W/m-°K	ΔT through specimen °K	Mean temperatu: of lower reference °K	Thermal conductivity of lower reference K_1 W/m-°K	ΔT through lower reference ΔT_1 °K	Mean temperature of upper reference °K	Thermal conductivity of upper reference K_2 W/m-°K	ΔT through upper reference ΔT_2 °K
Specimen 4F5000-5									
Run 1									
Density = 0.353 gm/cm^3									
Initial thickness = 2.401 cm									
Final thickness = 2.401 cm									
Initial weight = ----									
Final weight = 2.4820 gm									
1:00	379	2.22	35.8	342	3.80	19.7	419	3.60	22.9
8:30	670	2.29	48.0	615	3.31	32.6	726	3.21	33.9
8:00	758	2.47	54.4	695	3.24	37.6	827	3.11	46.5
3:45	920	2.62	72.7	829	3.11	59.4	1014	2.95	65.6

Notes:

1. All measurements made with helium purge. Apparatus was evacuated and backfilled [illegible] times prior to determination.
2. Thermal conductivity (k_S) of specimen calculated from following equation

$$k_S = \left[\frac{k_1 \Delta T_1}{l_1} + \frac{k_2 \Delta T_2}{l_2}\right] \frac{l_S}{2 \Delta T_S}$$

where subscripts 1, 2, and s refer to top reference, bottom reference, and specimen, respectively.

3 Gage lengths: l_S = 1.905 cm, l_1 = 1.892 cm, l_2 = 1.887 cm

TABLE 51

THE THERMAL CONDUCTIVITY OF PHENOLIC-NYLON CHARRED AT 3033°K FOR 300 MINUTES–MEASURED IN COMPARATIVE ROD APPARATUS WITH PYROCERAM REFERENCES

Specimen and time	Mean temperature of specimen °K	Thermal conductivity of specimen K_S W/m-°K	ΔT through specimen °K	Mean temperature of lower reference °K	Thermal conductivity of lower reference K_1 W/m-°K	ΔT through lower reference ΔT_1 °K	Mean temperature of upper reference °K	Thermal conductivity of upper reference K_2 W/m-°K	ΔT through upper reference ΔT_2 °K
Specimen 4F-5000-5 Run 4985-66 Density = 0.353 gm/cm³ Initial thickness = 2.540 cm Final thickness = 2.5415 cm Initial weight = 2.4823 gm Final weight = 2.4935 gm									
8:00 am	492	2.22	69.0	412	3.62	38.8	572	3.37	48.5
9:00 am	489	2.21	67.3	416	3.60	38.3	567	3.37	46.4
2:25 am	774	2.39	43.8	725	3.21	29.5	629	3.11	36.0
3:00 pm	772	2.39	48.7	715	3.21	35.2	831	3.11	37.6

Notes:

1. All measurements made with nitrogen purge. Apparatus was not evacuated prior to determination.
2. Thermal conductivity (k_S) of specimen calculated from following equation

$$k_S = \left[\frac{k_1 \Delta T_1}{l_1} + \frac{k_2 \Delta T_2}{l_2}\right] \frac{l_S}{2\Delta T_S}$$

   where subscripts 1, 2, and s refer to top reference, bottom reference, and specimen, respectively.
3. Gage lengths: l_S = 1.905 cm, l_1 = 1.892 cm, l_2 = 1.887 cm

TABLE 52

THE THERMAL CONDUCTIVITY OF PHENOLIC-NYLON CHARRED AT 3033°K FOR 30 MINUTES—STRIP SPECIMEN CONFIGURATION IN RADIAL INFLOW APPARATUS - ARGON PURGE

Specimen and runno.	Time	Outer face temp. °K	Outside hole temperature No. 1	Outside hole temperature No. 2	Inside hole temperature No. 1	Inside hole temperature No. 2	Specimen AT °K	Heat to calorimeter watts	Mean temperature °K	Thermal conductivity watts/meter-°K
ipecimen TC-5										
Run 4985-28-5										
2 = 0.351 " "	On									
3 = 0.344 " "	9:15							25.9		
4 = 0.350 " "	11:00							29.6		
Lverage 0.349 " "								28.4		
Run 3								23.4		
	Avg.	1205	1139	1123	1001	1008	126.5	26.8	1068	1.86
	12:30							40.6		
								41,3		
								40.3		
								41.3		
	Avg.	1822	1634	1637	1486	1482	151,5	40.9	1661	2.38
	1:45							62.4		
								60.5		
								59.3		
								60.3		
	Avg.	2439	2223	2214	2024	2010	201.5	60.6	2224	2.65
	3:15							95.0		
								97,5		
								92.0		
								91.6		
	Avg.	2944	2700	2620	a444	2394	241	94.0	2607	3.44
	4:00							141.4		
								138.8		
								139.6		
	Avg.	3309						135.6		
	Avg.	3309	2945	2881	2699	2619	138.9	138.9	3038	4.82

Notes:

1. Inside and outside hole temperatures below 1500°K are true temperatures as measured with thermocouples. All other inside and outside hole temperatures are observed optical temperatures not true temperatures.
2. Mean temperature below 1500°K calculated as the average of thermocouple readings,
3. Mean temperature above 1500°K = T_{OF} - 1.065 AT: T_{OF} - outer face temperature

$$k = \frac{tQ}{A\Delta T}$$

where

k = thermal conductivity
t = distance between outside and inside hole = 0.427 cm
Q = heat to calorimeter gage section
A = area of specimen = 4.839 cm^2 (total for 4 strips)
ΔT = temperature drop from outside to inside hole

TABLE 53

THE THERMAL CONDUCTWITY OF PHENOLIC-NYLON CHARRED AT 3033°K FOR 30 MINUTES-
IMPREGNATED WITH THERMATOMIC CARBON (4 to 7% BY WT)
STRIP SPECIMEN CONFIGURATION IN RADIAL INFLOW APPARATUS - ARGON PURGE

Specimen and run no.	Time	Outer face temp. °K	Outside hole temperature °K		Inside hole temperature °K		Specimen AT °K	Heat to calorimeter watts	Mean temperature °K	Thermal conductivity watts/meter-°K
			No. 1	No. 2	No. 1	No. 2				
Specimen TC-13										
Run 4985-72-5										
Density										
strip 1 = 0.351 gm/cm³										
2 = 0.356 " "	On									
3 = 0.348 " "	10:00							37.7		
4 = 0.350 " "	12:15							36.3		
Average 0.351 " "								38.0		
								50.0		
								54.4		
	Avg.	1394	1317	1311	1176	1158	147	43.3	1241	2.60
	1:30							56.7		
								59.8		
								67.0		
	Avg.	1978	1714	1716	1561	1561	154	61.2	1814	3.50
	2:30							96.8		
								96.5		
								111.2		
	Avg.	2639	2270	2239	2026	2022	230.5	101.2	2394	3.87
	4:30							138.9		
								142.0		
								142.2		
	Avg.	3100	2485	2480	2259	2266	220	141.1		5.66
								136.9		
								155.2		
								134.8		
	Avg.	3255	2808	2791	2561	2546	246	142.3	2993	5.10

Notes:

1. Inside and outside hole temperatures below 1500°K are true temperatures as measured with thermocouples. All other inside and outside hole temperatures are observed optical temperatures. not true temperatures.
2. Mean temperature below 15WK calculated as the average of thermocouple readings,
3. Mean temperature above 1500°K = T_{OF} - 1,065 AT; T_{OF} - outer face temperature

$$k = \frac{tQ}{A \Delta T}$$

where

k = thermal conductivity
t = distance between outside and inside hole = 0.427 cm
Q = heat to calorimeter gage section
A = area of specimen = 4.839 cm² (total for 4 strips)
AT = temperature drop from outside to inside hole

TABLE 54

THE THERMAL CONDUCTIVITY OF PHENOLIC-NYMN CHARRED AT 3033°K FOR 120 MINUTES—
STRIP SPECIMEN CONFIGURATION IN RADIAL INFLOW APPARATUS - HELIUM PURGE

Specimen and run no.	Time	Outer face temp. °K	Outside hole temperature °K		Inside hole temperature °K		Specimen AT °K	Heat to calorimeter watts	Mean temperature °K	Thermal conductivity watts / meter - °K
			No. 1	No. 2	No. 1	No. 2				
Specimen 2F5000-2	Read									
Run 4985-4-23	12:00		1254	1253	923	916		79.4		
Graphite Packing			1258	1257	926	919		79.1		
Density			1263	1261	929	922		77,1		
Strip 1 0.36 gm/cm³			1260	1243	936	921		77.1		
2 0.35 " "	Up		1263	1246	938	923				
3 0.35 " "	12:45		1264	1246	937	922				
4 0.35 " "	Avg.		1260	1251	932	921	329	78.2	1092	2.33
0.353" "										
Run 1	Read									
	2:oo	2061	1747	175%	1333	1294		123		
			1750	175%	1339	1294		121		
			1736	1750	1308	1291		121		
			1772	1758	1361	1322		117		
		2072	1769	1755	1358	1336		117		
	Avg.	2067	1755	1756	1340	1307	432	120	1631	2.73
	Read									
	4:00	2566	2302	2294	1839	1833		155		
			2339	2300	1877	1805		154		
			2277	2300	1855	1839		153		
			2319	2344	1841	1836		154		
			2344	2327	1880	1822		155		
		2577	2330	2350	1875	1808				
	Avg.	2572	2319	2319	1861	1824	476	154	2091	3.18
	Read									
	6:00	3089	2698	2655	2272	2244		190		
			2711	2744	2305	2272		190		
			2700	2678	2272	2250		190		
			2667	2694	2305	2283		172		
		3094	2689	2683	2305	2283		171		
	Avg.	3092	2693	2691	2292	2266	413	183	2675	4.35
	Temperature dropped to 2811°K before obtaining next data point									
		3311	2811		2422	-		193		
			2867	-	2405	-		198		
		337%	2883		2450	-		193		
		3361	2844	2855	2455	2428		188		
		3392	2844	2822	2455	2467		192		
								190		
								188		
	Avg.	3361	2850	2839	2437	2448	402	192	2955	4.69

Notes:

1. Inside and outside hole temperatures below 1500°K are true temperatures as measured with thermocouples. All other inside and outside hole temperatures are observed optical temperature, not true temperatures.
2. Mean temperature below 1500°K calculated as the average of thermocouple readings.
3. Mean temperature above 1500°K = T_{OF} 1 008 AT; T_{OF} - outer face temperature

$$k = \frac{tQ}{A\Delta T}$$

where

k = thermal conductivity
t = distance between outside and inside hole = 0.475 cm
Q = heat to calorimeter gage
A = area of specimen = 4.839 cm² (total for 4 strips)
AT = temperature drop from outside to inside hole

TABLE 55

THE THERMAL CONDUCTIVITY OF PHENOLIC–NYLON CHARRED AT 3033°K FOR 30 MINUTES–STRIP SPECIMEN CONFIGURATION IN RADIAL INFLOW APPARATUS - ARGON PURGE

Specimen and run no.	Time	Outer face temp. °K	Outside hole temperature °K No. 1	Outside hole temperature °K No. 2	Inside hole temperature °K No. 1	Inside hole temperature °K No. 2	Specimen ΔT °K	Heat to calorimeter watts	Mean temperature °K	Thermal conductivity watts/meter-°K
Specimen 2F-5000-2										
Run 4985-36-5	On									
Density	9:30							20.3		
trip 1 = 0.30 gm/cm	0:45							20.7		
2 = 0.35 " "								20.3		
3 = 0.35 " "								28.1		
4 = 0.35 " "	Avg.	1228	1169	1171	1046	1040	127	20.9	1107	2.08
Average 0.353 " "	2:30							49.0		
Run 2								50.9		
								48.5		
								53.0		
	Avg.	1803	1641	1669	1450	1473	193.5	50.4	1608	2.56
	1:45							62.3		
								08.8		
								65.5		
								64.6		
	Avg.	2183	1964	1975	1739	1750	222	65.3	1959	2.89
	2:00							90.0		
								81.5		
								82.0		
								83.9		
	Avg.	2530	2276	2270	2033	2022	245.5	84.4	2289	3.37
	4:30							104.1		
								97.0		
								90.2		
								103.1		
	Avg.	2828	2535	2533	2273	2270	262.5	100.1	2563	3.74
	5:30							118.3		
								116.3		
								113.0		
								123.0		
	Avg.	3033	2702	2705	2427	2422	279	117.8	2752	4.14
								140.8		
								145.0		
								147.8		
								150.0		
	Avg.	3311			2030	2022	302.5	147.4	3006	4.78

Notes:

1. Inside and outside hole temperatures below 1500°K are true temperatures as measured with thermocouples, All other inside and outside hole temperatures are observed optical temperatures. not true temperatures.
2. Mean temperature below 1500°K calculated as the average of thermocouple readings.
3. Mean temperature above 1500°K = T_{OF} - 1.008 AT; T_{OF} - outer face temperature

$$k = \frac{tQ}{A\Delta T}$$

where

k = thermal conductivity
t = distance between outside and inside hole = 0.475 cm
Q = heat to calorimeter gage section
A = area of specimen = 4.839 cm^2 (total for 4 strips)
AT = temperature drop from outside to inside hole

TABLE 56

THE THERMAL CONDUCTIVITY OF PHENOLIC-NYLON CHARRED AT 3023°K FOR 180 MINUTES--
STRIP SPECIMEN CONFIGURATION IN RADIAL INFLOW APPARATUS - HELIUM PURGE

Specimen and run no.	Time	Outer face temp. °K	Outside hole temperature °K No. 1	Outside hole temperature °K No. 2	Inside hole temperature °K No. 1	Inside hole temperature °K No. 2	Specimen AT °K	Heat to calorimeter watts	Mean temperature °K	Thermal conductivity watts/meter - °K
Specimen 3F5000-3	On									
Run 4985-8-5	8:00									
Zirconia Packing	Read									
Density:	9:45		1406	1414	1289	1294				
strip 1 = 0.36 gm/cm³			1406	1414	1289	1298		32.8		
2 = 0.36 " "			1409	1417	1293	1298		30.6		
3 = 0.36 " "			1410	1419	1294	1299		33.1		
4 = 0.37 " "			1410	1419	1294	1299		33.1		
Average 0.363 " "	Avg.		1408	1417	1292	1297	118	32.5	1354	2.70
	Read									
	12:15	2225	1969	1975	1786	1727		49.2		
			1972	1952	1814	1741		51.0		
		2230	1939	1966	1791	1766		48.9		
			2000	1944	1811	1805		51.9		
			1972	1964	1822	1822				
		2230	1958	1952	1811	1805				
	Avg.	2228	1968	1959	1806	1778	172	50.3	2054	2.87
	Read									
	2:15		2455	2497	2302	2300		67.7		
			2494	2500	2283	2311		72.7		
			2489	2500	2305	2308		69.1		
		2783	2494	2477	2327	2339		67.1		
		2783	2472	2477	2344	2355		73.2		
		2783	2489	2489	2350	2352				
	Avg.	2783	2486	2490	2319	2328	164	70.0	2617	4.19
	Read									
	3:45		2772	2833	2589	2555		134		
			2821	2844	2611	2539		135		
			2816	2833	2605	2577		133		
		3372								
		3339								
			2844	2869	2583	2605				
			2850	2855	2616	2572				
		3372	2866	2900	2589	2583				
	Avg.	3381	2827	2859	2599	2572	257	134	3101	5.12

Notes:

1. Inside and outside hole temperatures below 1500°K are true temperatures as measured with thermocouples. All other inside and outside hole temperatures are observed optical temperatures, not true temperatures.
2. Mean temperature below 1500°K calculated as the average of thermocouple readings.
3. Mean temperature above 1500°K = T_{OF} - 1.008 AT; T_{OF} - outer face temperature

$$k = \frac{tQ}{A\Delta T}$$

where

k = thermal conductivity
t = distance between outside and inside hole = 0.475 cm
Q = heat to calorimeter gage
A = area of specimen = 4.839 cm² (total for 4 strips)
AT = temperature drop from outside to inside hole

TABLE 57

THE THERMAL CONDUCTIVITY OF PHENOLIC-NYLON CHARRED AT 3033°K FOR 5 MINUTES—
MEASURED IN COMPARATIVE ROD APPARATUS WITH PYROCERAM REFERENCES

Specimen and time	Mean temperature of specimen °K	Thermal conductivity of specimen K_S W/m-°K	ΔT through specimen °K	Mean temperature of lower reference °K	Thermal conductivity of lower reference K_1 W/m-°K	ΔT through lower reference ΔT_1 °K	Mean temperature of upper reference °K	Thermal conductivity of upper reference K_2 W/m-°K	ΔT through upper reference ΔT_2 °K
Specimen 5000R1 Run 4985-55 Density = 0.210 gm/cm^3 Initial thickness = 2.538 cm Final thickness = ---- Initial weight = 1.4770 gm Final weight = ----									
12:30 pm	541	3.26	42.3	488	3.4[illegible]	38.[illegible]	597	3.34	42.3
8:15 pm	817	2.80	32.4	776	3.1[illegible]	27.[illegible]	859	3.09	29.7
9:15 pm	820	2.81	32.1	780	3.1[illegible]	28.o	862	3.08	29.7

Notes:

1. ll measuredme made h h m purge. Appar s was evacu d tw prior to determination.
2. hermal conduc y (k_S spe ien calcu ted fro following eq ion

$$k_S = \left[\frac{k_1 \Delta T_1}{l_1} + \frac{k_2 \Delta T_2}{l_2}\right] \frac{l_S}{2 \Delta T_S}$$

where subscripts 1, 2, and s refer to top reference, bottom reference, and specimen, respectively.

3. Gage lengths: l_S = 1.905 cm, l_1 = 1.892 cm, l_2 = 1.887 cm
4. Specimen was charred in a cylindrical configuration and the charring direction was radially inward. Measurements were made normal to the charring direction.

TABLE 58

THE THERMAL CONDUCTIVITY OF PHENOLIC-NYLON CHAR PREPARED IN THE FURNACE AT A RAPID HEATING RATE TO 3033°K— MEASURED IN COMPARATIVE ROD APPARATUS WITH PYROCERAM REFERENCES

Specimen and time	Mean temperature of specimen °K	Thermal conductivity of specimen K_s W/m-°K	ΔT through specimen °K	Mean temperature of lower reference °K	Thermal conductivity of lower reference K_1 W/m-°K	ΔT through lower reference ΔT_1 °K	Mean temperature of upper reference °K	ty reference K_2 W/m-°K	ΔT through upper reference ΔT_2 °K
Specimen 5000-R2									
Run 5053-70									
Density = 0.233 gm/cm³									
Initial thickness = 0.765 cm									
Final thickness = 0.765 cm									
Initial weight = 2.191 gm									
Final weight = 1.065 gm									
6:20 pm	479	8.49	6.02	447	3.55	30.7	514		35.8
9:00 pm	808	7.05	9.43	762	3.17	44.2	858		52.4
9:30 pm	821	6.97	9.78	774	3.16	46.4	873		53.0
3:40 pm	1087	6.47	7.07	1054	2.93	32.3	1125		39.5

Notes:

1. All measurements made with helium purge. Apparatus was not evacuated prior to determination.
2. Thermal conductivity (k_s) of specimen calculated from following equation

$$k_s = \left[\frac{k_1 \Delta T_1}{l_1} + \frac{k_2 \Delta T_2}{l_2} \right] \frac{l_s}{2 \Delta T_s}$$

where subscripts 1, 2, and s refer to top reference, bottom reference, and specimen, respectively.

3. Gage lengths: l_s = 0.447 cm, l_1 = 1.016 cm, l_2 = 1.016 cm
4. This specimen was made from the strips which comprised Specimen 5000-R2 which was used for the measurements in the radial inflow apparatus. The strips were glued together with RTV-731 silicone rubber and then the specimen was machined.

TABLE 59

THE THERMAL CONDUCTIVITY OF PHENOLIC-NYLON CHAR PREPARED IN THE FURNACE AT A RAPID HEATING RATE TO 3033°K — MEASURED IN COMPARATIVE ROD APPARATUS WITH PYROCERAM REFERENCES

Specimen and time	Mean temperature of specimen °K	Thermal conductivity of specimen K_S W/m-°K	ΔT through specimen °K	Mean temperature of lower reference °K	Thermal conductivity of lower reference K_1 W/m-°K	ΔT through lower reference ΔT_1 °K	Mean temperature of upper reference °K	Thermal conductivity of upper reference K_2 W/m-°K	ΔT through upper reference ΔT_2 °K
Specimen 5000-R3 Run 5053-68 Density = 0.236 gm/cm^3 Initial thickness = 0.702 cm Final thickness = 0.705 cm Initial weight = 0.460 gm Final weight = 0.492 gm									
6:45 pm	464	4.19	14.9	423	3.59	45.8	507	3.46	48.3
10:50 pm	825	3.98	15.4	783	3.16	47.8	875	3.07	57.9
1:00 pm	1090	3.77	16.1	1046	2.93	52.6	1144	2.85	59.6
1:55 pm	1094	3.94	14.8	1052	2.93	51.4	1146	2.85	56.3

Notes:

1. All measurements made with helium purge. Apparatus was not evacuated prior to determination.
2. Thermal conductivity (k_S) of specimen calculated from following equation

$$k_S = \left[\frac{k_1 \Delta T_1}{l_1} + \frac{k_2 \Delta T_2}{l_2}\right] \frac{l_S}{2\Delta T_S}$$

   where subscripts 1, 2, and s refer to top reference, bottom reference, and specimen, respectively.
3. Gage lengths: l_S = 0.705 cm, l_1 = 1.892 cm, l_2 = 1.887 cm
4. The surface temperatures of the specimen were measured. This was done by coating the surface of the specimen with a graphite paste and placing the thermocouple wires about 0.157 cm apart on the surface. Thus, the surface served as the junction of the thermocouple lead wires.

TABLE 60

THE THERMAL CONDUCTIVITY OF PHENOLIC–NYLON CHAR PREPARED IN THE FURNACE AT A RAPID HEATING RATE TO 3033°K — STRIP SPECIMEN CONFIGURATION IN RADIAL INFLOW APPARATUS - HELIUM PURGE

Specimen and run no.	Time	Outer face temp. °K	Outside hole temperature °K No. 1	Outside hole temperature °K No. 2	Inside hole temperature °K No. 1	Inside hole temperature °K No. 2	Specimen AT °K	Heat to calorimeter watts	Mean temperature °K	Thermal conductivity watts/meter-°K
Specimen 5000-R2 Run 4985-5-78	On 6:55							38.4		
=								37.5		
								36.9		
								36.9		
"								36.0		
"	Avg.	1147	1088	1090	1035	1034	54.5	37 1	1062	6.00
	10:30							65		
								58		
								64		
								59		
	Avg.	1750	1630	1634	1512	1508	122	62	1620	4.45
	12:30							82		
								81		
								80		
								78		
								79		
	Avg.	2289	2053	2061	1900	1896	159	80	2120	4.44
	2:00							107		
								105		
								107		
								105		
								106		
	Avg.	2811	2475	2473	2310	2291	174		2026	5.37
	3:00							135		
								133		
								139		
								136		
								139		
	Avg.	3144	2800	2839	2536	2555	274	136	2852	4.38

Notes:

1. Inside and outside hole temperatures below 1500°K are true temperatures as measured with thermocouples. All other inside and outside hole temperature are observed optical temperatures not true temperatures.
2. Mean temperature below 1500°K calculated as the average of thermocouples readings.
3. Mean temperature above 1500°K = T_{OF} - 1.065 AT; T_{OF} - outer face temperature

$$k = \frac{tQ}{A\,T}$$

where

k = thermal conductivity
t = distance between outside and inside hole = 0.427 cm
Q = heat to calorimeter gage section
A = area of specimen = 4.839 cm^2 (total for 4 strips)
AT = temperature drop from outside hole

TABLE 61

THE THERMAL CONDUCTIVITY OF PHENOLIC-NYLON CHARRED IN ARC-JET
AT A HEAT FLUX DENSITY OF 113 x 10^4 W/m^2
MEASURED IN COMPARATIVE ROD APPARATUS WITH PYROCERAM REFERENCES

Specimen and time	Mean temperature of specimen °K	Thermal conductivity of specimen K_S W/m-°K	ΔT through specimen °K	Mean temperature of lower reference °K	Thermal conductivity of lower reference K_1 W/m-°K	ΔT through lower reference ΔT_1 °K	Mean temperature of upper reference °K	Thermal conductivity of upper reference K_2 W/m-°K	ΔT through upper reference ΔT_2 °K
Specimen Arc-Jet 1 Run 4985-58 Density = 0.22 gm/cm^3 Initial thickness = 0.795 cm Final thickness = ---- Initial weight = 1.6368 gm Final weight = 0.4793 gm									
1:15 pm	599	0.46	63.0	445	2.81	47.2	900	2.56	63.8
6:33 pm	796	0.45	72.3	616	2.63	67.0	922	2.40	85.6

Notes:

1. Specimen was impregnated with polyalphamethylethylstyrene when built up in apparatus. Specimen was baked in apparatus at 741°K for 1 hour under roughing vacuum, prior to measurements, to remove impregnant.
2. All measurements made with nitrogen purge.
3. Thermal conductivity (k_S) of specimen calculated from following equation

$$k_S = \left[\frac{k_1 \Delta T_1}{l_1} + \frac{k_2 \Delta T_2}{l_2} \right] \frac{l_S}{2 \Delta T_S}$$

where subscripts 1, 2, and s refer to top reference, bottom reference, and specimen, respectively.

4. Gage lengths: l_S = 0.320 cm, l_1 = 1.892 cm, l_2 = 1.887 cm

TABLE 62

THE THERMAL CONDUCTIVITY OF PHENOLIC-NYLON CHARRED IN ARC-JET
AT A HEAT FLUX DENSITY OF 227 x 10^4 W/m^2
MEASURED IN COMPARATIVE ROD APPARATUS WITH PYROCERAM REFERENCES

Specimen and time	Mean temperature of specimen °K	Thermal conductivity of specimen K_S W/m-°K	ΔT through specimen °K	Mean temperature of lower reference °K	Thermal conductivity of lower reference K_1 W/m-°K	ΔT through lower reference ΔT_1 °K	Mean temperature of upper reference °K	Thermal conductivity of upper reference K_2 W/m-°K	ΔT through upper reference ΔT_2 °K
Specimen Arc-Jet 2 Run 4985-56 Density = 0.304 gm/cm^3 Initial thickness = 0.876 cm Final thickness = 0.868 cm Initial weight = 2.0685 gm Final weight = 0.7240 gm									
1:15 pm	526	1.29	30.7	416	3.61	49.2	585	3.35	57.8
2:15 pm	546	1.35	32.2	430	3.58	53.4	610	3.33	61.3
8:00 am	769	1.59	22.8	680	3.26	47.6	821	3.12	55.3
2:00 pm	1114	1.59	18.6	1043	2.92	40.9	1163	2.83	57.5

Notes:

1. Specimen was impregnated with polyalphamethylethylstyrene when built up in apparatus. Specimen was baked out at 643°K for $1\frac{1}{2}$ hours under roughing vacuum, prior to measurements, to remove impregnant.
2. All measurements made with nitrogen purge.
3. Thermal conductivity (k_S) of specimen calculated from following equation

$$k_S = \left[\frac{k_1 \Delta T_1}{l_1} + \frac{k_2 \Delta T_2}{l_2} \right] \frac{l_S}{2 \Delta T_S}$$

where subscripts 1, 2, and s refer to top reference, bottom reference, and specimen, respectively.

4. Gage lengths: l_S = 1.404 cm, l_1 = 1.892 cm, l_2 = 1.887 cm

TABLE 63

THE THERMAL CONDUCTIVITY OF THERMATOMIC CARBON-
MEASURED IN RADIAL **INFLOW** APPARATUS WITH APPARATUS A

Specimen and run no.	Time	Outer face temp. °K	Outside hole temp. °K	Inside hole temp. °K	Specimen A T °K	Heat to calorimeter watts	Mean temperature °K	Thermal conductivity $\frac{W}{m\text{-}°K}$
Specimen 1 Calorimeter A-5	On 11:30					19.9		
						19.3		
						19.6		
	12:10					19.9		
		1201	----	417	784	19.7	809	0.088
	1:30					77.6		
						76.5		
						75.9		
						76.5		
		2033	----	695	1338	76.6	1364	0.200

Notes:

1. Mean temperature calculated as the average of face (optical pyrometer) and thermocouple readings.

2. $K = \frac{\ln (D_o/D_i)}{2\pi L} \quad \frac{Q}{\Delta T}$

where

K = thermal conductivity
D_o = outside radius = 1.196 cm
D_i = inside radius = 0.904 cm
Q = heat to calorimeter
A T = temperature drop from hot to cold hole
L = gage length of calorimeter = 1.27 cm

3. Measurements made in helium purge.

TABLE 64

THE THERMAL CONDUCTIVITY OF ATJ GRAPHITE POWDER (LESS THAN 44 MICRONS PARTICLE SIZE)—MEASURED IN RADIAL INFLOW APPARATUS WITH APPARATUS A

Specimen and run no.	Time	Outer face temp. °K	Outside hole temp(1) °K	nside hole temp(1) °K	Specimen A T °K	Heat to calorimeter watts	Mean emperature °K	Thermal onductivity W/m-°K
Specimen 1 Calorimeter A-5 Density = 0.95 g/cm³						97.7 91.1 91.3 91.8		
	10:30	1160	923	681	242	93.8	802	1.34
						200 202 199 202		
	11:45	1615	1479	1041	438	201	1396	1.60
						377 379 381 381		
	1:05	2233	----	1415	818	380	1824	1.63
						416 418 419 417		
	1:40	2350	----	1496	854	418	1923	1.71

Notes:

1. Chromel/alumel thermocouples readings.
2. Mean temperature calculated as the average of thermocouples readings or as average of face and inside thermocouple reading.
3. $K = \frac{\ln (D_o/D_i)}{2\pi L} \frac{Q}{\Delta T}$

   where

   K = thermal conductivity
   D_o = outside radius = 1.196 cm
   D_i = inside radius = 0.904 cm
   Q = heat to calorimeter
   ΔT = temperature drop from hot to cold hole
   L = gage length of calorimeter = 1.27 cm
4. Measurements made in helium purge.

TABLE 65

THE THERMAL CONDUCTIVITY OF AT3 GRAPHITE POWDER (LESS THAN 44 MICRONS PARTICLE SIZE)– MEASURED IN RADIAL INFLOW APPARATUS WITH APPARATUS B

Specimen and run no.	Time	Outer face temp. °K	Outside hole temp. (1) °K	Inside hole temp. (1) °K	Specimen ΔT °K	Heat to calorimeter watts	Mean temperature °K	Thermal conductivity W/m-°K
Specimen 2 Calorimeter A-5 Density = 1.13 g/cm³						117 116 113 110		
	8:45	----	984	648	336	114	816	0.88
						195 192 186 182		
	10:00	1334	1360	825	535	189	1093	0.92
						274 270 269 270		
	11:10	1648	1694	1005	689	271	1350	1.02
						425 417 420 425		
	12:20	2034	----	1229	805	422	1632	1.36
						463 464 461 465		
	1:00	2185	----	1330	855	463	1758	1.41

Notes:

1. Pt/Pt-10 Rh thermocouple readings.
2. Mean temperature calculated as the average of thermocouple readings or as the average of the face and inside thermocouple readings.
3. $K = \frac{\ln (D_o/D_i)}{2\pi L} \frac{Q}{\Delta T}$

   where

   K = thermal conductivity
   D_o = outside radius = 1.905 cm
   D_i = inside radius = 1.549 cm
   Q = heat to calorimeter
   ΔT = temperature drop from hot to cold hole
   L = gage length of calorimeter = 1.27 cm
4. Apparatus was evacuated and backfilled with helium twice prior to making the measurements in a helium purge.

TABLE 66

THE THERMAL CONDUCTIVITY OF ATJ GRAPHITE POWDER (LESS THAN 44 MICRONS PARTICLE SIZE)-MEASURED IN RADIAL INFLOW APPARATUS WITH APPARATUS B

Specimen and runno.	Time	Outer face temp. °K	Outside hole temp.(1) °K	Inside hole temp.(1) °K	Specimen ΔT °K	Heat to calorimeter watts	Mean temperature °K	Thermal conductivity W/m-°K
Specimen 3 Calorimeter A-5 Density = 1.13 gm/cm³						133 133 123 111		
	2:50	---	1020	660	360	125	840	0.90

Notes:

1. Pt/Pt-10 Rh thermocouple readings.
2. Mean temperature calculated as the average of the thermocouple readings.
3. $K = \frac{\ln (D_o/D_i)}{2\pi L} \frac{Q}{\Delta T}$

   where

   K = thermal conductivity
   D_o = outside radius = 1.905 cm
   D_i = inside radius = 1.549 cm
   Q = heat to calorimeter
   AT = temperature drop from hot to cold hole
   L = gage length of calorimeter = 1.27 cm

4. Apparatus was evacuated and backfilled with helium twice prior to making the measurements in a helium purge.

TABLE 67

THE THERMAL CONDUCTIVITY OF POWDER MADE FROM PHENOLIC-NYLON CHARRED AT 3033°K FOR 30 MINUTES (LESS THAN 44 MICRONS PARTICLE SIZE)— MEASURED IN RADIAL INFLOW APPARATUS WITH APPARATUS B

Specimen and run no.	Time	Outer face temp. °K	Outside hole temp. °K	Inside hole temp. °K	Specimen A T °K	Heat to calorimeter watts	Mean temperature °K	Thermal conductivity $\frac{W}{m\text{-}°K}$
Specimen 1 Calorimeter A-23 Density = 1.05 gm/cm^3						62.2 61.2 63.2		
	2:30	1133	1120[1]	581[1]	539	62.2	851	0.30
						154.1 153.0 151.3		
	3:50	1971	----	896[1]	1075	152.8	1433	0.37
						249.3 254 254 263		
	5:00	2626	2569[2]	1169[2]	1400	255	1926	0.41
						523 527 521		
	6:30	3003	2886[2]	1562[2]	1324	524	2341	1.03

Notes:

1. Chromel/alumel thermocouple readings.
2. Optical pyrometer readings.
3. Mean temperature calculated as the average of thermocouple readings or as face reading minus one-half the temperature difference when all measurements were made with optical pyrometers.
4. $K = \frac{\ln (D_o/D_i)}{2\pi L} \frac{Q}{\Delta T}$

   where

   K = thermal conductivity
   D_o = outside radius = 1.905 cm
   D_i = inside radius = 1.549 cm
   Q = heat to calorimeter
   ΔT = temperature drop from hot to cold hole
   L = gage length of calorimeter = 1.27 cm
5. Measurements made in helium purge.

TABLE 68

THE THERMAL CONDUCTIVITY OF POWDER MADE FROM PHENOLIC–NYLON CHARRED AT 3033°K FOR 30 MINUTES (LESS THAN 44 MICRONS PARTICLE SIZE)– MEASURED IN RADIAL FLUX WITH APPARATUS B

Specimen and runno.	Time	Outer face temp. °K	Outside hole temp. °K	Inside hole temp. °K	Specimen ΔT °K	Heat to calorimeter watts	Mean temperature °K	Thermal conductivity $\frac{W}{m-°K}$
Specimen 2 Calorimeter A-23 Density = 0.975 gm/cm³						111.3 119.3 113.2		
	2:15	1094	1065[1]	539[1]	526	114.6	802	0.57
						272 270 270		
	3:15	1924	----	918[1]	1006	271	1421	0.70
						429 429 427		
	4100	2533	----	1132[1]	1401	428	1833	0.79
						718 727 725		
	4:30	3012	2872[2]	1501[2]	1371	723	2327	1.37

Notes:

1. Chromel/alumel thermocouple readings.
2. Optical pyrometer readings.
3. Mean temperature calculated as the average of thermocouple readings or as average of face and inside thermocouple reading. When hole temperatures were read with optical pyrometer the mean temperature was calculated as the face reading minus one–half the temperature difference.
4. $K = \frac{\ln (D_o/D_i)}{2\pi L} \frac{Q}{\Delta T}$

   where

   K = thermal conductivity
   D_o = outside radius = 1.905 cm
   D_i = inside radius = 1.549 cm
   Q = heat to calorimeter
   ΔT = temperature drop from hot to cold hole
   L = gage length of calorimeter = 1.27 cm
5. Measurements made in a helium purge.

TABLE 69

THE ELECTRICAL RESISTIVITY OF PHENOLIC-NYLON CHARRED AT 3033°K FOR 180 MINUTES

Specimen mean temperature °K	Time	Specimen circuit amps	Specimen circuit millivolts	Open circuit gage length potential millivolts	Closed circuit gage length potential millivolts	Resistivity 10^{-3}-Ω - cm	$(1 - P^{2/3})$ x Resistivity 10^{-3} - Ω- cm
Specimen machined from strip taken from thermal conductivity specimen 3F-5000-3 Density = 0.36 gm/cm^3 Gage length = 1.588 cm Diameter = 0.483 cm							
294	12:30	0.142	33.18	0.00	33.18	26.9	4.36
294		0.1235	28.80	0.00	28.80	26.9	4.36
294		0.104	24.22	0.00	24.22	26.8	4.35
1176	1:26	0.140	19.55	-0.32	19.87	16.4	2.66
1176		0.501	70.48	-0.27	70.75	16.3	2.64
1178		0.505	70.54	-0.27	70.81	16.2	2.62
1503	2:02	0.522	64.48	-0.30	64.78	14.3	2.32
1506		0.607	74.79	-0.22	75.01	14.2	2.30
1519		0.490	59.96	-0.20	60.16	14.1	2.28
1975	2:30	0.609	64.08	-1.24	65.32	12.4	2.01
1989		0.510	53.22	-1.53	54.75	12.4	2.01
2000		0.500	52.84	-1.62	54.46	12.6	2.04
2328	3:08	0.608	43.06	-17.33	60.39	11.4	1.85
2339		0.707	53.64	-16.06	69.70	11.4	1.85
2339		0.810	63.35	-16.62	79.97	11.4	1.85

Note: 1. Assumed true density was 1.5 gm/cm^3 to calculate porosity, P.

TABLE 70

THE PERMEABILITY OF PHENOLIC-NYLON CHARRED IN FURNACE AT 812°K FOR 30 MINUTES

Time	Permeating gas	Atmospheric pressure 10^3 N/m^2	Pressure drop through specimen $(P_2 - P_1)$ ΔP 10^3 N/m^2	Absolute downstream pressure P_1 10^3 N/m^2	Absolute upstream pressure P_2 10^3 N/m^2	Absolute mean specimen pressure P_m 10^3 N/m^2	Volumetric flow rate corrected to STP Q_{STP} cm^3/sec	(1) $\frac{P_m \Delta PM}{LRT\mu G}$ 10^8 cm^{-2}	(1) $\frac{G}{\mu}$ cm^{-1}
Specimen P1 A = 1.986 cm^2 L = 1.272 cm Density = 0.337 gm/cm^3									
8:35	Nitrogen	101.8	16.88	101.8	118.7	110.3	1.00	164.31	3.33
			101.5	101.8	203.3	152.6	4.42	309.24	14.70
			118.5	101.8	220.3	161.1	5.00	337.00	16.65
9:15	Helium	101.8	34.00	101.8	135.8	118.8	2.49	126.99	1.05
			67.59	101.8	169.4	135.6	5.25	136.69	2.22
			101.8	101.8	203.6	153.0	8.70	139.87	3.67
2:45	Nitrogen	101.6	118.5	101.6	220.1	160.8	5.00	336.53	16.60
8:00	Nitrogen	101.8	34.30	101.8	136.1	118.9	1.85	194.68	6.17
			50.70	101.8	152.5	127.1	2.61	218.07	8.71
			68.09	101.8	169.4	135.8	3.20	255.15	10.68
9:00	Helium	101.8	101.9	101.8	203.7	152.7	8.70	140.04	3.67
			118.8	101.8	220.6	161.2	10.01	149.71	4.23

1. $G = \frac{Q_{STP}\rho_{STP}}{A}$

TABLE 71

THE PERMEABILITY OF PHENOLIC-NYLON CHARRED IN FURNACE AT 1366°K FOR 30 MINUTES

Time	Permeating gas	Atmospheric pressure 10^3 N/m^2	Pressure drop through specimen $(P_2 - P_1)$ ΔP 10^3 N/m^2	Absolute downstream pressure P_1 10^3 N/m^2	Absolute upstream pressure P_2 10^3 N/m^2	Absolute mean specimen pressure P_m 10^3 N/m^2	Volumetric flow rate corrected to STP Q_{STP} cm^3/sec	(1) $\frac{P_m \Delta PM}{LRT \mu G_2}$ 10^8 cm^{-2}	(1) $\frac{G}{\mu}$ cm^{-1}
Specimen P2 A = 1.978 cm^2 L = 1.272 cm Density = 0.387 gm/cm^3									
9:30	Helium	101.92	35.55	101.92	137.47	119.68	0.3215	103.61	0.136
			68.53	101.92	170.45	136.19	0.7462	97.93	0.315
			102.33	101.92	204.25	153.07	1.0000	122.63	0.422
			119.14	101.92	221.06	161.47	1.4000	107.58	0.591
			102.12	101.92	204.05	152.97	1.0638	114.97	0.449
10:00	Nitrogen	101.92	16.95	101.92	118.87	110.40	0.1490	111.70	0.497
			34.57	101.92	136.49	119.21	0.3378	107.70	1.127
			51.15	101.92	153.07	127.48	0.4484	128.37	1.496
			68.09	101.92	170.02	135.95	0.6097	134.07	2.034
			102.06	101.92	203.98	152.93	0.8928	154.34	2.979
			119.04	101.92	220.96	161.44	0.9803	173.31	3.270
			34.23	101.92	136.15	119.04	0.3105	115.86	1.040

1. $G = \frac{Q_{STP} \rho_{STP}}{A}$

TABLE 72

THE PERMEABILITY OF PHENOLIC-NYLON CHARRED IN FURNACE AT 1922°K FOR 30 MINUTES

Time	Permeating gas	Atmospheric pressure 10^3 N/m^2	Pressure drop through specimen $(P_2 - P_1)$ ΔP 10^3 N/m^2	Absolute downstream pressure P_1 10^3 N/m^2	Absolute upstream pressure P_2 10^3 N/m^2	Absolute mean specimen pressure P_m 10^3 N/m^2	Volumetric flow rate corrected to STP QSTP cm^3/sec	(1) $\frac{P_m \Delta PM}{LRT\mu G}$ 10^8 cm^{-2}	(1) $\frac{G}{\mu}$ cm^{-1}
Specimen P3 A = 2.011 cm^2 L = 1.271 cm Density = 0.327 gm/cm^3									
8:30	Nitrogen	101.62	17.52	101.62	119.14	110.36	0.2500	68.28	0.834
			34.37	101.62	135.99	118.80	0.4761	75.71	1.588
			50.84	101.62	152.46	127.04	0.6896	82.69	2.300
			68.50	101.62	170.12	135.72	0.8771	93.66	2.926
			102.23	101.62	202.84	152.73	1.2500	110.27	4.170
			118.50	101.62	220.12	160.87	1.4492	116.12	4.840
9:30	Helium	101.62	34.10	101.62	135.72	118.67	0.4694	67.49	0.198
			68.03	101.62	169.64	135.61	1.0204	70.78	0.431
			102.02	101.62	203.64	152.63	2.0000	60.96	0.844
			118.60	101.62	220.22	160.90	2.4000	62.25	1.013

1. $G = \frac{Q_{STP}\rho_{STP}}{A}$

TABLE 73

THE PERMEABILITY OF PHENOLIC-NYLON CHARRED IN FURNACE AT 2480°K FOR 30 MINUTES

Time	Permeating gas	Atmospheric pressure 10^3 N/m^2	Pressure drop through specimen ($P_2 - P_1$) ΔP 10^3 N/m^2	Absolute downstream pressure P_1 10^3 N/m^2	Absolute upstream pressure P_2 10^3 N/m^2	Absolute mean specimen pressure P_m 10^3 N/m^2	Volumetric flow rate corrected to STP Q_{STP} cm^3/sec	(1) $\frac{P_m \Delta P M}{LRT\mu G}$ 10^8 cm^{-2}	(1) $\frac{G}{\mu}$ cm^{-1}
Specimen P4 A = 1.982 cm^2 L = 1.271 cm Density = 0.320 [illegible]/cm^3									
1:00	Nitrogen	101.89	17.45	101.89	119.34	110.60	0.5747	29.65	1.92
			34.44	101.89	136.32	119.11	1.0204	35.48	3.40
			51.42	101.89	153.30	127.58	1.4285	40.54	4.77
			68.47	101.89	170.35	136.12	1.7241	47.72	5.75
			67.86	101.89	169.75	135.82	2.0100	40.79	6.71
			101.89	101.89	203.78	152.83	2.8000	49.10	9.34
			119.27	101.89	221.16	161.51	3.2000	53.15	10.68
			51.48	101.89	153.37	127.61	1.5625	37.12	5.21
			68.30	101.89	170.18	136.02	1.8518	44.29	6.18
3:00	Helium	101.89	68.40	101.89	170.29	136.09	2.75	26.500	1.161
			102.19	101.89	204.08	152.97	4.51	27.136	1.904
			118.80	101.89	220.69	161.27	5.50	27.273	2.322
			34.37	101.89	136.26	119.07	1.25	25.631	0.528

1. $G = \frac{Q_{STP} \rho_{STP}}{A}$

TABLE 74

THE PERMEABILITY OF PHENOLIC-NYLON CHARRED IN FURNACE AT 3033°K FOR 30 MINUTES

Time	Permeating gas	Atmospheric pressure 10^3 N/m^2	Pressure drop hrough specimen $(P_2 - P_1)$ ΔP 10^3 N / m^2	Absolute downstream pressure P_1 10^3 N/m^2	Absolute upstream pressure P_2 10^3 N/m^2	Absolute mean specimen pressure P_m 10^3 N/m^2	Volumetric flow rate corrected to STP Q_{STP} cm^3/sec	(1) $\frac{P_m \Delta P M}{LRT\mu G}$ 10^8 cm^{-2}	(1) $\frac{G}{\mu}$ cm^{-1}
Specimen P5 A = 1.993 cm^2 L = 1.270 cm Density = 0.310 gm/cm^3									
12:30	Helium	101.55	34.06	101.55	135.61	118.57	1.923	16.443	0.812
			102.36	101.55	203.91	152.73	6.100	20.065	2.575
			119.61	101.55	221.16	161.34	7.500	20.145	3.167
1:15	Nitrogen	101.55	17.28	101.55	118.84	110.19	0.9009	18.665	3.006
			34.40	101.55	135.95	118.73	1.5151	23.801	5.055
			17.39	101.55	118.94	110.23	0.8264	20.473	2.757
			33.93	101.55	135.48	118.50	1.1405	24.140	4.905
			51.28	101.55	152.83	127.17	2.0000	28.788	6.673
			40.51	101.55	142.06	121.81	1.6129	27.010	5.381
			44.83	101.55	146.38	123.97	2.0000	24.533	6.673

1. $G = \frac{Q_{ST}\ \rho_{STP}}{}$

TABLE 75

THE PERMEABILITY IN CHARRING DIRECTION OF PHENOLIC-NYLON CHARRED IN FURNACE AT RAPID RATE TO 3033°K

Time	Permeating gas	Atmospheric pressure 10^3 N/m^2	Pressure drop through specimen $(P_2 - P_1)$ ΔP 10^3 N / m^2	Absolute downstream pressure P_1 10^3 N/m^2	Absolute upstream pressure P_2 10^3 N/m^2	Absolute mean specimen pressure P_m 10^3 N/m^2	Volumetric flow rate corrected to STP Q_{STP} cm^3/sec	(1) $\frac{P_m \Delta P M}{LRT \mu G}$ 10^6 cm^{-2}	(1) $\frac{G}{\mu}$ cm^{-1}
Specimen 5000-R3 A = 1.606 cm^2 L = 0.704 cm Density = 0.266 gm/cm^3									
8:35	Helium	99.45	1.05	99.58	100.63	100.11	89	1.34	46
			2.41	99.72	102.13	100.92	195	1.42	102
			4.21	99.91	104.12	102.01	334	1.46	174
			1.53	99.62	101.14	100.38	130	1.34	68
9:30	Nitrogen	99.45	0.717	99.61	100.32	99.96	58	1.58	239
			1.28	99.73	101.01	100.37	108	1.53	444
			2.30	99.89	102.21	101.05	148	2.02	609
			4.23	99.99	104.22	102.10	234	2.37	962
			6.17	100.01	106.18	103.09	309	2.64	1271
			7.71	100.03	107.74	103.89	366	2.81	1505

1. $G = \frac{Q_{STP} \rho_{STP}}{A}$

TABLE 76

THE PERMEABILITY IN CHARRING DIRECTION OF PHENOLIC-NYLON CHARRED IN ARC-JET AT 227×10^4 W/m²

Time	Permeating gas	Atmospheric pressure (10^3 N/m²)	Pressure drop through specimen ($P_2 - P_1$) ΔP (10^3 N/m²)	Absolute downstream pressure P_1 (10^3 N/m²)	Absolute upstream pressure P_2 (10^3 N/m²)	Absolute mean specimen pressure P_m (10^3 N/m²)	Volumetric flow rate corrected to STP Q_{STP} (cm³/sec)	(1) $\frac{P_m \Delta PM}{LRT\mu G}$ (10^6 cm^{-2})	(1) $\frac{G}{\mu}$ (cm^{-1})	Remarks
Specimen 1										
A = 2.029 cm²										
L = 0.833 cm										
Density = 0.295 gm/cm³										
10:50	Helium	99.9	0.522	100.0	100.5	100.2	70	0.91	29	RTV 735 silastic sealant used
			1.057	100.0	101.1	100.5	145	0.89	60	
			1.555	100.1	101.6	101.0	207	0.92	85	
			2.015	100.2	102.2	101.2	265	0.94	109	
11:00			2.537	100.3	102.8	101.6	337	0.94	139	
11:10	Nitrogen	99.9	0.522	100.0	100.5	100.3	70	1.03	228	
			1.057	100.2	101.3	100.7	127	1.15	413	
			1.505	100.4	101.9	101.1	163	1.28	531	
			2.053	100.4	102.5	101.4	208	1.37	677	
			2.525	100.4	102.9	101.7	245	1.44	798	
1:45	Nitrogen	99.6	0.801	99.8	101.6	100.2	101	1.09	329	
			1.306	100.0	101.3	100.7	148	1.22	482	
			1.766	100.1	101.9	101.0	184	1.33	599	
			2.281	100.1	102.4	101.3	227	1.39	739	
2:15	Helium	99.6	0.784	99.7	100.5	100.1	107	0.89	44	
			1.284	99.8	101.1	100.4	173	0.91	71	
			1.761	99.9	101.7	100.7	239	0.90	98	
			2.296	100.0	102.3	101.1	304	0.93	128	

1. $G = \frac{Q_{STP}\,\rho_{STP}}{A}$

TABLE 77

THE PERMEABILITY IN CHARRING DIRECTION OF PHENOLIC-NYLON CHARRED IN ARC-JET AT 227×10^4 W/m^2

Time	Permeating gas	Atmospheric pressure (10^3 N/m^2)	Pressure drop through specimen $(P_2 - P_1)$ ΔP (10^3 N / m^2)	Absolute downstream pressure P_1 (10^3 N/m^2)	Absolute upstream pressure P_2 (10^3 N/m^2)	Absolute mean specimen pressure P_m (10^3 N/ m^2)	Volumetric flow rate corrected to STP Q_{STP} (cm^3 / sec)	(1) $\frac{P_m \Delta PM}{LRT\mu G}$ (10^6 cm^{-2})	(1) $\frac{G}{\mu}$ (cm^{-1})
Specimen 2									
A = 1.978 cm^2									
L = 0.683 cm									
			0.488	99.7	100.2	99.9	72	0.98	30
3:30	Helium	99.5	0.769	99.7	100.5	100.0	114	0.98	48
			0.995	99.7	100.7	100.2	145	0.99	61
			1.261	99.7	101.0	100.3	178	1.03	75
			1.513	99.8	101.3	100.5	212	1.04	90
			1.809	99.8	101.6	100.7	255	1.03	108
			2.055	99.9	102.0	100.9	287	1.04	121
			2.264	99.9	102.2	101.0	314	1.05	133
			3.020	100.1	103.1	101.6	401	1.11	169
			0.525	99.7	100.2	99.9	76	1.12	254
4:00	Nitrogen	99.5	0.774	99.8	100.6	100.1	104	1.21	347
			1.020	99.9	100.9	100.4	132	1.26	441
			1.259	100.0	101.3	100.6	152	1.36	508
			1.520	100.1	101.6	100.8	175	1.43	584
			1.764	100.1	101.9	100.9	198	1.46	661
			2.015	100.1	102.1	101.1	217	1.53	725
			2.269	100.1	102.4	101.2	241	1.55	805
			2.513	100.1	102.6	101.3	262	1.58	875

$$G = \frac{Q_{STP}\ \rho_{STP}}{A}$$

TABLE 78

SUMMARY OF PERMEABILITY DATA

Specimen	Char conditions	Density gm/cm^3	Darcy's constant K in $10^{-10} cm^2$	Inertial flow coefficient β_g in 10^{-1} cm
Arc-jet 1	Charred in arc-jet at 227×10^4 W/m^2	0.295	11,800	0.00076
Arc-jet 2	Charred in arc-jet at 227×10^4 W/m^2	-----	10,500	0.00076
5000-R3	Charred in furnace at rapid rate to 3033°K	0.266	7,750	0.0010:3
P1	Charred in furnace at slow rate to 812°K	0.337	0.95	1400
P2	Charred in furnace at slow rate to 1366°K	0.387	1.05	2100
P3	Charred in furnace at slow rate to 1922°K	0.327	1.82	1300
P4	Charred in furnace at slow rate to 2480°K	0.320	4.17	270
P5	Charred in furnace at slow rate to 3033°K	0.310	6.72	200

TABLE 79

SUMMARY OF SONIC VELOCITY MEASUREMENTS

Specimen	Char preparation	Bulk density, gm/cm^3	Velocity 10^4 cm/sec	ρV^2 $0^9 N/m^2$
TC1-spare	Slow heating rate to 812°K - 30 minutes at temp.	0.303	22.0 - a[1]	1.47
	" "	0.303	18.1 - borc	0.99
	" "	0.303	18.7 - borc'	1.06
TC8S	Slow heating rate to 1366°K - 30 minutes at temp,	0.365	27.4 - borc	2.73
TC6S	Slow heating rate to 1922°K - 30 minutes at temp.	0.321	26.0 - borc'	2.17
3000-1A	" "	0.330	29.1 - a'	2.79
	" "	0.330	25.4 - borc	2.13
	" "	0.330	27.7 - borc	2.53
3000-1B	" "	0.330	25.9 - borc	2.21
	" "	0.330	27.0 - borc	2.41
3000-1C	" "	0.330	25.2 - borc	2.10
	" "	0.330	24.9 - borc	2.05
	" "	0.330	27.8 - borc	2.55
	" "	0.330	26.9 - borc	2.39
TC7S	Slow heating rate to 2480°K - 30 minutes at temp	0.330	26.1 - c	2.24
4F5000-5	Slow heating rate to 3033°K - 5 hours at temp.	0.353	24.7 - c	2.14
Rapid furnace char	Rapid heating rate to 3033°K - 5 minutes at temperature, measured in charring direction	0.266	23.6 - c	1.47
Arc-jet char	Prepared in arc-jet at 2.27 MW/m^2	0.300	21.3 - c	1.35

Note::

1. Configuration of blanks charred

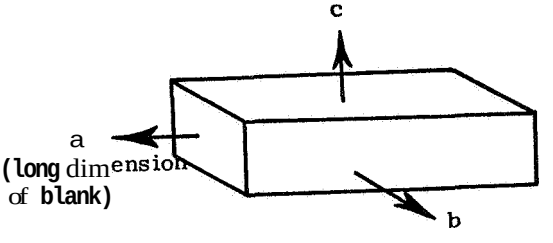

"a" direction represents "a-b" plane in virgin billet. The "b-c" directions are the charring directions where one or the other was in the "c" direction of the virgin billet.

REFERENCES

1 Kratsch, K M., Hearne, L F., and McChesney, H. R · Thermal Performance of Heat Shield Composites During Planetary Entry. Presented at AIAA-NASA National Meeting (Palo Alto, Calif.), Sept. 30 - Oct. 1, 1963.

2. Wilson, R. Gale: Thermophysical Properties of Six Charring Ablators from 140" to 700°K and Two Chars from 800" to 3000°K NASA TN D-2991, October 1965.

3. Nagler, Robert G The Thermal Conduction Process in Carbonaceous Chars JPL Technical Report 32-1010, February 1, 1967

4. Swann, Robert T , Pittman, Claud M.; and Smith, James C , Jr One-Dimensional Numerical Analysis of the Transient Response of Thermal Protection Systems. NASA TN D-2976, 1965.

5 Pittman, Claud M , and Brewer, William D.· Analytical Determination of the Effect of Thermal Property Variations on the Performance of a Charring Ablator. NASA TN D-3486, 1966.

6 McLain, Allen G.; Sutton, Kenneth; and Walberg, Gerald D,· Experimental and Theoretical Investigation of the Ablative Performance of Five Phenolic-Nylon-Based Materials. NASA TN D-4374, 1968.

7. Keller, L. B Development of Characterized and Reproducible Syntactic Foam of Phenolic-Nylon for Heat Shields. NASA CR-73041, 1966.

8. Gillis, Gerald F., Pears, Coultas D., and Oglesby, Sabert: Thermal and Mechanical Properties of Low Density Phenolic-Nylon and Filled Silicone Resin, 6617-1531-1-V NAS 1-2078, T O 1

9. Smyly, E D.; Pyron, C M. ,Jr , and Pears, C. D. An Investigation of the Mechanisms of Heat Transfer in Low-Density Phenolic-Nylon Chars. NASA CR-966, 1967.

10. Pears, C D.; and Allen, J G. The Thermal Properties of Twenty-Six Solid Materials to 5000°F or Their Destruction Temperatures ASD TDR 62-765, August 1962.

11 Greenberg, D. B ; and Weger, E.· An Investigation of the Viscous and Inertial Coefficients for the Flow of Gases through Porous Sintered Metals with High Pressure Gradients. Chemical Engineering Science, Vol. 12, Pergamon Press, Ltd., London, 1969, pp. 8-19.

12 Russell, H. W. Principles of Heat Flow in Porous Insulations Journal of the American Ceramic Society, Vol, 18, No. 1, 1935, pp. 1-5.

13. Jakob, Max: Heat Transfer - Volume II, John Wiley and Sons, Inc , New York, 1957, pp. 54-62.

14 Gardon, R. The Apparent Thermal Conductivity of Diathermanous Materials. Proceedings of the Second Conference on Thermal Conductivity, Division of Applied Physics, National Research Council, Ottawa, Ontario, 1962, pp 167-188

15. Larkin, Bert K., and Churchill, Stuart W Heat Transfer by Radiation through Porous Insulations, Journal of the American Institute of Chemical Engineers, Vol. 5, No. 4, 1959, pp. 467-474.

16 Deissler, R. G., and Boegli, J S An Investigation of Effective Thermal Conductivities of Powders in Various Gases. Transactions of the A S, M. E., Vol. 80, 1958, pp. 1417-1425.

17 Stevens, D. W. Thermal Conductivity of Beds of Coated Fuel Particles Nuclear Applications, Vol. 3, 1967, pp. 626-634.

18, Yagi, S , and Kunii, D. Studies on Effective Thermal Conductivities in Packed Beds. Journal of the American Institute of Chemical Engineers, 3, 373, 1957

19 Perry, H. A , Anderson, H. C.; and Mihalow, F A. Behavior of Reinforced Plastics in Contact with Hot Gases. Part III. Experiments. Fifteenth Annual Technical Conference of the Society of Plastic Engineers, Vol. 5, New York, 1959, p 70-111-1

20. Kobayashi, K. ; Sugawara, S. ; Toyoda, S., and Honda, H An X-Ray Diffraction Study of Phenol-Formaldehyde Resin Carbons Carbon, Vol. 6, No. 3, June 1968, pp. 359-364.

21. Dollimore, D., and Heal, G. R. The Degradation of Selected Polymers to Carbons in an Inert Atmosphere. Carbon, Vol. 5, No. 1, February, 1967, pp. 65-72,

22. Mizushima, S. On the Crystallite Growth of Carbon, Proceedings of the Fourth Conference on Carbon. Pergamon Press, New York, 1960, pp. 417-422.

23. Kotlensky, W. V.; and Walker, P L., Jr. Crystallographic and Physical Changes of Some Carbons upon Oxidation and Heat Treatment, Proceedings of the Fourth Conference on Carbon. Pergamon Press, New York, 1960, pp. 423-442.

24. Clayton, W.A., Kennedy, P.B., Evans, R.J., Cotton, J E., and Francisco, A. C., of The Boeing Company Aerospace Group; Fabish, T. J.; Eldridge, E. A ; and Lagedrost, J. F., of Battelle Memorial Institute, Columbus Laboratories Thermal Properties of Ablative Chars Air Force Materials Laboratory Report No. TR-67-413, January, 1968.

25. Ruben, Samuel: The Elements. Howard W. Sams and Company, Inc., The Bobbs-Merrill Company, Inc., 1965.

26. Engelke, W. T.; Pyron, C M, , Jr.; and Pears, C D. Thermophysical Properties of a Low-Density Phenolic-Nylon Ablation Material. NASA CR-809, 1967.

27 Davidson, H. W , and Losty, H. H. W Impermeable Cellulose Carbon G. E C Journal, Vol. 30, No. 1, 1963, pp. 22-30.

28 Strauss, Howard E Studies of Thermal Conductivity of Polycrystalline Graphite at High Temperature Proceedings of the Fourth Conference on Carbon, Pergamon Press, New York, 1960, pp. 473-482.

29. Ho, C Y., Powell, R. W ; and Liley, P E. Thermal Conductivity of Selected Materials, Part 2. NSRDS-NBS16 National Standard Reference Data Series - National Bureau of Standards - 16 (Category 5 - Thermodynamics and Transport Properties). U S. Government Printing Office, Washington, D C., February 1968. pp. 82-88.

REFERENCES - Continued

30. Mason, I. B. ; and Knibbs, R. H. : The Thermal Conductivity of Artificial Craphites and Its Relationship to Electrical Resistivity. UKAEA Report AERE-R 3973, 1-22, 1962.

31. Autio, G. W. ; and Scala, E. : The Normal Spectral Emissivity of Isotropic and Anisotropic Materials. Carbon, Vol. 4, No. 1, May 1966, pp. 13-28.

32. Tompkins, Stephen S. : A Study of the Simulation of the Flight Performance of Charring Ablators. Masters Thesis presented to the Faculty of the School of Engineering and Applied Science, University of Virginia, June 1968.

33. Grindle, Shirley L. : Thermal Testing of Government-Furnished Models. Space General Corporation Report No. SGC 1038-F1. Space General Corporation, El Monte, California, July 1966.

34. Kreith, Frank: Principles of Heat Transfer. International Textbook Company, Scranton, Pennsylvania, 1962, pp. 318-319.

35. Thermophysical Properties Research Center: Data Book, Volume 2, Nonmetallic Elements, Compounds, and Mixtures, Purdue University, Lafayette, Indiana, 1964.

36. Powell, R. W. ; Ho, C. Y. ; and Liley, P. E. : Thermal Conductivity of Selected Materials. NSRDS-NBS8 (Category 5 - Thermodynamic and Transport Properties). U. S. Government Printing Office, Washington, D. C., November, 1966.

37. Yamada, Shigehiko: A Review of Glasslike Carbon. DCIC Report 68-2. DCIC, Columbus, Ohio. April 1968.

APPENDIX

APPENDIX A

DOCUMENTATION SUPPLIED BY HUGHES AIRCRAFT FOR THE FORMULATION AND MOLDING CONDITIONS OF THE LOW-DENSITY PHENOLIC-NYLON SUPPLIED UNDER CONTRACT NAS 1-6832

1. Composition

Zytel 103 (-120 mesh)	40 PBW
Phenolic Microballoons (-50 to +230 mesh fraction)	23 PBW
Hughes HFN Novolac	37 PBW

The above composition is corrected for the amount of volatiles in each constituent, as follows:

$$\text{Corrected Wt} = W/100-X \times 100$$

where W = weight of the constituent and X is the volatiles content of the constituent

2. Formulation for 3" Thick x 12" Diameter Billets

Constituent	Uncorrected Weight, gm	Volatile Content, %		Corrected Weight, gm
Zytel 103	1264	1.36		1281
Phenolic Microballoons	727	2.54		746
Hughes HFN Novolac	1169	2.56		1200
			Total	3227
				28
			Total	3255 gm

(The billet loses approximately 95 gm during postcure to give an approximate final weight of 3160 gm)

3. Mixing of Formulation

Sufficient Zytel 103, Microballoons and Novolac HFN is blended to mold three billets. Each constituent is sifted through a 40 mesh sieve into a drum tumbler. The mixture is tumbled for 30 minutes.

4. Preparation of Preform

The corrected charge weight (3255 gm) is carefully distributed into a $12\frac{1}{2}$" diameter cylindrical, polypropylene container by sifting through a 40 mesh sieve. Leveling of the material in the preform is accomplished by sweeping the surface lightly with a special tool mounted in a standard drill press. Under no circumstance is the material leveled by compaction.

5. Dielectric Preheating

Preheating is accomplished in a Votator CP-30A dielectric heater. The initial reading should be 0.3 to 0.4 ma. The material is heated dielectrically until the reading is 1.4 ma. (approximately 55 seconds, depending on volatiles content). As a result of preheating, the Novolac resin particles will soften sufficiently to fuse the powdered charge into one large cylindrical preform. During this heating, the diameter of the preform will decrease to approximately 12 inches.

6. Molding

The hot preform is placed in a 12-inch diameter cylindrical mold maintained at a temperature of 275°F. Sufficient pressure is applied to close the mold to 3-inch lands. Total time is 3 hours at 275°F, after which the part is ejected hot.

7. Postcure

Postcuring is accomplished in a sealed canister in an atmosphere of argon. The oven temperature is increased from room temperature to 350°F over a period of 12 hours and from 350°F to room temperature over a period of 4 - 6 hours.

APPENDIX B

DESCRIPTION OF CONSTITUENTS (OR SIMILAR MATERIALS) USED IN FORMULATING THE BILLETS OF LOW-DENSITY PHENOLIC-NYLON

The following detailed description of each constituent within the low-density phenolic-nylon was supplied by the NASA Langley Research Center.

Union Carbide BRP-5549 Phenolic Resin

The properties of the resin as published by the manufacturer are shown in the table below

Property	Property Value
Density	16.8 to 19.4 lb/ft^3 (270 to 310 kg/m^3)
Sieve Analysis (U. S. Std. Mesh)	
on 40 mesh	0.0%
on 100 mesh	0.6%
on 200 mesh	2.0%
through 200 mesh	98.0%
Hexamethylene tetramine content	8.7 - 9.5%

Measurements with a Coulter Counter (Coulter Electronics Industrial Division) at the Langley Research Center indicate that the range of diameters of the phenolic resin powder particles is 0.0001 to 0.0048 in. (2 to 120 μm) with about 80 percent by volume of powder having diameters ranging from 0.0003 to 0.0023 in. (6 to 58 pm).

Phenolic Microballoons

The properties of the Microballoons as published by the manufacturer are given in the following table:

Property	Property Value
Density (liquid displacement)	15.6 lb/ft^3 (250 kg/m^3)
Density (air displacement)	18.7 lb/ft^3 (300 kg/m^3)
Flotation in toluene dupanol solution	Not less than 90% must float
Average particle size (dia)	0.0017 in. (43 μm)
Size range (dia)	0.002 to 0.0005 in. (13 to 51 pm)

Measurements with the Coulter Counter indicate that the range of diameters of the phenolic Microballoons is 0.0004 to 0.0100 in. (10 to 250 pm), with approximately 85 percent by volume of the Microballoons having diameters ranging from 0.0024 to 0.0080 in. (60 to 200 pm).

Nylon

Properties of the nylon powder as given by the manufacturer are listed in the table below:

Property	Property Value
Specific Gravity	1.3 - 1.15
Melting Point	482 - 500°F (523 - 533°K)
Tensile Strength	11,800 psi (81.4 MN/m^2)
Coefficient of Linear Thermal Expansion	45.0 x 10^{-6} in. /in. -°F (81.1 x 10^{-6} m/m-°K)$_2$
Thermal Conductivity	1.31 x 10^{-4} Btu-in. /ft^2-sec-°F 0.068 W/m-°K
Specific Heat	0.3 - 0.5 Btu/lb-°F 1.25 to 2.09 kJ/kg - "K

Preliminary studies using a Coulter Counter indicate that about 85 percent by volume of the nylon powder lies in the range from about 0.0012 to 0.0157 in. (30 to 400 μm) in diameter, with about 5 percent below 30 μm and 10 percent above 400 μm.

APPENDIX C

ULTIMATE STRENGTH, ELASTIC MODULUS, AND POISSON'S RATIO TO 5500°F IN TENSION

A typical tensile facility is shown in the photograph in figure C1 and in the schematic in figure C2. The primary components are the gas-bearings, the load frame, the mechanical drive system, the 5500°F furnace, the optical strain analyzers, and associated instrumentation for measurement of load and strain The load capacity is 15,000 pounds

The load frame and mechanical drive system are similar to those of many good facilities The upper crosshead is positioned by a small electric motor connected to a precision screw jack This crosshead is stationary during loading and is moved only when assembling the load train The lower crosshead is used to apply the load to the specimen through a precision screw jack chain driven by a variable speed motor and gear reducer.

Nonuniaxial loading, and therefore bending stresses, may be introduced in tensile specimens not only from (1) misalignment of the load train at the attachment to the crossheads, but also from (2) eccentricity within the load train, (3) unbalance of the load train, and (4) external forces applied to the load train by such items as electrical leads and clip-on extensometers. Although the bending moments from some of these sources may seem relatively slight, the resulting stress distortions are quite significant in the evaluation of the extremely sensitive brittle materials Now consider each individually

To confirm that the gas-bearings had eliminate nonuniaxial loading at the point of attachment of the load train to the crossheads, the frictional moment was determined at a load of 5000 pounds by measuring the torque required to produce initial motion within the system with the bearings in operation This torque was found to be a maximum of 6 6 x 10^{-3} inch-pounds, The equation

$$M_o = \frac{2\mu P}{3} \left[\frac{R_2^3 - R_1^3}{R_2^2 - R_1^2} \right] \qquad (1)$$

was then applied to the system to calculate the kinetic friction where M_o was the resisting moment due to kinetic friction and μ represented the coefficient of kinetic friction. The calculated value of μ was then equal to

a maximum of only 4.5×10^{-7}.

The classic equation

$$S = \frac{Mc}{I} \qquad (2)$$

was then employed to obtain the stress that could be induced in the specimen due to this bending moment. This value was 0.16 psi, or less than 0,002 percent of the tensile stress produced within a typical graphite specimen. These low values clearly indicate the elimination of problems of bending stress in the specimen imposed by misalignment at the crosshead attachments, either initially or during loading.

Emphases in the design of the load train were placed on (1) large length-to-diameter ratios at each connection, (2) close sliding fits (less than 0.005 inch) of all mating connections, (3) the elimination of threaded connections, (4) the use of pin connections wherever possible, and (5) increasing the size of components to permit precise machining of all mating surfaces. All members were machined true and concentric to within 0.0005 inch, and the entire load train was checked regularly to ensure overall alignment following assembly of the individual members. This process ensures concentricity and no kinks in the system.

The problems of unbalance within the load train and of external forces applied to the load train have been explored and corrected. The entire load train is statically balanced to less than 0.01 inch-pound for normal operation.

One configuration of the tensile specimen is shown in figure C3. This specimen provides a relatively large L/D ratio in the gripping are to ensure good alignment. All surfaces in the gripping area are cylindrical in order to make precision machining easier and repeatable from specimen to specimen. This specimen also has double breakdown radii from the gripping area to the gage section. This double breakdown allows a uniform transition of the stress pattern and reduces the frequency of radius (out of gage) fractures. This specimen provides a uniform gage section which gives a definable volume of material under stress and permits accurate measurements of strain, The flags for the measurement of axial strain are positioned one inch apart so that unit strain is recorded directly, The flag attachment for measurement of lateral strain is positioned between the flags for axial strain; see figure C4.

A schematic of the precision tensile grip is shown in figure C5. The design is much like the jaws of a lathe head or the chuck of a drill motor made with precision. Observe from the figure the long surface contact of the mating parts and the close fits to establish precise alignment with the specimen. As the load is applied, the wedges maintain alignment to fracture.

Figure C6 is a sketch of the 5500°F furnace used for tension showing the basic components. The furnace consists of a resistively heated graphite element insulated from a water-cooled shell by thermatomic carbon. The furnace and specimen are purged with helium to provide an inert atmosphere. Ports with visual openings are provided on opposite sides of the furnace as a means of allowing the strain analyzers to view the gage flags on the specimen. Specimen temperatures are determined by optical pyrometer readings taken through another small sight port containing a sapphire window. A calibration curve was established for the loss through the sapphire window, and since the furnace cavity acts essentially as a blackbody, true temperature readings are obtained. Power is supplied to the heating element by means of a 25 KVA variable transformer.

Strain measurement consists of measuring optically the elongation between two flags, or targets, which are mounted on the specimen and separated initially by a predetermined gage length. The travel of the targets is measured by sensing the displacement of the image of the edge of the targets and then electromechanically following the image displacement. The relative travel of the two targets provides the strain. Readout is continuous and automatic on a millivolt recorder. A schematic of the analyzer is shown in figure C7.

A brief summary of the mechanical motions of the components involved in monitoring the strain is helpful in understanding the detailed performance. A tracking telescope follows the upper target and carries a second telescope mounted on its carriage. The second telescope is capable of independent motion to follow the lower target. The relative displacement between the upper and lower telescope, as strain occurs, defines the strain. The system usually is operated so that the tracking telescope follows the upper target and the strain is monitored by the relative displacement of the aperture rather than the telescope following the lower target. With this procedure the maximum range is the maximum displacement available for the lower aperture, or about $\frac{1}{8}$ inch, and the sensitivity is limited by the optics and the noise level of the detector. Using both telescopes, the range is about $\frac{3}{4}$ inch.

To provide optical references on the specimens, targets are affixed to the test specimen as mentioned. When the specimen is heated to temperature, the targets are self-luminous and are observed optically. The optics view past the luminous targets into a cooled cavity in the opposite furnace wall. The self-luminous targets are then visible against a dark background. To obtain data below 2000°F, a light beam is directed from behind the flags providing a shadow image for the detection system.

The image of the flowing target is focused through a rotating shutter (chopper) and onto a rectangular aperture. Small slits in the aperture pass a portion of the upper and lower edges of the light beam. A photocell receives the light thus transmitted, and an electronic circuit detects whether the energy passed by the two slits is equal. A servo drives the apertures to let a balanced quantity of light pass through the two slits and thus maintains an optical null.

To obtain lateral strain, a strain analyzer is supported horizontally on the tensile frame to view the diametrical or lateral strain of the specimen. A flag attachment, with the general configuration as shown in figure C8, was developed to follow and transmit lateral motions of up to a few mils. The three-piece assembly consists of a ring and two rams bearing on the specimen.

Calibrations of the analyzers are performed in various ways including absolute correlations to precision micrometers, strain gage extensometers, and direct plots of stress-strain for reference materials such as steel, Plexiglas, magnesium, and aluminum. Precision is within ± 0.000020 inch.

Instrumentation includes primarily a stress-strain measurement system composed of a 1000-pound SR-4 Baldwin load cell, constant d. c. voltage power supply, two optical strain analyzers, and two X-Y recorders. Specimen temperature is monitored with an optical pyrometer. Stress (load) is measured by a commercial load cell. The cell receives a constant d. c. voltage input from the power supply and transmits a millivolt signal (directly proportional to load) to an X-Y recorder. Simultaneously, the optical strain analyzers measure both the axial and lateral strain and transmit a millivolt signal (proportional to strain) to the X-Y recorders. Thus, continuous plots of stress-axial strain and axial strain-lateral strain are recorded simultaneously.

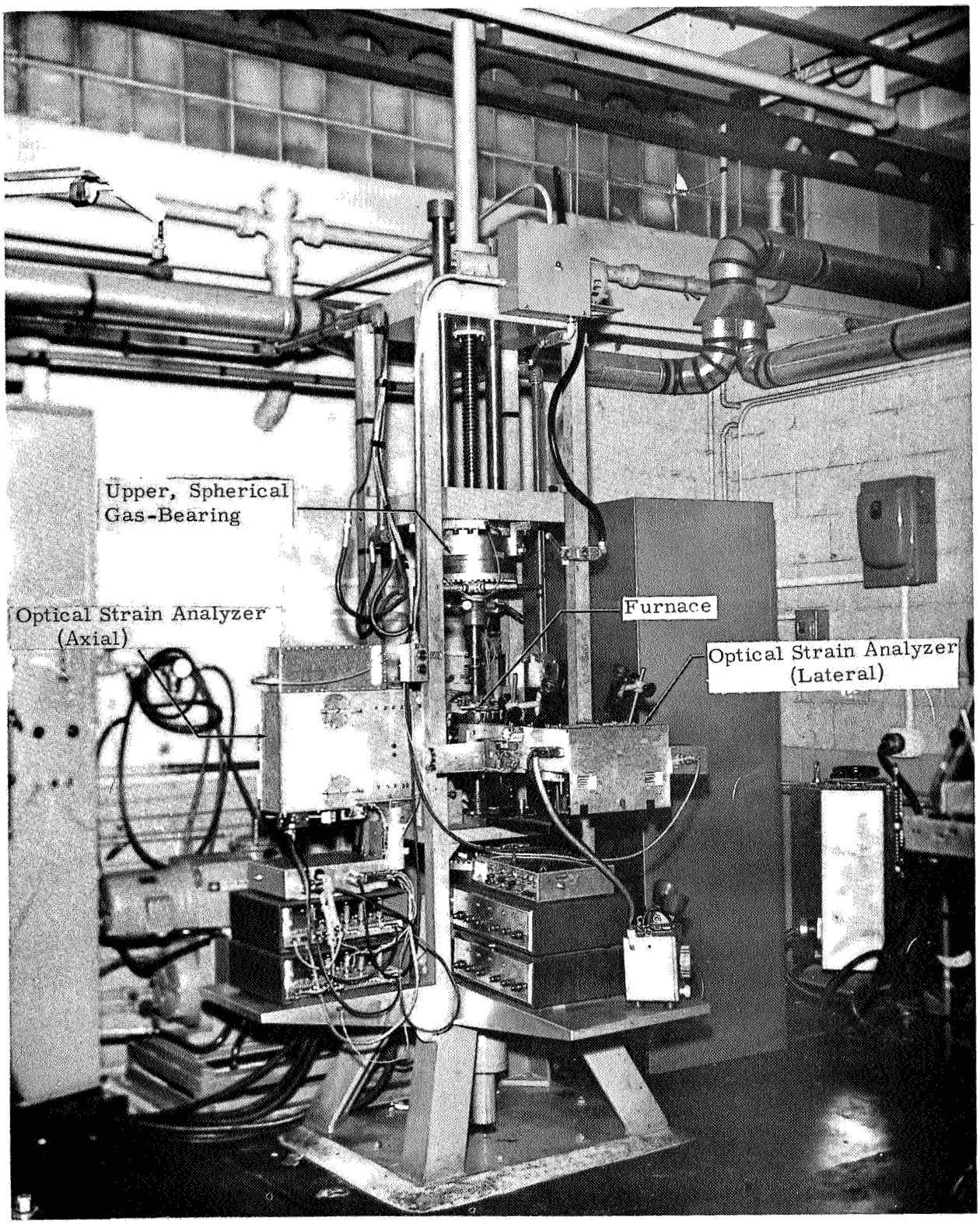

Figure C1. Picture of a tensile stress-strain facility

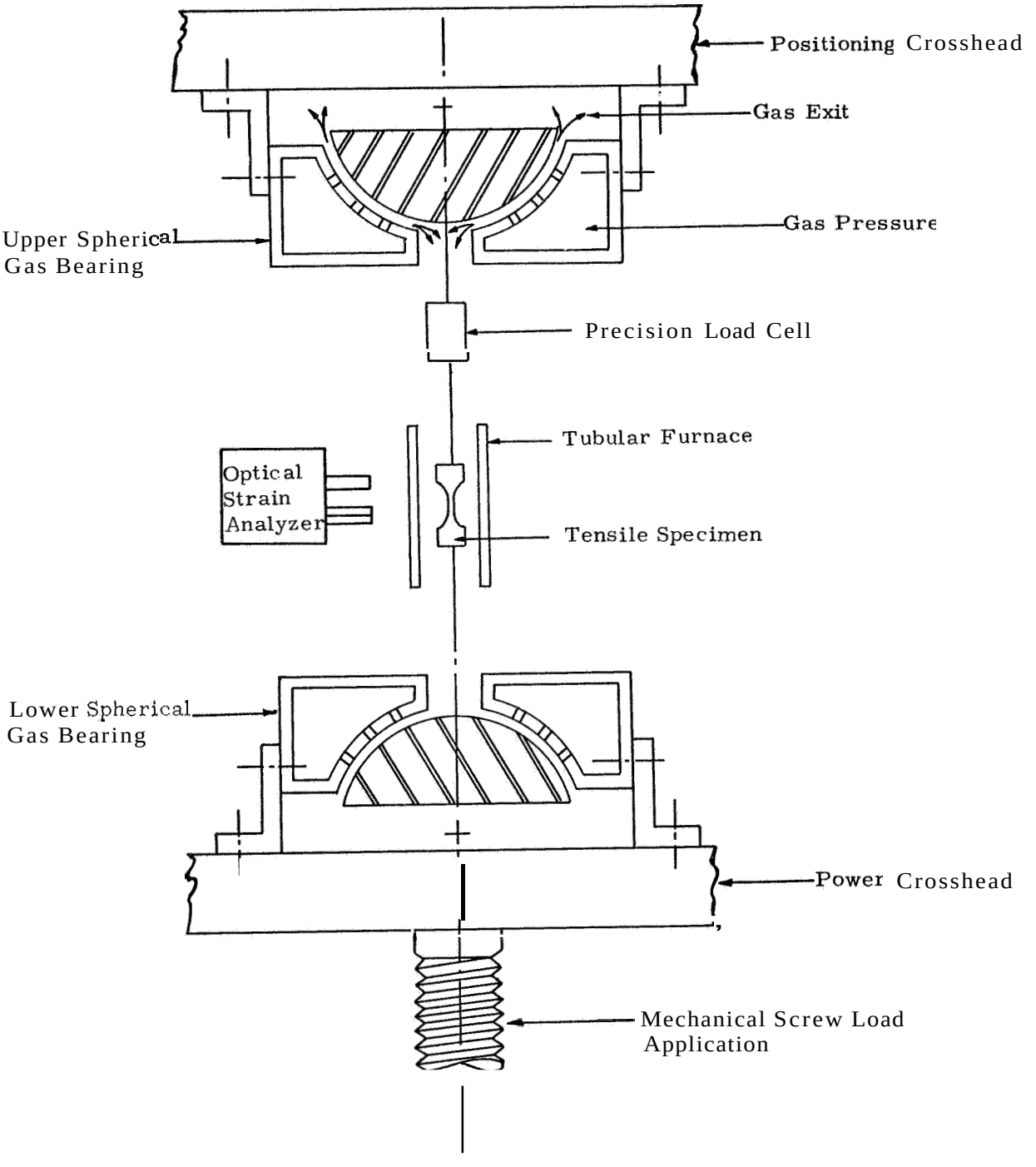

Figure **C2.** Schematic of the gas bearings and load train for the tensile apparatus

Notes:

1. All Diameters True and Concentric to Within 0.0005"
2. Do Not Undercut Radii At Tangent Points
3. Both Ends Flat and Perpendicular to and to Within 0.0005"
4. All Dimensions are in Inches
5. Tolerances are $\pm$ 0.001 on Diameters
   $\pm$ 0.005 on Lengths
   $\pm \frac{1}{64}$ on Fractions

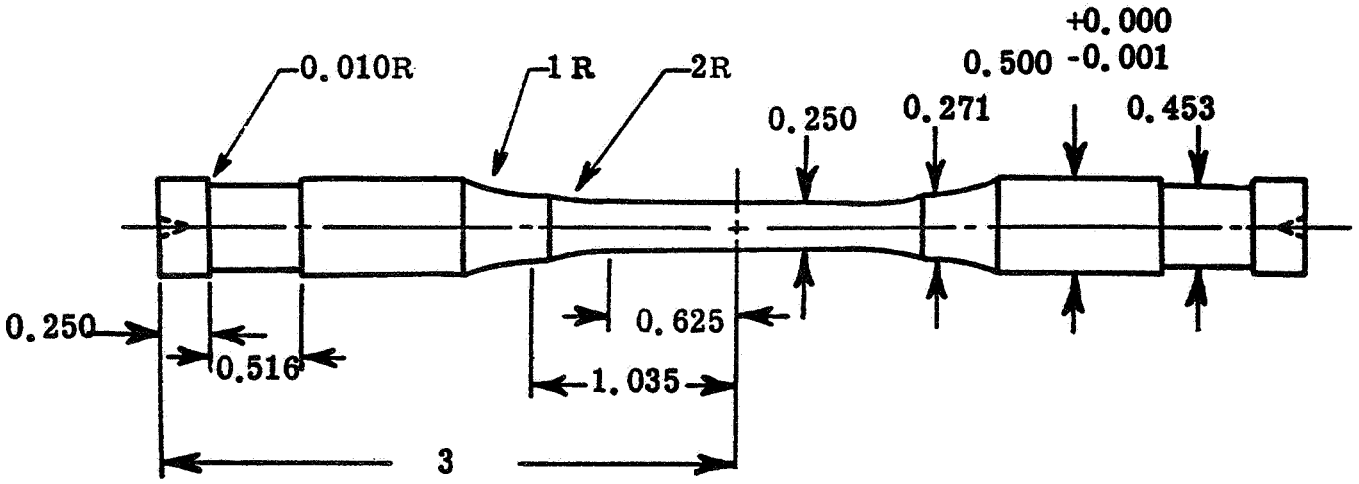

Figure C3. Tensile specimen configuration

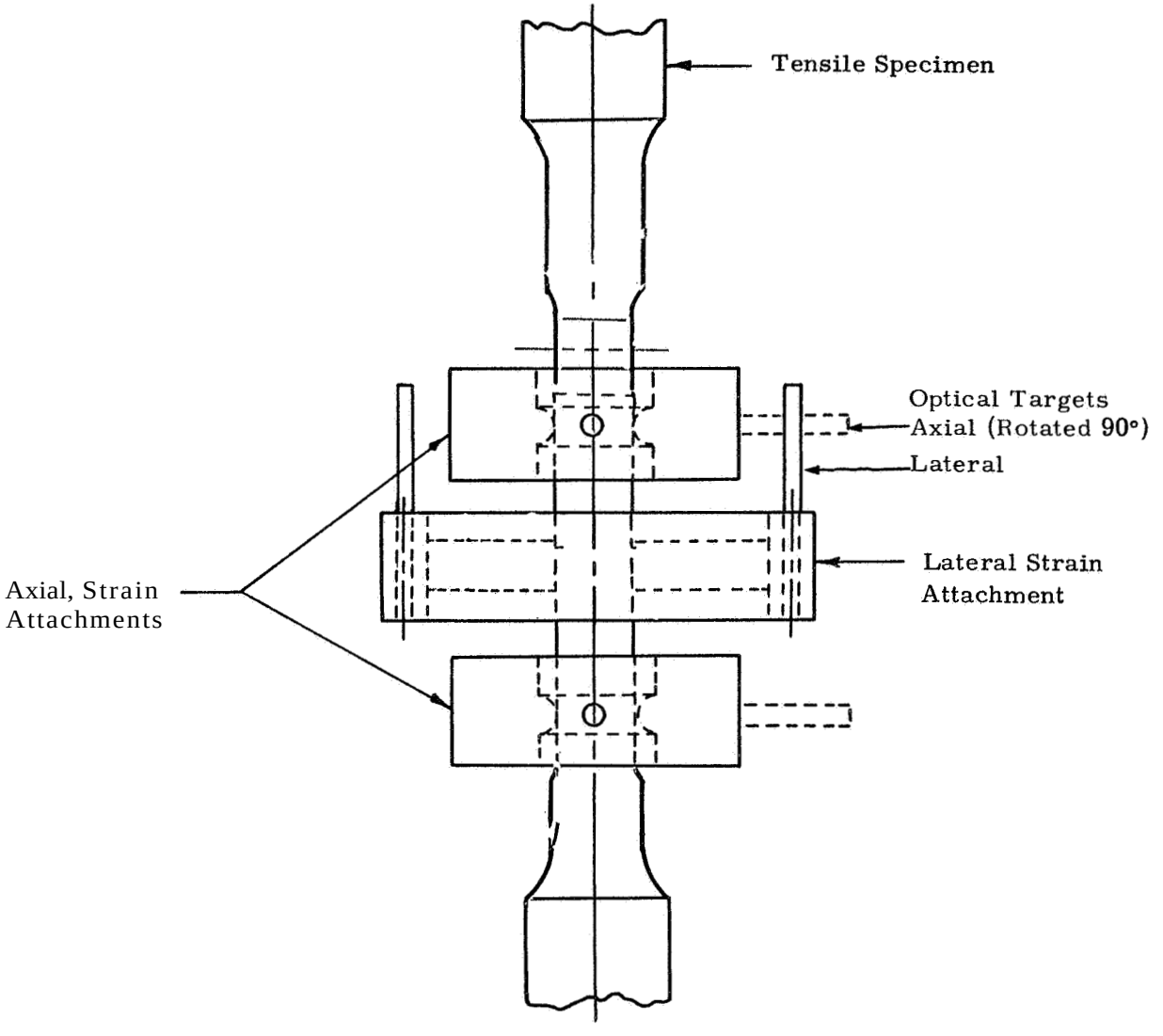

Figure C4. Location of the flag attachments on the tensile specimens

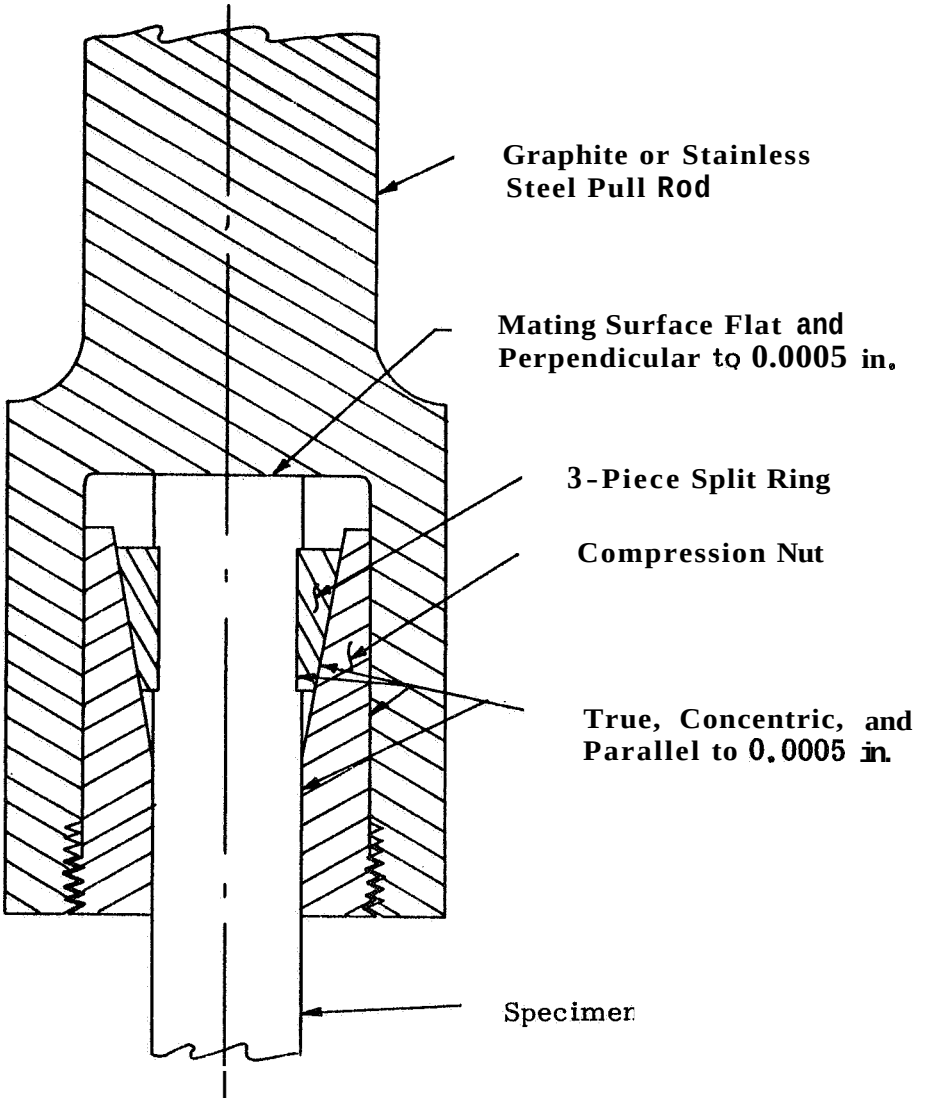

Figure C5. Precision collet grip for tensile specimens 2:1 scale

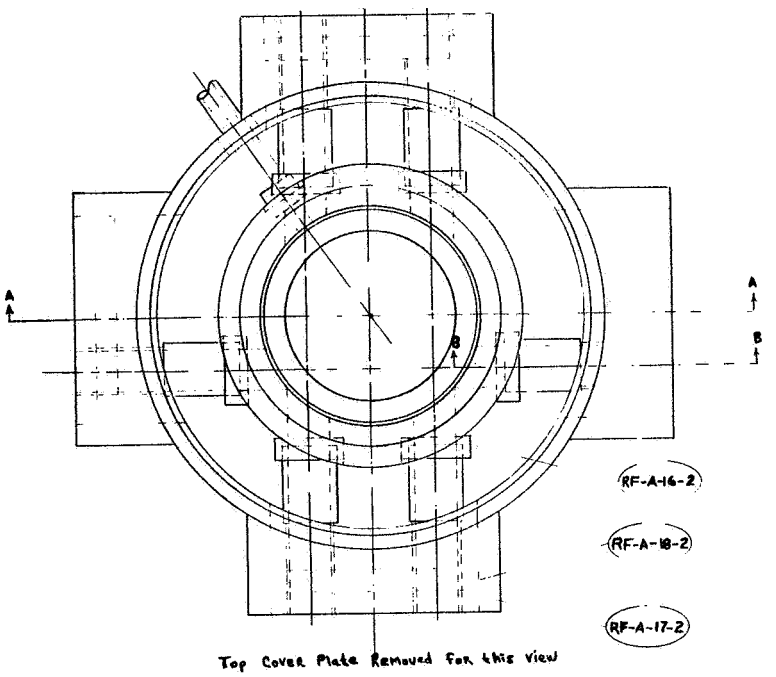

isy.	Item	uan.	Description
	۱-2	1	Top pyrolytic graphite ring
	L-3	1	Bottom pyrolytic graphite ring
	۱-4	1	Pyrolytic graphite temperature sight plate
	۱-5A	1	CS graphite protector tube
	۱-6	1	CS graphite temperature sight tube
	۱-7	1	Bottom Mlcarta insulating disc
	2-8	1	Top steel base plate
	3-BA	1	Steel shell
	4-10	1	Top Micarta insulating disc
	A-11	1	Top zirconia disc
	A-12	1	Bottom steel base plate
	A-13	1	Bottom zirconia disc
	A-14A	1	CS graphite heater tube
	A-15	2	Steel sight port tube
	A-16-1	2	CS graphite slght port plate
	A-16-2	2	CS graphite sight port plate
	A-17-1	2	Firebrick sight port plate
	A-11-2	2	Firebrick sight port plate
	A-18-1	2	Zirconia sight port disc
	A-18-2	2	Zirconia sight port disc
	A-19	4	CS graphite slght tube
	A-20	2	Fiberfrax insulator
	A-21	1	Top electrode
	A-22	1	Bottom electrode
	A-23	1	Thermatomic carbon

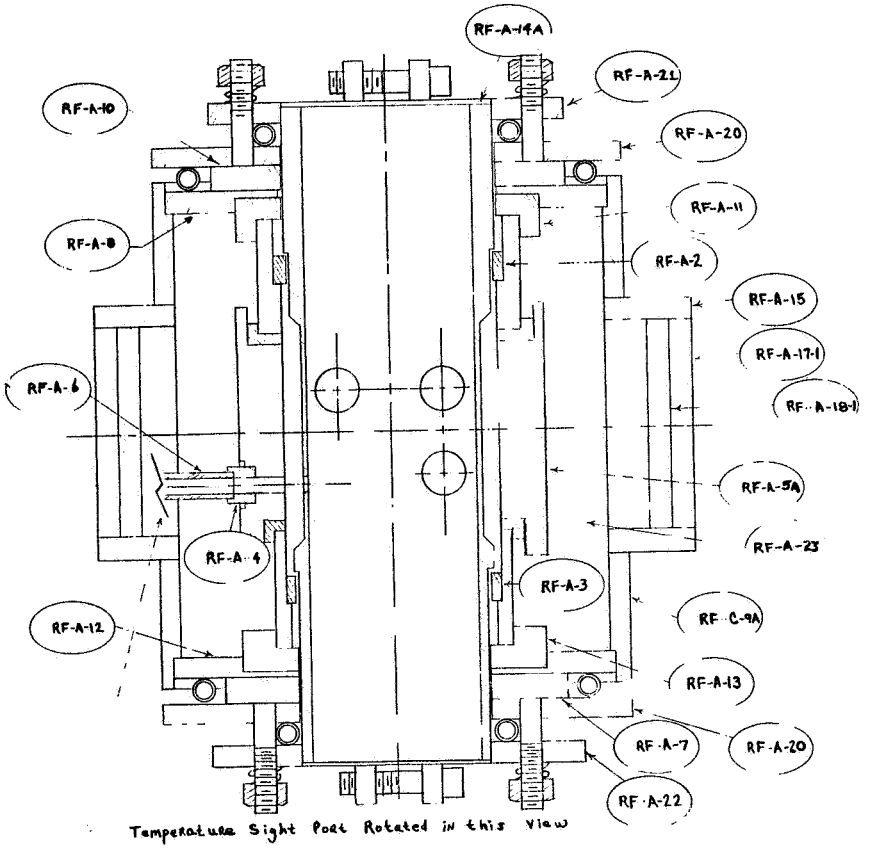

Section A A

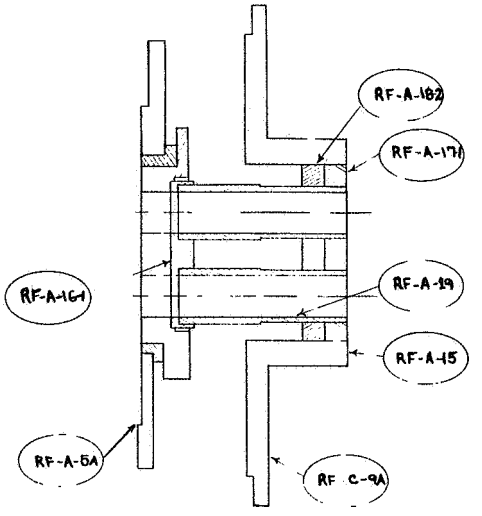

Section B-B

Figure C6. Small 5500°F graphite resistance furnace

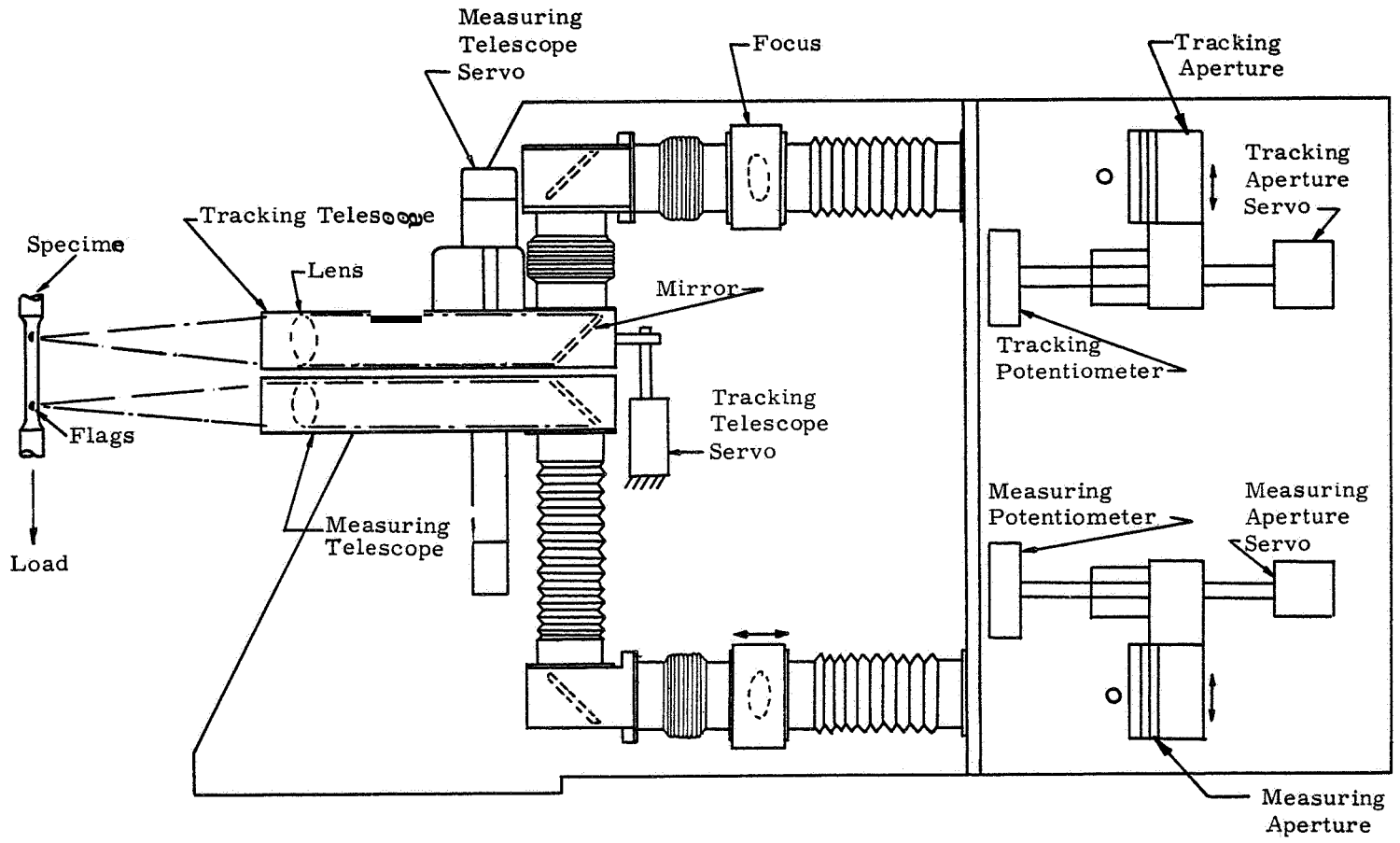

Figure C7. Arrangement of optical strain analyzer

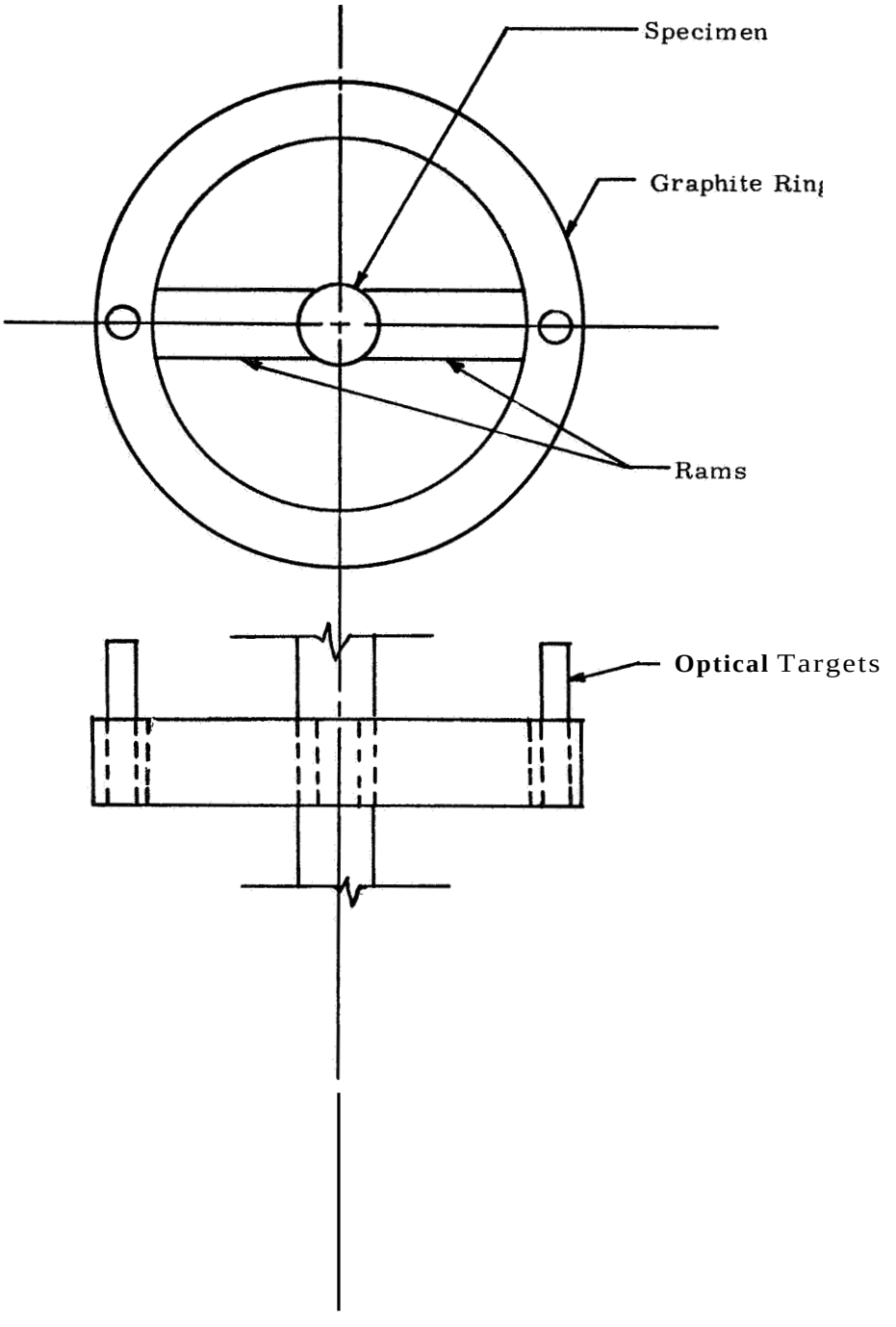

Figure C8. General configuration of the flag attachment to monitor lateral strain in tension

APPENDIX D

ULTIMATE STRENGTH, ELASTIC MODULUS, AND POISSON'S RATIO TO 5500°F IN COMPRESSION

The compressive apparatus is shown in the photograph in figure D1 and in the schematic infigure D2 and consists primarily of a load frame, gas-bearings, load train, 50-ton screw jack, variable speed mechanical drive system, strain analyzers, 5500°F furnace, and associated instrumentation for the measurement of load and strain.

The load frame is similar to most standard frames. It was designed to carry a maximum load of 100,000 pounds and to support the furnace, optical strain analyzers, and other related equipment.

Gas bearings are installed at each end of the load train to permit precise alignment of the loading train to the specimen. The upper bearing is spherical on a radius of 6.5 inches. This radius is the distance from the top of the specimen to the spherical bearing surface. The load train, not the specimen, shifts to maintain radial alignment. The lower bearing is flat and is about 6 inches in diameter. The lower bearing permits transverse alignment of the load train. The gas-bearings are floated for only a small initial amount of load so that precise alignment of the load train can be attained.

The load train near the furnace consists of the specimen loaded on each side by graphite and watercooled steel push rods. The graphite push rods are counter-bored to permit insertion of a pyrolytic graphite disc which serves as a heat dam and to align the specimen to the center-line of the load train. Extreme care is exercised in the preparation of all parts of the load train to ensure concentricity of the mating parts to less than 0.0005 inch.

The 50-ton jack is a power screw type. The mechanical drive system consists of a gear reducer driven by a Louis Allis Synchro-Spede Unit (300-3000 rpm). The gear reducer is connected to the Synchro-Spede Unit through a chain coupling and to the 50-ton jack by a single roller chain and sprocket system. Different load rates are obtained by adjustment of the variable speed setting on the Synchro-Spede and by changeout of sprockets on the gear reducer and screw jack.

Figure D3 shows details of the "dumbbell" specimen which maintains a 0.500 inch diameter over the 1.2 inch long gage section. The specimen provides sufficient room for the flag attachments that follow the axial and lateral strains and also minimizes the influence of end restraint.

The flag attachments for the measurement of axial strain are positioned one inch apart so that unit strain is recorded directly. The flag attachment for the measurement of lateral strain is positioned between the flags for axial strain; see figure D4. The lateral flag attachment used in compression is shown in figure D5. The 4-piece assembly consists of a ring, two rams bearing on the specimen, and a screw to adjust the contact pressure. The ring was designed to track lateral motions as great as 0.030 inch without breaking.

Figure D6 is a sketch of the 5500°F furnace used for compression showing the basic components. The furnace consists of a resistively heated graphite element insulated from a water-cooled shell by thermatomic carbon. The furnace and specimen are purged with helium to provide an inert atmosphere. Ports with visual openings are provided on opposite sides of the furnace as a means of allowing the strain analyzers to view the gage flags on the specimen. Specimen temperatures are determined by optical pyrometer readings taken through another small sight port containing a sapphire window. A calibration curve was established for the loss through the sapphire window, and since the furnace cavity acts essentially as a blackbody, true temperature readings are obtained. Power is supplied to the heating element by means of a 25 KVA variable transformer.

Strain measurement consists of measuring optically the elongation between two flags, or targets, which are mounted on the specimen and separated initially by a predetermined gage length. The travel of the targets is measured by sensing the displacement of the image of the edge of the targets and then electromechariically following the image displacement. The relative travel of the two targets provides the strain. Readout is continuous and automatic on a millivolt recorder. A schematic of the analyzer is shown in figure D7.

A brief summary of the mechanical motions of the components involved in monitoring the strain is helpful in understanding the detailed performance. A tracking telescope follows the upper target and carries a second telescope mounted on its carriage. The second telescope is capable of independent motion to follow the lower target. The relative displacement between the upper and lower telescope, as strain occurs, defines the strain. The system usually is operated so that the tracking

telescope follows the upper target and the strain is monitored by the relative displacement of the aperture rather than the telescope following the lower target. With this procedure the maximum range is the maximum displacement available for the lower aperture, or about $\frac{1}{8}$ inch, and the sensitivity is limited by the optics and the noise level of the detector. Using both telescopes, the range is about $\frac{3}{4}$ inch,

To provide optical references on the specimens, targets are affixed to the test specimen as mentioned. When the specimen is heated to temperature, the targets are self-luminous and are observed optically. The optics view past the luminous targets into a cooled cavity in the opposite furnace wall. The self-luminous targets are then visible against a dark background. To obtain data at below 2000° F, a light beam is directed from behind the flags providing a shadow image for the detection system.

The image of the glowing target is focused through a rotating shutter (chopper) and onto a rectangular aperture. Small slits in the aperture pass a portion of the upper and lower edges of the light beam. A photocell receives the light thus transmitted, and an electronic circuit detects whether the energy passed by the two slits is equal. A servo drives the apertures to let a balanced quantity of light pass through the two slits and thus maintains an optical null.

To obtain lateral strain, a strain analyzer is supported horizontally on the load frame to view the diametrical or lateral strain of the specimen.

Calibrations of the analyzers are performed in various ways including absolute correlations to precision micrometers, strain gage extensometers, and direct plots of stress-strain for reference materials such as steel, Plexiglas, magnesium, and aluminum. Precision is ± 0.000020 inch.

Instrumentation includes primarily a stress-strain measurement system composed of a 20,000-pound SR-4 Baldwin load cell, constant d. c. voltage power supply, two optical strain analyzers, and two X-Y recorders. Specimen temperature is monitored with an optical pyrometer. Stress (load) is measured by a commercial load cell. The cell receives a constant d. c. voltage input from the power supply and transmits a millivolt signal (directly proportional to load) to an X-Y recorder. Simultaneously, the optical strain analyzers measure both the axial and lateral strain and transmit a millivolt signal (proportional to strain) to the X-Y recorders. Thus, continuous plots of stress-axial strain and axial strain-lateral strain are recorded simultaneously.

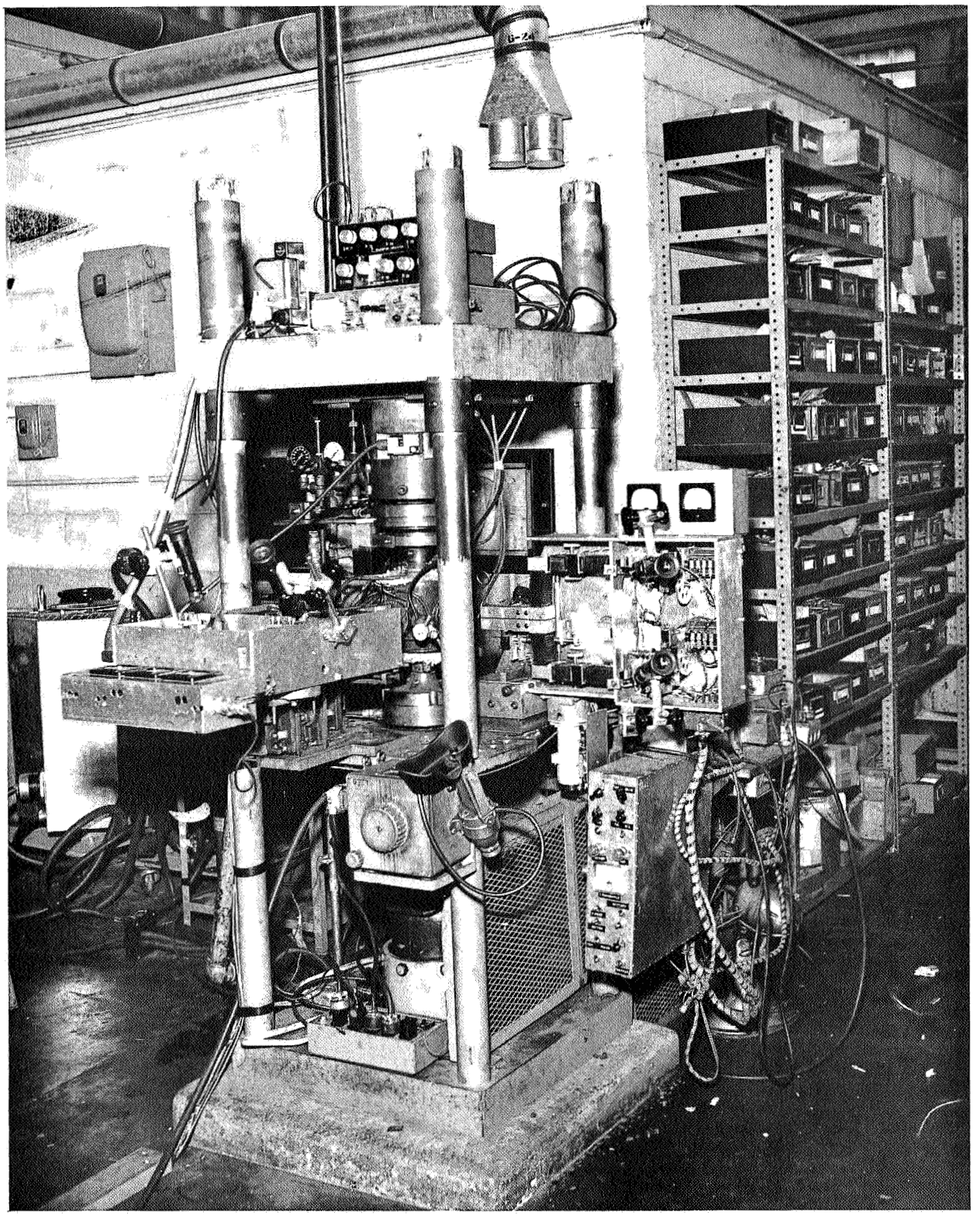

Figure D1. Picture of the compressive facility with gas-bearings and optical strain analyzer

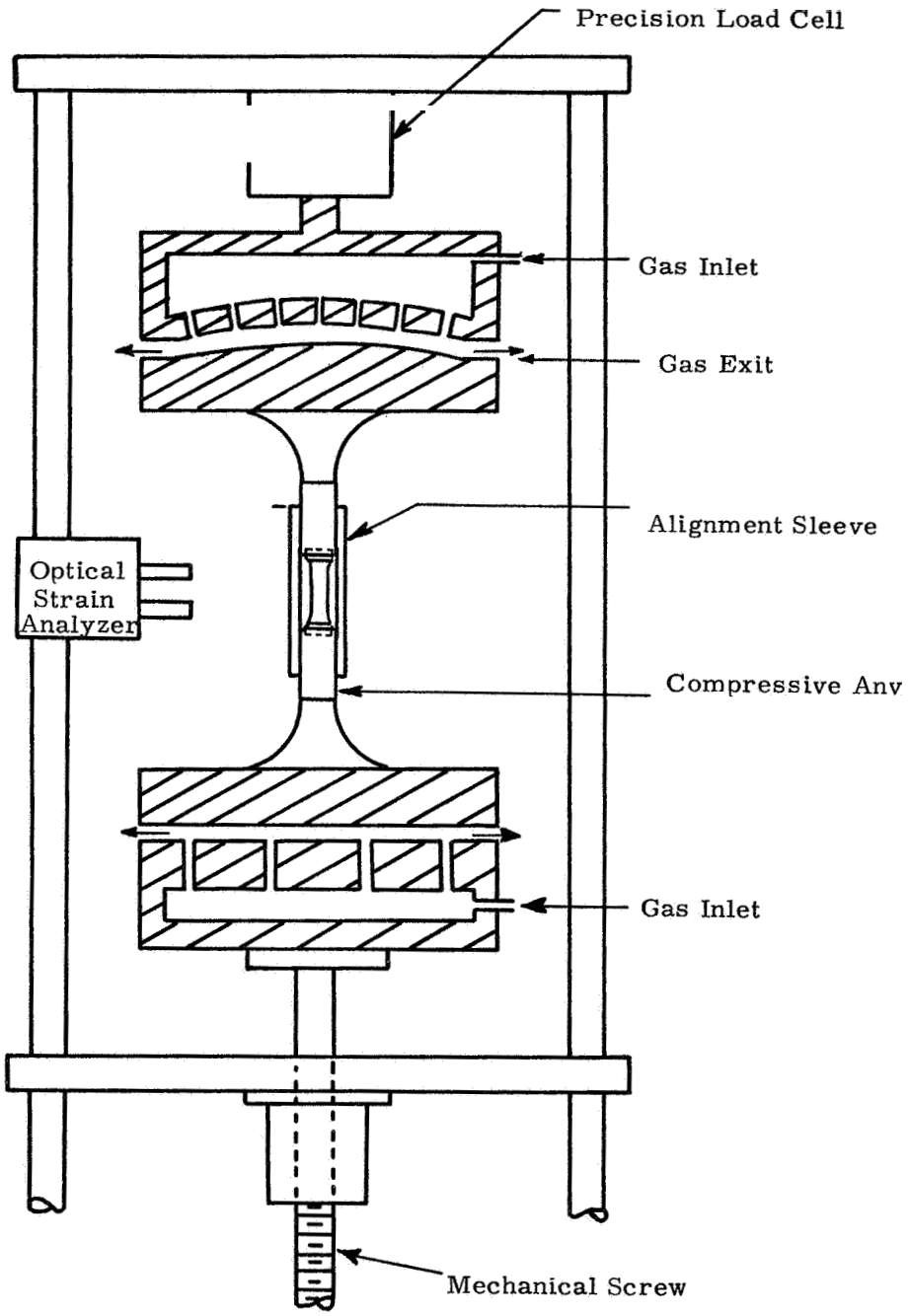

Figure D2. Schematic arrangement of gas-bearing universals, specimen, and load train

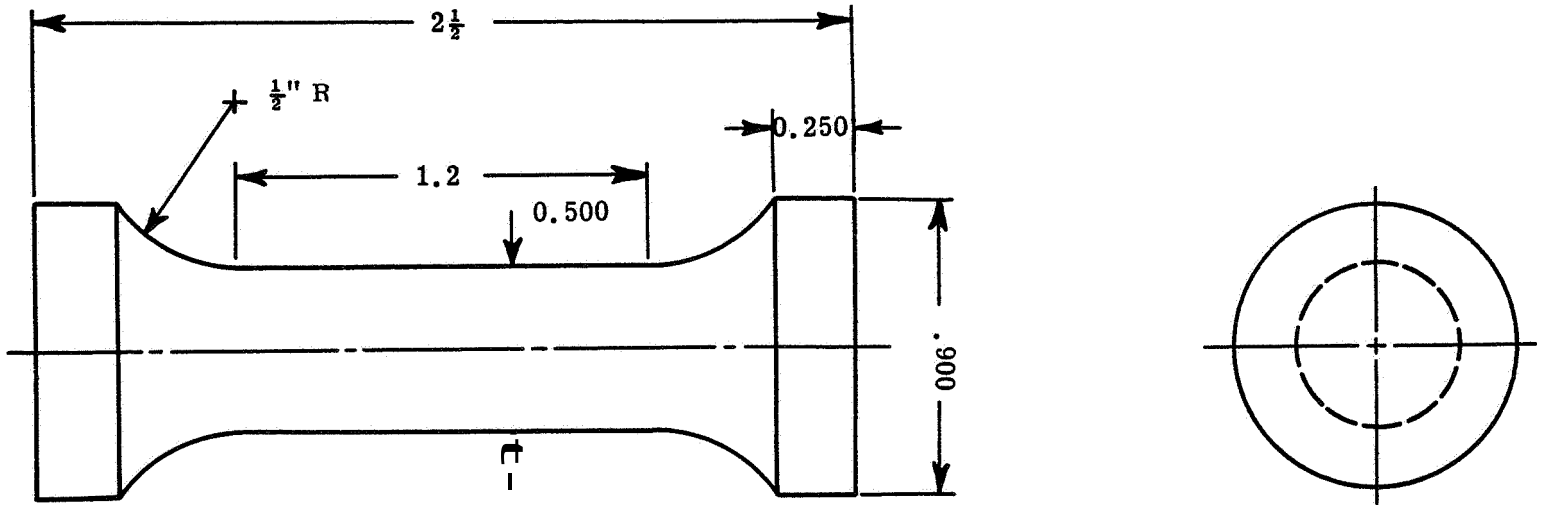

Figure D3. Compressive specimen configuration

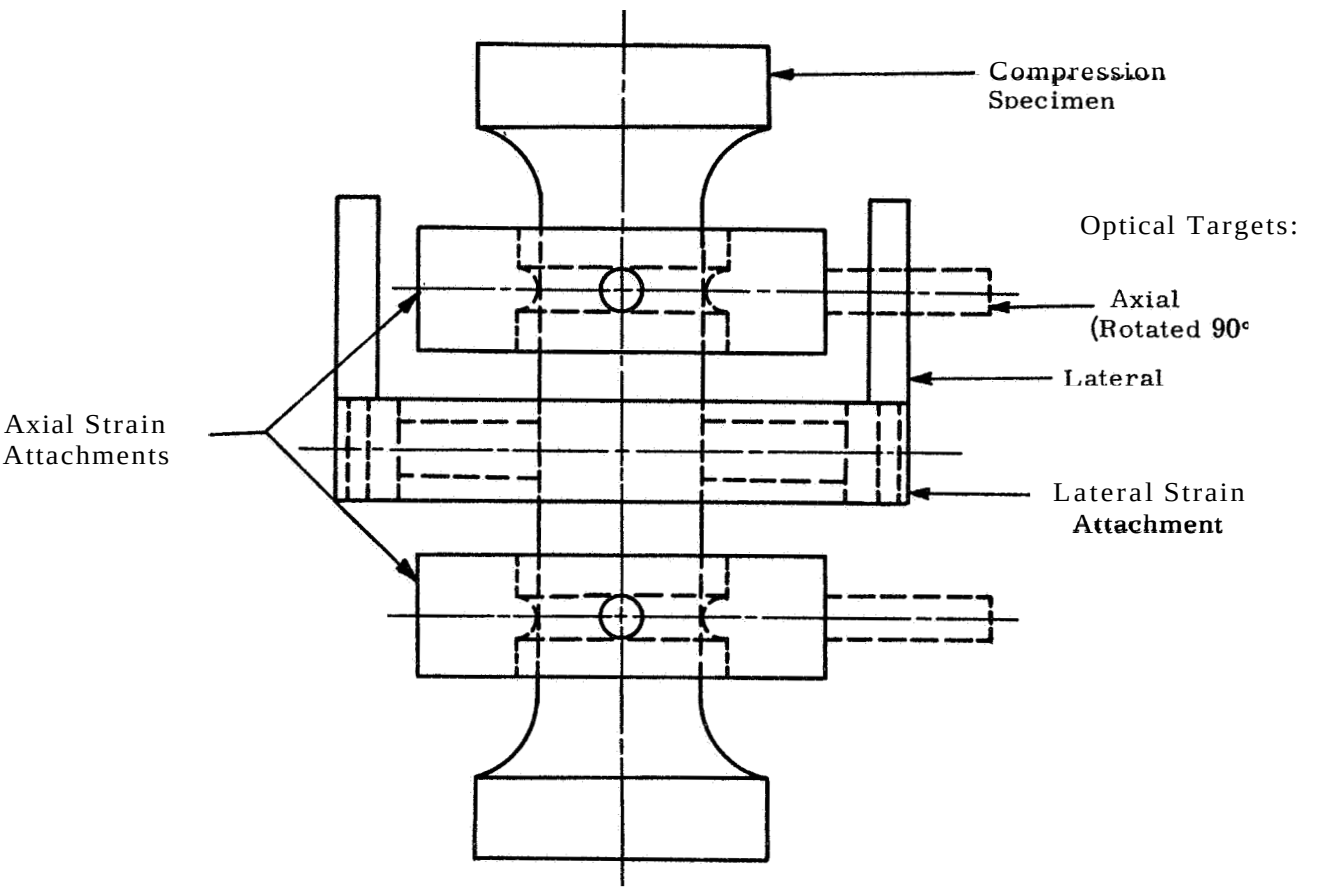

Figure D4. Location of the flag attachments on the compressive specimen

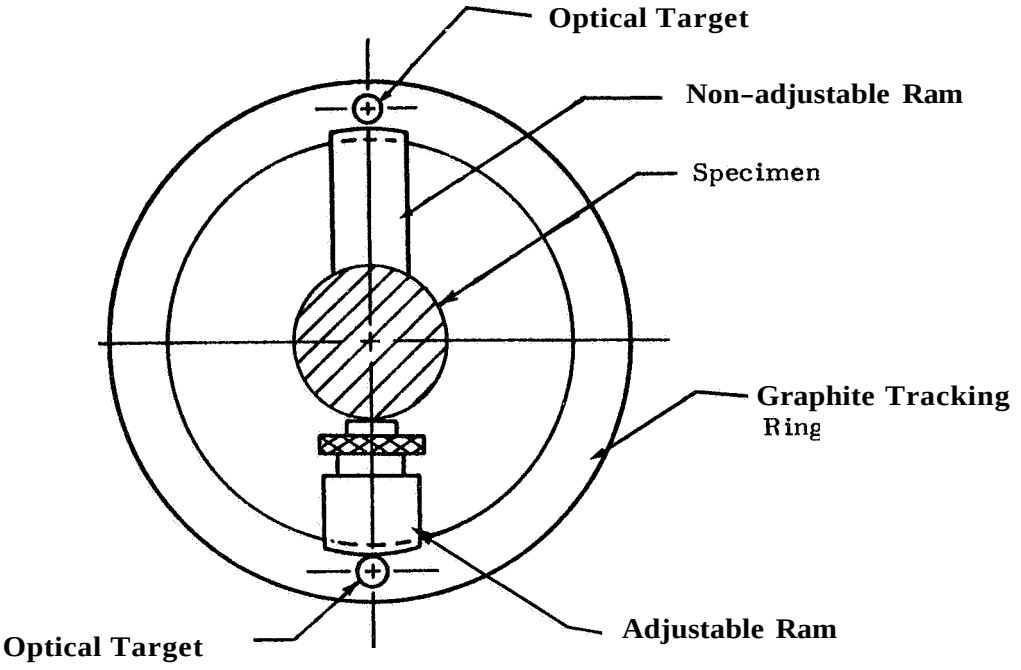

Figure 05. Lateral strain flag attachment for compressive specimen

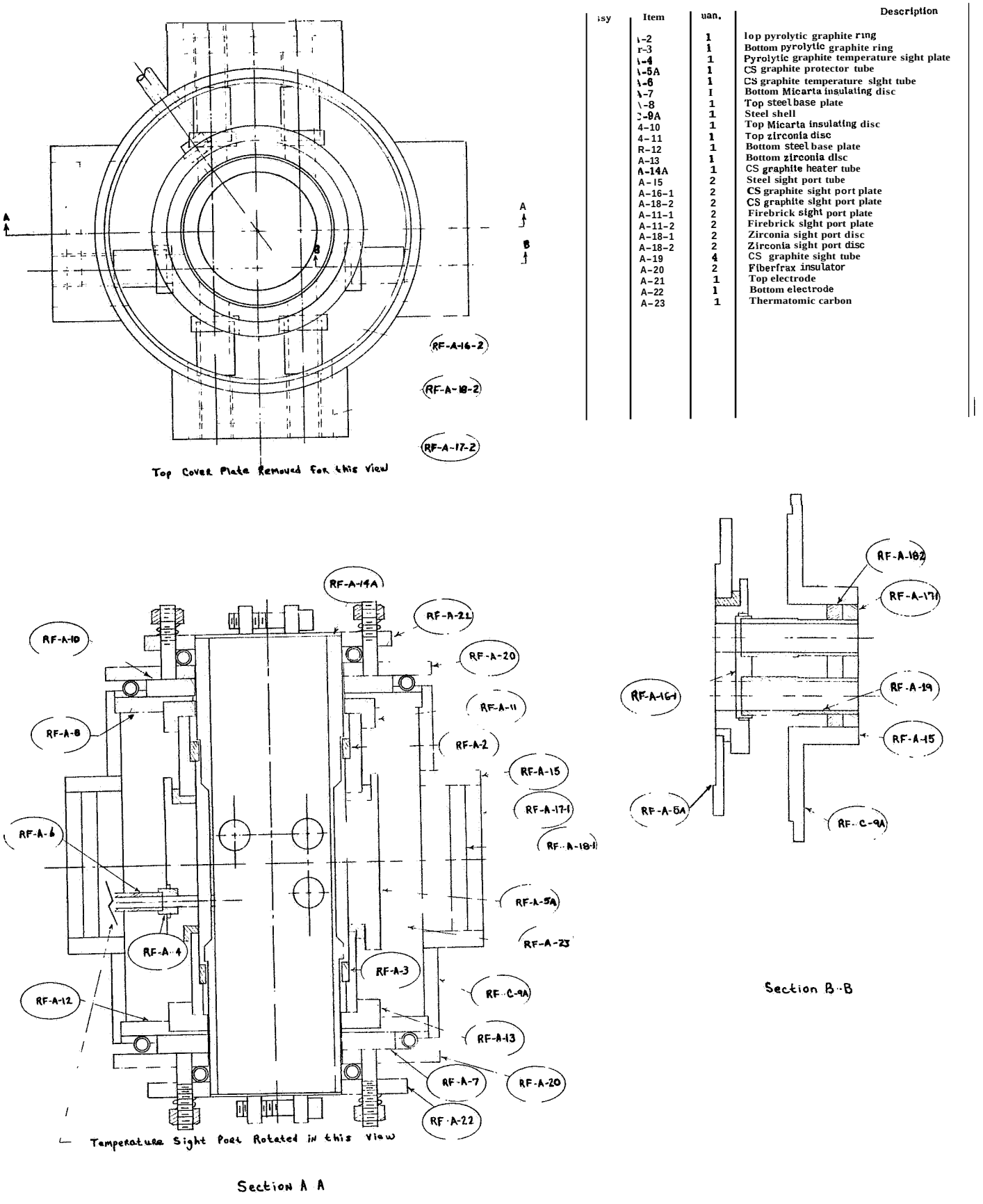

Figure D6. Small 5500°F graphite resistance furnace

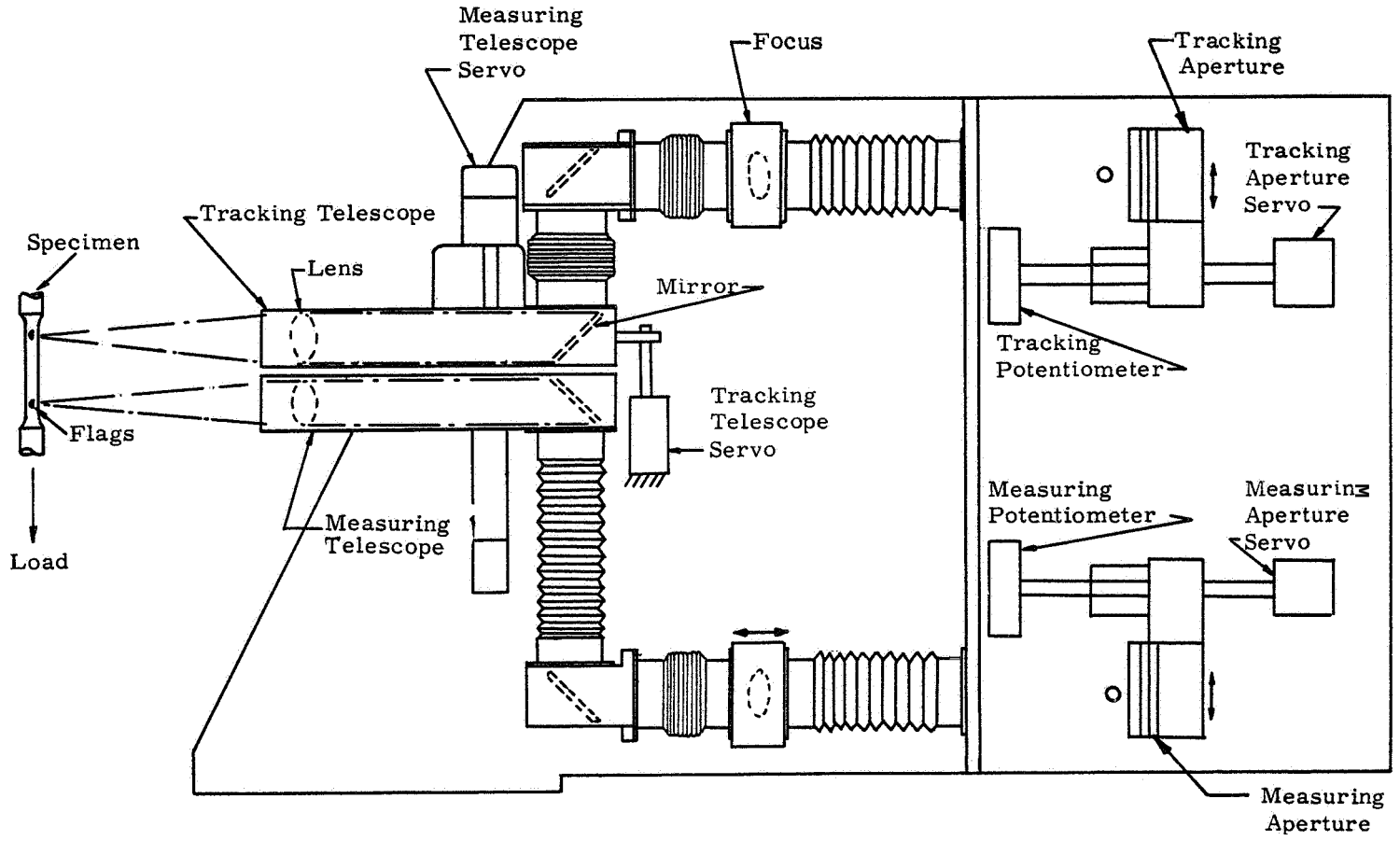

Figure 7 Arrangement of optical strain analyzer

APPENDIX E

THE HIGH TEMPERATURE FURNACES AND TEMPERATURE MEASUREMENT TO 5000°F

The graphite furnaces have been designed, built, and operated by Southern Research Institute personnel at temperatures up to 5100°F and beyond to over 5400°F for short periods; see figures E1 and2 for pictures of two of the furnaces.

A graphite helix is used as the heating element. It has most of the desired features for high temperature operation. After cutting the helix on a lathe, it is extended or stretched slightly. This action assures that the expansion of the helix does not permit the turns to short out, and also provides for the necessary thermal motions. The graphite actually has good strength up to about 6000°F. Up to 5000°F, the graphite is stable in an atmospheric argon, or helium environment. Beyond 5500°F, it is necessary to pressurize the furnace to about 100 psig to suppress excessive graphite vaporization. By this technique, short excursions to 6500°F have also been reported in the literature.

The water-cooled copper electrodes provide good electrical contact to the ends of the helix. No difficulties have been experienced when operating at current densities up to 300 amps per square inch.

Temperatures in the furnace are determined with chromel-alumel thermocouples to 2000°F and by optical pyrometer readings through optical sight glasses with sapphire windows to 5000°F. Cross checks are obtained during data runs between the optical pyrometer and the thermocouples above 1500°F.

Earlier investigations with the high-temperature thermocouples of tungsten-iridium, tungsten-molybdenum, and tungsten-rhenium established these couples to be internally inconsistent and unreliable when compared with the optical pyrometer. True temperatures above 1500°F are taken as the optical readings corrected for the sapphire sight glass (see figure EQ).

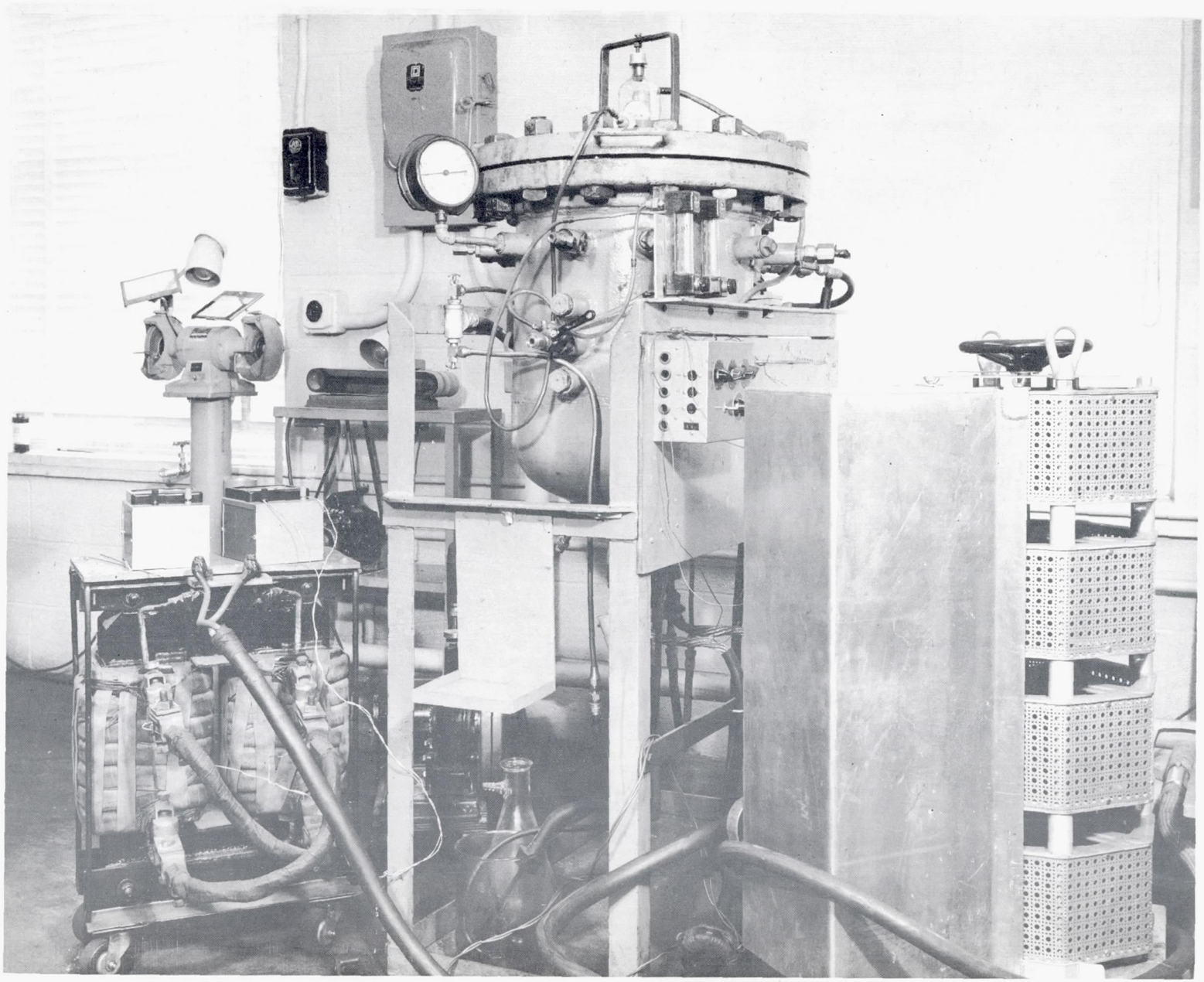

Figure E1. Furnace No. 1 with expansion apparatus installed

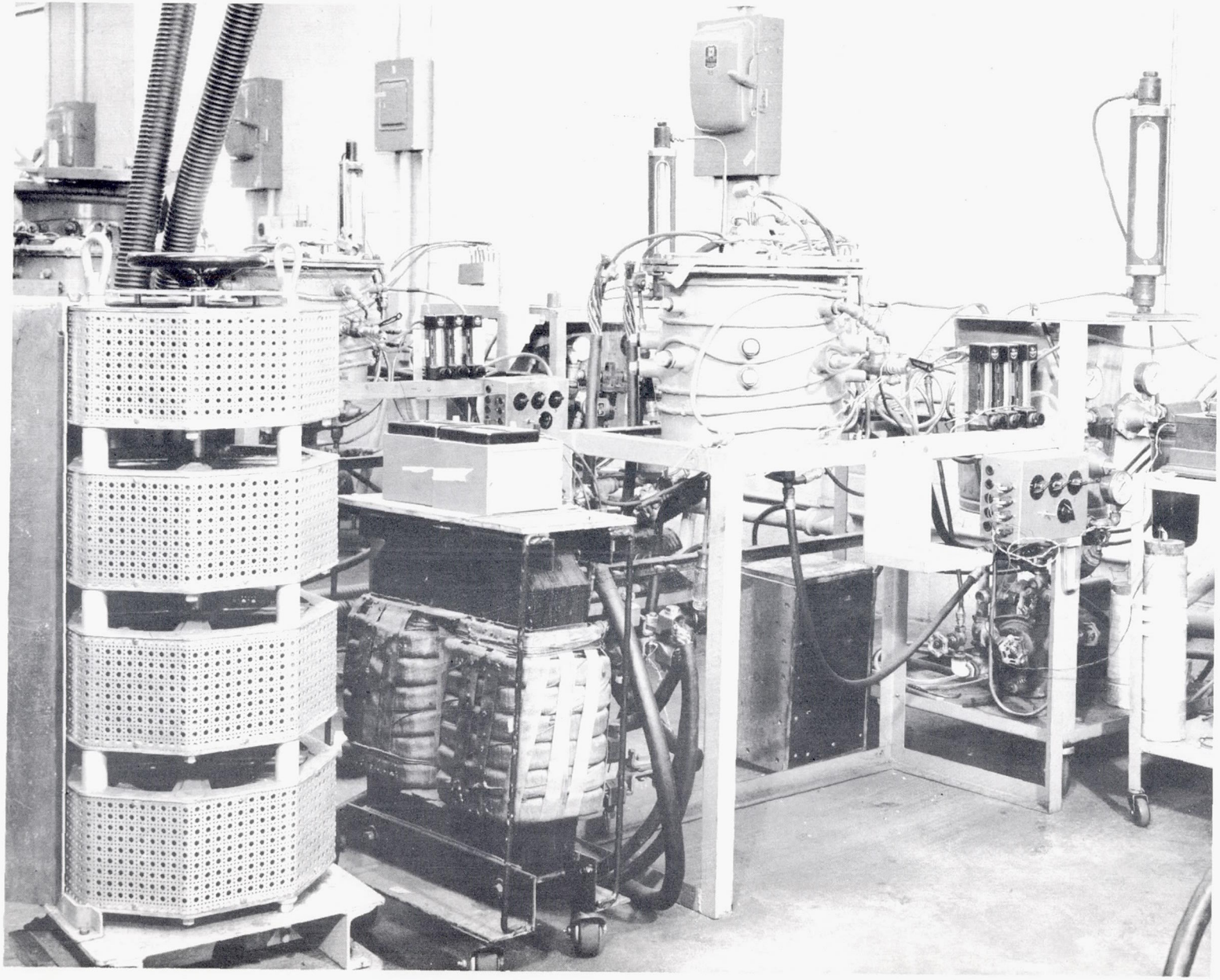

Figure E2. Furnace No. 8 with thermal conductivity apparatus installed

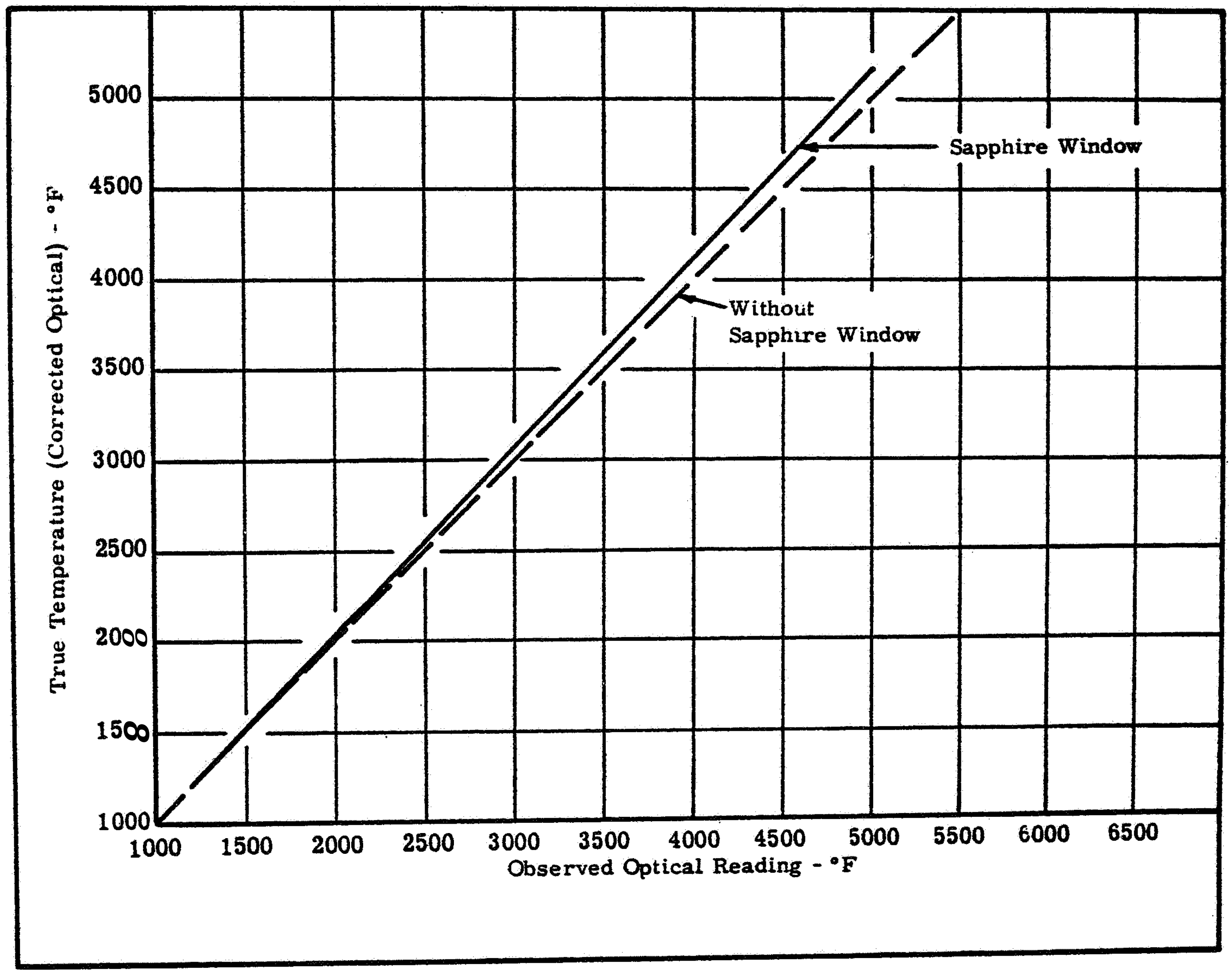

Figure E3 rature calibration curves for optical pyrometer

APPENDIX F

A COMPARATIVE ROD APPARATUS FOR MEASURING THERMAL CONDUCTIVITY TO 2000°F

Southern Research Institute's comparative rod apparatus is used to measure thermal conductivities of a wide variety of materials from -300°F to 2000°F. This apparatus, shown schematically in figure F1, consists basically of two cylindrical reference pieces of known thermal conductivity stacked in series with the cylindrical specimen. Heat is introduced to one end of the rod, composed of the references and specimen, by a small electrical heater. A cold sink or heater is employed at the opposite end of the rod as required to maintain the temperature drop through the specimen at the preferred level. Cylinders of zirconia may be inserted in the rod assembly to assist in controlling the temperature drop. Radial losses are minimized by means of radial guard heaters surrounding the rod and consisting of three separate coils of 26-gage Kanthal wire wound on a 2-inch diameter alumina core. The annulus between the rod and the guard heaters is filled with diatomaceous earth. Surrounding the guard is an annulus of diatomaceous earth enclosed in an aluminum shell.

The specimens and references (see figure F2) are 1-inch diameter by 1-inch long. Thermocouples located $\frac{3}{4}$ inch apart in radially drilled holes measure the axial temperature gradients. Thermocouples located at matching points in each guard heater are used to monitor guard temperatures, which are adjusted to match those at corresponding locations in the test section.

In operation, the apparatus is turned on and allowed to reach steady state. The guard and rod heaters are adjusted to minimize radial temperature gradients between the rod and guard sections consistent with maintaining equivalent functions of K_r times AT in the references. Temperatures are measured on a Leeds and Northrup Type K-3 potentiometer, and the temperature gradients calculated. A typical temperature profile in the test section is shown in figure F3.

The thermal conductivity of the specimen is calculated from the relation

$$K_S = \frac{K_1 \Delta T_1 + K_2 \Delta T_2}{2 \quad \Delta T_S} \quad \frac{\Delta X_S}{\Delta X_r}$$

where K_1 and K, are the thermal conductivities of the upper and lower references; ΔT_1, ΔT_2, and ΔT_S are the temperature gradients in the upper and lower references and specimens, respectively; ΔX_S and ΔX_r are the distances between thermocouples in the specimen and references.

Note that for purely axial heat flow, the products $K_1 \Delta T_1$ and $K_2 \Delta T_2$ should be equal. Due to imperfectly matched guarding and other factors, this condition is seldom attained in practice; therefore, the averageof the two values is

used in the calculations. Their difference is maintained as small as possible, usually within 5 percent of the smaller.

For identical specimens, the ratio $\Delta X_s/\Delta X_r$ should be unity but may vary due to the uncertainty in hole locations. To prevent introducing an additional error in calculations, ΔX is determined as follows: the depth of the hole is measured by inserting a snugly fitting drill rod in the hole, measuring the projecting length and subtracting it from the total length of the rod. The slope, or angle the hole makes with the perpendicular to the specimen axis, is determined by making measurements to the face of the hole and the outer end of the drill rod with respect to a datum plane, using a dial gage. From these measurements, the location of the bottom of the hole can be calculated.

For reference materials, Armco iron or copper is used with high conductivity specimens, 316 stainless steel with specimens of intermediate conductivities, and Teflon, Pyroceram 9606, or Pyrex with low conductivity specimens. Extensive calibration of the apparatus, using these reference materials as standards, has yielded accuracies to about 5 percent error, when sufficient care is exercised to maintain closely matched temperatures between the guard and test sections. Even with careless matching, the error is only about 10 percent so the system is not particularly sensitive to minor unbalances.

To establish the accuracy of the apparatus, some initial runs were made on 316 stainless steel, using Armco iron as the reference. The data, shown in Figure 4, are somewhat higher than those reported by Lucks and Deem[1], but agree well with values reported by several steel manufacturers. Note that the data scatter is less than 5 percent. The data on stainless steel were confirmed by evaluating Armco iron, using 316 stainless steel as reference. These data are shown in Figure 5 in comparison with values reported by Powell[2], who compiled his curve from the data of numerous investigators, and estimated its accuracy to be within ± 2 percent over the range from 0° to 1000°C. The comparative rod data for Armco iron, which were computed using the solid curve of Figure 4 for the thermal conductivity of the stainless steel reference, agree with Powell's data within 5 percent, thus confirming the data obtained for stainless steel.

---

[1]WADC TR 58-476, "The Thermophysical Properties of Solid Materials," Armour Research Foundation, November 1960

[2]Powell, R. W., ~~Proc. 3rd Conf. on~~ Thermal Conductivity, 322-341 (1963)

Some additional data obtained on the comparative rod apparatus are shown in figures F6 and 7. Figure F6 shows thermal conductivity data for ATJ graphite, with grain, using Armco iron as the reference material. These data show excellent agreement with earlier data obtained here and by other sources[3-5]. The maximum scatter of the comparative rod points was about 5 percent.

Figure F7 shows data for thermocouple grade constantan obtained on the comparative rod apparatus using Armco iron references, and on Southern Research Institute's high temperature radial inflow apparatus. Note the excellent agreement. These data also show close agreement with data obtained by Silverman[1] on an alloy of very similar composition.

---

[3]ASD-TDR-62-765, "The Thermal Properties of Twenty-Six Solid Materials to 5000°F or Their Destruction Temperatures," Southern Research Institute, August 1962

[4]Pears, C. D., ~~Proc. 3rd Conf. on~~ Thermal Conductivity, 453-479 (1963)

[5]Fieldhouse, et al, WADC TR 55-495, Part 3 (1955)

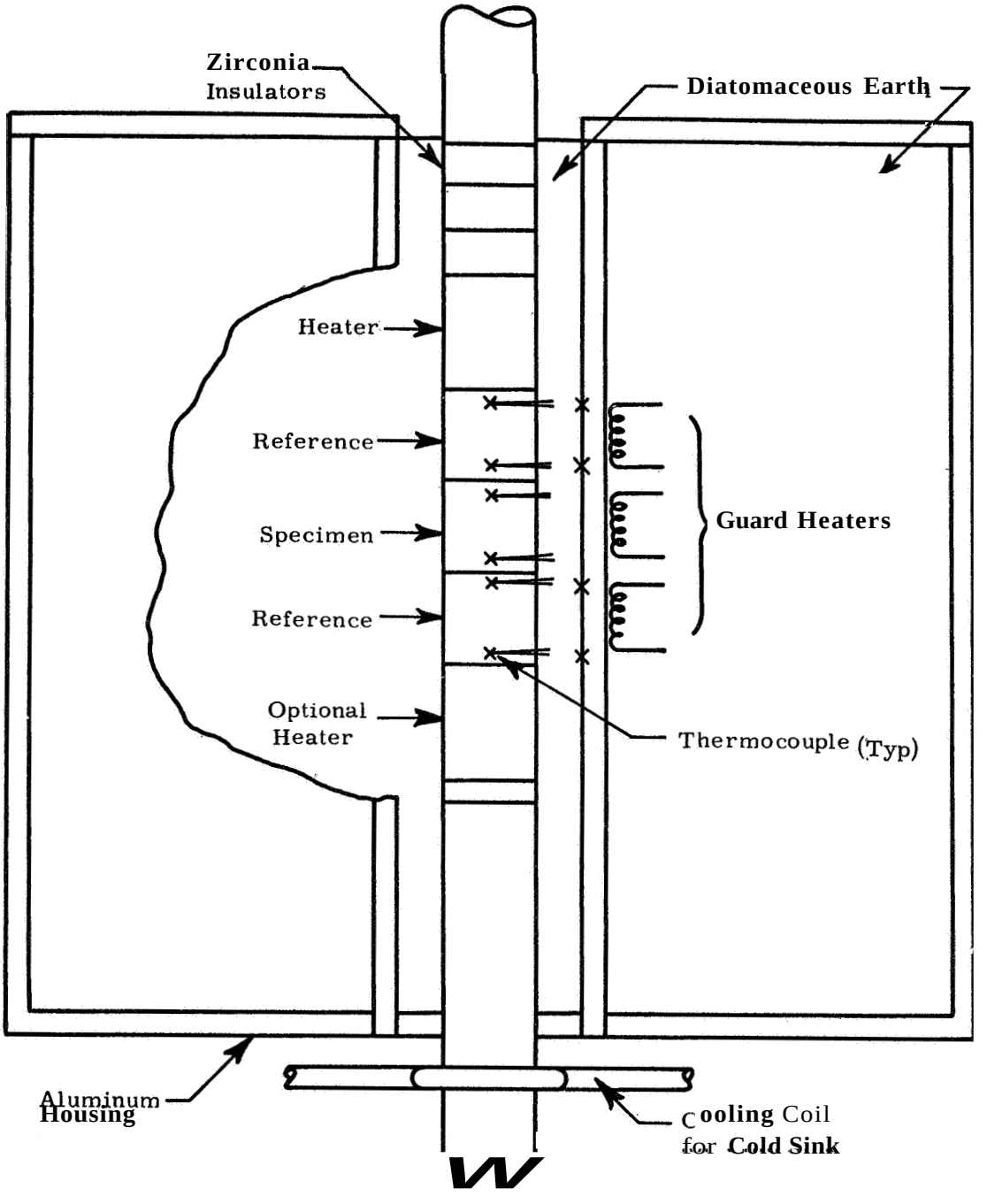

Figure F1. Schematic of comparative rod thermal conductivity apparatus

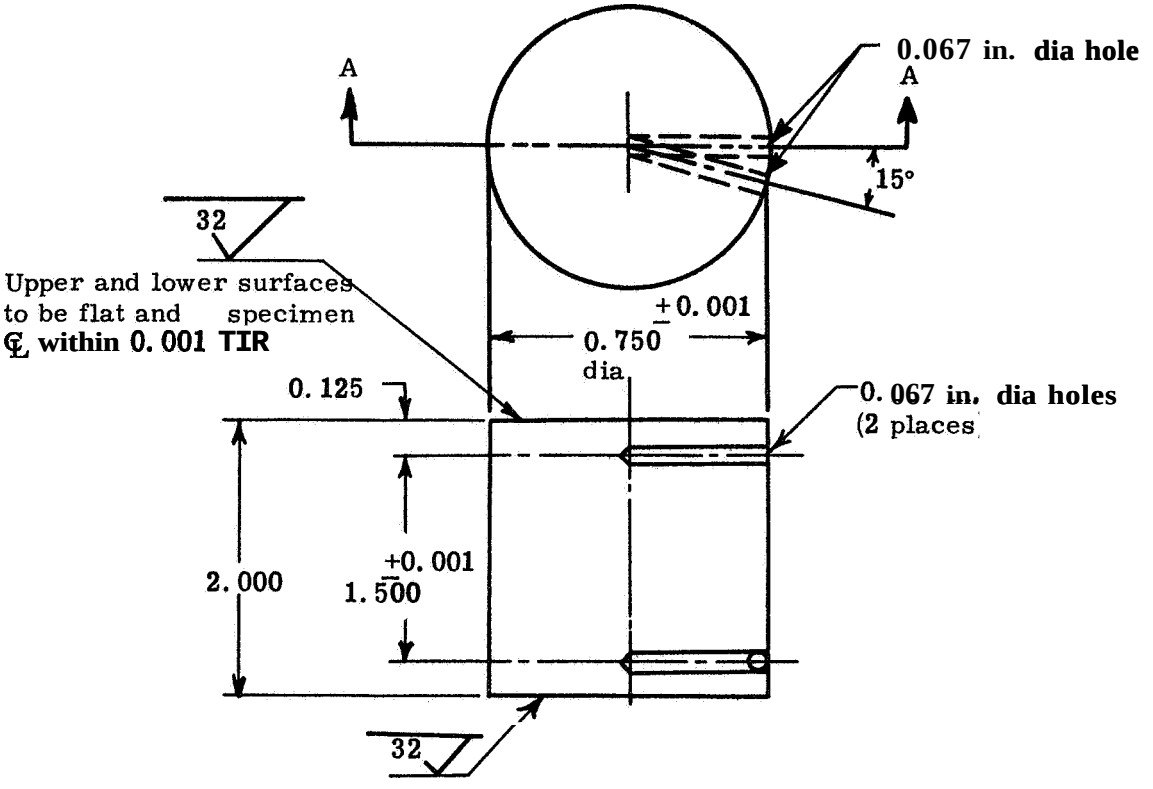

Tolerances ± 0.003 unless otherwise noted

Figure F2. Specimen configuration for comparative rod thermal conductivity apparatus

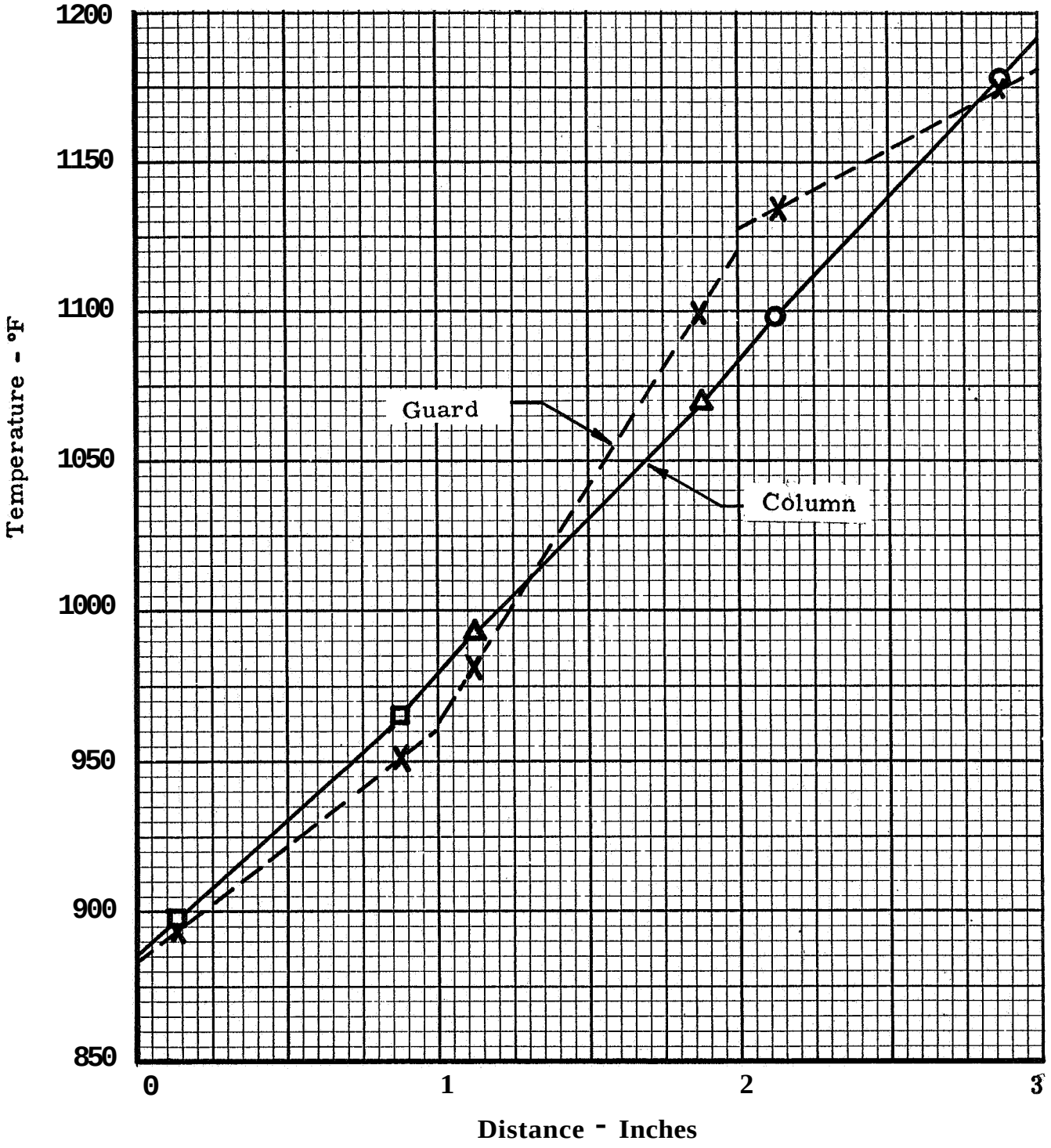

Figure F3. Typical temperature profile in test section

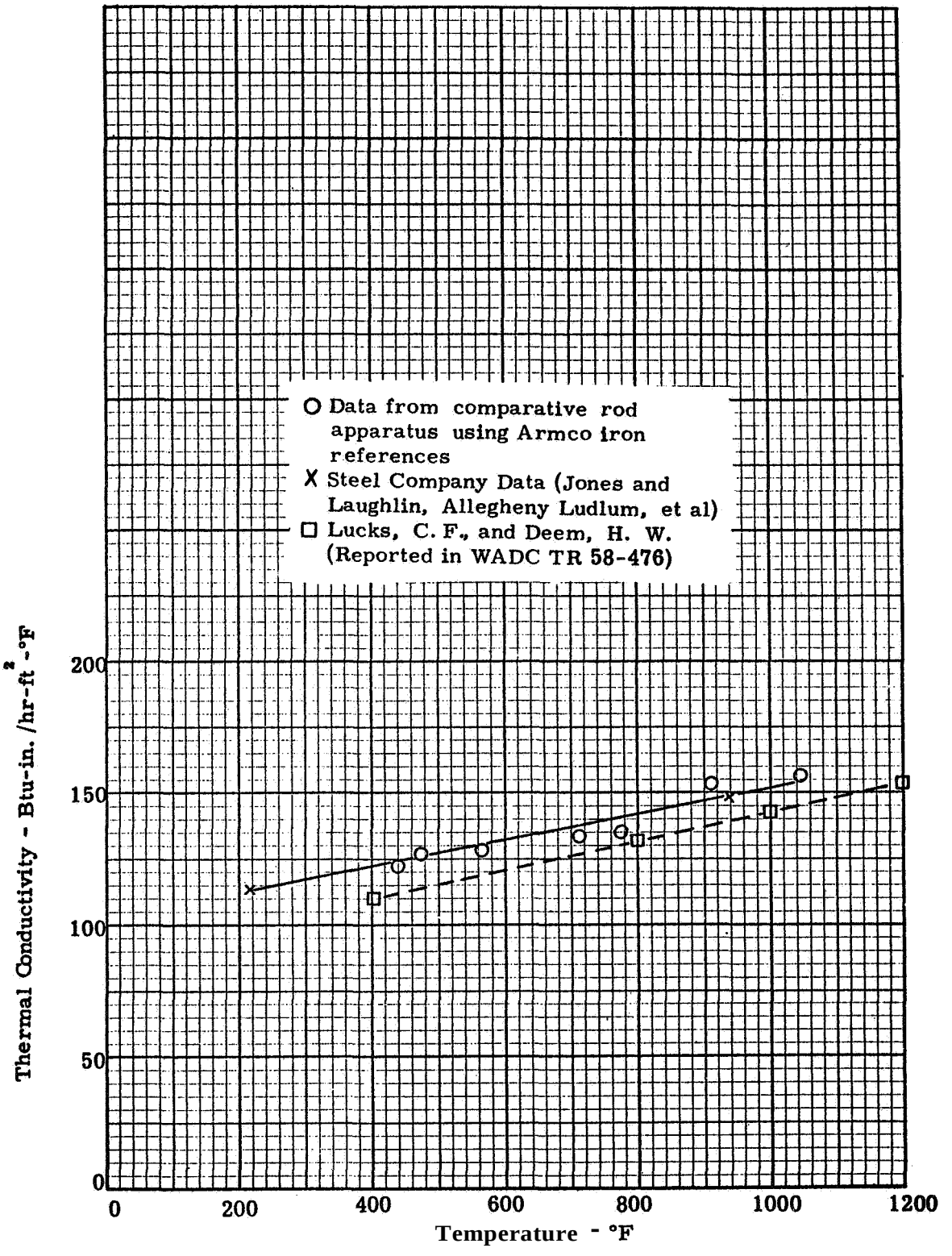

Figure F4. The thermal conductivity of type **316** stainless steel

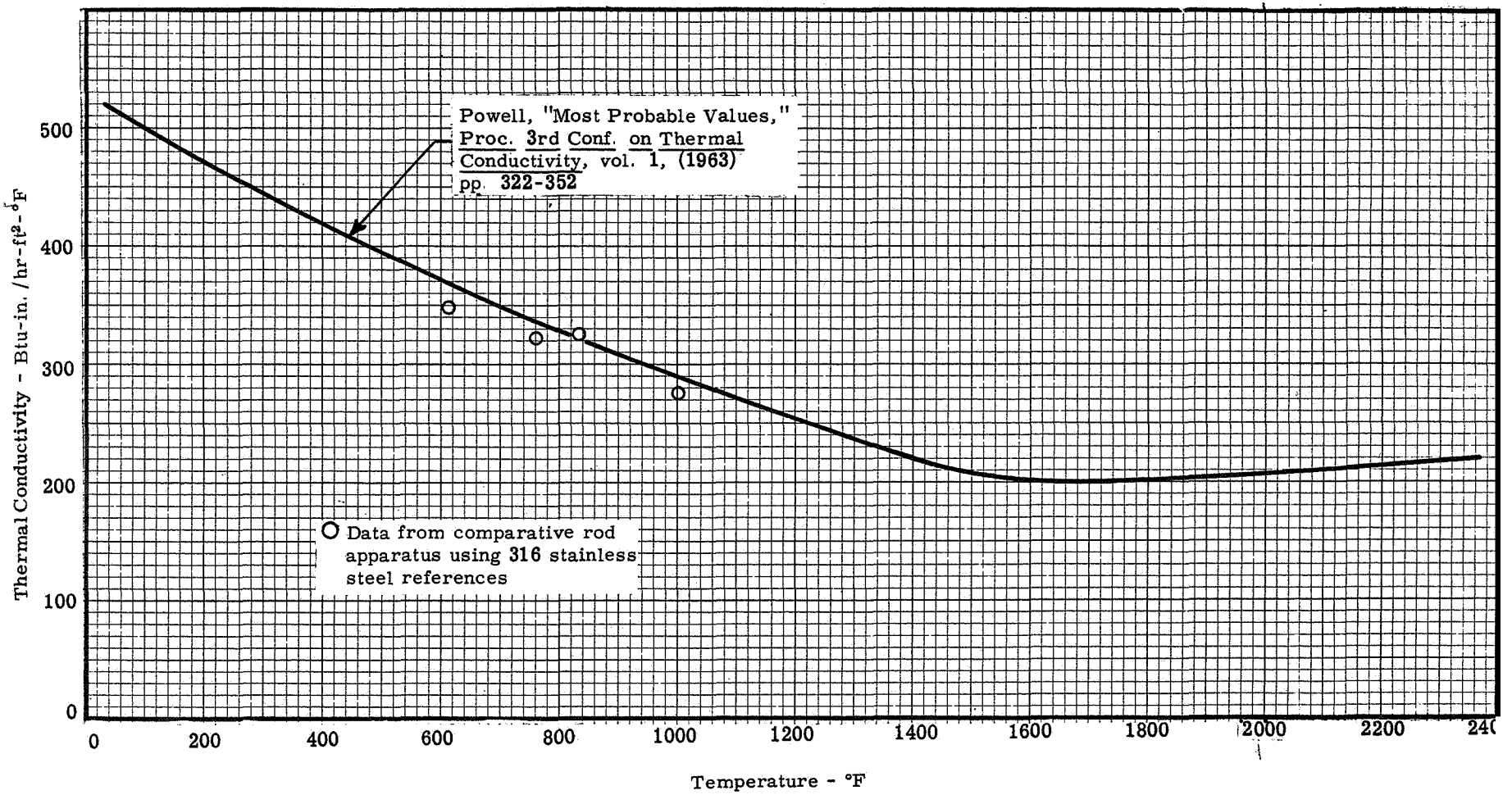

Figure F5. The thermal conductivity of Armco iron

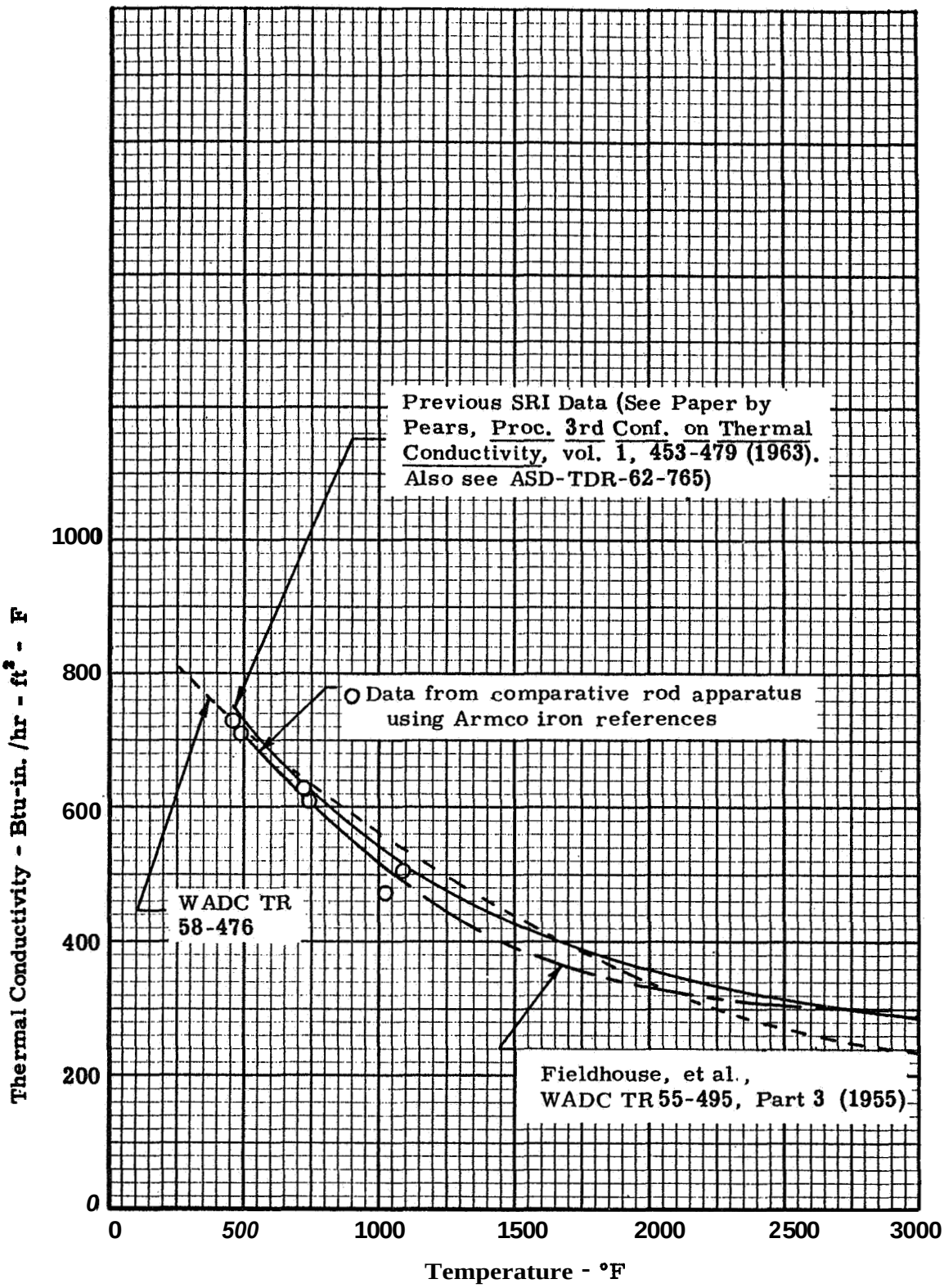

Figure F6. Thermal conductivity of ATJ graphite, with grain

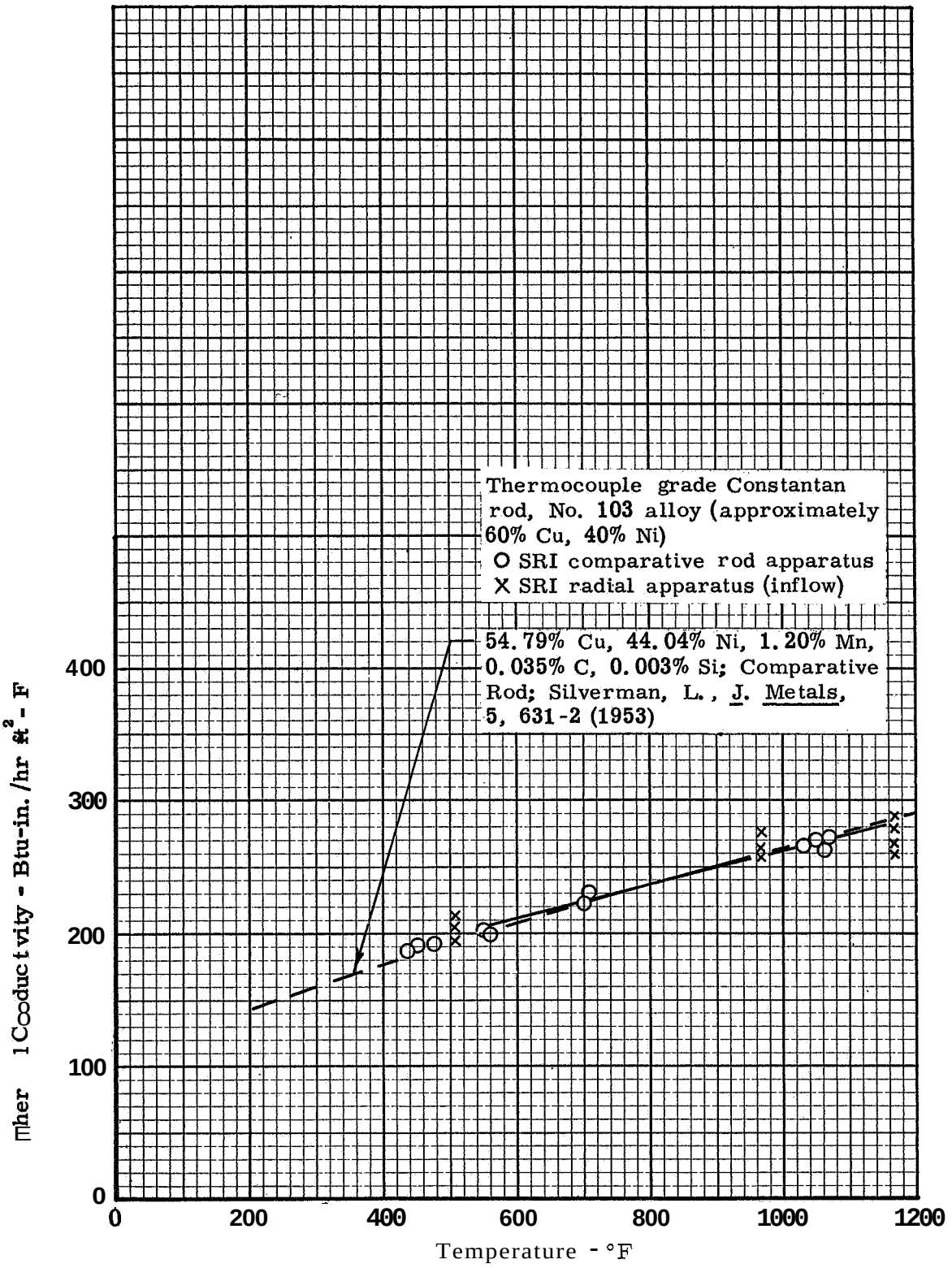

Figure F7. The thermal conductivity of thermocouple grade constantan rod

APPENDIX G

PERMEABILITY TO 1000°F

We have two apparatus in which to make permeability measurements. One apparatus is designed for operation to 1000°F and the other is designed for room temperature measurements. These apparatus are basically the same in principle, except for the method in which pressure measurements are made. Static pressures across the specimen are measured with the room temperature apparatus, whereas the total pressure is measured in the 1000°F apparatus.

Room Temperature Apparatus

This apparatus is shown schematically in figure G1. It consists of a copper housing and a copper specimen holder. An O-ring is used as a seal between the housing and the specimen holder Gas is supplied to the specimen from a commercial gas cylinder. Static pressures are measured at the inlet and exit points to the housing. Flow rates are measured with either a bubble type flowmeter, a variable area flowmeter or a wet test meter; the type of instrument used to measure the flow rate depending upon the magnitude of the flow.

The specimen, which is 1 inch in diameter by 1/2 inch thick, is mounted in the housing as shown in figure G2. The specimen is mounted on a shoulder approximately 1/64 inch wide and 1/64 inch deep. On the upstream side the specimen holder is bored out to a diameter of 1.5 inches and the annulus between the specimen and the holder is filled with silicone rubber (Dow Corning RTV-731 Silastic). This silicone rubber has been employed successfully as a sealant in prior permeability measurements.

High Temperature Apparatus

This apparatus is shown schematically infigure G2. A detail cutaway view of the housing and specimen holder is shown infigure G3. The apparatus as shown in these figures was designed for operation to 1000°F. Gas is supplied to the apparatus from a commercial gas cylinder. The volumetric flow rate is measured with a variable area flowmeter. The inlet pressure to the flowmeter is read with a mercury filled U-tube manometer. This pressure measurement is used to correct the indicated flowmeter reading to the volumetric flow rate at standard pressure. Between the flowmeter and the specimen housing, the gas passes through a preheater section. This consists of thin-walled stainless steel tubing which is resistively heated using low voltage and high current. Power is supplied

from a 25 KV step-down transformer, the input of which is regulated by a 220 V Powerstat. The gas then passes through the specimen and is exhausted to the atmosphere.

The pressures upstream and downstream of the specimen are measured with total pressure probes. These pressure monitors are connected to U-tube manometers such that the manometers read the pressure difference across the specimen and the gage pressure on the downstream side of the specimen.

Temperatures are measured with two chromel alumel thermocouples One thermocouple is mounted in the stainless steel specimen holder The other thermocouple is used to monitor the temperature of the gas leaving the downstream side of the specimen, The exposed junction of the gas thermocouple is placed so that the hot gas leaving the specimen impinges directly upon it

Knife edges are machined on the faces of the housing and specimen holder A copper gasket is used between these knife edges to provide a leak tight seal

The specimen is mounted in a stainless steel housing as shown in figure G4. The specimen rests in a recess approximately 1/64 inch wide by 1/32 inch deep Above this recess the holder is bored out to a diameter of 1.5 inches Normally, specimens used for the measurements are 1 inch in diameter by 1/2 inch thick Smaller specimens may also be accommodated The annulus between the specimen and the housing is filled with a sealing compound A silicone rubber (Dow Corning RTV-731 Silastic) is used as the sealing compound for low temperature measurements. For high temperature runs, Sauereisen 31 cement is used as a sealant. Both of these sealing compounds have been used successfully in prior evaluations. A stainless steel washer is mounted on the exposed surface of the Sauereisen cement while it is still wet This washer reduces the exposed area of the cement and serves as a secondary seal.

The procedure for setting up the specimen using the Sauereisen cement is as follows. The annulus is filled about 3/4 full with a fairly dry mix of the cement and then cured for about four hours at 250°F. Next, a wet wash is applied and the washer placed on top. The assembly is then cured for about four hours at 700° F

Procedure

Ambient Temperature Runs.- The procedure in making the runs at ambient temperature is as follows: when the wet test meter is used, the system is purged for about 30 minutes to remove residual gases from the meter. The pressure regulator is adjusted to give the desired pressure difference across the specimen. Several minutes are allowed for the system to stabilize, Then the measurements are made.

Elevated Temperature Runs.- The procedure in making the runs at elevated temperatures is as follows: the housing is brought up to temperature with no gas flow through the apparatus. After the housing temperature stabilizes, the gas flow is turned on and the pressure regulator is set to give the desired pressure drop across the specimen. The gas preheater is then turned on and the input power is increased until the gas reaches the same temperature as the housing At least two data points are taken at each pressure level to monitor that the two temperatures are in equilibrium and to reduce the risk of obtaining spurious readings.

General

During the runs the following data are recorded:

1. Atmospheric pressure.
2. Differential pressure across specimen.
3. Downstream gage pressure.
4. Pressure at flow instrument (at inlet to wet test meter or flowmeter; when flowmeter is used on the downstream side of housing no readings are taken because of the small pressure drop through the flowmeter venting to atmosphere)
5. Flowmeter readings,
6. Housing temperature.
7. Gas temperature.
8. Temperature at wet test meter (when used).

All flowmeter readings are converted to the volumetric flow rate at standard pressure

DATA CORRELATION

Theory

Greenberg and Weger[1] concluded from a review of some of the literature on permeability that most of the data could be correlated with an equation of the type:

$$-\frac{dP}{dx} = \alpha \mu V + \beta \rho V^n \qquad (1)$$

where

$\frac{dP}{dx}$ = pressure gradient in the direction of flow

α = viscous flow coefficient (reciprocal of Darcy's constant, k)

V = instantaneous gas velocity

β = inertial flow coefficient

ρ = instantaneous gas density

μ = absolute viscosity

and where n is some number between 1 and 2.

Carman[2] selected the value of n as 2 to account for turbulent flow. Greenberg and Weger[1] also state that correlations of the data of Cornell and Katz indicate that the value of n should be 2 to account for inertial flow through consolidated media.

In equation (1), the first term on the right-hand side represents the resistance due to viscous flow. The second term on the right-hand side represents the resistance due to inertial flow. Inertial flow results from turbulence induced by the tortuous path the gas must follow through the porous material and also by high velocities. Both of these phenomena depend upon the kinetic energy of the fluid per unit volume, ρV^2 Thus, in developing equation (1) it was assumed that the expression for the inertial resistance could be superimposed upon the expression for the viscous resistance.

---

[1]See Refererences

Under steady-state conditions, the mass velocity of gas (for one-dimensional flow) through a porous media must be constant. By letting $\rho V = G$ and $n = 2$, equation (1) becomes

$$-\rho \frac{dP}{dx} = \alpha \mu G + \beta G^2 \tag{2}$$

where G = mass velocity.

Now, for an ideal gas

$$\rho = \frac{PM}{RT} \tag{3}$$

where

P = absolute pressure

M = molecular weight of gas

R = universal gas constant

T = absolute temperature

Substituting equation (3) into equation (2) and rearranging yields

$$-\frac{PM}{RT\mu G}\frac{dP}{dx} = \alpha + \frac{\beta G}{\mu} \tag{4}$$

or

$$-\frac{M}{RT\mu G}\int_{P_1}^{P_2} P\,dP = \left(\alpha + \frac{\beta G}{\mu}\right)\int_0^L dx$$

Integrating and rearranging equation (4) yields

$$\frac{MP_m\Delta P}{LRT\mu G} = \alpha\gamma + \beta\left(\frac{G}{\mu}\right) \tag{5}$$

where

$P_m = \frac{1}{2}(P_1 + P_2)$ = mean specimen pressure

$\Delta P = (P_1 - P_2)$ = differential pressure

L = thickness of specimen

Since G is a constant, one may write

$$G = \frac{QSTP\ \rho STP}{A} \tag{6}$$

where

Q_{STP} = volumetric flow rate at standard conditions

ρ_{STP} = gas density at standard conditions

A = total cross section of porous media normal to flow

Data Reduction

The dependent and independent variables in equation (5) are calculated for each data point. Then a plot of $MP_m\Delta P/LRT\mu G$ versus G/μ is made. Such a presentation is known as a Cornell and Katz plot. A straight line is drawn through the points thus plotted and the viscous and inertial coefficients obtained from the intercept and slope of the curve, respectively. Thus, for each specimen evaluated one viscous and one inertial coefficient are calculated at a given temperature level. Data are obtained over a sufficient range of the parameter (G/μ) to allow a good correlation and reduce the effects of spurious readings. The uncertainty in the reduced data is estimated to be ± 5 percent.

Some reduced data for a low-density phenolic-nylon char are presented infigure *G3.* This figure shows typical data scatter about a straight line plotted through the data points. It has been our experience that the equation shown plotted in figure *G3,* equation (5), correlates the data for porous materials which we have evaluated,

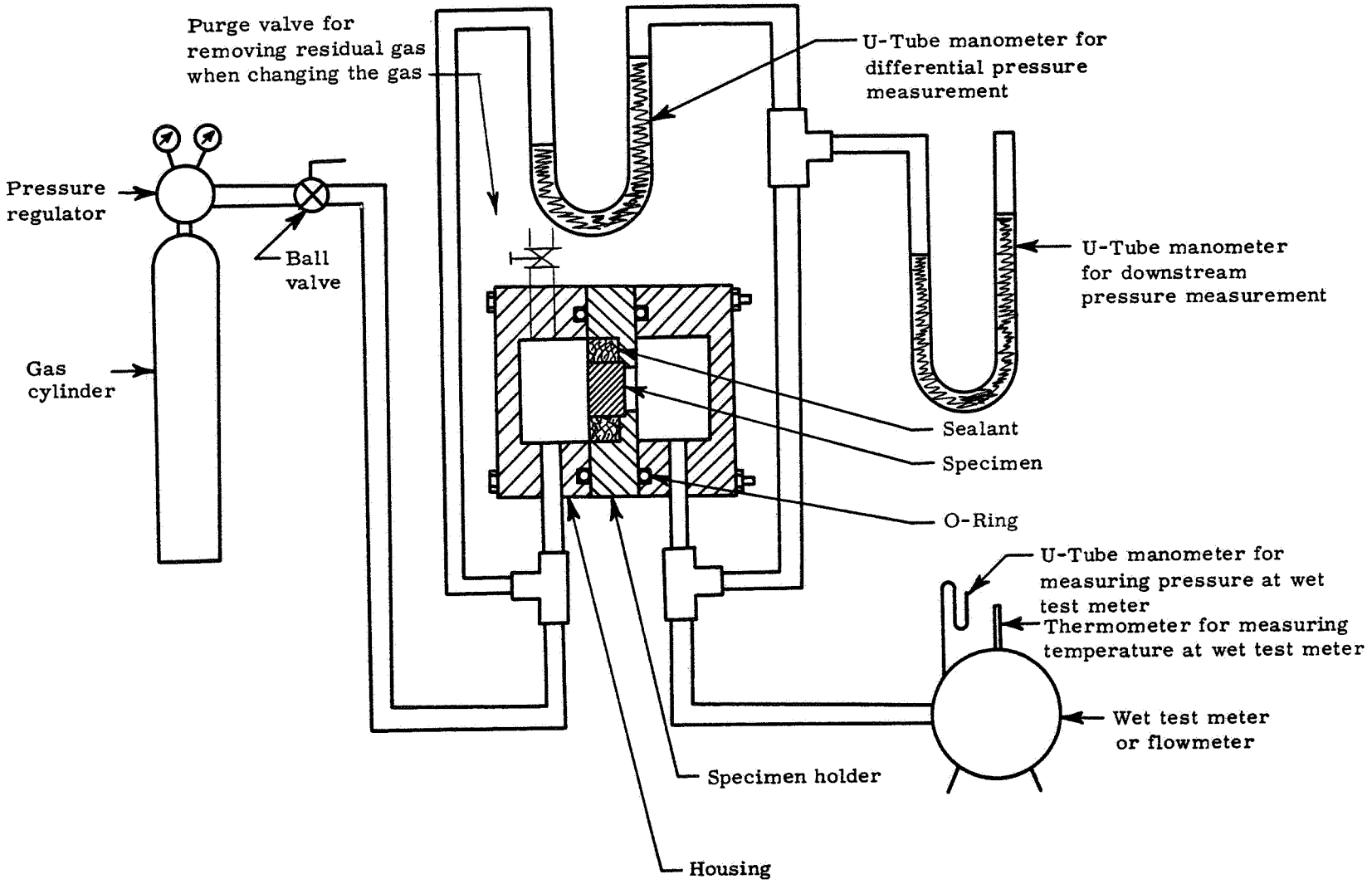

Figure G1. Permeability apparatus for low permeability materials

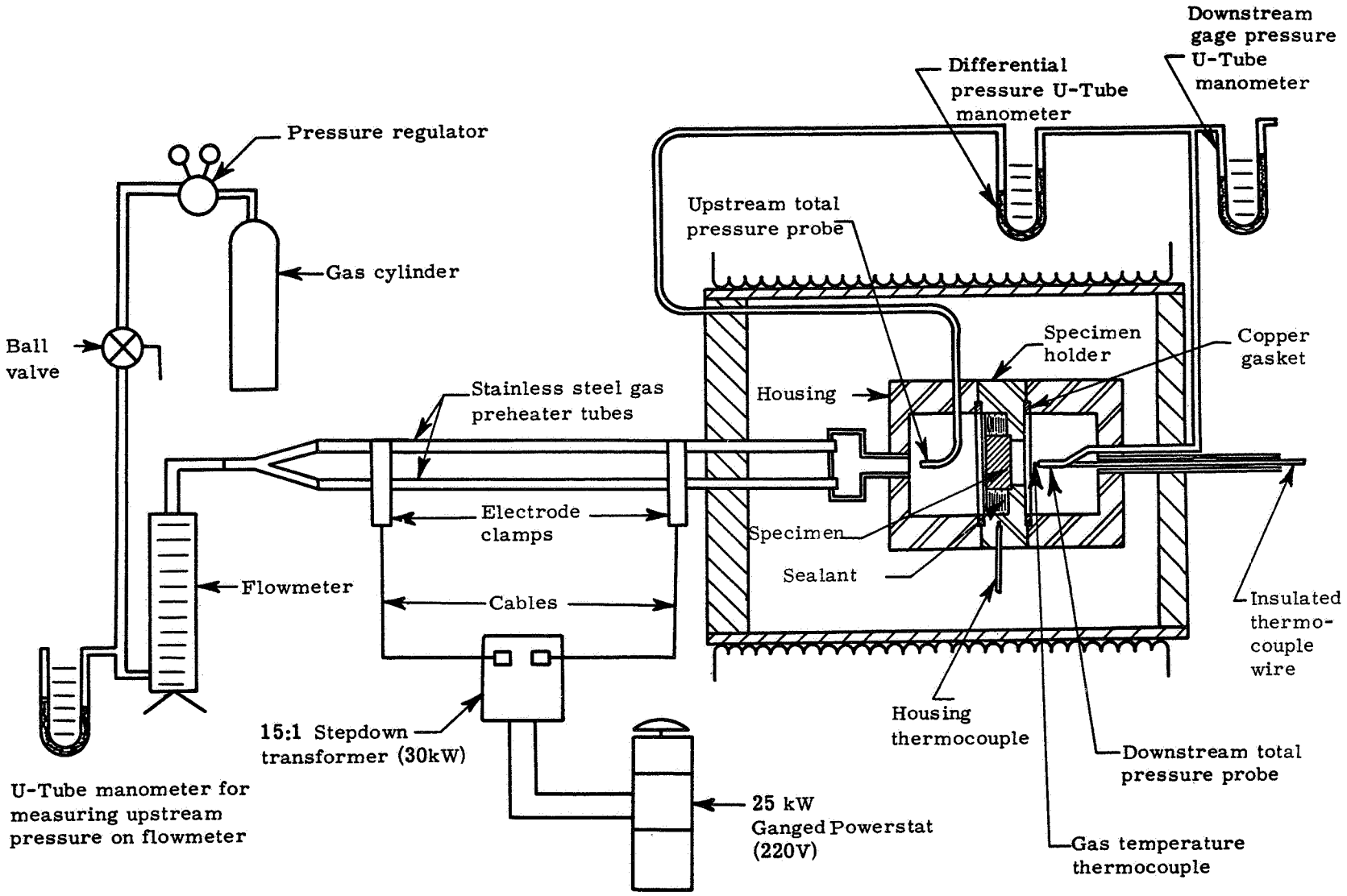

Figure G2. Permeability apparatus for measurements to 1000°F

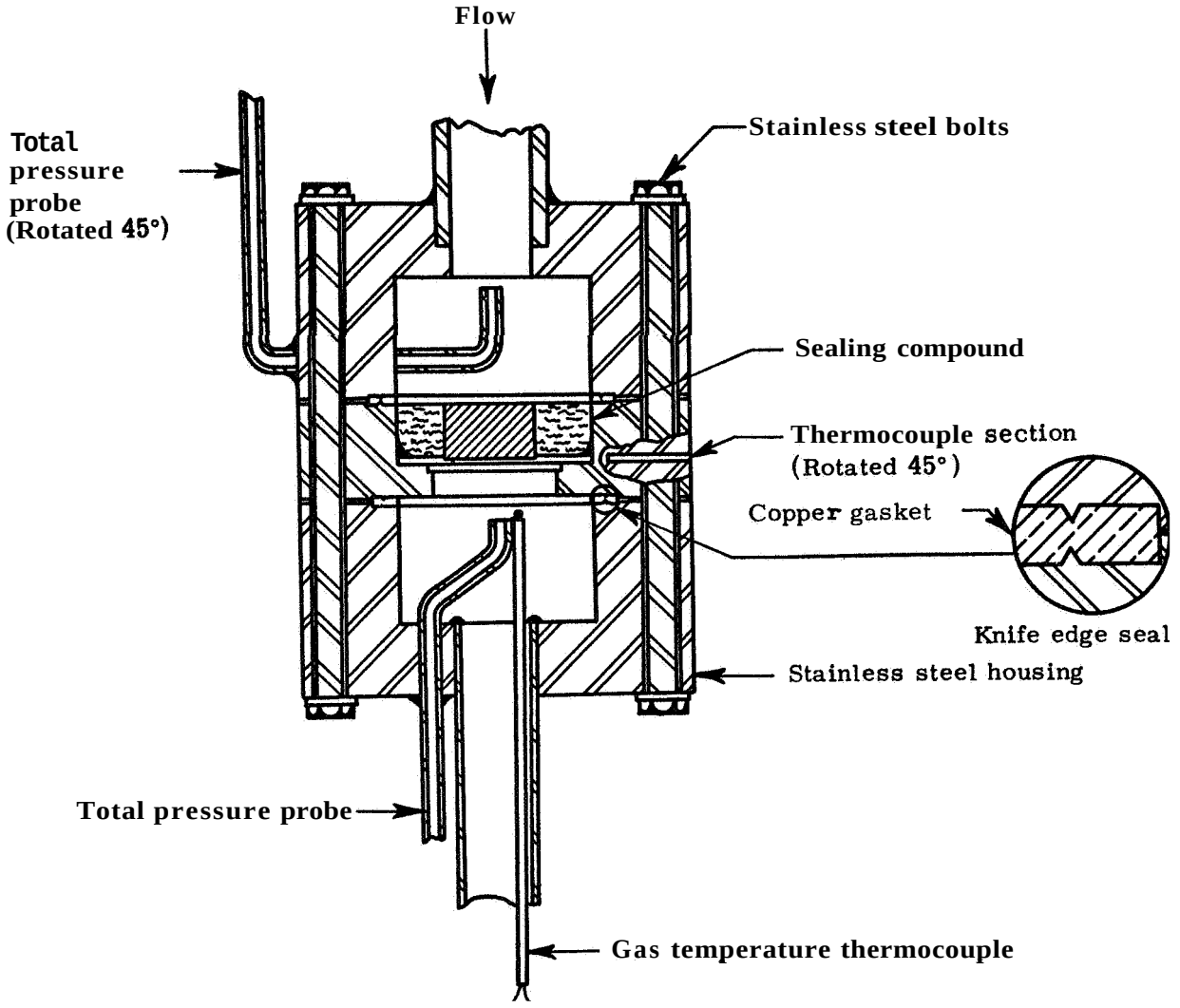

Figure G3. Details of specimen holder for high temperature permeability materials

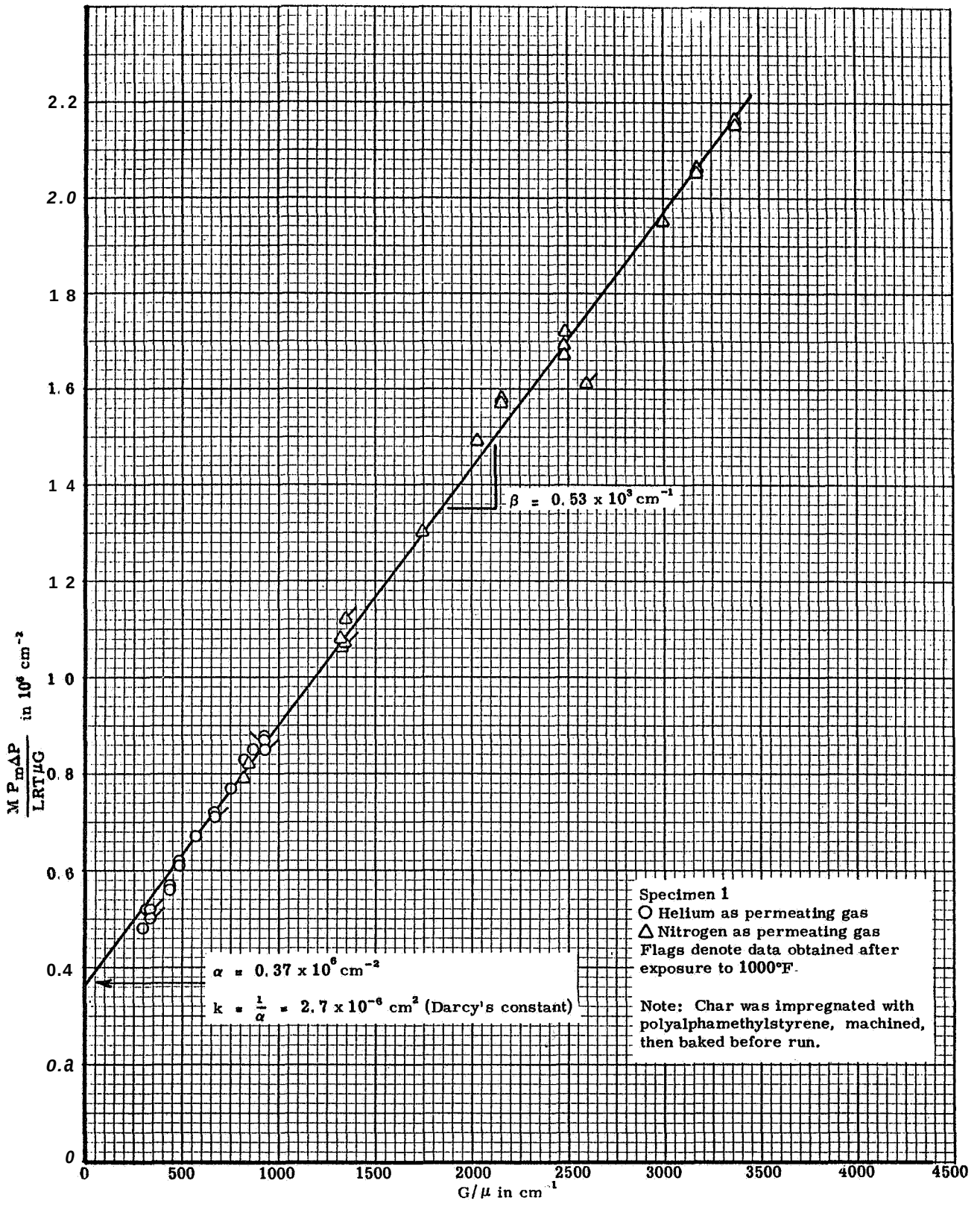

Figure G4. Cornell and Katz plot for low-density phenolic-nylon char perpendicular to the charring direction at room temperature

REFERENCES

1. Greenberg, D. B. and E. Weger, "An Investigation of the Viscous and Inertial Coefficients for the Flow of Gases through Porous Sintered Metals with High Pressure Gradients," Chemical Engineering Science 12, Pergamon Press Ltd., London, pp 8-19, 1960.

2. Carman, P. C., Flow of Gases through Porous Media, Academic Press, Inc., New York, 1956.

APPENDIX H

NATURE OF THE PHENOLIC-NYLON CHARRED IN THE FURNACE AT A RAPID HEATING RATE (Cold Wall Heat Flux of About 4.9 MW/m²)

General

The nature of the phenolic-nylon charred in the furnace to a rapid heating exposure was quite different from that charred to the slow heating cycle. Even though these two chars are called "rapid" chars and "slow" or "furnace" chars, respectively, do not infer that the rate of heating was the only difference. There were other environmental differences including elapsed time at different temperatures, exact gas chemistry immediately surrounding the char at any instant, impurity leaks into the furnace and impurities evolved from different graphite heaters in the furnace. Thus the terms rapid and slow (or furnace) chars refer to the total process or total environmental history during their formation.

In the text several references were made to the fact that the chars prepared in the furnace at a rapid heating cycle to high temperatures (3033°K) were more graphite-like than those prepared in the arc-jet on the furnace at a low heating cycle. The prime reason for that conclusion was that the rapid chars exhibited a thermal conductivity response which was graphite-like (higher values which decreased with increasing temperature at low temperatures) while the other chars did not exhibit a character or level consistent with graphite behavior. Other monitors such as true density provided similar evidence. Additional X-ray diffraction measurements were made after the fact to investigate whether or not this behavior of thermal conductivity was related to the structure. This appendix summarizes the conditions leading to and the results of the X-ray diffraction measurements.

The slow furnace char (S) was prepared by heating to 3033°K at a rate of 10°K/min., holding at temperature for one hour, and cooling at 10°K/min. The rapid char (5000-R2) was prepared by immersing a cylinder of phenolic-nylon in a furnace which was preheated to 3033°K (cold wall heat flux of about 4.9 MW/m²). The sample reached 3033°K in about 100 seconds (it was calculated that this was about the time required to achieve 3033°K throughout the material) and it remained at this temperature for 5 minutes. At the end of the 5 minute soak, power to the furnace was shut off and the sample cooled below 2000°K in about 10 - 15 minutes. Pictures of a rapid char are shown in figure 132.

The surface of the rapid char had a more dense appearance than the interior as if some deposition might have occurred in the vicinity of the surface. Perhaps the thought of a deposition occurs because of considerable information in the literature that deposition does occur at the outer surface of an ablative material as the gases reach the hotter deposition temperatures. Thermal conductivity strips were cut from the rapid char and thermal conductivity was measured to 3033°K (about one hour hold during measurements at highest temperature) with the radial inflow apparatus. The cylinder surface was cut away in making the strips for the radial inflow and hence the specimen was taken from the interior. Subsequently, the strips were machined into specimens for the comparative rod and thermal conductivity was again measured to 1000°K.

Three X-ray diffraction samples were taken from the rapid char. Two were taken from the "as-charred" material; (RO) was the sample from the surface (to a depth of about 2 mm) and (RI) was the sample from the interior (at a depth of more than 2 mm). The thermal conductivity sample used for the radial inflow and comparative rod apparatuses (5000-R2) was also used for X-ray diffraction (RK). These identifications have been maintained for the X-ray diffraction measurements, (S) - slow char, (RK)- rapid char specimen 5000-R2 used for thermal conductivity measurements, (RO)- outside of rapid char and (RI)- interior of rapid char.

Before discussing the X-ray diffraction results the other observations about the rapid char will be reviewed, During charring the weight loss of the rapid char was less than that of the slow chars; about 53 percent as compared to about 75 percent for the slow chars. The bulk density of the rapid char was about 0.23 gm/cm^3 as compared to 0.35 gm/cm^3 for the slow char prepared at 3033°K and the true density value for the rapid char was 1.78 gm/cm^3 as compared to 1.46 gm/cm^3 for the slow furnace chars. Finally, the experimental thermal conductivity curve for the rapid char was graphitic in character and the reduced values of matrix thermal conductivity were within the range of values normally associated with graphite-like materials (see figures 151 and 169). At this point, it appeared that the rapid char was more graphite-like than the slow char. Now, the results of the X-ray diffraction measurements will be discussed.

The results of the X-ray diffraction measurements are presented in the table at the end of this appendix. The results have been presented in terms of the lattice spacing of the graphite basal planes. The d_c lattice spacing (002,004, etc.) is that of the graphite basal planes and is the most important measure of "degree of graphitization." ASTM card 12-212 assigns this spacing a value of 3.37 Å for synthetic graphite to give a unit cell value of 6.74 Å. ASTM card 13-148 assigns the d spacing a value of 3.35 Å for a

natural graphite to give a unit cell value of **6.70** Å. The value of **3.354** Å is taken by most investigators as that corresponding to complete ordering. In contrast, a value of **3.44** Å or above is normally associated with complete disorder. The slow furnace chars and the arc-jet chars all exhibited $d_{c(002)}$ values of **3.44** Å or above which indicates complete disorder (see text). The slow furnace char for which data are included in this appendix had a value for d_c of **3.428** Å (see table) which indicates some order. This value is different than the value of **3.44** Å reported in the text because it was calculated from the second-order diffraction peaks **(004)** whereas for the measurements reported in the text the first-order reflections (002) were used. Nevertheless, both measurements indicate that the slow char was poorly graphitized.

Observe in the table that the $d_{c(004)}$ lattice spacings for the rapid char were all lower than for the slow char, decreasing *from* **3.410** Å for sample TO to **3.396** Å for sample RI and **3.391** Å for sample RK (taken from thermal conductivity specimen after re-exposure to **3033°K).** These values indicate that the rapid char was significantly more graphite-like than the slow char. The high values of $p_{c(004)}$, **0.66** to **0.81** as opposed to less than **0.2** for very well-graphitized material make the X-ray results less striking than the, thermal conductivity results. Values of d spacings of **3.360** and **3.361** Å (p_c = **0.26** and **0.29** calculated) have been reported for ATJ and ATJ-S graphites.[1] Further, measurements here on ATJ-S graphite have shown d lattice spacings of **3.375**, **3.380**, **3.370** Å (p_c = **0.43**), **3.385** Å (p_c = **0.60**) and **3.395** Å (p_c = **0.69).** No precise history has been kept on these specimens. The latter two values were obtained on the same piece of material. The fact that graphite has shown values of p_c near those for the rapid char indicates that the thermal conductivity of the char should not necessarily be lower than that of graphite.

Note in the table that the material near the surface of the rapid char was less graphite-like than that in the interior as indicated by a higher value for $d_{c(004)}$. The interior of the rapid char in the "as-charred" condition (RI) was only slightly less graphite-like than the char which was reheated to **3033°K** during a thermal conductivity evaluation. Since the thermal conductivity

---

1. Maahs, Howard G., "Crystallographic Data on Selected Artificial Graphites with Comments on the Role of the Degree of Crystal Development in Oxidation," NASA TN D-4888, November **1968.**

specimen from the rapid char exhibited graphite-like behavior at the first data point (1070°K) and since the absolute values of the first few points were quite high, it appears that the material was graphite-like in the "as-charred" condition and was not made much more graphite-like by the exposure.

The X-ray diffraction measurements do not offer positive proof that a graphite was produced by rapid charring. However, the X-ray measurements do support the thermal conductivity results and together they suggest that the rapid char was more graphite-like. Unfortunately, no one can yet conclusively assign a value of thermal conductivity to a given value of p_C (probability of disorder between adjacent graphite layers).

The data suggest that the trend toward enhanced graphite-like behavior for the rapid char results from lattice changes rather than a deposition phenomena if it occurred. More deposition probably would occur near the heated face since there would be more possibility of chemical cracking or mechanical deposition at this location. The X-ray data suggest that any deposition near this face was not more highly ordered than the char.

Characterization by X-ray Diffraction of Two Char Specimens

The data herein reported and the associated comments were requested of the Inorganic Materials Section because a difference in thermal conductivity was observed between two char specimens which differed only in the rate at which the char temperature was reached and the time of soak at 3033°K. The rapidly charred-short soak time specimen possessed the higher K value.

The data acquired are presented in the accompanying table. This information is presented in a form similar to that used by other investigators whose work appears in the literature. However, the data are only suitable for comparison of the four samples examined. The techniques used are imperfect compared to those which would be used if this type of characterization were to be a specific facet of an investigation. In the present work no internal standard was used, no corrections applied, peaks were not electronically quantitized, etc., and one should therefore not attempt to relate the numbers to other literature.

The characteristics listed in the attached table can be defined as follows:

d_c - This is the lattice spacing for the graphite basal planes. This value multiplied by **2** gives the value of the unit cell along the "c" axis, c_0. The subscript Miller index (004) signifies it was calculated from the second-order reflection. The calculation is made from the angular position of the diffraction line using the Bragg equation - $n\lambda = 2d \sin 8$. The d_c value is the most important measure of degree of graphitization. The value for d_c of **3.440** indicates complete disorder, while **3.354** shows complete ordering.

p_c - The value p_c is an expression of the probability of adjacent graphite layers being disordered, In the attached table, p_c was calculated from the expression

$$d_c = 3.440 - 0.086\ (1 - p^2)$$

taken from Franklin, Acta Cryst. **4, 1951,** pp **253-261.** Again, the subscript **(004)** means the second-order basal plane reflection was used. Within the range of p_c values determined, this expression is considered suitable,

$I_{(002)}$ - This value has no fundamental meaning. In this table it merely relates, on a percentage basis, the intensities of the most intense line (002) for the four patterns run. Film 217 gave the most intense 002 line.

L_c - This is a measure of the crystallite size in Angstroms and was calculated from the Scherrer equation

$$L_{(hkl)} = \frac{0.89\lambda}{\beta_{\frac{1}{2}} \cos\theta}$$

The subscript c (002) means it refers to the crystallite height and was calculated from the (002) diffraction line.

$d_{a(110)}$ - This is the d spacing for the (110) diffraction planes and two times this value gives the other unit cell dimension, a_0. Normally for graphitic carbons this value is invariant at **1.2307** Å.

The tabulated data justify the following observations:

1. The slowly charred material is less well graphitized than that which was rapidly charred.

2. The peripheral $\frac{1}{16}$" skin of the rapidly charred material is not graphitized to the same degree as the inside material. (In the case of the slowly charred material, no record was kept regarding geometric position; sample acquired a year ago.)

3. The additional thermal exposure during conductivity measurement apparently increases the degree of graphitization.

4. Although none of these specimens would be considered a well-graphitized material, the rapidly charred specimen, which had been subjected to K measurements, possesses the greatest degree of graphitization of a char that has been examined in this laboratory. The high p_c values and small values for L_c indicate poor graphitization.

The above observations are interesting but do not contribute to unequivocable conclusions. They do induce much speculation.

It has been noted that differences in color and physical structure exist between the peripheral layer and inner core of the rapidly charred specimen. Furthermore, the separation of these two regions was not complete in acquiring X-ray samples. Therefore, it is quite possible that the inner material (Film 219) should have more closely approximated the data for the specimen which had been measured for thermal conductivity and that the thermal input due to K determination did not influence the degree of graphitization. Also, had the separation been perfect, the data for the peripheral layer (Film 218) may have more closely resembled those of the slow char (Film 216).

It is the writer's understanding that the conductivity specimen for the rapidly charred material was taken in a manner which excluded the peripheral layer, while the specimen representing the slowly charred material was precut to size before charring. If it is assumed that the depth of the peripheral layer is time-dependent, one might conclude that the values in the table for the slowly charred specimen are representative of the whole conductivity specimen. It would seem that on the one hand, higher thermal conductivity was recorded for a material having a d_c of 3.39 to 3.40 and a denser structure (rapidly charred) and on the other, lower conductivity was recorded for a specimen having a less dense structure and a d_c of 3.42 to 3.43 (slowly

charred). The magnitude of the effect of (1) the degree of graphitization and (2) physical structure on conductivity is beyond the scope of this discussion. The point is that, in addition to the difference in graphitization, there probably is a difference in physical structure between the two specimens and that the whole of the slowly charred specimen probably is similar to the outer layer of the rapidly charred specimen. To have a chance to separate these effects, more complete characterization would be required.

Even if one's thoughts are restricted to the degree of graphitization versus thermal exposure, only speculative explanations result. Factors such as maximum temperature, time at maximum temperature, rate of heating, environmental conditions, etc., influence the degree of graphitization for a given starting material. The obvious differences in charring conditions for the specimens of interest are the heating rate and soak time. One can readily picture a potential effect of rapid heating. One could assume a complex intermediate state could be created or avoided by rapid heating, the presence or absence of which contributes to enhanced graphitization. The review of literature pertaining to the thermal degradation of phenolic resin and nylon separately and in combination as a function of heating rate and atmosphere probably would offer assistance. Heating rate may also determine the effluent species which, in turn, could affect the degree of graphitization, A fast rate may also have the result of somewhat inhibiting outgassing, which could promote graphitization.

The information which causes difficulty with respect to the speculation concerning heating rate is that the outer surface of the rapidly charred material resembles that of the bulk of the slowly charred material. This would suggest that soak time may be an important parameter. One might visualize the vaporization of a species which promotes graphitization occurring at a relatively low temperature or during the prolonged exposure at the soak temperature. In other words, would the outer surface of the rapidly charred specimen resemble the slowly charred speci-men if the reaction were only dependent on rate of heating? Would the rapidly charred specimen have had different characteristics if it had been allowed to remain at temperature for one hour?

On the other hand, one might consider the potential effect of some environmental agent. If one assumes a very short exposure time is required at 3000°K to carbonize and partially graphitizes the phenolic-nylon composite, any additional time used to raise the temperature or soak the specimen in a nocuous atmosphere could adversely influence the graphitization procedure. Graphite reacts with many other materials; for example, by processes of oxidation and intercalation. Since these processes can influence thermal,

mechanical, electrical properties, etc, , they probably affect lattice parameters. Therefore, one could speculate that slow heat up and/or long soak time allows undesirable minor environmental agents to have a role in the ultimate character of the char.

If one wishes to understand the observations and leave the area of speculation, one needs additional accurately controlled experimental evidence, the consultation of organic chemists, and the background of literature pertaining to the degradation of phenolics and nylon.

Before drawing conclusions regarding the anomalous thermal conductivity values, it might be well to reproduce the information starting with charring samples of similar geometry and providing detailed physical characterization data.

Summary of X-ray Diffraction Measurements on Phenolic-Nylon Charred in the Furnace (both Slow and Rapid Heating Rates)

	Film Number *				
Characteristic	(S) 216	(RK) 217	(RO) 218	(RI) 219	Very well-graphitized material
$d_{c(004)}$	3.428	3.391	3.410	3.396	3.354
$p_{c(004)}$	0.93	0.66	0.81	0.70	< 0.2
$I_{(002)}$	83	100	77	90	---
$L_{c(002)}$	33	63	69**	50	> 200
$d_{a(110)}$	1.225	1.232	1.230	1.230	1.2307

* 216 - (S) slow char; no subsequent thermal properties measured.
217 - (RK) rapid char; K measured to 5000°F.
218 - (RO) rapid char; no subsequent thermal properties measured. Sample came from outer edge (2mm) of the charred material.
219 - (RI) same as 218, but sample came from the interior of the charred material.

**This value is too high for no apparent reason. The peak breadth was checked for the (004) line and had it been used in the calculation of L_c, the value for Film 218 would have fallen between those of Film 216 and 219.

ERRATA

NASA CR-66731

AN INVESTIGATION OF SOME THERMAL AND MECHANICAL PROPERTIES OF A LOW-DENSITY PHENOLIC-NYLON ABLATION MATERIAL

By H. G. Sanders, E. D. Smyly, and C. D. Pears

February 1969

Page 216: In figure 114, the plane identified as (100) with a spacing of 2.13 Å is incorrectly shown. The plane shown is the (110) plane with a spacing of a_o = 2.46 Å. A revised figure is attached.

Inserted 7/29/05

Issue date: April 1,1969